

INFORMATION TO USERS

This manuscript has been reproduced from the microfilm master. UMI films the text directly from the original or copy submitted. Thus, some thesis and dissertation copies are in typewriter face, while others may be from any type of computer printer.

The quality of this reproduction is dependent upon the quality of the copy submitted. Broken or indistinct print, colored or poor quality illustrations and photographs, print bleedthrough, substandard margins, and improper alignment can adversely affect reproduction.

In the unlikely event that the author did not send UMI a complete manuscript and there are missing pages, these will be noted. Also, if unauthorized copyright material had to be removed, a note will indicate the deletion.

Oversize materials (e.g., maps, drawings, charts) are reproduced by sectioning the original, beginning at the upper left-hand corner and continuing from left to right in equal sections with small overlaps.

Photographs included in the original manuscript have been reproduced xerographically in this copy. Higher quality 6" x 9" black and white photographic prints are available for any photographs or illustrations appearing in this copy for an additional charge. Contact UMI directly to order.

**ProQuest Information and Learning
300 North Zeeb Road, Ann Arbor, MI 48106-1346 USA
800-521-0600**

UMI[®]

University of Alberta

Coordination Chemistry of the New Preorganized Polyphenoxide Ligand Tetrakis(2-hydroxyphenyl)ethene Derivatives. Attempts to Create Surface-Models for Classic Ziegler-Natta Olefin Polymerization Catalysts

by

Megumi Fujita



A thesis submitted to the Faculty of Graduate Studies and Research in partial fulfillment of the requirements for the degree of Doctor of Philosophy

Department of Chemistry

Edmonton, Alberta

Fall 2001



**National Library
of Canada**

**Acquisitions and
Bibliographic Services**

**395 Wellington Street
Ottawa ON K1A 0N4
Canada**

**Bibliothèque nationale
du Canada**

**Acquisitions et
services bibliographiques**

**395, rue Wellington
Ottawa ON K1A 0N4
Canada**

Your file Votre référence

Our file Notre référence

The author has granted a non-exclusive licence allowing the National Library of Canada to reproduce, loan, distribute or sell copies of this thesis in microform, paper or electronic formats.

The author retains ownership of the copyright in this thesis. Neither the thesis nor substantial extracts from it may be printed or otherwise reproduced without the author's permission.

L'auteur a accordé une licence non exclusive permettant à la Bibliothèque nationale du Canada de reproduire, prêter, distribuer ou vendre des copies de cette thèse sous la forme de microfiche/film, de reproduction sur papier ou sur format électronique.

L'auteur conserve la propriété du droit d'auteur qui protège cette thèse. Ni la thèse ni des extraits substantiels de celle-ci ne doivent être imprimés ou autrement reproduits sans son autorisation.

0-612-68932-8

Canada

University of Alberta

Library Release Form

Name of Author: Megumi Fujita

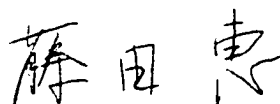
Title of Thesis Coordination Chemistry of the New Preorganized Polyphenoxide Ligand Tetrakis(2-hydroxyphenyl)ethene Derivatives. Attempts to Create Surface-Models for Classic Ziegler-Natta Olefin Polymerization Catalysts

Degree: Doctor of Philosophy

Year this Degree Granted: 2001

Permission is hereby granted to the University of Alberta Library to reproduce single copies of this thesis and to lend or sell such copies for private, scholarly or scientific research purposes only.

The author reserves all other publication and other rights in association with the copyright in the thesis, and except as herein before provided, neither the thesis nor any substantial portion thereof may be printed or otherwise reproduced in any material form whatever without the author's prior written permission.



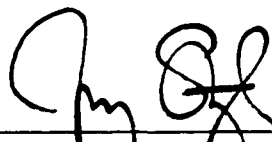
49-4-101 Matsugaya, Hachioji, Tokyo
192-0354, Japan

August 03, 2001

University of Alberta

Faculty of Graduate Studies and Research

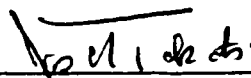
The undersigned certify that they have read, and recommended to the Faculty of Graduate Studies and Research for acceptance, a thesis entitled *Coordination Chemistry of the New Preorganized Polyphenoxide Ligand Tetrakis(2-hydroxyphenyl)ethene Derivatives. Attempts to Create Surface-Models for Classic Ziegler-Natta Olefin Polymerization Catalysts* submitted by Megumi Fujita in partial fulfillment of the requirements for the degree of Doctor of Philosophy.



Dr. Jeffrey M. Stryker (Supervisor)



Dr. Derrick L. J. Clive



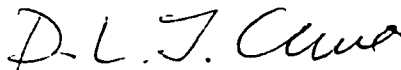
Dr. Josef Takats




Dr. Rik R. Tykwinski



Dr. Sieghard Wanke



Dr. Sandro Gambarotta

Approved July 30, 2001


Abstract

The derivatization of the newly developed preorganized tetraphenol ligand tetrakis(2-hydroxyphenyl)ethene, the coordination chemistry of the derived ligand systems, and verification of their potential as polymerization catalysts are described in this thesis.

Ortho-propylated analogue tetrakis(2-hydroxy-3-propylphenyl)ethene and selectively alkylated *E*- and *Z*-bis(2-hydroxyphenyl)-bis(2-methoxyphenyl)ethenes were synthesized as modified ligands of the parent system, tetrakis(2-hydroxyphenyl)ethene. The ability of these ligands to serve as templates for constructing polymetallic coordination complexes, especially hetero-polymetallic species, was examined by using three metal elements, titanium(IV), magnesium(II) and aluminum(III), as potential models of classic heterogeneous Ziegler-Natta catalysts.

The *ortho*-propylation of the ligand system contributed to the reduced tendency for intermolecular aggregation. Various coordination patterns and chemical reactivity were observed in the polynuclear complexes and were quite specific to the metal and other ligand groups. "All-up" trinuclear structures were always observed for magnesium complexes. "Up/down" dinuclear structures, mostly geminal, were preferred for titanium complexes. Aluminum complexes showed various coordination patterns, from six-membered crown ring systems to symmetrical and unsymmetrical dinuclear structures, depending upon the degree of exposure to a coordination solvent and the different substituents on the aluminum atoms. Several hetero-polymetallic complexes were also developed, starting from a magnesium complex.

The *E*-dialkylated ligand exhibited an ability to form well-organized titanium and aluminum complexes. The titanium complexes were all mononuclear, while both mono-

and dinuclear aluminum complexes were obtained. The latter, however, basically consisted of a core mononuclear structure appended to an alkylaluminum reagent through a dative interaction. Attempted synthesis for aluminum/titanium hetero-polynuclear complexes extended our understanding of the ligand's coordination tendency. The Z-dialkylated ligand, on the other hand, was found to be a poor template for the construction of discrete metal complexes.

The titanium complexes of these preorganized phenoxide ligands showed poor ethene polymerization activity. Meanwhile, when titanium precatalysts were prepared in situ from the corresponding magnesium complexes, high polymerization activity was observed. The active catalytic species must somehow involve magnesium in the newly formed titanium aryloxide. This "magnesium effect" was not specific to preorganized systems, but also true for simpler phenoxide systems. The preorganization of the designed ligand systems contributed to the narrower polydispersity of the product polyethene.

Acknowledgement

My sincere gratitude to my supervisor Dr. Jeff Stryker, for support and encouragement, and the colleague Udo Verkerk, who set the basis of this project. Also to the other past and present labmates, especially Dr. Makoto Yasuda for useful discussions and friendship, and Dr. Charles Carter and Dr. Sensuke Ogoshi for teaching various lab techniques in my early years. Many thanks to Dr. Bob McDonald in the X-ray lab and the skilled staff in the Analysis Lab, the NMR lab, the mass spectroscopy lab, the glass shop, and the machine shop. Acknowledgements to the Department of Chemistry and University of Alberta, for encouraging and giving chances to a foreign student with a B.A. degree. Special thanks to Dr. Lois Browne, for care and support in many ways, and my close friends who shared funny experiences as foreign students in Canada. Finally, the best gratitude to my family back in my home country.

Table of Contents

General Introduction	1
Chapter 1. Ligand Synthesis and Modification	2
1.0. Introduction	3
1.1. Modification of Tetrakis(2-hydroxyphenyl)ethene Framework	9
1.1.1. <i>Ortho</i> -Substituent Introduction	9
1.1.2. Partial Protection/Deprotection of Hydroxy Groups	13
1.1.3. Attempts to Introduce Other Heteroatoms	22
1.2. Synthesis of 2,7-Bis(1,1-dimethylethyl)-9H-fluorene-1,8-diol (4)	23
1.3. Conclusion	25
1.4. Experimental	26
1.5. References and Notes	45
Chapter 2. Preface to Chapter 3 and 4	47
Chapter 3. Metal Complexes Derived from Tetrakis(2-hydroxy-3-propylphenyl)ethene: Structure, Spectroscopic Features and Chemical Behavior	56
3.0. Introduction	58
3.1. Homo-polymetallic Complexes	61
3.1.1. Mg Complexes	61
3.1.2. Ti Complexes	77
3.1.3. Al Complexes	109
3.1.4. Na Complex	121
3.2. Hetero-polymetallic Complexes	124
3.1.1. Mg/Al Complexes	126
3.1.2. Mg/Ti Complex	134
3.1.3. Al/Ti Complex	136
3.1.4. Other Attempts to Prepare Hetero-Polymetallic Complexes	139
3.3. Conclusion	139
3.4. Experimental	141

3.5.	References and Notes	167
Chapter 4. Metal Complexes Derived from <i>E</i>- and <i>Z</i>-Bis(2-hydroxyphenyl)-bis(2-methoxyphenyl)ethene (3<i>E</i>/3<i>Z</i>): Structure, Spectroscopic Features and Chemical Behavior		
4.0.	Introduction	170
4.1.	Al Complexes	172
4.2.	Ti Complexes	182
4.3.	Attempts to Construct Al/Ti Complexes	192
4.4.	Conclusion	202
4.5.	Experimental	203
4.6.	References	212
Chapter 5. Ethene Polymerization by Derivatives of the Preorganized Polyaryloxy Ligands		
5.0.	Introduction and Overview	214
5.1.	Ti Complexes	215
5.2.	Magnesium Effect	222
5.3.	Conclusion	254
5.4.	Experimental	256
5.5.	References and Notes	282
General Conclusion		284
Apendices X-ray Crystallography Data		286

List of Tables

	page
Table 3.1. Selected bond distances and torsional angles of 26 and 28 .	68
Table 3.2. Distance from the least-squares plane of O1-O2-O1'-O2' (Å).	69
Table 3.3. Non-bonding interatomic distances between the proton at 6-position of each ring.	87
Table 3.4. Selected distances and angles for 41 and 42 .	129
Table 3.5. Distance from the least-squares plane of O1-O2-O1'-O2' or O1-O2-O3-O4 (Å): comparison of 25 , 41 and 42 .	131
Table 3.6. Chemical shifts (¹ H NMR) of the coordinating THF and ethyl groups on Mg or Al atoms in complexes 41 and 42 .	132
Table 3.7. Attempts to prepare Mg/Ti hetero-polymetallic species.	136
Table 4.1. Comparison of the electron counting for 52 and 59 .	195
Table 5.1. Ethene polymerization trials with titanium complexes derived from ligands 7 , 3E and 4 .	217
Table 5.2. The different conditions to produce a catalyst from the metal derivatives of 4 .	223
Table 5.3. Control experiments with Na salt of 7 (40).	226
Table 5.4. Control experiments with Al salts of 3E .	228
Table 5.5. Control experiments with Mg salt of 3Z (76).	228
Table 5.6. Control experiments with Na salt of phenol (80).	229
Table 5.7. Control experiments with Na salt of hydroquinone (81).	231
Table 5.8. Composition of the magnesium salts evaluated for the influence of halides on the magnesium effect.	238
Table 5.9. Composition of the magnesium salts evaluated for the influence of solvating molecules on the magnesium effect.	241
Table 5.10. Ethene polymerization activity by the precatalysts prepared from 41 and TiCl ₄ .	245
Table 5.11. Ethene polymerization activity by the precatalysts prepared from 42 and TiCl ₄ .	245

Table 5.12.	GPC analyses of the polyethene from high temperature polymerization reactions <i>I</i> and <i>II</i>.	247
Table 5.13.	GPC analyses of H₂-incorporated polyethene products.	248
Table 5.14.	Activity of ethene polymerization reactions in the presence and absence of hydrogen partial pressure.	250

List of Figures

		page
Figure 1.1.	(a) <i>para-tert</i> -Butylcalix[4]arene. (b) Tetrakis(2-hydroxyphenyl)ethene 2 .	3
Figure 1.2.	Titanium complexes reported for (a) <i>para-tert</i> -butylcalix[4]arene and (b) tetrakis(5- <i>tert</i> -butyl-2-hydroxyphenyl)ethene.	6
Figure 1.3.	Aluminum complexes reported for (a) <i>para-tert</i> -butylcalix[4]arene and (b) tetrakis(2-hydroxyphenyl)ethene.	7
Figure 1.4.	Suggested structure of the oxidation product of tetrakis(4-hydroxyphenyl)ethene.	18
Figure 1.5.	Oxidation product of <i>para-tert</i> -butylcalix[4]arene.	19
Figure 1.6.	The structure of 3X ?	20
Figure 1.7.	Triflates 15 , 16E , 16Z and 17 .	22
Figure 2.1.	Rotation axes of (a) tetrakis(2-hydroxyphenyl)ethene 2 and (b) calix[4]arene.	48
Figure 2.2.	Hydrogen-bonding illustrations based on the crystal structures: (a) tetrakis(2-hydroxyphenyl)ethene 2 ; (b) <i>para-tert</i> -butylcalix[4]arene.	49
Figure 2.3.	Ethyl aluminum complex of 2 (R = Et).	50
Figure 2.4.	Different conformations of tetrakis(2-hydroxyphenyl)ethene.	50
Figure 2.5.	Active site of a Ziegler-Natta catalyst showing incoming propylene; the growing isotactic polypropylene chain; part of the support; and the residue of the AlEt ₃ promoter.	52
Figure 2.6.	Metal complexes of sterically hindered bisaryloxides used for olefin polymerization (M = Ti and/or Zr). The main contributor, the publication year and the activity class assigned by Gibson are provided for each system.	53
Figure 2.7	Half-metallocene with phenoxide pendant group by Marks (1997).	53
Figure 3.1.	List of characterized compounds in Chapter 3.	59
Figure 3.2.	Verkerk's collapsed Mg salt of the parent ligand 2 .	63
Figure 3.3.	X-ray crystallographic structure of 25 .	66

Figure 3.4.	X-ray crystallographic structure of 26 . With side and top views.	67
Figure 3.5.	X-ray crystallographic structure of 28 . With side and top views.	67
Figure 3.6.	The "tweezer" complex by Mach et al.	70
Figure 3.7.	¹ H NMR spectra of (a) 25 and (b) 7 in THF-d ₈ .	72
Figure 3.8.	¹ H NMR spectrum of 25 in C ₆ D ₆ .	73
Figure 3.9.	A terminal THF in the shielding region of neighboring aryl rings.	74
Figure 3.10.	Isofield diagram of ring current effects by a benzene ring on a proton nucleus, provided by Haigh and Mallion. The unit of the axes is benzene radius (1.39 Å), and the unit of shifts in the chemical shift is ppm.	75
Figure 3.11.	(a) Positions of the central THF protons against the ligand framework's aryl rings in the crystal structure of complex 26 . (b) Illustration of complex 26 from the top view, with the central THF oriented orthogonal to the olefin double bond of the ligand (as in the crystal state). (c) Illustration of complex 26 from the top view, with the central THF aligned parallel to the olefin double bond of the ligand.	76
Figure 3.12.	X-ray crystallographic structure of 30a .	80
Figure 3.13.	X-ray crystallographic structure of 33a .	81
Figure 3.14.	X-ray crystallographic structure of 34 with different angle views.	83
Figure 3.15.	X-ray crystallographic structure of 35 with different angle views.	84
Figure 3.16.	"Tilted or distorted T-structure" of benzene dimer, by Jorgensen et al.	82
Figure 3.17.	¹ H-NMR spectrum of 30a (C ₆ D ₆).	86
Figure 3.18.	Selected atom labels in the complex 30a .	87
Figure 3.19.	Positions of the H-6 protons in 30a against the geminal(g) or vicinal(v) neighboring ring.	89
Figure 3.20.	Positions of the H-6 protons in 26 against the geminal or vicinal neighboring ring.	89
Figure 3.21.	Positions of the benzylic methylene groups in 35 against the ligand's aryl rings.	91

Figure 3.22.	Positions of the H16 and H26 protons in complex 34 against the same-side Cp ring (C31~C35) and the opposite Cp ring (C31'~C35').	93
Figure 3.23.	The sandwich-type complex 32 .	94
Figure 3.24.	X-ray crystallographic structure of 32 .	95
Figure 3.25.	¹ H NMR spectrum of 32 (C ₆ D ₆).	96
Figure 3.26.	¹ H NMR spectra (part of aromatic region) of 30a and 30b (C ₆ D ₆).	98
Figure 3.27.	X-ray crystallographic structure of 31 the vicinal "up/down" isomer.	99
Figure 3.28.	Positions of the aromatic protons of 31 (dark dots) and 30a (light dots) against the geminal or vicinal neighboring ring.	101
Figure 3.29.	One possible structure of 36 , the adduct of 35 and B(C ₆ F ₅) ₃ .	105
Figure 3.30.	X-ray crystallographic structure of the complex 38 with different angle views.	110
Figure 3.31.	Verkerk's eight-membered Al crown complex (R = Me or Et).	111
Figure 3.32.	¹ H NMR spectrum of 37 (C ₆ D ₆). The position of free Me ₃ Al (-0.36 ppm) is indicated with the dotted line.	112
Figure 3.33.	Proposed structure of E and different appearance in C ₆ D ₆ and THF-d ₈ .	117
Figure 3.34.	X-ray crystallographic structure of 39 .	119
Figure 3.35.	X-ray crystallographic structure of the sodium salt 40 .	123
Figure 3.36.	(a) View of a monomer in the trimer 40 . (b) Different angle view to show the distortion of the olefin plane. (c) Simplified illustration of the monomer.	123
Figure 3.37.	"Formal" description of 25 .	124
Figure 3.38.	X-ray crystallographic structure of 41 .	128
Figure 3.39.	X-ray crystallographic structure of 42 .	128
Figure 3.40.	Comparison of the side views of 25 , 41 and 42 and selected torsion angles.	131
Figure 3.41.	X-ray crystallographic structure of 45 .	135

Figure 3.42.	X-ray crystallographic structure of 46 or 46' .	138
Figure 4.1.	List of characterized or semi-characterized compounds in Chapter 4.	171
Figure 4.2.	X-ray crystallographic structure of 47 .	173
Figure 4.3.	The position above the central metal atom: in 47 and 25 .	174
Figure 4.4.	X-ray crystallographic structure of 50 .	178
Figure 4.5.	X-ray crystallographic structure of 52 .	184
Figure 4.6.	Mononuclear "CpTiCl" complex 54 .	185
Figure 4.7.	X-ray crystallographic structure of the "CpTiCl ₂ /OH" complex 53 .	186
Figure 4.8.	Internal and external ether coordination in mononuclear TiCl ₂ complexes 52 (<i>E</i> -ligand) and 56 (<i>Z</i> -ligand).	190
Figure 4.9.	X-ray crystallographic structure of 58 .	191
Figure 4.10.	X-ray crystallographic structure of the complex 59 with different angle views.	193
Figure 4.11.	The similarity in structural features of 59 and 50 .	194
Figure 4.12.	Suggested structures of N .	197
Figure 5.1.	Structures of the titanium complexes that appear in Table 5.1 .	216
Figure 5.2.	Ligand systems evaluated for the magnesium effect (drawn in deprotonated form).	225
Figure 5.3.	Ethene polymerization activity vs. mixing time: Mg salt of 7 (25) with TiCl ₄ .	226
Figure 5.4.	Ethene polymerization activity vs. mixing time: Mg salt of 3E (75) with TiCl ₄ .	227
Figure 5.5.	Ethene polymerization activity vs. mixing time: Mg salt of phenol (77) with TiCl ₄ .	229
Figure 5.6.	Ethene polymerization activity vs. mixing time: Mg salt of 3,3'-dimethyl-4,4'-biphenol (78) with TiCl ₄ .	230
Figure 5.7.	Ethene polymerization activity vs. mixing time: Mg salt of hydroquinone (79) with TiCl ₄ .	231

Figure 5.8.	Ethene polymerization activity by the precatalysts prepared in situ from Mg/Cl/(thf) salt (25) and Mg/Br/(thf) salt (26), derived from ligand 7 , with 2 equiv. of TiX ₄ .	239
Figure 5.9.	Ethene polymerization activity by the precatalysts prepared in situ from Mg/Cl/(thf) salt (77) and Mg/Br/(thf) salt (82) of phenol with 0.5 equiv. of TiX ₄ .	239
Figure 5.10.	Ethene polymerization activity by the precatalysts prepared from Mg/Cl/(thf) salt (25) and Mg/Cl/(OEt) ₂ salt(27), derived from ligand 7 , and TiX ₄ .	242
Figure 5.11.	Ethene polymerization activity by the precatalysts prepared from (PhO) ₂ Mg (83) + 0.1MgCl ₂ •(OEt) ₂ and TiX ₄ .	243
Figure 5.12.	Structures of 41 , 42 and 25 .	244
Figure 5.13.	Ethene polymerization activity vs. Ti/Mg ratio: from precatalysts prepared in situ from 41 , 42 , 25 or 77 with TiCl ₄ , and the isolated precatalysts [77 + nTiCl ₄] (n = 0.5, 1 and 2: 84 , 85 , and 86 respectively).	246
Figure 5.14.	Temperature/flow-rate profiles of the catalyst prepared from [7 – 4H]Mg ₃ Cl ₂ (thf) ₂ (25) and 4 equiv. of TiCl ₄ ; Mixing time 5 min.	252
Figure 5.15.	Temperature/flow-rate profiles of the catalyst prepared from C ₆ H ₅ OMgCl(thf) ₂ (77) + 0.5 TiCl ₄ ; Mixing time 10 min.	253
Figure 5.16.	Preliminary X-ray crystallographic structure of 77 .	259

List of Schemes

	page
Scheme 1.1. Oxidative coupling of diarylhydrazone with a heteroatom donor at every <i>ortho</i> -position by von Itter.	4
Scheme 1.2. Synthesis of tetrakis(2-hydroxyphenyl)ethene 2 .	4
Scheme 1.3. Acid-catalyzed coupling of the diazo compound.	5
Scheme 1.4. <i>Ortho</i> -propylation of tetrakis(2-hydroxyphenyl)ethene.	10
Scheme 1.5. Unaccomplished attempt at branch introduction at the allylic/benzylic position of 6 due to unstability of the methylated complex 24 .	12
Scheme 1.6. Synthesis of 3E and 3Z .	14
Scheme 1.7. Proposed mechanism of the formation of byproduct Y .	15
Scheme 1.8. An attempt to obtain a bridged dihydrazone for intramolecular coupling.	16
Scheme 1.9. Expected oxidation product of 2 and strategy for regioselective alkylation.	17
Scheme 1.10. DDQ oxidation of 2 to 13 .	17
Scheme 1.11. Proposed mechanism of the formation of 13 .	18
Scheme 1.12. Protection of 13 and attempts at back-reduction.	19
Scheme 1.13. Proposed route from 14 to 3X .	21
Scheme 1.14. Synthesis of 2,7-bis(1,1-dimethylethyl)-9H-fluorene-1,8-diol 4 .	23
Scheme 1.15. Triflation products from 4 . Triflate 22 and the major biproduct 23 , the pyridine adduct.	25
Scheme 3.1. Trinuclear magnesium complexes from 7 .	62
Scheme 3.2. Direct and indirect routes to the Mg(CH ₃) complex 28 .	64
Scheme 3.3. Suggested equilibrium to bring 25 to 28 .	65
Scheme 3.4. Mg(Bn) complex 29 .	65
Scheme 3.5. Geminal up/down titanium halide complexes.	78

Scheme 3.6.	Geminal up/down titanium halide complexes, THF-coordinated.	78
Scheme 3.7.	Geminal up/down benzyltitanium complex 35 .	79
Scheme 3.8.	Proposed solution behavior of 30a . The thick arrows represent the direction of the helices.	86
Scheme 3.9.	Relationship between 30a and 30b in solution.	97
Scheme 3.10.	Presumed interconversion of "geminal up/down" and "vicinal up/down" isomers.	102
Scheme 3.11.	Proposed interconversion mechanism of "geminal up/down" and "vicinal up/down" isomers.	103
Scheme 3.12.	Proposed mechanism of THF polymerization by 36 .	106
Scheme 3.13.	Proposed mechanism of formation of 36 from 35 plus $B(C_6F_5)_3$.	107
Scheme 3.14.	Formation of 37 and 38 from 7 and R_3Al .	109
Scheme 3.15.	"Collapsing" of the aluminum crown complexes upon leaching out R_3Al by a coordinating solvent with the proposed structure of A .	114
Scheme 3.16.	Proposed equilibrium between two enantiomers of A .	114
Scheme 3.17.	The THF-driven transformation of C into D and E .	117
Scheme 3.18.	Summary of the aluminum complexes and the chemical behavior in THF medium.	120
Scheme 3.19.	The preparation of (a) the Al-Mg-Mg complex 41 and (b) the Al-Mg-Al complex 42 .	126
Scheme 3.20.	Formation of 43 and 44 .	133
Scheme 3.21.	Formation of 46 from 41 and 42 .	137
Scheme 4.1.	Formation of 47 and 48 from reaction between ligand 3E and one or two equivalents of Et_3Al .	172
Scheme 4.2.	Equilibrium between 48 and 47 .	175
Scheme 4.3.	Formation of 49 and 50 from reaction between ligand 3E and one or two equivalents of Et_3Al .	176
Scheme 4.4.	Proposed mechanism for the formation of 50 .	179
Scheme 4.5.	Proposed structure of 48 and mechanism of the formation.	180

Scheme 4.6.	Aluminum abstraction by CD ₃ CN from 48 and 50 .	181
Scheme 4.7.	Addition of alkyl aluminum reagent to 47 .	182
Scheme 4.8.	Preparation of complex 52 .	183
Scheme 4.9.	Formation of "TiBn ₂ " complex 55 .	187
Scheme 4.10.	Proposed outcome of a reaction between 55 and B(C ₆ F ₅) ₃ .	188
Scheme 4.11.	Suggested structures of 56 and 57 .	189
Scheme 4.12.	Al/Ti hetero-polymetallic complex 59 .	192
Scheme 4.13.	Proposed mechanism of the formation of 59 .	196
Scheme 4.14.	Proposed structure of L formed from the reaction between 52 and Me ₃ Al.	198
Scheme 4.15.	Reactions between 47 or 48 and TiCl ₄ .	199
Scheme 4.16.	Proposed mechanism of the reaction between 48 and one equivalent of TiCl ₄ .	201
Scheme 5.1.	In situ formation of 30a and 30 accompanied by the formation of inorganic salts.	219
Scheme 5.2.	Reaction between 35 and B(C ₆ F ₅) ₃ and the proposed structure of 36 .	219
Scheme 5.3.	Formation of 59 from 52 and two equivalents of Et ₃ Al.	220
Scheme 5.4.	Proposed structure of precatalyst produced in <i>entry 24</i> : the 1 : 1 adduct of TiCl ₄ and the sodium salt of ligand 4 .	221
Scheme 5.5.	Proposed structure of precatalyst produced in <i>entry 3</i> : the 1 : 1 adduct of TiCl ₄ and the sodium salt of ligand 4 .	224
Scheme 5.6.	Suggested MgCl ₂ -incorporated phenoxytitanium chloride precatalysts produced from the reaction of 77 with TiCl ₄ .	235
Scheme 5.7.	Formal balanced equations of the reactions between 25 or 26 and TiCl ₄ or TiBr ₄ .	240
Scheme 5.8.	Formal balanced equations of the reactions between 77 or 82 and TiCl ₄ or TiBr ₄ .	240
Scheme 5.9.	The suggested transfer-steps of solvate molecules (solv) in the Mg/Ti precatalyst.	242

List of Abbreviations

Å	angstrom
Ac	acetyl, C(=O)CH ₃
<i>t</i> -AmOH	<i>tert</i> -amyl alcohol = 2-methyl-2-butanol
APT	attached proton test (a ¹³ C NMR spectroscopy method)
BB	broad band (a ¹³ C NMR spectroscopy method)
dba	1,5-diphenyl-3-pentadienone
BINAP	2,2'-bis(diphenylphosphino)-1,1'-binaphthyl
Bn	benzyl, PhCH ₂
bpy	bipyridine
Cp	η ⁵ -cyclopentadienyl
DDQ	2,3-dichloro-5,6-dicyano-1,4-benzoquinone
DMSO	dimethyl sulfoxide
Et	ethyl, C ₂ H ₅
eq.	equation
equiv.	equivalent(s)
ES	electrospray
Hz	hertz
HRMS	high resolution mass spectrometry
M	metal atom or ion; or a molecular mass in mass spectroscopy
Me	methyl, CH ₃
NMR	nuclear magnetic resonance
ORTEP	Oak Ridge Thermal Ellipsoid Program
Ph	phenyl, C ₆ H ₅
ppm	parts per million
Pr	propyl
psig	pounds per square inch gauge pressure
R	alkyl group
r.t.	room temperature
Tf	trifluoromethanesulfonyl, CF ₃ S(=O) ₂ -
THF	tetrahydrofuran
TMEDA	<i>N,N,N',N'</i> -tetramethylethanedi- <i>amide</i>
TMS	trimethylsilyl
TsOH	<i>para</i> -toluenesulfonic acid
UV	ultraviolet
X	halogen atom or halide ion

General Introduction

This thesis describes the modification of the newly developed preorganized tetradentate ligand, tetrakis(2-hydroxyphenyl)ethene, the metal coordination chemistry of several substituted ligands prepared, using Ti(IV), Al(III) and Mg(II) metals, and trials of the metal complexes in ethene polymerization catalysis.

Format of this thesis:

This thesis takes a paper format. Each of the major chapters (Chapters 1, 3, 4 and 5) is self-contained, having its own introduction, table of contents, conclusion, experimental and references/notes sections.

Thesis overview:

The synthesis and modification of tetrakis(2-hydroxyphenyl)ethene are described in Chapter 1. The synthesis, characterization and chemical behavior studies of the metal derivatives from the selected ligands are discussed in Chapter 3 and 4: Chapter 2 provides a preface of these two chapters. Ethene polymerization studies by selected metal derivatives are discussed in Chapter 5. Chapter 6 provides a general conclusion. Appendices are found in the second volume.

Chapter 1

Ligand Synthesis and Modification

Table of Contents

1.0. Introduction	3
1.1. Modification of Tetrakis(2-hydroxyphenyl)ethene Framework	9
1.1.1. Ortho-Substituent Introduction	9
1.1.2. Partial Protection/Deprotection of Hydroxy Groups	13
1.1.3. Attempts to Introduce Other Heteroatoms	22
1.2. Synthesis of 2,7-Bis(1,1-dimethylethyl)-9H-fluorene-1,8-diol (4)	23
1.3. Conclusion	25
1.4. Experimental	26
1.5. References and Notes	45

1.0. Introduction

A major goal of our research was to develop new preorganized polydentate ligands designed to hold more than one metal atom in proximity. We intended to create a well-defined surface-like platform on a discrete polydentate molecule to serve as a model of heterogeneous polymetallic catalyst systems. The re-creation of surface phenomena on a well-defined species will facilitate otherwise difficult mechanistic studies of such heterogeneous systems. We focused on potentially bimetallic or polymetallic catalytic systems such as the supported Ziegler-Natta catalysts (more details will be presented in Chapter 2).

Phenoxide-based preorganized ligand systems were chosen as our main target because of their affinity to early transition metals, in relation to classic Ziegler-Natta catalysts. A widely known example of a preorganized aryloxy-ligand type is the calixarene series,¹ in which four or more aryloxy rings are conjoined by methylene bridges (Figure 1.1-a). This cyclic ligand system and related derivatives have been investigated in various contexts, including coordination chemistry, host-guest chemistry and supramolecular chemistry.

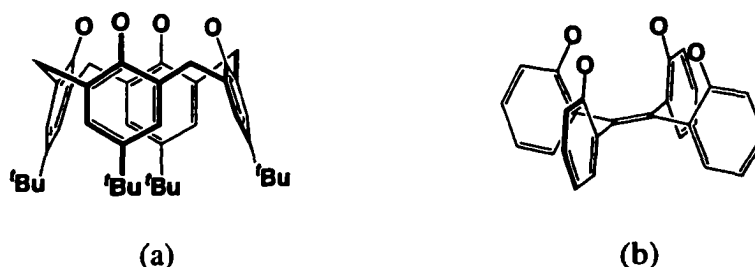
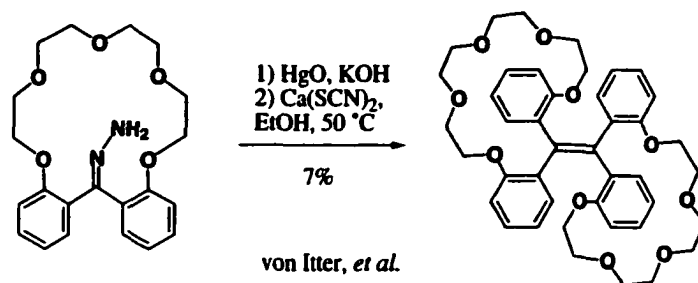


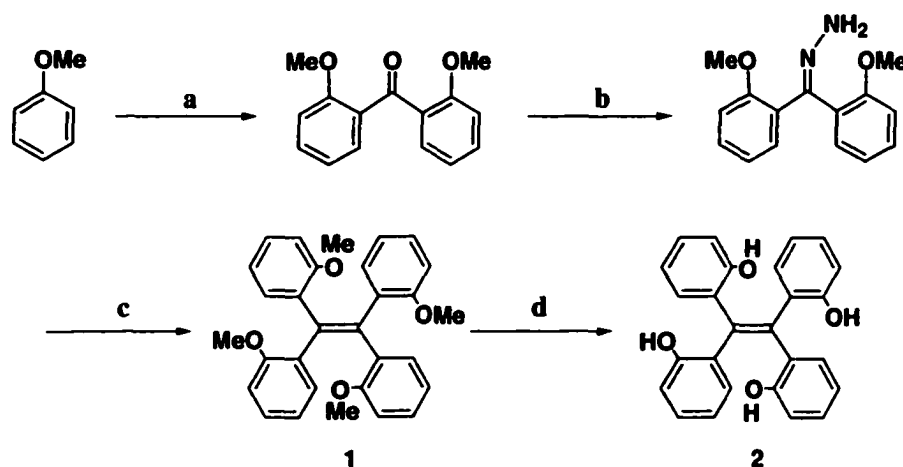
Figure 1.1. (a) *para-tert*-Butylcalix[4]arene. (b) Tetrakis(2-hydroxyphenyl)ethene 2.

As a new type of preorganized aryloxy ligands, tetrakis(2-hydroxyphenyl)ethene 2 (Figure 1.1-b)² was developed by Udo Verkerk in our group. Many tetraphenylethene compounds are known,³ but very few with a heteroatom donor at the 2-position of all the phenyl rings have been reported. The only example with heteroatoms at all 2-positions was prepared by von Itter et al., in which the low-yield oxidative coupling of the crown ether-macrocyclic hydrazone was reported (Scheme 1.1).⁴ No other heteroatom analogues have been prepared.

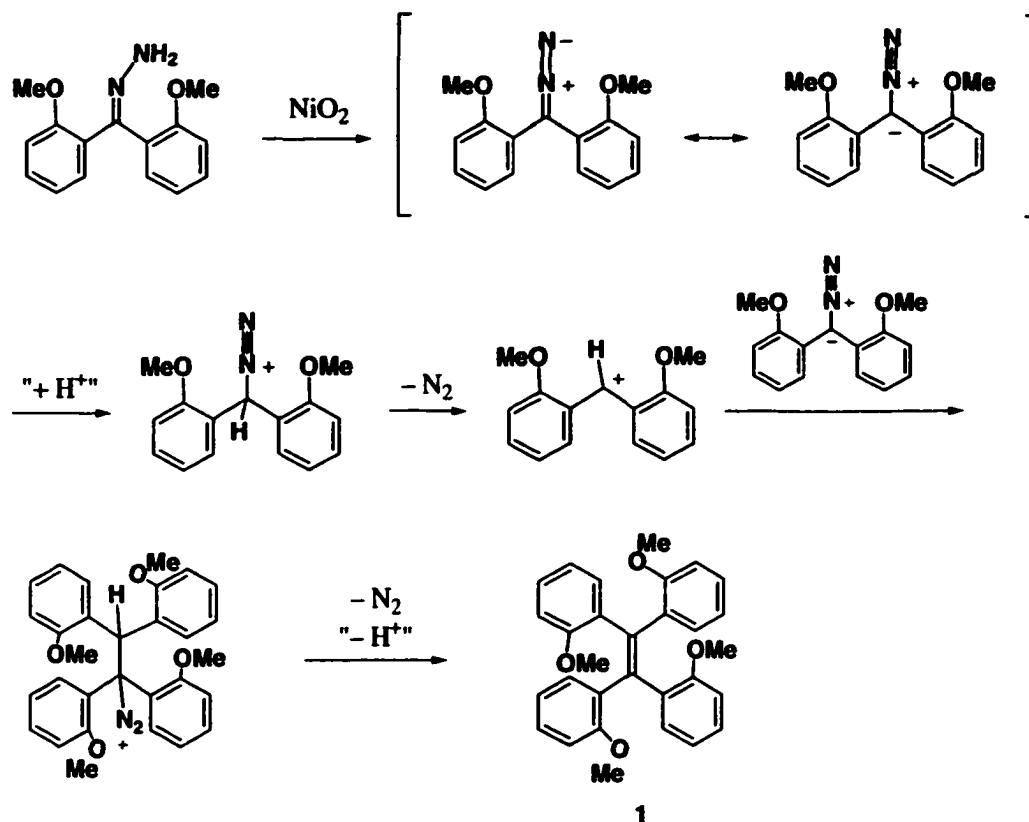


Scheme 1.1. Oxidative coupling of diarylhydrazone with a heteroatom donor at every *ortho*-position by von Itter.

Verkerk established an efficient synthetic route for tetrakis(2-hydroxyphenyl)ethene **2**, as described in **Scheme 1.2**. The yield of the key oxidative coupling of the hydrazone (step c) was greatly improved to 80 to 87% by the use of an acid catalyst.⁵ A mechanistic rationale for the coupling reaction is shown in **Scheme 1.3**.



Scheme 1.2. Synthesis of tetrakis(2-hydroxyphenyl)ethene **2**. Conditions: **a.** i) BuLi, TMEDA, Et₂O, -65 °C to r.t., ii) Me₂NC(O)Cl, iii) H₂O, HCl, 73%; **b.** H₂NNH₂·H₂O, *n*-BuOH, reflux, 16 h, 92%; **c.** i) NiO₂, CH₃CN, 0 °C, 1 h, ii) filtration, then iii) cat. TsOH, 80%; **d.** BBr₃, CH₂Cl₂, -65 °C to r.t., 16 h, 90%.



Scheme 1.3. Acid-catalyzed coupling of the diazo compound.

For some metals, ligand **2** shows coordination patterns similar to those of the calix[4]arene ligand. In the titanium(IV) complexes, for example, the *para-tert*-butylcalix[4]arene exhibits the coordination pattern drawn in **Figure 1.2-a**.⁶ The sandwich-like dimeric structure, in which the metals are buried in the oxygen coordination sites, is commonly observed with most other oxygen-bound metal complexes reported for *para-tert*-butylcalix[4]arene.^{1a} The *para-tert*-butylated analog of **2**, prepared analogously to parent ligand **2**,⁷ gave a titanium complex of a similar structure, shown in **Figure 1.2-b**.^{2a} The difference is that there are extra μ -oxygen bridges between two Ti atoms in the latter complex, making the Ti atoms pentacoordinate.

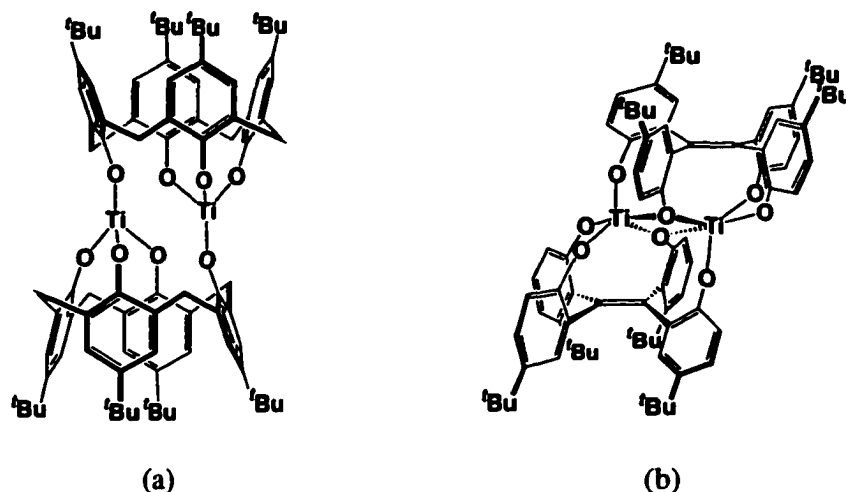


Figure 1.2. Titanium complexes reported for (a) *para-tert*-butylcalix[4]arene and (b) tetrakis(5-*tert*-butyl-2-hydroxyphenyl)ethene.

The aluminum complexes of *para-tert*-butylcalix[4]arene and tetrakis(2-hydroxyphenyl)ethene **2** also appear to be similar in some respects. Ligand **2** was reported to give an 8-membered aluminum-oxygen crown complex upon addition of excess R_3Al ($R = Et$ or Me) or Et_2AlCl , as shown in **Figure 1.3-b**.^{2a} Meanwhile, the adduct of excess Me_3Al to *para-tert*-butylcalix[4]arene was reported by Atwood et al. as $[(\text{ligand} - 4H)Al_4Me_8]_2$.⁸ This report, however, does not say how the researchers found it dimeric nor provide any details about structural information. At least, the formula is the same as that of the ligand **2** case.

The adduct of <1 equivalent of $[H_3Al(NMe_3)]_2$ is reported by Atwood et al. as the sandwich-type structure shown in **Figure 1.3-a**.⁸ The similar dimeric structure was also found for the ligand **2** case, when the above-mentioned crown complex (**Figure 1.3-b**) was dissolved in a coordinating solvent such as THF or acetonitrile. These coordinating solvents apparently deprive trialkyl aluminum molecules from the complex to force the ligand system to "collapse" to the aluminum-deficient sandwich structure shown in **Figure 1.3-c**. The core structure is remarkably similar to that of the calixarene case (**Figure 1.3-a**).

The "collapsed" dimeric structure of the metal complexes of the calix[4]arene and ligand **2** shows the limitation of the system as a surface-mimic platform. The "surface-

side" is completely covered with another ligand molecule, and the metal atoms are buried in aryloxy donors in the complex. The ligand **2**, however, still shows a promising surface-like structure in the crown complex, in which four aluminum metals are kept in proximity.

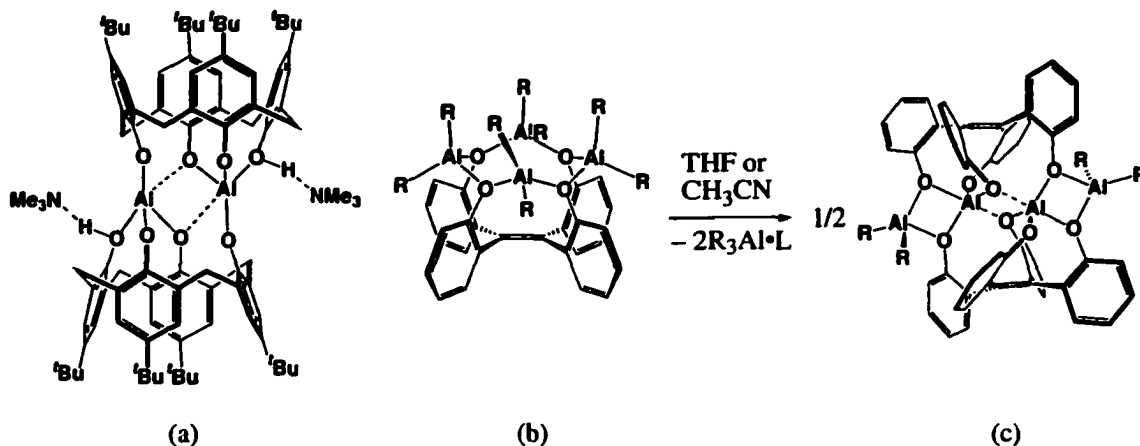


Figure 1.3. Aluminum complexes reported for (a) *para-tert*-butylcalix[4]arene and (b) tetrakis(2-hydroxyphenyl)ethene.

The ligand **2** has a structural advantage over the calixarene system in serving as a more efficient surface-like platform: the position *ortho* to the hydroxy group is available for further modifications. Introduction of a substituent with steric bulk at the *ortho* position would reduce the possibility of the dead-end sandwich structure formation or other random aggregation.

Another benefit from *ortho*-substituent introduction would be an improvement in the solubility of the compound. The poor solubility of ligand **2** itself and the metal derivatives in many common solvents have made analyzing and/or purifying the products difficult. Having no steric protection around the aryloxy groups or coordination sites may increase the intermolecular interactions, leading to aggregation of the complexes or the ligand itself.

This chapter will discuss various modifications of the parent tetraarylethene-based ligand **2**. The first theme of ligand modification is the introduction of *ortho*-substituents. The successful Claisen rearrangement route to introduce propyl group at the *ortho*

position will be described in detail. Other miscellaneous attempts, including bromination, lithiation and organobismuth-mediated phenylation, will also be described.

Partial protection of the tetrahydroxy ligand to give trihydroxy, dihydroxy, and monohydroxy ligands is another important theme of ligand modification. Adjusting the number of aryloxy and ethereal donors in the ligand allows the ligand framework to fit different metal or metal-containing groups with various oxidation numbers and available coordination sites.

Regioselective alkylation reactions of hydroxy groups in the calix[4]arene case have been established, from monoalkylation to selective dialkylation. Reaction conditions such as the base and the stoichiometry of reagents were carefully chosen to gain the desired selectivity. However, preliminary studies of selective protection of **2** or selective deprotection of the tetramethylether **1** by Verkerk were unsuccessful.^{2a,9} As an alternative pathway to *trans* or *cis* dialkylation products (**3E** and **3Z**, Section 1.1.2, page 13), a convergent synthesis starting from an unsymmetrical ketone was established and the details will be described in this chapter. Related attempts at selective desymmetrization included the oxidative-regioselective protection of parent ligand **2**. Mild oxidation of **2** resulted in an interesting fused-ring product **13** (Section 1.1.2-ii, page 17); the characterization of this compound as well as the attempts to utilize it for regioselective alkylation of **2** will be described.

Although not successful, some attempts to introduce heteroatom donors other than oxygen were made as the third theme of ligand modification (Section 1.1.3, page 22). Introduction of other heteroatoms on the tetraarylethene framework would broaden the range of usable metal species. Several failed attempts, including palladium-catalyzed amination of the triflate and catalytic phosphination, will be briefly described.

In the last part of this chapter, the bidentate aryloxy ligand 2,7-bis(1,1-dimethylethyl)-9H-fluorene-1,8-diol **4** (Section 1.2, page 23) will be discussed as a rigid bidentate platform for preorganizing bimetallic sites. The synthesis of ligand **4** was originally reported by Wuest et al.¹⁰ as a platform for "bidentate Lewis acids" upon coordination to Al(III) or Ti(IV) atoms.^{10,11} We attempted an alternative synthetic route to improve the synthetic efficiency of this ligand, but these attempts did not succeed. The alternate but not necessarily improved synthetic route and the problems encountered will be addressed.

1.1. Modification of Tetrakis(2-hydroxyphenyl)ethene Framework

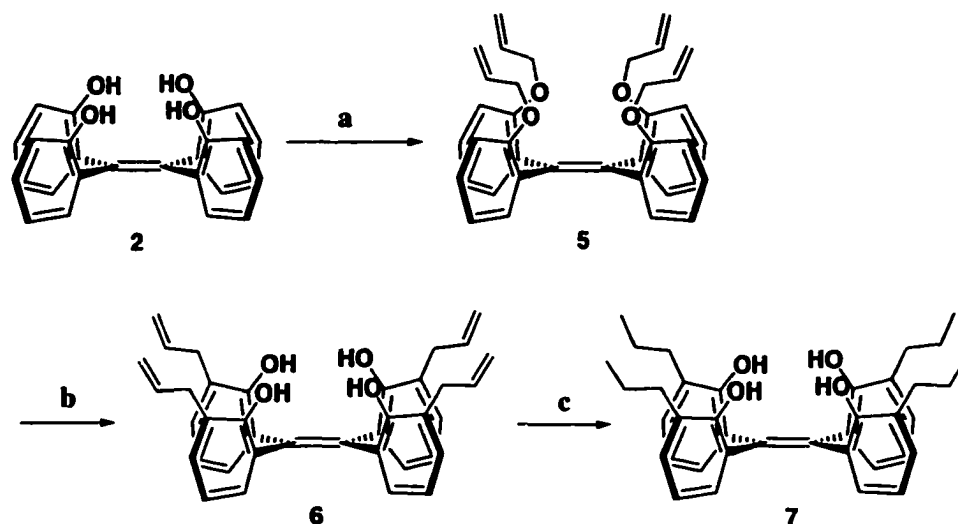
Accomplished or attempted modifications of the parent tetrakis(2-hydroxyphenyl)ethene ligand **2** are discussed in the following categories: (1) *ortho*-substituent introduction, (2) partial protection/deprotection of hydroxy groups, and (3) attempts to introduce other donor heteroatoms.

1.1.1. *Ortho*-Substituent Introduction

Because the same modification is required four times at all the four aryl rings in the ligand **2**, the modification reaction must be very clean and efficient. If inefficiency or the effect of side-reaction accumulates four times for a whole molecule, the yield of a desired product can be significantly reduced. The Claisen rearrangement route, the most successful *ortho*-alkylation route, will be described in the following section. A description of related attempts to modify the *ortho*-position will follow.

i) Claisen Rearrangement Route. The Claisen rearrangement of the allyloxy ether **5** followed by hydrogenation produced the tetrakis-*ortho*-propylated ligand **7** successfully (Scheme 1.4). All steps showed good to excellent yield with small and large scales.

The first acetylation step (step **a**) was clean and quantitative. A pure product was obtained by simple crystallizations without pre-purification by flash chromatography. The small scale reaction (up to 0.1 g) was completed overnight, but reactions of larger than a gram scale required as long as three days for completion, probably due to the heterogeneous nature of the reaction (especially the base, K₂CO₃, was scarcely dissolved in boiling acetone). The next Claisen rearrangement (step **b**) was not sensitive to the scale-up either, but was accompanied by more yellow-oily impurities. The yield of 80% was obtained from crystallization only, but the residue, still containing a considerable amount of the right product, would have required flash column chromatography treatment to further obtain pure substance. At the last step (c), a high pressure of hydrogen was important to bring the reaction to completion. Atmospheric pressure of hydrogen saturated only 40 to 50% of allyl groups after being applied overnight.



Scheme 1.4. *Ortho*-propylation of tetrakis(2-hydroxyphenyl)ethene. Conditions: **a.** $\text{CH}_2=\text{CHCH}_2\text{Br}$, K_2CO_3 , acetone, reflux, 3 days, 90%; **b.** mesitylene, 200°C , 16 h, 80%; **c.** H_2 (600 psig), cat. 10% Pd-C, MeOH, r.t., 16 h; 74%.

The solubility of ligand **7** in organic solvents was much better than that of parent ligand **2**. For example, **7** was readily soluble in hexane at room temperature, whereas **2** was mostly insoluble or only sparingly soluble in hexane, toluene or diethyl ether.

The ^1H NMR signals of **7** were all sharp, and only one kind of aromatic ring was observed at room temperature, indicating that the rotation of each ring was not hindered. No low temperature NMR spectroscopy was performed on this system to compare the rotation barrier with parent ligand **2**. The rotation of aryl rings was also found to be free for the precursors **5** and **6** at room temperature in CDCl_3 solution.

Interestingly, the ^1H NMR spectra of the propylated ligand **7** in various solvents (CDCl_3 , C_6D_6 and THF-d_8) all showed 3 to 3.5 equivalents of OH group relatively downfield (5.74, 5.80 and 7.53 ppm, respectively), and the remaining 1 to 0.5 equivalents were usually found mixed with the $\text{H}_2\text{O}/\text{HDO}$ signal at more upfield position (3.51 ppm by itself in CDCl_3 , 0.41 ppm with H_2O in C_6D_6 , and 2.48 ppm with H_2O in THF-d_8). This observation might suggest that a cyclic hydrogen bonding array is held among three out of the four hydroxy groups, and the remaining one hydroxy group is more rapidly exchanging the proton with the water in solution. In contrast, in parent ligand **2**, usually two hydroxy groups are found downfield and the other two are found together with the

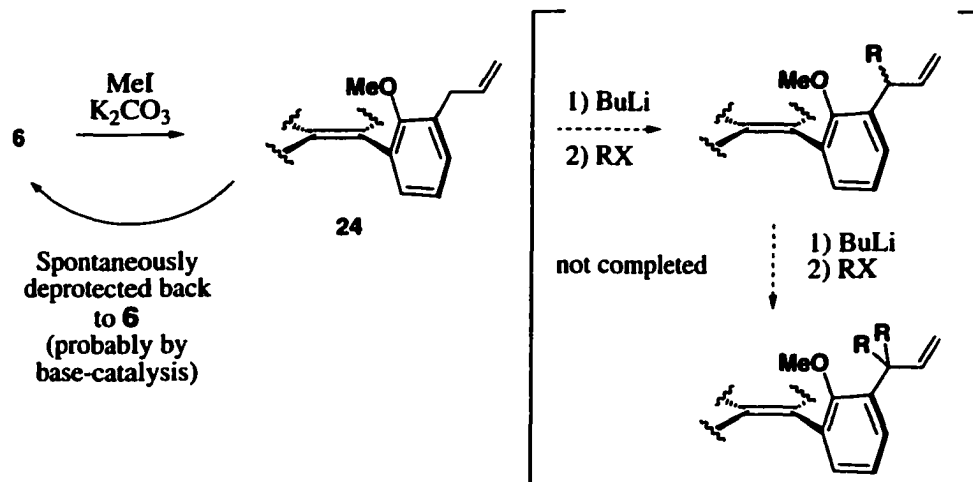
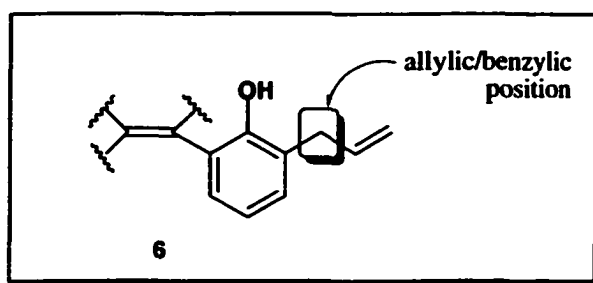
water signal.² This pairwise hydrogen bonding behavior was supported by the X-ray crystallographic structure.² Structural analysis by X-ray crystallography was desired for the propylated ligand **7** or its precursor **6** to confirm the suggested threesome hydrogen-bonding array, but growing X-ray-crystallographic quality crystals was not successful despite numerous trials.

The Claisen route was attempted to introduce more substituted allyl groups: crotyl (*cis/trans*-CH₃CH=CHCH₂-) and prenyl [(CH₃)C=CHCH₂-]. However, the *O*-crotylation or *O*-prenylation of parent ligand **2** did not proceed to completion under conditions analogous to step a in **Scheme 1.4**. All reactions gave mixtures of mono-, di-, tri- and a small amount of tetra-substitution. The fact that some amount of the tetra-substituted product was formed suggests that a complete reaction would still be possible under proper conditions, but no further attempts were made.

Branch-introduction at the allylic/benzylic position of the allyl branch in the *ortho*-allylated complex **6** (**Scheme 1.5**) was considered a good alternative to the above-mentioned attempts to introduce a more branched allylic group. The strategy was to protect the hydroxy groups in **6** first, then lithiate the allylic/benzylic position, followed by quenching with an alkyl halide such as CH₃I (**Scheme 1.5**).

The first methylation of **6** was successful: the product **24** was characterized by ¹H NMR spectroscopy, HRMS and TLC. However, in attempts at crystallization, this product decomposed back to the starting material **6** over several days in a slurry-solution. Why this decomposition happened is unclear, but having four methoxy groups with allyl groups next to them was probably too sterically demanding. Because the crystallization was being tried for the crude product without flash chromatography or other methods to remove the base completely, the demethylation may have been catalyzed by the base left in the crude product.

This observation suggests that introduction of alkyl branches at the allylic/benzylic position may be sterically too demanding in general. One small branch per allyl group may be possible, but this would lead to a mixture of many stereoisomers because the allylic/benzylic positions are diastereotopic. (The steric demand, however, may lead to diastereoselective branch formation.) Introduction of two alkyl branches at each site would solve the stereoisomer problem, but our results suggest that such compounds would be too crowded to form. No further attempts related to this approach were made.



Scheme 1.5. Unaccomplished attempt at branch-introduction at the allylic/benzylic position of **6** due to instability of the methylated complex **24**.

Other functionalizations may be possible at the double bond of the allyl branch in the 3-allylated ligand **6**, but the susceptibility of the parent system to unwanted side reactions must be taken into consideration. Oxidizing conditions cannot be used, because the conjugated phenol system will likely be affected (see Section 1.1.2-ii). Mild electrophilic addition conditions (in which highly substituted alkenes are not affected) may be a good choice, although this possibility was not pursued.

ii) Other *Ortho*-Functionalizations Attempts. The major problem in functionalizing the *ortho*-positions of parent ligand **2** was the prospect of obtaining *ortho/para* mixtures of products. The *para*-positions were often as susceptible as the *ortho*-positions under many electrophilic functionalization conditions, even under those known to have selectivity for the *ortho*-positions.

For example, under *ortho*-bromination conditions,¹² parent ligand **2** gave partly *para*-brominated mixtures. The *para*-position has to be blocked beforehand for clean *ortho*-bromination. Verkerk succeeded in clean *ortho*-bromination using the *para*-blocked (*para-tert*-butylated) analogs of **1** and **2**, using standard conditions.^{2a} Perbromination or octabromination of **1** or **2** at all the *ortho*- and *para*- positions were also tried by using bromination reagents of various kinds in excess, but these conditions usually resulted in mixtures of incomplete bromination products.

The *ortho*-directing photo-Fries rearrangement conditions reported by Garcia et al.¹³ looked promising to apply to the tetraacetate of **2** (= **2-OAc**) for introducing acetyl group at the *ortho*-positions. While tetrakis(2-acetoxyphenyl)ethene **2-OAc** was prepared quantitatively from parent ligand **2** by standard condition (acetic anhydride and pyridine), the rearrangement reaction resulted in a complicated mixture.

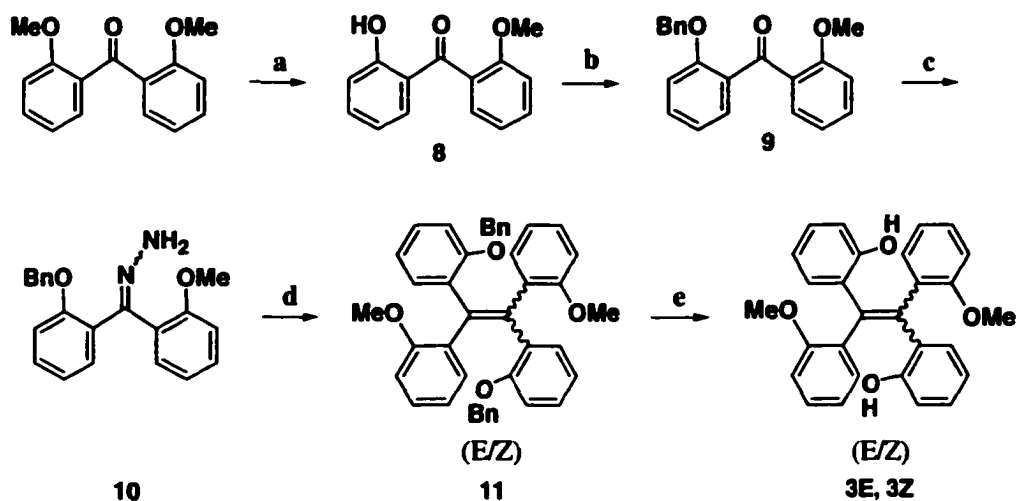
Alkoxy group-directed *ortho*-lithiation conditions, such as the one used for simple anisole (Scheme 1.2, step a), were not successful for conversion of the tetramethoxy ligand **1**. The poor solubility of the starting material, as well as the partially lithiated species, may have been a disadvantage for such reactions.

Some organobismuth reagents, such as Ph₃Bi, are known to *ortho*-phenylate the sodium salts of phenols.¹⁴ However, when used for the phenylation of parent ligand **2**, aryl-ring oxidation seems to have accompanied the reaction. The product mixture showed the HRMS signals (EI) of [**2** - 2H], [(**2** - 2H) + C₆H₄] and [(**2** - 2H) + 2(C₆H₄)], in which the core [**2** - 2H] is considered most likely to be the fused ring product **13**, the DDQ-oxidation product of **2** (*vide infra*). The last two masses are apparently of partially phenylated species of such oxidized product.

1.1.2. Partial Protection/Deprotection of Hydroxy Groups

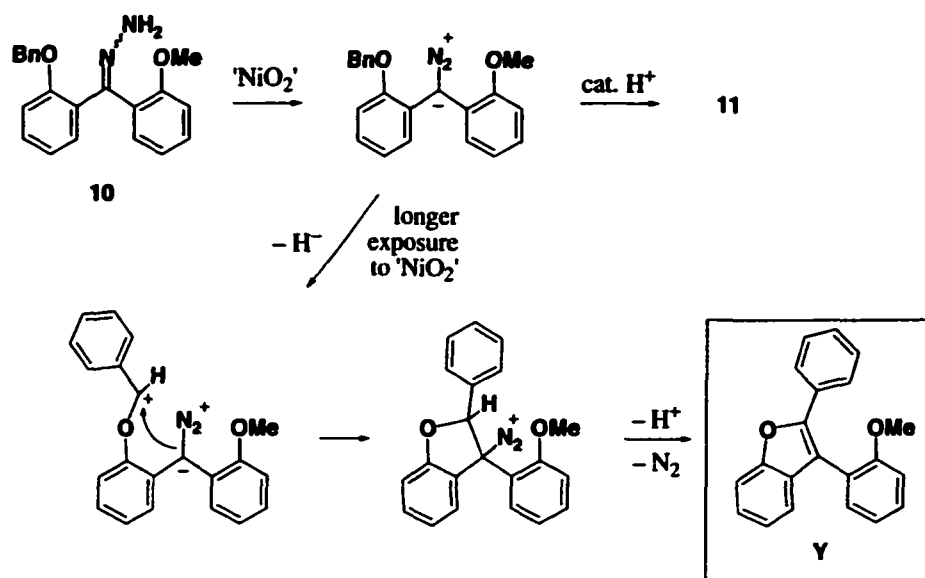
As mentioned in the Introduction, preliminary attempts at selective partial etherification of parent ligand **2** or selective deprotection of the tetramethoxy ligand **1** were not successful. The synthesis of *E*- and *Z*- dialkylated derivatives of **2** (**3E** and **3Z**) was, however, accomplished by differentiating the alkoxy groups at the ketone stage.

i) Convergent Synthesis of 3E/3Z. The alkoxy group differentiation of the starting bis(2-methoxyphenyl)methanone was performed in two steps: mono-deprotection to produce the ketone **8**, then benzylation of the freed hydroxy group to give the non-symmetrical (2-benzyloxyphenyl)(2-methoxyphenyl)methanone **9** (Scheme 1.6).



Scheme 1.6. Synthesis of **3E** and **3Z**. Conditions: **a.** i) BCl_3 /heptane, CH_2Cl_2 , -65°C to r.t., 75 min, ii) NaHCO_3 , H_2O , 99%; **b.** BnBr , K_2CO_3 , DMSO, r.t., overnight, 97%; **c.** $\text{H}_2\text{NNH}_2\cdot\text{H}_2\text{O}$, *n*-BuOH, reflux, overnight, 100%; **d.** i) NiO_2 , CH_3CN , 0°C , 40 min, ii) filtration, iii) cat. TsOH , 88.5%; **e.** H_2 (400 psig), cat. 10% Pd-C, EtOAc-MeOH, r.t., 17 h, >70%.

The standard coupling procedure of **9** produced a mixture of *E*- and *Z*-bis(2-benzyloxyphenyl)-bis(2-methoxyphenyl)ethene **11**. The *E*- and *Z*-isomers were neither separable nor distinguishable spectroscopically or by TLC at this stage. The coupling step (**d**) required careful attention: the first ' NiO_2 ' oxidation step should be as short as possible, because the benzyl group is apparently susceptible to ' NiO_2 '. A longer period of exposure to ' NiO_2 ' produced an increased amount of the byproduct **Y** (Scheme 1.7). The structure of **Y** is tentatively assigned based on the ^1H NMR spectroscopy and HRMS. The proposed mechanism of the formation of **Y** is given in Scheme 1.7. To minimize this side-reaction, the reaction must be carefully monitored by TLC, and as soon as all the starting material has been consumed, the next step (filtration to remove ' NiO_2 ') must be promptly performed.



Scheme 1.7. Proposed mechanism of the formation of the byproduct Y.

Extra care must also be taken during the work-up stage. When the acid-catalyzed coupling is complete, the catalytic amount of TsOH must be neutralized by adding KOH before removal of the solvent acetonitrile by rotary evaporation. When the acid was left in solution, the rotary evaporation of the mixture resulted in the formation of a significant amount of byproducts. These byproducts (at least two species) were not identified, but showed R_f values and spot colors TLC (UV visualization) similar to those of the desired product.

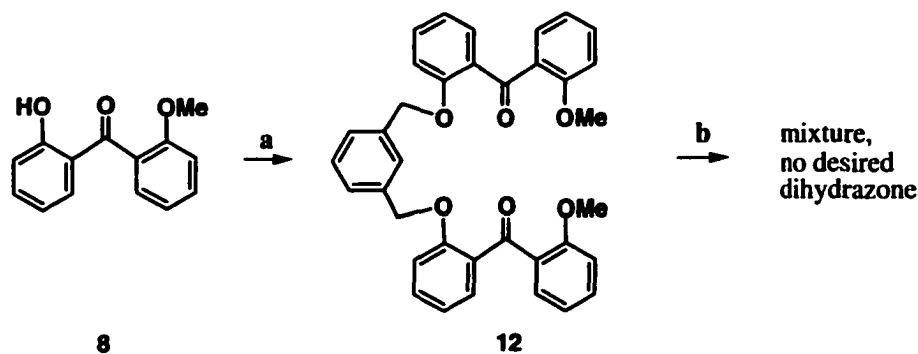
After de-benzylation by hydrogenolysis, a mixture of the deprotected *E*- and *Z*-isomers **3E** and **3Z** was obtained. Finding a suitable medium for this hydrogenolysis step was not simple: after trying several solvents and combination of solvents, a mixture of ethyl acetate and methanol at the ratio of 1 : 3 to 1 : 4 was found to be suitable. The reason why this particular system worked is not clear, but the reaction might have been sensitive to the solubility of the starting material **11**.

The ratio of **3E** and **3Z** in the product mixture varied in different runs, from 3/1 to 7/1, but **3E** was always the major isomer. The *E*-isomer was probably favored because the large benzyl groups prefer to avoid each other during the coupling step. This finding suggests that more diastereoselective coupling might be attained using larger protecting groups. However, since both alkenes were desired for evaluation of the coordination

ability of the tetraarylethene-based ligand system, no greater control over this coupling was investigated.

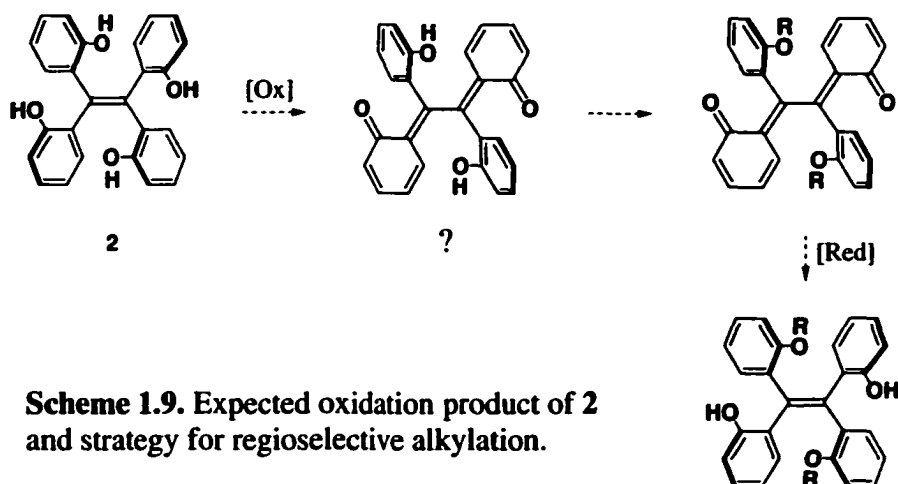
The mixture of **3E** and **3Z** was separated by careful flash chromatography or selective crystallization. The visibly different crystal morphology of these isomers helped to distinguish one from the other (each of the crystal portions was final-checked by TLC and/or ^1H NMR spectroscopy). Their tendency to adsorb colored contaminants was also different: a trace of blue "Sharpie" pen ink, which was accidentally introduced into the solution, was preferably adsorbed on **3E** upon crystallization, while a yellowish organic impurity present in the mixture tended to be adsorbed selectively onto **3Z**. The stereochemistry of **3E** and **3Z** was determined by X-ray crystallography of the *Z*-isomer (see Appendix A-1 for details).

An attempt was made to obtain a single coupling product of known stereochemistry. The coupling of the hydrazone corresponding to the bridging ketone **12** (Scheme 1.8) was expected to produce the *Z*-isomer exclusively. However, the desired dihydrazone was not produced from **12** under standard conditions, using excess hydrazine monohydrate (ca. 100 equivalents). This reaction resulted in a complicated mixture in which at least 15 to 20 kinds of methoxy signals were found in the ^1H NMR spectrum. Attempted intramolecular McMurry coupling of **12** also gave a complex mixture.

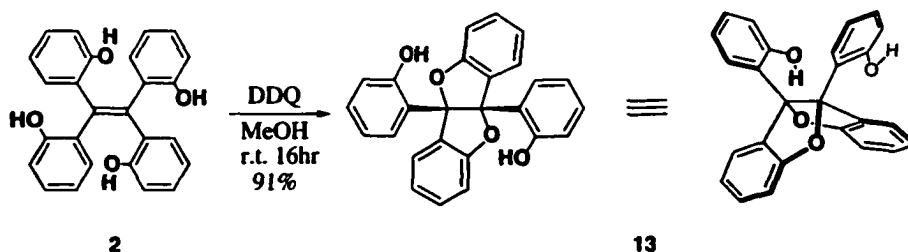


Scheme 1.8. An attempt to obtain a bridged dihydrazone for intramolecular coupling. Conditions: **a.** *m*-C₆H₄(CH₂Br)₂, K₂CO₃, DMSO, r.t., overnight, 85%; **b.** H₂NNH₂•H₂O (ca. 100 equiv), *n*-BuOH, reflux, overnight.

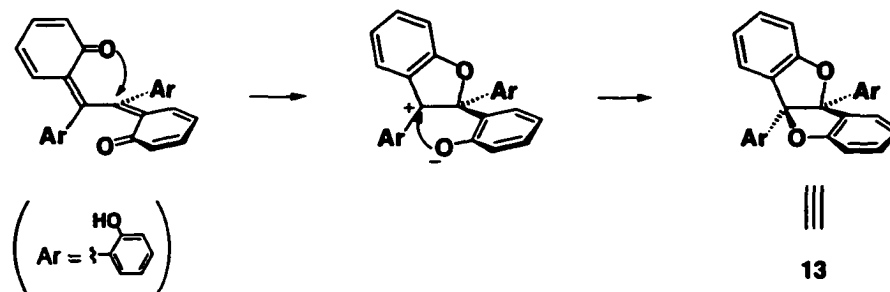
ii) Oxidation Strategy. One attempted strategy for regioselective partial protection of the hydroxy groups of parent ligand **2** was oxidation with a mild oxidant such as DDQ. It was expected that parent ligand **2**, technically a conjugated diphenol, would be oxidized to a conjugated quinone structure (Scheme 1.9). The protection of the remaining two hydroxy groups followed by back-reduction to the tetraarylethene state would give *cis*- or *trans*-dialkylated species.



The oxidation of **2** with DDQ, however, did not give a conjugated quinone, but instead gave the interesting fused-ring product **13** (Scheme 1.10). The structure of **13** was characterized by X-ray crystallography (see Appendix A-2). The skeleton of 6-, 5-, 5-, and 6-membered rings has the empirical name of *cis*-cumarocumaron. The official name given to **13** is *cis*-4b,9b-dihydro-4b,9b-bis(2-hydroxyphenyl)benzofuro(3,2-b)benzofuran, based on the nomenclature of a very similar compound.¹⁵



The conjugated quinone (as drawn in Scheme 1.9) may still be an intermediate in the formation of 13. The double nucleophilic cyclization of such a conjugated quinone would exclusively produce the *cis*-cumarocumaron framework over *trans*, as shown in Scheme 1.11, because the starting conjugated quinone would not be coplanar, but rather twisted at the central C-C bond, due to the steric hindrance.



Scheme 1.11. Proposed mechanism of the formation of 13.

The double cyclization of the possible conjugated quinone occurs in the case of the starting compound 2 because its hydroxy groups are at the 2-positions. A non-cyclized conjugated quinone would form if the hydroxy groups were at the 4-positions. Unlike the 2-hydroxy ligand 2, the 4-hydroxy version (= tetrakis(4-hydroxyphenyl)ethene) has been long known, with the oldest record being found in Behr's report in 1872.¹⁶ This article also describes the oxidation reaction of tetrakis(4-hydroxyphenyl)ethene by FeCl_3 ; the oxidation product had a formula of $\text{C}_{26}\text{H}_{18}\text{O}_4$, two H atoms less than the starting material. Although no structural information was available at that time, the author concluded that a quinohydrone-type compound was produced, based on the color of the oxidation product (it was green) and analogies to the color changes of quinohydrone-based dyes. These descriptions strongly suggest that they produced the conjugated quinone as drawn in Figure 1.4.

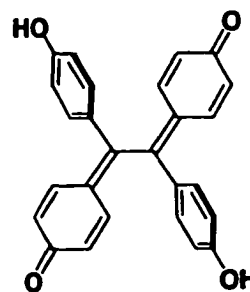


Figure 1.4. Suggested structure of the oxidation product of tetrakis(4-hydroxyphenyl)ethene.

Similar cyclization upon oxidation was observed with calixarenes. Mild oxidation of *para-tert*-butylcalix[4]arene, for example, resulted in the formation of the spiro-dienone from cyclization of each set of two neighboring rings (Figure 1.5).¹⁷

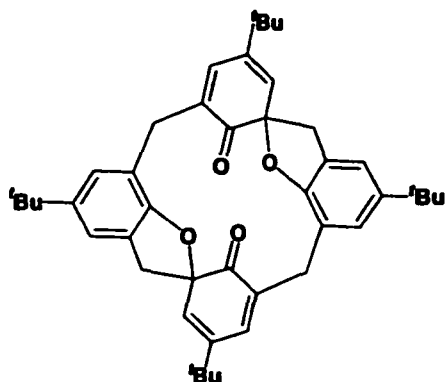
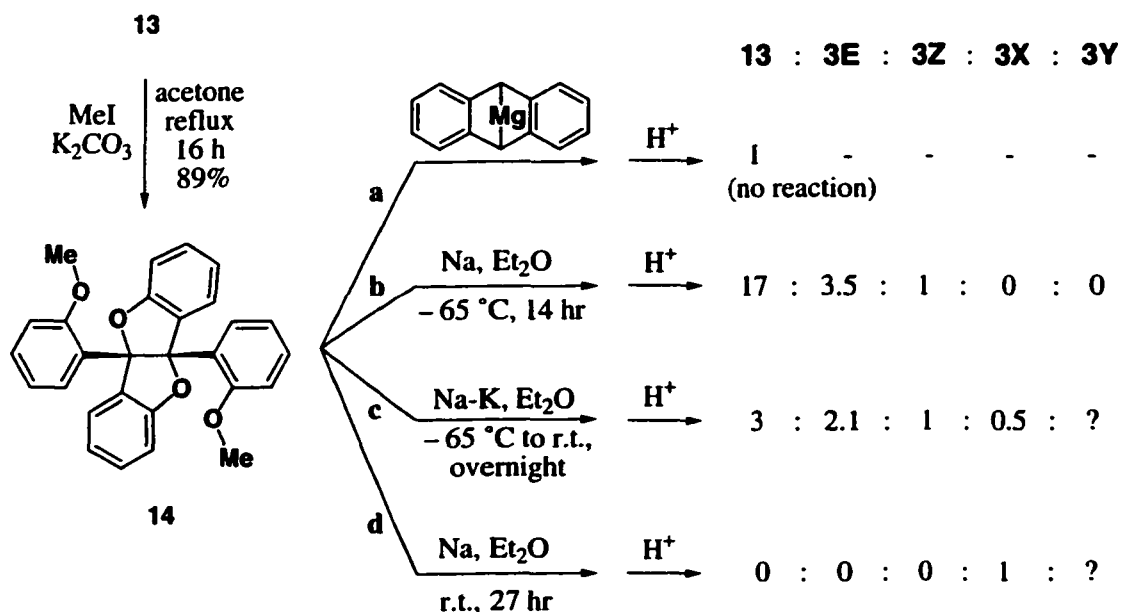


Figure 1.5. Oxidation product of *para-tert*-butylcalix[4]arene.

After protection of the hydroxy groups in the cumarocumaron **13**, the back-reduction to the tetraarylethene state was attempted. The evaluated conditions are listed in Scheme 1.12. Initially, magnesium anthracenide salt was used as a mild reducing agent, but no reaction occurred (eq. **a**). Use of Na or Na-K alloy to reduce a substituted cumarocumaron to the corresponding ethene was then evaluated in various conditions, including those reported by Rigaudy et al.¹⁸



Scheme 1.12. Protection of **13** and attempts at back-reduction.

Starting material **14** remained under milder conditions (eqs. **b**, **c**), but the formation of both **3E** and **3Z** were observed. Prolonged reduction at room temperature (eqs. **c**, **d**) gave the uncharacterized compounds **3X** and **3Y**.

Unknown **3X** showed ^1H NMR spectroscopic features similar to those of **3E/3Z**, except for a highly downfield, slightly broad doublet of doublet (dd) signal at 8.94 ppm. The ratio of unknown **3Y** relative to other products was unclear in the ^1H NMR spectrum due to the overlapping and probably complicated spectrum. The absence of the desired products (**3E** and **3Z**) in the last case (eq. **d**) was confirmed by TLC and ^1H NMR spectroscopy (some signals are close to those of **3E** or **3Z**, but there was no complete coincidence).

The HRMS (EI) of the mixture of the last entry (eq. **d**), a mixture of **3X** and **3Y**, exhibited two major parent signals, corresponding to $\text{C}_{28}\text{H}_{24}\text{O}_4$ (identical to **3E/3Z**) and $\text{C}_{26}\text{H}_{18}\text{O}_2$ ($\text{C}_{28}\text{H}_{24}\text{O}_4 - 2\{\text{OCH}_3\}$). The IR spectrum of the mixture showed an OH band. Assuming that both the formula of $\text{C}_{28}\text{H}_{24}\text{O}_4$ and the OH band belong to the unknown compound **3X**, we tentatively assigned its identity as 1,1-(2-hydroxyphenyl)-2,2-(2-methoxyphenyl)ethene (**Figure 1.6**), the third isomer of **3E** and **3Z**.

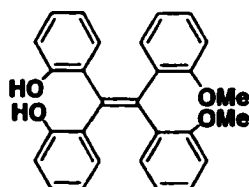
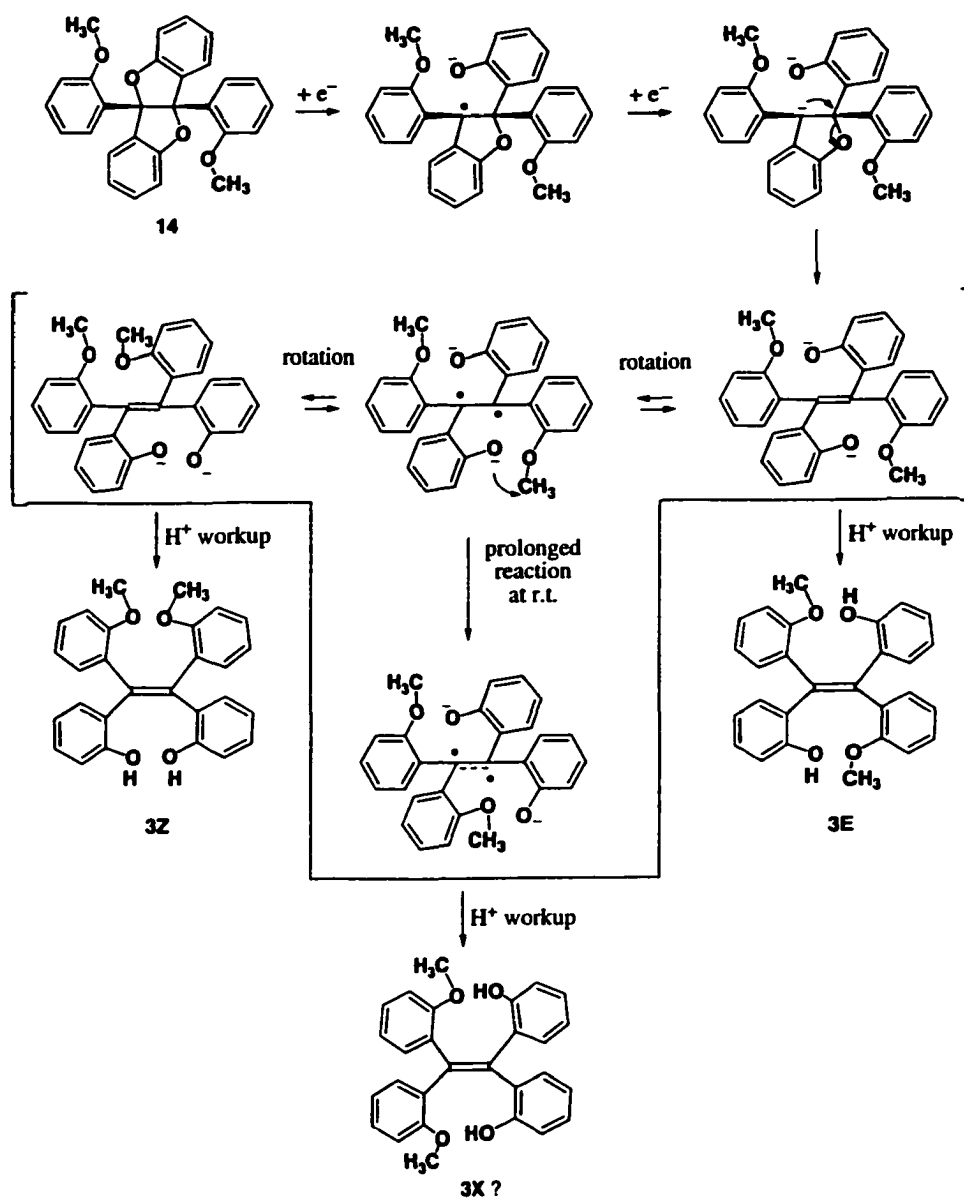


Figure 1.6. The structure of **3X**?

The possible mechanistic route to attain this isomer is provided in **Scheme 1.13**. The methyl migration is depicted as an intramolecular step. Intermolecular methyl migration is not likely because it would produce monomethoxy and trimethoxy species, the mass of which were not observed in the mass spectrometry.

However, even if the proposed structure of **3X** is correct, why this isomer is preferred over the *E*- and *Z*-isomers **3E** and **3Z** is unclear.



Scheme 1.13. Proposed route from **14** to **3X**.

1.1.3. Attempts to Introduce Other Heteroatoms

There are many known palladium-catalyzed or mediated amination¹⁹ or phosphination²⁰ reactions of aryl halides and aryl triflates. The triflate **15** (Figure 1.7) was prepared from **1** by using a standard condition (Tf₂O, Py) in attempt to replace the triflate groups with amino or phosphino groups. Various catalyst/phosphine/base/amine combinations were tried, including Pd(dba)₂/DPPF^a/*t*-BuONa/*t*-BuNH₂²¹ and Pd(dba)₂/BINAP^b/*t*-BuONa/aniline,²¹ but none of them worked. The problem was not only with the catalyst, because the same catalysts were confirmed to function for simpler aryl triflates such as 1-methyl-3-*tert*-butyl-4-triflyloxybenzene and 2-triflyloxynaphthalene. The amination reactions of the simpler triflates, however, were often incomplete and/or accompanied by a hydrolyzed product. These reactions might not work for the tetrakis-triflate **15** because (1) the solubility of the starting material is very poor, and (2) when a small degree of hydrolysis per each triflate is accumulated four times, the result is a mixture of partially hydrolyzed, partially aminated, and partially unreacted triflates.

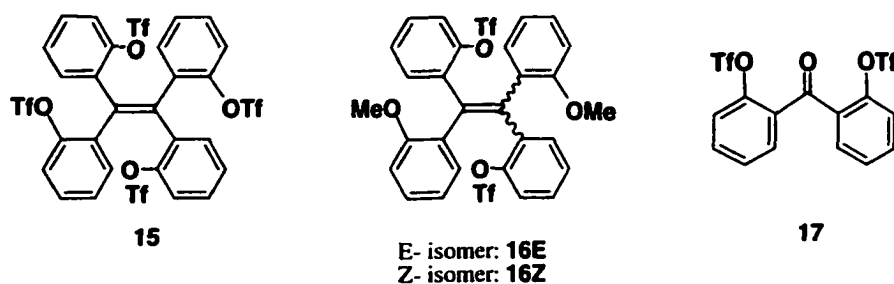


Figure 1.7. Triflates **15**, **16E**, **16Z** and **17**.

Although tetrakis-triflate was obtained for parent ligand **2**, triflation was not successful for the *ortho*-propylated ligand **7** under the standard reaction condition. This result was probably because the ligand framework, with propyl groups next to the hydroxy groups, does not readily accommodate four big triflate groups. The triflate **15** already experiences limited rotation freedom of each aryl ring in solution, as observed in

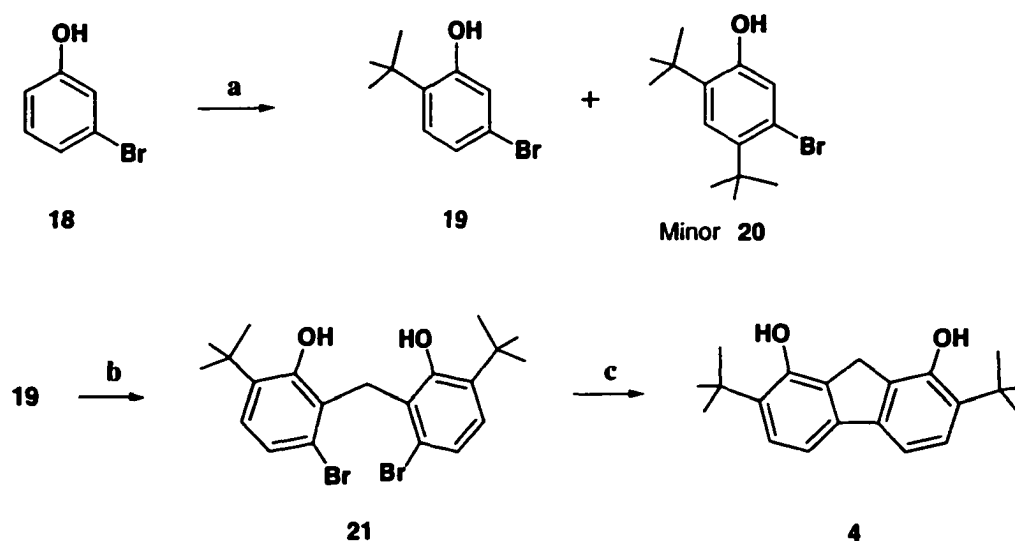
^a DPPF = 1,1'-bis(diphenylphosphino)ferrocene

^b BINAP = 2,2'-bis(diphenylphosphino)-1,1'-binaphthyl

the broadened ^1H NMR signals, obviously due to the big triflate substituents. The dialkylated ligand systems **3E** and **3Z**, on the other hand, were readily converted to the corresponding triflates **16E** and **16Z** (**16E** was only partially characterized by ^1H NMR spectroscopy, while **16Z** was completely characterized). Catalytic amination conditions, however, also did not work for the two bistriflates. Amination also failed for the bistriflate of 2,2'-dihydroxybenzophenone (**17**).

1.2. Synthesis of 2,7-Bis(1,1-dimethylethyl)-9H-fluorene-1,8-diol (**4**)

As mentioned in the Introduction, Wuest et al. reported the synthesis of the fluorene diol **4**.¹⁰ We also worked on this compound because it is an excellent system to enforce non-chelating coordination of two metal atoms held in proximity. Although the total efficiency did not improve greatly, the number of the reaction steps was reduced in the route we developed (Scheme 1.14).



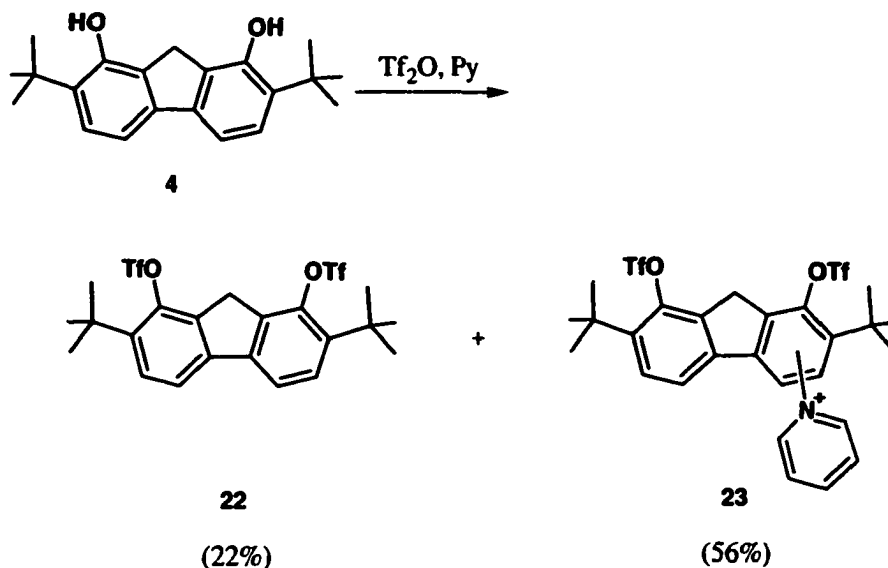
Scheme 1.14. Synthesis of 2,7-bis(1,1-dimethylethyl)-9H-fluorene-1,8-diol **4**. Conditions: a. 1 equiv. $(\text{CH}_3)_2\text{C}=\text{CH}_2$, cat. Me_3Al , benzene, $100\text{ }^\circ\text{C}$, 2 h, incomplete conversion, 50%; b. 0.5 equiv. $(\text{CH}_2\text{O})_n$, xylenes, $173\text{ }^\circ\text{C}$, 13.5 h, 77%; c. i) 2 equiv 'AmONa, 4 equiv. NaH, 1 equiv. $\text{Ni}(\text{OAc})_2$, 2 equiv. 2,2'-bipyridine, THF, benzene, reflux, ii) 1 equiv. KI, iii) **21**, 33%.

The efficiency of the condensation (step **b**) was slightly better than that in the case of Wuest et al. (77% vs. 56%), while the *tert*-butylation (step **a**)²² was much more efficient and simpler for their procedure (50% vs. 87%). We, however, could not reproduce their reaction (*t*-BuBr, SiO₂, Na₂CO₃, CCl₄, reflux). It is suspected that the reaction may be sensitive to the quality of the SiO₂, although Wuest et al. state that "SiO₂ of the type normally employed for flash chromatography could be used directly without special treatment" (see reference 10(a)).

In the aryl-aryl coupling stage (step **c**), we utilized the nickel-mediated reductive coupling in the presence of unprotected hydroxy groups,²³ thus eliminating the protection/deprotection steps in Wuest's procedure. However, the yield did not rise any higher than 33%, which is lower than the net yield of Wuest's protection-coupling-deprotection steps (50.5% overall). One of the major byproducts in our coupling procedure was over-reduced bis[2-hydroxy-3-(1,1-dimethylethyl)phenyl]methane, in which the bromine atoms in the starting material **21** were replaced with hydrogen atoms.

The inefficiency/difficulty of the synthesis and high price of the starting material discouraged us from pursuing this template for further research. However, some of the metal derivatives of this ligand showed promising ability as ethylene polymerization catalysts (see Chapter 5, Section 5.1). Our group is currently working on the alternative ligand system 3,3'-(1,1-dimethylethyl)-2,2'-dihydroxydibenzofuran to continue the polymerization catalyst project.²⁴

Triflation was also attempted for the fluorene-diol **4**, in hope of replacing the triflate groups with other heteroatom donor groups. However, the standard triflation condition using Tf₂O and pyridine did not give the desired product **22** quantitatively. The major product was tentatively assigned to a pyridine adduct **23**. The ¹H NMR and low resolution MS (FAB) data were consistent with the structure of **23** given in Scheme 1.15. Probably one aromatic proton in **22** was replaced by a pyridinyl group, but the position of the pyridine substitution was not confirmed. The mechanism of formation remains obscure. This type of problem may be avoided by the use of hindered pyridine, such as 2,6-di-*tert*-butyl-4-methylpyridine.



Scheme 1.15. Triflation products from **4**. Triflate **22** and the major byproduct **23**, the pyridine adduct.

Nevertheless, the palladium-catalyzed amination was attempted for the isolated bis-triflate **22**, using *n*-propylamine. The major spot in the product TLC represented a non-symmetrical species, which could be either a single unsymmetrical species or a 1 : 1 mixture of two compounds by the ¹H NMR spectroscopy, but the identity of this compound was not confirmed. No propyl group from *n*-propylamine, however, was incorporated on the structure.

1.3. Conclusion

The syntheses of the modified ligand **7**, the *ortho-n*-propylated derivative of tetrakis(2-hydroxyphenyl)ethene **2**, and the dihydroxy diether derivatives **3E/3Z** were established in the ligand modification project. These ligands were studied for their coordination chemistry (Chapters 2 to 4). Some of the metal derivatives from these ligands, along with the fluorene-diol **4**, were evaluated for ethene polymerization catalysis (Chapter 5).

1.4. Experimental

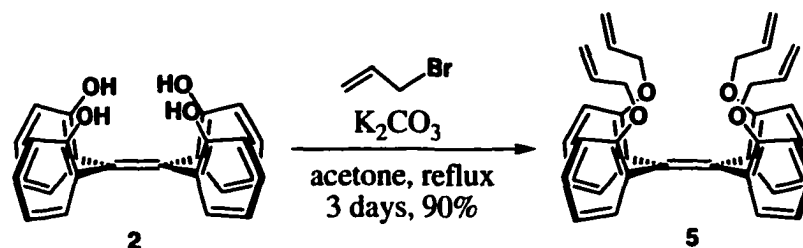
Instruments and Analysis: Nuclear magnetic resonance (NMR) spectra for ^1H and ^{13}C were recorded on Bruker AM-360, AM-400, AM-300, AM-200, Unity 500 and Unity Inova 500. NMR spectra were obtained at 25 °C unless otherwise noted. Chemical shifts are reported in parts per million (ppm, δ) relative to TMS, and coupling constants are reported as J in Hz. The "apparent" coupling constants of, for example, a doublet of doublets that appear as triplets, or broadened signals in which not all couplings are certain, are reported as J_{obs} or J . The assignment of quaternary (4°) or tertiary (3°) for aromatic carbons in ^{13}C NMR spectroscopy is either based on APT or relative intensity of the signals on BB analysis. The olefin C=C carbons are tentatively assigned to the smallest 4° signal in a proper region in most cases. Elemental analyses were performed by the University of Alberta Microanalytical Service Laboratory. Single crystal X-ray diffraction studies were performed at the X-ray Crystallography Laboratory at the University of Alberta Department of Chemistry by Dr. Robert McDonald. Details of the structure determinations are presented in Appendices. Mass spectra were obtained on Kratos MS-50 High Resolution Mass Spectrometer (EI, at 8kV), Micromass VG 7070E (CI, at 6kV), Kratos MS-9 (FAB at 6kV) or Micromass ZabSpec Sector-TOF (ES, at 4kV). FTIR spectra were obtained on Nicolet Magna IR 750 or Nicolet 20SX spectrophotometer. UV-Vis spectra were obtained on HP 8450A Diode Array Spectrophotometer.

Reaction Conditions and Supplemental Materials: Unless stated otherwise, all air- or moisture-sensitive manipulations were conducted under a nitrogen atmosphere by using standard Schlenk techniques. Flasks for moisture or air sensitive reactions were dried in the 120 °C oven overnight before use. Cylindrical Pyrex vessels equipped with Kontes k-826510 Teflon stopcocks are referred to as "reaction bombs." Some reactions and steps were performed in the drybox (Vacuum Atmospheres He-553-2 Dri-lab equipped with a Mo-41-1 inert gas purifier, a CD-882 Dri-Cold Freezer maintained at -35 °C, and a DK-3E Dri-Kool mechanical refrigeration unit). Flash column chromatographic separations were performed on silica gel 60 (230-400 mesh, SiliCycle). TLC (Silica Gel 60 F-254) was visualized by UV light or Morstein reagent.²⁵ Celite filtrations were performed by using Celite 545 on a fritted glass funnel under vacuum.

Materials: Unless indicated otherwise, solvents and reagents were purchased from commercial vendors and used as received (sensitive materials were kept and used under a

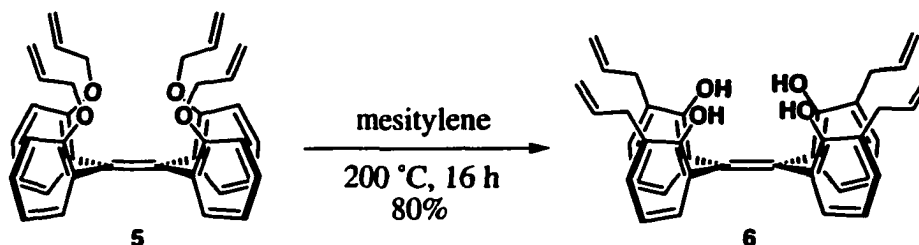
proper conditions to maintain quality). The following solvents/liquid reagents were dried and stored as indicated before use: THF, benzene and hexanes were purified by distillation from sodium benzophenone ketyl; toluene was distilled over potassium and degassed; acetonitrile was distilled from CaH₂ freshly before use; pyridine was distilled over calcium hydride and stored over 4Å molecular sieves; *t*-AmOH was dried over NaH, distilled, and kept in a bomb; and *n*-propylamine was dried, distilled from CaH₂, and stored under N₂ in a bomb. 3-Bromophenol (**18**) was dried by azeotropic distillation with benzene and degassed before use in the drybox. The solid materials KI and Ni(OAc)₂ were dried under reduced pressure by mild heating overnight with vigorous stirring and stored in the drybox. 2,2'-Bipyridine and BINAP were dried under reduced pressure overnight and stored in the drybox. NaH was washed with hexanes to remove the oil, dried, and stored in the drybox. The following complexes were prepared by following published procedures: tetrakis(2-hydroxyphenyl)ethene (**2**),² 2,2'-dimethoxybenzophenone,² nickel peroxide ('NiO₂'),²⁶ and Pd(dba)₂.²⁷

Tetrakis(2-propen-2-yloxyphenyl)ethene (5)



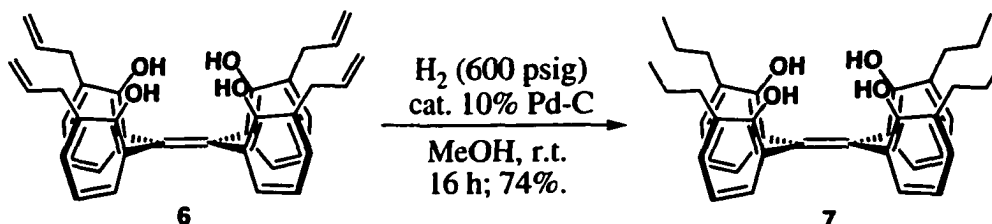
A mixture of tetrakis(2-hydroxyphenyl)ethene (2) (11.4 g, 0.0286 mol), allyl bromide (48.0 mL, 0.555 mol) and K₂CO₃ (61.5 g, 0.445 mol) in 300 mL of acetone was stirred under reflux for 2 days in a flask equipped with a CaCl₂ tube. Addition of 10 mL more of allyl bromide (0.116 mol) and 2 more days of stirring under reflux brought the reaction to completion, as determined by TLC analysis. The white precipitate, combined with the residue from the filtrate after removal of volatiles under reduced pressure, was washed with water to remove K₂CO₃, dissolved in hot CH₂Cl₂, filtered, concentrated, and ether was layered carefully on top of the solution. Slow diffusion gave 7.78 g (48.8%) of the pure crystalline product. The water washings were extracted with EtOAc and CH₂Cl₂, and the combined organic extract was dried over Na₂SO₄, filtered, and the volatiles were evaporated. Crystallization of the residue gave an additional 2.38 g (15.0%) of the pure product. From all the mother liquors, another 4.22 g (26.5%) was obtained by repeating crystallization (total yield: 90.3%). ¹H NMR (360 MHz, CDCl₃): δ 7.23 (4H, slightly br d, *J* = 7.5 Hz), 6.98 (4H, ddd, *J* = 8, 7.5, 1.7 Hz), 6.64 (4H, ddd, *J* = 7.5, 7.5, 1.0 Hz), 6.61 (4H, slightly br d, *J* = 8 Hz), 5.82 (4H, ddt, *J* = 17, 11, 5 Hz), 5.28 (4H, br d, *J* = 17 Hz), 5.12 (4H, br d, *J* = 10.5 Hz), 4.26 (8H, br). ¹³C NMR (75 MHz, CDCl₃, APT): δ 156.3 (4°, C-O), 137.0 (4°), 134.3 (3°), 132.6 (4°), 132.4 (3°), 127.3 (3°), 119.6 (3°), 116.4 (2°, -O-CH₂-C=), 111.9 (3°), 69.0 (2°, H₂C=C). Anal. Calcd for C₃₈H₃₆O₄: C, 81.99; H, 6.52. Found: C, 81.83; H, 6.35. HRMS (EI) *m/z*: Calcd for C₃₈H₃₆O₄: 556.26135. Found: 556.26202 (100%) [M⁺].

Tetrakis(3-propen-2-yl-2-hydroxyphenyl)ethene (6)



A mixture of tetrakis(2-propen-2-yloxyphenyl)ethene (5) (9.08 g, 0.0163 mol) in 35 mL of mesitylene was degassed in a bomb, which was refilled with nitrogen. The closed bomb was heated to 200 °C for 16 h with stirring. After concentrating the resulting mixture under reduced pressure, a white precipitate was formed, which was separated from the mixture by washing away the yellow oil with hexanes. The white precipitate was recrystallized from ethyl acetate-hexanes to yield 7.32 g (80%) of the pure product. ¹H NMR (360 MHz, CDCl₃): δ 7.01 (4H, dd, *J* = 7.5, 1.5 Hz), 6.87 (4H, dd, *J* = 7.5, 1.5 Hz), 6.70 (4H, dd, *J* = 7.5, 7.5 Hz) 5.99 (4H, br s, OH), 5.86 (4H, ddt, *J* = 17, 10, 6 Hz), 5.00 (4H, ddt, *J* = 10, 1.5, 1 Hz), 4.79 (4H, ddt, *J* = 17, 1.5, 1 Hz), 3.28 (8H, slightly br d, *J* = 6 Hz). ¹³C NMR (75 MHz, CDCl₃, APT): δ 150.6 (4°, C-O), 137.9 (C=C), 136.2 (3°), 129.7 (3°), 128.7 (4°), 128.4 (3°), 126.0 (4°), 120.6 (3°), 116.1 (2°, H₂C=C), 34.9 (2°, -O-CH₂-C=). Anal. Calcd for C₃₈H₃₆O₄: C, 81.99; H, 6.52. Found: C, 81.90; H, 6.50. HRMS (EI) *m/z*: Calcd for C₃₈H₃₆O₄: 556.26135. Found: 556.26152 (100%) [M⁺].

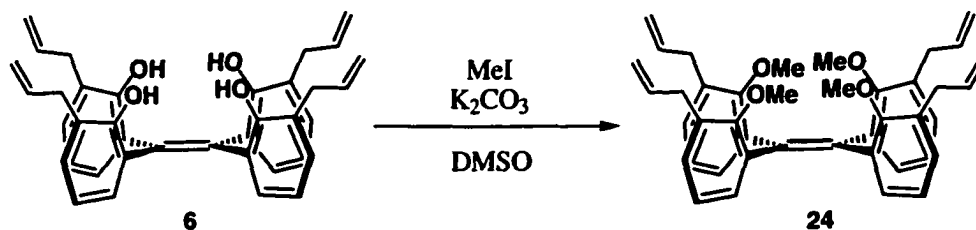
Tetrakis(3-propyl-2-hydroxyphenyl)ethene (7)



In a steel autoclave, a solution of tetrakis(3-propen-2-yl-2-hydroxyphenyl)ethene (6) (2.55 g, 4.57 mmol) in 120 mL of methanol was pressurized with H₂ (600 psig) in the presence of 10% Pd-C (0.052 g, 0.24 mmol) for 10 h at room temperature. After filtration through Celite and removal of the volatiles, the residue was passed through a silica gel column (eluent: hexanes/EtOAc = 2/1) to remove the dark-colored impurity. The product-

containing portions were collected and recrystallized from hexanes (hot to sub-zero) to give pure product (1.91 g, 74%). The mother liquor still contained the right product, which was purified by flash column chromatography together with the remnants from other runs (the yield of this portion was not recorded). $^1\text{H NMR}$ (360 MHz, CDCl_3): δ 6.94 (4H, dd, $J = 7.5, 1.5$ Hz), 6.88 (4H, dd, $J = 7.5, 1.5$ Hz), 6.68 (4H, t, $J_{\text{obs}} = 7.5$ Hz), 5.74 (3H, br s, OH), 3.51 (1H, s, OH), 2.45 (8H, t, $J = 7.5$ Hz), 1.44 (8H, sextet, $J = 7.5$ Hz), 0.80 (12H, t, $J = 7.5$ Hz). $^1\text{H NMR}$ (360 MHz, C_6D_6): δ 7.06 (4H, dd, $J = 7.5, 1.5$ Hz), 6.74 (4H, dd, $J = 7.5, 1.5$ Hz), 6.61 (4H, t, $J_{\text{obs}} = 7.5$ Hz), 5.80 (~3.5H, s, OH), 2.355 (8H, t, $J = 7.5$ Hz), 1.41 (8H, sextet, $J_{\text{obs}} = 7.5$ Hz), 0.75 (12H, t, $J = 7.5$ Hz), 0.41 (~3.5H, s, OH + H_2O). $^1\text{H NMR}$ (360 MHz, THF-d_8): δ 7.53 (3.3H, s, OH), 6.97 (4H, dd, $J = 7.5, 1$ Hz), 6.74 (4H, dd, $J = 7.5, 1$ Hz), 6.51 (4H, t, $J_{\text{obs}} = 7.5$ Hz), 2.48 (1.7H, s, OH + H_2O), 2.44 (8H, t, $J = 7.5$ Hz), 1.44 (8H, sextet, $J = 7.5$ Hz), 0.78 (12H, t, $J = 7.5$ Hz). $^{13}\text{C NMR}$ (125 MHz, CDCl_3 , APT): δ 150.3, 138.1 (C=C), 129.8, 129.6, 128.2, 127.9, 120.6, 32.2, 22.9, 13.8. HRMS (EI) m/z : Calcd for $\text{C}_{38}\text{H}_{44}\text{O}_4$: 564.32397. Found: 564.32246 (100%) [M^+]. Anal. Calcd for $\text{C}_{38}\text{H}_{44}\text{O}_4$: C, 80.82; H, 7.85. Found: C, 80.43; H, 7.71. UV/Vis (CH_2Cl_2): λ_{max} (ϵ_{max}) = 224 (36000), 284 (11000).

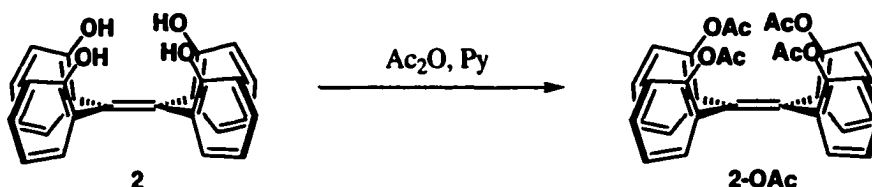
Tetrakis(3-propen-2-yl-2-methoxyphenyl)ethene (24)



Tetrakis(3-propen-2-yl-2-hydroxyphenyl)ethene (**6**) (0.119 g, 0.214 mmol), CH_3I (0.11 mL, 1.8 mmol) and K_2CO_3 (0.352 g, 2.55 mmol) were mixed in DMSO (2 mL) and stirred overnight in a flask equipped with a CaCl_2 drying tube and wrapped with aluminum foil to avoid light. The reaction mixture was then diluted with water, extracted with CH_2Cl_2 , and the combined extracts were washed with water and sat. NaCl and then dried over Na_2SO_4 . After removal of volatiles, the residue showed the $^1\text{H NMR}$ and mass spectroscopy results consistent with the structure of **24** (0.131 g, 100%, but not pure). Product from a larger scale run (2.2857 g of the starting material **6**) decomposed back to the starting material during recrystallization trials. $^1\text{H NMR}$ (360 MHz, CDCl_3): δ 7.02 (4H, br), 6.95 (4H, br d, $J = 7$ Hz), 6.75 (4H, t, $J_{\text{obs}} = 7$ Hz), 5.92 (4H, br m, $\text{H}_2\text{C}=\text{CHCH}_2^-$), 5.03 (4H, br d, $J_{\text{obs}} = 10$ Hz, $\text{H}_2\text{C}=\text{CHCH}_2^-$), 4.97 (4H, br d, $J_{\text{obs}} = 18$ Hz,

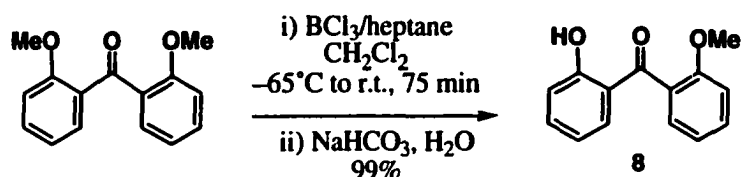
$\text{H}_2\text{C}=\text{CHCH}_2^-$), 3.36 (12H, s, OMe), 3.31 (8H, br, $\text{H}_2\text{C}=\text{CHCH}_2^-$). HRMS (EI) m/z : Calcd for $\text{C}_{42}\text{H}_{44}\text{O}_4$: 612.32397. Found: 612.32351 (100%) [M^+].

Tetrakis(2-acetoxyphenyl)ethene (2-OAc)



To a mixture of 1 mL of acetic anhydride and 1 mL of pyridine (distilled from calcium hydride and stored over 4Å molecular sieves), protected from moisture by a CaCl_2 drying tube, was added tetrakis(2-hydroxyphenyl)ethene (2) (0.0498 g, 0.126 mmol). The solid completely dissolved after stirring for 5 min. The reaction was followed by TLC. The completion of the reaction was confirmed in 15 min. The mixture was diluted with 10 mL of CH_2Cl_2 , washed with water (5 mL x 2) followed by 1N HCl (5 mL), 5% NaHCO_3 , water again (5 mL), and saturated NaCl. The organic solution was dried over anhydrous Na_2SO_4 , filtered, and the volatiles were removed. Pure product was obtained by recrystallization from acetone. The yield was quantitative. ^1H NMR (360 MHz, CDCl_3): δ 7.31 (4H, br), 7.16 (4H, td, $J = 7.5, 1.5$ Hz), 6.95-6.90 (8H, br), 1.98 (12H, s, OAc). ^{13}C NMR (75 MHz, CDCl_3 , APT): δ 169.2 (C=O), 149.2 (ipso) 133.9 (ipso), 133.5, 128.5, 125.1, 122.8, 20.9 (CH_3), C=C was not observed; Anal. Calcd for $\text{C}_{34}\text{H}_{28}\text{O}_8$: C, 72.33; H, 5.00. Found: C, 72.02; H, 4.97. HRMS (EI) m/z : Calcd for $\text{C}_{34}\text{H}_{28}\text{O}_8$: 564.17841. Found: 564.17867 (100%) [M^+], 522.16790 (53%) [$\text{M}^+ - \text{C}_2\text{H}_2\text{O}$], 480.15657 (39%) [$\text{M}^+ - 2(\text{C}_2\text{H}_2\text{O})$], 438.14581 (49%) [$\text{M}^+ - 3(\text{C}_2\text{H}_2\text{O})$], 396.13527 (40%) [$\text{M}^+ - 4(\text{C}_2\text{H}_2\text{O})$].

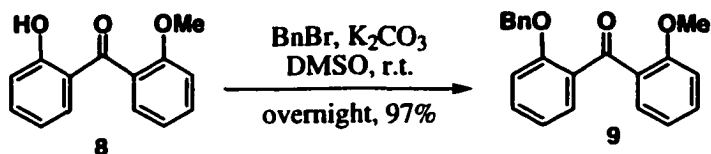
2-Hydroxy-2'-methoxybenzophenone (8)



This reaction was done based on a literature procedure.²⁸ To the solution of 2,2'-dimethoxybenzophenone (6.7 g, 0.028 mol) in CH_2Cl_2 (95 mL, freshly distilled from CaH_2) cooled to -65°C under nitrogen atmosphere, was added a solution of BCl_3 in

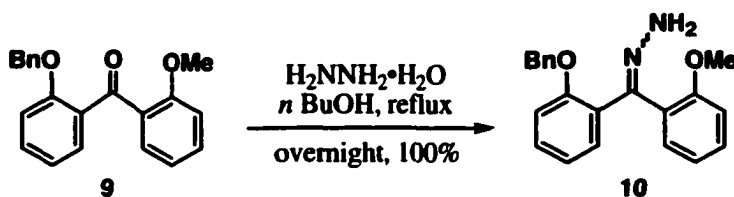
heptane (1.0 M, 52 mL, 0.052 mol). The mixture was allowed to warm to room temperature over 75 min. The mixture was slowly poured into a stirred sat. NaHCO₃ solution cooled in an ice bath. The organic compounds were extracted with CH₂Cl₂, and the extract was washed with water, followed by sat. NaCl, and dried over Na₂SO₄. After removal of the solvent, the residue was almost pure product, containing 3% of the starting material (6.3 g, 99%). This material was used as is in the next step. ¹H NMR (360 MHz, CDCl₃): δ 12.18 (~0.7H, s, OH), 7.48 (1H, ddd, *J* = 9, 7.9, 1.9 Hz), 7.47 (1H, ddd, *J* = 9, 7.5, 1.9 Hz), 7.33 (1H, dd, *J* = 7.6, 1.9 Hz), 7.30 (1H, dd, *J* = 7.6, 1.9 Hz), 7.06 (1H, td, *J* = 7.5, 1 Hz), 7.03 (1H, dd, *J* = 8.5, 1 Hz), 7.02 (1H, d, br, *J* = ~8.5 Hz), 6.80 (1H, ddd, *J* = ~9, 7.6, 1 Hz), 3.78 (3H, s, OMe), 1.56 (~0.5H, s, OH + H₂O?). ¹³C NMR (75 MHz, CDCl₃, APT): δ 202.2 (C=O), 163.0 (4°), 156.6 (4°), 136.5, 133.8, 131.9, 128.9, 127.9 (4°), 125.6, 120.3 (4°), 118.7, 118.1, 111.5, 55.7 (OCH₃). HRMS (EI) *m/z*: Calcd for C₁₄H₁₂O₃: 228.07864. Found: 228.07876 (35%) [M⁺], 197.06085 (100%) [M⁺ - OCH₃].

(2-Benzyloxyphenyl)(2-methoxyphenyl)methanone (9)



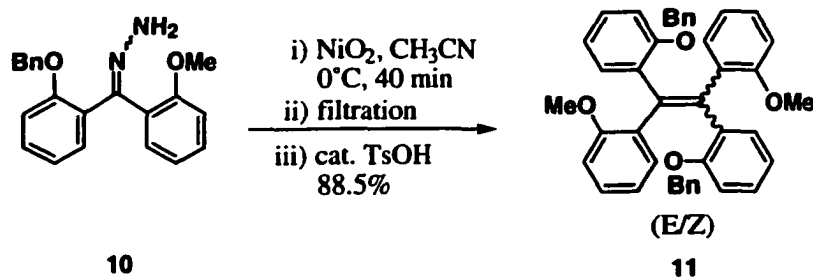
A mixture of **8** (8.08 g, 0.0354 mol), K₂CO₃ (24.5 g, 0.177 mol) and BnBr (4.4 mL, 0.037 mol) in 90 mL of DMSO was stirred at room temperature overnight. The mixture was diluted with diethyl ether and water. The aqueous layer was extracted with fresh diethyl ether, and the combined organic layers were washed with water followed by sat. NaCl and dried over Na₂SO₄. After purification by flash chromatography (eluent: CH₂Cl₂ / hexanes = 5/4 → 3/2), pure product (7.98 g, 97%) was obtained as clear oil. ¹H NMR (360 MHz, CDCl₃): δ 7.61 (1H, dd, *J* = 8, 1.8 Hz), 7.57 (1H, dd, *J* = 8, 2 Hz), 7.43 (1H, ddd, *J* = 8.5, 7.5, 2 Hz), 7.39 (1H, ddd, *J* = 8, 7.5, 1.8 Hz), 7.22~7.18 (3H, overlapping), 7.04 (1H, td, *J* = 7.5, 1 Hz), 6.98~6.94 (4H, overlapping), 6.84 (1H, d, br, *J* = 8 Hz), 5.45 (2H, s, PhCH₂), 3.60 (3H, s, CH₃). ¹³C NMR (75 MHz, CDCl₃, APT): δ 195.5 (C=O), 158.4 (4°), 157.2 (4°), 136.4 (4°), 132.6, 130.9 (4°), 130.6 (4°), 130.5, 130.3, 127.5 (two peaks overlapping), 126.7, 120.8, 120.4, 112.4, 111.7, 70.1 (OCH₂Ph), 55.7 (OCH₃). HRMS (EI) *m/z*: Calcd for C₂₁H₁₈O₃: 318.12558. Found: 318.12606 (22%) [M⁺], 287.10749 (16%) [M⁺ - OCH₃], 227.07093 (8%) [M⁺ - C₇H₇], 91.05485 (100%) [C₇H₇⁺].

(2-Benzyloxyphenyl)(2-methoxyphenyl)methanone hydrazide (10)



A mixture of **9** (7.98 g, 0.025 mol) and $\text{H}_2\text{NNH}_2 \cdot \text{H}_2\text{O}$ (16.0 mL, 0.328 mol) in 28 mL of butanol was stirred at reflux temperature overnight. The mixture was diluted with water, and the organic portion was extracted twice with a THF-acetonitrile (1 : 1). After washing the organic extracts with sat. NaCl and drying over Na_2SO_4 , the volatiles were removed by rotary evaporator to give a mixture of oil and solid. The solid part increased after being left under reduced pressure (vacuum pump) overnight. The resulting substance weighed more than >100% (8.78 g) and was used as is in the next step. The product gave a complicated ^1H NMR spectrum, probably due to the existence of *syn/anti* isomers. HRMS (EI) m/z : Calcd for $\text{C}_{21}\text{H}_{20}\text{N}_2\text{O}_2$: 332.15247. Found: 332.15233 (16%) [M^+], 316.13307 (31%) [$\text{M}^+ - \text{NH}_2$], 301.12286 (41%) [$\text{M}^+ - \text{N}_2\text{H}_3$], 91.05483 (100%) [C_7H_7^+].

E/Z-Bis(2-benzyloxyphenyl)-bis(2-methoxyphenyl)ethene (11)



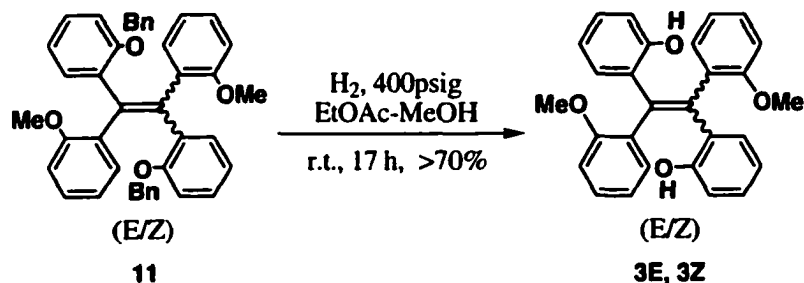
To a solution of **10** (5.60 g, 0.0168 mol) in acetonitrile (100 mL, freshly distilled from CaH_2), protected from moisture by a CaCl_2 drying tube and cooled to 0°C , the nickel peroxide " NiO_2 "²⁶ (active oxygen atom 2.69×10^{-3} mol/g, 17.3 g, 0.0464 mol) was added and stirred for 40 min (longer reaction time leads to the increase of formation of the byproduct Y). The mixture was filtered quickly through aluminum oxide (activated, basic, activity I), and the flask and the nickel peroxide cake were rinsed with fresh acetonitrile (total of 80 mL) until the washings were no longer pink-colored. To the deep pink filtrate was added a few drops of a solution of anhydrous *p*-toluenesulfonic acid in

benzene; the color immediately changed to yellow-brown. The catalytic amount of the acid was neutralized by adding a few drops of concentrated aqueous KOH solution to the mixture with stirring (the yellow color became lighter). This treatment was crucial to avoid the formation of unknown byproducts. After removal of volatiles and purification by flash chromatography (silica gel, eluent CH₂Cl₂/hexanes = 1/3 → 1/1 → 4/1), the analytically pure product was obtained (4.68 g, 88.5%). The product is either a single stereoisomer (*E* or *Z*) or a mixture of the diastereoisomers, but these are not distinguishable spectroscopically.

11 (*E/Z*). ¹H NMR (360 MHz, CDCl₃): δ 7.25~7.15 (6H, overlapping, br), 7.11 (1H, d, br), 7.03~6.97 (2H, overlapping, br), 6.68~6.59 (4H, overlapping, br), 4.83 (2H, s, br, PhCH₂), 3.39 (3H, s, br, OCH₃). ¹³C NMR (75 MHz, CDCl₃, APT and BB): δ 157.4 (4°), 156.4 (4°), 138.0 (4°), 137.0 (4°), 132.8 (4°), 132.4 (3°), 132.3 (3°), 128.1 (3°), 127.34 (3°), 127.28 (3°), 127.2 (3°), 127.1 (3°), 119.6 (3°), 111.8 (3°), 111.0 (3°), 69.7 (PhCH₂), 55.2 (CH₃), one 4° carbon and one 3° carbon are missing or overlapping with other peaks in the aromatic region. Anal. Calcd for C₄₂H₃₆O₄: C, 83.42; H, 6.00. Found: C, 83.24; H, 6.02. HRMS (EI) *m/z*: Calcd for C₄₂H₃₆O₄: 604.26135. Found: 604.26081 (85%) [M⁺], 513.20567 (5%) [M⁺ - C₇H₇], 422.15187 (24%) [M⁺ - 2(C₇H₇)], 91.05485 (100%) [C₇H₇⁺].

Byproduct Y. ¹H NMR (360 MHz, CDCl₃): δ 7.72 (2H, dd?), 7.62 (1H, dd, *J* = ~8.5, ~1 Hz) 7.49~7.33 (7H, overlapping), 7.27 (1H, td, *J* = ~7.5, ~1 Hz), 7.11 (2H, overlapping?), 3.70 (3H, s, OMe). HRMS (EI) *m/z*: Calcd for C₂₁H₁₆O₂: 300.11502. Found: 300.11511 (100%) [M⁺]. Based on this data, the byproduct is tentatively assigned structure Y (see Scheme 1.7).

E/Z-Bis(2-hydroxyphenyl)-bis(2-methoxyphenyl)ethene (**3E**, **3Z**)



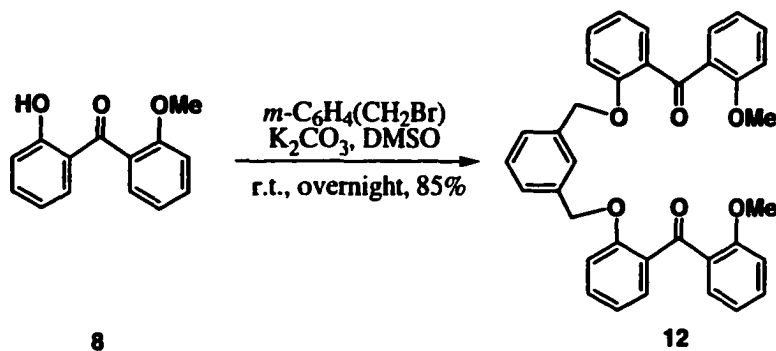
Due to the limited volume of the reaction apparatus, the reaction was done in two separate runs, and the resulting mixture was combined for purification.

In a steel autoclave, a mixture of **11** and 10% Pd-C in EtOAc and MeOH was pressurized with H₂ under 400 psig for 17 h. In the first run were used 2.01 g (3.32 mmol) of **11**, 0.355 g (0.334 mmol) of 10% Pd-C, 40 mL of EtOAc and 160 mL of MeOH. In the second run were used 2.48 g (4.10 mmol), 0.429 g (0.403 mmol), 50 mL and 155 mL, respectively. After the hydrogenation was complete, the mixture was filtered through Celite to remove the bulk of the catalyst, and the volatiles were removed. The *E/Z* mixture (crude ratio shown by ¹H-NMR spectroscopy was 7/1) was separated by flash chromatography (hexanes/EtOAc = 20/1, then 10/1). After crystallization of each of the *E*-dominant portion and the *Z*-dominant portion, 1.24 g (39%) of *E*-isomer **3E** and 0.3817 g (12%) of *Z*-isomer **3Z** were obtained. The *E/Z* mixture portion was 17%. By use of crystal seeding, **3E** or **3Z** were further crystallized individually from the mixture portion and the mother liquors. The stereochemistry of each isomer was assigned based on the X-ray crystallography of **3Z** (see Appendix A-1). The crystals of **3Z** used for X-ray analysis were grown from EtOAc-hexanes by slow diffusion.

3E. ¹H NMR (360 MHz, C₆D₆): δ 7.22 (2H, d, br, *J* = ~7.5 Hz), 7.07 (2H, br d, *J* = 7.5 Hz), 6.87~6.81 (2H+2H+2H, overlapping), 6.66 (2H, td, *J* = 7.5, 1 Hz), 6.56 (2H, ddd, *J* = ~7.5, ~7, 1.5~1.8 Hz), 6.27 (2H, dd, *J* = ~8, ~1 Hz), 3.21 (6H, s, OMe). ¹³C NMR (75 MHz, acetone-d₆, APT and BB): δ 156.9 (4°), 154.8 (4°), 138.2 (C=C), 131.5, 131.4 (4°), 131.1, 129.8 (4°), 129.1, 128.7, 121.0, 119.5, 115.8, 111.5, 55.8 (OMe). Anal. Calcd for C₂₈H₂₄O₄: C, 79.22; H, 5.70. Found: C, 78.94; H, 5.73. HRMS (EI) *m/z*: Calcd for C₂₈H₂₄O₄: 424.16745. Found: 424.16699 (100%) [M⁺]. UV/Vis (CH₂Cl₂): λ_{max} (ε_{max}) = 222 (29000), 284 (13000). IR (CHCl₃, cast) 3530 (br, s), 3440 (br, s) cm⁻¹.

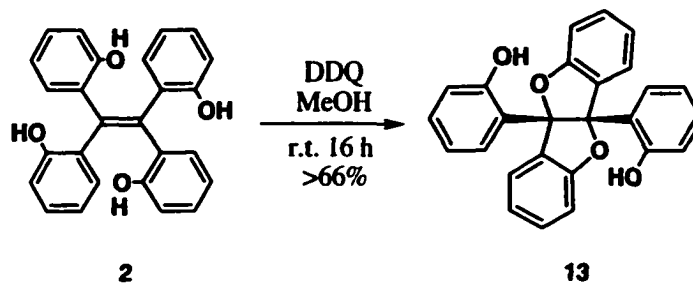
3Z. ¹H NMR (360 MHz, C₆D₆): δ 7.31 (2H, br d, *J* = ~7.5 Hz), 7.15 (2H, dd, overlapping with solvent), 6.91 (2H, dd, *J* = 8, 1.5 Hz), 6.86 (2H, ddd, *J* = ~8, 7, 1.7 Hz), 6.77 (2H, ddd, *J* = 8, 7.2, 1.8 Hz), 6.65 (2H, td, *J* = 7.2, 1.5 Hz), 6.59 (2H, td, *J* = 7.5, 1 Hz), 6.20 (2H, dd, *J* = 8, <1 Hz), 3.11 (6H, OMe). ¹³C NMR (75 MHz, acetone-d₆, APT and BB): δ 156.9 (4°), 154.9 (4°), 138.0 (C=C), 131.9 (4°), 131.3, 131.2, 129.7 (4°), 129.0, 128.9, 120.7, 119.6, 115.8, 111.4, 55.7 (OMe). Anal. Calcd for C₂₈H₂₄O₄: C, 79.22; H, 5.70. Found: C, 78.93; H, 5.50. HRMS (EI) *m/z*: Calcd for C₂₈H₂₄O₄: 424.16745. Found: 424.16685 (100%) [M⁺]. UV/Vis (CH₂Cl₂): λ_{max} (ε_{max}) = 222 (29000), 283 (13000). IR (CHCl₃, cast) 3424 (br, s) cm⁻¹.

Compound 12



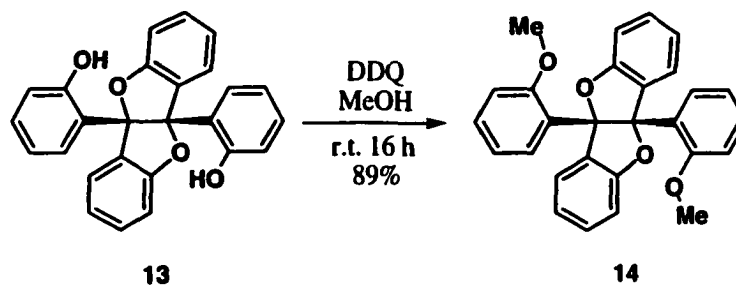
A mixture of 2-hydroxy-2'-methoxybenzophenone (**8**) (3.01 g, 13.2 mmol), K_2CO_3 (9.10 g, 65.9 mmol) and α,α' -dibromo-*m*-xylene (1.88 g, 7.11 mmol) in 30 mL of DMSO was stirred at room temperature overnight. The mixture was then diluted with diethyl ether and water. The aqueous layer was extracted with fresh diethyl ether, and the combined organic layers were washed with water, followed by sat. NaCl, and dried over Na_2SO_4 . After purification by flash chromatography (eluent: $\text{CH}_2\text{Cl}_2/\text{hexanes} = 1/0 \rightarrow 39/1 \rightarrow 29/1 \rightarrow 19/1$), pure product (2.96 g, 85%) was obtained as slightly yellow, clear oil. ^1H NMR (360 MHz, CDCl_3): δ 7.59 (2H, dd, $J = 7.5, 1.8$ Hz), 7.52 (2H, dd, $J = 7.5, 1.8$ Hz), 7.44 (2H, ddd, $J = 8.1, 7.5, 1.8$ Hz), 7.33 (2H, ddd, $J = 8.1, 7.5, 1.8$ Hz), 7.05 (2H, ddd, $J = 7.1, 7.5, 0.8$ Hz), 7.05' (1H, t, $J = 7.5$ Hz), 6.945 (2H, dd, $J = 8.1$ Hz, smaller J could not be determined), 6.94 (2H, ddd, $J = 7.5, 7.5, 0.8$ Hz), 6.80 (2H, br d, $J_{\text{obs}} = 7.5$ Hz), 6.79 (2H, br d, $J_{\text{obs}} = 8.1$ Hz), 6.61 (1H, br s), 4.85 (4H, s, $-\text{CH}_2\text{O}$), 3.56 (6H, s, CH_3O). ^{13}C NMR (75 MHz, CDCl_3 , APT): δ 195.3 (C=O), 158.5 (4°), 157.2 (4°), 136.4* (4°), 132.7, 132.6, 131.0 (4°), 130.5, 130.4, 128.6, 128.3, 126.0, 124.9, 120.9, 120.3, 112.4, 111.7, 70.0 (CH_2), 55.7 (CH_3); *Probably two 4° signals are overlapping. HRMS (EI) m/z : Calcd for $\text{C}_{36}\text{H}_{30}\text{O}_6$: 558.20422. Found: 558.20525 (1.5%) [M^+], 540.19326 (7%) [$\text{M}^+ - \text{H}_2\text{O}$], 331.13197 (61%) [$\text{C}_{22}\text{H}_{19}\text{O}_3$] $^+$, 330.12511 (63%) [$\text{C}_{22}\text{H}_{18}\text{O}_3$] $^+$, 211.11101 (66%), 210.10426 (92%), 135.04461 (100%) [$\text{C}_8\text{H}_7\text{O}_2$] $^+$, 105.07016 (93%), 104.06429 (80%).

Cis-4b,9b-dihydro-4b,9b-bis(2-hydroxyphenyl)benzofuro(3,2-b)benzofuran (13)



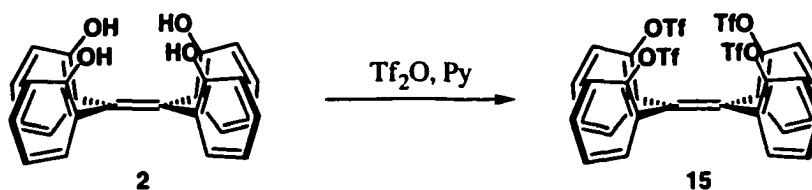
In 15 mL of methanol, tetrakis(2-hydroxyphenyl)ethene (**2**) (0.103 g, 0.259 mmol) and 2,3-dichloro-5,6-dicyano-1,4-benzoquinone (DDQ, 0.0899 g, 0.396 mmol) were dissolved and stirred for 16 h. Reaction progress was followed by TLC (hexane/EtOAc = 1/1). After removal of the volatiles, the product was separated by passing it through a short silica gel column with eluent (hexanes/EtOAc = 1/1). Pure portions yielded 0.068 g (66%). Impure portions also contained some of the product. The crystals for X-ray analysis was grown from Et₂O, warm to r.t., and slow evaporation. ¹H NMR (400 MHz, DMSO-d₆, 120°C): δ 8.24 (2H, br, OH), 7.50 (2H, br), 7.21 (2H, ddd, *J* = 8, 7.5, 1.5 Hz), 7.07 (2H, d, slightly br, *J* = 7.5 Hz), 6.92 (2H, d, *J* = 7.5 Hz), 6.89 - 6.87 (2H + 2H, overlapping, ddd & ddd), 6.64 (2H, dt, slightly br, *J*_{obs} = (7.5), 1 Hz), 6.35 (2H, dd, *J* = 8, 1 Hz). ¹³C NMR (125 MHz, DMSO-d₆, 100°C): δ 158.3 (4°), 153.9 (4°), 130.4 (4°), 129.2, 127.9, 127.7 (br), 124.6 (br), 124.0 (4°), 120.0, 116.7, 114.7, 109.3; One 4° carbon was not observed. HRMS (EI) *m/z* Calcd for C₂₆H₁₈O₄: 394.12051. Found: 394.12035 (100%) [M⁺]. Anal. Calcd for C₂₆H₁₈O₄: C, 79.17; H, 4.60. Found: C, 79.09; H, 4.59. UV/Vis (CH₃OH): λ_{max} (ε_{max}) = 279 (10941), 220 (hidden under solvent band). IR (cast): 3406 cm⁻¹ (OH), 1599, 1481, 1463, 749. X-ray crystallography: see **Appendix A-2**.

Cis-4b,9b-dihydro-4b,9b-bis(2-methoxyphenyl)benzofuro(3,2-b)benzofuran (14)



The mixture of **13** (0.206 g, 0.522 mmol), CH₃I (1 mL, 16 mmol) and K₂CO₃ (2.19 g, 15.8 mmol) in acetone (45 mL) was stirred under reflux. The reaction was followed by TLC (hexane/EtOAc = 5/1). After 16 h, a second aliquot of CH₃I (1 mL, 16 mmol) was added. After an additional 26 h, the mixture was cooled to r.t., volatiles were removed, water was added, and organic contents were extracted with EtOAc. The organic layer was washed with water followed by brine and dried over Na₂SO₄. After removal of the volatiles, pure product was obtained by crystallization from EtOAc/hexanes (0.196 g, 89%). ¹H NMR (360 MHz, CDCl₃): most peaks are slightly broadened; δ 8.01 (2H, d, *J* = 7.5 Hz), 7.19 (2H, t, *J*_{obs} = 7.5 Hz), 7.07~7.06 (2H & 2H), 6.95~6.94 (2H & 2H), 6.82 (2H, t, *J*_{obs} = 7.5 Hz), 6.33 (2H, d, *J* = 8 Hz), 3.96 (6H, s); some unassigned broad peaks were present. ¹³C NMR (75 MHz, CDCl₃): δ 158.8 (4°), 155.7 (4°), 131.3 (4°), 129.6, 128.7, 128.1 (4°), 127.3, 124.6, 120.7, 119.0, 110.3, 109.8, 54.2. One 4° carbon was not found. HRMS (EI) *m/z* Calcd for C₂₈H₂₂O₄: 422.15179. Found: 422.15158 (100%) [M⁺]. Anal. Calcd for C₂₈H₂₂O₄: C, 79.60; H, 5.25. Found: C, 79.70; H, 5.21.

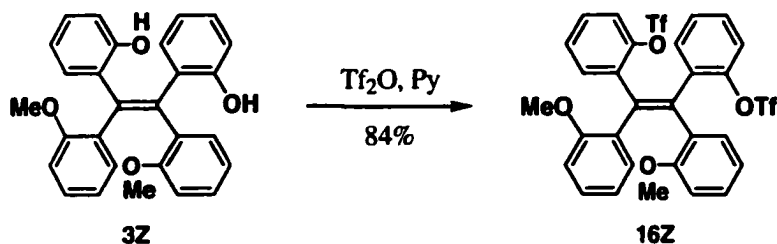
Tetrakis(2-trifluoromethanesulfonyloxyphenyl)ethene (**15**)



The mixture of 4.30 g (0.0108 mol) of tetrakis(2-hydroxyphenyl)ethene (**2**) in 24 mL of pyridine was prepared and placed under nitrogen atmosphere. To the mixture cooled to 0 °C was slowly added 1/3 portion of trifluoromethanesulfonic anhydride (total added: 9.0 mL, 15.5 g, 0.055 mol) via syringe. The remaining anhydride was added after letting the initial mixture stir for several minutes. The white solid that formed on the side of the vial was dissolved by immersing the reaction mixture in an ultrasound bath. The dark brown solution was allowed to warm to room temperature, then stirred for 24 h. The mixture was then diluted with 60 mL of water, which was accompanied by the formation of a precipitate. The mixture was extracted with 50 to 100 mL of diethyl ether five times until no product was observed by TLC. The combined ether extracts were washed with 50 mL of water, followed by 10% HCl, water again, and sat. NaCl. The combined aqueous washings were re-extracted with diethyl ether (20 mL x 2). The combined organic layers were dried over MgSO₄, filtered, and the solvent was evaporated. The yellow color impurities were removed from the residue by passing through a silica gel packed column

(with eluent: $\text{CCl}_4/\text{CH}_2\text{Cl}_2 = 2/1$). The colorless crude product was purified by recrystallization from acetone or acetone-acetonitrile. The yield was quantitative. ^1H NMR (360 MHz, CDCl_3): δ 7.44 (4H, br), 7.30 (4H, ddd, $J = 9, 7.3, 1.8$ Hz), 7.22 (4H, br), 6.84 (4H, br). ^{13}C NMR (125 MHz, CDCl_3): δ 147.9 (br, 4°), 135.4 (br, 3°), 134.3 (br, 4°), 132.5 (br, 4°), 130.3 (sharp, 3°), 127.9 (br, 3°), 121.0 (br, 3°), 118.3 (q, $J_{\text{C-F}} = 443$ Hz, CF_3). Anal. Calcd for $\text{C}_{30}\text{H}_{16}\text{F}_{12}\text{O}_{12}\text{S}_4$: C, 38.97; H, 1.74; S, 20.76. Found: C, 38.76; H, 1.45; S, 1.36. MS (ES) m/z : Calcd for $\text{C}_{30}\text{H}_{16}\text{F}_{12}\text{O}_{12}\text{S}_4$: 923.9. Found: 946.9 (55%) [$\text{M} + \text{Na}$] $^+$, 813.8 (40%) [$\text{M} - \text{SO}_2\text{CF}_3$] $^+$, 736.7 (100%), 603.7 (65%) [$736.7 - 2(\text{SO}_2\text{CF}_3)$] $^+$, 474.7 (45%).

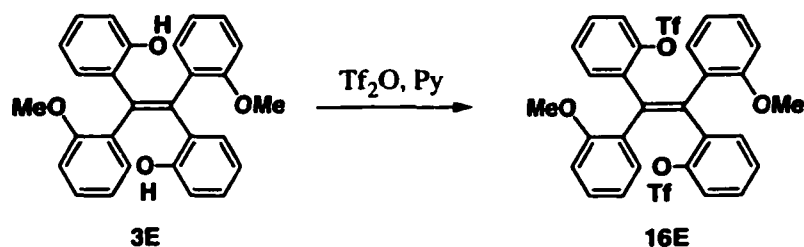
Z-Bis(2-trifluoromethanesulfonyloxyphenyl)-bis(2-methoxyphenyl)ethene (16Z)



To the solution of Z-bis(2-hydroxyphenyl)-bis(2-methoxyphenyl)ethene (**3Z**) (0.504 g, 1.19×10^{-3} mol) in pyridine (2 mL) in an oven-dried flask, which was cooled to 0°C and protected from moisture by a CaCl_2 drying tube, was slowly added trifluoromethanesulfonic anhydride (1.1 mL, 6.71×10^{-3} mol). Vigorous reaction with white smoke was observed, and the reaction mixture became reddish immediately. After the addition, more pyridine (2 mL) was added to dilute the mixture and permit continued stirring. The mixture was allowed to warm to room temperature and stirred overnight. The mixture was then diluted with water, extracted with ether until the extract showed no product by TLC analysis, and the combined extracts were washed with 1N HCl (x 2), water, sat. NaCl, then dried over Na_2SO_4 . After removal of the volatiles, the residue was crystallized from CH_2Cl_2 -hexanes to give pure product (0.657 g, 84%). ^1H NMR (360 MHz, DMSO-d_6): δ 7.32-7.27 (2H + 2H, overlapping, br), 7.13-7.03 (2H + 2H + 2H, overlapping, br), 6.98 (2H, br d, $J = \sim 7$ Hz), 6.84 (2H, br d, $J_{\text{obs}} = 8$ Hz), 6.70 (2H, br t, $J_{\text{obs}} = 7.5$ Hz). ^{13}C NMR (125 MHz, DMSO-d_6 , 100°C): δ 156.8, 145.7 (4°), 135.2 (4°), 134.1, 132.0 (4°), 130.6, 130.2 (4°), 128.8, 128.7, 126.8, 119.35, 119.32, 117.5 (q, $J = 319$ Hz, CF_3), 111.0, 54.5 (OCH_3), one 4° carbon missing. Anal. Calcd for $\text{C}_{30}\text{H}_{22}\text{F}_6\text{O}_8\text{S}_2$: C, 52.33; H, 3.22; S, 9.31. Found: C, 52.16; H, 3.15; S, 9.71. HRMS (EI) m/z : Calcd for

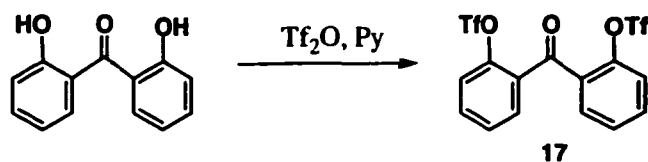
$C_{30}H_{22}F_6O_8S_2$: 688.0661. Found: 688.06529 (100%) [M^+], 555.10877 (13%) [$M - SO_2CF_3$] $^+$, 422.15122 (29%) [$M - 2(SO_2CF_3)$] $^+$.

E-Bis(2-trifluoromethanesulfonyloxyphenyl)-bis(2-methoxyphenyl)ethene (16E)



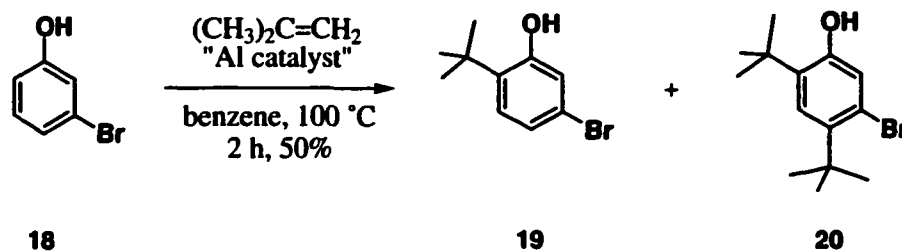
This product was prepared from **3E** in the same way as **16Z** was from **3Z**. From 0.0568 g of **3E** (0.134 mmol) with 1 mL of pyridine and 0.11 mL (0.67 mmol) of trifluoromethanesulfonic anhydride, the crude product **16E** was obtained quantitatively (crude yield: 0.0928 g, 101%). Crystallization from CH_2Cl_2 -hexanes gave clear prism crystals. 1H NMR (360 MHz, $CDCl_3$): δ 7.32 (2H, br d, $J = 6\sim 7$ Hz), 7.16-7.02 (2H x 5, overlapping, br), 6.71 (2H, br t, $J = \sim 7$ Hz), 6.67 (2H, br d, $J = 8\sim 8.5$ Hz), 3.48 (6H, s, OMe). The structure was tentatively assigned based on the symmetry of the product shown in 1H NMR spectroscopy and comparison with the *Z*-analogue.

2,2'-Dihydroxybenzophenone bistriflate (17)



This product was prepared from commercially purchased 2,2'-dihydroxybenzophenone in the same way as **16Z** was from **3Z**. From 1.50 g of 2,2'-dihydroxybenzophenone (7.0 mmol) with 6.5 mL of pyridine and 2.7 mL (16.5 mmol) of trifluoromethanesulfonic anhydride, the crude product **17** was obtained. Flash chromatography did not purify the product completely, as seen in the >100% yield (3.27 g, 113%). 1H NMR (360 MHz, $CDCl_3$): δ 7.67 (2H + 2H, overlapping, dd and dt), 7.51 (2H, t, $J_{obs} = 8.5$ Hz). HRMS (EI) m/z : Calcd for $C_{15}H_{18}F_6O_7S_2$: 477.96157. Found: 477.96324 (100%) [M^+], 329.00438 (47%) [$M - OSO_2CF_3$] $^+$.

5-Bromo-2-(1,1-dimethylethyl)phenol (**19**)²⁹



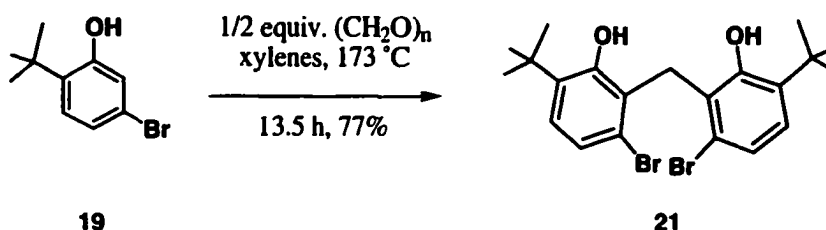
Catalyst preparation: Tris(5-bromophenoxy)aluminum was prepared in the drybox by slowly adding dropwise 3-bromophenol (**18**) (2.75 g, 21.7 mmol) to the solution of Me_3Al (0.491 g, 6.81 mmol) in pentane (35 mL) prepared in a 50 mL Schlenk flask. A small amount of toluene was used to rinse the container that contained **18**. Gentle reflux was maintained while a weak vacuum was applied on the sidearm of the Schlenk flask to reduce the amount of evolving gas escaping to the box's atmosphere. A white precipitate started to form when about 3/4 of **18** had been added. After completion of the addition, the mixture was stirred for 5 more minutes, and then the volatiles were removed in vacuo. The white powder was collected, rinsed with pentane, followed by a small amount of toluene (to remove remaining **18**), rinsed again with pentane, and dried in vacuo. The yield was > 95%.

Small scale: Under inert atmosphere, 2-methylpropene was introduced to a coldfinger cooled with dry ice, to condense in a preweighed bomb. The bomb with condensed 2-methylpropene was closed, warmed to room temperature, and reweighed to obtain the mass of 2-methylpropene (0.895 g, 0.0160 mol). In the drybox, **18** (2.76 g, 0.0160 mol) and the catalyst tris(5-bromophenoxy)aluminum (0.437 g, 8.05×10^{-4} mol) were weighed based on the mass of 3-methylpropene and mixed in benzene in a second reaction bomb. The second bomb had to be large enough to contain all the reagents. Out of the drybox, 2-methylpropene was transferred to the bomb containing **18** by connecting the two bombs under inert atmosphere, isolating the system, cooling the latter bomb to -60 °C and opening the valves to both bombs. After the transfer, the bomb was closed, allowed to warm to r.t., then heated in an oil bath (immersed to the neck level for even heating) at 100-110 °C for longer than 27 h. After the heating period, the bomb was cooled to r.t., opened to the atmosphere, and 10% HCl was added to liberate the phenoxides from the catalyst. The organic layer was separated from the aqueous layer, which was further extracted with additional benzene. The combined organic layer was washed with 10% HCl, followed by water, dried over MgSO_4 , and filtered. The volatiles were removed from the filtrate in vacuo to give the crude product mixture, in which **18** (unreacted), **19**

and **20** (overreacted) were found at the ratio of [6 : 58 : 30], according to the ^1H NMR spectroscopy.

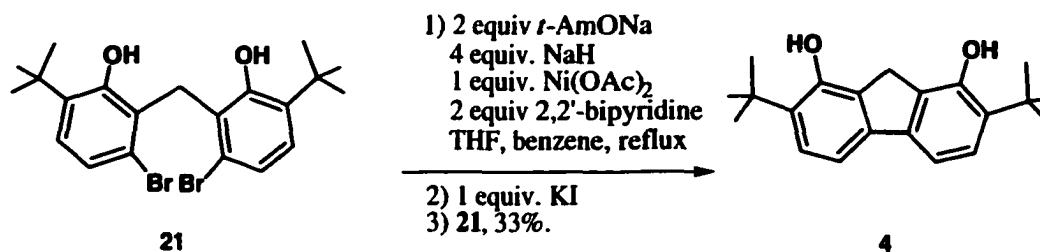
Large scale: Two separate reactions were performed following the small-scale procedure, and the product mixtures were combined for purification. Reaction (I): 2-methylpropene (6.24 g, 0.111 mol), **18** (17.1 g, 0.0988 mol), the Al catalyst (5.24 g, 9.65×10^{-3} mol), and benzene (80 mL) were used. The heating temperature was 170-180 °C using heating tape instead of oil bath, and the heating period was 40 h. Reaction (II): 2-methylpropene (9.0 g, 0.16 mol), **18** (27.7 g, 0.160 mol), the catalyst (4.36 g, 8.03×10^{-3} mol), and benzene (85 mL) were used. The heating temperature was 176-178 °C using an oil bath, and the heating period was 24h. The product mixture ratio [**18** : **19** : **20**] was [2 : 41 : 57] and [3 : 46 : 50], respectively. The separation/purification by careful flash chromatography was performed on the combined product mixtures by using hexanes/EtOAc = 1/0 \rightarrow 100/1 \rightarrow 50/1 \rightarrow 20/1 \rightarrow 10/1 \rightarrow 2/1. The purest portion of **19** (31.1g, 50%) still contained up to 5% of the byproduct **20**. The yield was calculated based on the starting material **18** and the total amount of the phenol contained in the catalyst.

Bis[5-bromo-3-(1,1-dimethylethyl)-2-hydroxyphenyl]methane (21**)**³⁰



In a reaction bomb, 3-bromo-5-(1,1-dimethylethyl)phenol (**19**) (11.1 g, 0.0484 mol) was weighed, and then paraformaldehyde (0.725 g, 0.0242 mol) and xylenes (5.14 g, 0.0484 mol) were added. The closed bomb was heated to 173 °C for 13.5 h. The color turned from almost colorless to yellowish-orange. After removal of the bulk of the volatiles in vacuo, the thick residue was purified by flash chromatography (eluent: hexane/EtOAc = 1/0 \rightarrow 500/1 \rightarrow 30/1). The reasonably pure portion yielded 4.6 g (40%). Less pure portions provided an additional 4.3g (37%). These products were recrystallized from hexane prior to use in the next step. The identity of the product was confirmed by ^1H NMR spectroscopy and was identical to the data reported by Wuest et al. See reference **10**.

2,7-Bis(1,1-dimethylethyl)-9H-fluorene-1,8-diol (4)



The procedure of Caubère et al. was adapted.²³ The following three mixtures were prepared in separate Schlenk flasks in the drybox: (a) Suspension of NaH (0.288 g, 0.0120 mol), Ni(OAc)₂ (0.354 g, 2.00 mmol) and 2,2'-bipyridine (0.625 g, 4.00 mmol) in THF-benzene (5 + 5 mL); (b) THF-benzene (1 + 1 mL) to which *t*-AmOH (0.44 mL, 4.0 mmol) was added outside of the drybox later; and (c) bis[5-bromo-2-hydroxy-3-(1,1-dimethylethyl)phenyl]methane (21) (0.471 g, 1.00 mmol) in THF-benzene (1.2 + 1.2 mL). The Schlenk flasks were taken out of the drybox and placed under nitrogen atmosphere. Flask (a) was equipped with a condenser and brought to reflux. The color became darker. The contents of flask (b) were then transferred to flask (a); gas evolution was observed. Anhydrous KI (0.338 g, 2.03 mmol) was quickly weighed and added to the mixture. After keeping the mixture at reflux for 1.5 h, the contents of flask (c) were added. Vigorous reaction was observed with the color turning to dark greenish purple. The reaction was monitored by TLC. After 13 h, the dark purple mixture was cooled to r.t. A small amount of EtOH was added dropwise to quench excess hydride. The mixture was then acidified with 5% HCl (25 mL); the exothermic reaction was accompanied by a color change to greenish brown and precipitate formation. The mixture was extracted with ether (25 mL x 2). The combined extracts were dried over MgSO₄. After removal of the solvent, the residue was purified by flash chromatography (eluent: hexanes/EtOAc = 20/1). Fairly pure product 4 was obtained (0.104 g, 33%) and identified by spectroscopic comparison to the known compound (see reference 10). This product was further purified by crystallization (toluene-hexane) prior to use in the preparation of metal derivatives. The byproducts included uncoupled, over-reduced product Bis[2-hydroxy-3-(1,1-dimethylethyl)phenyl]methane, tentatively assigned by ¹H NMR spectroscopy and HRMS analysis.

h with stirring. The TLC (hexanes / EtOAc = 15/1) a new major spot, accompanied by several minor spots, with no starting material. After removal of the volatiles, the major species was isolated by flash chromatography (eluent: hexanes → hexanes / EtOAc = 200/1 → 150/1). No propyl group from *n*-propylamine was incorporated on the structure, as confirmed by ¹H NMR spectroscopy.

1.5. References and Notes

-
- ¹ (a) Wieser, C.; Dieleman, C. B.; Matt, D. *Coord. Chem. Rev.* **1997**, *165*, 93-161. (b) Böhmer, V. *Angew. Chem. Int. Ed.* **1995**, *34*, 713-745.
- ² (a) Verkerk, U. Ph.D. Dissertation, University of Alberta, 2001. (b) US Patent Application: US Serial Number 09/336,388 (filed on 06/18/99).
- ³ Based on literature search in Beilstein database.
- ⁴ (a) von Itter, F. A.; Vögtle, F. *Ber. Dtsch. Chem. Ges.* **1985**, *118*, 2300-2313. (b) von Itter, F. A.; Vögtle, F.; Weber, G.; Sheldrick, G. M. *Z. Naturforsch.* **1983**, *38b*, 262-264.
- ⁵ (a) Roberts, J. D.; Watanabe, W. *J. Am. Chem. Soc.* **1950**, *72*, 4869-4871. (b) Bethell, D.; Callister, J. D.; *J. Chem. Soc.* **1963**, 3801-3815.
- ⁶ Olmstead, M. M.; Sigel, G.; Hope, H.; Xu, X.; Power, P. P. *J. Am. Chem. Soc.* **1985**, *107*, 8087-8091.
- ⁷ Dzwiniel, T., unpublished results.
- ⁸ Atwood, J. L.; Bott, S. G.; Jones, C.; Raston, C. L. *J. Chem. Soc. Chem. Commun.* **1992**, 1349-1351.
- ⁹ Verkerk, U., unpublished results.
- ¹⁰ (a) Saied, O.; Simard, M.; Wuest, J. D. *Inorg. Chem.* **1998**, *37*, 2620-2625. (b) Sharma, V.; Bachand, B.; Simard, M.; Wuest, J. D. *J. Org. Chem.* **1994**, *59*, 7785-7792.
- ¹¹ Saied, O.; Simard, M.; Wuest, J. D. *Organometallics* **1998**, *17*, 1128-1133.
- ¹² Pearson, D. E.; Wylson, R. D.; Breder, C. U. *J. Org. Chem.* **1967**, *32*, 2358-2360.
- ¹³ Garcia, H.; Primo, J. *Synthesis* **1985**, 901-902.
- ¹⁴ Barton, D. H. R.; Bhathagar, N. Y.; Blazejewski, J-C.; Charpiot, B.; Finet, J-P., Lester, D. J.; Motherwell, W. B.; Papoula, M. T. B.; Stanforth, S. P. *J. Chem. Soc. Perkin Trans I* **1985**, 2657-2665.
- ¹⁵ Ramakanth, S.; Narayanan, K.; Balasubramanian, K. K. *Tetrahedron* **1986**, *42*, 863-876.

-
- ¹⁶ (a) Behr, A. *Chem. Ber.* **1872**, *5*, 277-280. (b) The position of the hydroxy groups at the 4-positions were confirmed in this report. Buckles, R. E.; Womer, W. D. *J. Am. Chem. Soc.* **1958**, *80*, 5055-5058.
- ¹⁷ (a) Litwak, A. M.; Biali, S. E.; *J. Org. Chem.* **1992**, *57*, 1943-1945. (b) Litwak, A. M.; Grynszpan, F.; Aleksyuk, O.; Cohen, S.; Biali, S. E. *J. Org. Chem.* **1993**, *58*, 393-402. (c) Grynszpan, F.; Biali, S. E. *J. Chem. Soc. Chem. Commun.* **1994**, 2545-2546.
- ¹⁸ Rigaudy, J.; Scribe, P.; Brelière, C. *Tetrahedron* **1981**, *37*, 2585-2593.
- ¹⁹ Hartwig, J. F. *Angew. Chem. Intl. Ed.* **1998**, *37*, 2046-2067 and references within.
- ²⁰ (a) Cai, D.; Payack, J. F.; Bender, D. R.; Hughes, D. L.; Verhoeven, T. R.; Reider, P. J. *J. Org. Chem.* **1994**, *59*, 7180-7181. (b) Lipshutz, B. H.; Buzard, D. J.; Yun, C. S. *Tetrahedron Lett.* **1999**, *40*, 201-204.
- ²¹ Louie, J.; Driver, M. S.; Hamann, B. C.; Hartwig, J. F. *J. Org. Chem.* **1997**, *62*, 1268-1273. Also referred: Wolfe, J. P.; Buchwald, S. L. *J. Org. Chem.* **1997**, *62*, 1264-1267.
- ²² To avoid overalkylation, acid-catalyzed *O*-*tert*-butylation* of 5-bromo-2-(1,1-dimethylethyl)phenol (100% yield) followed by thermal rearrangement to the *ortho*-position was also attempted. The latter step, however, also resulted in a mixture of **19** (58%), **18** (42%) and trace of **20**. *Holcombe, J. L.; Livinghouse, T. *J. Org. Chem.* **1986**, *51*, 111-113.
- ²³ Lourak, M.; Vanderesse, R.; Fort, Y.; Caubère, P. *J. Org. Chem.* **1989**, *54*, 4840-4844.
- ²⁴ Dzwiniel, T. and Qi, G., unpublished results.
- ²⁵ Components of the Morstein reagent are: 20 g of ammonium molybdate, 0.4 g of cerium (IV) sulfate, and 500 mL of 10% H₂SO₄. *Europ. J. Org. Chem.* **2000**, 1745-1758.
- ²⁶ Nakagawa, K.; Konaka, R.; Nakata, T. *J. Org. Chem.* **1962**, *27*, 1597-1601.
- ²⁷ Rettig, M. F.; Maitlis, P. M. *Inorg. Synth.* **1990**, *28*, 110-112.
- ²⁸ Dean, F. M.; Goodchild, J.; Houghton, L. E.; Martin, J. A.; Morton, R. B.; Parton, B.; Price, A. W.; Somvicien, N. *Tetrahedron Lett.* **1966**, *35*, 4153-4159.
- ²⁹ Based on (a) Von Stroh, R.; Seydel, R.; Harn, W. *Angew. Chem.* **1957**, *69*, 699-746; (b) Kolka, A. J.; Napolitano, J. P.; Filbey, A. H. Ecke, G. G. *J. Org. Chem.* **1957**, *22*, 642-646; and (c) Verkerk, U., unpublished results.
- ³⁰ Based on (a) Casiraghi, G.; Casnati, G.; Pochini, A.; Puglia, G. Ungero, R. Sartori, G. *Synthesis* **1981**, 143-146; (b) Verkerk, U., unpublished results.

Chapter 2

Preface to Chapters 3 and 4:

Basic Concepts and Strategies for the Coordination Studies of the Tetrakis(2-hydroxyphenyl)ethene-Derived Preorganized Ligands

In the following two chapters (Chapters 3 and 4), the synthesis, structure, spectroscopic features, and chemical behavior of metal complexes prepared from the modified tetrakis(2-hydroxyphenyl)ethene-based ligands will be discussed.

Prior to this work, little was known about this new ligand system's ability to coordinate to metal atom(s). After establishing a few successful modification routes of parent ligand **2** as described in Chapter 1, the next goal was to evaluate the coordination behavior of those modified tetraarylethene systems. The effect of *ortho*-alkylation (as in **7**), as well as the effect of partial etheration of hydroxy groups (as in **3E** and **3Z**) on the coordination behavior, needed to be examined.

Before going into the details and specifics of each metal complex, it is useful to review the basic features of the parent ligand system **2** related to its coordination behavior, and to define some concepts and terms. The first section of this chapter will outline the flexibility, symmetry, ring-tilting tendency and classification of conformations of the tetrakis(2-hydroxyphenyl)ethene-based ligand system, with specific comparisons to the calix[4]arene system.

The latter part of this chapter will describe the concepts and background of the "surface-mimic" study using these ligands. Many of the coordination studies presented in this thesis are related to our attempts to create a well-defined mimic of heterogeneous MgCl_2 -supported TiCl_4 olefin polymerization catalysts. The proposed structure of the catalytic center of such heterogeneous catalysts and phenoxide-based olefin polymerization catalysts will be reviewed, followed by a description of the general

approach taken to obtain a surface-mimic of such systems by using tetrakis(2-hydroxyphenyl)ethene-based ligands.

2.A. Flexibility and Symmetry of the Tetrakis(2-hydroxyphenyl)ethene System as a Coordination Platform

2.A.1. Ring Rotation. The rotation dynamic of each aryl ring is one of the unique features of tetrakis(2-hydroxyphenyl)ethene-based ligands. The calixarene system also has rotatory freedom and flexibility, but the nature of the rotation is obviously different. **Figure 2.1** shows the rotation axes of tetrakis(2-hydroxyphenyl)ethene (a) and calix[4]arene system (b). The former rotates each ring about the ethene plane by "tilt" rotation, while the latter flexes on an inward/outward manner.

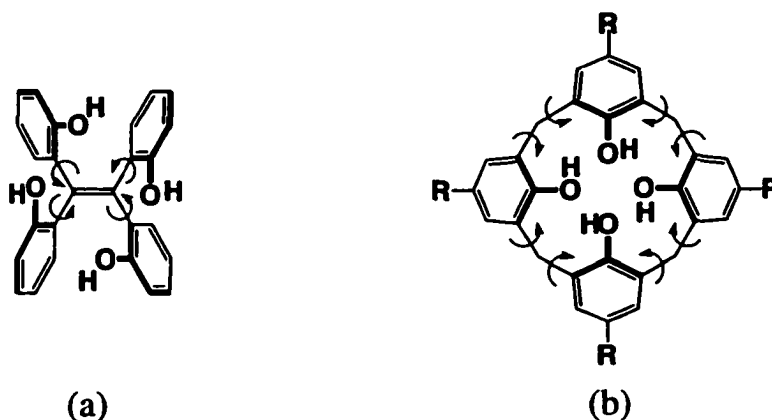


Figure 2.1. Rotation axes of (a) tetrakis(2-hydroxyphenyl)ethene **2** and (b) calix[4]arene.

2.A.2. Backbone-Rigidity and Symmetry. The ethene-backbone gives some degree of rigidity to the ligand framework. However, the tilt rotation of each ring allows flexibility for the ligand system **2** to adjust to the coordination requirements of different metal atoms.

The ethene-backbone also gives a different symmetry to the ligand system **2**. The C_{2v} symmetry (if all the hydroxy groups are on the same side) makes two kinds of "proximal" relationships: "geminal" and "vicinal." Meanwhile, calix[4]arene has C_{4v}

symmetry and has only one kind of "proximal" relationship between two neighboring aryl rings.

2.A.3. Tilting Angle of Each Ring. Although each ring in parent ligand **2** (as well as in the *para-tert*-butylated analogue or the *ortho*-propylated ligand **7**) rotates freely in solution phase, the solid-state structure of **2** suggests certain conformational preferences. Unlike calix[4]arenes, which are always found in the "cone" conformation in crystal structures,¹ the crystal structure of **2** reveals a "two-up/two-down" conformation, with or without the *para-tert*-butyl groups (Figure 2.2)².

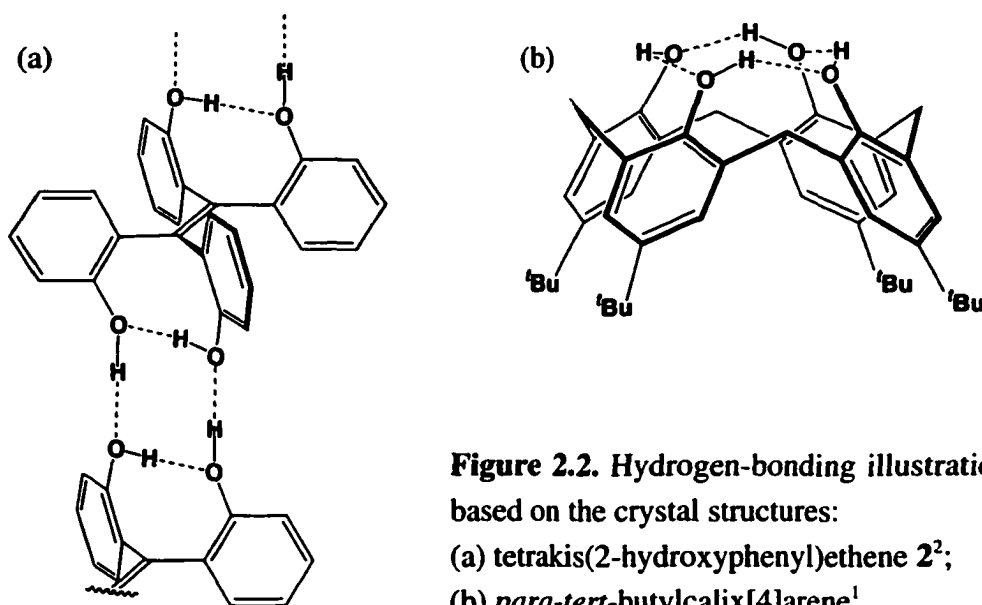


Figure 2.2. Hydrogen-bonding illustrations based on the crystal structures:

(a) tetrakis(2-hydroxyphenyl)ethene **2**²;

(b) *para-tert*-butylcalix[4]arene¹.

In the calix[4]arene system, the cyclic hydrogen bonding array among the four hydroxy groups is the major factor stabilizing this particular "cone" conformation. In the tetrakis(2-hydroxyphenyl)ethene system, in contrast, intramolecular hydrogen bonding is seen only pairwise: between each geminal pair of hydroxy groups. The intermolecular hydrogen bonding then forms from an infinite one-dimensional array.

Cyclic intramolecular hydrogen bonding could form theoretically in the tetrakis(2-hydroxyphenyl)ethene system, if the aryl rings tilt to a certain degree. The ligand, however, seems to prefer to have the aryl rings as perpendicular to the olefin plane as possible, rather than deviating markedly from the perpendicular. When the rings

are all roughly perpendicular, the distance between the vicinal pair of hydroxy groups is too great to allow hydrogen bonding.

The cyclic bridging among the four aryloxy groups is, however, attained when the protons are replaced with stronger bridging groups. For example, the alkyl aluminum complex of **2** (Figure 2.3) forms such a cyclic structure.² The aryl rings are nearly perpendicular to the olefin plane. The longer Al–O bond lengths make the cyclic structure possible while keeping the aryl rings nearly perpendicular.

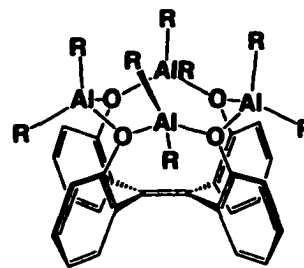


Figure 2.3. Ethyl aluminum complex of **2** (R = Me or Et).

2.A.4. Classification of Ligand Conformations. Theoretically, the tetrakis(2-hydroxyphenyl)ethene framework can take five different basic conformations: "all-up," "geminal up/down," "vicinal up/down," "alternating up/down," and "three-up/one-down" (Figure 2.4). All patterns have been observed in the metal derivatives obtained from the *ortho*-propylated ligand **7** or dialkylated ligands **3E** or **3Z** (Chapters 3 and 4).

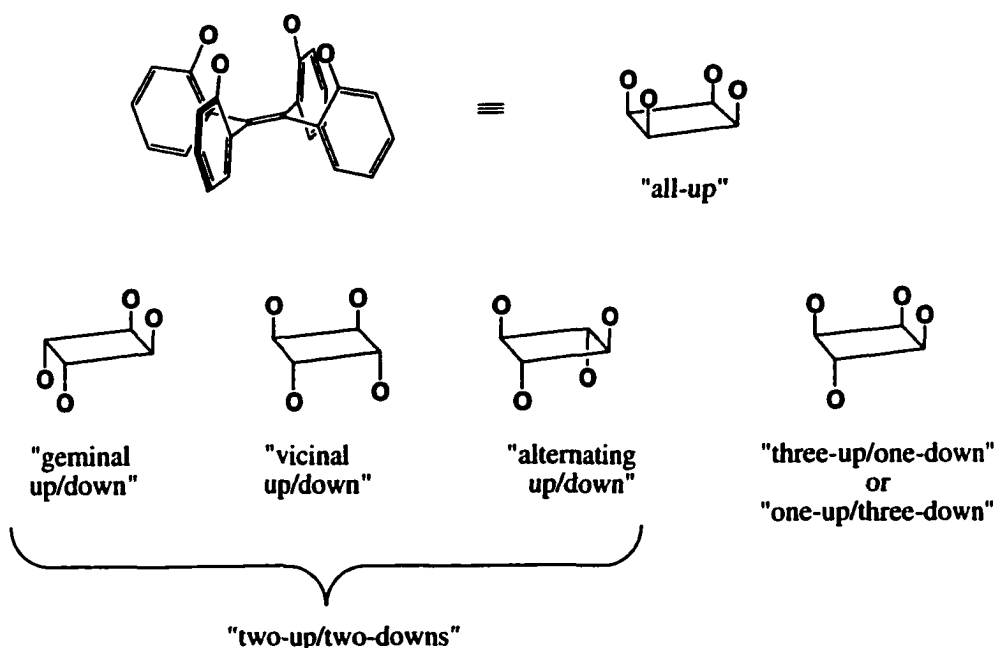


Figure 2.4. Different conformations of tetrakis(2-hydroxyphenyl)ethene.

Although the "all-up" case is further classified in calix[4]arene cases according to the tilting of the rings and the resultant overall symmetry, such further classification of the "all-up" case is not discussed for the tetrakis(2-hydroxyphenyl)ethene system in this thesis.

2.B. Direction of the Coordination Studies

The focus of the initial coordination studies of the new tetrakis(2-hydroxyphenyl)ethene system as a potential surface-model system was placed on the construction of structural models for heterogeneous catalytic species. Supported Ziegler-Natta olefin polymerization catalysts became the special target.

2.B.1. Supported Ziegler-Natta catalysts. Supported Ziegler-Natta catalysts, typically TiCl_4 supported on silica or MgCl_2 activated by alkylaluminum reagents, are still most widely used in industrial olefin polymerization.³ Many researchers have proposed structures for the active site(s) of these catalysts, but their heterogeneous nature has prevented their true structure from being determined.

It has been suggested that the catalytic centers of such systems consist of several metal atoms (typically Ti, Mg, and possibly Al) bridged with halide or other ligands, including some from solid supporting matrices. Such constructions are considered capable of forming stereoregulating catalytic centers to produce, for example, isotactic poly- α -olefins (Figure 2.5).⁴

In response to this proposal, the focus of the metal coordination studies using the modified tetrakis(2-hydroxyphenyl)ethene ligands was placed on the development of polymetallic systems by using the following three metals: Ti(IV), Mg(II), and Al(III). Hetero-polymetallic species, in which different metal atoms combine to form one discrete complex, were of special interest as potential catalytic site models for silica- and MgCl_2 -supported Ziegler-Natta catalysts.

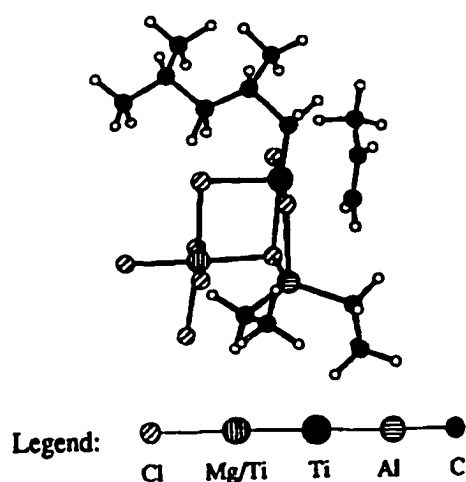


Figure 2.5. Active site of a Ziegler-Natta catalyst showing incoming propylene; the growing isotactic polypropylene chain; part of the support; and the residue of the AlEt_3 promoter (from reference 4).

2.B.2. Aryloxy-based ligands in olefin polymerization. Titanium or zirconium complexes of some sterically hindered chelating bisaryloxy ligands are known to be good olefin polymerization precatalysts. Articles about and patents for such complexes appeared from 1987-1998, describing aryloxy-based bidentate ligands as one possible post-metallocene support-ligand for α -olefin polymerization catalysts. Schaverien et al. in 1995 compared ethene polymerization activity by Group 4 complexes of various hindered bisaryloxides.⁵ The review by Gibson et al. in 1999 summarized the bisphenoxides as one successful post-metallocene system for Group 4 catalysts.⁶ **Figure 2.6** shows the representative examples of such bisaryloxy precatalyst complexes that appeared in Gibson's review.

Steric hindrance is important to protect the aryloxy oxygen atoms or the central cationic metal atom from unwanted aggregation or interactions with co-catalysts or other species. Extra donors seem useful for both steric protection and electronic tuning of the catalysts, as are incorporated into those in the second row of **Figure 2.6**. Still, these bisaryloxides do not provide a well-defined single site catalyst, as indicated by the broad polydispersity of the product polyethenes.⁵

The review by Gibson also cited a few half-metallocene complexes with a pendant alkoxide donor. The system reported by Marks et al. had a phenoxide donor that showed very high activity (**Figure 2.7**).

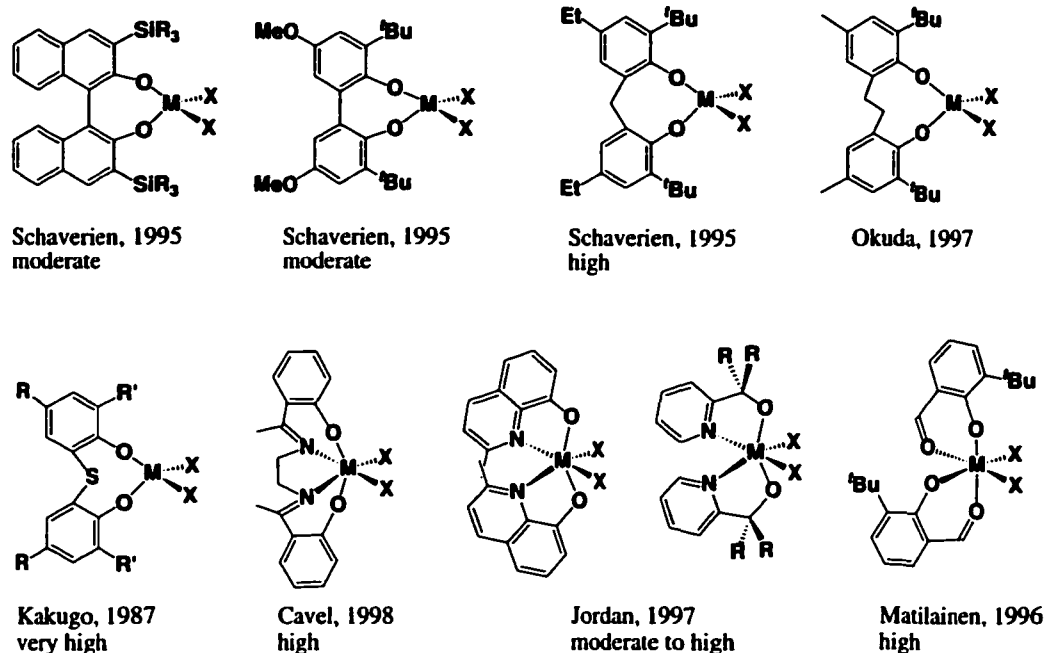


Figure 2.6. Metal complexes of sterically hindered bisaryloxides used for olefin polymerization (M = Ti and/or Zr). The main contributor, the publication year and the activity class assigned by Gibson are provided for each system.

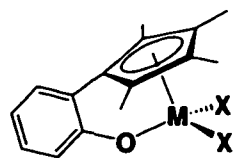


Figure 2.7. Half-metallocene with phenoxide pendant group by Marks (1997).

Such phenoxide-based systems are, however, not the most promising in the latest studies of post-metallocene olefin polymerization catalysts. The ligands for the "hottest" post-metallocene catalysts all contain nitrogen-based donors, especially imines.⁷ Many of the imine-based ligands are effective with late transition metals, many of which are neutral species. Some of these catalysts accomplish polymerization productivity higher than that of the metallocene catalysts. These systems also allow structural fine-tuning of the catalysts for molecular weight control and co-polymerization degree.

Nevertheless, in combination with the polymetallic "nucleation" and the potential surface-mimic template, these preorganized phenoxide ligands may still be interesting as polymerization catalyst templates. The modified tetrakis(2-hydroxyphenyl)ethene ligands do not exert much steric hindrance, but constructing polymetallic catalytic sites may replace the requirement for steric protection (the polymerization-related investigation of the metal derivatives will be discussed in Chapter 5).

2.C. General Approach

Our basic strategy for investigating the coordination chemistry of these ligand systems was first to prepare single-kind metal complexes of each ligand, with a special focus on the ligands **7** and **3E**, using metal reagents of Ti(IV), Mg(II), and Al(III). The basic connectivity patterns and chemical behavior were examined for each case. Construction of hetero- or mixed-polymetallic complexes was then attempted, starting with some of the single-kind metal complexes. The hetero-polymetallic combinations were also among the above-mentioned three metals. Chapter 3 discusses the coordination studies using tetrakis(2-hydroxy-3-propylphenyl)ethene **7**. Chapter 4 then covers the derivatives of *E*- and *Z*- bis(2-hydroxyphenyl)-bis(2-methoxyphenyl)ethene **3E** and **3Z**.

2.D. References and Notes

¹ Böhmer, V. *Angew. Chem. Int. Ed.* **1995**, *34*, 713-745.

² Verkerk, U. Ph. D. Dissertation, University of Alberta, 2001.

³ Tsutsui, T. *Organomet. News*, **1998**, 82-85.

⁴ Parshall, G. W.; Ittel, S. D. *Homogeneous Catalysis The Application and Chemistry of Catalysis by Soluble Transition Metal Complexes*, 2nd ed., John Wiley & Sons, Inc., New York; **1992**.

⁵ Van der Linden, A.; Schaverien, C. J.; Meijboom, N.; Christian, G.; Orpen, A. G. *J. Am. Chem. Soc.* **1995**, *117*, 3008-3021.

⁶ Britovsek, G. J. P.; Gibson, V. C.; Wass, D. F. *Angew. Chem. Int. Ed.* **1999**, *38*, 428-447 and references therein.

⁷ Reviews: (a) Ittel, S. D.; Johnson, L. K.; Brookhart, M. *Chem. Rev.* **2000**, *100*, 1169-1203; (b) Matsui, S.; Inoue, Y.; Fujita, T. *J. Synth. Org. Chem. Jpn.* **2001**, *59*, 232-240; and references within.

Chapter 3

Metal Complexes Derived from Tetrakis(2-hydroxy-3-propylphenyl)ethene: Structure, Spectroscopic Features and Chemical Behavior

Table of Contents

3.0. Introduction	58
3.1. Homo-polymetallic Complexes	61
3.1.1. Mg Complexes	61
3.1.1.A. MgX Complexes of 7	61
3.1.1.B. MgR Complexes of 7	64
3.1.1.C. Crystallographic Features of the Tri-Magnesium Complexes	66
3.1.1.D. Spectroscopic Features of the Tri-magnesium Complexes	71
3.1.2. Ti Complexes	77
3.1.2.A. Geminal Up/Down Complexes	77
3.1.2.B. Crystallographic Features of the Geminal Up/Down Ti Complexes	79
3.1.2.C. Spectroscopic Features of the Geminal Up/Down Ti Complexes	85
3.1.2.D. The Collapsed "Sandwich" Complex	94
3.1.2.E. Isomerization of "Geminal Up/Down" to "Vicinal Up/Down"	97
3.1.2.F. Dinuclear Cationic Complex from 35 ?	104
3.1.3. Al Complexes	109
3.1.3.A. Al Complexes Obtained in Non-Coordinating Medium	109
3.1.3.B. Chemical Behavior in THF Medium	113
3.1.3.C. Conclusion of the Aluminum Chemistry of Ligand 7	121
3.1.4. Na Complex	121
3.2. Hetero-polymetallic Complexes	124
3.2.1. Mg/Al Complexes	126
3.2.1.A. Addition of Et ₂ AlCl to 25	126
3.2.1.B. Addition of EtAlCl ₂ to 25	133

3.2.2. Mg/Ti Complex	134
3.2.3. Al/Ti Complex	136
3.2.4. Other Attempts to Prepare Hetero-polymetallic Complexes	139
3.3. Conclusion	139
3.4. Experimental	141
3.5. References and Notes	167

3.0. Introduction

This chapter describes the synthesis, structure, spectroscopic features, and chemical behavior of metal complexes derived from tetrakis(2-hydroxy-3-propylphenyl)ethene **7**. We focused on the creation of homo- and hetero-polymetallic complexes by using the metals Mg(II), Ti(IV) and/or Al(III) potentially relevant to the proposed catalytic-site structure of heterogeneous Ziegler-Natta catalysts (see Chapter 2).

Ligand **7** proved its potential to form various discrete polymetallic complexes. **Figure 3.1** provides a list of the structurally characterized complexes that appear in this chapter. All of the complexes depicted, except for those in parentheses, have been characterized by X-ray crystallography.

The introduction of the *ortho*-propyl groups on the parent ligand framework (**2**) obviously contributed to the development of various discrete and characterizable complexes. The formation of many discrete complexes results from the *ortho*-substituents' effect, reducing the possibility of random aggregation or "collapsing" (i.e., forming a "sandwich-type" complexes, which is a dead-end in the search for oxo-surface mimics) of the complexes. The improved solubility resulting from the *ortho*-alkylation also enabled sufficient spectroscopic characterization and an expanded investigation of the chemistry of the metal complexes.

Various coordination patterns were observed by using different metal elements. The coordination patterns are determined by the metal's oxidation number, the number of available coordination sites, and the number and the size of the ancillary ligands. Additional coordination patterns were observed for some of the mixed-metal systems.

Generally speaking, the phenolato-oxygen atoms often bridge between two metal atoms. This bridging nature of the oxygen atoms is the major contributor in the formation of rigid oxo-surface like structures in the metal derivatives. When the oxygen atoms are not used for bridging, the aryloxy groups functions pairwise to form geminal or vicinal up/down structures (as was observed in many Ti complexes). The metals are rather preorganizing the ligand backbone than the ligand is preorganizing the metals.

Hence, not all the metal elements lead to the formation of oxo-surface-like complexes of potential use for surface-model studies. However, even these metal atoms can still be placed on the "all-up" shaped ligand through the preparation of mixed-metal (hetero-polymetallic) systems. For example, both Ti/Mg and Ti/Al hetero-polymetallic complexes maintained the Ti atom on an oxo-surface-like platform of the ligand.

In this chapter, we first describe the homo-polymetallic complexes composed of Mg, Ti, Al, or Na atoms. The hetero-polymetallic systems of Mg/Al, Mg/Ti and Al/Ti combinations will follow.

Figure 3.1. List of characterized compounds in Chapter 3.

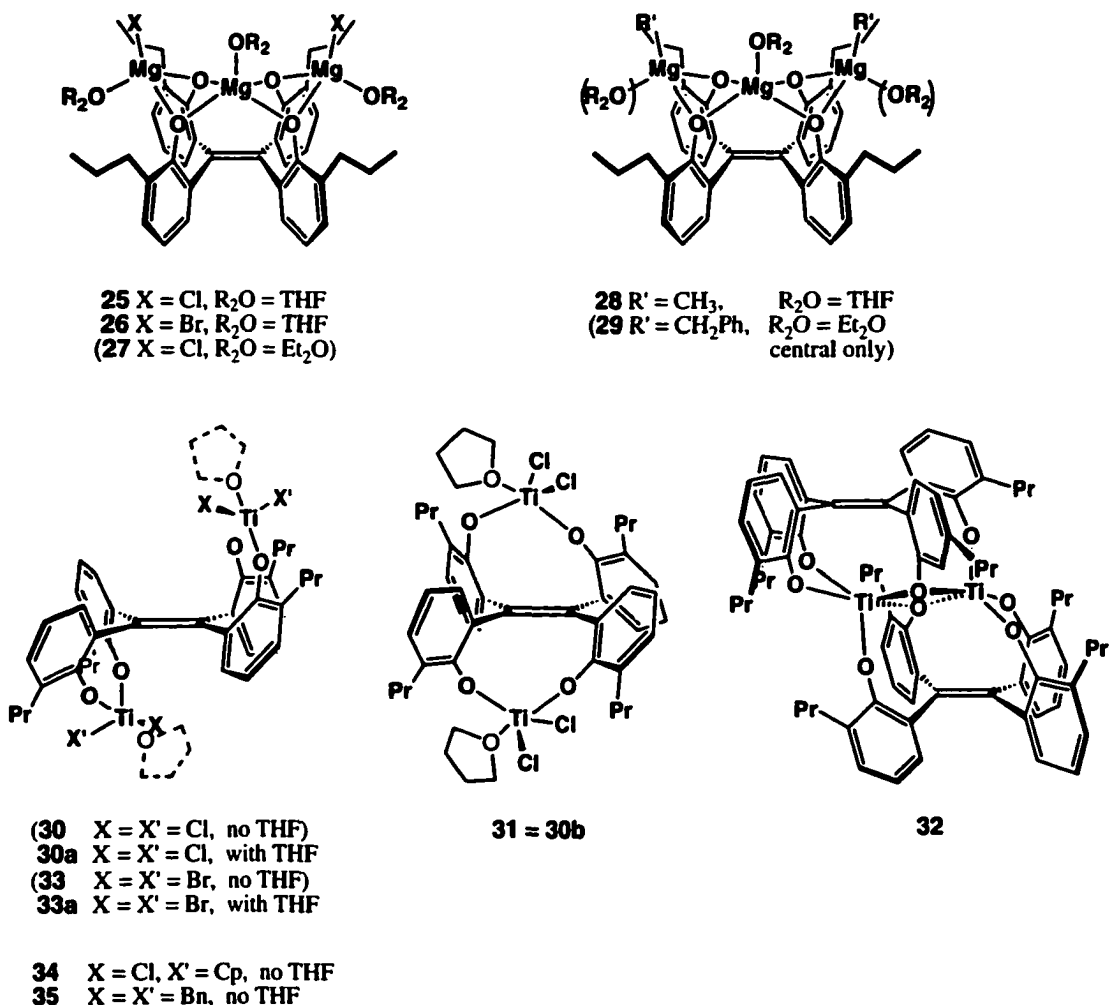
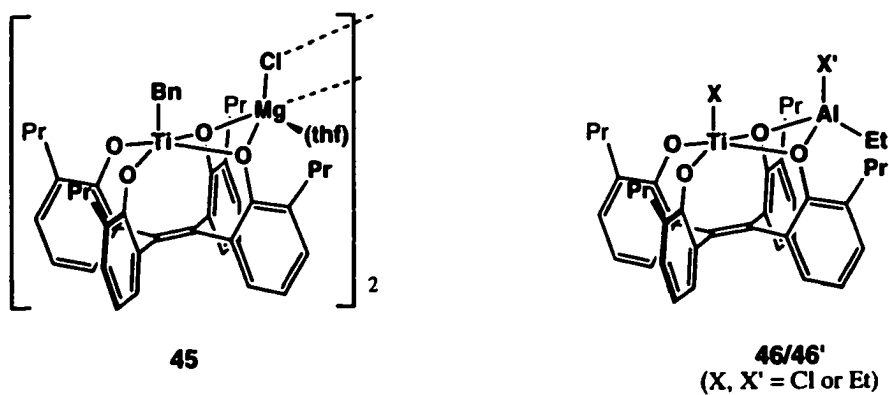
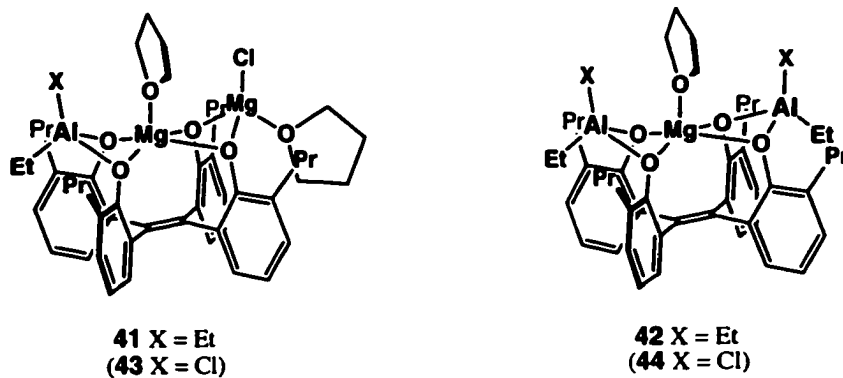
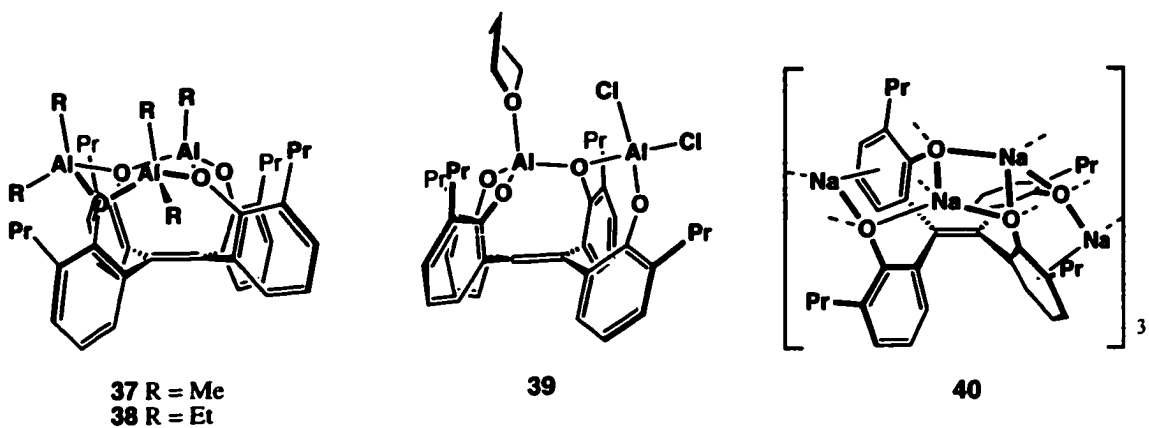


Figure 3.1. (continued)



3.1. Homo-polymetallic Complexes

Many discrete homo-polymetallic complexes were prepared from the *ortho*-propylated tetrakis(2-hydroxyphenyl)ethene **7** that contains Mg(II), Ti(IV) or Al(III) atoms. Ligand **7** exhibits various conformation and coordination patterns, which, in many cases, are unique to the metal. Varieties are also often observed within the same metal species: different ancillary groups on the metal atom sometimes result in different connectivity and reactivity in the product. For example, Et₃Al and Et₂AlCl apparently produce differently coordinated polynuclear aluminum complexes.

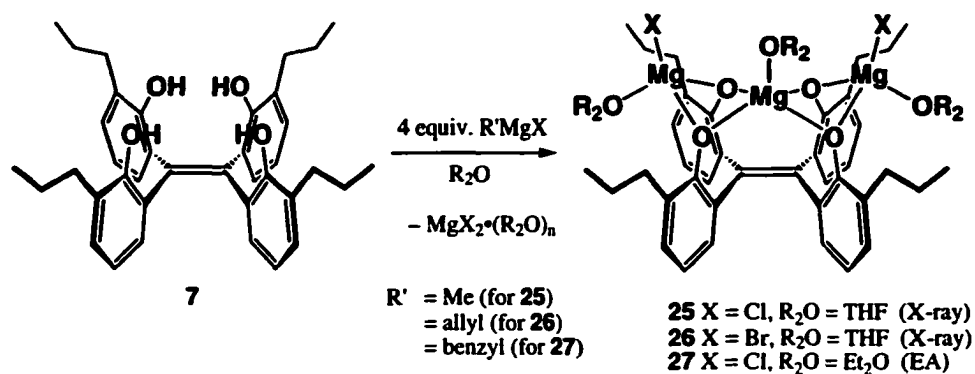
The general synthetic routes are the following: (1) addition of a metal halide reagent to ligand **7** with or without pre-deprotonation, and (2) addition of an alkyl metal reagent to ligand **7** for protonolysis. The reactions were all performed in a drybox and at room temperature.

For the Mg(II) complexes, route (2) was used exclusively with various Grignard reagents. For the Ti(IV) complexes, route (1) was taken for the reagents TiCl₄, TiBr₄ and CpTiCl₃, and route (2) was used for TiBn₄. For the Al(III) complexes, route (2) was exclusively used with alkyl aluminum reagents R₃Al (R = Me or Et), Et₂AlCl and EtAlCl₂. For a comparison, a low-valent, non-oxophilic Na(I) complex, often used as a deprotonated precursor for route (1) reactions, was also structurally examined.

3.1.1. Mg Complexes

3.1.1.A. MgX Complexes of **7**

Deprotonation of the tetraphenol **7** by four equivalents of a Grignard reagent gives a series of trinuclear magnesium complexes (**Scheme 3.1**). The Grignard reagent can be anything that produces a volatile and removable hydrocarbon R'H. R' was methyl for complex **25**, allyl for **26**, and benzyl for **27**.



Scheme 3.1. Trinuclear magnesium complexes from **7**.

Although the reaction conditions were all similar, the purification procedure varied for complexes **25** to **27**. In the case of the Mg(Cl) complex **25**, the product was less soluble in THF than the byproduct, MgCl₂(thf). This factor made it possible to crystallize the product from a hot THF solution of the 1 : 1 mixture of **25** and MgCl₂(thf). The mother liquor after the first crystallization, still containing some product but now with a higher concentration of MgCl₂·(thf)_n, was evaporated and triturated with toluene. In toluene, the solubility is higher for the product **25** than the inorganic byproduct, in contrast to THF. Upon repeating the crystallization of the toluene extract, 73% of the purified product was isolated in total. The amount of [MgCl₂(thf)] as a minor component increased in later crops of crystals.

In the case of the Mg(Br) complex **26**, the product was more soluble in THF than was MgBr₂·(thf)₂. The byproduct MgBr₂(thf) crystallized out in the first crystallization from THF. The crystals of the product **26** were obtained from the mother liquor from the first crystallization, after removal of THF and crystallization from toluene/hexanes. The crystals contained some amount of a byproduct that was most likely a dibenzylated species, analogous to complex **29** (*vide infra*). This overreaction is attributed to the use of excess Grignard reagent in this reaction. With exactly four equivalents of Grignard reagent, the reaction is expected to give **26** quantitatively.

The structures of the compounds **25** and **26** were determined by X-ray crystallography (see Section 3.1.1.C). Complex **27** gave an elemental analysis and ¹H/¹³C NMR spectroscopy consistent with the given structure.

The introduction of the *ortho*-propyl substituent at the 3-position of each aryl ring contributes to the formation of the discrete trinuclear structure. According to Verkerk, with no *ortho*-substituents (i.e., in the case of **2**), the same reaction conditions as that for the Mg(Cl) complex **25** gave a half-collapsed pentamagnesium structure (Figure 3.2).¹ The steric influence of the propyl groups in **7** must be effective enough to avoid such aggregation.

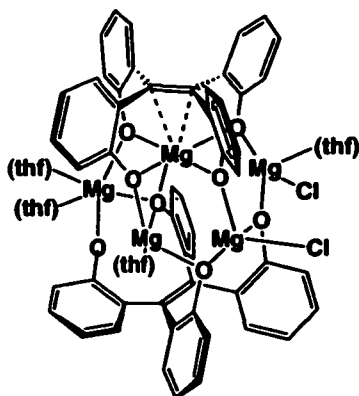


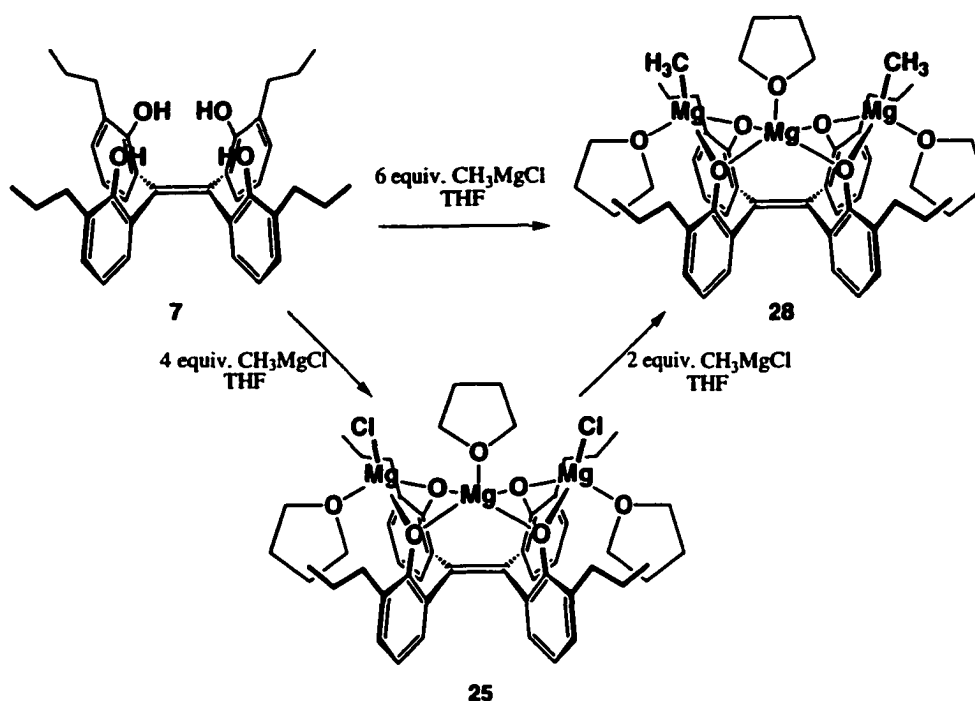
Figure 3.2. Verkerk's collapsed Mg salt of parent ligand **2**.

Although we initially expected the ligand to hold all four magnesium atoms on the "all-up" tetraaryloxy platform, one equivalent of MgCl₂•(thf) is excluded from the system to form the trinuclear structure. It seems that the steric effect of the propyl groups not only prevents the collapse of two molecules but also prevents the ligand from retaining all four Mg atoms.

The structure of the tri-magnesium complexes on the oxo-surface-like ligand platform was promising as a potential surface model and as a starting point to construct different surface models. Subsequently, we found that complex **25** is also an excellent starting material to produce hetero-polymetallic complexes (*vide infra*).

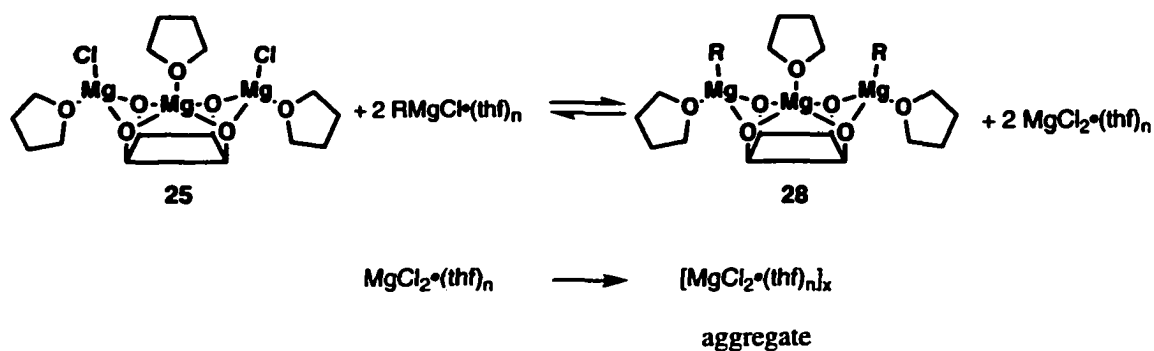
3.1.1.B. MgR Complexes of 7

In the presence of excess methyl magnesium chloride, the halides on the terminal magnesium atoms of **25** are replaced with methyl groups to give the $\text{Mg}(\text{CH}_3)$ complex **28** (Scheme 3.2). Complex **28** was obtained either by addition of six equivalents of methyl magnesium chloride to the protonated ligand **7**, or by adding two equivalents of methyl magnesium chloride to the preformed magnesium derivative **25**. Both routes cleanly gave the product **28**. This complex was also characterized crystallographically (Section 3.1.1.C).



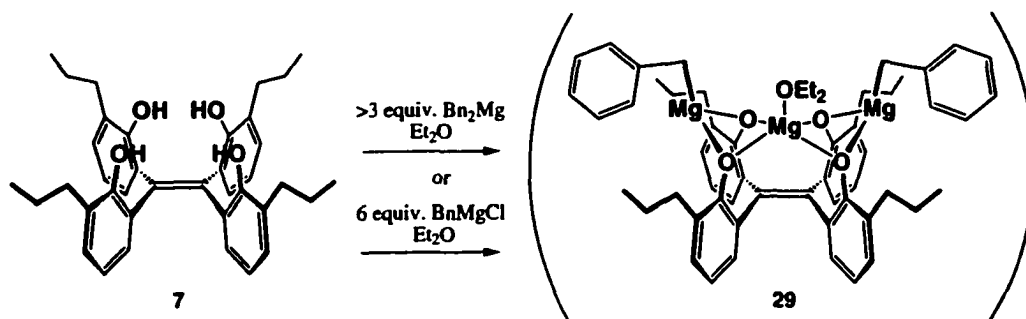
Scheme 3.2. Direct and indirect routes to the $\text{Mg}(\text{CH}_3)$ complex **28**.

As is known for Grignard reagents and other magnesium compounds in solution, the alkyl and halide anions exchange in equilibrium.² Apparently, the equilibrium was shifted to the direction of the formation of MgCl_2 and the dialkylated product **28**. The self-aggregation of MgCl_2 to precipitate, bringing itself out of the system, is probably the driving force for the completion of the reaction.



Scheme 3.3. Suggested equilibrium to bring **25** to **28**.

When six equivalents of benzyl Grignard reagents are added to ligand **7** in diethyl ether medium, dibenzyl compound **29** is obtained (**Scheme 3.4**). The ^1H NMR spectrum of the crystallized material in THF-d_8 indicates that **29** retains only one equivalent of coordinating ether. This one molecule of ether is probably at the central position. The large size of the terminal benzyl groups may prevent the coordination of ether molecules. It is not confirmed, however, whether or not the benzyl groups have a hapticity of greater than one.



Scheme 3.4. $\text{Mg}(\text{Bn})$ complex **29**.

3.1.1.C. Crystallographic Features of the Tri-Magnesium Complexes

The X-ray crystallographic determination of the solid-state structures of complexes **25**, **26** and **28** were obtained (see Appendices A-3 and A-4 for details). **Figure 3.3** shows the ORTEP plot of complex **25**. The data set was too weak to be refined to the adequate level, yet the basic connectivity of the atoms was provided.

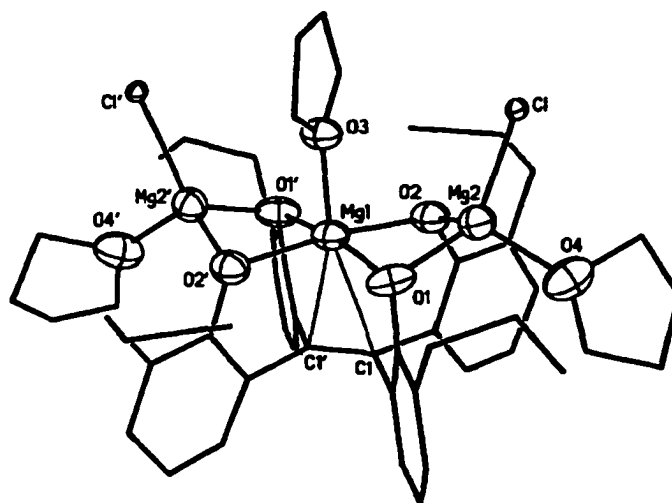


Figure 3.3. X-ray crystallographic structure of **25**.

Both complexes **26** and **28** gave good quality crystal structures (**Figure 3.4** and **3.5**). As shown in the ORTEP plots, the structures of these three complexes are very similar. Selected bond lengths and angles are provided in **Table 3.1**.

The conformation of the ligand framework in each complex is hardly affected by the different groups on the terminal Mg atoms. In these structures, the four aryl rings are nearly perpendicular to the olefin plane. The "ring torsion against olefin plane" in the table shows the relative angle of the C11-C16 ring and C21-C26 ring against the olefin double bond. These torsional angles are close to 90°. The deviation from perpendicularity is approximately 3° and 1°, respectively.

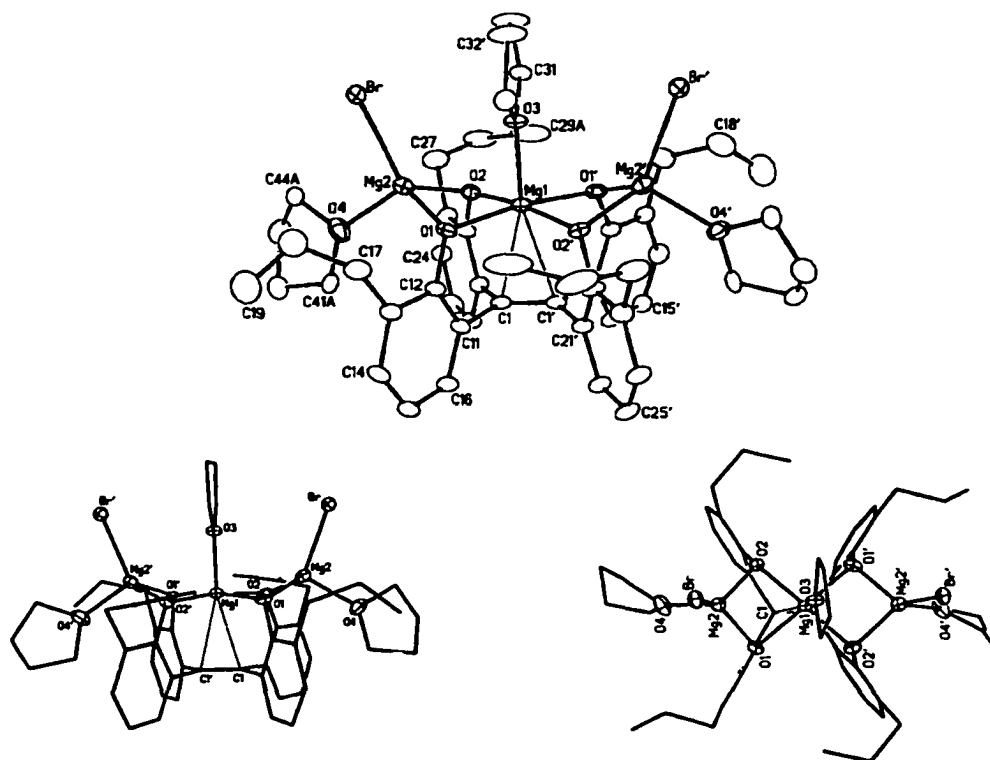


Figure 3.4. X-ray crystallographic structure of **26**. With side and top views.

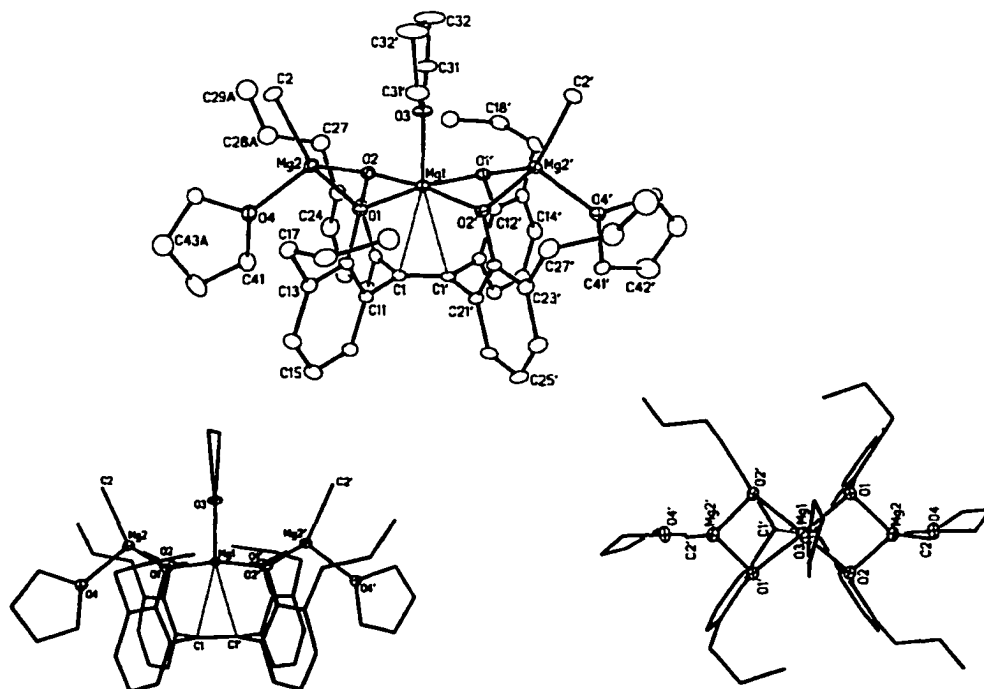


Figure 3.5. X-ray crystallographic structure of **28**. With side and top views.

Table 3.1. Selected bond distances and torsional angles of 26 and 28.

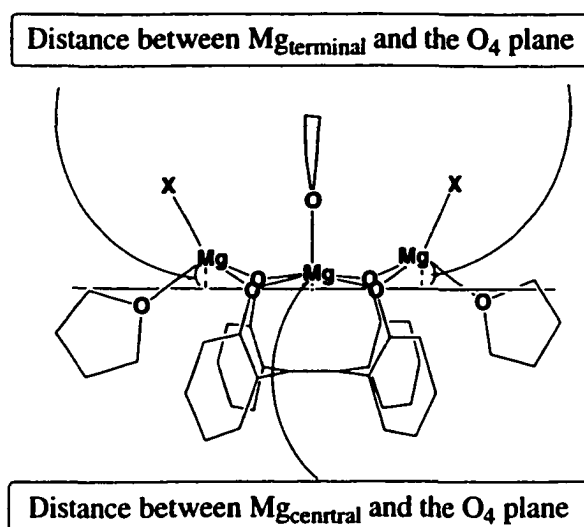
	Complex 26	Complex 28
R_1	0.0959	0.0569
wR_2	0.3405	0.1487
Mg1 – O3 ($O_{\text{thf-central}}$) (Å)	2.015(8)	2.015(3)
Mg2 – O4 ($O_{\text{thf-terminal}}$) (Å)	2.005(8)	2.053(2)
Mg1 – O1 (Å)	2.081(6)	2.0491(17)
Mg1 – O2 (Å)	2.047(6)	2.0719(16)
Mg2 – O1 (Å)	1.942(7)	2.0111(19)
Mg2 – O2 (Å)	1.996(7)	1.989(2)
Mg2 – X (Å)	(X = Br) 2.424(3)	(X = $\underline{\text{C}}\text{H}_3$) 2.112(3)
Mg1 – C1 (C_{olefin}) (Å)	2.581(8)	2.583(3)
C1 – C1' (Å)	1.355(19)	1.347(5)
Interatomic Angles (deg)		
O1 – Mg2 – X	(X = Br) 121.3(2)	(X = $\underline{\text{C}}\text{H}_3$) 126.85(11)
O2 – Mg2 – X	(X = Br) 122.8(2)	(X = $\underline{\text{C}}\text{H}_3$) 125.48(10)
O4 – Mg2 – X	(X = Br) 102.3(3)	(X = $\underline{\text{C}}\text{H}_3$) 103.63(11)
O1 – Mg2 – O2	85.9(3)	83.59(8)
O1 – Mg2 – O4	113.5(4)	106.61(8)
O2 – Mg2 – O4	111.2(3)	108.77(8)
Torsional Angles of Olefin Plane (deg)		
C11–C1–C1'–C11'	–175.1(10)	175.7(3)
C11–C1–C1'–C21'	0.3(5)	–0.72(16)
Ring Torsion Angles* (deg)		
C1'–C1–C11–C12	93.2(9)	91.1(2)
C1'–C1–C11–C16	–87.3(9)	–91.3(3)
C1'–C1–C21–C22	–90.4(9)	–94.1(2)
C1'–C1–C21–C26	91.3(9)	88.5(3)

*Ring torsion angle is defined as the torsional angle of CX1-CX2 bond or CX1-CX6 bond (in this case, X = 1 or 2) in an aromatic ring and the olefin C=C bond (in this case C1-C1'). The aryl ring CX1~CX6 is perpendicular to the olefin plane when [C=C]-CX1-CX2 and [C=C]-CX1-CX6 are $\pm 90^\circ$ ([C=C] is either C1-C1' or C1'-C1 in this case).

As is observed in the side views of **26** and **28**, the Mg atoms are located above the O₄ plane. The central Mg atom (Mg1) is only slightly above the reference plane, while the two crystallographically equivalent terminal Mg atoms (Mg2) are considerably more "uplifted." **Table 3.2** summarizes the distance of the central or terminal Mg atoms from the O₄ plane in **25**, **26** and **28**.

Table 3.2. Distance from the least-squares plane of O1-O2-O1'-O2' (Å).

	25	26	28
Mg _{central} (Mg1)	0.15	0.148	0.147
Mg _{terminal} (Mg2)	0.60	0.616	0.688



The terminal Mg atoms are more "uplifted" partly because of the van der Waals repulsion between the equatorial THF and the neighboring aryl rings. When the terminal groups are "AlEt₂" instead of "MgCl(thf)," as in the complexes **41** and **42** (*vide infra*, Section 3.2.1.A), the terminal aluminum atoms are significantly closer to the O₄ plane than the terminal magnesium atoms in complexes **25**, **26**, and **28**.

Still, in both all-magnesium and aluminum/magnesium complexes, the central magnesium atom is lower than the terminal metal atoms. The central Mg atom takes pseudo-octahedral geometry with the four phenolato-oxygen atoms at the equatorial positions. Although the central Mg atom is located slightly "away" from the olefin double

bond at the axial position, the interatomic distance between the central Mg and the olefin carbon atom (2.58 Å) suggests a weak interaction between them. Presumably, this interaction with the olefin π -electrons contributes to the "flattening" of the central Mg atom.

The pseudo-tetrahedral geometry of each terminal Mg atom is distorted in two ways: firstly, at the O1-Mg2-O2 angle (83 to 86°) due to constraints in the ligand structure; and secondly, at the X group (Br or CH₃), which is angled away from the central THF by van der Waals repulsion.

Disorder was noted for the terminal THF molecules. The terminal THF has two possible orientations: the illustrations in Figure 3.4 and 3.5 represent only one of them. Details can be found in Appendices A-3 and A-4.

There are very few reported examples of crystallographically characterized interactions between a Mg atom and π electrons of carbon-carbon double/triple bonds. Mach et al. reported the titanocene diacetylide "tweezer" complex shown below (Figure 3.6).³

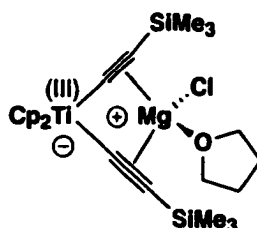


Figure 3.6. The "tweezer" complex by Mach et al.³

Bond distances: C-C = 1.22 Å, Mg-C_{inner} (average) = 2.27 Å, Mg-C_{outer} (average) = 2.46 Å.

The Mg-C_{olefin} distances found in **26** and **28** are longer than those in the Mach's complex, but they are still comparable to some of the known Mg-(μ -C) bond lengths in Cp-Mg or indenyl-Mg complexes cited in this reference.

3.1.1.D. Spectroscopic Features of the Tri-magnesium Complexes

The ^1H -NMR spectroscopic features of tri-magnesium complexes **25**, **26**, **27**, **28** and **29** are very similar to each other. When compared in the same deuterated solvent (THF-d_8), the ligand framework signals appear at very similar positions. The similarity in the solution phase suggests that the electronic effects of the different groups attached to the terminal Mg atoms is minimal on the ligand framework, as was observed for the solid state structure of these complexes.

For all five complexes, the four aryl rings (including the propyl substituent) are all equivalent. The α - CH_2 and β - CH_2 methylene protons in each propyl group are diastereotopic (i.e., the protons in each CH_2 group are non-equivalent) due to the rigid structure. This feature contrasts with that of the enantiomeric α - CH_2 and β - CH_2 methylene protons in the free phenolic ligand, in which each aryl ring is freely rotating.

As an example, the ^1H NMR spectrum of complex **25** in THF-d_8 is provided in **Figure 3.7-a**. The THF molecules that were coordinating to the complex are liberated upon dissolving in THF-d_8 , completely being replaced with the deuterated solvent. For comparison, the spectrum of the free phenolic ligand **7** is given as **Figure 3.7-b**. Complex **25**'s signal pattern in the aromatic region is quite similar to that of **7**, but slightly shifted upfield. This difference is obviously due to the ionization of the OH groups to aryloxides, which become more electron rich and provide more electron density to the ring.

The chemical shifts of the alkylmagnesium groups in **28** (CH_2Ph) and **29** (CH_3) are comparable to the shifts of corresponding alkyl groups of typical Grignard reagents, only slightly downfield-shifted. For example, the chemical shift of the " CH_2Ph " proton of **28** is 1.46 ppm while $\text{PhCH}_2\text{MgCl}(\text{ether})_n$ appears at 1.33 ppm in THF-d_8 , and the chemical shift of the " CH_3 " group in **29** is -1.53 ppm while $\text{CH}_3\text{MgCl}(\text{thf})_n$ appears at -1.70 ppm.^a

^a The chemical shifts of the Grignard reagents were obtained by removing volatiles from the solution of the corresponding commercial Grignard reagents, then redissolving in THF-d_8 .

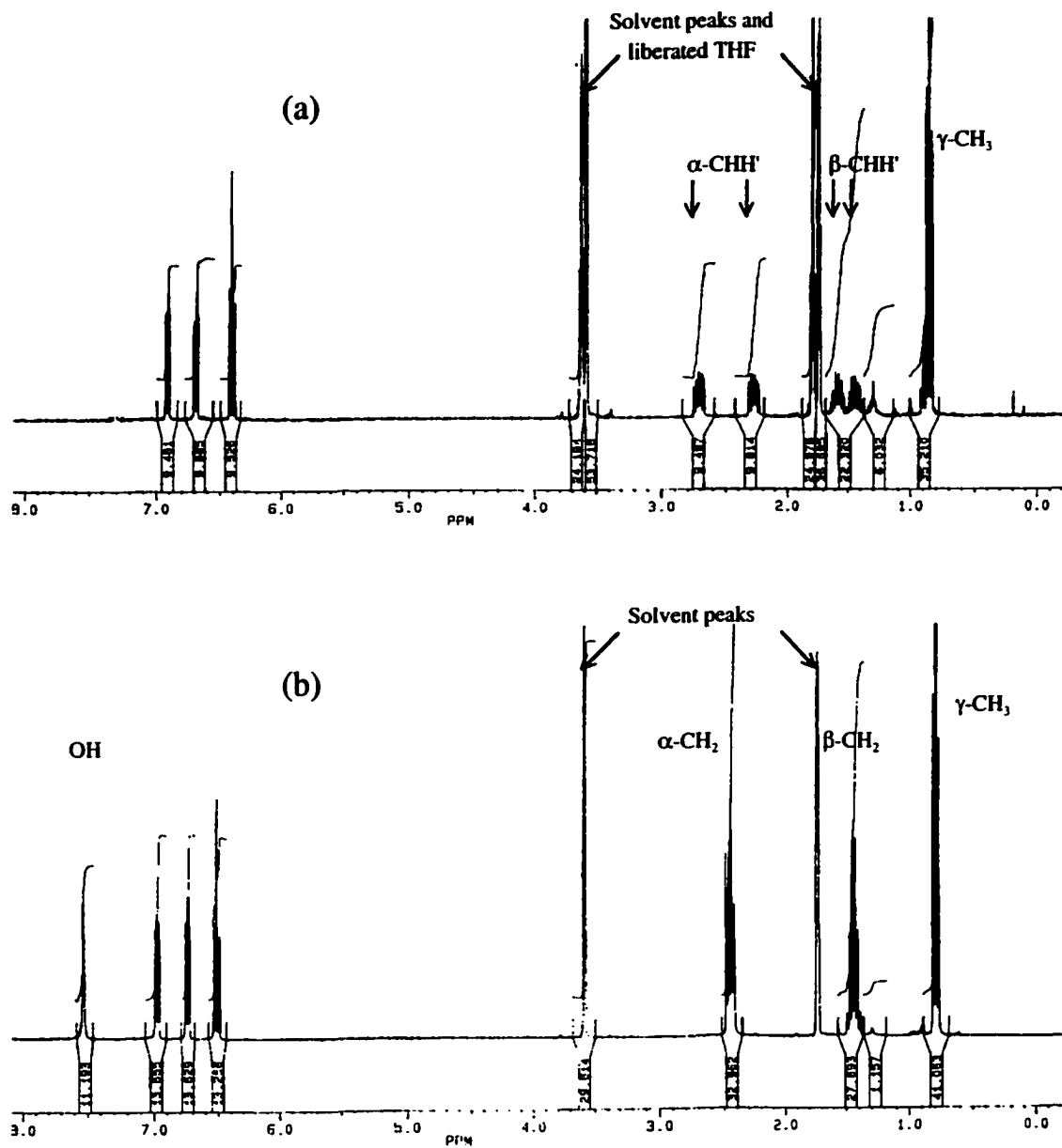


Figure 3.7. ¹H NMR spectra of (a) **25** and (b) **7** in THF-d₈.

In a non-coordinating medium, such as C_6D_6 , the coordinating THF molecules on **25** remain intact on the complex. The central and terminal THF molecules are clearly differentiated in the 1H NMR spectrum (Figure 3.8).

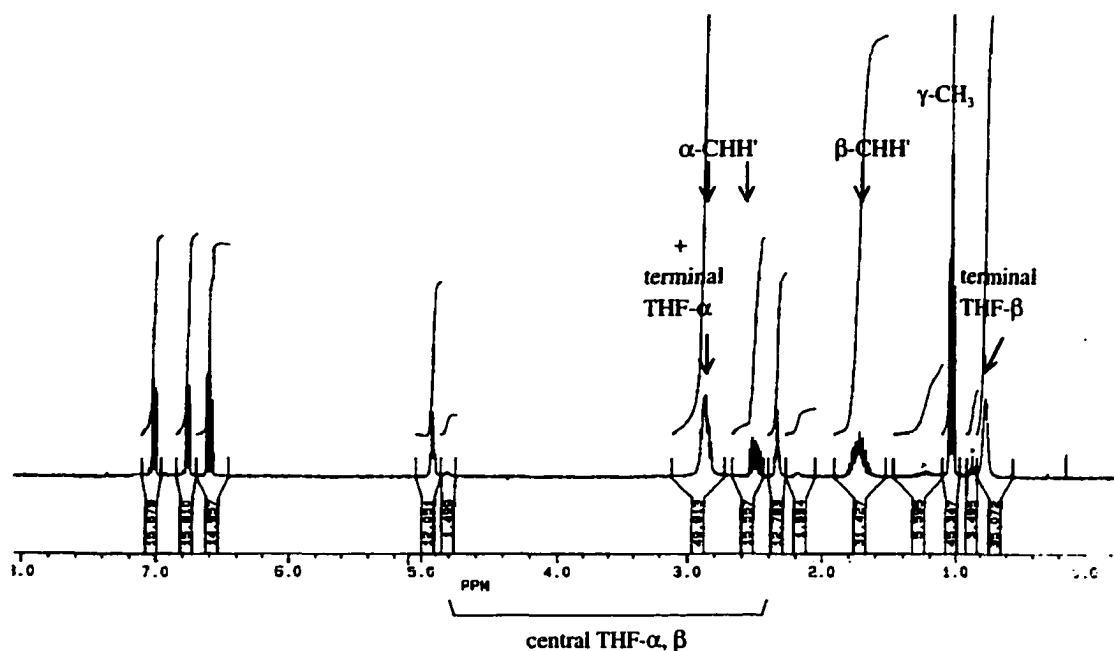


Figure 3.8. 1H NMR spectrum of **25** in C_6D_6 .

In C_6D_6 , the central-THF signals are sharp and highly downfield-shifted. The chemical shifts are 4.92 and 2.34 ppm, whereas free THF appears at 3.57 and 1.40 ppm. On the other hand, the terminal THF's are broad and upfield-shifted (2.86 and 0.76 ppm).

The upfield shift of the terminal THF ligands is best explained as an anisotropic effect exerted by the neighboring aromatic rings. Each terminal THF is placed in between a pair of geminal aromatic rings, in the shielding region of both rings. **Figure 3.9-a** provides some idea about the position of the terminal THF ligand from the top view. **Figures 3.9-b** and **-c** are different perspective ORTEP plots of complexes **26** and **28**, in which the positions of a terminal THF and one aryl ring are viewed.

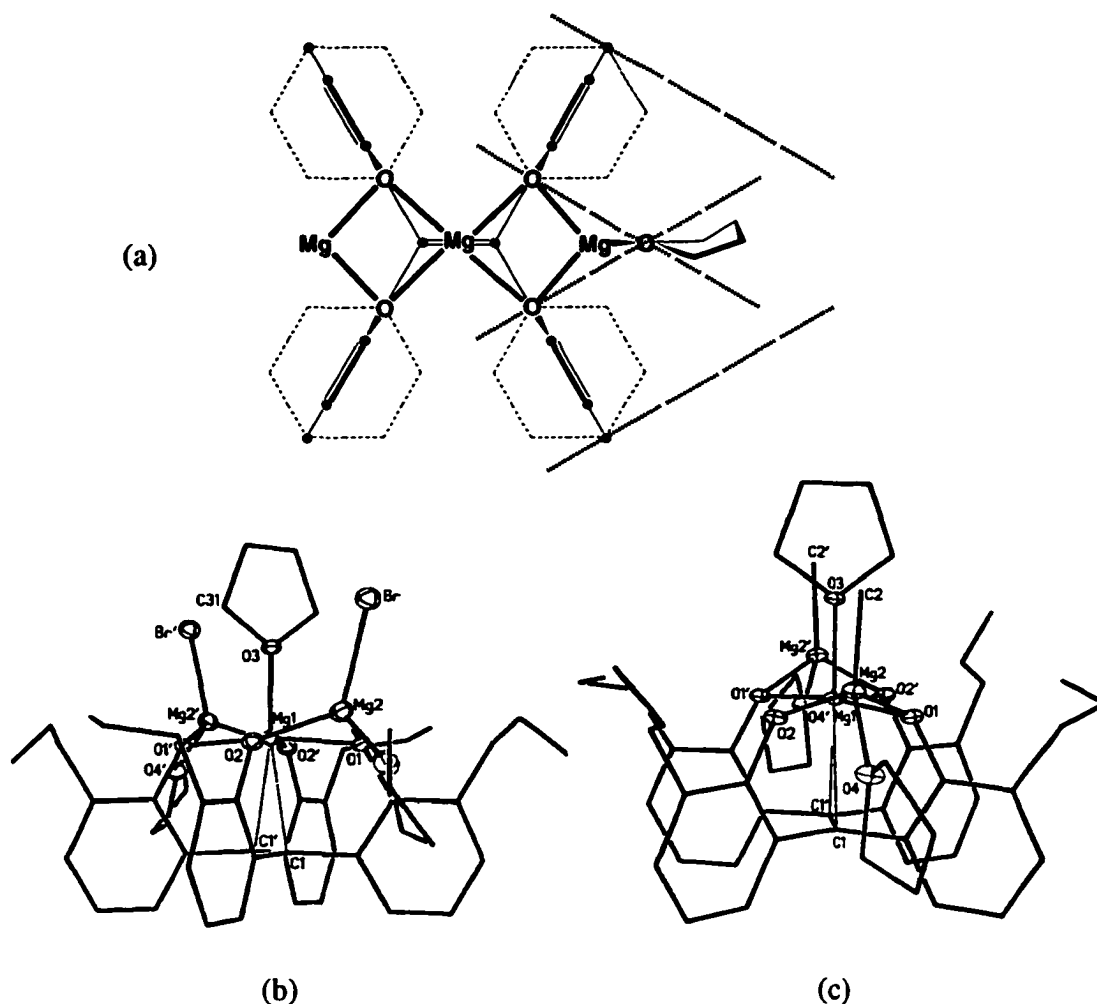


Figure 3.9. A terminal THF in the shielding region of neighboring aryl rings.
 (a) Top view with perpendicular aryl rings. Propyl groups are omitted for clarity. The thin dotted lines show the position of the aryl rings when they are coplanar with the double bond.
 (b) A terminal THF and one aryl ring in **26**'s ORTEP plot.
 (c) A terminal THF and one aryl ring in **28**'s ORTEP plot.

Why the central THF appears so downfield is less clear at a glance. The coordination to a Mg(II) ion by itself is definitely not sufficient to cause the signals to shift by ca. 1.3 ppm. For example, the THF molecules coordinated to the simple phenoxymagnesium chloride, $[\text{PhOMgCl}(\text{thf})_2]_2$, appear at 3.62 and 1.15 ppm in C_6D_6 , quite close to the chemical shifts of free THF.

The aryl rings are the only possible source of this deshielding effect. To examine the anisotropic effect of the aryl rings on the protons of the central THF molecule, the positions of the protons against each of the aryl rings were measured in the crystal structure of the Mg(Br) complex **26**, and compared with the theoretical calculation of shielding/deshielding effects of a benzene ring by Haigh and Mallion (Figure 3.10).⁴

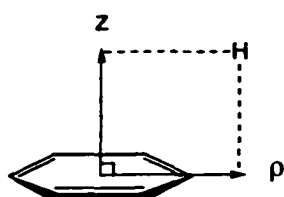


Figure 3.10. Isofield diagram of ring current effects by a benzene ring on a proton nucleus, provided by Haigh and Mallion.⁴ The unit of the axes is benzene radius (1.39 Å), and the unit of shifts in the chemical shift is ppm.

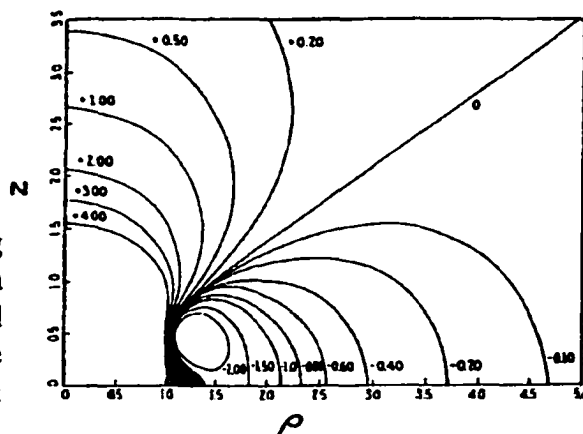


Figure 3.11-a summarizes the positions of α -protons (light dots) and β -protons (dark dots) against each aryl ring in the crystal structure of complex **26**. The two connected dots are of a pair protons on the same methylene group, pointing inward or outward. The α -protons of the central THF are located in the deshielding region of each of the four aryl rings, although the distance is 5.4 Å or longer to the centroid of each ring. According to the Haigh-Mallion diagram, the deshielding effect is still effective by ca. $\Delta 0.4$ ppm at 4 Å and $\Delta 0.2$ ppm at 5 Å along the ρ -axis. The additive effect of all the four rings may thus be noticeable. However, it is questionable if this effect alone can explain the shift of $\Delta 1.3$ ppm in this conformation.

If the central THF is positioned in a different way, the THF-protons accept the deshielding effect more efficiently. Presumably, the central THF is rotating in solution, while the crystal structure represents only the state in which it is placed orthogonal to the olefin double bond (**Figure 3.11-b**). If the central THF is placed along the olefin double bond axis, it brings the α -THF protons closer to the plane of the adjacent ring (**Figure 3.11-c**). If the contribution of the latter state is not small, a larger deshielding effect is expected for the central THF than that suggested by the crystal structure (**Figure 3.10-b**).

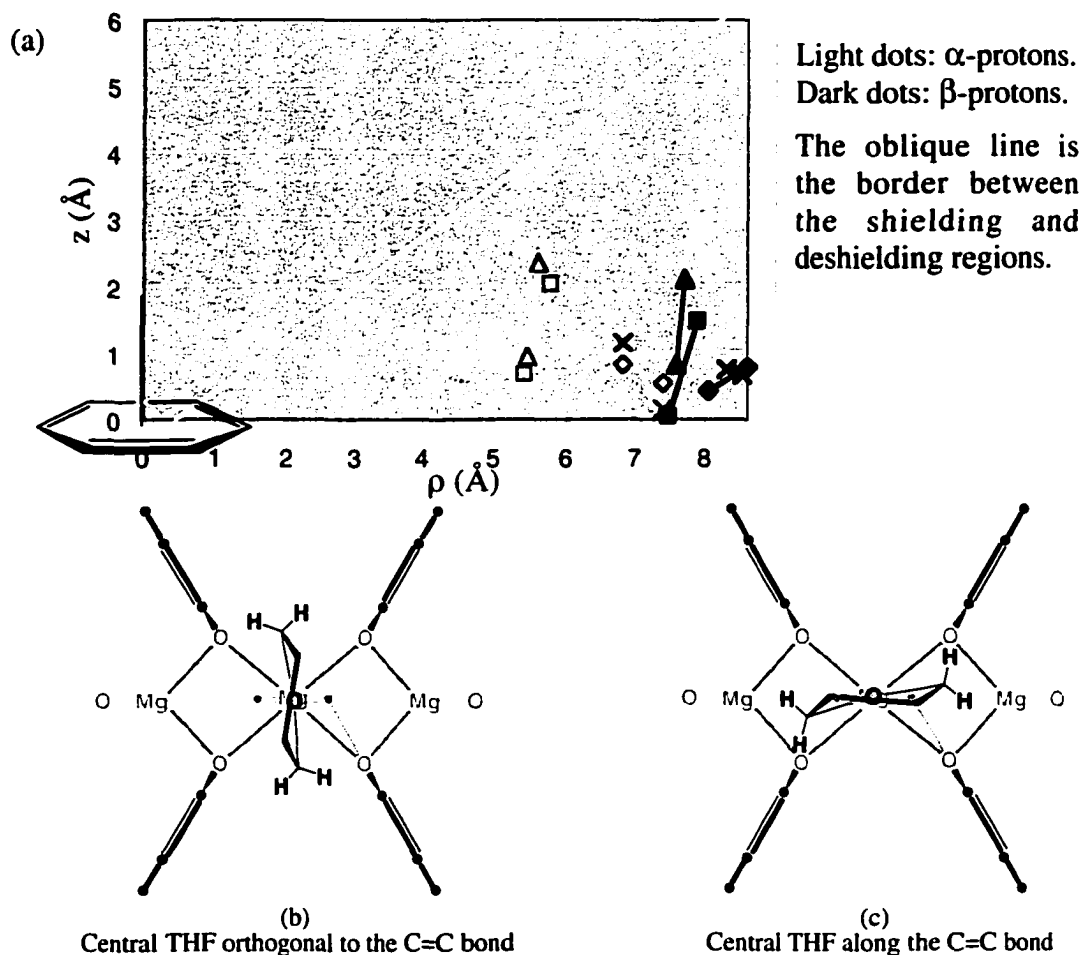


Figure 3.11.

- (a) Positions of the central THF protons against the ligand framework's aryl rings in the crystal structure of complex **26**.
- (b) Illustration of complex **26** from the top view, with the central THF oriented orthogonal to the olefin double bond of the ligand (as in the crystal state).
- (c) Illustration of complex **26** from the top view, with the central THF aligned parallel to the olefin double bond of the ligand.

The ^1H NMR spectrum of **25** in C_6D_6 shows additional differences between the central and terminal THF molecules. When excess free THF is present in C_6D_6 solution, only the terminal THF signals are averaged with free THF. The averaged signals of the free and terminal THF molecules appear as broad bands (both the α and β protons). The central THF signals remain unaffected in the presence of excess free THF.

3.1.2. Ti Complexes

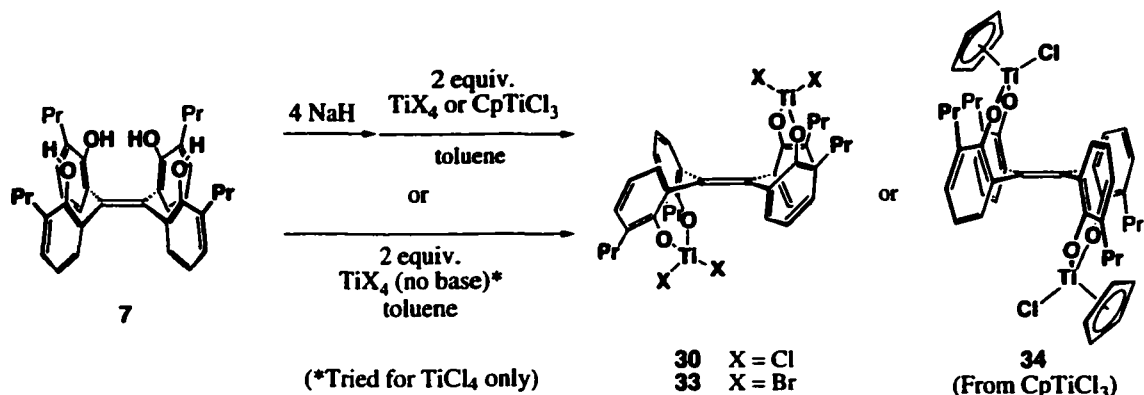
Most dinuclear titanium complexes of ligand **7** show a "two up/two down" ligand conformation, not an "all-up" oxo-surface-like structure. The "geminal up/down" complexes obtained from the reaction with titanium halides or alkyltitanium reagents are presented in the first three sections (3.1.2.A to 3.1.2.C), followed by a section about a 1 : 1 adduct of ligand **7** and TiCl_4 , the collapsed "sandwich-type" complex **32** (Section 3.1.2.D). Interestingly, the geminal up/down di- $\text{TiCl}_2(\text{thf})$ complex **30a** showed isomerization behavior to a vicinal up/down analogue **30b**: this chemical behavior will be discussed (Section 3.1.2.E). In the final section, the spectroscopic features of these titanium complexes will be discussed, with a focus on the significant effects caused by the tilting of aryl rings on the NMR chemical shifts (3.1.2.F).

3.1.2.A. Geminal Up/Down Complexes

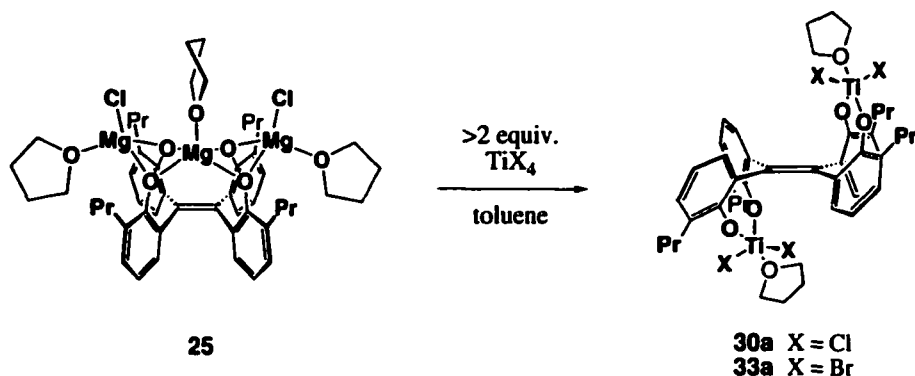
The reactions of ligand **7** with two equivalents of titanium halides TiCl_4 , TiBr_4 or CpTiCl_3 , after prior deprotonation, produced geminal up/down dinuclear complexes **30**, **33**, and **34**, respectively (Scheme 3.5). Although the reactions were fairly clean, minor impurities were always found in the crude products. The reaction with TiCl_4 without prior deprotonation also resulted in producing a reasonably clean product (the no-base reaction was attempted for TiCl_4 only).

When two equivalents of TiCl_4 or TiBr_4 were added to the trinuclear magnesium complex **25**, similar geminal up/down complexes **30a** and **33a** were produced (Scheme 3.6). The only difference from **30** and **33** was that each Ti atom is coordinated by one THF molecule in complexes **30a** and **33a**, as was confirmed by ^1H NMR spectroscopy and X-ray crystallography (*vide infra*). The coordinating THF molecules came from the starting material. Use of the $\text{Mg}(\text{Br})(\text{thf})$ complex **26**, instead of the above-mentioned $\text{Mg}(\text{Cl})(\text{thf})$ complex **25**, resulted in the same product, as was established for complex **30a**.

The initial intention for performing the reactions between the magnesium salts **25** or **26** and TiCl_4 was to obtain Mg/Ti hetero-polymetallic species. However, no magnesium remained in the product.



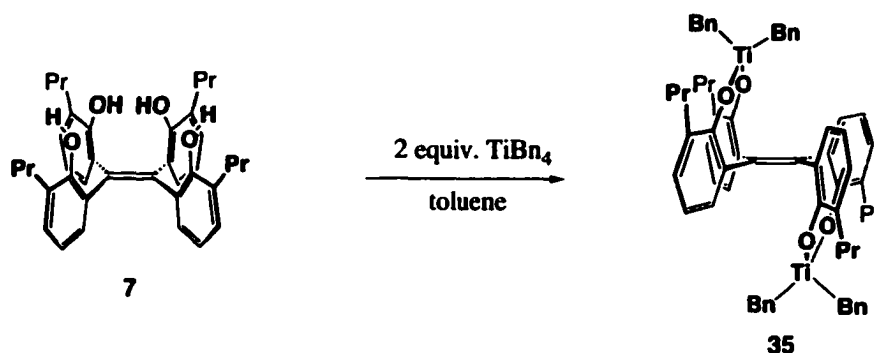
Scheme 3.5. Geminal up/down titanium halide complexes.



Scheme 3.6. Geminal up/down titanium halide complexes, THF-solvated.

The reactions between the magnesium complex **25** and the titanium halides were also fairly clean, but the products were often accompanied by minor unidentified byproducts. A longer reaction time seemed to increase the impurities. The CpTiCl complex **34** was difficult to obtain impurity-free in the bulk, although X-ray quality crystals were produced by careful crystallization.

The alkane elimination reaction between ligand **7** and two equivalents of TiBn_4 also resulted in a geminal up/down complex (**35**, **Scheme 3.7**). The reaction was clean; crystallization was relatively easy and produced pure material in good yield.



Scheme 3.7. Geminal up/down benzyltitanium complex 35.

In the formation of these dinuclear titanium complexes, the *ortho*-propylation in ligand **7** again contributes to the formation of a non-aggregated discrete products. The parent tetrakis(2-hydroxyphenyl)ethene **2**, with no alkyl substituents, does not give analyzable products under similar conditions, probably due to the poor solubility of the starting material, and possibly, the aggregation of the Ti adduct into oligomeric clusters.

3.1.2.B. Crystallographic Features of the Geminal Up/Down Ti Complexes

The structures of the complexes **30a**, **33a**, **34** and **35** were confirmed by X-ray crystallography.

The thf-solvated chloro complex **30a** and the bromo analogue **33a** show quite similar structural features (**Figures 3.12** and **3.13**). Each Ti atom assumes trigonal bipyramidal geometry in both cases, with the THF molecule and one aryloxy group at axial positions. The olefin plane of the ligand framework is slightly distorted. The aryl rings are tilted from the position perpendicular to the C=C olefin plane (i.e., $\pm 90^\circ$) by 10° - 30° (**30a**) or 7° - 35° (**33a**), as shown by the ring torsion angles. The direction of the tilting is helical: the top edge of one ring is over the bottom edge of the neighboring ring.

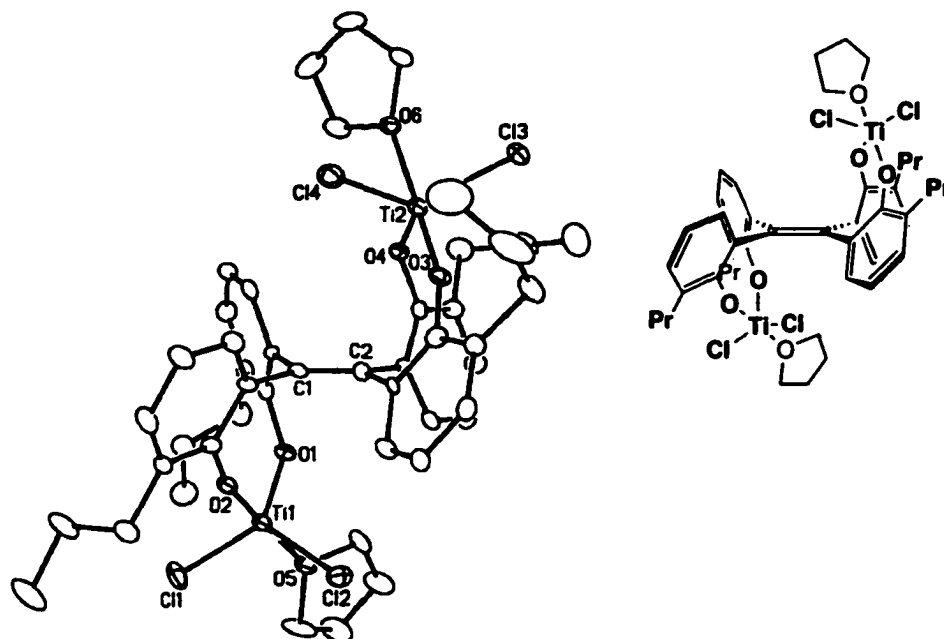


Figure 3.12. X-ray crystallographic structure of **30a**. The label for the aromatic carbon attached to OX is CX2.

Bond lengths (Å): C1-C2 = 1.322(8), Ti1-Cl1 = 2.255(2), Ti1-O1 = 1.800(4), Ti1-O2 = 1.763(4), Ti1-O51 = 2.169(4). Interatomic angles (deg): O1-Ti1-O2 = 96.66(18), O3-Ti2-O4 = 97.52(19). Torsional angles about C1-C2 bond (deg): C11-C1-C2-C31 = 175.0(5), C11-C1-C2-C41 = -10.5(9), C21-C1-C2-C31 = -1.4(10), C21-C1-C2-C41 = 173.1(5). Ring torsion angles (deg): C2-C1-C11-C12 = 82.0(8), C2-C1-C11-C16 = -101.1(7), C2-C1-C21-C22 = -109.6(7), C2-C1-C21-C26 = 70.3(9), C1-C2-C31-C32 = -120.1(7), C1-C2-C31-C36 = 61.9(10), C1-C2-C41-C42 = 78.2(9), C1-C2-C41-C46 = -101.8(8).

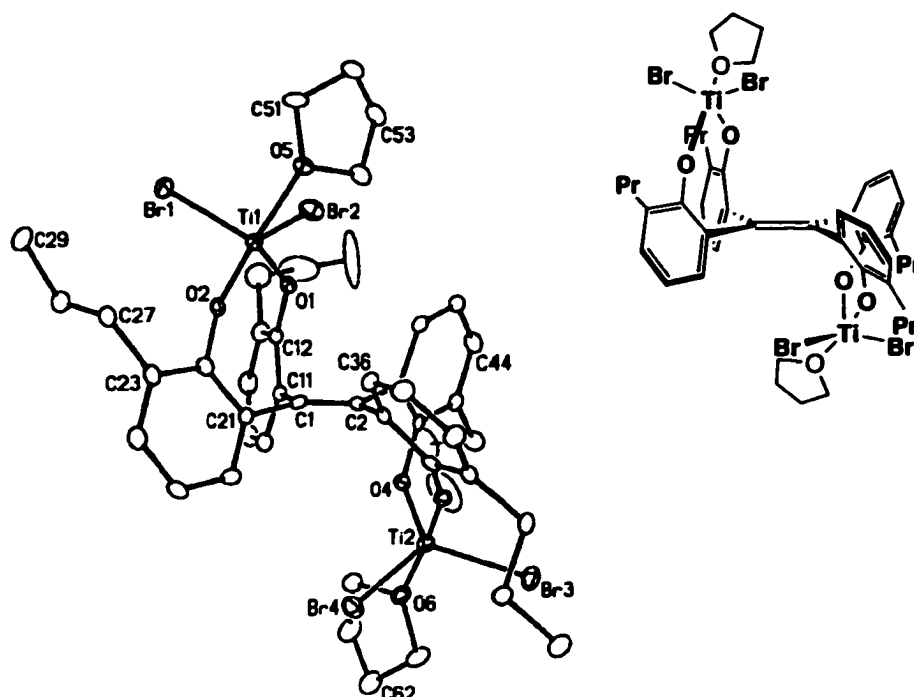


Figure 3.13. X-ray crystallographic structure of **33a**.

Bond lengths (Å): C1-C2 = 1.338(7), Br1-Ti1 = 2.4041(11), Ti1-O1 = 1.794(3), Ti1-O2 = 1.765(4), Ti-O5 = 2.171(4). Interatomic angles (deg): O1-Ti1-O2 = 97.11(16), O3-Ti2-O4 = 95.22(16). Torsional angles about C1-C2 bond (deg): C11-C1-C2-C31 = -177.4(5), C11-C1-C2-C41 = 10.9(7), C21-C1-C2-C31 = -3.9(8), C21-C1-C2-C41 = -175.6(5). Ring torsion angles (deg): C2-C1-C11-C12 = -82.7(6), C2-C1-C11-C16 = 98.9(6), C2-C1-C21-C22 = 111.7(6), C2-C1-C21-C26 = -71.2(8), C1-C2-C31-C32 = 128.8(6), C1-C2-C31-C36 = -53.8(8), C1-C2-C41-C42 = -83.7(6), C1-C2-C41-C46 = 96.3(6).

The structures of the THF-free products **30** and **33** are considered to be analogous to **30a** and **33a**, based on their similar ^1H NMR spectroscopic features (*vide infra*). Crystallization of the non-THF complexes **30** and **33** was difficult due to solubility problems. In contrast to the THF-solvated versions, the non-solvated analogues had "inconsistent" solubility in toluene and other non-coordinating hydrocarbon solvents. After triturating with toluene, the residual solid after removal of toluene from the triturate

does not become completely soluble again. Removing the volatiles or even concentrating the toluene solution accelerates the aggregation or disproportionation of the complexes to form less soluble species, a process that may be irreversible. The coordination by THF in **30a** apparently helps to prevent such aggregation.

In contrast to the tilting aryl rings in **30a** or **33a**, the aryl rings in the di-CpTiCl complex **34** and the di-TiBn₂ complex **35** are nearly perpendicular (Figures 3.14 and 3.15). The ring tilting angles are 5°-8° (**34**) and 6°-10° (**35**) from perpendicularity, which are significantly smaller than those of **30a** and **33a**. The major difference between the former two complexes and the latter two complexes is in the coordination geometry of each Ti atom, trigonal bipyramidal for the former, and tetrahedral (**35**) or pseudo-tetrahedral (**34**) for the latter. The olefin distortion degree is also small for **34** and **35**. Probably the tetrahedral geometry of Ti atoms on the geminal up/down configuration is more "fitting" to the ligand framework, without requiring as much distortion or ring-tilting as the trigonal bipyramidal cases require.

In the crystal structure of the benzyltitanium complex **35**, the orientation of each pair of benzyl groups (on each titanium atom) provides a good example of a so-called "tilted (or distorted) T-shaped" aromatic-aromatic interaction, the most favorable interaction of the benzene dimer, according to Jorgensen et al.⁵ Although no detailed distances and angles are provided in the reference, the ring center-ring center distance of 4.99 Å and the relative positions of the two interacting benzene rings illustrated in the reference (Figure 3.16) are remarkably similar to the proximal benzyl/benzyl relationship in the structure of **35**. The centroid-centroid distance in **35** is 4.95 Å, quite close to the Jorgensen's "tilted T" relationship. The perspective view of **35** in Figure 3.15-b gives a good idea of the orientation of these two phenyl rings.

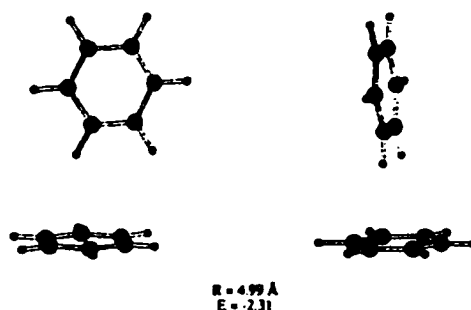


Figure 3.16. "Tilted or distorted T-structure" of benzene dimer, by Jorgensen et al. R is the ring center-ring center distance and E is the interaction energy in kcal/mol.

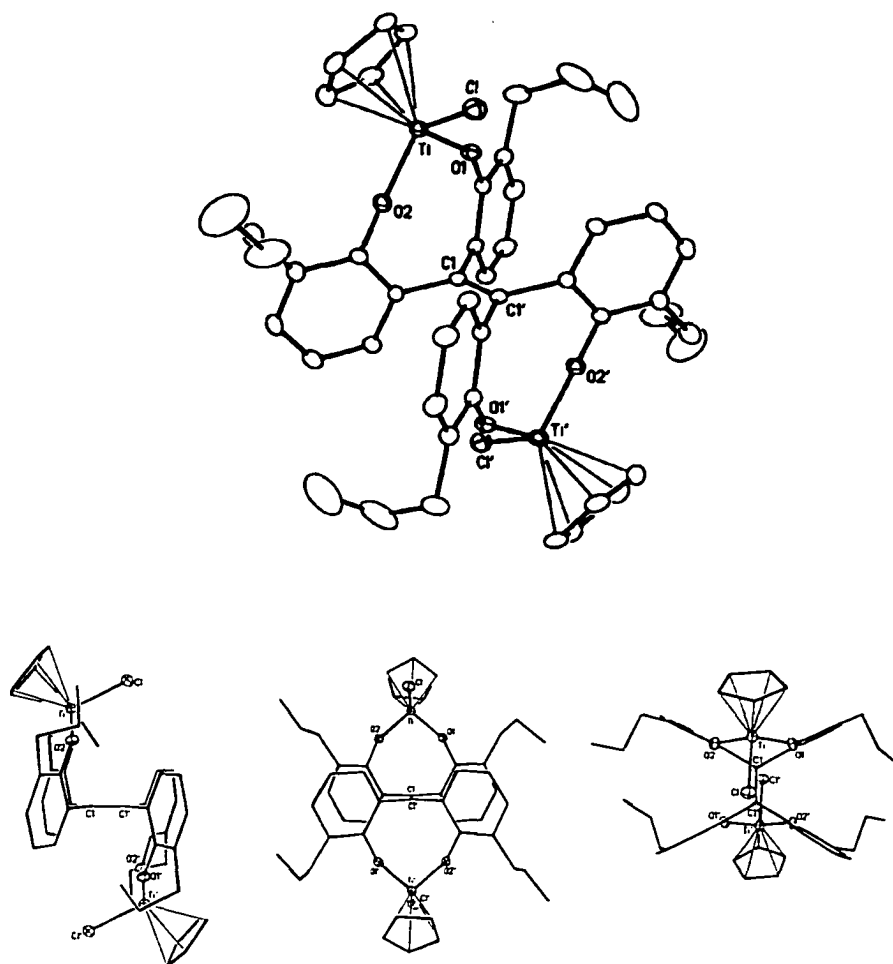
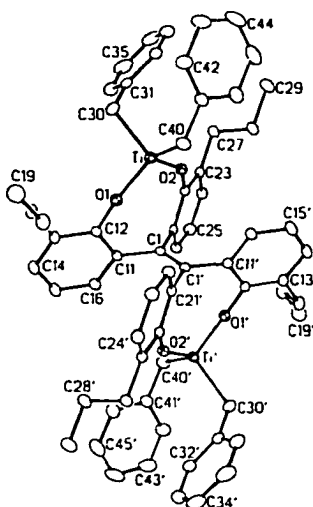
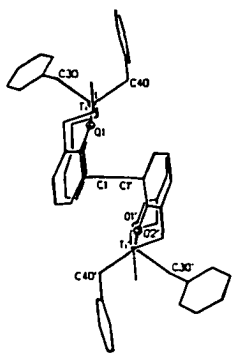


Figure 3.14. X-ray crystallographic structure of **34** with different angle views.

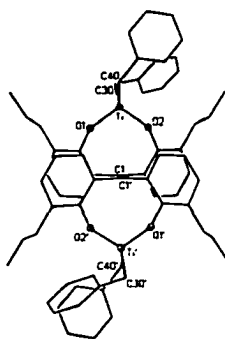
Bond lengths (Å): Cl-Cl' = 1.344(8), Ti-Cl = 2.2903(14), Ti-O1 = 1.804(3), Ti-C31 = 2.402(4), Ti-C32 = 2.389(4), Ti-C33 = 2.354(5), Ti-C34 = 2.330(5), Ti-C35 = 2.351(4), Ti-C36 = 1.361(4). Interatomic angles (deg): O1-Ti-O2 = 101.68(12), O1-Ti-Cl = 104.73(10), O2-Ti-Cl = 102.41(10), Ti-O1-C12 = 149.2(3), Ti-O2-C22 = 148.6(2). Torsional angles about C1-C2 bond (deg): C11-C1-Cl'-C21' = 2.1(7); C11-C1-Cl'-C21' = 0° by definition. Ring torsion angles (deg): Cl'-C1-C11-C12 = -85.2(5), Cl'-C1-C11-C16 = 92.3(6), Cl'-C1-C21-C22 = 84.1(6), Cl'-C1-C21-C26 = -93.9(5).



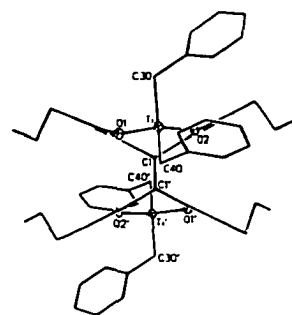
(a)↑



(b)



(c)



(d)

Figure 3.15. X-ray crystallographic structure of **35** with different angle views.

Bond lengths (Å): C1-C1' = 1.341(5), Ti-O1 = 1.7917(18), Ti-O2 = 1.7923(17), Ti-C30 = 2.086(3), Ti-C40 = 2.103(3). **Interatomic angles (deg):** O1-Ti-O2 = 112.40(8), O1-Ti-C30 = 104.25(10), O1-Ti-C40 = 107.56(10), O2-Ti-C30 = 109.93(10), O2-Ti-C40 = 112.17(10), C30-Ti-C40 = 110.22(12), Ti-O1-C12 = 143.88(16), Ti-O2-C22 = 145.33. **Torsional angles about C1-C2 bond (deg):** C11-C1-C1'-C21' = 0.0(5), C11-C1-C1'-C21' = 0° by definition. **Ring torsion angles (deg):** C1'-C1-C11-C12 = 77.9(4), C1'-C1-C11-C16 = 99.5(3), C1'-C1-C21-C22 = 80.6(4), C1'-C1-C21-C26 = 96.2(3).

3.1.2.C. Spectroscopic Features of the Geminal Up/Down Ti Complexes

i) Di-(TiX₂) Complexes. Complexes **30a** and **33a**, the geminal up/down di-TiCl₂(thf) and di-TiBr₂(thf) complexes, showed very similar ¹H NMR spectra. The spectra of the non-THF solvated analogues **30** and **33** were also quite analogous.

Figure 3.17 presents the ¹H-NMR spectrum of **30a** in C₆D₆ at 25 °C as an example. The four aryl rings are all equivalent, indicating that the helical ring tilting observed in the X-ray structure is not retained in solution phase at room temperature. Helical ring tilting in both directions may co-exist, but each must be alternating rapidly in solution (**Scheme 3.8**). The basic geminal up/down structure remains unchanged, for the α- and β-methylene groups of the propyl chains show diastereotopic features (i.e., splitting), indicating the rigidity of the structure.

The characteristic feature of the spectrum is that one aromatic proton signal is highly downfield-shifted. This double doublet (dd) signal appears at 7.88 ppm for **30a**. This downfield shift is remarkable compared to that of the tri-magnesium complexes **25-29**: the most downfield signal of **25**, for example, is 7.01 ppm (**Figure 3.8**). This downfield dd is assigned to the H-6 proton of each aryl ring because this position is anisotropically most influenced by the ring rotation or tilting.

Because a similar kind of highly downfield dd signal is commonly observed in many (but not all) "up/down" metal complexes, the proximity of an aromatic proton to the metal atoms was first suspected as the source of the deshielding effect. With geminal or vicinal "up/down" structures, H-6, the aromatic protons at the 6-position (H16, H26, H36 and H46: see **Figure 3.18**) are brought spatially close to the metal coordination site on the opposite side. Note that in the magnesium complexes **25-29**, no aromatic proton is near the coordination site.

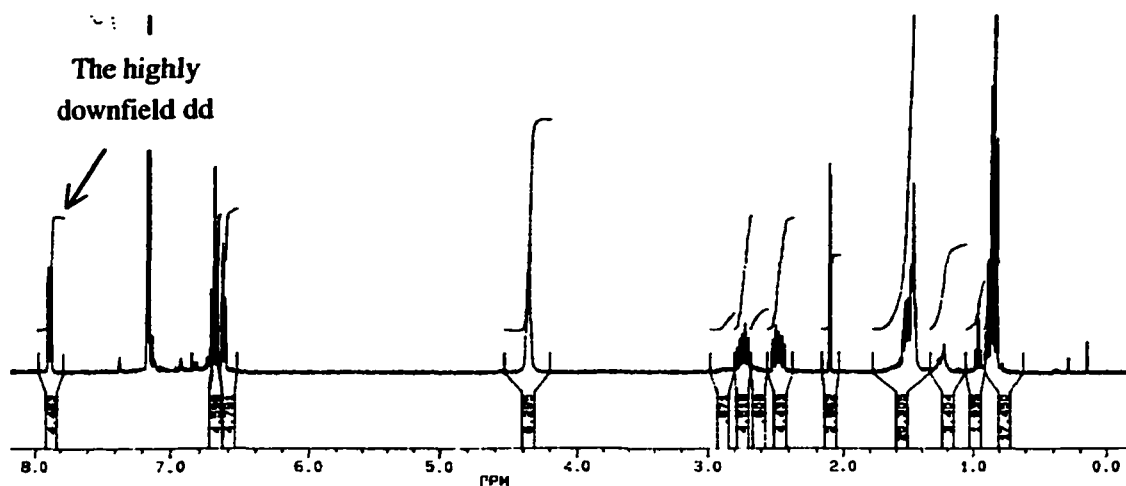
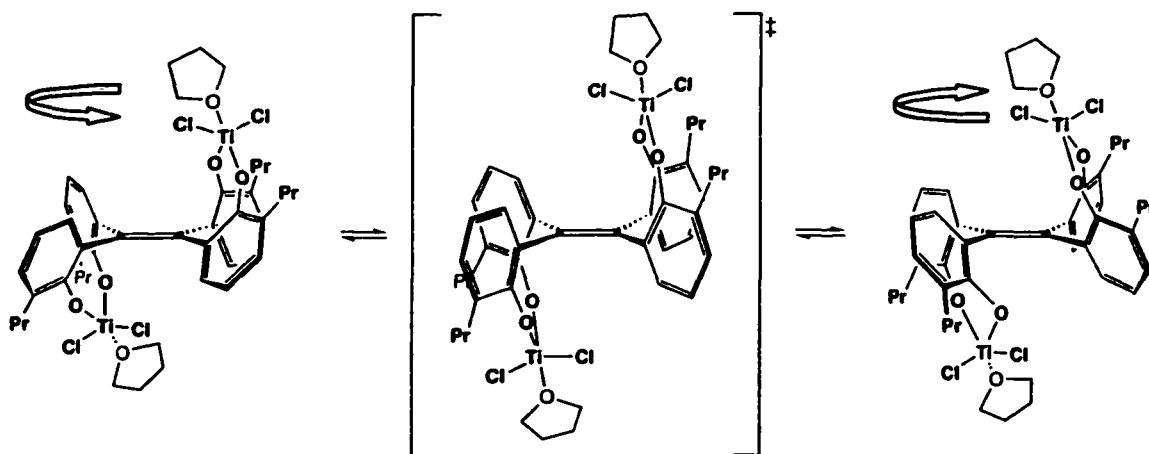


Figure 3.17. $^1\text{H-NMR}$ spectrum of **30a** (C_6D_6).



Scheme 3.8. Proposed solution behavior of **30a**. The thick arrows represent the direction of the helices.

Table 3.3. Non-bonding interatomic distances between the proton at 6-position of each ring.

<i>Interatomic distance (Å)</i>	
Ti...H	
Ti1...H36	3.93
Ti1...H46	3.67
Ti2...H16	3.82
Ti2...H26	4.14
H...Cl	
H36...Cl2	2.90
H46...Cl2	3.10
H16...Cl4	3.32
H26...Cl4	2.85

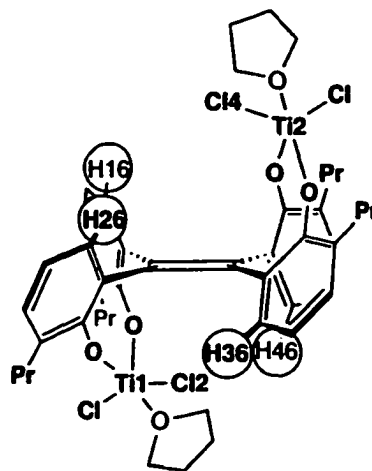


Figure 3.18. Selected atom labels in the complex 30a.

The possibility of the H-6 proton having an *agostic interaction*⁶ with the closest titanium atom and the possibility of *hydrogen bonding* to the closest chloride ligand were examined for 30a. Table 3.3 presents the distances between an H-6 and the closest Ti or Cl atoms in 30a. The relevant atom labels are provided in Figure 3.15. Based on these non-bonded interatomic distances, no meaningful interaction is expected between any H-6 and the Ti atoms nor between H-6 and any Cl atoms. The Ti...H distances are too long to allow any interaction, and the H...Cl distances are no shorter than the van der Waals distances.

A more plausible explanation for the highly downfield shift is that the tilting of the aryl rings causes a change in the local magnetic environment. Unlike aryl rings in the magnesium complexes, the aryl rings in complex 30a are not perpendicular to the olefin plane in the crystal structure. In solution, as discussed earlier, the direction of the helical ring tilting should be switching rapidly from one way to another (Scheme 3.8).

Nevertheless, the ^1H NMR spectrum will reflect mainly the two tilted extremes and not the all-perpendicular transition state. The two tilted extremes are enantiomeric; therefore, the ^1H NMR signals from each are identical. These tilted extremes are assumed to be close to those observed in the crystal structure.

To examine the effect of the ring tilting on the magnetic environment, the positions of each H-6 from the neighboring rings (geminal and vicinal) were measured in the crystal structure of **30a**, and are summarized in **Figure 3.19**. For comparison, the corresponding data for the magnesium complex **26** are given in **Figure 3.20** as an example of a nearly perpendicular species.

While the positions of H16 and H46 in **30a** relative to the neighboring rings are not as deviated as the "nearly perpendicular" cases of **26**, H26 and H36 are greatly affected by the geometry change. These are the protons tilting toward the vicinal neighboring ring (or the vicinal neighboring ring is tilting toward these protons). Apparently, the ring-tilting brings these protons into a more deshielding region of the vicinal neighbor. The distance between the centroid of the vicinal aryl ring and these protons is nearly 5 Å, but the deshielding effect may still be effective by ca. +0.4 ppm, according to the Haigh-Mallion ring-current calculation.⁴

ii) Di-(TiBn₂) Complex 35. The ring tilting theory described above is further supported by the spectroscopic features of benzyltitanium complex **35**. Unlike the titanium halide complexes **30/30a** and **33/33a**, complex **35** does NOT show a highly downfield dd signal near 8 ppm. The most downfield chemical shift of the ligand's aryl rings is 7.16 ppm (C_6D_6). This shift is most likely due to the relatively small tilting angles of the aryl rings, which are apparently not great enough to bring any H-6 proton into the effective deshielding region of neighboring rings. The phenyl rings of the benzyl groups cannot be the source of deshielding because in solution, they are freely rotating: their net shielding/deshielding effects (if any) presumably average out to nil. The tetraarylethene framework of complex **35** in solution is probably closer to that of the nearly perpendicular tri-magnesium complexes **25-29** rather than other ring-tilted geminal up/down complexes **30-33a**.

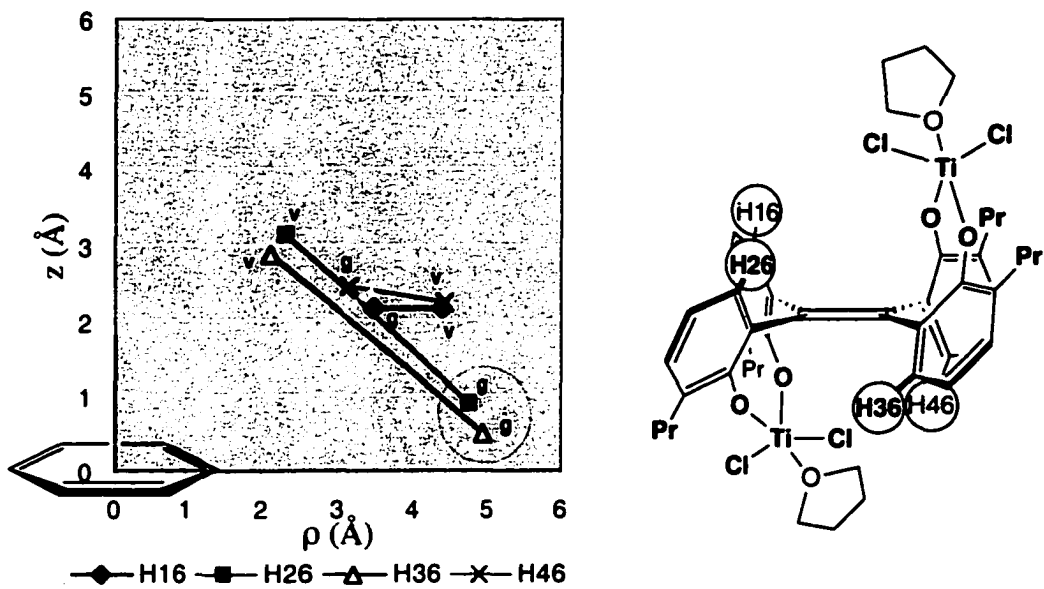


Figure 3.19. Positions of the H-6 protons in **30a** against the geminal(g) or vicinal(v) neighboring ring.

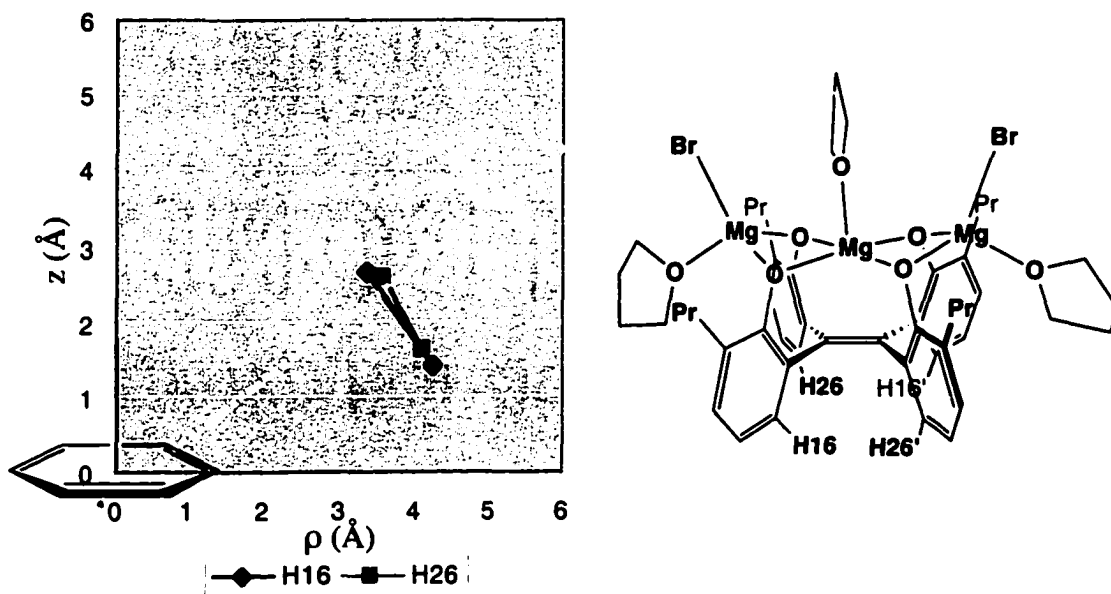


Figure 3.20. Positions of the H-6 protons in **26** against the geminal or vicinal neighboring ring.

In the ^1H NMR spectrum of **35**, the two benzyl groups on each Ti atom are clearly differentiated in the ^1H NMR spectrum. Compared to the chemical shifts of TiBn_4 ,^b the methylene signal of one benzyl group is ca. 0.5 ppm downfield, and the other is ca. 0.5 ppm upfield. The benzyl groups must be rotating freely through the C30-Ti or C40-Ti axes, because each pair of methylene protons shows a sharp singlet.

The large chemical shift difference (ca. 1 ppm) between the two benzyl methylene groups can also be attributed to the anisotropic effects of the ligand aryl rings. The positions of the "outward" and "inward" benzylic methylene groups from ligand aryl rings are compared in **Figure 3.21**. In this comparison, the "inward" methylene group is clearly more in the deshielding region than is the "outward" methylene group. The former is quite far away from the centroid, by ca. 4.7-6.7 Å, but still in the effective deshielding region of some of the aryl groups.

This observation also supports the hypothesis that the position directly above the olefin double bond receives considerable deshielding from all four aryl rings, as was suggested for the centrally coordinated THF in the tri-magnesium complex **25-29** (**Figure 3.10**) The position of the inward benzylic methylene group relative to the ligand aryl rings in **35** is similar to the position of the central THF in **26** described in **Figure 3.10**.

^b Chemical shifts of TiBn_4 in C_6D_6 (ppm): 7.77 (*o*), 6.93 (*p*), 6.61 (*m*), 2.82 ($-\text{CH}_2\text{Ph}$).

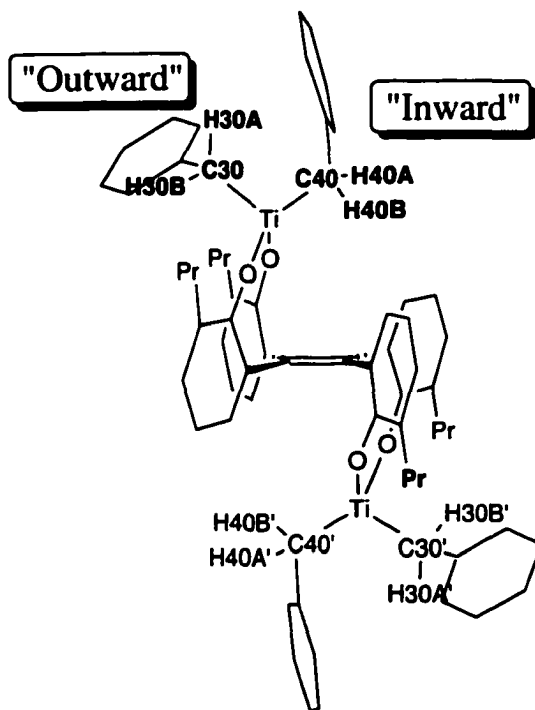
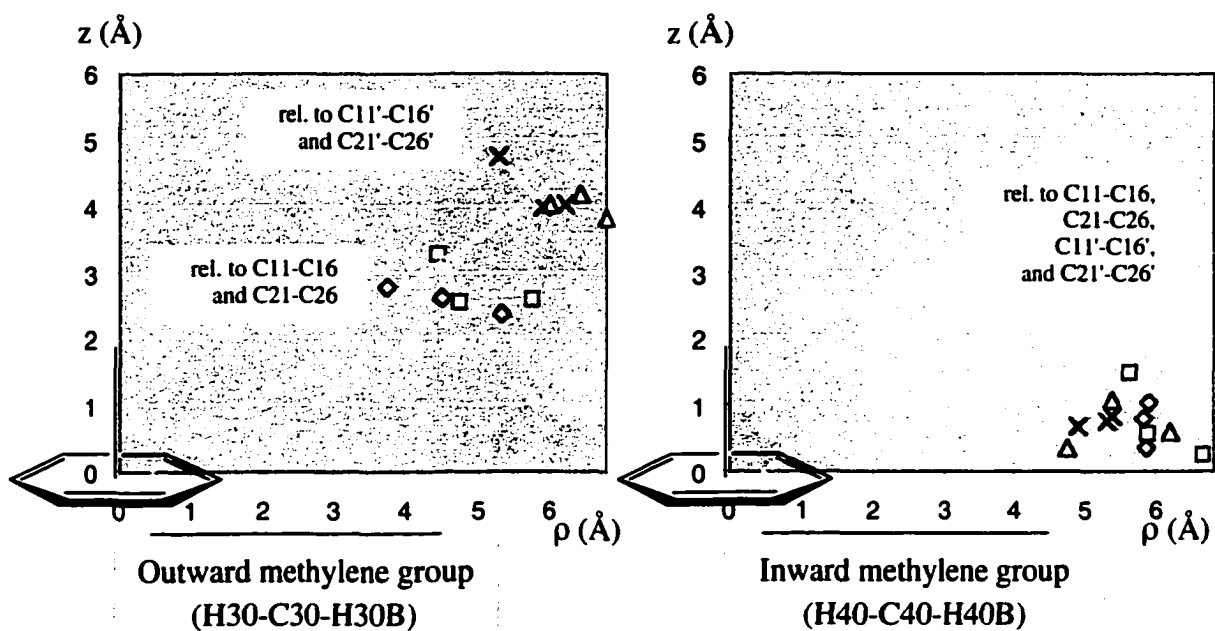


Figure 3.21. Positions of the benzylic methylene groups in **35** against the ligand's aryl rings. The double bonds in the aromatic rings are omitted for clarity.

iii) Di-(CpTiCl) Complex 34. The basic ^1H NMR spectroscopic features are very similar to those of the geminal up/down di- $\text{TiX}_2(\text{thf})_n$ complexes **30/30a** and **33/33a**. The four aryl rings are all equivalent, α - and β -methylene groups in the propyl group are diastereotopic, and the chemical shifts of the aromatic protons are quite similar.

Although the aryl rings of complex **34** are nearly perpendicular to the olefin plane, unlike the rings in **30a** and its analogues, the spectrum still shows a highly downfield-shifted aromatic dd signal at 8.21 ppm (H-6). This signal is even more downfield, by ca. 0.2 to 0.3 ppm, than that of the Cp-free titanium halide complexes. Meanwhile, the H-4 and H-5 signals are also more downfield than those in **30a**, but only by ca. 0.08 ppm (H-4) and 0.15 ppm (H-5).

The source of this deshielding effect on the H-6 protons, however, is not clear. If it is from the ligand aryl rings, they must be tilted in solution phase, in contrast to how they are present in the crystal structure. As discussed earlier for the trinuclear magnesium complex **25**, the deshielding effect on the H-6 protons is not significant when the aryl rings are near perpendicular. The Cp rings of the titanium fragment were thus suspected as possible source of anisotropic effects. However, in the crystal structure, the positions of the H16 or H26 protons relative to the same-side Cp ring (C31~C35) or opposite side Cp (C31'~C35') do not indicate a clear deshielding effect (**Figure 3.22**). If anything, these H-6 protons seem rather in the shielding region of the opposite Cp ring.

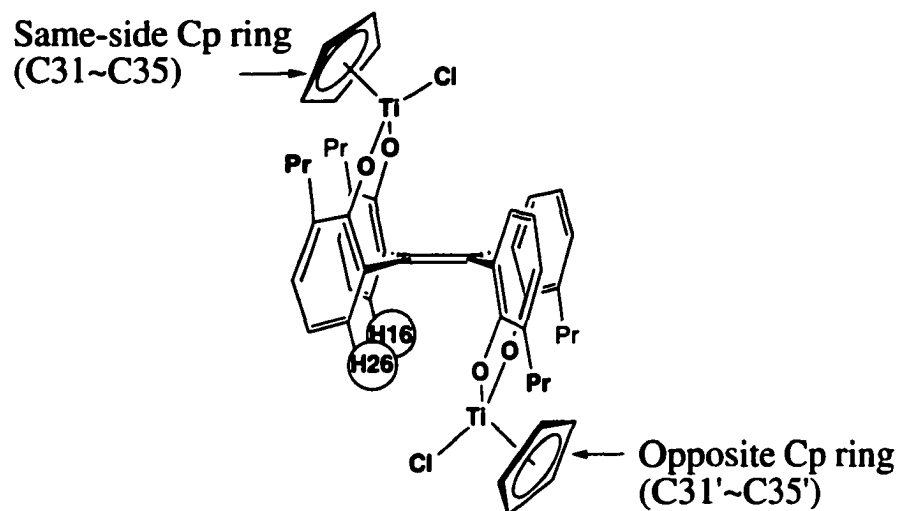
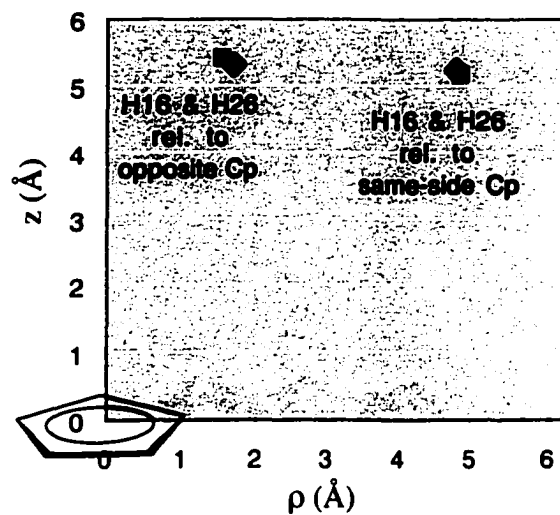


Figure 3.22. Positions of the H16 and H26 protons in complex **34** against the same-side Cp ring (C31~C35) and the opposite Cp ring (C31'~C35').

3.1.2.D. The Collapsed "Sandwich" Complex

i) **Synthesis and Structure of 32.** The collapsed sandwich-type complex **32** (Figure 3.23) was obtained cleanly by adding one equivalent of TiCl_4 to the Na salt of **7** in toluene. The reaction was also reasonably clean without prior deprotonation, but small amounts of impurities were found in the ^1H NMR spectrum of the crude product. Using THF as a solvent instead of toluene (with beforehand deprotonation by NaH) darkened the color of the reaction mixture to almost black, and the product was considerably less pure. The darkened color suggests some reduction of Ti(IV) to Ti(III). It is not surprising that ligand **7**, a phenolic species, may be oxidized by Ti(IV); the more polar THF may assist the electron transfer. THF may also slow the reaction between TiCl_4 and the salt of **7** by coordinating to TiCl_4 .

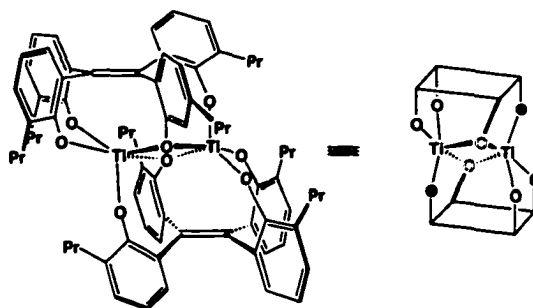


Figure 3.23. The sandwich-type complex **32**.

This sandwich complex has only one Ti atom per ligand. All of the chlorides from TiCl_4 are replaced with aryloxy groups. The reaction gives a 2 : 2 adduct because apparently a single ligand cannot provide a suitable coordination environment to a Ti(IV) atom. The same sandwich-type compound was also reported for the tetrakis(5-*tert*-butyl-2-hydroxyphenyl)ethene ligand by Verkerk (see also Chapter 1, Section 1.0).¹ Apparently, the *ortho*-propyl groups are not bulky enough to prevent the collapse of two ligand units in the case of titanium derivatives (in contrast to aluminum complexes, *vide infra*).

Figure 3.24 provides the crystal structure of **32** obtained by X-ray crystallographic analysis of the co-crystal of **32** and the 2 : 1 adduct **30a** (1 : 2 molar

ratio), obtained from one of many crystallization trials of **30a** (*vide infra*). In the molecule of **32**, the two ligands are equivalent, as are the Ti atoms. Within each ligand, the four aryl rings are all non-equivalent.

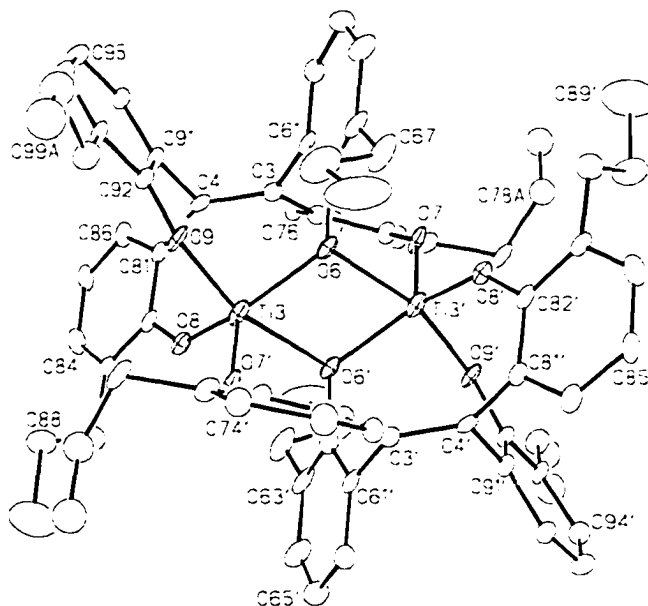


Figure 3.24. X-ray crystallographic structure of **32**.

Torsional angles about C3-C4 bond (deg): C61-C3-C4-C81 = $-172.7(7)$, C61-C3-C4-C91 = $8.8(9)$, C71-C3-C4-C81 = $15.9(11)$, C71-C3-C4-C91 = $-162.5(6)$. Ring torsion angles (deg): C4-C3-C61-C62 = $84.9(7)$, C4-C3-C61-C66 = $-90.9(8)$, C4-C3-C71-C72 = $-149.5(7)$, C4-C3-C71-C76 = $39.8(10)$, C3-C4-C81-C82 = $90.9(8)$, C3-C4-C81-C86 = $-99.1(8)$, C3-C4-C91-C92 = $-86.2(8)$, C3-C4-C91-C96 = $98.1(7)$.

The olefin plane is notably distorted, as is seen in the figure and in the torsional angles about the C3-C4 bond of up to 16° . The degree of ring-tilting varies. Among the three rings that are coordinated to the same Ti atom, those diagonally positioned (C61~C66 and C81~C86) are almost perpendicular to the ethene plane, while the other two rings are more tilted, especially the C71~C76 ring. The tilting angle of this ring is ca 50° from the perpendicular position.

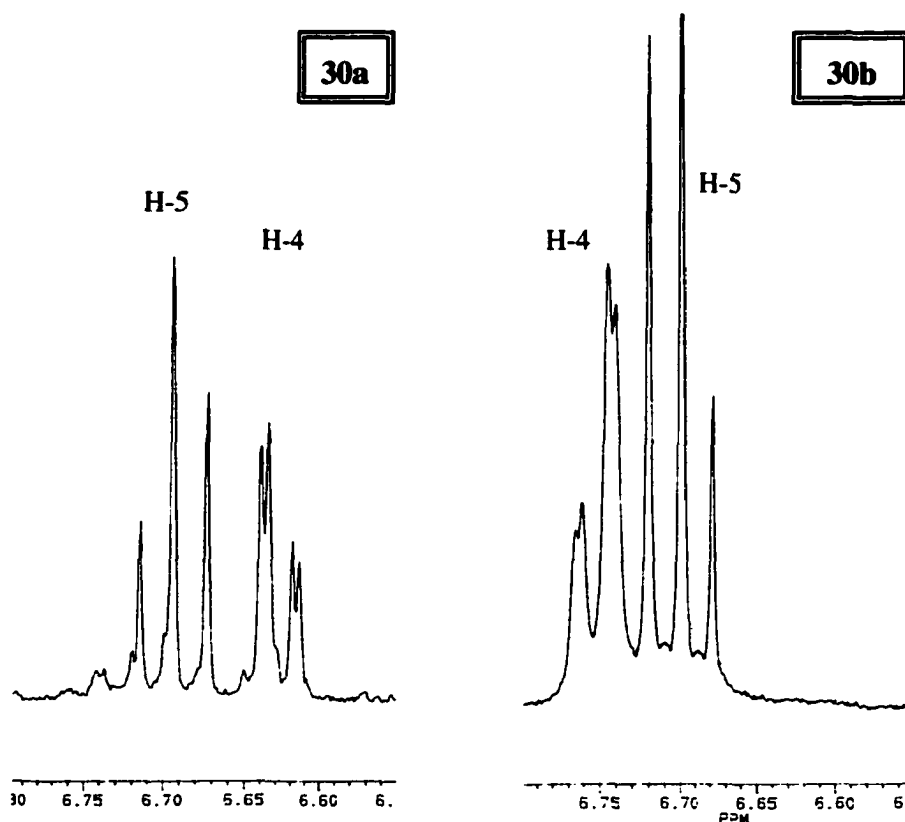


Figure 3.26. ^1H NMR spectra (part of aromatic region) of **30a** and **30b** (C_6D_6).

Two major spectroscopic differences exist between **30a** and **30b**. First, while the α -methylene protons of the propyl group are both sharp for **30a**, isomer **30b** has one broad (the more downfield one) and one sharp α -methylene proton. Second, the relative position of the aromatic protons H-5 and H-4 are switched between **30a** and **30b**. **Figure 3.26** presents part of the aromatic regions of ^1H NMR spectra of **30a** and **30b**. The chemical shift of the H-5 triplet signal is very similar (only $\Delta 0.01$ ppm difference), but the H-4 dd signal is more downfield for **30b**, compared to that of **30a**. The difference is ca. $\Delta 0.13$ ppm.

Interestingly, such isomerization and equilibration were not observed without the presence of THF (i.e., for **30**). Apparently, the interconversion between **30a** and **30b** is assisted by the coordinating THF.

Separately from these isomerization reactions, the crystal structure of a *vicinal up/down* isomer of the di-TiCl₂(thf) complex, named **31**, was serendipitously obtained (**Figure 3.27**). The crystal was obtained from one of many crystallization attempts for the *geminal up/down* isomer **30a**, from toluene-pentane medium by slow evaporation.

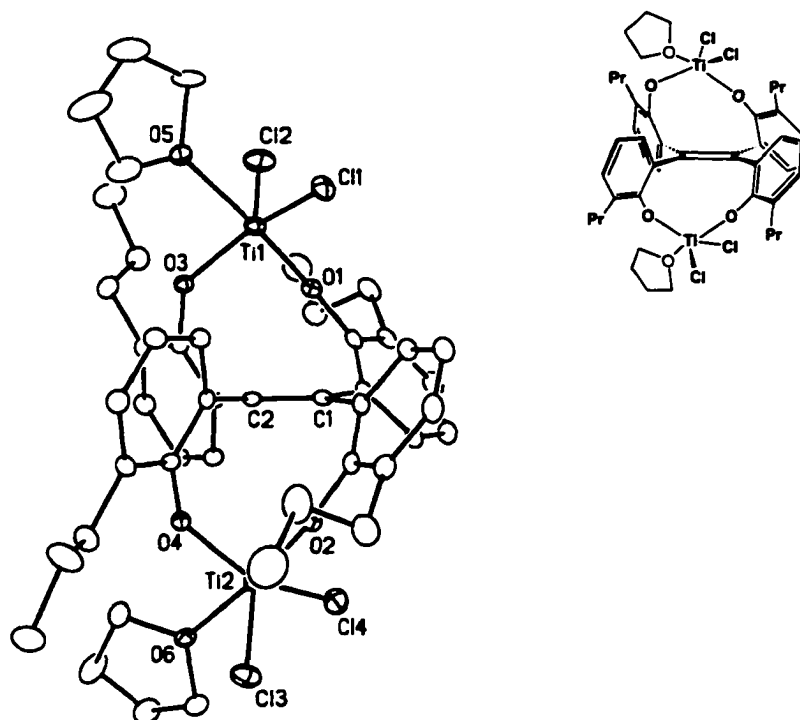


Figure 3.27. X-ray crystallographic structure of **31** the vicinal "up/down" isomer. The label for the aromatic carbon attached to OX is CX2.

Bond length C1-C2 = 1.339(6) Å, Ti1-Cl1 = 2.2646(16) Å, Ti1-O1 = 1.764(3) Å, Ti1-O3 = 1.826(3) Å, Ti1-O5 = 2.177(4) Å. Interatomic angle O1-Ti1-O3 = 95.13(14)°, O2-Ti2-O4 = 93.71(14)°. Torsional angle through C1-C2 bond: C11-C1-C2-C31 = 6.9(6)°, C11-C1-C2-C41 = 174.0(4)°, C21-C1-C2-C31 = -173.8(4)°, C21-C1-C2-C41 = 5.3(6)°. Ring torsion angle against C1-C2 bond: C2-C1-C11-C12 = 52.0(6)°, C2-C1-C11-C16 = -127.2(5)°, C2-C1-C21-C22 = 57.4(6)°, C2-C1-C21-C26 = -120.5(5)°, C1-C2-C31-C32 = -110.4(5)°, C1-C2-C31-C36 = 70.8(6)°, C1-C2-C41-C42 = -106.2(5)°, C1-C2-C41-C46 = 71.9(6)°.

In the crystal structure of **31**, each Ti atom takes a trigonal bipyramidal structure, with interatomic angles quite similar to those of the *geminal up/down* isomer **30a**.⁷ To keep the Ti coordination geometry unchanged, the aryl rings are more tilted from the

perpendicular position compared to those of **30a**: the ring torsion angles are 20 to 40° off the perpendicular angle ($\pm 90^\circ$). The topology of the tilting is again helical. The distortion of the olefin double bond away from coplanarity is roughly 5-7° (by torsional angles about the C1-C2 bond), a level similar to that of **30a**.

The situation leading to the formation of crystals of **31** was quite similar to the conditions leading to the formation of crystals of the mysterious equilibrium isomer **30b**. Moreover, both are isomeric with **30a**. However, unfortunately, no direct evidence was obtained to connect **30b** and **31**. Due to the small amount of the crystals of **31** that were obtained, an insufficient amount was left for ^1H NMR spectroscopy after selecting some for X-ray analysis. The mother liquor, after removal of volatiles, showed a ^1H NMR spectrum of a mixture containing a symmetrical species with rather broad and (probably) diastereotopic propyl groups, but *no* highly downfield dd signal in aromatic region. However, it was not certain if these signals belonged to isomer **31**.

Nevertheless, it is most logical to conclude that **30b** is the vicinal up/down isomer **31**. Besides the similarity of the crystallization situation, the crystal structure of **31** is quite consistent with the spectroscopic features of **30b**. The major spectroscopic difference of **30b** from **30a** was, as mentioned earlier, the chemical shift of the H-4 signal. **Figure 3.28** compares the crystallographic positions of the aromatic protons (H-4, H-5 and H-6) in **31** and **30a** relative to their neighboring aryl rings (geminal or vicinal). The difference between **31** and **30a** is very small for H-5 and H-6, as shown in **Figure 3.28-b** and **-c**. In contrast, the difference in H-4 between **31** and **30a** is clear (**Figure 3.28-a**): some H-4 protons in **31** (circled) are positioned more toward the deshielding region. These are the H14 and H24 protons in **31**, affected by the geminal neighboring ring in both cases. This factor explains the further downfield shift of H-4 signal of **30b**, compared to **30a** (**Figure 3.27**).

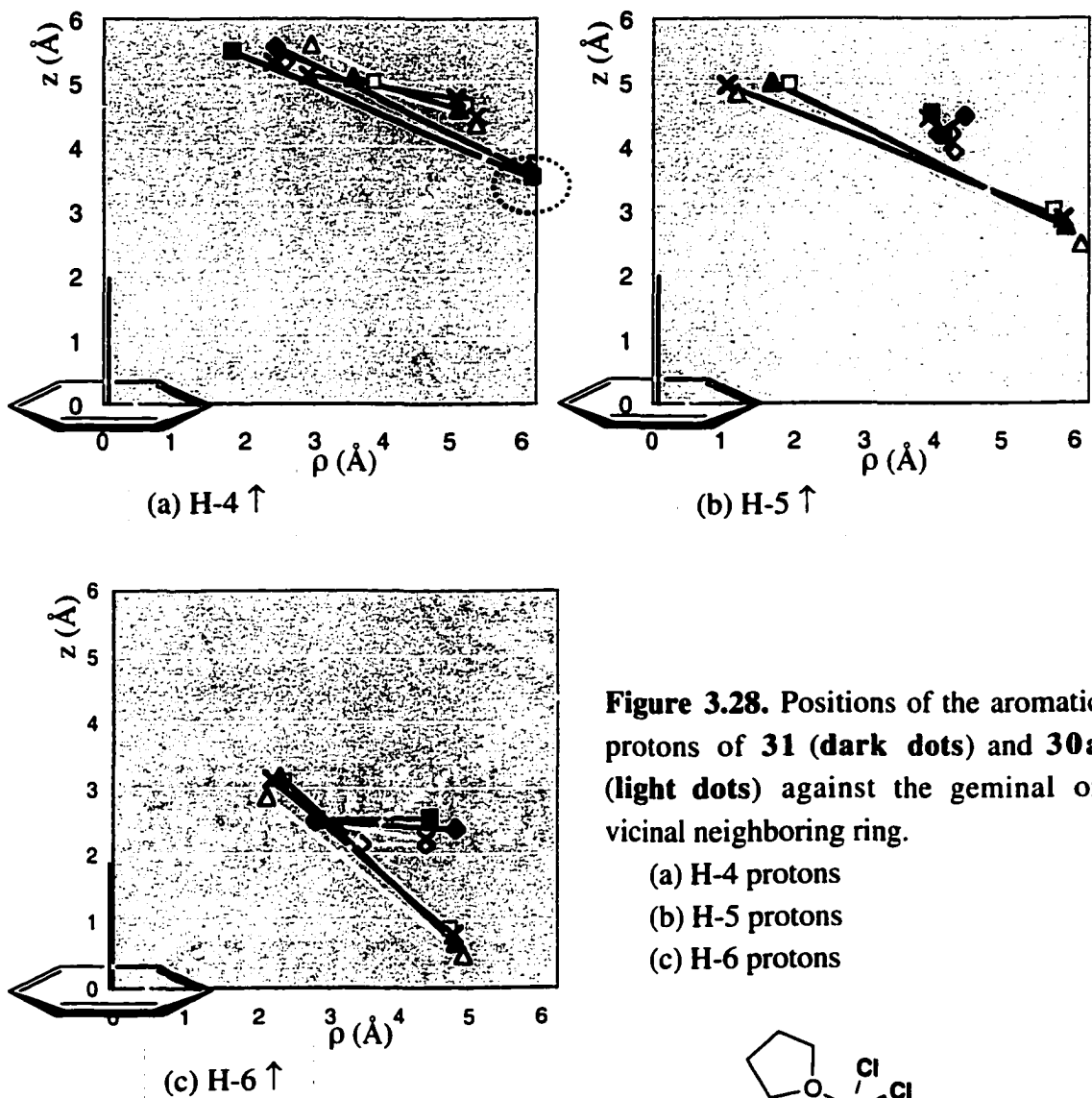
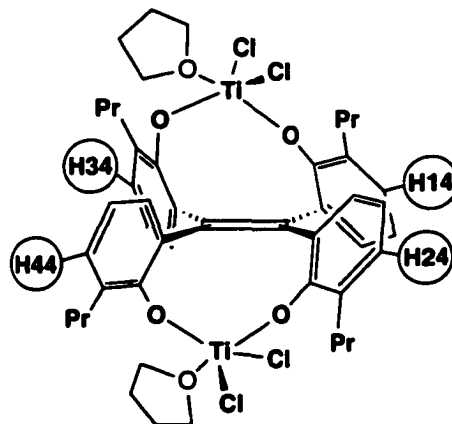
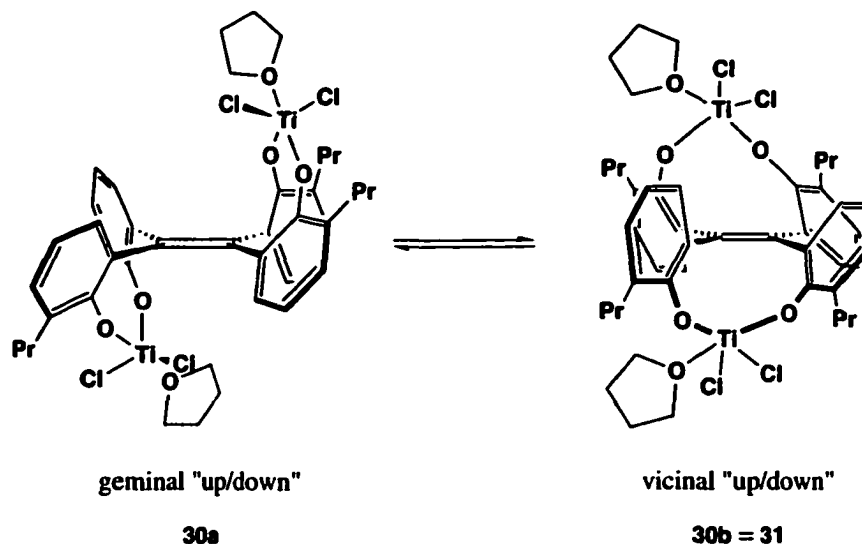


Figure 3.28. Positions of the aromatic protons of **31** (dark dots) and **30a** (light dots) against the geminal or vicinal neighboring ring.

- (a) H-4 protons
- (b) H-5 protons
- (c) H-6 protons



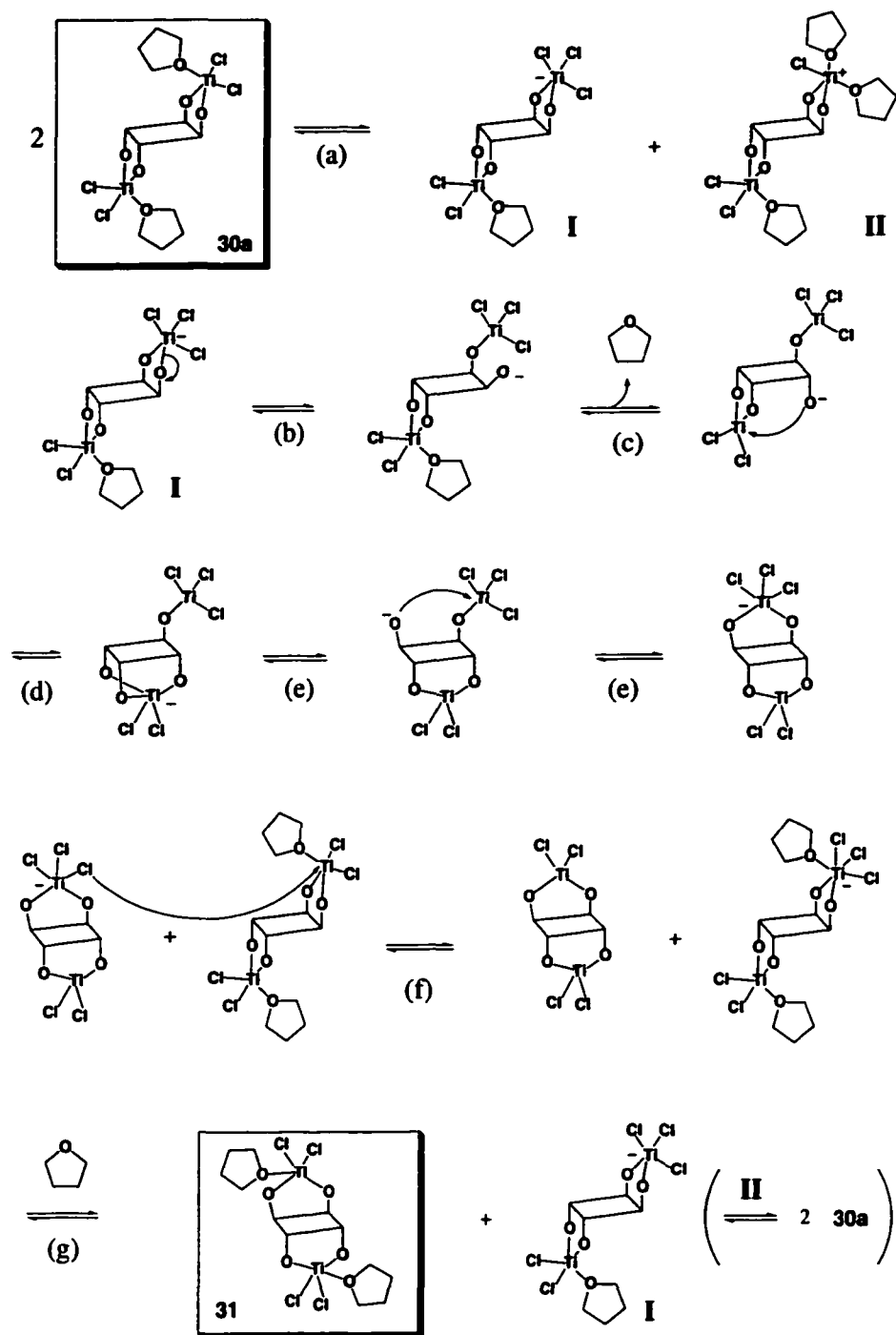
It is then presumed that the geminal up/down di-TiCl₂(thf) complex **30a** and the vicinal analogue **30b/31** exist as an equilibrium mixture at 1 : 1 ratio in hydrocarbon solution (Scheme 3.10).



Scheme 3.10. Presumed interconversion of "geminal up/down" and "vicinal up/down" isomers.

It is interesting to consider the mechanism of the interconversion of **30a** and **31**. Breaking a Ti-O bond is required for **30a** and **31** to interconvert, although Ti-O bonds are usually quite strong and not easy to break. One possibility is that the interconversion is assisted by THF. As mentioned earlier, the non-THF version **30** did not isomerize to a vicinal analogue.

One proposed mechanism for the interconversion is shown in Scheme 3.11. The first step (a) is a disproportionation between two (ArO)₂TiCl₂(thf) centers from different molecules (this cannot happen intramolecularly due to the non-interacting ends of the structure). The exchange of THF and "Cl⁻" is proposed, probably consisting of two steps: first, THF transfers from one metal center to the other, then Cl⁻ transfers from the sterically crowded THF recipient "(ArO)₂TiCl₂(thf)₂" back to the now unsaturated metal. Thus one titanium becomes titanate "(ArO)₂TiCl₃⁻," and the other cationic "(ArO)₂TiCl(thf)₂⁺," in which the positive charge is stabilized by the extra THF coordination, both electronically and sterically.



Scheme 3.11. Proposed interconversion mechanism of "geminal up/down" and "vicinal up/down" isomers.

Isomerization further proceeds from the titanate **I**: the electron rich Ti^- center undergoes Ti-O cleavage (step **b**). The "liberated" ArO^- then can rotate to the "down" side of the molecule, encountering the other " $(\text{ArO})_2\text{TiCl}_2(\text{thf})$ " center (step **d**). Dissociation of THF may be a prerequisite for the aryloxy attack on the Ti center to form a triaryloxy titanate center " $(\text{ArO})_3\text{TiCl}_2^-$ " (step **c**). Any of the three aryloxy residues can leave and rotate to the "up" side, either reforming the geminal $(\text{ArO})_2\text{TiCl}_2$ or forming the vicinal " $(\text{ArO})_2\text{TiCl}_2$ " center (step **e**).

The remaining steps achieve the loss of the extra Cl^- and gain a sufficient amount of THF to become the final "vicinal up/down" di- $\{(\text{ArO})_2\text{TiCl}_2(\text{thf}) \}$ complex **31**. The recovered titanate **I** can either initiate further isomerization or recombine with the initial cationic species (**II**) to form the original state. In this proposed mechanism, THF plays an important role in several steps, stabilizing intermediates and associating/dissociating flexibly to provide coordination sites for other donor groups.

This type of isomerization to vicinal analogue is observed for only the di- $\text{TiCl}_2(\text{thf})$ system **30a** and **31**. Other geminal up/down species, including the bromo analogue **33a**, do not show such chemical behavior. The reason why the isomerization does not occur for the bromo analogue is not clear.

3.1.2.F. Dinuclear Cationic Complex from **35**?

There are many known examples of alkyltitanium complexes that can be converted into active ethylene polymerization catalysts. Typically, one alkyl group is abstracted by a strongly Lewis acidic reagent to form a cationic titanium species.⁸ Many discrete cationic species have been isolated and structurally well-characterized.⁸ This section describes our attempts to produce a discrete cationic titanium species from the di- TiBn_2 complex **35** and the promising result with $\text{B}(\text{C}_6\text{F}_5)_3$. The ethylene polymerization experiments using **35**, however, were not successful (details will be discussed in Chapter 5).

In an attempt to abstract one benzyl group from **35**, a 1 : 1 mixture of **35** and $\text{B}(\text{C}_6\text{F}_5)_3$ was prepared in C_6D_6 . The ^1H NMR spectrum was complicated after 15 minutes reaction time, but after longer than one day, the spectrum showed a symmetrical species (**36**) as a major product. The aromatic region was complicated due to severe peak overlap

(from both the ligand framework and the benzyl groups), but the four propyl groups seemed all equivalent, i.e., all the aryl rings are apparently equivalent. The benzyl methylene singlets were also present in the ratio of 2 : 1 : 1.

One possible structure for **36** that meets these spectroscopic features is a dinuclear cationic complex, as shown in **Figure 3.29**. Attempts to crystallize this product, however, were not successful.

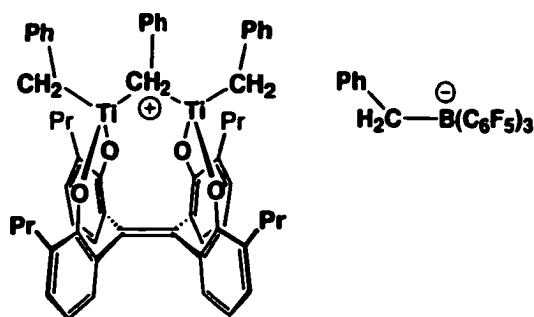
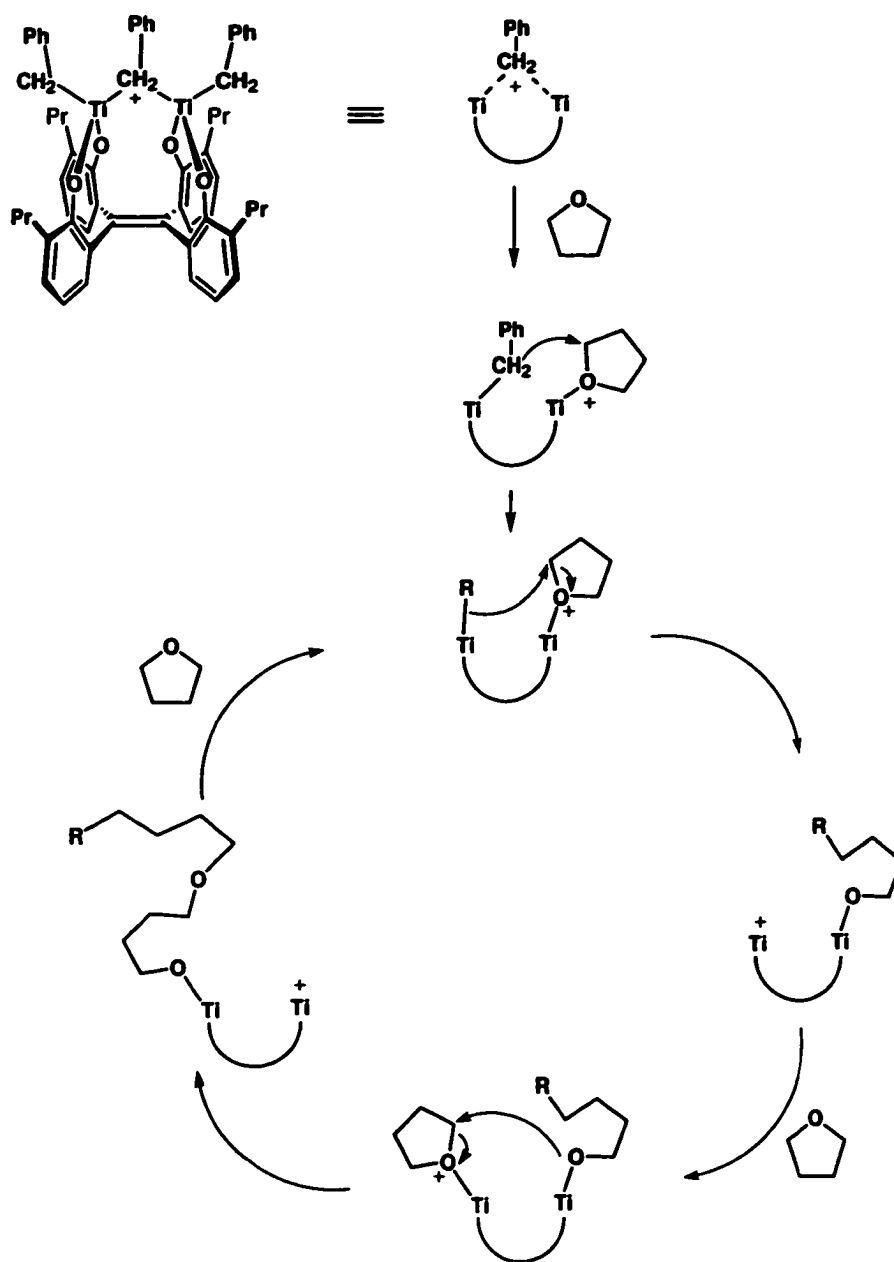


Figure 3.29. One possible structure of **36**, the adduct of **35** and $B(C_6F_5)_3$.

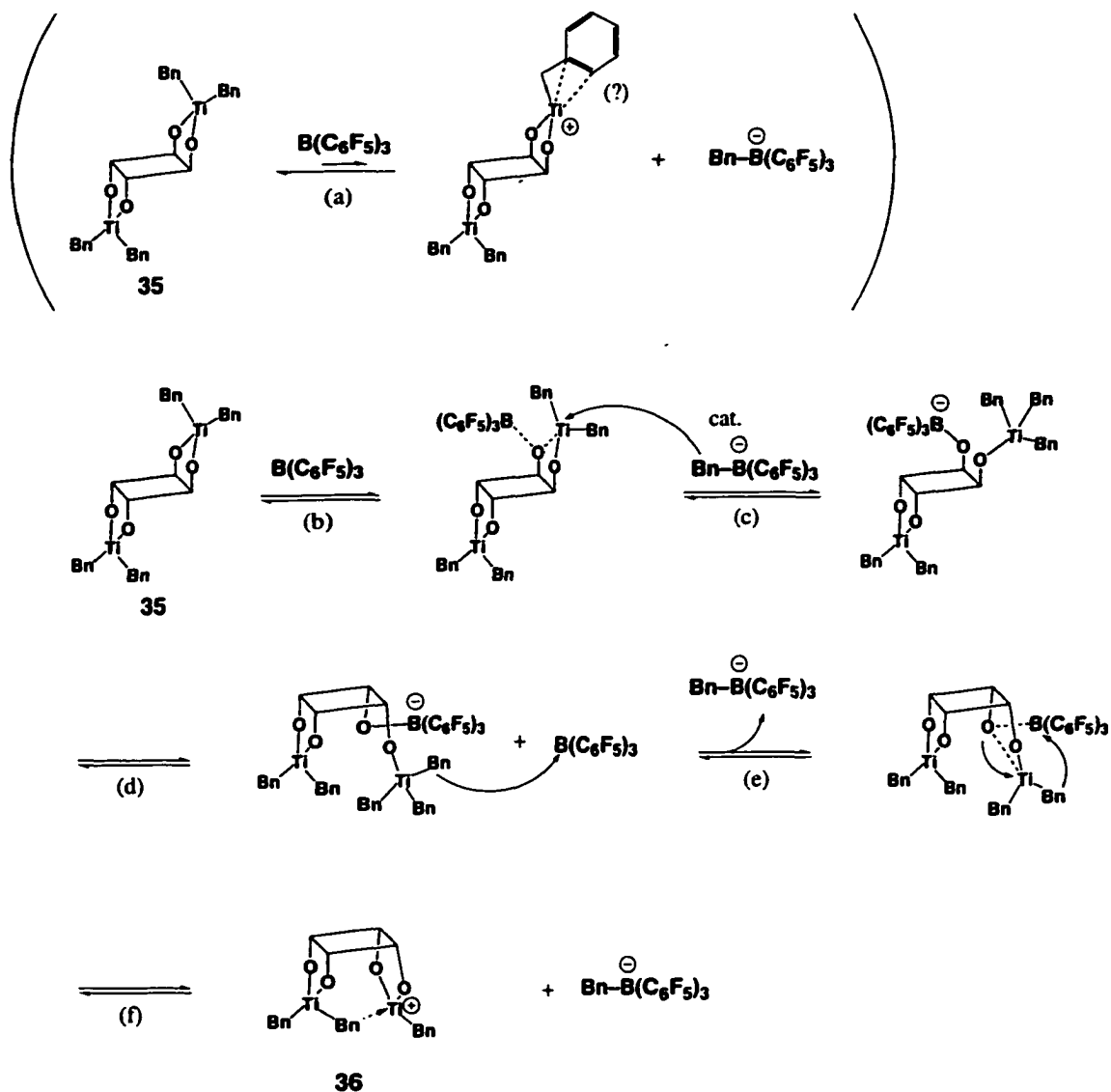
When THF was used as one component of the crystallization solvents, along with toluene, a layer of clear colorless viscous oil formed after being kept overnight at -30°C . This viscous oil, although not confirmed, was presumably polymerized THF, because addition of more THF to this mixture resulted in an increase of the clear oil layer after >16 hours. The polymerization of THF must have been catalyzed by **36**, because $B(C_6F_5)_3$ alone does not polymerize THF, nor does **35** by itself. A combination of $B(C_6F_5)_3$ and an alkylzirconium complex does not generally polymerize THF either. For example, Mattheis et al. reported the reaction between $(\eta^5:\eta^1\text{-Cp}')ZrMe_3$ ($\text{Cp}' = \text{C}_5\text{H}_4\text{CH}_2\text{CH}_2\text{OMe}$) and $B(C_6F_5)_3$ in THF, which affords a cationic zirconium complex $[(\eta^5:\eta^1\text{-Cp}')ZrMe_3(\text{THF})][\text{MeB}(C_6F_5)_3]$. Neither of the ions, nor the combination of them, polymerizes THF.⁹

A proposed mechanism for THF polymerization by **36** is given in **Scheme 3.12**. Polymerization of THF requires a Lewis acid to activate the THF and a nucleophilic reagent to initiate a polymerization. Compound **36** would be not only capable of playing both roles, but also its proposed dinuclear structure would provide an excellent platform for both THF activation and polymer chain growth by alternating the two roles between the two Ti centers.



Scheme 3.12. Proposed mechanism of THF polymerization by 36.

Formation of the dinuclear cationic structure proposed for **36** from the reaction of **35** and $\text{B}(\text{C}_6\text{F}_5)_3$ requires a conformational change of the ligand framework from "geminal up/down" to "all-up." This change is plausible with the assistance of Lewis acidic $\text{B}(\text{C}_6\text{F}_5)_3$. A proposed mechanism for this transformation is described in Scheme 3.13.



Scheme 3.13. Proposed mechanism of formation of **36** from **35** plus $\text{B}(\text{C}_6\text{F}_5)_3$.

Scheme 3.13 proceeds as follows: the boron reagent can either abstract a benzyl group from **35** (step **a**) or interact with a phenolato oxygen atom (step **b**). The latter, with assistance by a catalytic amount of $[\text{BnB}(\text{C}_6\text{F}_5)_3]^{(-)}$ formed in step **a**, allows for cleavage of a Ti-O bond, followed by flipping the affected aryloxytitanium and aryloxyborate groups to the other face of the ligand (steps **c**, **d** and **e**). The transformation is auto-catalytic because once formation of **36** is completed, an equimolar amount of $[\text{BnB}(\text{C}_6\text{F}_5)_3]^{(-)}$ is also produced.

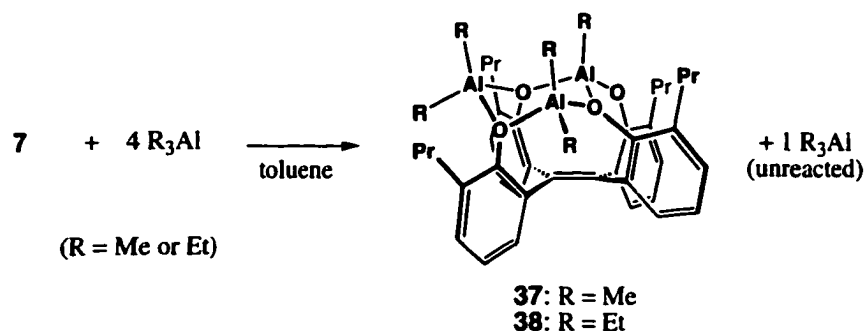
Other boron reagents commonly used to activate alkyltitaniums did not give discrete products. Attempted protonolysis by $[\text{PhEt}_2\text{NH}]^+[\text{Cl}]^-$ in C_6D_6 did not proceed cleanly. After more than one day, the ^1H NMR spectrum still showed signals from the starting material. The reaction with $[\text{PhEt}_2\text{NH}]^+[\text{B}(\text{C}_6\text{F}_5)_4]^-$ in C_6D_6 showed the starting materials and a new compound after 30 minutes at room temperature. After more than one day, a precipitate had formed and the solution showed PhEt_2N signals only. The precipitate, obviously the product, unfortunately could not be identified. When the precipitate was redissolved in THF-d_8 , only broad and complicated signals were observed. One-electron oxidation using either $[\text{Ph}_3\text{C}]^+[\text{B}(\text{C}_6\text{F}_5)_4]^-$ or $[\text{Cp}_2\text{Fe}]^+[\text{B}(\text{C}_6\text{F}_5)_4]^-$ in toluene did not proceed cleanly, perhaps because of the poor solubility of the reagents. Transferring the mixture to a bomb, adding THF and heating to $100\text{ }^\circ\text{C}$ to promote the reaction, resulted in only broad ^1H NMR signals in C_6D_6 . No tractable product could be isolated from these reaction mixtures.

3.1.3. Al Complexes

Reactions of ligand **7** and R_3Al ($R = Me$ or Et) resulted in the formation of discrete tri-aluminum complexes in non-coordinating medium. The analogous reactions with Et_2AlCl and $EtAlCl_2$ result in indiscrete tetra-aluminum adducts. These products show interesting chemical behavior in a THF medium. This section first describes the products in a non-coordinating medium, then the THF-driven alteration of these products.

3.1.3.A. Al Complexes Obtained in Non-Coordinating Medium

i) Adducts of R_3Al . Mixing the phenolic ligand **7** and four equivalents of R_3Al in toluene gives a non-symmetrical trinuclear aluminum complex **37** ($R = Me$) or **38** ($R = Et$) (Scheme 3.14). The fourth equivalent of the reagent is left unreacted in both cases.



Scheme 3.14. Formation of **37** and **38** from **7** and R_3Al .

The structure of **38** was determined by X-ray crystallography (Figure 3.30). The structure of **37** is considered to be analogous to that of **38**, based on the similarity of the 1H NMR spectroscopic features. In the six-membered " Al_3O_3 " chair-form crown ring, each aluminum atom holds an axial and an equatorial substituent. The Al_2 and Al_3 atoms hold two ethyl groups, while the Al_1 atom has one ethyl group at the axial position, with an ArO group (that is not participating the " Al_3O_3 " crown ring) at the equatorial position. Overall, three axial and two equatorial ethyl groups are found in the crystal structure.

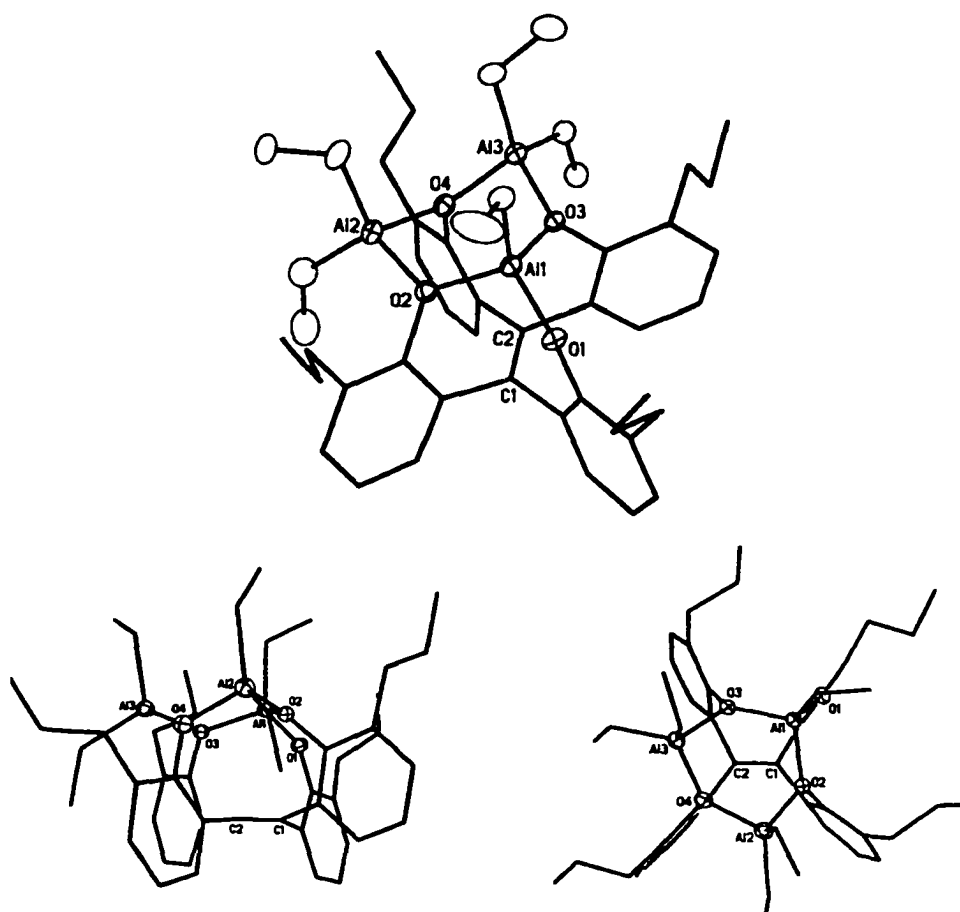


Figure 3.30. X-ray crystallographic structure of the complex **38** with different angle views. The label for the aromatic carbon attached to OX is CX2.

Bond lengths (Å): Al1-O1 = 1.699(2), Al1-O2 = 1.863(2), Al1-O3 = 1.855(2), Al1-C50 = 1.943(3), Al2-O2 = 1.893(2), Al2-O4 = 1.885(2), Al2-C52 = 1.955(4), Al2-C54 = 1.943(4), Al3-O3 = 1.887(2), Al3-O4 = 1.867(2), Al3-C56 = 1.960(3), Al3-C58 = 1.954(3). Interatomic angles (deg): O1-Al1-O2 = 109.88(10), O1-Al1-O3 = 110.24(10), O2-Al1-O3 = 108.91(9), O3-Al1-C50 = 107.08(12), O2-Al2-O4 = 92.93(10), O3-Al3-O4 = 92.36(10), O3-Al3-C56 = 112.02(13). Torsional angle of olefin plane (deg): C11-C1-C2-C31 = -9.8(4), C11-C1-C2-C41 = 166.1(3), C21-C1-C2-C31 = 164.1(3), C21-C1-C2-C41 = -20.0(5). Ring torsion angles (deg): C2-C1-C11-C12 = 93.8(4), C2-C1-C11-C16 = -94.7(4), C2-C1-C21-C22 = -78.0(4), C2-C1-C21-C26 = 118.0(4), C1-C2-C31-C32 = -92.4(4), C1-C2-C31-C36 = 87.1(4), C1-C2-C41-C42 = 105.0(4), C1-C2-C41-C46 = -82.2(4).

The olefin plane is distorted, especially at the aryl ring that holds the O2 atom, as shown in the side view (Figure 3.30, bottom left). This ring is quite lifted in order to bridge between the Al1 and Al2 atoms and become a part of the "Al₃O₃" crown ring. The aryl ring with the O1 atom is, on the other hand, pushed down from the olefin plane to take the equatorial position of the Al1 atom.

The structure of the trinuclear aluminum complex **38** is not analogous to the R₃Al adducts of parent ligand **2**. Verkerk confirmed that a similar reaction with **2** leads to an "Al₄O₄" eight-membered crown ring (Figure 3.31)¹ as mentioned in Chapter 1. In the case of ligand **7**, the *ortho*-propyl groups evidently limit the coordination site sterically, leaving insufficient room to accommodate four [AlEt₂] groups.

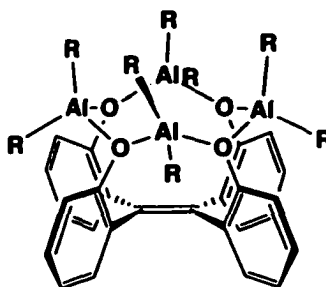


Figure 3.31. Verkerk's eight-membered Al crown complex (R = Me or Et).

As mentioned, complexes **37** and **38** showed common ¹H NMR spectroscopic features in C₆D₆. The four aryl rings are all different, as expected from the unsymmetrical crystal structure. Three out of five alkyl groups (Me or Et) are quite downfield compared to Me₃Al (-0.36 ppm in C₆D₆), and the other two are quite upfield. Figure 3.32 shows the ¹H NMR spectrum of the complex **37**.

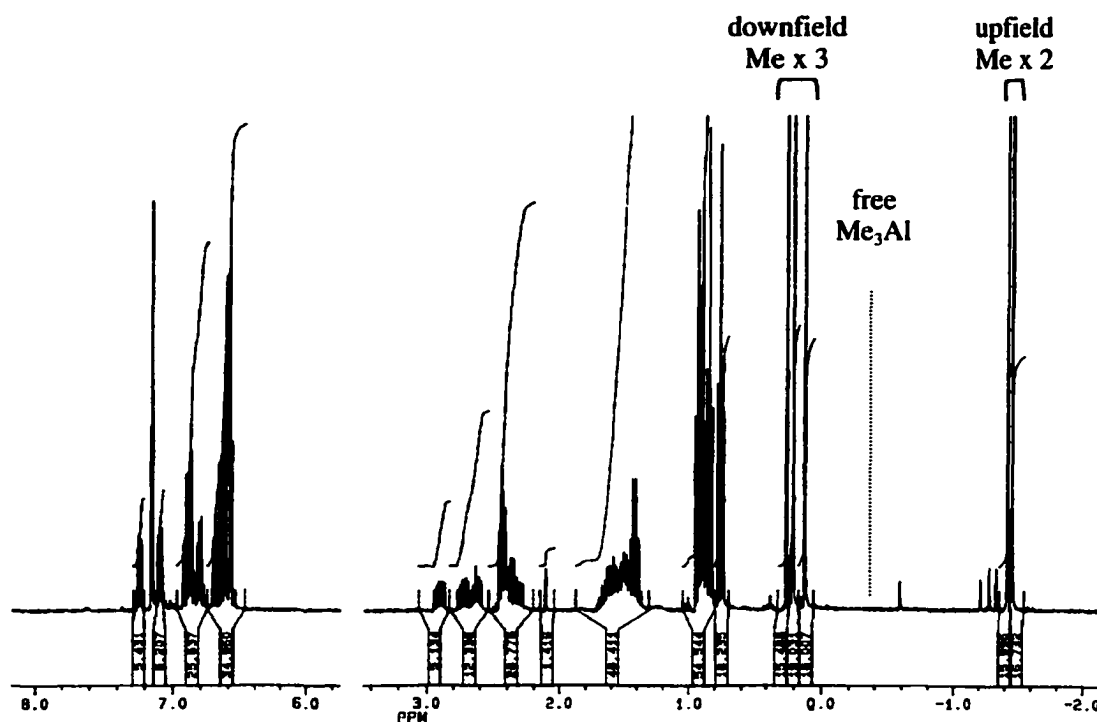


Figure 3.32. ^1H NMR spectrum of **37** (C_6D_6). The position of free Me_3Al (-0.36 ppm) is indicated with the dotted line.

The three downfield methyl groups are assigned to the three axial groups, and the two upfield ones to the equatorial methyl groups. Among the metal complexes from ligand **7**, the position "above" the olefin plane generally receives a deshielding effect from the aryl rings, while the positions in between neighboring aryl rings are shielded. Although this case is the first example of a complex having an equatorial group between *vicinal* pair of aryl rings, the effect seems similar to the cases where a substituent is between a *geminal* pair of aryl rings.

Complex **38** is totally inert toward one equivalent of TiCl_4 in C_6D_6 . The ArO groups are presumably too stable and kinetically protected by the tight bindings to the Al atoms in the crown structure to attack the titanium atom.

ii) Adduct of Et_2AlCl . The reaction of ligand **7** and four equivalents of Et_2AlCl is not as straightforward as the R_3Al case. The ^1H NMR spectrum of the product(s), labeled **C**,

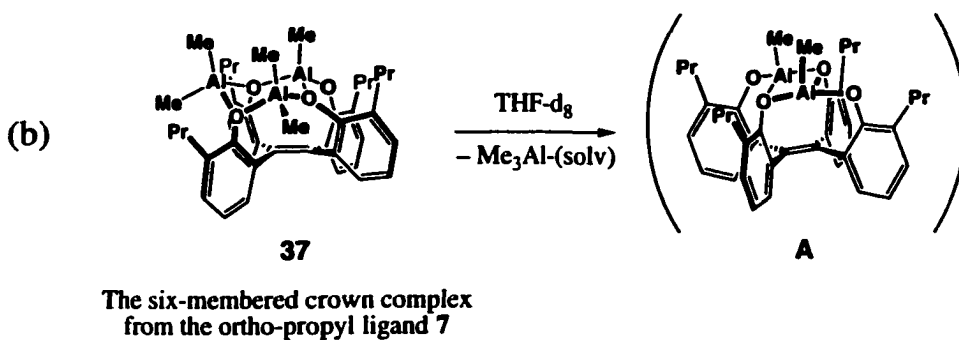
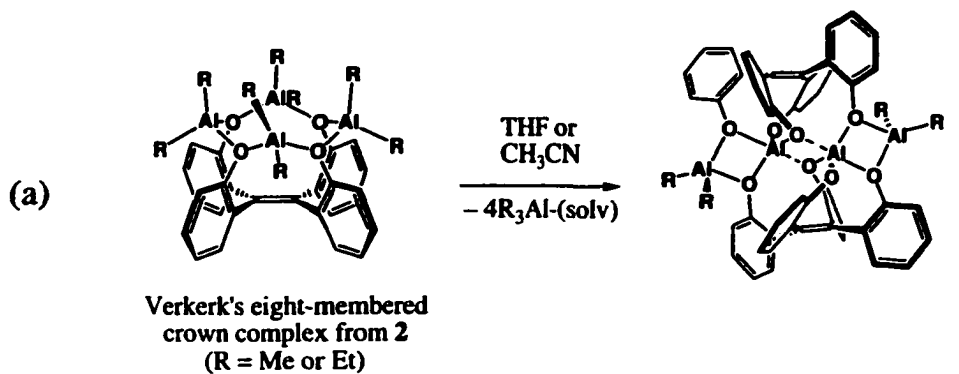
in C_6D_6 is quite complicated. The elemental analysis of the crystallized product, however, proposes the formula of $[C_{38}H_{40}O_4Al_4Et_4Cl_4]$ ($C_{38}H_{40}O_4 = [7 - 4H]$), consistent with an adduct of **7** and four equivalents of Et_2AlCl . Unlike what occurs in the R_3Al case, all the four equivalents of the aluminum reagent seem reacted to provide "AlEtCl" fragments to the product. The complicated 1H NMR spectrum in C_6D_6 suggests that it is a mixture of many different species.

ii) **Adduct of $EtAlCl_2$.** Unlike the adducts in the previous two cases, the adduct between ligand **7** and four equivalents of $EtAlCl_2$ is insoluble in toluene or other non-coordinating hydrocarbon solvents. The precipitated product, labeled **F**, gives the C/H and Cl elemental analysis results quite close to the calculated values of the four-equivalent adduct $[C_{38}H_{40}O_4Al_4Cl_8]$ ($C_{38}H_{40}O_4 = [7 - 4H]$).

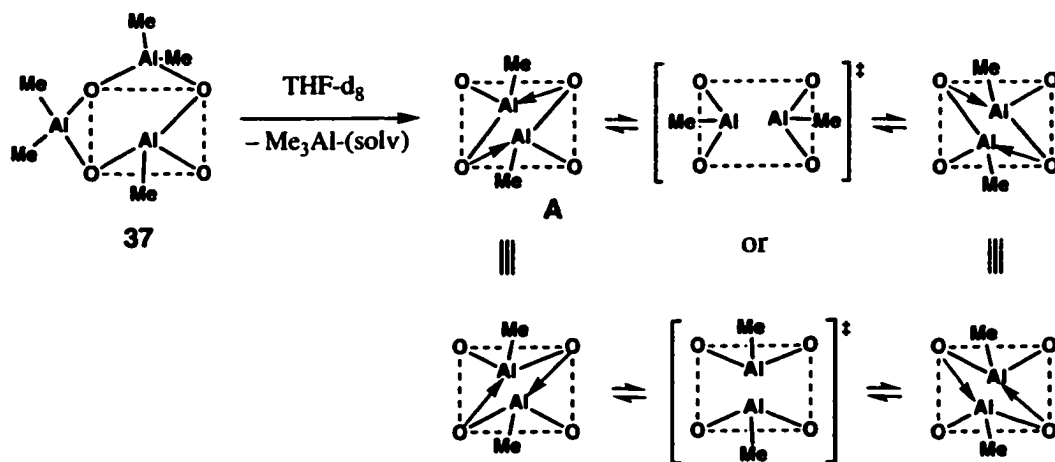
3.1.3.B. Chemical Behavior in THF Medium

i) **From Al_3R_5 Complexes (37/38).** No reaction occurs when two equivalents of THF are added to **38** in C_6D_6 medium. The aluminum-crown complex is apparently inert to a small amount of THF in solution. The same result was reported by Verkerk for the eight-membered aluminum crown complex of parent ligand **2**.¹

However, Verkerk reported that dissolving in THF or acetonitrile medium converts the eight-membered crown aluminum complex of parent ligand **2** into the sandwich-type complex, as shown in **Scheme 3.15-a** (see also Chapter 1 and reference 1). The collapsed complex has only two equivalents of aluminum and two alkyl groups per ligand. The coordinating solvents apparently "leach out" three equivalents of R_3Al from each tetranuclear crown system.



Scheme 3.15. "Collapsing" of the aluminum crown complexes upon leaching out R₃Al by a coordinating solvent with the proposed structure of **A**.



Scheme 3.16. Proposed equilibrium between two enantiomers of **A**.

Dissolving the six-membered crown complex **37** (Scheme 3.15-b) in THF- d_8 results in a new compound, labeled **A**. The ^1H NMR spectrum of the THF- d_8 solution shows a completely symmetrical ligand framework (i.e., all aryl rings are equivalent) with diastereotopic propyl methylene protons and two identical methyl groups per ligand. The methyl signal appears at -0.35 ppm, more downfield than that of free Me_3Al (-0.94 ppm in THF- d_8). The solution also shows one equivalent of liberated Me_3Al (as fully coordinated by solvent THF- d_8).

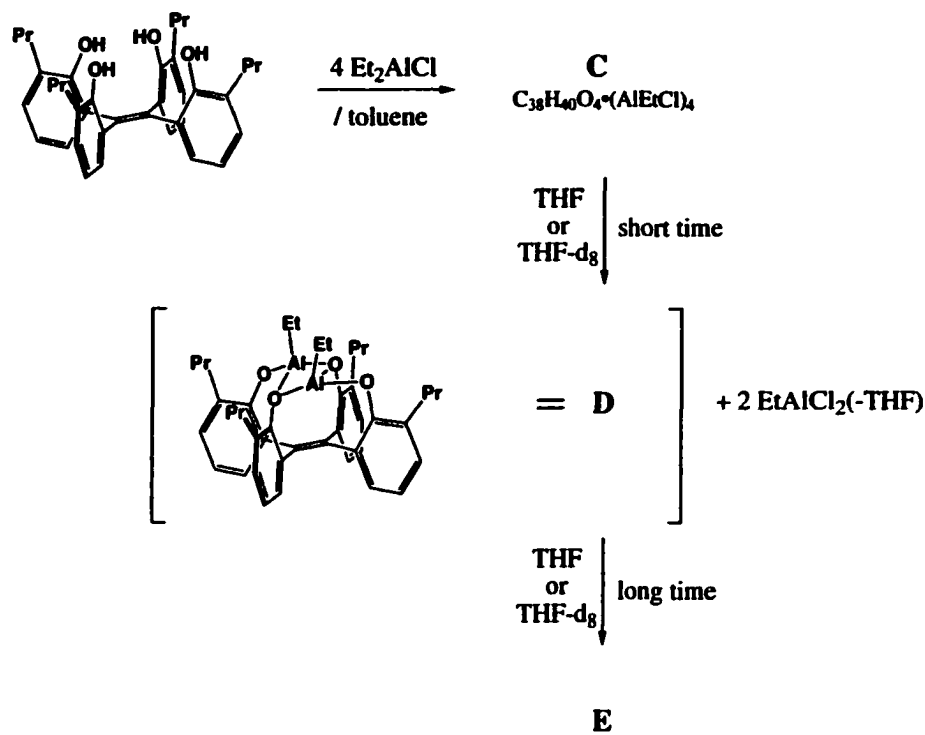
Although X-ray crystallography or other decisive structural determination is unavailable, the structure of **A** is proposed as shown in Scheme 3.15-b. The dinuclear aluminum structure is consistent with the ^1H NMR spectroscopic features: the stoichiometry of methyl groups and the deshielding effect caused by the axial methyl positions. To meet the ligand symmetry requirement, the equilibration of two enantiomers is proposed (Scheme 3.16). The exchange must be fast to make all the aryl rings equivalent. Note that the connectivity of the bottom-right Al atom in **37** (in Scheme 3.16) is retained in the structure of **A**. The ^1H NMR spectrum hardly changes when the temperature is lowered to -60 °C: the equilibration is still fast for the NMR time-scale at this temperature.

ii) From $\text{Al}_4\text{Et}_4\text{Cl}_4$ Adduct **C**. The THF- d_8 solution of **C**, the $\text{Al}_4\text{Et}_4\text{Cl}_4$ adduct or adduct mixture also shows a new compound, labeled **D**, immediately after preparation of the solution. This product **D** has very similar spectroscopic features to those of the previously discussed **A**. The ligand framework is all-symmetric with two identical ethyl groups, which are downfield-shifted. The chemical shifts of the ligand protons are very similar to those of **A**. The solution also shows two equivalents of liberated EtAlCl_2 . It is considered that the structure of **D** is analogous to that of **A**, differing only by the alkyl group (Et vs. Me).

The same mixture, however, showed a completely different spectrum after remaining in THF- d_8 overnight. The resulting ^1H NMR spectrum in THF- d_8 was not simple, possibly showing a mixture. The resulting species or mixture is labeled **E**. Scheme 3.17 tentatively summarizes the alteration of **C** to **D**, and then to **E**.

The product **E**, the result of prolonged exposure to THF medium, was separately prepared by dissolving **C** in normal THF and stirring overnight. After removal of volatiles, the C_6D_6 solution of the resulting product (**E**) showed a ligand framework with σ -symmetry with one downfield THF molecule and two different ethyl groups: one

upfield and one in the normal region; also observed were liberated aluminum reagents. The THF- d_8 solution of the same product showed the same ^1H NMR spectrum that matched the first THF- d_8 dissolution experiment after being kept overnight.



Scheme 3.17. The THF-driven transformation of **C** into **D** and **E**.

Figure 3.33 provides the proposed structure of **E**, which meets the ^1H NMR spectroscopic features in C_6D_6 . The ligand framework in the proposed structure can be σ -symmetric if the full and dative Al-O bonds between the central and terminal Al atoms exchange rapidly in solution. The two ethyl groups, one upfield and one in normal region, are assigned to the equatorial and axial ethyl groups on the terminal Al atom. A similar terminal "AlEt₂" fragment was found in other crystallographically characterized complexes **41** and **42** (*vide infra*, section 3.2.1.A). Finally, the THF coordinated on the central Al atom can account for the highly downfield-shifted THF signals.

The different spectroscopic appearance of **E** when dissolved in THF- d_8 is partly explained by the desymmetrization induced by excess THF- d_8 . Unlike what occurs in C_6D_6 , the presence of excess THF- d_8 causes both central and terminal Al atoms to coordinate THF- d_8 , breaking the dative Al-O bonds completely: this process makes the

ligand framework unsymmetrical (**Figure 3.33-b**). The spectrum, however, is more complicated than was expected for a single unsymmetrical species. The reversible transformation from monomeric to dimeric species upon further alkyl reagent abstraction is suggested in **Figure 3.33-b**, as one possible explanation to account for the complicated ^1H NMR spectrum in THF-d_8 .

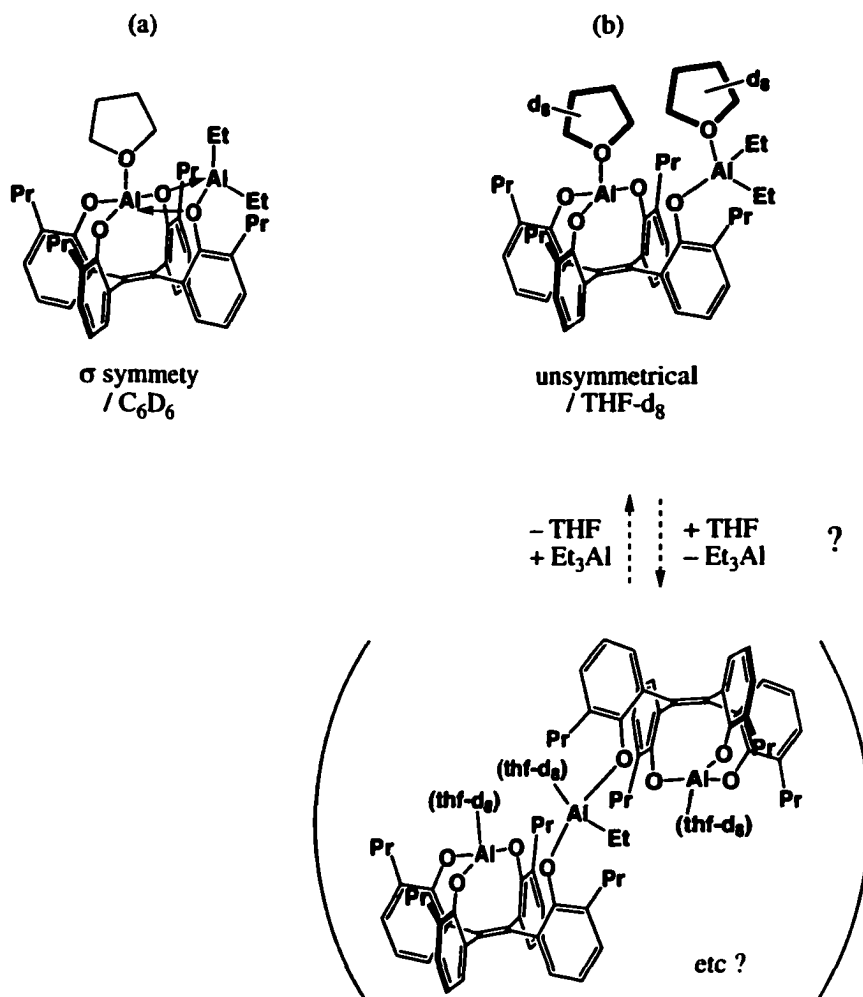


Figure 3.33. Proposed structure of **E** and different appearance in (a) C_6D_6 and (b) THF-d_8 .

Crystallization of **E** was, unfortunately, unsuccessful. It tends to oil out from hydrocarbon medium (e.g., pentane). However, the similarly-obtained complex **39** gave a crystal structure that supports the suggested structure of **E** (*vide infra*).

It is interesting that the dinuclear *diethyl* complex **D** further disproportionates to the pseudo- σ -symmetry species **E** in a THF medium, while the *dimethyl* complex **A** remains unchanged. The disproportionation of **D** is probably promoted by the larger size of the ethyl group. If the suggested structures of **A** and **D** are correct, the two alkyl groups are both at the axial positions on an Al_2O_2 four-membered ring, probably close enough to each other to experience repulsive van der Waals interactions. Having larger ethyl groups on these positions makes **D** less stable.

The conversion of **D** to **E** upon prolonged exposure to THF- d_8 is, in other words, the intramolecular disproportionation of two " $(\text{ArO})_2\text{EtAl}$ " units into " $(\text{ArO})_3\text{Al}(\text{thf})$ " and " $(\text{ArO})\text{Et}_2\text{Al}(\text{thf})$ " units. The above-mentioned steric repulsion is probably the driving force.

In summary, we have observed a stepwise alteration from the initial four-equivalent Et_2AlCl adduct **C** to **D**, and then to **E**. The transformation of **C** to **D** is driven by aluminum scavenging by the coordinating solvent, and **D** to **E** is an intramolecular disproportionation of the aluminum centers.

iii) From Al_4Cl_8 Adduct **F.** The THF-driven conversion of **F**, the Al_4Cl_8 adduct, partly parallels that of the ethyl-group containing analogue **C**. Because no ethyl groups are in **F**, the information provided by ^1H NMR studies was more limited. Nevertheless, the symmetry change in the ligand framework was often quite informative, allowing for a reasonable analogy to be made the previously discussed aluminum complexes.

The toluene-insoluble product **F** is well-soluble in THF- d_8 . Immediately after the solution was prepared, the ^1H NMR spectrum showed two species: one a σ -symmetry compound **G**, with all sharp signals; the other **H**, consisting of rather broad signals. The ratio of **G** : **H** was ca. 1.5~2 : 1, made imprecise by the broadness and overlapping of signals.

After being kept overnight in THF- d_8 , the ^1H NMR spectra no longer showed either **G** or **H**, but gives a complicated spectrum, seemingly a mixture of at least two compounds. The product after prolonged exposure to THF- d_8 is labeled **39**. The same product **39** obtained from separate reaction^c showed the same complicated ^1H NMR

^c The compound **39** was separately prepared by mixing the ligand **7** and four equivalents of EtAlCl_2 in THF and crystallized from toluene-pentane.

spectrum in THF- d_8 , but showed a σ -symmetry ligand framework in C_6D_6 , accompanied by one deshielded coordinating THF molecule (α proton signal at 4.25 ppm). The solid-state structure was obtained as shown in **Figure 3.34** (for detailed data, see Appendix A-12).

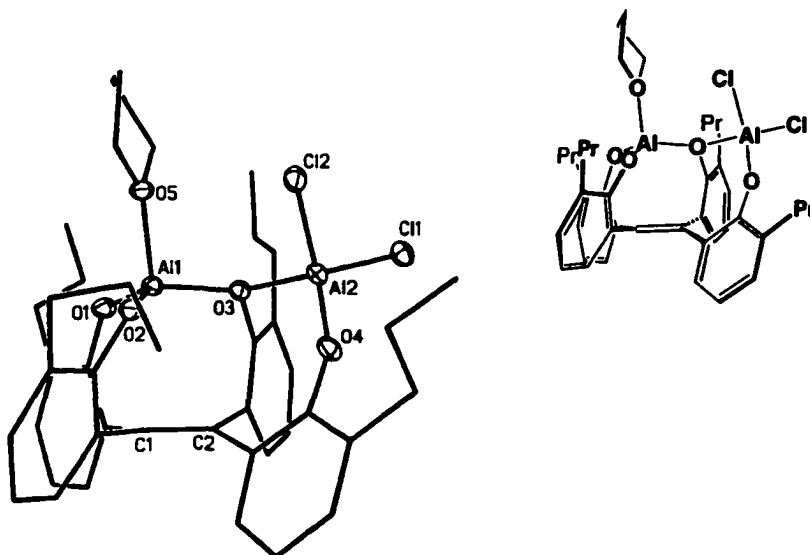
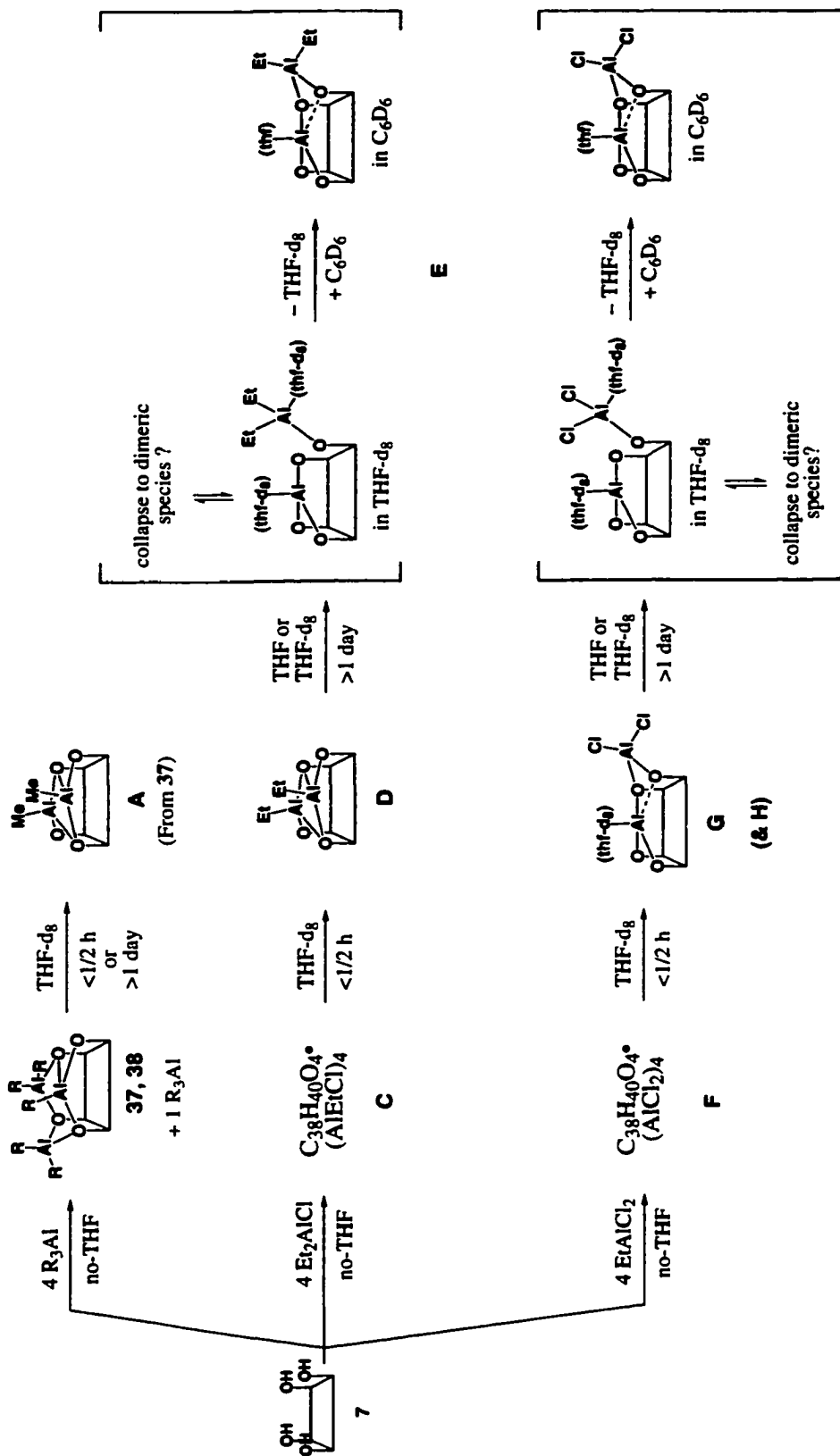


Figure 3.34. X-ray crystallographic structure of **39**.

The crystal structure of **39** provided very useful information relevant to the THF-driven alteration of aluminum complexes derived from ligand **7**. This information further supports the proposed structure of the similarly-produced diethyl analogue **E** (**Figure 3.33**) described in the previous section. The resemblance between the 1H NMR spectroscopic features of **39** and the diethyl analog **E** in C_6D_6 also complements the analogy. Although the crystal structure of **39** is not symmetrical, it may equilibrate the Al-O bonds between the central and the terminal Al atoms in solution, becoming pseudo- σ -symmetrical, as observed in the 1H NMR spectrum in C_6D_6 .

Scheme 3.18 summarizes all the THF-driven aluminum abstraction chemistry of **37**, **C** and **F** with proposed structures.



Scheme 3.18. Summary of the aluminum complexes and the chemical behavior in THF medium.

The structure of **G**, the result of brief THF- d_8 exposure of **F**, is suggested to be the same as **39**, to meet the σ -symmetry requirement. This assignment is based on the hypothesis that either **F** does *not* go through a symmetrical intermediate prior to intramolecular disproportionation (as observed for **37** or **C**), or it does so too quickly to be observed spectroscopically. To meet this hypothesis, the coordination of THF to desymmetrize **G** must be slow, although it may be unusual in the presence of excess THF- d_8 . However, after being kept in THF- d_8 overnight, the desymmetrization (and possible further conversion as also suggested for **E**) is complete in THF. Upon removal of THF and re-dissolution in C_6D_6 , the complex reverts to the σ -symmetric **39**.

The identity of **H**, which showed broad signals observed together with the complex assigned as **G**, remains unclear. Possibly, it is an intermediate stage between the all-symmetric stage (analogous to **D** or **A**) and **G**, or between **G** and the desymmetrized stage (**39**) by a second coordination of THF to the terminal Al atom.

3.1.3.C. Conclusion of the Aluminum Chemistry of Ligand 7

The aluminum complexes derived from ligand **7** showed various connectivity patterns, depending on the degree of exposure to excess THF. The reactivity toward THF is clearly affected by the different groups bonded to aluminum (methyl, ethyl, ethyl/chloro or chloro).

3.1.4. Na Complex

Although sodium is not a metal typically used for heterogeneous Ziegler-Natta catalysts, the sodium salts of various phenoxide ligands were prepared and studied as precatalysts for ethene polymerization, mainly to compare with the corresponding magnesium salts (Chapter 5). In this section, the solid-state structure of the sodium salt of ligand **7** (**40**) is examined to compare the coordination tendency of this "+1" cation with that of previously discussed titanium(IV), aluminum(III) or magnesium(II) ions.

The sodium salt **40** was prepared by adding four equivalents of NaH to the phenolic ligand **7** in toluene. The resulting solution was slightly cloudy and pale yellow-green. After filtration and concentration of the solution, crystallization from toluene-hexane gave light yellow-green crystals. The elemental analysis (C/H) gave the best match to the formula of $C_{38}H_{40}O_4 \cdot Na_4 \cdot (toluene)_{1/2}$ ($C_{38}H_{40}O_4 = [7 - 4H]$).

The X-ray crystal structure of complex **40** revealed the trimeric structure in the solid state (Figure 3.35). The Na/O cluster consists of a "Na₆O₆" inner core and three "Na₂O₂" outer subunits. Each sodium atom in the inner core assumes a trigonal pyramidal coordination geometry. The inner core consists of two nearly eclipsed "Na₃O₃" hexagons.

Each sodium atom in the outer subunits also has pseudo-trigonal bipyramidal geometry,^d receiving η⁶-coordination from one aryl ring at one of the equatorial positions. The second equatorial position and the axial position are occupied by phenolato oxygens. The remaining equatorial ligand is not quite resolved. Some electron density was found at the position, but it was not possible to identify this molecule due to the weak data set (4444 observed data out of 13097 total unique data; R₁ = 15.7 %). This molecule is suspected, however, to be a toluene molecule, since it is the only possibility included in the crystal of **40** available for coordination.

In each ligand unit (Figure 3.36), two diagonal oxygen atoms are used in the inner core, and the other two in the outer subunits. The aryl rings attached to the oxygen atoms constructing the inner core are the same rings that are used for η⁶-coordination to the outer-sodium atoms.

The ¹H NMR spectrum of **40** in C₆D₆ shows broad peaks at room temperature: three in the aromatic region and three in the propyl region. The integrals are consistent with the ligand framework. The broadness suggests that the trimer structure of the sodium salt **40** is not retained in solution phase. Upon dissolution, the solvent toluene or benzene molecules must aid in the dissociation of the trimer into monomers by occupying the vacant coordination sites, and/or assisting a different kind of association of monomers.

^d Selected interatomic angles (deg): O1-Na1-O1' = 87.4, O1-Na-[centroid of C21-C26] = 100.8, O1'-Na-[centroid of C21-C26] = 120.6; O3-Na6-O5 = 86.4, O3-Na6-[centroid of C61-C66] = 122.0, O5-Na6-[centroid of C61-C66] = 102.6; O3-Na5-O5 = 86.6, O3-Na5-[centroid of C41-C46] = 102.7, O5-Na5-[centroid of C41-C46] = 119.6.

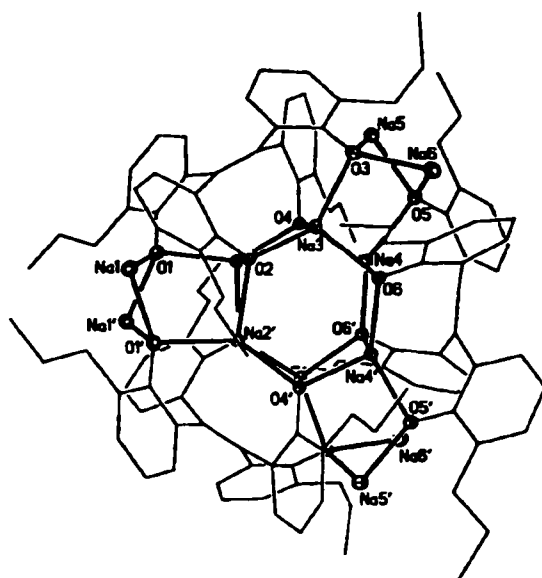


Figure 3.35. X-ray crystallographic structure of the sodium salt **40**.

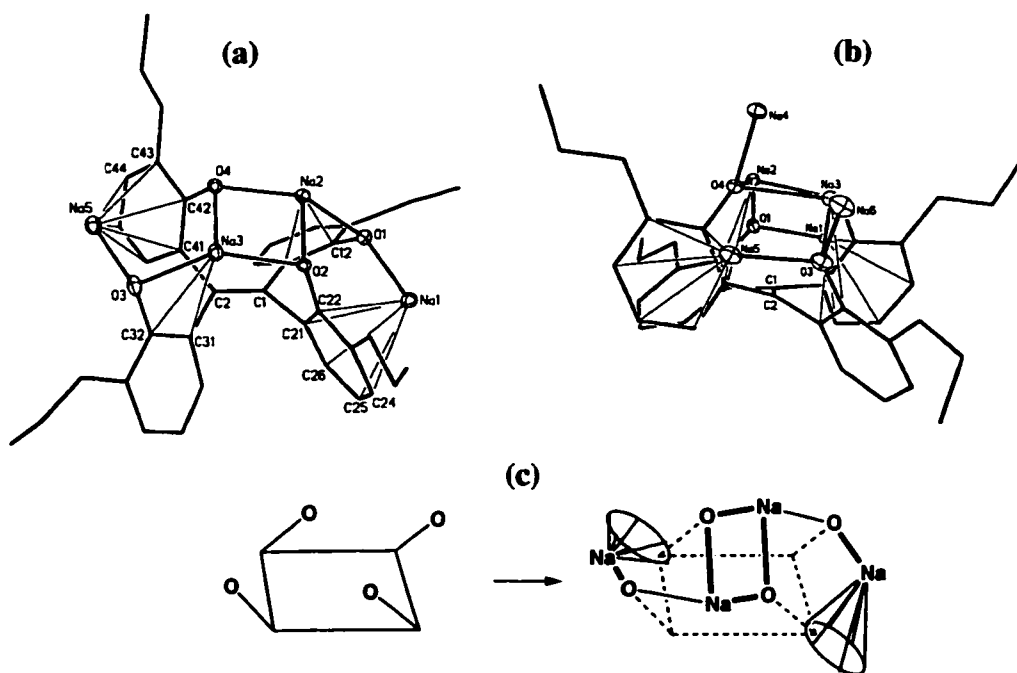


Figure 3.36. (a) View of a monomer in the trimer **40**. (b) Different angle view to show the distortion of the olefin plane. (c) Simplified illustration of the monomer.

The solid-state structure and the solution behavior of the Na(I) complex **40** showed the compound's relatively weak tendency to form a monomeric discrete complex, compared to the previously discussed Mg(II), Al(III), and Ti(IV) cases. The critical factor is the number of metal centers per ligand. Each ligand must hold four Na(I) centers, each of which has certain coordination demands. This leads to intermolecular interactions because a single ligand cannot provide sufficient Lewis bases to satisfy all four metal centers, even with the π -electrons of the aryl rings.

3.2. Hetero-polymetallic Complexes

Because it is believed that the active sites of classic heterogeneous Ziegler-Natta catalysts are not monometallic but consist of titanium (IV or III) bridging to other metals such as aluminum (III) and/or magnesium (II) atoms (Chapter 2), the construction of characterizable hetero-polymetallic complexes was a major goal of this research, as potential models for such heterogeneous systems. As discussed, ligand **7** was found to give various polymetallic complexes consisting of one kind of metal atom. The next goal was to build hetero-polymetallic species on the ligand system.

Several Mg/Al, Mg/Ti and Al/Ti hetero-polymetallic complexes were obtained and structurally characterized. All of them were prepared using the tri-magnesium complex **25** as a starting material. The essential feature of **25** that made these syntheses possible is that it has formally two kinds of magnesium phenoxides (Figure 3.37). The central magnesium is a magnesium diaryloxyde, and the terminal ones are aryloxymagnesium chlorides. The nucleophilicity of all the four aryloxides is equivalent due to the dative coordination, but the magnesium metals' lability toward replacement by other metals is different. Apparently, the terminal magnesium atom is more labile to replacement by other metals than is the central magnesium atom.

The general strategy for building a hetero-polymetallic complex from **25** was, therefore, the addition of one or two equivalents of R_mMX_n (m and n are integers; R is any alkyl group; $m + n =$ the metal's oxidation number; M is a metal other than magnesium; and X is halide or any leaving group). To avoid overreaction, i.e., complete replacement of all magnesium atoms, the number of X groups on the reagent (n) must be limited. In relation to the composition of classic heterogeneous Ziegler-Natta catalysts, the metal in our investigation (M) is limited to Al(III) and Ti(IV).

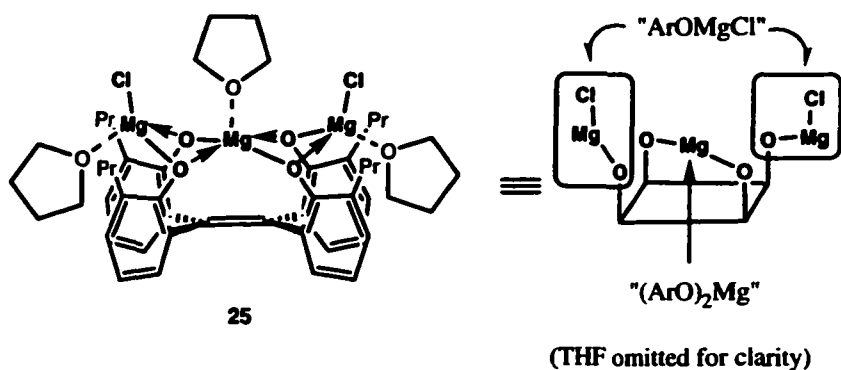


Figure 3.37. "Formal" description of **25**.

The balance between the nucleophilicity of the magnesium aryloxides and reactivity of metal chloride reagent is important, especially when an excess number of potential leaving groups X are present on the reagent. To replace the terminal magnesium (chloride) of **25** while keeping the central magnesium atom on the ligand, the metal halide should be reactive enough for the former but inert toward the latter. There are not many options, however, because the reactivity of metal halides toward an aryloxymagnesium is largely determined by the metal, which we limited to titanium and aluminum only. Titanium halides were found to be so reactive that no excess halide could be on the reagent. Aluminum reagents, on the other hand, showed a great selectivity toward the terminal aryloxymagnesium centers.

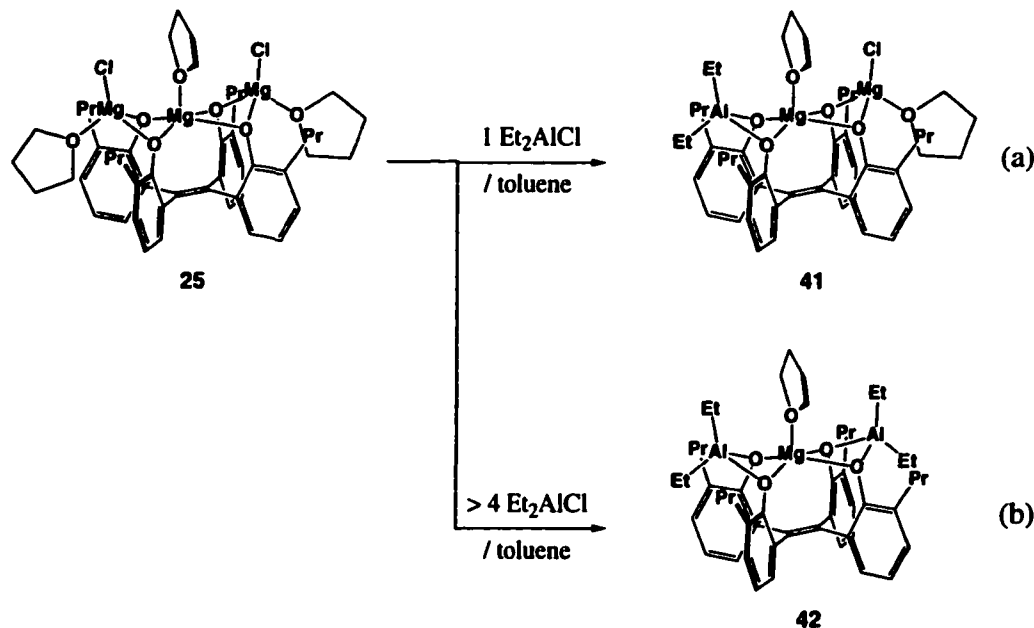
In the following sections, the syntheses and structural/spectroscopic features of Mg/Al, Mg/Ti, and Al/Ti hetero-polymetallic complexes will be discussed. Most of these complexes were evaluated for ethylene polymerization activity; these results will be discussed in Chapter 5.

3.2.1. Mg/Al Complexes

Addition of one or two equivalents of Et_2AlCl or EtAlCl_2 to the tri-magnesium complex **25** resulted in the formation of discrete Mg/Al hetero-polymetallic complexes. The difference in lability between the central and terminal Mg atoms is exploited in this reactivity.

3.2.1.A. Addition of Et_2AlCl to **25**

The addition of one equivalent of Et_2AlCl to **25** in toluene successfully produced the Al-Mg-Mg complex **41** within 3 hours (Scheme 3.19-a). The clean formation of **41** in these conditions demonstrates the large reactivity difference between the terminal and central magnesium atoms in **25**. Furthermore, the lability of the first and second terminal magnesium atoms is also apparently quite different, because no overreaction product (i.e., formation of **42**) was observed.



Scheme 3.19. The preparation of (a) the Al-Mg-Mg complex **41** and (b) the Al-Mg-Al complex **42**.

The difference between the first and the second replacement of the terminal Mg atoms was further confirmed when two equivalents of Et_2AlCl were added to **25** in toluene. When the reaction was worked-up within 15 minutes, ^1H NMR spectroscopy of the product showed a mixture of **41** and **42** in a 2.8 : 1 ratio. When a reaction under the same conditions was continued for 3 days, the ratio was reversed to 1 : 2.5, but the reaction remained incomplete. This observation suggests that the second replacement is not only slow but also never goes to completion with only two equivalents of the reagent. The addition of four equivalents of Et_2AlCl was required to obtain the Al-Mg-Al complex **42** exclusively (Scheme 3.19-b). The reason for the slow second addition is probably that the second equivalent of Et_2AlCl is deactivated by the byproduct $\text{MgCl}_2(\text{thf})$ formed in the first replacement, by either THF or chloride transfer to the Al atom. If this conclusion were true, four equivalents of the reagent would be required to complete the second aluminum addition to compensate for the consumption of reagent by the $\text{MgCl}_2(\text{thf})$, of which two equivalents would be formed.

When four equivalents of Et_2AlCl were used, the formation of **42** was indeed complete within a day. An NMR-tube reaction under the same conditions in C_6D_6 confirmed that no **41** remained after 5 hours of reaction, but instead of clean **42**, a mixture of **42** and other unknown species was observed. The same reaction mixture, after 28 hours, showed **42** exclusively. The identity of the intermediate species was not clear.

The structures of **41** and **42** were confirmed by X-ray crystallography, as shown in Figures 3.38 and 3.39 (with selected data in Table 3.4, for details see Appendices A-13 and A-14). Both structures are quite similar to the starting material **25**: tri-nuclear connectivity on the "all-up" ligand platform, aryl rings nearly perpendicular to the olefin plane, and even the positioning of the four propyl groups in the crystal.

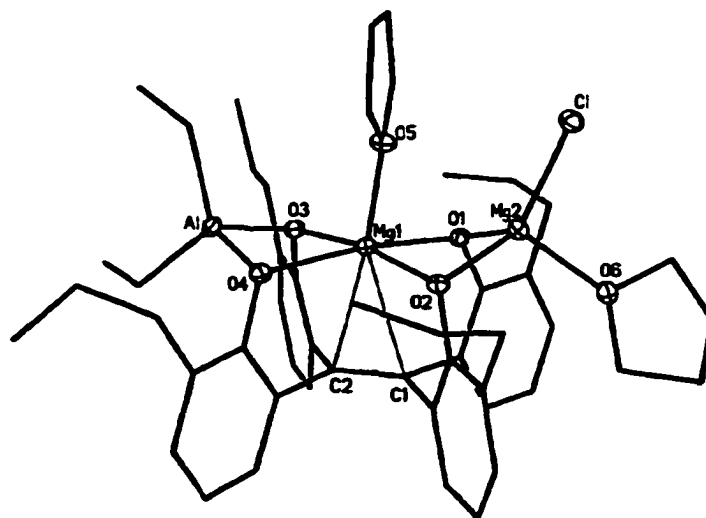


Figure 3.38. X-ray crystallographic structure of **41**.

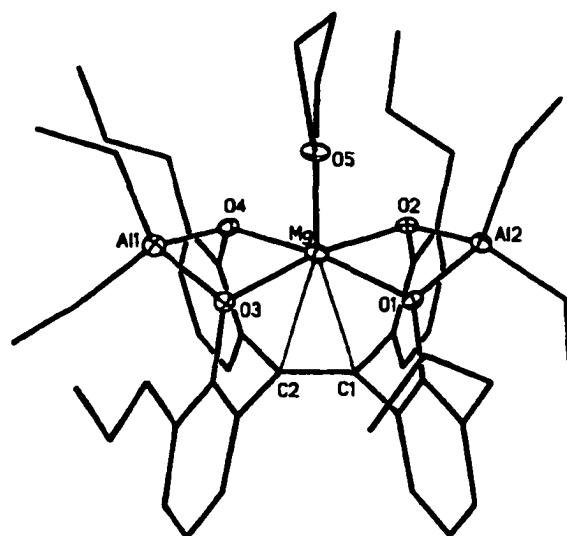


Figure 3.39. X-ray crystallographic structure of **42**.

Table 3.4. Selected distances and angles for **41** and **42**.

	Complex 41	Complex 42
R_1	0.0602	0.0647
wR_2	0.1557	0.1754
C1 – C2 (Å)	1.345(3)	1.344(4)
Bond length related to Mg(1) (Mg_{central})		
Mg1 – C1 (C_{olefin}) (Å)	2.631(3)	2.636(3)
Mg1 – C2 (C_{olefin}) (Å)	2.593(3)	2.638(3)
Mg(1) – O5 ($O_{\text{thf-central}}$) (Å)	2.027(2)	2.001(2)
Mg(1) – O1 (Å)	2.0402(18)	2.066(2)
Mg(1) – O2 (Å)	2.0453(19)	2.076(2)
Mg(1) – O3 (Å)	2.0943(19)	2.070(2)
Mg(1) – O4 (Å)	2.094(2)	2.061(2)
Bond length related to Mg2 (Mg_{terminal})		
Mg2 – O1 (Å)	1.9918(18)	-
Mg2 – O2 (Å)	1.9732(19)	-
Mg2 – O6 ($O_{\text{thf-terminal}}$) (Å)	2.019(2)	-
Mg2 – Cl (Å)	2.2694(12)	-
Bond length related to Al(1) or Al2		
Al(1) – O3 (Å)	1.848(2)	1.852(2)
Al(1) – O4 (Å)	1.852(2)	1.860(2)
Al(1) – C3 (Å)	1.961(3)	1.954(4)
Al(1) – C5 (Å)	1.970(4)	1.970(3)
Al2 – O1 (Å)	-	1.856(2)
Al2 – O2 (Å)	-	1.847(2)
Al2 – C7 (Å)	-	1.951(3)
Al2 – C9 (Å)	-	1.966(3)
Interatomic angles (deg)		
Cl – Mg2 – O1	125.27(7)	-
Cl – Mg2 – O2	124.83(7)	-
Cl – Mg2 – O6	100.57(7)	-
O1 – Mg2 – O2	85.30(8)	-
O1 – Mg2 – O6	108.15(9)	-
O2 – Mg2 – O6	112.36(9)	-

Table 3.4. (continued)

	Complex 41	Complex 42
Interatomic Angles (cont'd)		
O3 – Al1 – O4	88.21(9)	87.52(9)
O3 – Al1 – C3	113.40(13)	114.81(13)
O3 – Al1 – C4	110.79(17)	112.60(13)
O4 – Al1 – C3	111.95(13)	110.56(13)
O4 – Al1 – C5	108.16(16)	113.94(14)
C3 – Al1 – C5	119.80(15)	114.56(16)
O1 – Al1 – O2	-	87.52(9)
O1 – Al1 – C7	-	113.86(13)
O1 – Al1 – C9	-	113.85(12)
O2 – Al1 – C7	-	119.46(13)
O2 – Al1 – C9	-	111.66(12)
C7 – Al1 – C9	-	109.22(15)
Olefin Plane Torsional Angles (deg)		
C11–C1–C2–C31	0.7(4)	0.1(4)
C11–C1–C2–C41	176.6(2)	-177.5(3)
C21–C1–C2–C31	-177.3(2)	177.7(2)
C21–C1–C2–C41	-1.5(4)	0.1(4)
Ring Torsion against Olefin Plane (deg)		
C2–C1–C11–C12	85.7(3)	-92.3(4)
C2–C1–C11–C16	-96.3(3)	84.4(4)
C2–C1–C21–C22	-92.5(3)	91.8(3)
C2–C1–C21–C26	90.4(3)	-83.8(4)
C1–C2–C31–C32	-96.1(3)	90.8(4)
C1–C2–C31–C36	82.6(3)	-86.1(4)
C1–C2–C41–C42	93.1(3)	-92.6(4)
C1–C2–C41–C46	-83.4(3)	85.7(4)

The distance of the metal atoms from the O_4 plane is considerably different for a terminal "MgCl(thf)" group (in **25** and **41**) and a terminal "AlEt₂" group (in **41** and **42**): the former is more "uplifted" than the latter. The side view projections of **25**, **41** and **42** reveal the degree of uplifting (Figure 3.40). Table 3.5 presents the distance of each metal atom from the O_4 plane. The degree of uplifting most likely differs because of the different equatorial groups: the THF molecule on a terminal Mg atom requires more space than the ethyl group does on the Al atoms.

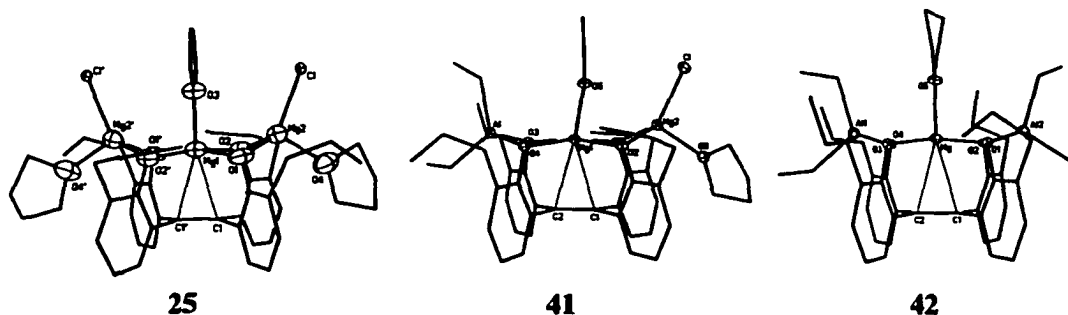


Figure 3.40. Comparison of the side views of **25**, **41** and **42** and selected torsion angles.

Table 3.5. Distance from the least-squares plane of O1-O2-O1'-O2' or O1-O2-O3-O4 (Å): comparison of **25**, **41** and **42**.

	25	41	42
Mg _{central}	0.154	0.170	0.182
Mg _{terminal}	0.600	0.672	-
Al _{terminal}	-	0.389	0.381 (av.)

The symmetry and composition of the Al-Mg-Mg complex **41** and the Al-Mg-Al complex **42** are all consistent with the ¹H NMR spectroscopic features (C₆D₆). The basic features, such as the diastereotopicity of the propyl groups and the relative order of chemical shifts of the aromatic protons, are all analogous to those of the tri-magnesium complex **25**.

The axial and equatorial ethyl groups are clearly differentiated, as are the central and terminal THF molecules, based on the assignments for the tri-magnesium complex **25**. **Table 3.6** summarizes the chemical shifts of the THF and ethyl groups in **41** and **42** (with the data of **25** as a reference). These chemical shifts clearly indicate the positions of these groups (i.e., central/terminal or axial/equatorial).

Table 3.6. Chemical shifts (^1H NMR) of the coordinating THF and ethyl groups on Mg or Al atoms in complexes **41** and **42**. Chemical shifts of **25**, free THF and free Et_3Al are given for comparison.

	THF _{central}		THF _{terminal}		Ethyl (axial)		Ethyl (equatorial)	
	α	β	α	β	CH_3	CH_2	CH_3	CH_2
25	4.92	2.34	2.86	0.76	-	-	-	-
41	4.87 / 4.50	2.24 / 1.83	2.69	0.64	1.51	0.30	0.62	-0.62
42	4.37	1.74	-	-	1.39	0.18	0.47	-0.90
THF	3.57(α)		1.40 (β)					
Et_3Al					1.10 (CH_3)		0.27 (CH_2)	

The α - and β - methylene protons of the central THF of complex **41** are each quite split, by ~ 0.4 ppm, reflecting the different terminal groups. These peaks are broadened, possibly from slow rotation of the central THF molecule. Although the THF should mainly remain at the sterically least-demanding angle, as in the crystal structure (i.e., C51-O5-C54 plane twisted by 90° from the C=C bond), the space between the terminal " $\text{MgCl}(\text{thf})$ " or " AlEt_2 " groups seems wide enough to allow for the rotation.

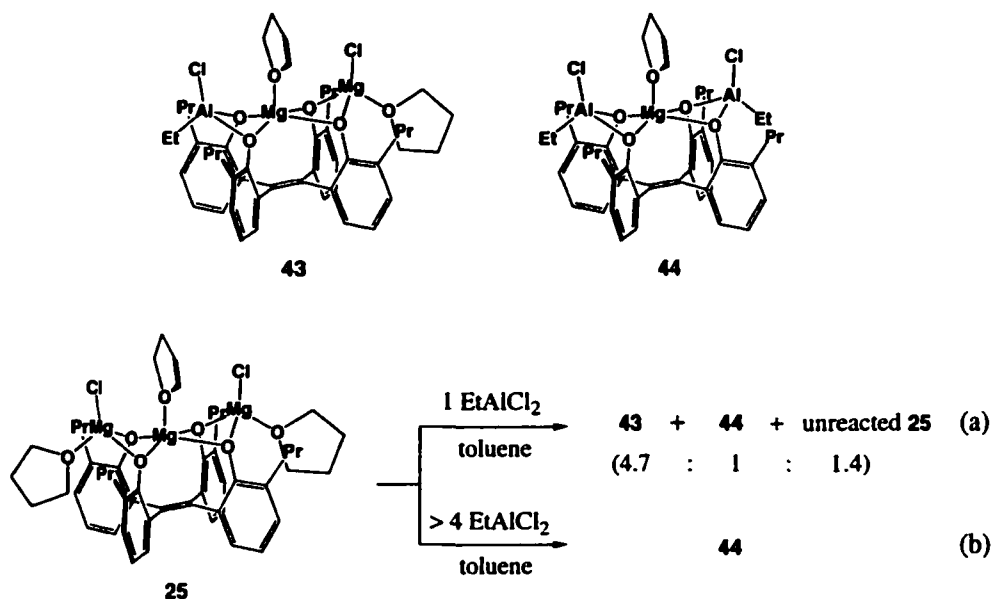
The central THF molecule in the Al-Mg-Al complex **42** is still downfield-shifted (α - CH_2 : 4.37 ppm), but not as downfield as that in **25** (α - CH_2 : 4.92 ppm). This difference is probably because the terminal " AlEt_2 " groups are not as electron-withdrawing as the " $\text{MgCl}(\text{thf})$ " groups. The central THF molecule of **41** has the chemical shifts^c inbetween those determined for **25** and **42**.

^c Average of the two split signals.

The highly upfield ethyl group(s) in **41** or **42** are assigned to the equatorial ethyl group(s), because they are in the shielding region of the neighboring aryl rings. The other set of ethyl signals appears in the normal region, and is therefore assigned to the axial ethyl group(s). Apparently, the anisotropic effects on these positions exerted by the ligand aryl rings are minimal.

3.2.1.B. Addition of EtAlCl₂ to **25**

The addition of EtAlCl₂, instead of Et₂AlCl, to **25** resulted in the analogous products **43** and **44** (Scheme 3.20). However, the one-equivalent adduct **43** did not form cleanly, even when one equivalent of the reagent was used. In an NMR-tube reaction, the 1 : 1 mixture of **25** and EtAlCl₂ produced a mixture of **25** : **43** : **44** one day after the solution was prepared. Apparently, the first and the second replacements of the terminal Mg units are less differentiated for the more electrophilic reagent.



Scheme 3.20. Formation of **43** and **44**.

The use of at least four equivalents of EtAlCl₂ was required to produce the double substitution product **44** free from any incomplete adduct **43**. This finding is analogous to that in the case of **42**, as discussed in the previous section. The scale-up of this reaction

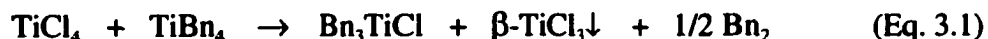
and all attempts at crystallization, however, resulted in the formation of less pure material for unknown reasons. Complexes **43** and **44**, therefore, were not isolated.

The structures of **43** and **44** were identified from ^1H NMR spectroscopy alone. The ethyl groups in the terminal "AlEtCl" units were determined to be equatorially positioned, based on the upfield chemical shift of the ethyl signals. Other spectroscopic features were similar to those observed for **41** and **42**.

3.2.2. Mg/Ti Complex

Our first attempt to produce a Mg/Ti complex was by mixing the tri-magnesium complex **25** with one or two equivalents of TiCl_4 , but these reactions failed. As discussed earlier, in Section 3.1.2.A., titanium-only complexes (such as **32** and **30a**) were formed, leaving no magnesium in the complex. Aryloxymagnesium groups are simply so nucleophilic toward titanium chlorides that the substitution does not end until no Ti-Cl or no aryloxymagnesium moieties remain in the system. To leave a magnesium atom in the ligand framework, the number of chlorides (leaving groups) on the titanium reagent must be restricted.

Tribenzyltitanium chloride (Bn_3TiCl) was therefore selected as a titanium reagent with a minimal number of leaving groups. Syntheses and physical properties of Bn_4Ti , Bn_4Zr and mixed halogen/alkoxy derivatives were reported several decades ago by Zucchini and others.¹⁰ Because thermal instability in solution was reported for Bn_3TiCl , it was prepared *in situ* using the conditions reported by Ivanova et al. They reported that a 1 : 1 mixture of TiCl_4 and TiBn_4 in toluene at $-50\text{ }^\circ\text{C}$ results in a mixture of Bn_3TiCl , $\beta\text{-TiCl}_3$ (precipitate) and bibenzyl (Eq. 3.1).¹¹ Apparently, the reaction mixture does not produce the conproportionation product Bn_2TiCl_2 , but instead leads to irreversible reduction of titanium(IV) to titanium (III).



Assuming that the precipitated $\beta\text{-TiCl}_3$ is innocent in solution phase reactions, we used this method to produce Bn_3TiCl in situ. After mixing TiBn_4 and TiCl_4 for 10 to 20 minutes in toluene at $-50\text{ }^\circ\text{C}$, the toluene solution of **25** (" Bn_3TiCl " : **25** = 1 : 1) was

slowly added to the reagent mixture. After work-up and crystallization, a clean Mg/Ti dinuclear complex **45** (Figure 3.41) was obtained in a 45% yield. X-ray crystallography of the compound established the dimeric structure (for details see Appendix A-15).

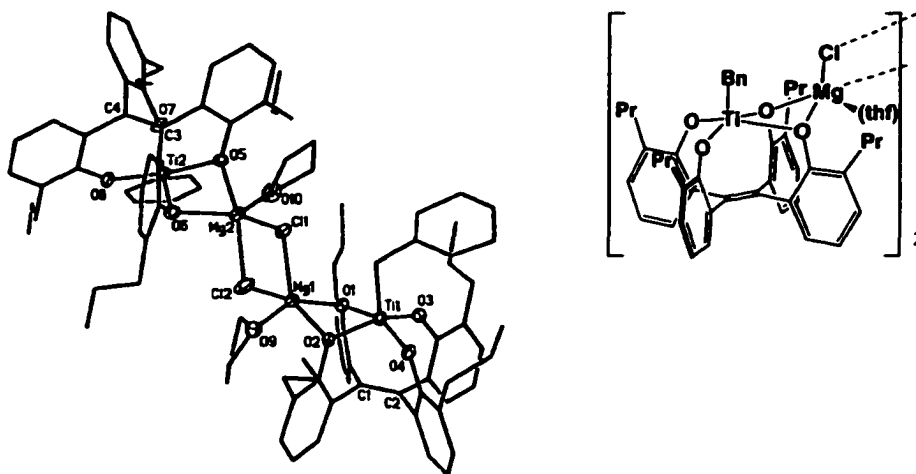


Figure 3.41. X-ray crystallographic structure of **45**.

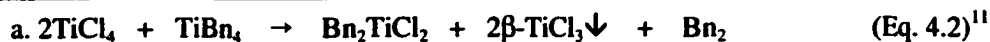
The structure of **45** was not what had been anticipated from the reaction. The titanium atom was expected to lose a chloride and gain aryloxyde(s), but the three benzyl groups were not expected to be replaced. However, one equivalent of "Bn₂Mg(thf)" apparently leaves the system, resulting in **45**.

Nevertheless, **45** is the first and the only Mg/Ti hetero-polymetallic complex obtained for ligand system **7** or any other of the preorganized ligands developed and used in this research. Unfortunately, complex **45** does not polymerize ethene upon standard activation (Chapter 5).

Several combinations of stoichiometry and different benzyltitanium chlorides Bn_xTiX_{4-x} were tested, but none but the above-mentioned case was successful. The examined cases are summarized in Table 3.7. The condition that led to the preparation of **45** is entry 1. In entries 5 and 6, the trinuclear dibenzyl magnesium complex **29** (see section 4.1.1.B) was used as a starting material. The intention was either to exchange the benzyl groups in **29** with the chlorides of TiCl₄ *in situ* to generate Bn₂TiCl₂. The product mixture from entry 6 contained sharp signals on ¹H NMR spectroscopy, but it was a mixture. The broad signals observed in most other cases could be due to the reduced Ti(III) species.

Table 3.7. Attempts to prepare Mg/Ti hetero-polymetallic species.

Entry	(A) Starting material	(B) Reagent	(C) (A) : (B)	(D) Comments ^d	(E) Product description (¹ H NMR/C ₆ D ₆)
1	25	"Bn ₃ TiCl"	1 : 1	(small scale only)	45 (>45 %)
2	25	"Bn ₃ TiCl"	1 : 2		broad signals
3	25	"Bn ₂ TiCl ₂ " ^a	1 : 1		broad signals
4	25	"Bn ₃ TiBr" ^b	1 : 1		starting material & broad signals
5	29 ^c	TiCl ₄	1 : 1 ^c	r.t. /toluene	broad signals
6	29 ^c	TiCl ₄	1 : 1 ^c	-50°C → r.t. /THF, toluene	broad and sharp



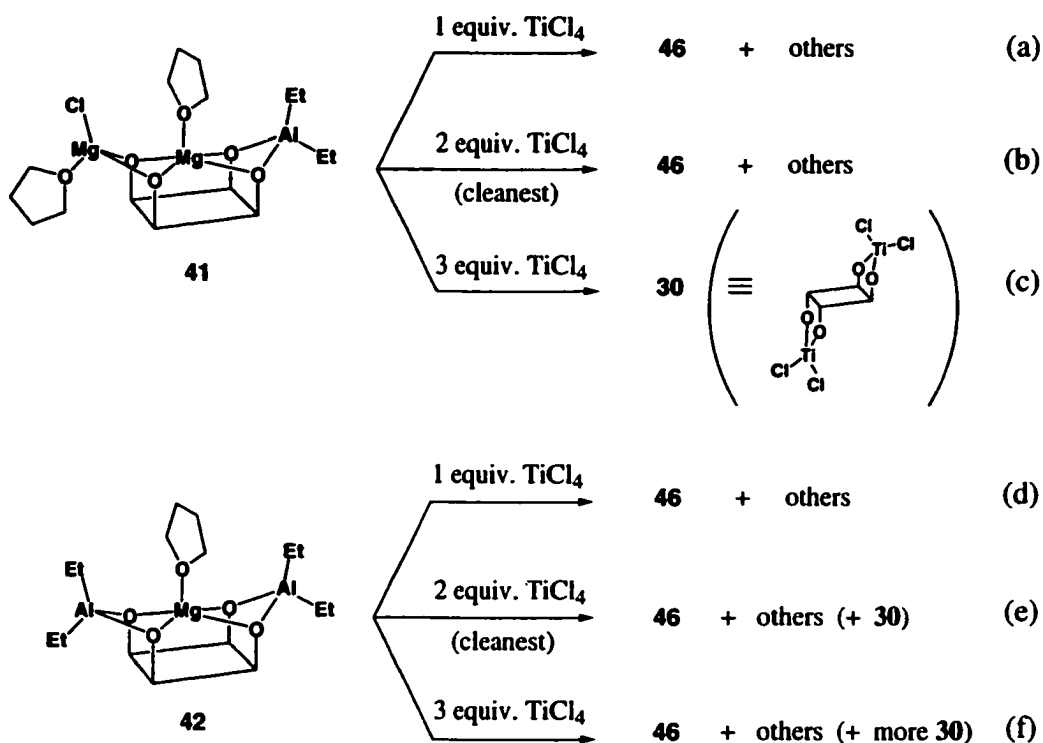
c. The complex **29** is the trinuclear magnesium complex with two benzyl groups on the terminal magnesium atoms. The formula of **29** is only approximate, thus the (A) : (B) ratio is not very precise.

d. Unless otherwise stated, the reagent was prepared in situ at -50°C in toluene medium and the starting material was added at this temperature.

3.2.3. Al/Ti Complex

Preliminary attempts to construct Al/Mg/Ti or Al/Ti hetero-polymetallic complexes were made by adding TiCl₄ to the Al/Mg complexes **41** and **42**. Replacing one Mg atom in the Al-Mg-Mg complex **41** with one Ti atom was anticipated to produce a Al/Mg/Ti system. If the second Mg atom is too easily replaced, the reaction could still produce an Al/Ti hetero-polymetallic species. Replacing an Mg atom in the Al-Mg-Al complex **42** with a Ti atom could also result in an Al-Ti species.

The following NMR-tube experiments were performed in C_6D_6 to find good reaction conditions. The starting material, either **41** or **42**, was mixed with one, two or three equivalents of $TiCl_4$ and the products were examined by 1H NMR spectroscopy after being kept overnight. **Scheme 3.21** summarizes the combinations of starting material, stoichiometry and the results from those reactions.



Scheme 3.21. Formation of **46** from **41** and **42**.

Both starting materials, **41** and **42**, resulted in a product mixture containing common compound(s), labeled **46**, in all runs, except for condition (c). These results suggest that starting with the Al-Mg-Mg complex **41** did not help to maintain Mg in the complex. Under condition (c), not only the Mg but also the Al was completely replaced by titanium to form the familiar geminal up/down Ti complex **30**.

The X-ray diffractable crystals of the common product **46** were obtained from reaction using the condition (e) at larger scale. This reaction still did not produce a single

compound: the ^1H NMR spectrum of the crystals showed a mixture of two major products (1 : 1) and other minor species. One of the major products was **46**, and the other was labeled **46'**, which was not as dominant as **46** in the preliminary NMR-tube reactions.

The crystal structure shown in **Figure 3.42** was obtained for these crystals by X-ray crystallographic analysis from a weak data set (see Appendix A-16). However, it was not clear which of the two species, **46** or **46'**, gave the crystal structure. The two chlorides in the crystal structure are only tentatively assigned: one or both could be ethyl groups. Given the weak data, it was not possible to determine the identity of these groups based on the observed electron density.

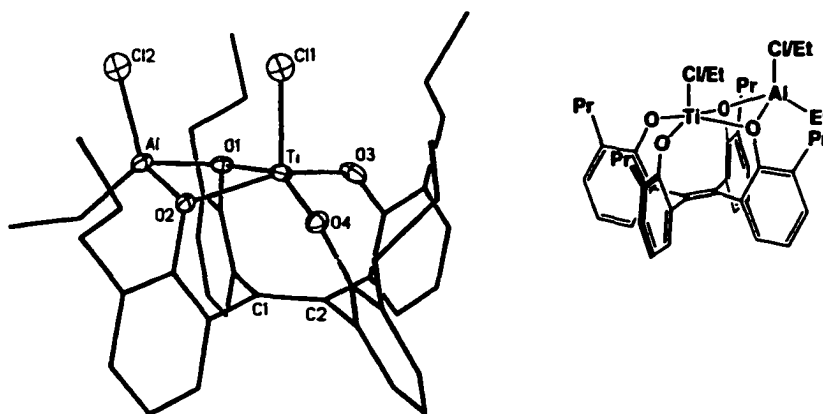


Figure 3.42. X-ray crystallographic structure of **46** or **46'**. Cl 1 and Cl 2 may be either chlorides or ethyl groups.

Spectroscopically, both **46** and **46'** seem like σ -symmetry species, based on the number of propyl- γ - CH_3 groups and integration. The σ symmetry of **46'** is further assured by the aromatic signals; the aromatic signals of **46** remain ambiguous due to the severe overlapping. Both species seem to have one upfield ethyl group, which is considered to be equatorial at the terminal aluminum atom. From the features described above, both are reasonable candidates for the X-ray structure determination (**Figure 3.46**). From the similarities in spectroscopic features, the difference between **46** and **46'** may only be in the two ambiguous axial groups, which can be either Cl or Et.

Although many ambiguities remain, **46** (or **46'**) is the only crystallographically characterized Al-Ti hetero-polymetallic complex obtained from ligand **7**. Its crystal structure is quite similar to that of the Mg-Ti complex **45** discussed in the previous section. A Ti atom occupies the central position in both cases. Apparently, the central position, surrounded by all four oxygen donors, is a preferred place for the strongly oxophilic Ti(IV).

3.2.4. Other Attempts to Prepare Hetero-polymetallic Complexes

The addition of a range of aluminum reagents to a preformed titanium complex was investigated as an alternative route to Al/Ti hetero-polymetallic systems. The reaction between the "vicinal up/down" di-TiCl₂(thf) complex **31** and two equivalents of Me₃Al gave a fairly clean product that had σ or *i* symmetry (i.e., two kinds of aryl rings were found). This reaction could not be reproduced, however, at least partly because the starting material may have converted to the "geminal up/down" di-TiCl₂(thf) complex **30a**. Use of **33a**, the bromo-analogue of **30a**, did not give a clean product either; therefore, the symmetrical product observed from **31** was probably specific to the vicinal isomer. This approach was not further investigated due to the unavailability of the clean starting material (either **31** or **30a**).

3.3. Conclusion

In this chapter, the capability of ligand **7** to form well-defined polymetallic complexes with Mg, Ti and Al atoms, both homo- and hetero-metallic, has been demonstrated. Various bonding patterns were observed for different metal atoms and different combinations. The coordination variability arose from differences in metal's oxidation number and the number of available coordination sites.

Most of the Ti-only complexes formed two-up/two-down structures (**30/30a**, **33/33a**, **34** and **35**), with a "geminal up/down" dinuclear structure as the most favorable coordination pattern. The ligand was also capable of forming a "vicinal up/down" structure (**31**). The energy difference between "geminal up/down" and "vicinal up/down"

structures can be quite small when appropriate coordinating groups are attached, as seen in the equilibrium between **30a** and **31**.

The magnesium-only complexes (**25** to **29**) formed rigid trinuclear structures on an "all-up" oxo-surface-like ligand platform. The same structure was maintained in the mixed Mg-Al derivatives (**41** to **44**).

Some aluminum-only complexes showed a six-membered crown structure (**37** and **38**), but exposure of the aluminum complexes (**37**, **C** and **F**) to excess THF resulted in a variety of different connectivities, a few of which were structurally confirmed. One of these structurally confirmed aluminum complexes (**39**) retained a dinuclear structure on an "all-up" ligand platform.

Dinuclear "all-up" structures were also found in Ti-containing hetero-bimetallic complexes (the Mg-Ti complex **45** and the Al-Ti complex **46/46'**). In both cases, the titanium assumed the central position, surrounded by four oxygen donors, while the other metal atom took the terminal position.

In the construction of all hetero-polymetallic species, the balance in oxophilicity of the second-introduced metal and the nucleophilicity of the ArO[M] fragment from the first-introduced metal was important to avoid substituting all the first-contained metals with the incoming metals.

The basic knowledge of the reactivity and connectivity patterns imposed by these metals on ligand **7** provides a strong foundation for further exploration of coordination chemistry and catalysis using this newly developed ligand system.

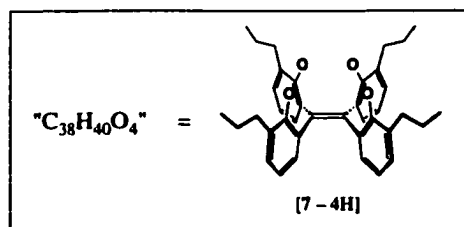
3.4. Experimental

Instruments and Analysis: See the experimental Section of Chapter 1 (1.4).

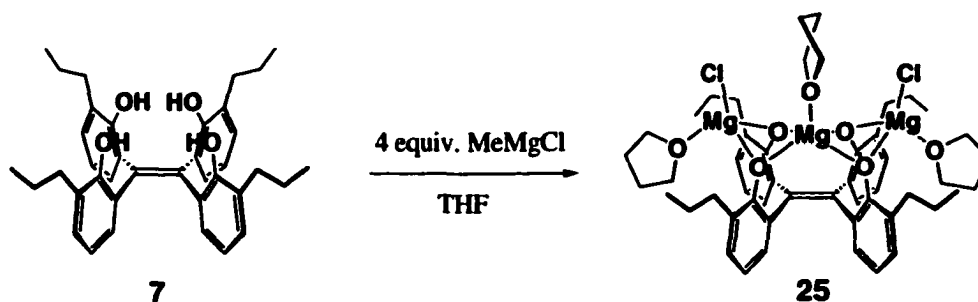
General: All experiments were carried out in the drybox (see Chapter 1, Section 1.4). Most reactions were performed in 3-dram vials with plastic caps, stirred with a magnetic rod on a stirrer. "NMR-tube reaction" in this thesis means a reaction performed in an NMR tube in a deuterated solvent, mainly to monitor the reaction progress. Celite used for filtration was Celite 545, dried in a vacuum oven (50 °C) at least three days. "Celite-packed pipette" was prepared by packing the dried Celite in a disposable pipette plugged with small piece of glass wool, and used for small-scale filtration. A glass-fritted funnel packed with the dried Celite was used for larger scale filtration. All glassware was dried at 120 °C in an oven at least overnight right before bringing into the drybox.

Materials: Tetrakis(2-hydroxy-3-propylphenyl)ethene (**7**) was prepared as described in Chapter 1. THF, diethylether (ether), benzene, pentane and hexanes were purified by distillation from sodium benzophenone ketyl, degassed and stored in the drybox. Toluene was distilled over potassium, degassed and stored in the drybox. "Ethereal-solvent-free Toluene" was kept in a separate bottle, opened only when the drybox atmosphere was free of ethereal solvent vapor. All Grignard reagents, TiCl₄ and alkylaluminum reagents (Me₃Al, Et₃Al, Et₂AlCl and EtAlCl₂) were purchased from commercial vendors, stored in the drybox and used as is. The alkylaluminum reagents (kept in the original Aldrich Sure/Pac™ metal cylinder) and TiCl₄ were used under no-THF/ether atmosphere. TiBr₄ was purified by triturating with hexanes to remove hydrate and other impurities, then recrystallizing from hexanes. NaH was freed from the oil in the drybox by washing with hexanes, dried under reduced pressure and kept in the drybox. Bn₂Mg•OEt₂,¹³ CpTiCl₃,¹⁴ and TiBn₄¹⁵ were prepared by following published procedures.

Note: "C₃₈H₄₀O₄" represents the fully deprotonated ligand **7** i.e. [**7** - 4H] (see the figure). The conformation is not restricted to the "all-up" form.



25: C₃₈H₄₀O₄•Mg₃•Cl₂•(thf)₃

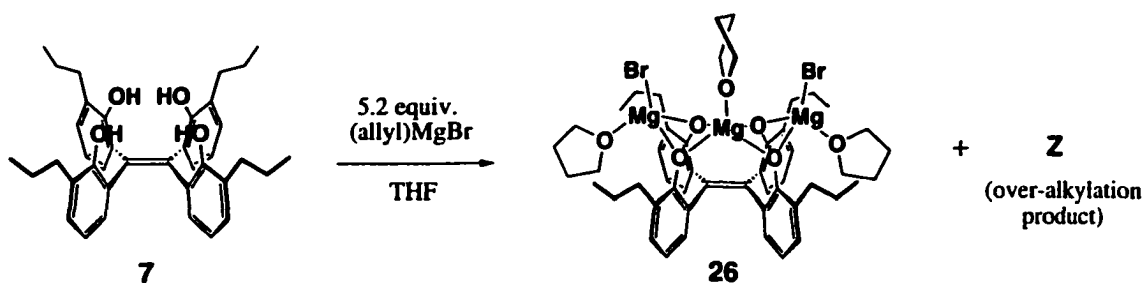


To a solution of tetrakis(2-hydroxy-3-propylphenyl)ethene (**7**) (1.8432 g, 3.2637 mmol) in 8 mL of THF was added a solution of CH₃MgCl/THF (3M, 4.4 mL, 13 mmol) dropwise at room temperature. A vigorous reaction with gas evolution, followed by the formation of white precipitate was observed. The color became yellow initially, but turned nearly colorless again upon completion of addition. After 10 more min. of stirring, the mixture was cooled to -30 °C overnight. The precipitated solid was collected and recrystallized to yield the desired product: Crop 1 (MW = '920.4,' 1.515 g, 38%); Crop 2 (MW = '968.7,' 0.6895 g, 22%); Crop 3 (MW = '1036,' 0.2016 g, 6%). The mother liquor and the solution portion after the first cooling were combined, evaporated and triturated with toluene, filtered, concentrated and cooled to -30 °C to yield Crop 4 (0.2378 g, 7%). Total yield was 73%. The composition of each crop based on C/H analysis¹⁶ is summarized in **Table 3.11**. The product from a separate small-scale reaction was crystallized from hot THF to give X-ray crystallographic quality crystals (**Figure 3.3**). Although the X-ray crystallography provided enough information of the connectivity of the atoms, the data was not worth further refinement because of the large residual factor (26%). ¹H NMR (360 MHz, C₆D₆): δ 7.01 (4H, dd, *J* = 7.4, 1.8 Hz), 6.76 (4H, dd, *J* = 7.4, 1.8 Hz), 6.60 (4H, t, *J* = 7.4 Hz), 4.92 (3.2H, m, central THF-α-CH₂), 2.86 (4+9.3H, overlapping terminal THF-α-CH₂ and propyl-α-CH₂), 2.50 (4H, m, propyl-α-CH₂), 2.34 (3.2H, m, central THF-β-CH₂), 1.72 (8H, m, propyl-β-CH₂H_b), 1.03 (12H, t, *J* = 7.2 Hz, propyl-β-CH₂H_b), 0.76 (9.3H, br, terminal THF-β-CH₂). ¹H NMR (360 MHz, THF-d₈): δ 6.91 (4H, dd, *J* = 7.5, 1.8 Hz), 6.69 (4H, dd, *J* = 7.5, 1.8 Hz), 6.40 (4H, t, *J* = 7.5 Hz), 3.62 (~11H, m, liberated THF), 2.71 (4H, m, α-CH₂), 2.27 (4H, m, α-CH₂), 1.78 (~11H, m, liberated THF), 1.58 (4H, m, β-CH₂), 1.43 (4H, m, β-CH₂), 0.85 (12H, t, *J* = 7.2 Hz, γ-CH₃). ¹³C NMR (125 MHz, APT, C₆D₆): δ 156.8 (4°), 148.4 (C=C), 133.0 (4°), 131.8 (4°), 129.1, 127.1 (3°), 118.2 (3°), 71.6 (thf), 70.0 (thf), 33.6, 26.1 (thf), 24.7 (thf), 23.5, 14.3. Anal. Calcd for C₃₈H₄₀O₄•Mg₃•Cl₂•(thf)₃: C, 65.21; H, 7.01; Cl, 7.70. Found: see **Table 3.11**.

Table 3.11. C/H analysis and calculated composition of Crops 1 to 4.

	C/H analysis	Composition	Formula Mass
Crop 1	C, 65.40; H, 7.03	$C_{38}H_{40}O_4 \cdot Mg_{2.97} \cdot Cl_{1.95} \cdot (thf)_{3.03}$	920.4
Crop 2	C, 65.57 (± 0.03)*; H, 7.26 (± 0.02)*.	$C_{38}H_{40}O_4 \cdot Mg_{2.96} \cdot Cl_{1.91} \cdot (thf)_{3.72}$	968.7
Crop 3	C, 61.11; H, 6.70	$C_{38}H_{40}O_4 \cdot Mg_{3.69} \cdot Cl_{3.39} \cdot (thf)_{3.67}$	1035.8
Crop 4	C, 61.75 (± 0.21)*; H, 6.94 (± 0.09)*	$C_{38}H_{40}O_4 \cdot Mg_{3.6} \cdot Cl_{3.2} \cdot (thf)_{4.1}$	1060.3

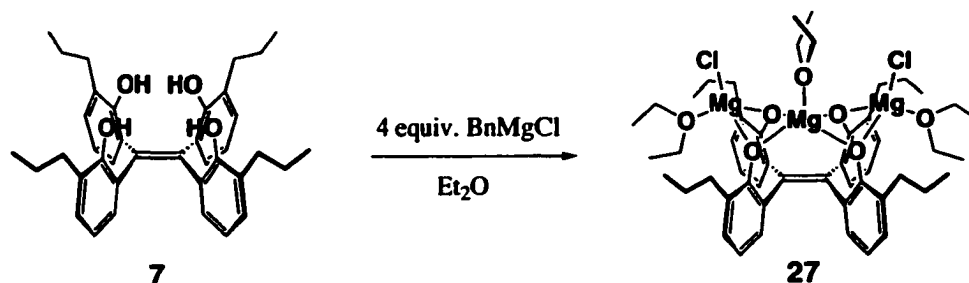
* average of two runs

26: $C_{38}H_{40}O_4 \cdot Mg_3 \cdot Br_2 \cdot (thf)_3$ 

To a solution of tetrakis(2-hydroxy-3-propylphenyl)ethene (**7**) (0.3323 g, 0.5884 mmol) in 6–7 mL of THF was added a solution of RMgCl / Et₂O (R = allyl, 1M, 3.08 mL, 3.1 mmol) dropwise at room temperature. A vigorous reaction with gas evolution was observed with color becoming yellow. The mixture became cloudy within 30 minutes. After 2 h, tiny crystals started to form. After cooling to –30 °C more crystals were formed. The isolated crystals were MgBr₂·(thf)₂, as determined by C/H and Br elemental analysis. The volatiles were removed from the mother liquor, and the residue crystallized from toluene-hexane by slow diffusion and cooling to –30 °C. The crystals obtained proved to be **26** (the yield was not recorded). More product was obtained from the mother liquors. The mother liquor after the crystallizations contained a byproduct **Z**, that was most likely the alkylated complex (Br replaced by allyl) due to the excess amount of the Grignard reagent used in the reaction. ¹H NMR (360 MHz, C₆D₆): δ 6.99 (4H, dd, *J* = 7.5, 1.8 Hz), 6.75 (4H, dd, *J* = 7.5, 1.8 Hz), 6.59 (4H, t, *J* = 7.5 Hz), 4.93 (4H, br, central THF-α-CH₂), 3.50 (31H, br, terminal THF-α-CH₂ plus free THF-α-CH₂), 2.88 (4H, m, propyl-α-CH₂), 2.50 (4H, m, propyl-α-CH₂), 2.38 central THF-β-CH₂), 1.72 (8H, m,

propyl- β -CH₂H_b), 1.20 (31H, br, terminal THF- β -CH₂ plus free THF- β -CH₂), 1.03 (12H, t, $J = 7.5$ Hz). ¹H NMR (360 MHz, THF-d₈): δ 6.91 (4H, dd, $J = 7.5, 1.8$ Hz), 6.70 (4H, dd, $J = 7.5, 1.8$ Hz), 6.42 (4H, t, $J = 7.5$ Hz), 3.62 (~16H, m, liberated THF), 2.74 (4H, m, α -CH₂), 2.29 (4H, m, α -CH_b), 1.78 (~16H, m, liberated THF), 1.58 (4H, m, β -CH₂), 1.45 (4H, m, β -CH_b), 0.86 (12H, t, $J = 7.2$ Hz, γ -CH₃). ¹³C NMR (75 MHz, APT, C₆D₆): δ 156.7 (4°), 148.4 (C=C), 133.1 (4°), 131.8 (4°), 129.1, 127.1, 118.3, 71.7 (thf), 70.4 (thf), 33.7, 26.1 (thf), 24.6 (thf), 23.6, 14.3. Anal. Calcd for C₃₈H₄₀O₄•Mg₃•Br₂•(thf)₃: C, 59.47; H, 6.39; Br, 15.83. Found: C, 56.5797 (av. of two runs, ± 0.0795); H, 6.3284 (av. of two runs, ± 0.0927); Br, 19.75 (av. of two runs, ± 0.995). Composition obtained from the C/H elemental analysis:¹⁶ C₃₈H₄₀O₄•Mg_{3.42}•Br_{2.85}•(thf)_{3.99}; MW = 1145.4. X-ray crystallography: see Appendix A-3.

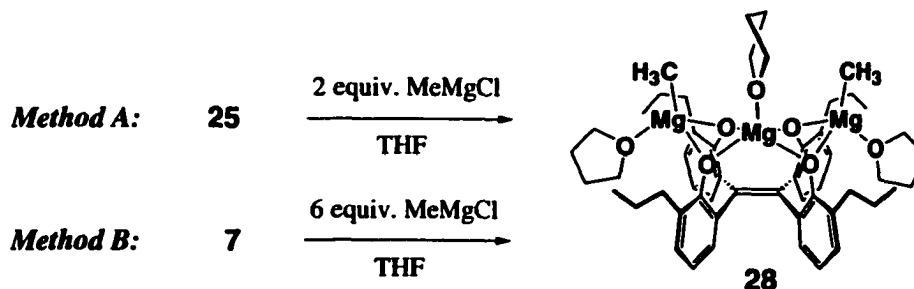
27: C₃₈H₄₀O₄•Mg₃•Cl₂•(Et₂O)₃



To a solution of tetrakis(2-hydroxy-3-propylphenyl)ethene (**7**) (0.2092 g, 0.3704 mmol) in 2 mL of Et₂O was added a solution of BnMgCl / Et₂O (1.0M, 1.48 mL, 1.48 mmol) dropwise at room temperature. A vigorous reaction with gas evolution, a color change to yellow, and subsequent precipitate formation were observed. After stirring the mixture overnight, the solids redissolved and the solution became less colored (pale yellow). The solution was passed through Celite and evaporated. The residue did not dissolve in Et₂O completely, thus it was triturated with Et₂O. After filtration and concentration, the mixture was heated slightly then cooled to r.t.; and then -30 °C. The partly powdery crystals were collected and dried under reduced pressure (0.0363 g, 11%). The mother liquor still contained considerable amount of the product but no further crystallization was performed. The ¹H NMR spectrum of the compound in THF-d₈ showed peaks of the ligand framework identical to those of C₃₈H₄₀O₄•Mg₃•Cl₂•(thf)₃ (**25**) with approximately three equivalents of liberated Et₂O; which means that these two compounds were identical except for the coordinating solvent, which was liberated and replaced

completely by THF- d_8 in both cases to show the identical spectrum. Anal. Calcd for $C_{38}H_{40}O_4 \cdot Mg_3 \cdot Cl_2 \cdot (OEt_2)_3$: C, 64.79; H, 7.61; Cl, 7.65. Found: C, 65.04; H, 7.69; Cl, 7.58.

28: $C_{38}H_{40}O_4 \cdot Mg_3 \cdot (CH_3)_2 \cdot (thf)_x$



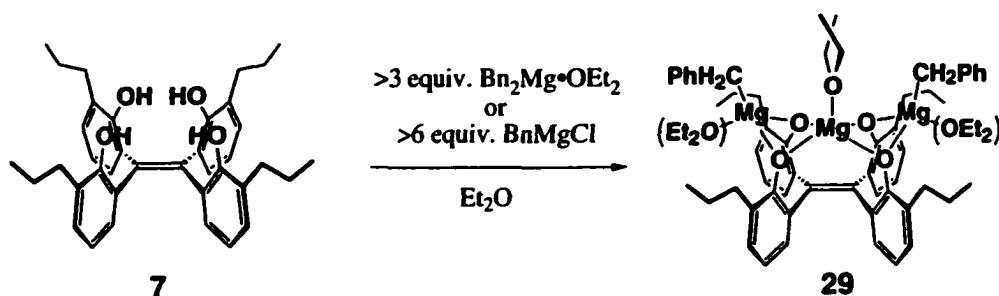
Method A. To a solution of **25** (0.0604 g, 0.0626 mmol) in 2–3 mL of THF was added the CH_3MgCl/THF (3M, 0.05 mL, 0.15 mmol) and stirred for overnight. No visible change was observed. The volatiles were removed in vacuo. The solution of the residue in THF- d_8 showed a clean single product in the 1H -NMR spectrum, together with a peak from some Grignard reagent(s). The residue was recrystallized together with the **Method B** product.

Method B. To a solution of tetrakis(2-hydroxy-3-propylphenyl)ethene (**7**) (0.0484 g, 0.0857 mmol) in 0.5 mL of THF was added CH_3MgCl/THF (3M, 0.17 mL, 0.51 mmol) dropwise at room temperature. A vigorous reaction with gas evolution was observed. The color became slightly yellow initially, but turned nearly colorless again upon completion of the addition. After stirring overnight, the volatiles were removed from the solution in vacuo. The residue showed the same signals as the **Method A** product in the 1H -NMR spectrum, except that there was little Grignard reagent signal left. The residue was triturated with toluene, filtered through Celite-packed pipette, and the volatiles were removed. The residue was combined with the product of the **Method A** and crystallized from toluene (r.t. \rightarrow -30 °C). Shiny block crystals among tiny particles were grown. X-ray crystallography confirmed the structure. The solid was removed from the mother liquor, washed with cold toluene and dried under reduced pressure. The product yield was 0.0657 g (50%) although the elemental analysis for C/H did not give a good match with the calculated values, probably due to contamination by the residual Grignard reagents and/or $MgCl_2 \cdot (thf)_x$.

1H NMR (360 MHz, THF- d_8): δ 6.90 (4H, dd, $J = 7.5, 1$ Hz), 6.66 (4H, dd, $J = 7.5, 1$ Hz), 6.36 (4H, t, $J = 7.5$ Hz), 3.62 (~29H, m, THF liberated from the complex combined with excess free THF), 2.60 (4H, m, α - CH_2), 2.29 (4H, m, α - CH_2), 1.78 (~29H, m, THF)

liberated from the complex combined with excess free THF), 1.57 (4H, m, β -CH₂), 1.47 (4H, m, β -CH₂), 0.83 (12H, t, J = 7.2 Hz, γ -CH₃), -1.53 (6H, br s, CH₃). ¹³C NMR (100 MHz, BB, THF-d₈): δ 158.3 (4°), 148.9 (4°), 132.9 (4°), 132.6 (4°), 128.9 (3°), 127.6 (3°), 117.5 (3°), 68.2 (liberated THF), 34.3, 26.4 (liberated THF), 23.9, 14.5, -17.3 (MgCH₃). Anal. Calcd for C₃₈H₄₀O₄•Mg₃•(CH₃)₂•(thf)₃: C, 70.97; H, 8.02. Found: C, 66.61; H, 7.57. X-ray crystallography: see Appendix A-4.

29: C₃₈H₄₀O₄•Mg₃•Bn₂•(OEt₂)



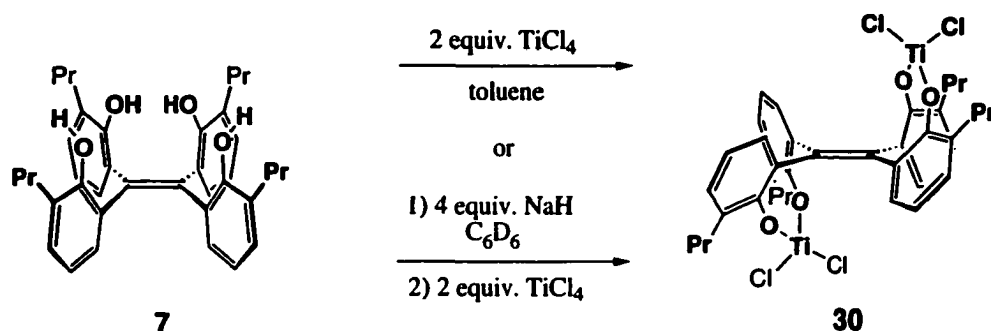
Method A. The reaction mixture and the products were kept from any contact with THF throughout the procedure. To a solution of tetrakis(2-hydroxy-3-propylphenyl)ethylene (**7**) (0.1105 g, 0.1957 mmol) in 1 mL of Et₂O was added the solution of Bn₂Mg•OEt₂ (0.2775 g, 0.7821 mmol) in 3 mL of Et₂O dropwise. A vigorous reaction with gas evolution and immediate precipitation were observed. The color became slightly yellow initially, but turned nearly colorless again upon completion of the addition. After stirring for 3 h, the cloudy mixture was cooled to -30 °C. The big crystals among a white powder were Bn₂Mg•OEt₂, and the powder was identified as the product based on ¹H-NMR spectroscopy in THF-d₈. The powder was collected and washed twice with a small amount of Et₂O using the centrifuge, then dried under reduced pressure. The washings contained only Bn₂Mg•OEt₂. The washed and dried powder (0.1040 g, 85% if the formula is as expected) showed a fairly clean product with only 1 equiv. of liberated Et₂O per ligand in the ¹H-NMR spectrum in THF-d₈. Elemental analysis for this compound is ambiguous, because the weight of the sample was changing while weighing the sample.

Method B. To a solution of tetrakis(2-hydroxy-3-propylphenyl)ethylene (**7**) (0.1810 g, 0.3205 mmol) in diethyl ether (1.5 mL) was added BnMgCl (1.0 M/ether, 2.2 mL, 2.2 mmol). Gas evolution was noted, with color turning more yellow and precipitate formation. After stirring the mixture for 4 h, all the precipitate was found to have dissolved. After a total of 18 h, the volatiles were removed from the reaction mixture to give a foamy, sticky residue. The ¹H NMR spectrum in THF-d₈ showed the same product

as the result from *Method A*. Crystallization from different combinations of ether, toluene and hexanes has not been successful.

^1H NMR (360 MHz, THF- d_6): δ 6.86 (4H, dd, $J = 7.5, 1.8$ Hz), 6.79 (8H, m, Bn), 6.65 (4H, dd, $J = 7.5, 1$ Hz), 6.39 (2H, overlapping, Bn), 6.36 (4H, t, $J = 7.5$ Hz), 3.38 (4H, q, $J = 7$ Hz, liberated Et₂O), 2.67 (4H, m, α -CH₂), 2.30 (4H, m, α -CH₂), 1.64 (4H, m, β -CH₂), 1.54 (4H, m, β -CH₂), 1.46 (4H, s, benzyl-CH₂), 1.12 (6H, t, $J = 7$ Hz, liberated Et₂O), 0.93 (12H, t, $J = 7.5$ Hz, γ -CH₃). ^{13}C NMR (125 MHz, THF- d_6): δ 157.8 (4°), 156.2 (4°), 149.1 (4°), 132.8 (4°), 132.7 (4°), 128.8 (3°), 128.5 (3°), 127.6 (3°), 124.7 (3°), 117.9 (3°), 117.5 (3°), 66.3 (liberated Et₂O), 34.2, 23.7, 21.6 (PhCH₂), 15.7 (liberated Et₂O), 14.6. Anal. Calcd for C₃₈H₄₀O₄•Mg₃•(C₇H₇)₂•O(C₂H₅)₂: C, 75.57; H, 7.25. Found:^f (1) C, 69.79; H, 7.07. (2) C, 73.16; H, 7.52.

30: C₃₈H₄₀O₄•(gem-TiCl₂)₂ (geminal up/down)



(A) *Without pre-deprotonation.* The reaction mixture and the products were kept from any contact with THF or Et₂O throughout the procedure. To a solution of tetrakis(2-hydroxy-3-propylphenyl)ethylene (**7**) (0.0546 g, 0.0967 mmol) in 1 mL of toluene was added TiCl₄ (0.0373 g, 0.197 mmol) dissolved in 2 mL of toluene. The color turned ruby-red immediately. After stirring the mixture for 30 minutes, the volatiles were removed in vacuo. The red residue was washed with pentane, triturated with toluene and filtered through Celite-packed pipette. The triturate was evaporated to give dark red powder. The ^1H NMR spectroscopy of this crude product showed fairly clean desired complex **30**. The

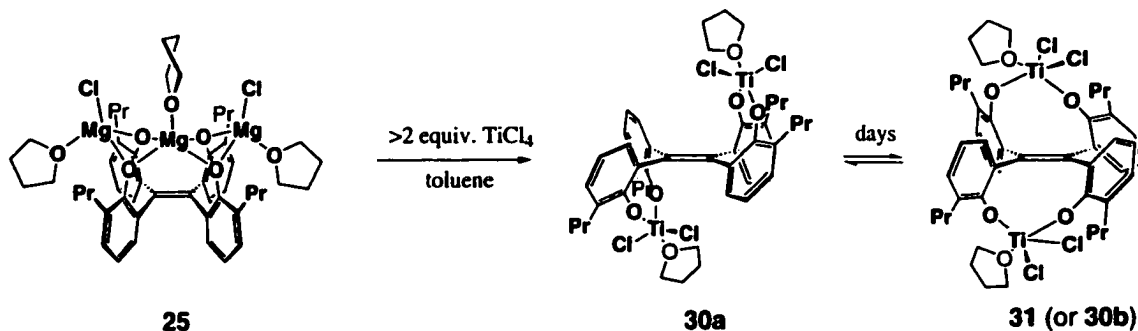
^f The weight of the sample was changing during the weighing, thus did not allow accurate analysis, according to the elemental analysis technician. The samples were wrapped doubly in preweighed tin boats in the drybox and brought out for quick weighing and analysis. This method works for most air- and moisture-sensitive compounds. This particular sample, however, may have reacted with oxygen or moisture in the atmosphere.

yield was not recorded. The structure was determined by analogy to the THF-coordinated version, **30a** (next section), based on the similarity of the ^1H NMR spectroscopy.

(B) With pre-deprotonation (NMR-tube reaction only). Tetrakis(2-hydroxy-3-propylphenyl)ethylene (**7**) (0.0457 g, 0.0809 mmol) and NaH (0.0078 g, 0.32 mmol) were mixed in ca. 0.5 mL C_6D_6 in an NMR tube for 6 h, then TiCl_4 (0.0312 g, 0.164 mmol) was added with small amount of additional C_6D_6 . The color turned ruby-red immediately. Due to the cloudiness of the sample, the mixture was filtered through Celite-packed pipette, and the solution part was checked by ^1H NMR spectroscopy at 20 minutes after the addition of TiCl_4 . The spectrum showed the product **30** as a major product, accompanied by other unidentified species. After one day, the same solution showed a cleaner spectrum of **30**.

^1H NMR (360 MHz, C_6D_6): δ 7.88 (4H, dd, $J = 7.5, \sim 1$ Hz), 6.74 (4H, t, $J = 7.5$ Hz), 6.49 (4H, dd, $J = 7.5, \sim 1$ Hz), 2.60 (4H, m, $\alpha\text{-CH}_2$), 2.31 (4H, m, $\alpha\text{-CH}_2$), 1.40-1.38 (8H, m, $\beta\text{-CH}_2\text{H}_b$), 0.73 (12H, t, $J = 7.5$ Hz, $\gamma\text{-CH}_3$).

30a and 30b/31: geminal and vicinal up/down $\text{C}_{38}\text{H}_{40}\text{O}_4 \cdot \{\text{TiBr}_2(\text{thf})\}_2$



Three slightly different conditions are presented as follows: (1) the conditions under which "**30a**" was isolated, (2) the conditions under which "**30b**" was isolated, and (3) the conditions under which the crystals of "**31**" were obtained. These conditions are not optimized.

(1) Conditions under which "30a" was isolated. To a solution of **25** (FW = 965 based on the elemental analysis; 0.0848 g, 0.879 mmol) in 3 mL of toluene was added TiCl_4 (0.0345 g, 0.182 mmol) dissolved in 1 mL of toluene. The color turned ruby-red immediately. After overnight, the volatiles were removed in vacuo. The residue was triturated with toluene and filtered through a Celite-packed pipette. The residue after

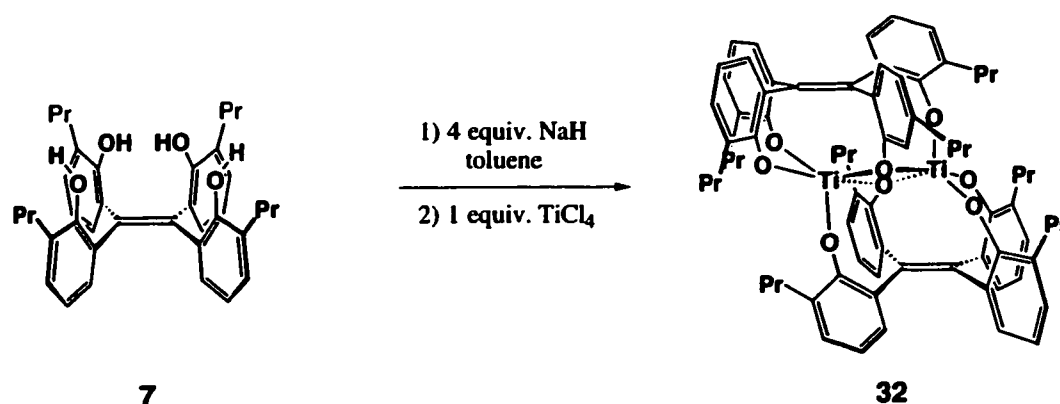
removal of the volatiles in vacuo was fairly pure product **30a** (0.080 g, 96%). Analytically pure product as a bulk could not be obtained due to the isomerization of **30a** to **30b/31**, as well as the gradual formation of **32**. Co-crystals of **30a** and **32** (2 : 1 ratio) were obtained from one of many crystallization attempts, mainly from toluene-pentane or toluene-hexane by slow diffusion or slow-evaporation. The crystallization batch that produced the light-red co-crystals of **30a** and **32** also produced dark-red crystals, which were single crystals of **30a**, according to the ¹H NMR spectrum. ¹H NMR (360 MHz, C₆D₆): δ 7.88 (4H, dd, *J* = 7.5, 1.8 Hz), 6.69 (4H, t, *J* = 7.5 Hz), 6.70 (4H, dd, *J* = 7.5, 1.8 Hz), 4.35 (4H, m, THF-α-CH₂), 2.73 (4H, m, α-CH₂), 2.47 (4H, m, α-CH₆), 1.50 (8H, m, β-CH₂H₆), 1.46 (4H, m, THF-β-CH₂), 0.83 (12H, t, *J* = 7.3 Hz, γ-CH₃). ¹³C NMR: A clean spectrum could not be obtained due to the tendency to isomerize to **30b/31**. X-ray crystallography: see Appendix A-5 (co-crystal of **30a** and **32**).

(2) **Conditions under which "30b" was isolated.** To a solution of **25** (FW = 965 based on the elemental analysis; 0.2196 g, 0.227 mmol) in 4 mL of toluene was added TiCl₄ (0.0959 g, 0.506 mmol) dissolved in 1 mL of toluene. The color turned ruby-red immediately. After overnight, the volatiles were removed in vacuo. The residue was triturated with toluene and filtered through a Celite-packed pipette. After removal of the volatiles in vacuo from the triturate, the residue was crystallized from toluene (hot to r.t.) followed by slow diffusion of hexanes layered on top of the toluene solution. A total of 0.0477 g (23%) of analytically pure vicinal up/down isomer **30b** was obtained as the first and the second crops of the slow-process crystallization. The isomer **30b** was identified as "**31**" as discussed in Section 3.1.2.E. ¹H NMR (360 MHz, C₆D₆): δ 7.875 (4H, dd, *J* = 7.5, 1.8 Hz), 6.75 (4H, dd, *J* = 7.5, 1.8 Hz), 6.70 (4H, t, *J* = 7.5 Hz), 4.38 (4H, m, THF-α-CH₂), 2.81 (4H, br, α-CH₂), 2.68 (4H, m, α-CH₆), 1.49 (8H, m, β-CH₂H₆), 1.40 (4H, m, THF-β-CH₂), 0.88 (12H, t, *J* = 7.3 Hz, γ-CH₃). ¹³C NMR: A clean spectrum was not obtained due to partial isomerization to **30a**. Anal. Calcd for C₃₈H₄₀O₄•Ti₂•Cl₄•(C₄H₈O)₂: C, 58.62; H, 5.99; Cl, 15.05. Found: C, 58.44; H, 5.81; Cl, 14.98.

(3) **Conditions that gave the X-ray quality crystals of "31."** To a solution of **25** (FW = 1235 based on the elemental analysis; 0.162 g, 0.0178 mmol) in 1 mL of toluene was added TiCl₄ (0.0071 g, 0.037 mmol) dissolved in 0.5 mL of toluene. The color turned ruby-red immediately. After overnight, another portion of TiCl₄ (0.0069 g, 0.036 mmol) was added with 0.5 mL of toluene. After 15 minutes, the volatiles were removed in vacuo. The residue was triturated with toluene, filtered through a Celite-packed pipette, concentrated in vacuo and cooled to -30 °C. Light orange crystals were formed, which turned out to be [Cl₃(thf)Ti-μ-Cl]₂, as confirmed by preliminary X-ray analysis. The mother liquor was then removed from the crystals, evaporated, and the residue was

washed with pentane. The residue was then redissolved in toluene, small amount of pentane was layered on, and set aside for slow diffusion/slow evaporation. This batch, however, did not give good quality crystals. The pentane washings, after concentrating slightly and allowing slow evaporation, produced red-orange crystals that were analyzed by X-ray crystallography as the vicinal up/down complex **31**. The ^1H NMR spectroscopy of the evaporated mother liquor, after removing the crystals for X-ray analysis, was of questionable identity (Section 3.1.2.E). X-ray crystallography: see **Appendix A-7 (31)**.

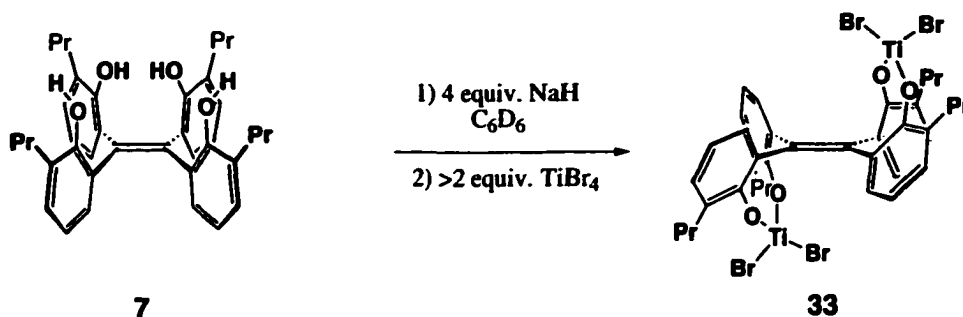
32: $(\text{C}_{38}\text{H}_{40}\text{O}_4)_2 \cdot \text{Ti}_2$



To a solution of tetrakis(2-hydroxy-3-propylphenyl)ethylene (**7**) (0.0163 g, 0.0289 mmol) in 1 mL of toluene was added NaH (0.0030 g, 0.125 mmol) dissolved in 1 mL of toluene. The color turned slightly yellow. After stirring the mixture for 5 minutes, TiCl_4 (0.0056 g, 0.030 mmol) was added with 2 mL of toluene. After overnight, the red mixture was almost clear, with some fuzzy stuff at the bottom. After removal of the volatiles, the residue was triturated with toluene, filtered through Celite-packed pipette, and the volatiles were removed to give quite clean product as confirmed by ^1H NMR spectroscopy. The yield was 0.0173 g (99%). The structure was identified by X-ray crystallography of the co-crystal of **30a** and **32** (see previous section). ^1H NMR (360 MHz, C_6D_6): δ 8.01 (1H, dd, $J = 7.8, 1.8$ Hz), 7.45 (1H, dd, $J = 7.5, 1.8$ Hz), 6.88 (4H, t, $J = 7.5$ Hz), 6.85~6.79 (5H, overlapping), 6.72 (1H, dd, $J = 7.5, 1.5$ Hz), 6.58~6.55 (3H, overlapping), 3.57 (1H, m, α -CH), 2.57~2.44 (3H, m, overlapping, α -CH), 2.42 (2H, t, $J = 8$ Hz, α - CH_2), 2.17~2.13 (2H, m, overlapping, α -CH), 1.53~1.29 (8H, m, overlapping, β -CH), 0.87 (3H, t, $J = 7.5$ Hz, γ - CH_3), 0.84 (3H, t, $J = 7.5$ Hz, γ - CH_3), 0.77 (3H, t, $J = 7.5$ Hz, γ - CH_3), 0.37 (3H, t, $J = 7.5$ Hz, γ - CH_3). MS (ES) m/z : Calcd for $\text{C}_{76}\text{H}_{80}\text{O}_8\text{Ti}_2$: 1216.48. Found: 1239 (55%) $[\text{M} + \text{Na}]^+$.

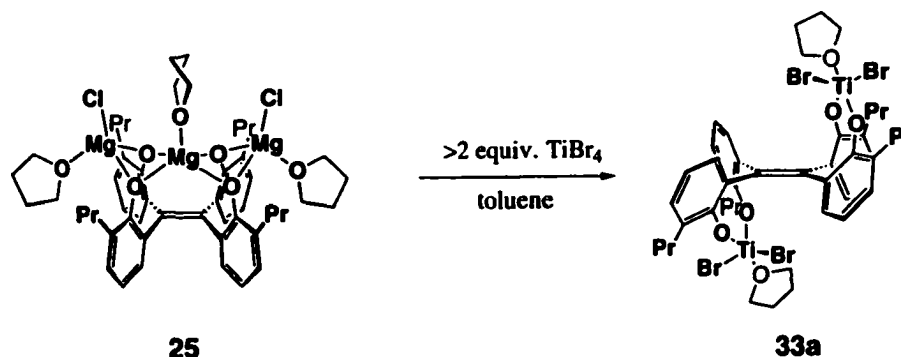
X-ray crystallography: see **Appendix A-5** (co-crystal of **30a** and **32**) and **A-6** (obtained from one of the failed attempts to produce **45**).

33: C₃₈H₄₀O₄•(gem-TiBr₂)₂•(thf)₂ (geminal up/down)



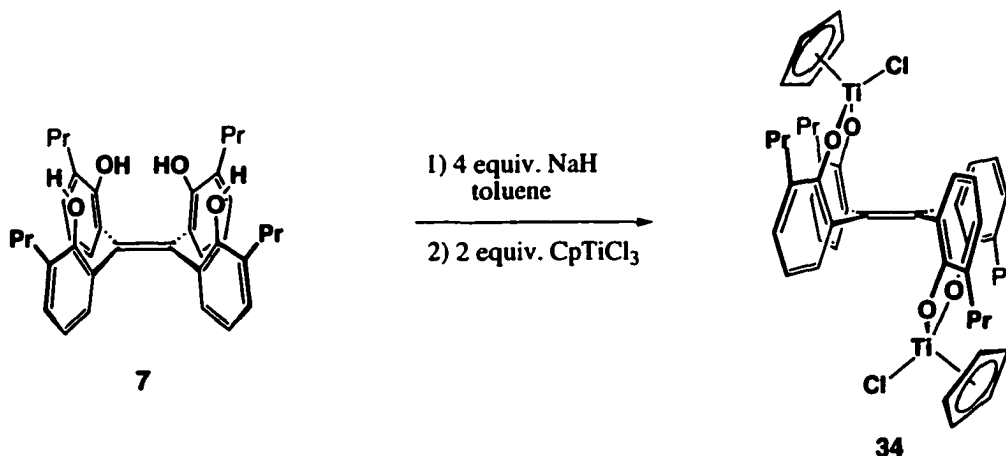
The reaction mixture and the product were kept from any contact with THF or Et₂O throughout the procedure. Tetrakis(2-hydroxy-3-propylphenyl)ethylene (**7**) (0.0409 g, 0.0724 mmol) and NaH (0.0070 g, 0.29 mmol) were mixed in ca. 0.5 mL of C₆D₆ in an NMR tube. After 4 h, TiBr₄ (0.0537 g, 0.146 mmol) was added, dissolved in a small amount of additional C₆D₆. The ¹H NMR spectrum observed 5 minutes after the TiBr₄ addition showed clean **33** (the inorganic byproduct, NaBr, precipitated to the bottom of the solution so NMR spectroscopy was possible). The same solution showed an increase in minor unidentified byproducts over time. The structure was determined by analogy to the THF- coordinated version, **33a** (next section), based on the similarity of ¹H NMR spectra. ¹H NMR (360 MHz, C₆D₆): δ 7.86 (4H, dd, *J* = 7.5, 1.3 Hz), 6.765 (4H, t, *J* = 7.5 Hz), 6.51 (4H, dd, *J* = 7.5, 1.3 Hz), 2.705 (4H, m, α-CH₂), 2.36 (4H, m, α-CH₂), 1.45 (8H, m, β-CH₂H_b), 0.765 (12H, t, *J* = 7.2 Hz, γ-CH₃).

33a: C₃₈H₄₀O₄•(gem-TiBr₂)₂•(thf)₂ (geminal up/down)



To a solution of **25** (FW = 965 based on the elemental analysis; 0.0358 g, 0.0371 mmol) in 2 mL of toluene was added TiBr_4 (0.0295 g, 0.0803 mmol) dissolved in 1 mL of toluene. The color turned dark-red immediately. After overnight, the volatiles were removed in vacuo. The residue was triturated with toluene, filtered through a Celite-packed pipette, and concentrated. Cooling the concentrated solution to $-30\text{ }^\circ\text{C}$ produced ruby-red prism crystals of **33a**. The yield was not recorded, but the NMR-tube reaction of the same reaction in C_6D_6 medium showed that the reaction is clean and quantitative. ^1H NMR (360 MHz, C_6D_6): δ 7.87 (4H, dd, $J = 7.2, 2$ Hz), 6.69 (4H, t, $J = 7.2$ Hz), 6.70 (4H, dd, $J = 7.2, 2$ Hz), 4.46 (4H, m, THF- α - CH_2), 2.88 (4H, m, α - CH_2), 2.55 (4H, m, α - CH_2), 1.58 (8H, m, β - CH_2H_b), 1.57 (4H, m, THF- β - CH_2), 0.88 (12H, t, $J = 7.3$ Hz, γ - CH_3). ^{13}C NMR (75 MHz, APT, C_6D_6): δ 166.4 (4° , C-O), 138.6 (4° , C=C), 134.9 (4°), 130.3 (4°), 129.0 (3°), 128.8 (3°), 124.0 (3°), 74.2 (THF- α), 33.1 (propyl- α), 25.4 (THF- β), 24.2 (propyl- β), 14.2 (propyl- γ). Anal. Calcd for $\text{C}_{38}\text{H}_{40}\text{O}_4 \cdot \text{Ti}_2 \cdot \text{Br}_4 \cdot (\text{C}_4\text{H}_8\text{O})_2$: C, 49.32; H, 5.04. Found: C, 49.12; H, 4.49. X-ray crystallography: see Appendix A-8.

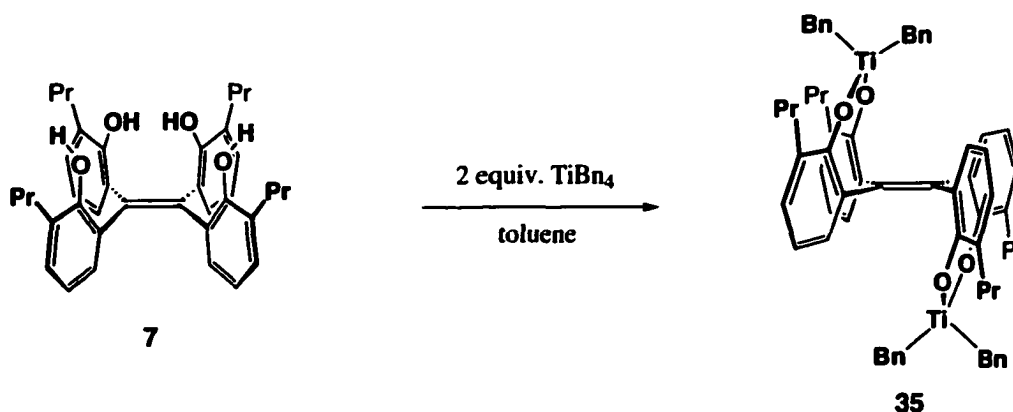
34: $\text{C}_{38}\text{H}_{40}\text{O}_4 \cdot (\text{gem-CpTiCl})_2$ (geminal up/down)



To a solution of tetrakis(2-hydroxy-3-propylphenyl)ethene (**7**) (0.0234 g, 0.0414 mmol) in 1 mL of toluene was added NaH (0.0042 g, 0.18 mmol) suspended in 1 mL of toluene. After stirring the mixture for 2.5 h, CpTiCl_3 (0.0192 g, 0.0876 mmol) was added, dissolved in 1 mL of toluene. The color turned orange immediately, then light red. After overnight, the volatiles were removed in vacuo. The residue was triturated with toluene, filtered through a Celite-packed pipette, and the toluene was removed in vacuo. Crystallization from hexane-toluene, cooling from elevated temperature to r.t., then to

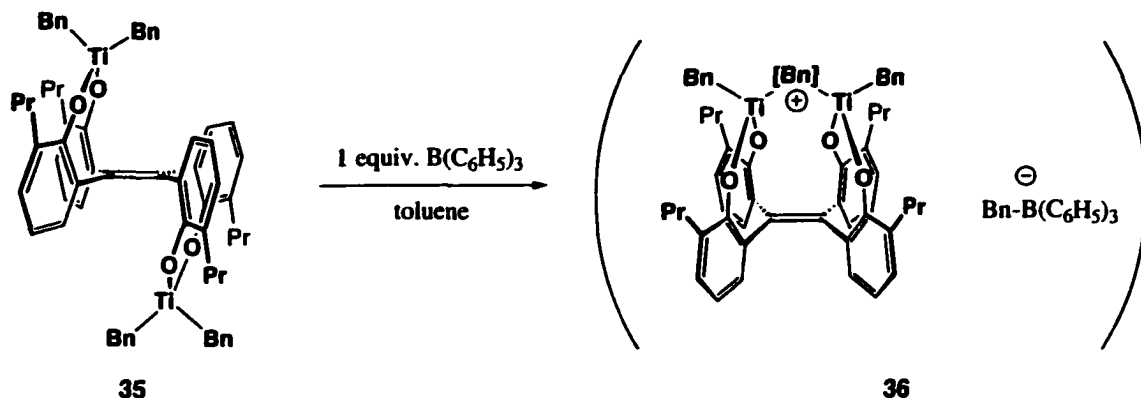
-30 °C, yielded light orange prism-needle crystals of **34**. The structure was confirmed by X-ray crystallography, although the crystallized material as a bulk still contained impurities, mainly Cp-based species. ¹H NMR (360 MHz, C₆D₆): δ 8.21 (4H, dd, *J* = 7.5, 1.8 Hz), 6.82 (4H, t, *J* = 7.5 Hz), 6.72 (4H, dd, *J* = 7.2, 2 Hz), 6.18 (10H, s, Cp), 2.83 (4H, m, α-CH₂), 2.23 (4H, m, α-CH₆), 1.50 (8H, m, β-CH₂H₆), 0.78 (12H, t, *J* = 7.3 Hz, γ-CH₃). X-ray crystallography: see Appendix A-9.

35: C₃₈H₄₀O₄•(gem-TiBn₂)₂ (geminal up/down)



To a solution of tetrakis(2-hydroxy-3-propylphenyl)ethene (**7**) (0.2004 g, 0.3548 mmol) in toluene (4 mL) was added TiBn₄ (0.3078 g, 0.7464 mmol) dissolved in 1 to 2 mL toluene. After 30 minutes, the solution was concentrated and cooled to -30 °C to produce crystals. By repeating crystallization from toluene-hexanes, more crystals were obtained. All of the crystals were washed with a small amount of hexanes to remove the remaining unreacted reagent. Analytically pure product **35** was obtained as orange-brown crystals (0.290 g, 66 %). ¹H NMR (360MHz, C₆D₆): δ 7.40 (4H, br d, *J* = 7.5 Hz, Bn₂-ortho), 7.31 (4H, br t, *J* = 7.5 Hz, Bn₂-meta), 7.16 (4H, dd, *J* = 7, 2.2 Hz), 7.06 (2H, br t, *J* = 7.5 Hz, Bn₂-para), 6.83 (4H, br t, *J* = 7.5 Hz, Bn₆-meta), 6.78 (4H, dd, *J* = 7, 2.2 Hz), 6.75 (4H, t, *J* = 7 Hz), 6.67 (2H, br t, *J* = 7.5 Hz, Bn₆-para), 6.51 (4H, br d, *J* = 7.5 Hz, Bn₆-ortho), 3.30 (4H, s, PhCH₂) 2.84 (4H, m, propyl-α-CH₂), 2.34 (4H, s, PhC'H₂), 2.21 (4H, m, propyl-α-CH₆), 1.57 (8H, m, propyl-β-CH₂H₆), 0.91 (12H, t, *J* = 7.2 Hz, propyl-γ-CH₃). ¹³C NMR (125MHz, BB, C₆D₆): δ 159.1, 144.5, 140.9, 139.7, 131.5, 130.2, 130.0, 129.1, 128.6, 128.3, 127.0, 126.9, 125.6, 123.3, 122.1, 84.2, 82.9, 33.1, 23.6, 14.2. Anal. Calcd for C₃₈H₄₀O₄•Ti₂•(C₇H₇)₄: C, 77.64; H, 6.71. Found: C, 77.38; H, 6.64.

36: $[(C_{38}H_{40}O_4)(TiBn)_2(\mu-Bn)][BnC(C_6F_5)_3]$?

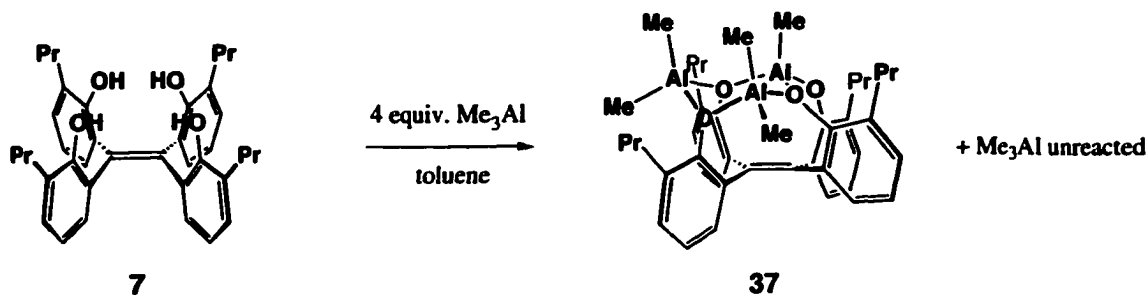


NMR-tube reaction. The geminal-up/down di-TiBn₂ complex **35** (0.0032 g, 0.0031 mmol) and B(C₆F₅)₃ (0.0016 g, 0.0031 mmol) were dissolved in ca. 0.5 mL of C₆D₆. The ¹H NMR spectrum at 15 minutes after mixing showed broad "intermediate" signals. After a day, the spectrum showed the compound designated as **36**, with a symmetric (C_{2v} or C_{iv}) ligand framework and 2 : 1 : 1 ratio of benzyl groups, as the major product. The structure of **36** is suggested as shown in the equation above, based on the symmetry and the number of different benzyl groups. ¹H NMR (360MHz, C₆D₆): δ 7.14~6.99 (integral not clear due to overlap with contaminant toluene), 6.94~6.81 (integral not clear due to minor impurities), 6.83 (4H, t, *J* = 7.5 Hz, H-5 of ligand framework), 6.69 (4H, dd, *J* = 7.5, 1.5 Hz, H-4 of ligand framework), 3.28 (4H, s, PhCH₂) 2.88 (2H, s, PhC''H₂), 2.78 (2H, s, PhC'''H₂), 2.76 (4H, m, propyl-α-CH₂), 2.40 (4H, m, propyl-α-CH₂), 1.59 (8H, m, propyl-β-CH₂H₆), 0.88 (12H, t, *J* = 7~7.5 Hz, propyl-γ-CH₃).

Attempts to crystallize. The above-mentioned reaction was repeated using **35** (0.0688 g, 0.0674 mmol) and B(C₆F₅)₃ (0.0345 g, 0.0674 mmol) in 2.5 mL toluene, under conditions free of THF and ether. Crystallization from toluene (r.t. to -30 °C) or THF-toluene was not successful. The use of THF as a crystallization solvent resulted in the polymerization of THF.

Polymerization of THF by 36. In one of the crystallization attempts for **36**, a solution of **36** (unknown amount) in THF was prepared, concentrated, a few drops of toluene was added to it, and cooled to -30 °C. After overnight, the mixture had become two layers: a dark layer and a viscous colorless layer. A few more drops of THF was added to dilute the dark layer and the mixture was left at r.t.. Next day, the colorless viscous layer increased. It is thus tentatively concluded that THF was polymerized.

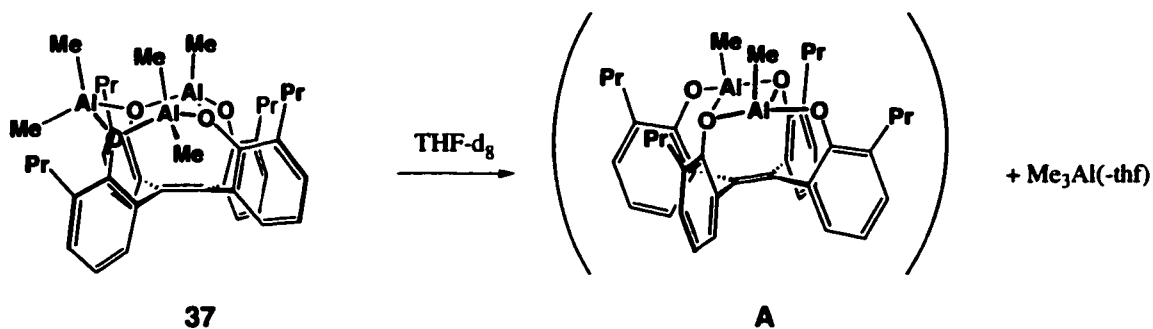
37: C₃₈H₄₀O₄·Al₃·Me₃



To a solution of tetrakis(2-hydroxy-3-propylphenyl)ethylene (**7**) (0.0386 g, 0.0683 mmol) in 1 mL of toluene was added Me₃Al (0.0207 g, 0.287 mmol) dissolved in 1 mL of toluene. The color turned slightly yellow immediately and gas evolution was observed. After 5 min. of stirring, the volatiles were removed in vacuo. The residue did not redissolve in toluene, thus the mixture was filtered and the filtrate was concentrated.⁵ Adding pentane to the oily solution and cooling to -30 °C yielded crystals. After removal of the mother liquor, rinsing with small amount of cold pentane, and drying under reduced pressure, the analytically pure product was obtained (0.0243 g, 50%). ¹H NMR (360 MHz, C₆D₆): δ 7.24 (1H, dd, *J* = 7.2, 2 Hz), 7.09 (1H, dd, *J* = 6, 3.5 Hz), 6.91~6.87 (3H, overlapping), 6.81 (1H, dd, *J* = 5.5, 3.8 Hz), 6.70 (1H, dd, *J* = 7.5, 2 Hz), 6.65~6.58 (5H, overlapping), 2.90 (1H, m, propyl-α-CH), 2.73 (1H, m, propyl-α-CH), 2.63 (1H, m, propyl-α-CH), 2.43~2.31 (5H, overlapping, propyl-α-CH), 1.63~1.41 (8H, overlapping, propyl-β-CH), 0.92 (3H, t, *J* = 7.3 Hz, propyl-γ-CH₃), 0.89 (3H, t, *J* = 7.3 Hz, propyl-γ-CH₃), 0.84 (3H, t, *J* = 7.3 Hz, propyl-γ-CH₃), 0.75 (3H, t, *J* = 7.3 Hz, propyl-γ-CH₃), 0.26 (1H, s, AlCH₃), 0.21 (1H, s, AlCH₃), 0.12 (1H, s, AlCH₃), -1.42 (1H, s, AlCH₃), -1.46 (1H, s, AlCH₃). ¹³C NMR (125MHz, BB, C₆D₆): δ 153.1, 149.4, 149.2, 148.6, 142.9, 140.9, 136.2, 136.1, 134.6, 134.2, 133.3, 132.7, 132.1, 131.3, 129.9, 129.7, 129.5, 129.4, 129.2, 128.3, 128.1, 126.0, 125.1, 124.84, 123.79, 118.7, 34.2 (propyl-α), 32.9 (propyl-α, two signals overlapping), 32.6 (propyl-α), 23.8 (propyl-β), 23.4 (propyl-β), 22.9 (propyl-β), 21.9 (propyl-β), 14.22 (propyl-γ), 14.15 (propyl-γ), 14.0 (propyl-γ), 13.9 (propyl-γ), -5.7 (AlCH₃), -6.7 (AlCH₃), -10.1 (AlCH₃), -10.2 (AlCH₃), -11.2 (AlCH₃). Anal. Calcd for C₄₈H₆₅Al₃O₄: C, 73.26; H, 8.33. Found: C, 73.39; H, 8.33.

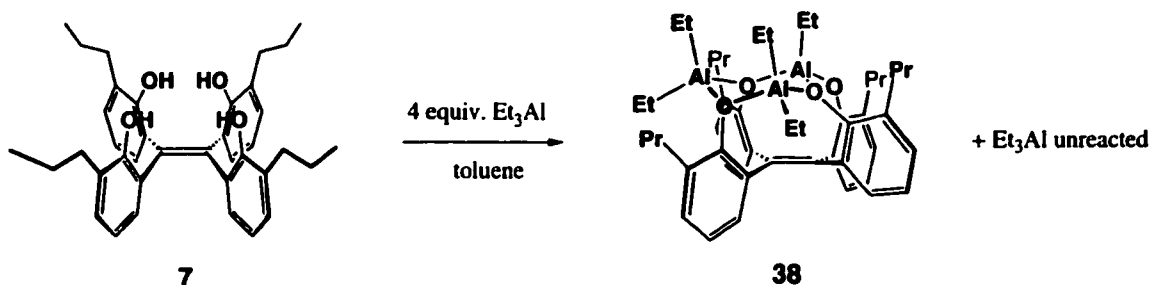
⁵ Complete removal of toluene from the mixture made it difficult to dissolve again.

Formation of "A": THF-driven abstraction of Me₃Al from 37.



A solution of complex **37** (undetermined amount) in THF-d₈ was prepared in an NMR tube. The ¹H NMR spectrum at 15 minutes after preparation showed a single aromatic ring for the ligand framework, accompanied by two identical deshielded methyl groups. The spectrum remained unchanged after 2 days. One molecule of Me₃Al was freed from the complex: the identity of the liberated Me₃Al was confirmed by adding small amount of Me₃Al to the solution and observing an increase in the intensity of the signal assigned to the liberated Me₃Al. ¹H NMR (300 MHz, THF-d₈): δ 7.07 (4H, dd, *J* = 7.3, 1.5 Hz), 6.62 (4H, dd, *J* = 7.3, 1.5 Hz), 6.32 (4H, t, *J* = 7.3 Hz), 2.64 (4H, m, propyl-α-CH₂), 2.17 (4H, m, propyl-α-CH₂), 1.42 (8H, m, propyl-β-CH₂H₆), 0.77 (12H, t, *J* = 7.3 Hz, propyl-γ-CH₃), -0.35 (6H, s, AlCH₃), -0.94 (9H, s, freed Me₃Al). ¹³C NMR (100 MHz, THF-d₈): δ 155.0, 142.5, 133.1, 130.6, 128.32, 128.31, 117.5, 34.1 (propyl-α), 23.9 (propyl-β), 14.4 (propyl-γ), -9.1 (AlCH₃, of freed Me₃Al), -13.3 (AlCH₃, of A). The structure of A is suggested by these spectroscopic features.

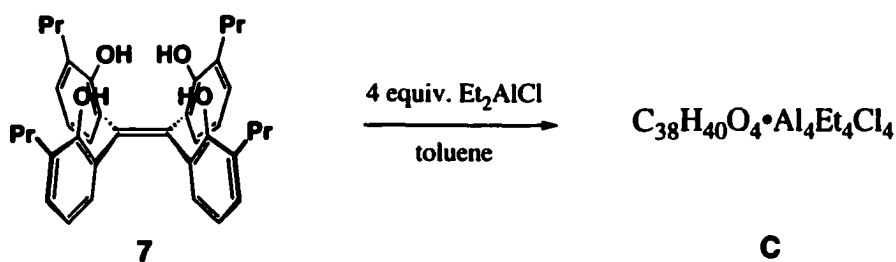
38: C₃₈H₄₀O₄•Al₃•Et₅



To a solution of tetrakis(2-hydroxy-3-propylphenyl)ethane (**7**) (0.0595 g, 0.105 mmol) in 1 mL of toluene was added a solution of Et₃Al in toluene (1.105 mmol/mL, 0.42 mL, 0.46 mmol) slowly. The color turned slightly yellow immediately and gas evolution was

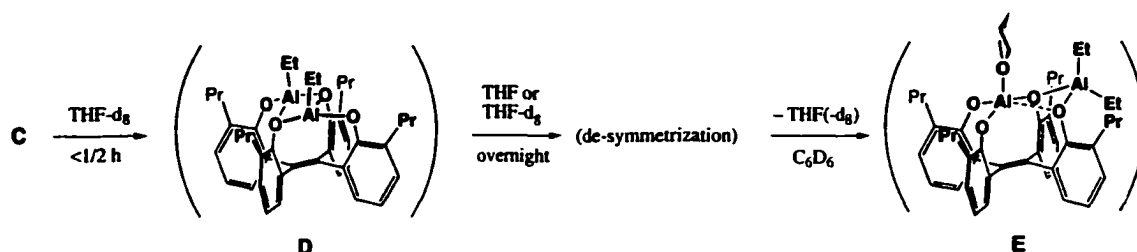
observed. After 5 min. of stirring, the volatiles were removed in vacuo, and the residue was crystallized from benzene (r.t., slow evaporation). The crystals, which were separated from the mother liquor, washed with hexanes, and dried in vacuo, were analytically pure product **38** (0.0503 g, 61%). The structure was confirmed by X-ray crystallography. The residue from the mother liquor after evaporation was also mainly the product, accompanied by unreacted Et_3Al . ^1H NMR (360 MHz, C_6D_6): δ 7.25 (1H, dd, $J = 5.5, 4$ Hz), 7.08 (1H, dd, $J = 6.5, 2.8$ Hz), 6.94 (2H, overlapping), 6.85 (1H, dd, $J = 7.5, 2$ Hz), 6.79 (1H, dd, $J = 5.5, 3.5$ Hz), 6.69 (1H, dd, $J = 7.5, 2$ Hz), 6.65 (3H, overlapping), 6.59 (2H, overlapping), 3.03 (1H, m, propyl- α - CH_2), 2.92 (1H, m, propyl- α -CH), 2.69 (2H, overlapping m, propyl- α - CH 's), 2.43 (4H, overlapping m, propyl- α - CH 's), 1.66 (3H, t, $J = 8.2$ Hz, axial- AlCH_2CH_3), 1.56~1.53 (4H, overlapping m, propyl- β - CH 's), 1.53 (3H, t, $J = 8.2$ Hz, axial- AlCH_2CH_3), 1.52 (3H, t, $J = 8.2$ Hz, axial- AlCH_2CH_3), 1.40 (4H, overlapping m, propyl- β - CH 's), 0.97~0.86 (2H + 2H + 2H, overlapping m, axial- AlCH_2CH_3), 0.97 (3H, t, $J = 7$ Hz, propyl- γ - CH_3), 0.95 (3H, t, $J = 7$ Hz, propyl- γ - CH_3), 0.93 (3H, t, $J = 7$ Hz, propyl- γ - CH_3), 0.79 (2H, m, axial- AlCH_2CH_3), 0.78 (3H, t, $J = 7$ Hz, propyl- γ - CH_3), 0.46 (3H, t, $J = 8$ Hz, equatorial- AlCH_2CH_3), 0.08 (3H, t, $J = 7.8$ Hz, equatorial- AlCH_2CH_3), -0.56 (1H, m, equatorial- AlCH_2CH_3), -0.68 (2H, overlapping m, equatorial- AlCH_2CH_3), -0.93 (1H, m, equatorial- AlCH_2CH_3). ^{13}C NMR (125 MHz, BB, C_6D_6): δ 152.9, 148.9, 148.8, 148.0, 142.7, 140.8, 136.6, 136.3, 134.4, 134.2, 133.5, 132.6, 132.2, 131.5, 129.9, 129.6, 129.20, 129.18, 128.5, (128.3?), 126, 2, 125.2, 124.8, 124.8, 118.7, 33.8 (propyl- α), 32.8 (propyl- α), 32.5 (propyl- α), 32.4 (propyl- α), 24.0 (propyl- β), 23.3 (propyl- β), 23.1 (propyl- β), 21.5 (propyl- β), 14.4 (propyl- γ), 14.14 (propyl- γ), 14.06 (propyl- γ), 13.9 (propyl- γ), 9.9 (AlCH_2CH_3), 9.6 (AlCH_2CH_3), 9.4 (AlCH_2CH_3), 8.4 (AlCH_2CH_3), 7.6 (AlCH_2CH_3), 3.5 (AlCH_2CH_3), 2.3 (AlCH_2CH_3), 0.95 (AlCH_2CH_3), 0.69 (AlCH_2CH_3), -0.88 (AlCH_2CH_3). One carbon signal was missing or overlapping with another in the aromatic region. The peak at 128.3 ppm is questionable. Anal. Calcd for $\text{C}_{48}\text{H}_{65}\text{Al}_3\text{O}_4$: C, 73.26; H, 8.33. Found: C, 73.39; H, 8.33. X-ray crystallography: see **Appendix A-11**.

C: $\text{C}_{38}\text{H}_{40}\text{O}_4 \cdot (\text{AlEtCl})_4$



To a solution of tetrakis(2-hydroxy-3-propylphenyl)ethene (**7**) (0.0716 g, 0.127 mmol) in 1 mL of toluene was slowly added Et₂AlCl (0.0629 g, 0.522 mmol) diluted with total of 2.5 mL toluene. The color immediately turned slightly yellow, then reddish orange, accompanied by gas evolution. After overnight, the color became pale yellow. After removal of the volatiles in vacuo, the product was crystallized from toluene (warm → r.t.). After tiny shiny crystals were formed, some hexanes was layered on for slow diffusion. Later more hexanes was added and cooled to -30 °C for several days. The mother liquor was removed from the crystals, which were washed with pentane and dried in vacuo. The yield was 0.0534 g (45%). The ¹H NMR spectrum in C₆D₆ was complicated, probably of a mixture of isomers. Anal. Calcd for C₃₈H₄₀O₄•(AlC₂H₅Cl)₄: C, 59.62; H, 6.53; Cl, 15.30. Found: C, 59.72; H, 6.30; Cl, 14.59.

D and E: THF-driven abstraction of aluminum from C



NMR-tube reaction. The product **C** from the previous reaction (amount unrecorded) was dissolved in THF-d₈, placed in an NMR-tube, and the ¹H NMR spectrum was taken immediately after preparation of the sample. A symmetrical complex **D** with liberated aluminum, presumably EtAlCl₂ (2 equiv.), was observed. After overnight, the same solution showed a mixture of **D** and a newly emerging unsymmetrical species **E**.

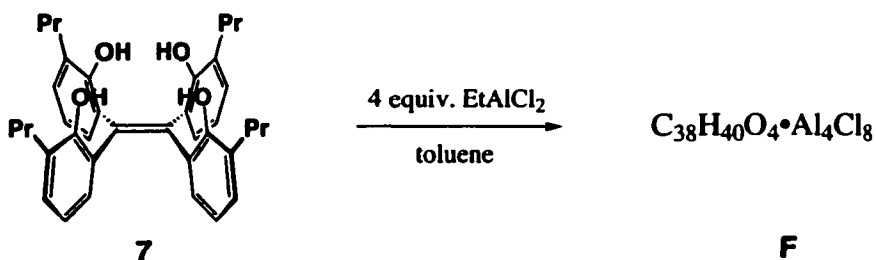
Isolation of E. The product **E** was exclusively obtained by mixing tetrakis(2-hydroxy-3-propylphenyl)ethene (**7**) (0.0558 g, 0.0988 mmol) and Et₂AlCl (0.0496 g, 0.411 mmol) in THF (2 mL) for a day. After removal of the volatiles in vacuo, ¹H NMR spectroscopy of the remaining viscous pale yellow oil in C₆D₆ showed clean σ-symmetry compound **E**. The THF-d₈ solution of **E** showed a complicated spectrum, probably a mixture of at least two compounds. At least one of them is unsymmetrical.

D. ¹H NMR (360 MHz, THF-d₈): δ 7.09 (4H, dd, $J = 7.5, 2$ Hz), 6.60 (4H, dd, $J = 7.5, 2$ Hz), 6.32 (4H, t, $J = 7.5$ Hz), 2.63 (4H, m, propyl-α-CH₂), 2.14 (4H, m, propyl-α-CH₂), 1.42 (8H, m, propyl-β-CH₂H_β), 1.30 (6H, t, $J = 8$ Hz, AlCH₂CH₃), 0.75 (12H, t, $J = 7.3$ Hz), 0.40 (4H, q, $J = 8$ Hz, AlCH₂CH₃). The liberated aluminum is presumed to be

EtAlCl₂: 1.03 (6H, slightly br t, *J* = 8 Hz, AlCH₂CH₃), 0.07 (4H, slightly br q, *J* = 8 Hz, AlCH₂CH₃).

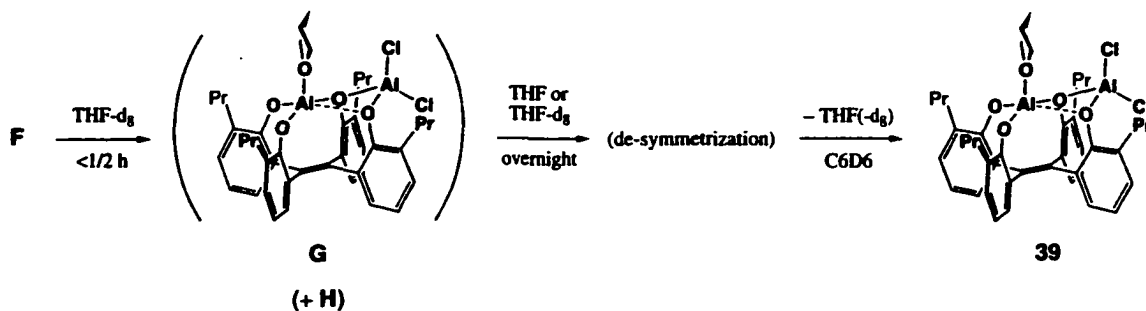
E. ¹H NMR (360 MHz, C₆D₆): δ 7.09 (2H, dd, *J* = 7.3, 1.8 Hz), 6.99 (2H, dd, *J* = 7.3, 1.8 Hz), 6.80 (2H, dd, *J* = 7.3, 1.8 Hz), 6.76 (2H, dd, *J* = 7.3, 1.8 Hz), 6.66 (2H, t, *J* = 7.3 Hz), 6.61 (2H, t, *J* = 7.3 Hz), 4.74 (4H, m, THF-α), 2.81 (2H, m, propyl-α-CH), 2.56~2.46 (6H, m, propyl-α-CH), 1.69 (4H, m, propyl-β-CH₂H_b), 1.53~1.51 (4H+4H, m, propyl-β-CH₂H_b plus THF-β), 1.28 (3H, t, *J* = 8 Hz, axial AlCH₂CH₃), 0.97 (6H, t, *J* = 7.3 Hz), 0.84 (6H, t, *J* = 7.3 Hz), 0.67 (3H, t, *J* = 8 Hz, equatorial AlCH₂CH₃), 0.29 (3H, t, *J* = 8 Hz, axial AlCH₂CH₃), -0.35 (3H, t, *J* = 8 Hz, equatorial AlCH₂CH₃). The liberated aluminum is presumed to be EtAlCl₂(thf): 1.36 (6H, t, *J* = 8 Hz, AlCH₂CH₃), 0.24 (4H, q, *J* = 8 Hz, AlCH₂CH₃); the coordinated THF molecule exchanges with free excess THF: 3.45 (14~15H, α), 0.99 (14~15H, β). ¹³C NMR (50 MHz, BB, C₆D₆): δ 154.9, 150.0, 133.2, 132.0, 130.1, 130.0, 129.1, 128.8, 128.3, 123.9, 123.5, 123.14(?), 113.0, 73.9 (coordinated THF-α), 71.1 (excess THF-α), 33.7 (propyl-α), 33.0 (propyl-α), 25.2 (coordinated THF-β), 24.8 (excess THF-β), 23.1 (propyl-β), 22.9 (propyl-β), 14.3 (propyl-γ), 14.2 (propyl-γ), 9.2 (AlCH₂CH₃, liberated EtAlCl₂?), 8.5 (AlCH₂CH₃, axial?), 8.0 (AlCH₂CH₃, equatorial?); "AlCH₂CH₃" signals are not clearly observed, probably due to broadening.

F: C₃₈H₄₀O₄•(AlCl₂)₄



To a solution of tetrakis(2-hydroxy-3-propylphenyl)ethene (**7**) (0.1558 g, 0.2759 mmol) in 1.5 mL of toluene was added EtAlCl₂ (0.1499 g, 1.181 mmol) dissolved in 2 mL of toluene. The color turned dark immediately, with gas evolution. The color soon turned greenish, and became lighter as the mixture became cloudy. After overnight, the milky light orange-brown precipitate was collected, washed with toluene followed by pentane, and dried in vacuo to give the off-white, slightly pink powder **F** (0.1995 g, 76%). Anal. Calcd for C₃₈H₄₀O₄Al₄Cl₈: C, 47.93; H, 4.23; Cl, 29.78. Found: C, 48.57; H, 4.36; Cl, 28.02.

G/H and 39: THF-driven abstraction of aluminum reagent(s) from F



NMR-tube reaction. A solution of F (amount unrecorded) in THF-d₈ was prepared in an NMR tube. The ¹H NMR spectrum immediately after the preparation of the sample showed a σ-symmetry species G and a broad, intermediate set of signals (H) in a ratio of ca. 1.5~2 : 1. After overnight, the same solution showed a complicated spectrum of probably a mixture of at least two compounds.

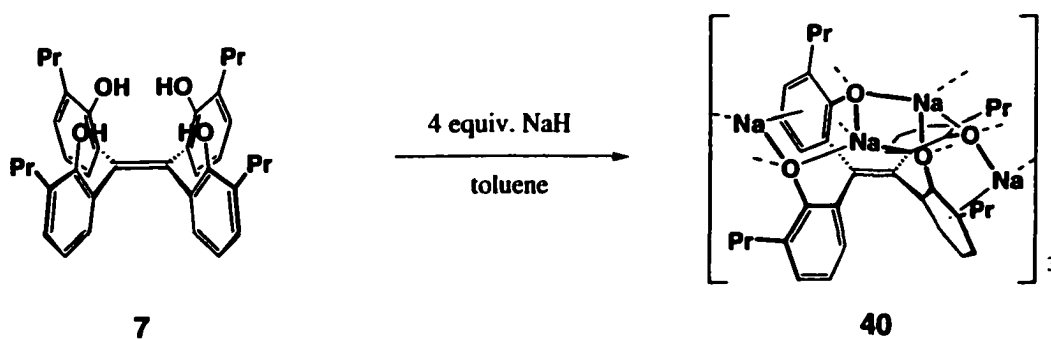
Isolation of 39. Tetrakis(2-hydroxy-3-propylphenyl)ethene (7) (0.0551 g, 0.0975 mmol) and EtAlCl₂ (0.0514 g, 0.405 mmol) were mixed in THF (2 mL) for a day. After removal of the volatiles in vacuo, the pale orange crude product 39 showed a ¹H NMR spectrum in THF-d₈ identical to the above-mentioned complicated spectrum. The crude product was crystallized from toluene (r.t. → -30 °C), growing tiny shiny less-colored crystals. The crystals were further grown by layering pentane on to allow slow diffusion at -30 °C, producing pale orange prism crystals that were used to obtain the X-ray crystallographic structure of 39 (Appendix A-12). The prisms, along with an orange-colored and less-crystalline solid, were isolated from the mother liquor, washed with a small amount of pentane and dried in vacuo (0.0790 g). The mass of the isolated material is larger than a quantitative yield of 39 (0.0790 g expected), most likely because the less crystalline part contains inorganic byproduct AlCl₃(thf)_n, or [AlCl₂(thf)₄][AlCl₄].

G. ¹H NMR (360 MHz, THF-d₈, tentatively assigned): δ 6.97 (2H, dd, J = 7.5, 1.5 Hz), 6.90? (2H, br d, J = ~7 Hz), 6.81 (2H, br d, J = ~7 Hz), 6.74 (2H, slightly br dd, J = ~7, ~1 Hz), 6.51 (2H, t, J = 7.5 Hz), 6.51 (2H, t, J = 7.5 Hz), 2.73 (2H, m, propyl-α-CH), 2.44 (2H+2H, m, propyl-α-CH), 2.13 (2H, m, propyl, propyl-α-CH), 1.44 (4H, m, propyl-β-CH₂H_b), 1.26 (4H, m, propyl, β-CH₂H_b), 0.78 (6H, t, J = 7.3 Hz, propyl-γ-CH₃), 0.78 (6H, t, J = 7.5 Hz, propyl-γ-CH₃).

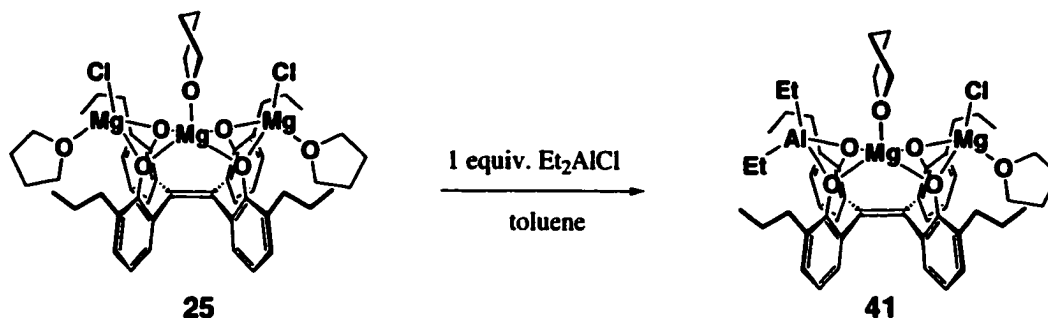
H. ¹H NMR (360 MHz, THF-d₈, tentatively assigned as σ-symmetry species with broad signals): δ 7.03 (2H, br), 6.81 (2H, br), 6.71 (4H, br), 6.59 (2H, br t, J = ~7.5 Hz), 6.46 (2H, br), 2.50~2.44 (8H?, br, propyl-α-CH), 1.60~1.44 (8H?, br, propyl-β-CH), 0.87 (12H?, br t, overlapping? J = ~7 Hz, propyl-γ-CH₃)

39. $^1\text{H NMR}$ (360 MHz, C_6D_6): δ ~7.14[?] (2H, br, overlapping with solvent signal), 7.09 (2H, br d, $J = 7\text{--}8$ Hz), 6.83 (2H, dd, $J = 7.5, 1.8$ Hz), 6.71 (2H, t, $J = 7.3$ Hz), 6.64 (2H, $J = 7.5, 1.8$ Hz), one aromatic dd (2H) is not located due to the overlapping; 2.75 (4H, m, propyl- α -CH), 2.51 (2H, m, propyl- α -CH), 2.40 (2H, m, propyl- α -CH), 1.62 (4H, m, propyl- β - CH_2H_b), 1.49 (4H, m, propyl- β - $\text{C}'\text{H}_2\text{H}_b$), 0.92 (6H, t, $J = 7.3$ Hz, propyl- γ - CH_3), 0.78 (6H, t, $J = 7.3$ Hz, propyl- γ - CH_3). MS (ES) m/z : Calcd for $\text{C}_{42}\text{H}_{48}\text{Al}_2\text{Cl}_2\text{O}_5$: 756.25. Found: 863 (88%, unidentified parent signal with Cl_2 pattern). X-ray crystallography: see Appendix A-12.

40: $(\text{C}_{38}\text{H}_{40}\text{O}_4 \cdot \text{Na}_4 \cdot (\text{C}_7\text{H}_8)_{1/2})$

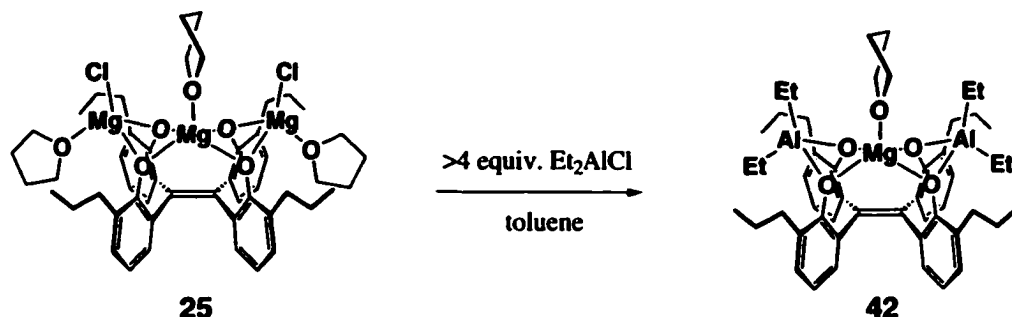


To a solution of tetrakis(3-propyl-2-hydroxyphenyl)ethene (**7**) (0.1106 g, 0.1958 mmol) in toluene (2 mL), was added NaH (0.0191 g, 0.796 mmol) suspended in 0.5 mL of toluene and the mixture was stirred overnight. The greenish yellow mixture was filtered through Celite-packed pipette. After removal of the volatiles from the filtrate, the crude yield was 0.148 g (108%). The $^1\text{H NMR}$ spectrum in C_6D_6 showed a set of broad signals. After crystallization from toluene, pale greenish-yellow crystals were obtained (yield not recorded). $^1\text{H NMR}$ (360 MHz, C_6D_6): δ 7.332 (4H, br), 6.81 (4H, br), 6.53 (4H, br), 2.21 (8H, br, α - CH_2), 1.39 (8H, br, β - CH_2), 0.70 (12H, br, γ - CH_2). Anal. Calcd for $\text{C}_{38}\text{H}_{40}\text{O}_4 \cdot \text{Na}_4$: C, 69.93; H, 6.18. Calcd for $\text{C}_{38}\text{H}_{40}\text{O}_4 \cdot \text{Na}_4 \cdot (\text{C}_7\text{H}_8)_{1/2}$: C, 71.33; H, 6.35. Found: C, 71.14; H, 6.33. X-ray crystallography: a trimer structure (see Section 3.1.4) was provided, but data were not refined due to the large residual factor.

41: C₃₈H₄₆O₄•(AlEt₂)•[Mg(thf)]•[MgCl(thf)]

To a suspension of **25** (FW = 920.4 based on the elemental analysis, 0.1995 g, 0.2168 mmol) in 3 mL of toluene was added Et₂AlCl (0.0261 g, 0.216 mmol) dissolved in 3.5 mL of toluene. After 15 min. of stirring, the volatiles were removed from the mixture, the residue was triturated with toluene, filtered, and the filtrate was evaporated. Crystallization of the residue from toluene-pentane (slow mixing, r.t. → -30° C) produced large (1~2 mm) block crystals among some powdery precipitate. The block crystals, after isolation, washing with pentane, and drying in vacuo for >2 h, were found to be analytically pure (0.0856 g, 45%). A second crystallization from the residue yielded a less pure portion of the product (0.0534 g, 28%). The structure was confirmed by X-ray crystallography. ¹H NMR (360 MHz, C₆D₆): δ 6.97 (2H, dd, *J* = 7.5, 1.8 Hz), 6.92 (2H, dd, *J* = 7.3, 1.8 Hz), 6.83 (2H, dd, *J* = 7.5, 1.8 Hz), 6.72 (2H, t, *J* = 7.5 Hz), 6.70 (2H, dd, *J* = 7.3, 1.8 Hz), 6.56 (2H, t, *J* = 7.3 Hz), 4.87 (2H, br, central thf-α), 4.50 (2H, br, central thf-α), 2.86 (2H, m, propyl-α-CH), 2.79 (2H, m, propyl-α-CH), 2.69 (4H, br, terminal thf-α), 2.48 (2H, m, propyl-α-CH), 2.43 (2H, m, propyl-α-CH), 2.24 (2H, br, central thf-β), 1.83 (2H, br, central thf-β), 1.73~1.68 (8H, m, propyl-β-CH's, overlapping), 1.51 (3H, t, *J* = 8 Hz), 0.99 (6H, t, *J* = 7.5 Hz), 0.97 (6H, t, *J* = 7.5 Hz), 0.64 (4H, br, terminal thf-β), 0.62 (3H, t, *J* = 8 Hz), 0.30 (3H, q, *J* = 8 Hz), -0.62 (3H, q, *J* = 8 Hz). ¹³C NMR (125 MHz, APT, C₆D₆): δ 156.0 (4°), 153.3 (4°), 150.2 (4°), 147.0 (4°), 133.6 (4°), 132.7 (4°), 131.9 (4°), 131.7 (4°), 129.5 (3°), 129.1 (3°), 127.9 (3°), 126.8 (3°), 121.2 (3°), 118.5 (3°), 71.4 (thf), 70.3 (thf), 33.5, 33.4, 25.9 (thf), 24.5 (thf), 23.4, 23.1, 14.3, 14.2, 9.8, 8.7, 0.05, -1.8. Anal. Calcd for C₃₀H₄₆AlClMg₂O₆: C, 68.70; H, 7.61; Cl, 4.06. Found: C, 68.30; H, 7.63, Cl, 3.52. X-ray crystallography: see **Appendix A-13**.

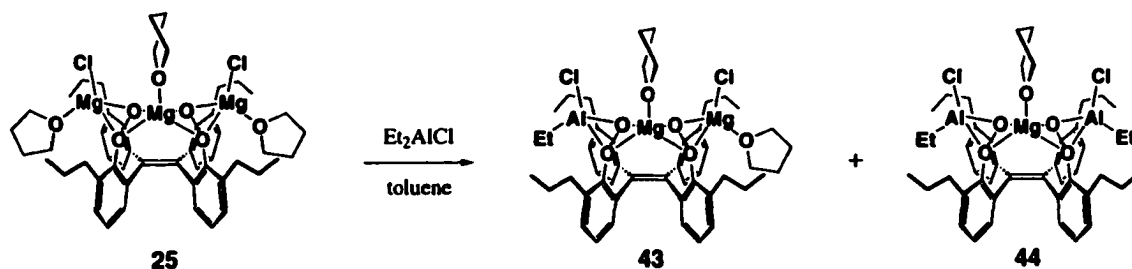
42: C₃₈H₄₀O₄•(AlEt₂)₂•[Mg(thf)]



To a suspension of **25** (FW = 968.7 based on the elemental analysis, 0.4536 g, 0.4683 mmol) in 7 mL of toluene was added Et₂AlCl (0.2295 g, 1.903 mmol) dissolved in 2 mL of toluene. The mixture became clear within a few minutes, then turned cloudy again upon longer stirring. After 16 h the volatiles were removed from the mixture, the residue was triturated with toluene, filtered, and the filtrate was concentrated. By adding some hexanes to the concentrate and cooling to -30 °C, analytically pure crystals were obtained (0.1611 g, 41.6%). Repeating the crystallization yielded an additional 0.087 g (23%).

¹H NMR (400 MHz, C₆D₆): δ 6.89 (4H, dd, *J* = 7.5, 1.8 Hz), 6.77 (4H, dd, *J* = 7.5, 1.8 Hz), 6.70 (4H, t, *J* = 7.5 Hz), 4.40 (4H, m, thf), 2.77 (4H, m, propyl-α-CH₂), 2.41 (4H, m, propyl-α-CH₂), 1.70 (4H, m, thf), 1.63 (8H, m, propyl-β-CH₂H_b), 1.44 (6H, t, *J* = 8.2 Hz), 0.98 (12H, t, *J* = 7.3 Hz, propyl-γ-CH₃), 0.56 (6H, t, *J* = 8.2 Hz), 0.18 (4H, q, *J* = 8.2 Hz), 0.80 (4H, q, *J* = 8.2 Hz). ¹³C NMR (100 MHz, APT, C₆D₆): δ 152.6 (4°), 149.0 (C=C), 133.2 (4°), 131.8 (4°), 129.4 (3°), 127.6 (3°), 121.3 (3°), 70.5 (thf), 31.2, 25.6 (thf), 23.1, 14.2, 9.8, 8.6, 0.24, -1.9. Anal. Calcd for C₅₀H₆₈Al₂MgO₅: C, 72.59; H, 8.28. Found: C, 72.73; H, 8.46. X-ray crystallography: see Appendix A-14.

43 and 44: C₃₈H₄₀O₄•(AlEtCl)•Mg(thf)•MgCl(thf) and C₃₈H₄₀O₄•(AlEtCl)₂•Mg(thf)



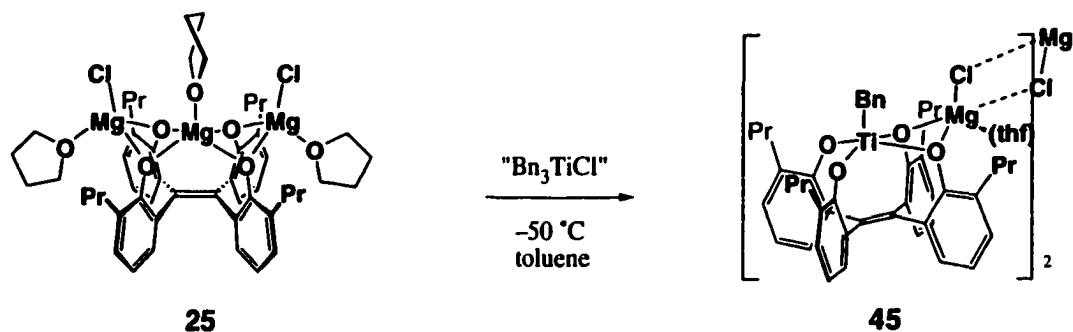
NMR-tube reaction 1. In ca. 0.5 mL of C₆D₆, **25** (FW = 998, 0.0063 g, 0.0063 mmol) and EtAlCl₂ (0.0009 g, 0.007 mmol) were mixed. The starting material was not well dissolved initially, but became mostly dissolved during 1.3 h of occasional shaking. After overnight, the solution showed three compounds: **25**, **43** and **44** in a 1.4 : 4.7 : 1 ratio by ¹H NMR spectroscopy.

NMR-tube reaction 2. In ca. 0.5 mL of C₆D₆, **25** (FW = 920, 0.0057 g, 0.0062 mmol) and EtAlCl₂ (0.0024 g, 0.019 mmol) were mixed. The reaction was complete within 4 h as determined by ¹H NMR spectroscopy. The mixture showed a 2 : 1 ratio of **43** : **44**. After an additional portion of EtAlCl₂ (0.0020 g, 0.016 mmol) was added, the product became **44** exclusively within 45 min (accompanied by some minor unknown species).

43. ¹H NMR (360 MHz, C₆D₆): δ 6.83 (4H, dd, *J* = 7.2, 1.9 Hz), 6.73 (4H, dd, *J* = 7.4, 1.9 Hz), 6.67 (4H, t, *J*_{obs} = 7.4 Hz), 4.69 (4H, m, thf-α), 2.81 (4H, m, α-CH₂), 2.43 (4H, m, α-CH₂), 1.94 (4H, m, thf-β), 1.61 (8H, m, β-CH₂H_b), 0.91 (12H, t, *J* = 7.2 Hz, γ-CH₃), 0.56 (6H, t, *J* = 8 Hz, CH₃CH₂Al), (4H, q, *J* = 8 Hz, CH₃CH₂Al).

44. ¹H NMR (360 MHz, C₆D₆): δ 6.94 (2H, dd, *J* = 7.5, 1.8 Hz), 6.89 (2H, dd, *J* = 7.5, 1.8 Hz), 6.79 (2H, dd, *J* = 7.5, 1.8 Hz), 6.71 (2H, t, *J*_{obs} = 7.5 Hz), 6.70 (2H, dd, *J* = 7.5, 1.8 Hz), 6.56 (2H, t, *J*_{obs} = 7.5 Hz), 4.82 (4H, m, thf-α), 2.90 (2H, m, α-CH₂), 2.78 (2H, m, α-CH₂), 2.50 (2H, m, α-C'H_a), 2.43 ((2H, m, α-C'H_b), 2.155 (4H, m, thf-β), 1.71 (4H, m, β-CH₂H_b), 1.62 (4H, m, β-C'H_aH_b), 0.97 (6H, t, *J* = 7.4 Hz, γ-C'H₃), 0.96 (6H, t, *J* = 7.4 Hz, γ-C'H₃), 0.59 (6H, t, *J* = 8 Hz, CH₃CH₂Al), -0.43 (4H, q, *J* = 8 Hz, CH₃CH₂Al).

45: {C₃₈H₄₀O₄•[Ti(CH₂C₆H₅)]•[Mg(Cl)(thf)]}₂

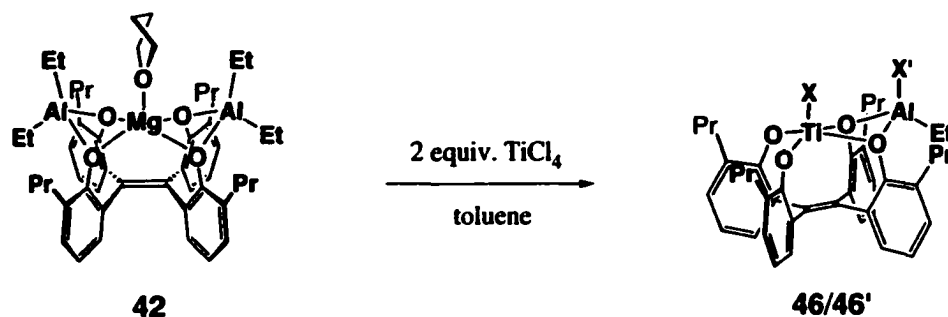


The *in situ* formation of Bn₃TiCl used in this procedure was based on the report by Ivanova et al.¹¹ In the drybox, a solution of TiBn₄ (0.0214 g, 0.0519 mmol) in toluene (5 mL) and a solution of **25** in toluene (3 mL) were prepared in separate reaction bombs. A solution of TiCl₄ in toluene was measured in a polyethylene syringe (2.08 mmol/mL, 1.0 mL, 2.08 mmol) with the needle tip stuck into a rubber stopper to protect the contents

from air. All solutions were taken out of the drybox, kept under N₂ atmosphere using the Schlenk line. The TiBn₄ solution was cooled to -50 °C, and the solution of TiCl₄ was injected into it. After 18 min. of stirring, the solution of **25** was transferred by cannula into the mixture. The temperature was raised very slowly and the mixture was stirred overnight. The final color was brown, lighter than in the beginning, and slightly cloudy. The volatiles were removed in vacuo, the bomb brought into the drybox, and the residue was triturated with toluene. After filtration through Celite-packed pipette, the filtrate was concentrated and recrystallized by adding a few drops of hexane and cooling to -30 °C. After removing the mother liquor, washing the crystals with pentane, and drying under reduced pressure, analytically pure crystalline product was obtained (0.0193 g, 45 %). The mother liquor still contains considerable amount of the product, according to the ¹H NMR spectroscopy. ¹H NMR (360 MHz, C₆D₆): δ 7.62 (2H, br d, *J* = 7.7 Hz), 7.30 (2H, br t, *J* = 7.7 Hz), 6.94 (1H, br t, *J* = 7.3 Hz), 6.85 (2H + 2H, overlapping), 6.72 (2H, dd, *J* = 7.5, 1.7 Hz), 6.63 (2H, dd, *J* = 7.5, 1.7 Hz), 6.58 (2H, t, *J* = 7.4 Hz), 6.50 (2H, t, *J* = 7.5 Hz), 3.86 (2H, br, α-CH₂), 3.62 (2H, s, PhCH₂), 3.05 (4H, br, thf), 2.71 (2H, m, α-C'H₂), 2.47 (2H, m, β-CH₂), 2.26 (2H, m, β-CH₂), 2.17 (2H, br-m, α-CH₂), 1.84 (2H, b, α-C'H₂), 1.45 (4H, m, β-C'H₂H₂), 1.27 (6H, t, *J* = 7.3 Hz), 0.88 (6H, t, *J* = 7.3 Hz), 0.77 (4H, br, thf). ¹³C NMR (125 MHz, BB, C₆D₆): δ 161.0, 160.0, 158.3, 148.1, 146.0, 133.6, 132.7, 132.0, 129.7, 128.7, 128.5, 128.1, 127.5, 127.2, 124.3, 123.8, 121.2, 120.5, 88.6 (PhCH₂), 70.0 (thf), 34.2, 32.4, 24.6 (thf), 23.5, 23.0, 14.8, 14.3. Anal. Calcd for {C₃₈H₄₀O₄•[Ti(CH₂C₆H₅)]₂•[Mg(Cl)(OC₄H₈)]₂: C, 70.77; H, 6.67. Found: C, 69.90; H, 6.48. X-ray crystallography: see **Appendix A-15**.

The scale-up of this reaction was not successful. The major problem was probably external, the degradation of TiCl₄ due to the use of a Schlenk flask instead of a reaction bomb. It is often observed that maintaining TiCl₄ neat or in toluene in a Schlenk flask under nitrogen causes a yellow precipitate to separate out of the liquid/solution. The rubber septum (or the plasticizer in the septum) is suspected to cause this problem, even without direct contact. It is also suspected that normal pre-purified nitrogen is not innocent either, as long as it comes through a rubber tube connecting the Schlenk line to the flask. Although the period of exposure was minimized to <15 minutes to avoid this situation, some precipitate formation was still observed. The failed scale-up run resulted in a mixture of the titanium-sandwich complex **32** (Section 3.1.2.D) and unidentified species that showed broad signals in the ¹H NMR spectrum. The formation of **32** suggests that the reaction between TiCl₄ and TiBn₄ was possibly incomplete. No further scale-up was attempted.

46/46': $C_{38}H_{48}O_4 \cdot (TiX) \cdot (AlEtX')$ (X, X' = Cl or Et)



To a suspension of **42** (0.0569 g, 0.0688 mmol) in 0.5 mL of toluene was added $TiCl_4$ (0.0261 g, 0.138 mmol) dissolved in 1 mL of toluene. The mixture became dark red immediately. After 2 h, the volatiles were removed from the mixture and the residue was triturated with pentane, filtered, and the filtrate was concentrated. The crude yield was 0.0474 g (% yield is not calculated because the molecular weight of the product was uncertain). Repeated crystallization from pentane (r.t. \rightarrow -30 °C) yielded ruby-red crystals that was analyzed by X-ray crystallography. After removing some crystals for elemental analysis, the rest of the crystals along with dried remnant from mother liquor, was analyzed by 1H and ^{13}C NMR spectroscopy. The spectrum showed **46** and **40'** in a 1 : 1 ratio as major species, accompanied by other minor species.

1H NMR (360 MHz, C_6D_6): the signals are tentatively assigned to either **46** or **46'** or unclassifiable, based on the comparison to the results from other reactions (Section 3.2.3, **Scheme 3.18**) containing different ratios of these species. Signals from the liberated aluminum species are not listed.

46. 1H NMR (360 MHz, C_6D_6): δ 6.80 (2H, dd, $J = 7.7$ Hz), 6.76 (2H, dd, $J = \sim 8$, 1~1.5 Hz), the other 2H x 4 signals are in the regions 6.79~6.75 or 6.65~6.55 ppm, but not clearly identified; 2.84 (2H, m, propyl- α -CH), 2.65 (2H, m, propyl- α -CH), 2.49 (2H, m, propyl- α -CH), 2.37 (2H, m, propyl- α -CH), 1.74 (2H, m, propyl- β -CH), 1.64 (2H, m?, propyl- β -CH?), 1.44 (4H, m, propyl- β -CH₂), 0.98 (6H, t, $J = 7.3$ Hz, propyl- γ -CH₃), 0.77 (6H, t, $J = 7.3\text{--}7.5$ Hz, propyl- γ -CH₃), 0.585 (3H, t, $J = 8$ Hz, $AlCH_2CH_3$), -0.65 (2H, q, $J = 8$ Hz, $AlCH_2CH_3$). **46':** 1H NMR (360 MHz, C_6D_6): δ 6.79~6.75 ppm and 6.65~6.55 ppm (2H x 6, overlapping themselves and with signals from **46**), 3.00 (2H, m, propyl- α -CH), 2.98 (2H, m, propyl- α -CH), 2.55 (4H, overlapping m, propyl- α -CH), 2.35 (2H, m, propyl- α -CH), 2.88~1.55 (8H, overlapping m, propyl- β -CH), 1.04 (6H, t, $J = 7.3$ Hz, propyl- γ -CH₃), 0.86 (6H, t, $J = 7.3$ Hz, propyl- γ -CH₃), 0.605 (3H, t, $J = 8$ Hz, $AlCH_2CH_3$), -0.38 (2H, q, $J = 8$ Hz, $AlCH_2CH_3$). **Unclassified signals:** 3.42 (4H, m, THF- α), 3.36 (2H, q, $J = 7.3$ Hz, $TiCH_2CH_3$), 2.19 (3H, t, $J = \sim 7.5$ Hz, $TiCH_2CH_3$), 1.55 (4H, m, THF- β).

¹³C NMR (100 MHz, BB, C₆D₆) of **46** + **46'** (not specifically classified): δ 162.1 (4°), 160.4 (4°), 160.2 (4°), 158.6 (4°), 154.6 (4°), 152.5 (4°), 145.7 (4°), 141.8 (4°), 135.9 (4°), 135.2 (4°), 133.5 (4°), 132.6 (4°), 131.7 (4°), 131.2 (4°), 130.5 (3°), 130.4 (3°), 130.0 (3°), 129.7 (3°), 129.0 (3°), 128.5 (3°), 128.4 (3°), 124.3 (3°), 124.0 (3°), 123.7 (3°), 123.2 (3°), 121.8 (3°), 33.5 (?), 33.4 (propyl-α), 33.3 (propyl-α), 33.1 (propyl-α), 32.4 (propyl-α), 24.5 (?), 23.4 (propyl-β), 23.3 (propyl-β), 23.1 (2 x propyl-β), 19.7 (?), 14.2 (2 x propyl-γ), 14.1 (propyl-γ), 13.8 (propyl-γ), 13.3 (?), 9.5 (AlCH₂CH₃ or ?), 8.5 (AlCH₂CH₃ or ?), 8.2 (AlCH₂CH₃ or ?), 7.8 (AlCH₂CH₃ or ?), 0.8 (AlCH₂CH₃), -1.1 (AlCH₂CH₃).

Elemental analysis did not match any possible formula for **46/46'**, probably due to incomplete removal of solvents or reagents/byproducts.

X-ray crystallography: see **Appendix A-16**.

3.5. References and Notes

¹ Verkerk, U. Ph.D. Dissertation, University of Alberta, 2001.

² Markies, P. R.; Akkerman, O. S.; Bickelhaupt, F.; Smeets, W. J. J.; Spek, A. L. *Adv. Organomet. Chem.* **1991**, *32*, 147-226.

³ Toroyanov, S. I.; Varga, V.; Mach, K. *Organometallics* **1993**, *12*, 2820-2824.

⁴ Haigh, C. W.; Mallion, R. B. *Org. Mag. Res.* **1972**, *4*, 203-228.

⁵ Jorgensen, W. L.; Severance, D. L. *J. Am. Chem. Soc.* **1990**, *112*, 4758-4774.

⁶ Typical interatomic length of agostic interaction is 2 to 2.5 Å, according to: Brookhart, M.; Green, M. L. H.; Wong, L-L. *Prog. Inorg. Chem.* **1988**, *36*, 1-124.

⁷ See Appendix A-5 (**30a**) and A-7 (**31**).

⁸ A recent review of co-catalysts for metal-catalyzed olefin polymerization: Chen, E. Y-X.; Marks, T. J. *Chem. Rev.* **2000**, *100*, 1391-1434.

⁹ Mattheis, C.; van der Zeijden, A. A. H.; Frohlich, R. *J. Organomet. Chem.* **2000**, *602*, 51-58.

¹⁰ Zucchini, U.; Albizzati, E.; Giannini, U. *J. Organomet. Chem.* **1971**, *26*, 357-372 and references 1 to 5 therein.

¹¹ Ivanova, V. P.; Estrin, A. S. *J. Gen. Chem. USSR*, **1990**, *60*, 18-21.

¹² Reduction of Ti does not seem to occur to TiBr₄, when mixed with TiBn₄, unlike the TiCl₄ case. Zucchini *et al.* prepared Bn₂TiBr₂ by mixing TiBr₄ and TiBn₄ at 1 : 1 ratio. See reference 10.

¹³ Schrock, R. R. *J. Organomet. Chem.* **1976**, *122*, 209-225.

¹⁴ (a) Cardoso, A. M.; Clark, R. J. H.; Moorhouse, S. J. *Chem. Soc. Dalton Trans.* **1980**, 1156-1160. (b) Hart, S. L.; Duncalf, D. J.; Hastings, J. J.; McCamley, A.; Taylor, P. C. *J. Chem. Soc. Dalton Trans.* **1996**, 2843-2849.

¹⁵ Van der Linden, A.; Schaverien, C. J.; Meijboom, N.; Ganter, C.; Orpen, A. G. *J. Am. Chem. Soc.* **1995**, *117*, 3008-3021.

¹⁶ See Chapter 5, section 5.4.

Chapter 4

Metal Complexes Derived from *E*- and *Z*-Bis(2-hydroxyphenyl)-bis(2-methoxyphenyl)ethene (3*E*/3*Z*): Structure, Spectroscopic Features and Chemical Behavior

Table of Contents

4.0. Introduction	170
4.1. Al Complexes of Ligand 3<i>E</i>	172
4.1.A. Adducts of Et ₃ Al	172
4.1.B. Adducts of Et ₂ AlCl	176
4.1.C. Aluminum Abstraction by Coordinating Solvent	180
4.1.D. From Mononuclear to Dinuclear	181
4.2. Ti Complexes of Ligands 3<i>E</i>/3<i>Z</i>	182
4.2.A. TiCl ₂ Complex of 3 <i>E</i>	183
4.2.B. CpTiCl ₂ Complexes of 3 <i>E</i>	185
4.2.C. TiBn ₂ Complex of 3 <i>E</i>	187
4.2.D. Ti Chemistry of Ligand 3 <i>Z</i>	188
4.3. Attempts to Prepare Al/Ti Complexes of Ligand 3<i>E</i>	192
4.3.A. Reactions of a Ti Complex 52 with Al Reagents	192
4.3.B. Reactions of Al Complexes with TiCl ₄	199
4.4. Conclusion	202
4.5. Experimental	203
4.6. References	212

4.0. Introduction

The coordination chemistry of the di-hydroxy-di-methoxy ligands **3E** and **3Z**, *E*- and *Z*-bis(2-benzyloxyphenyl)-bis(2-methoxyphenyl)ethene, was studied using Al(III), Ti(IV) and Mg(II) metal atoms, following the general direction of our research (Chapter 2). The synthesis, structural and spectroscopic features, and chemical behavior of metal complexes prepared from ligands **3E** and **3Z** are presented in this chapter.

Many discrete Al(III) and Ti(IV) complexes were obtained for the *E*-ligand **3E**, including hetero-polymetallic Al/Ti species. The preliminary titanium chemistry of *Z*-ligand **3Z**, however, showed that this ligand is less suitable for creating discrete complexes. Only one Ti complex was structurally characterized for ligand **3Z**. Neither **3E** nor **3Z** gave discrete Mg salts, in contrast to the *ortho*-propylated tetrahydroxy ligand **7**, which provided well-defined tri-nuclear magnesium complexes and derivatives (Chapter 3).

In this chapter, mono- and dinuclear aluminum complexes derived from **3E** and their chemical interconversions are discussed first. Coordinating solvents induced aluminum-abstraction chemistry to convert dinuclear complexes into mononuclear species. A similar chemistry was discussed for the aluminum complexes of ligand **7** (Chapter 3, Section 3.1.3). The aluminum chemistry of ligand **3E** also showed the *reverse* of the aluminum abstraction when a second aluminum center was added to a mononuclear complex to form dinuclear species.

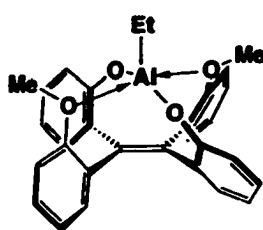
The titanium chemistry of ligands **3E** and **3Z** is presented in the next section. Several mononuclear titanium complexes of **3E** were synthesized and structurally characterized. The *Z*-ligand **3Z**, in contrast, exhibited poor chelating and organizing behavior in the formation of discrete complexes.

Our attempts to construct hetero-polymetallic species on the **3E** system are described in the final section. Hetero-polymetallic targets were restricted to the combination of Al and Ti metal atoms. One Al/Ti hetero-polymetallic complex was cleanly obtained and structurally characterized.

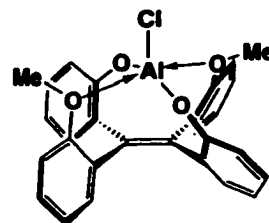
Figure 4.1 provides the list of compounds derived from ligand **3E** and discussed in Chapter 3. Those characterized by X-ray crystallography are indicated in the figure.

Figure 4.1. List of characterized or semi-characterized compounds in Chapter 4.

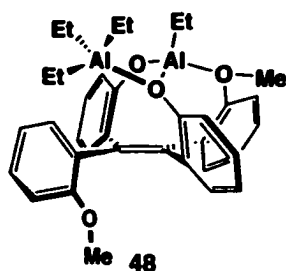
Aluminum complexes from 3E



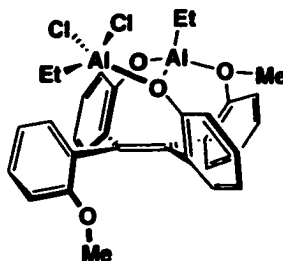
47
(X-ray)



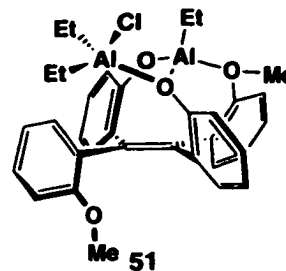
49



48

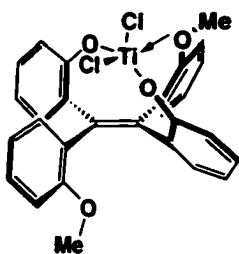


50
(X-ray)

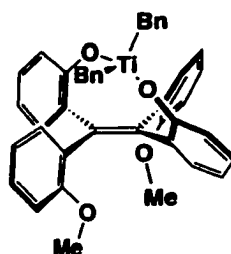


51

Titanium complexes from 3E

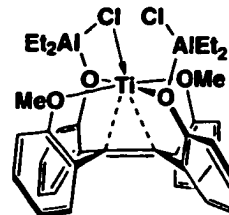


52
(X-ray)

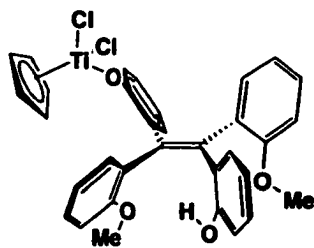


55

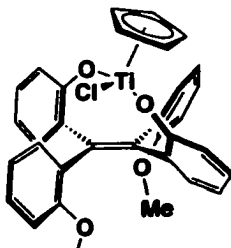
Aluminum/titanium complex from 3E



59
(X-ray)

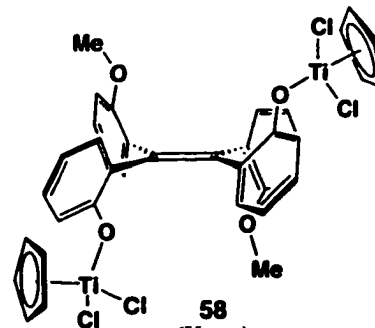


53
(X-ray)



54

Titanium complex from 3Z



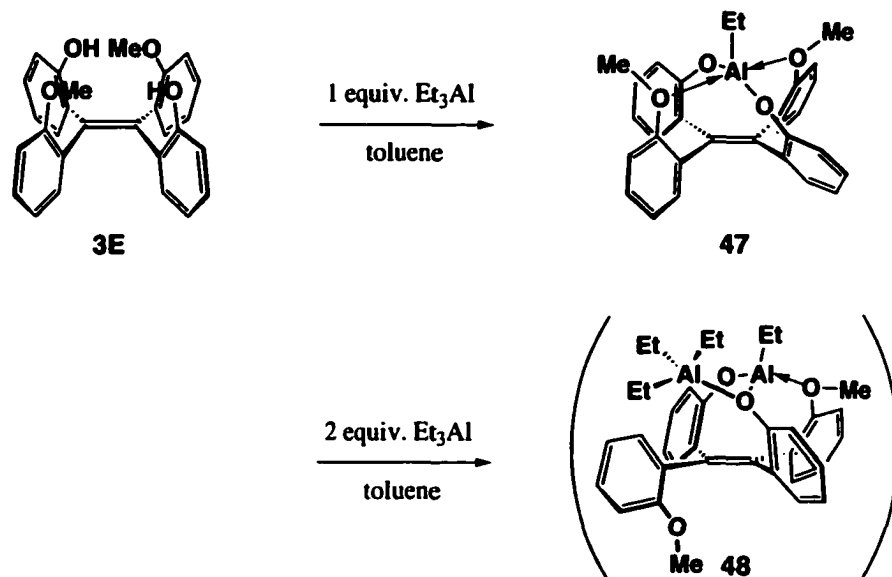
58
(X-ray)

4.1. Al Complexes of Ligand 3E

Mononuclear and dinuclear aluminum complexes were prepared from ligand **3E** and Et_3Al or Et_2AlCl with appropriate stoichiometry. The interconversions of the dinuclear and mononuclear aluminum complexes were investigated.

4.1.A. Adducts of Et_3Al

The addition of one or two equivalents of Et_3Al to ligand **3E** in toluene resulted in the formation of the mononuclear ethylaluminum complex **47** and the dinuclear adduct **48** (Scheme 4.1). The structure of **48** is tentatively assigned (*vide infra*).



Scheme 4.1. Formation of **47** and **48** from the reaction between ligand **3E** and one or two equivalents of Et_3Al .

i) Mononuclear "AlEt" complex 47. The reaction that gave complex **47** was clean, and analytically pure crystals were obtained by simple crystallization from benzene. The structure of complex **47** was confirmed by X-ray crystallography (Figure 4.2).

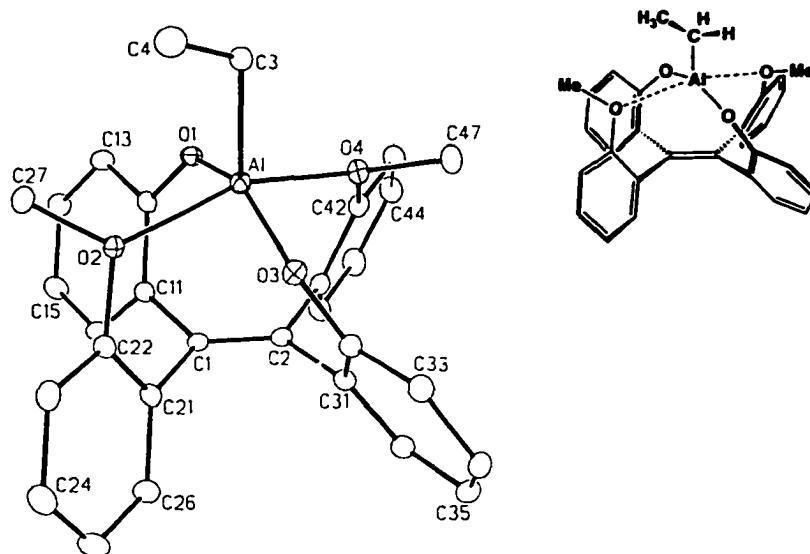


Figure 4.2. X-ray crystallographic structure of **47**.

Bond length (Å): C1-C2 = 1.345(3), Al-O1 = 1.7883(13), Al-O2 = 2.0956(14), Al-O3 = 1.7912(14), Al-O4 = 2.0862(13), Al-C3 = 1.9671(17). **Interatomic angle (deg):** O1-Al-O2 = 87.60(6), O1-Al-O3 = 148.47(6), O1-Al-O4 = 85.01(5), O1-Al-C3 = 105.33(7), O2-Al-O3 = 85.59(6), O2-Al-O4 = 155.66(5), O2-Al-C3 = 102.66(7), O3-Al-O4 = 88.67(6), O3-Al-C3 = 106.20(8), O4-Al-C3 = 101.66(7). **Torsional angle through C1-C2 bond (deg):** C11-C1-C2-C31 = 172.56(15), C11-C1-C2-C41 = -1.4(3), C21-C1-C2-C31 = -1.9(3), C21-C1-C2-C41 = -175.89(15). **Ring torsion angle against C1-C2 bond (deg):** C2-C1-C11-C12 = -65.6(2), C2-C1-C11-C16 = 112.8(2), C2-C1-C21-C22 = 105.4(2), C2-C1-C21-C26 = -74.8(3), C1-C2-C31-C32 = -66.3(2), C1-C2-C31-C36 = 116.8(2), C1-C2-C41-C42 = 104.9(2), C1-C2-C41-C46 = -75.2(3).

In the crystal structure, both of the methoxy groups are coordinated to the Al atom to form pseudo-square pyramidal geometry. The O₄ plane is obviously not square, but diamond-shaped with two long and two short Al-O bonds. The Al atom is located above the O₄ plane, with no indication of interaction with the olefin double bond. The four aryl rings are tilted in a helical way. The rings with phenolato oxygen donors (C11-C16 and C31-C36 rings) are tilted by ca. 25° from the position perpendicular to the olefin ring. The other two rings with the methoxy groups are tilted by ca. 15°.

The ^1H NMR spectroscopic features are all consistent with the crystallographic structure: all-sharp signals reflecting the rigid structure; symmetrical ligand framework; and slightly split (by ~ 2 Hz) methylene proton signals of the ethyl group reflecting the diastereotopicity. The methoxy signal appears at 3.18 ppm, close to the methoxy signal in the starting material **3E** (3.21 ppm).

The ethyl group on the Al atom (CH_3 : 1.68 ppm and CH_2 : 0.60 ppm) is more downfield than is typical, roughly by 0.3 to 0.7 ppm.* The position right above the central metal atom was found to be deshielded in the trinuclear magnesium complexes **25** to **29**, as discussed in Chapter 3, Section 3.1.1 (Figure 4.3): the deshielding for the THF molecule at the central Mg atom was by over 1.4 ppm. The deshielding for the ethyl group in **47** is much weaker: the greater distance from the aryl rings (the central Al atom in **47** is more "above" than the Mg atom in **25**) may be partly responsible. The tilting of the aryl rings may also orient the most effective deshielding region away from the ethyl group.

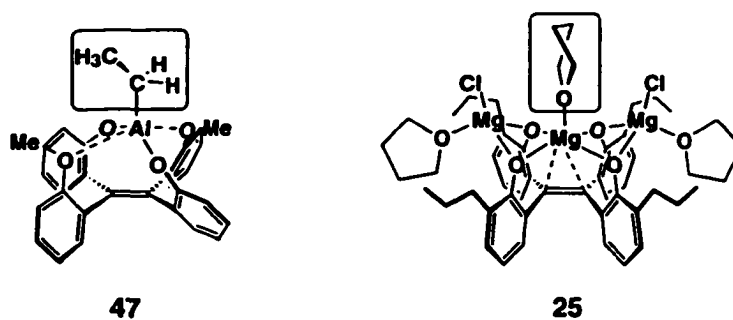


Figure 4.3. The position above the central metal atom: in **47** and **25**.

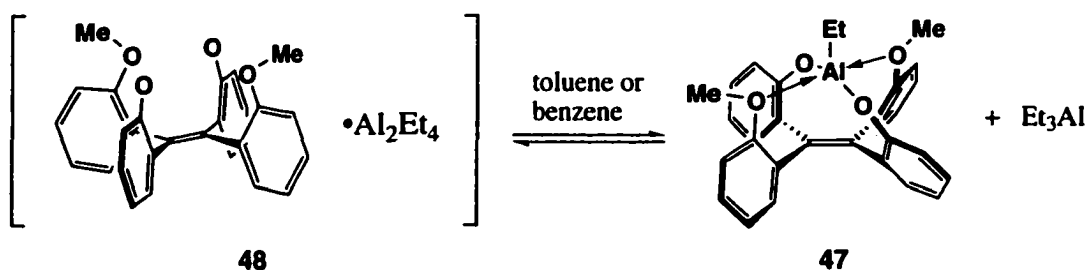
ii) **Dinuclear complex 48.** An unsymmetrical dinuclear structure is tentatively assigned to **48**, based on the analogy to the related dinuclear complex **50** (*vide infra*). The analytically pure product was obtained by rather quick crystallization/precipitation: adding hexane to a concentrated and already partly cloudy toluene solution, then cooling to -30 °C. The white, opaque but not crystalline precipitate showed the C/H elemental analysis perfectly matching the expected values for a dinuclear product $\text{C}_{28}\text{H}_{22}\text{O}_4\text{Al}_2\text{Et}_4$ ($\text{C}_{28}\text{H}_{22}\text{O}_4 = [3\text{E} - 2\text{H}]$).

* Compared to Et_3Al (CH_3 : 1.10 and CH_2 : 0.28 ppm) and EtAlCl_2 (CH_3 : 0.89 and CH_2 : 0.14 ppm).

^1H NMR spectroscopy was not helpful in determining the structure of **48**. The ^1H NMR spectrum in C_6D_6 consists of broad and complicated signals at room temperature, although the integrals of the aromatic region, methoxy and ethylaluminum regions are consistent with the expected formula of **48**. At $75\text{ }^\circ\text{C}$, the signals became sharp and simplified, showing a symmetrical, or completely averaged ligand framework.

Interestingly, slow crystallization of **48** yielded crystals of the aforementioned mononuclear complex **47**. When the analytically pure compound **48** was dissolved in toluene and recrystallized by layering on hexanes for slow diffusion, with simultaneous cooling to $-30\text{ }^\circ\text{C}$, a few big, clear prism crystals were formed in the hexanes layer overnight. The crystals turned out to be the mononuclear "AlEt" complex **47**, confirmed by ^1H NMR spectroscopy and X-ray crystallography (the ORTEP provided in Figure 4.2 was actually from these crystals). The residue after removal of the volatiles from the mother liquid showed a broad and complicated ^1H NMR spectrum, but the pattern does not match that of **48**.

The broadness of the ^1H NMR signals of **48** and the formation of the mononuclear crystal **47** from the solution suggest that the dinuclear species **48** exists in equilibrium with **47** in solution (Scheme 4.2).

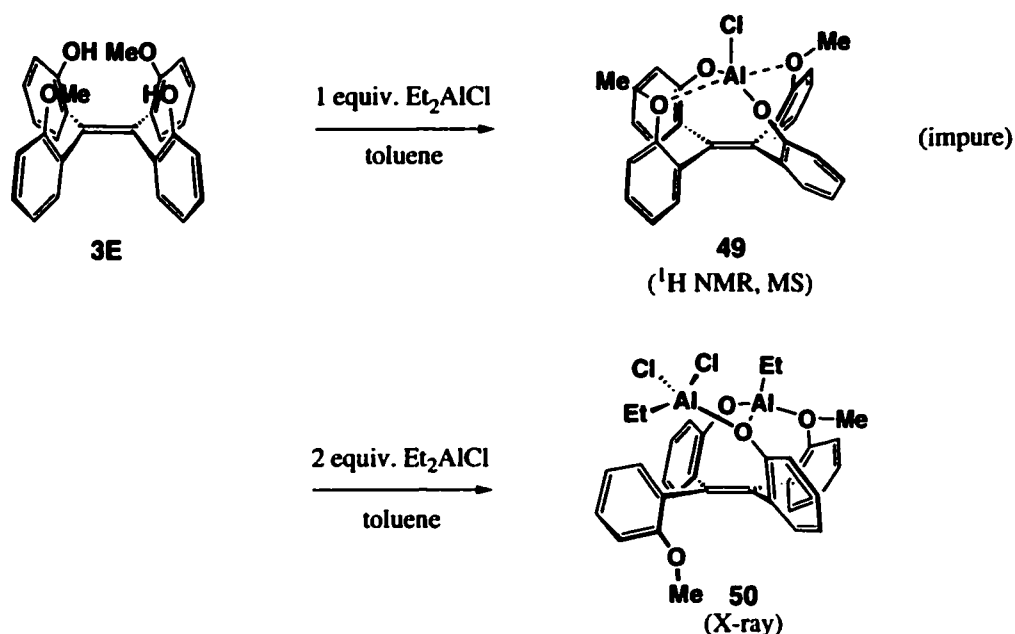


Scheme 4.2. Equilibrium between **48** and **47**.

The equilibrium was confirmed by a reaction between **47** and one equivalent of Et_3Al in C_6D_6 to produce **48**. The resulting mixture showed broad ^1H NMR signals very similar to those of **48**. The mother liquor of the crystallization of **47** from a solution of **48** must have contained a higher stoichiometry of Et_3Al , affecting the equilibrating system and producing a different appearance.

4.1.B. Adducts of Et₂AlCl

The results from the addition of one or two equivalents of Et₂AlCl to ligand **3E** were mostly analogous to the addition of Et₃Al described in the previous section. The one-equivalent addition resulted in a mononuclear "AlCl" complex **49**, and the two-equivalent addition produced the dinuclear complex **50** (Scheme 4.3). The unsymmetrical structure of **50**, confirmed by X-ray crystallography, provided useful information about the chemical behavior of the two-equivalent aluminum adducts **48** and **50**.



Scheme 4.3. Formation of **49** and **50** from the reaction between ligand **3E** and one or two equivalents of Et₂AlCl.

i) Mononuclear adduct 49. The addition of one equivalent of Et₂AlCl to **3E** in toluene resulted in the formation of a white precipitate. The high-resolution mass spectrometry of the precipitate showed a parent peak of C₂₈H₂₂O₄AlCl (100%). The ¹H NMR spectroscopy of a dilute solution in CD₃CN cleanly showed a symmetrical ligand framework with no ethyl group. Both data are consistent with the proposed structure of **49** (Scheme 4.3). A concentrated solution of the precipitate in CD₃CN, however, showed a mixture of **49** and

another unidentified species (**X**) in about a 1 : 1 ratio. In the spectrum, compound **X** showed the symmetrical ligand framework and relatively broad methoxy groups, a result suggesting a non-rigid structure. Why compound **X** was not observed in the initial spectrum of the dilute solution is not clear.

Compound **X** was also found in the reaction of **3E** with two equivalents of EtAlCl_2 . This recipe was expected to give a dinuclear " Al_2Cl_4 " complex. The crude product, however, was a mixture of **49** and **X** in a ~1 : 2 ratio, according to ^1H NMR spectroscopy in CD_3CN . Thus, compound **X** might have been the expected dinuclear " Al_2Cl_4 " complex. However, this hypothesis was not supported by the observation of **X** in the above-mentioned [**3E** + 1 Et_2AlCl] experiment (see Scheme 4.3), in which not enough chloride equivalents were provided. The identity of this symmetrical byproduct **X** thus remains unclear.

ii) **Dinuclear complex 50.** Addition of two equivalents of Et_2AlCl to ligand **3E** gave the formally dinuclear " $(\text{AlEtCl})_2$ " complex **50** as a major product, with a small amount of a mononuclear " AlCl " complex **49** as a byproduct (2 to 14 %). The formation of **49** is presumably the result of the 1 : 1 reaction between **3E** and Et_2AlCl . The C/H elemental analysis of the crystallized portion of the product mixture showed the values expected for $\text{C}_{28}\text{H}_{22}\text{O}_4 \cdot \text{Al}_2 \cdot \text{Et}_2 \cdot \text{Cl}_2$ ($\text{C}_{28}\text{H}_{22}\text{O}_4 = [\text{3E} - 2\text{H}]$). The unsymmetrical structure of **50** was confirmed by X-ray crystallography (Figure 4.4). The structure may be described as a "core" mononuclear unit, equivalent to the " AlEt " complex **47**, attached to one equivalent of EtAlCl_2 at the second lone pair of one of the " ArO " groups coordinated to the central aluminum atom. One methoxy ether group remains as a spectator. It is interesting that the EtAlCl_2 unit stays intact on the core molecule, with no dissociation.

Unlike the " Al_2Et_4 " analogue **48**, complex **50** shows sharp ^1H NMR signals (in C_6D_6) at room temperature. The ^1H NMR spectrum is consistent with the unsymmetrical ligand framework shown in the crystal structure, with two inequivalent ethyl groups. The sixteen aromatic signals (from four different aryl rings) are widely spread between 7.73 and 6.11 ppm. The sharpness of the signals supports the conclusion that EtAlCl_2 does not dissociate, but is tightly bound to the core. At 75 °C, the signals become slightly broadened, possibly indicating partial dissociation of " EtAlCl_2 " unit, but the unsymmetrical structure still being preserved.

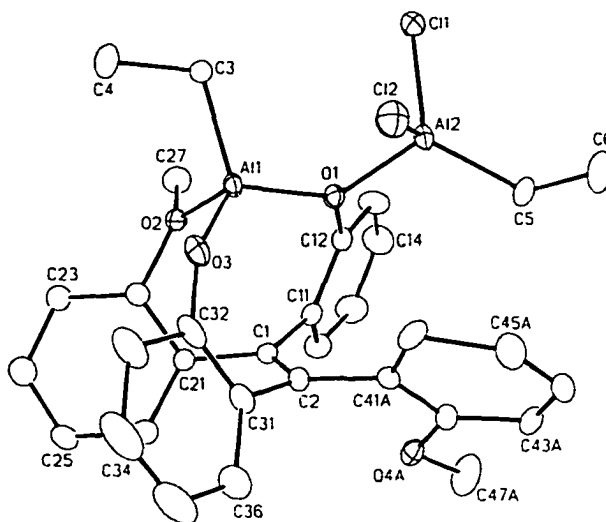
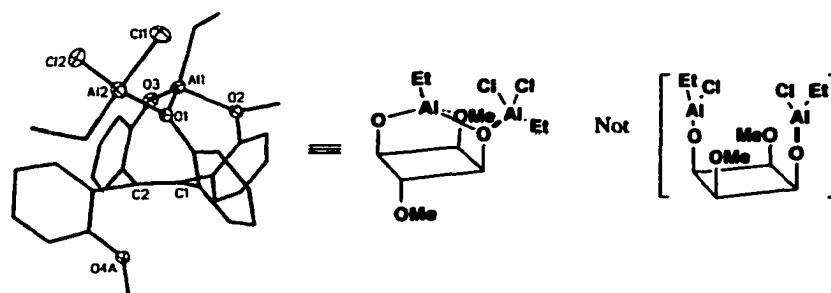
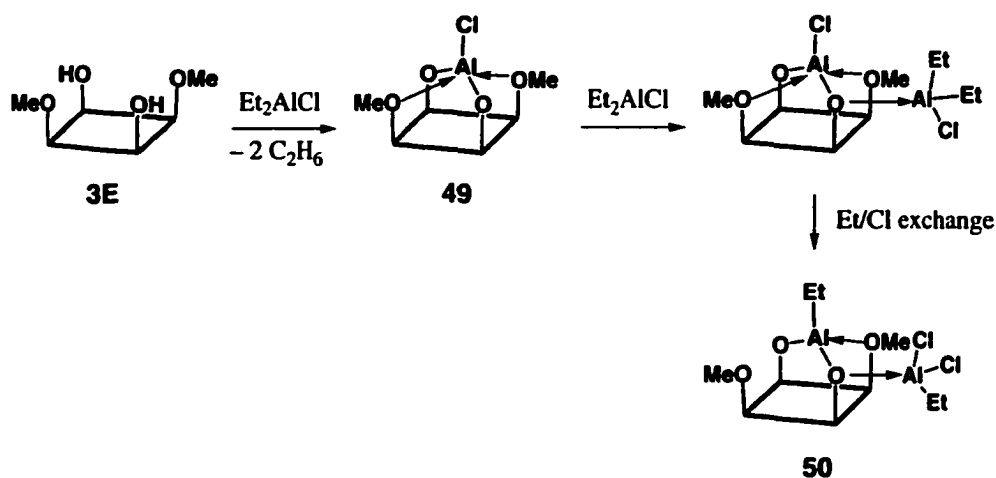


Figure 4.4. X-ray crystallographic structure of **50**.

Bond lengths (Å): C11-Al2 = 2.156(2), Cl2-Al2 = 2.142(3), Al1-O1 = 1.852(4), Al1-O2 = 1.920(4), Al1-O3 = 1.707(4), Al1-C3 = 1.934(5), Al2-O1 = 1.864(4), Al2-C5 = 1.942(6), C1-C2 = 1.328(8). Interatomic angles (deg): O1-Al1-O2 = 197.40(17), O1-Al1-O3 = 1122.0(2), O1-Al1-C3 = 1112.3(2), O2-Al1-O3 = 1102.40(19), O2-Al1-C3 = 1101.1(2), O3-Al1-C3 = 1116.3(2), C11-Al2-Cl2 = 1107.44(10), C11-Al2-O1 = 1105.41(14), C11-Al2-C5 = 1113.2(2), Cl2-Al2-O1 = 199.15(14), Cl2-Al2-C5 = 1118.3(2), O1-Al2-C5 = 1111.8(2). Torsional angles of olefin plane (deg): C11-C1-C2-C31 = 162.8(5), C11-C1-C2-C41A = -2.3(11), C11-C1-C2-C41B = -32.3(10), C21-C1-C2-C31 = -14.3(8), C21-C1-C2-C41A = -179.4(7), C21-C1-C2-C41B = 150.6(8). Ring torsion angles (deg): C2-C1-C11-C12 = -70.0(7), C2-C1-C11-C16 = 117.7(7), C2-C1-C21-C22 = 118.2(7), C2-C1-C21-C26 = -59.9(8), C1-C2-C31-C32 = -61.1(8), C1-C2-C31-C36 = 119.3(7), C1-C2-C41A-C42A = -56.3(11), C1-C2-C41A-C46A = 124.3(11), C1-C2-C41B-C42B = 141.5(13), C1-C2-C41B-C46B = -25(2).

The methylene protons of both ethyl groups, one on the central Al atom and the other in the terminal AlEtCl₂ unit, are notably split, reflecting the highly unsymmetrical structure. The chemical shifts and appearance of these two ethyl groups are quite different: one is sharp and downfield-shifted compared to free EtAlCl₂ (by 1.1 to 0.6 ppm), and the other is upfield-shifted (by 0.8 to 1 ppm) and slightly broad.^b The former is assigned to the ethyl group on the central Al atom, from the similar chemical shift to the ethyl group in the mononuclear complex **47**. The latter is therefore the ethyl group in the terminal "AlEtCl₂" unit. Its upfield-shift relative to free EtAlCl₂ obviously comes from the additional dative coordination by the oxygen donor of the core complex. The broadness of the terminal ethyl signals comes most likely from the slow rotation around the O–AlEtCl₂ bond.

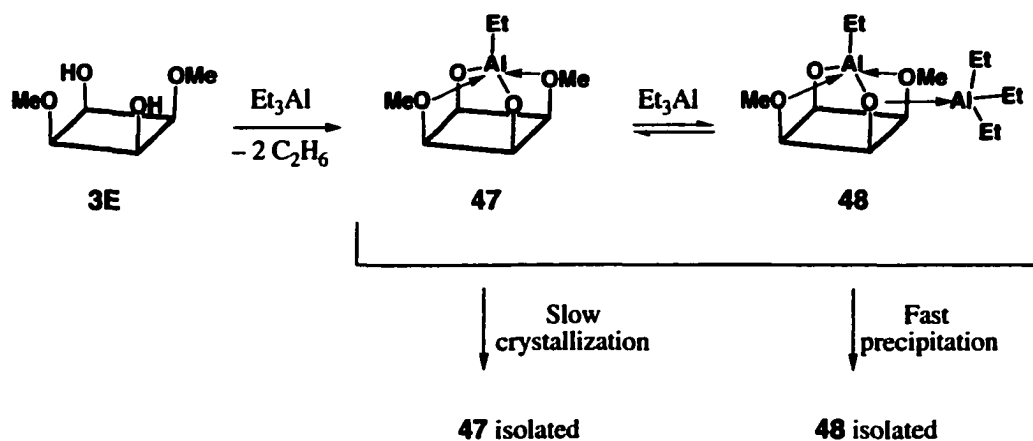
The formation of the dinuclear (AlEt)(AlEtCl₂) complex **50** may be explained as a stepwise reaction of **3E** with Et₂AlCl, as suggested in Scheme 4.4. In this scheme, the reaction of **3E** with the first equivalent of Et₂AlCl gives **49**, the mononuclear "AlCl" complex. The second equivalent of Et₂AlCl first interacts at the second lone pair of an aryloxy oxygen, then replaces the chloride in **49** with an ethyl group to give **50**.



Scheme 4.4. Proposed mechanism for the formation of **50**.

^b Chemical shift of EtAlCl₂ (CH₃: 0.89 ppm and CH₂: 0.14 ppm).

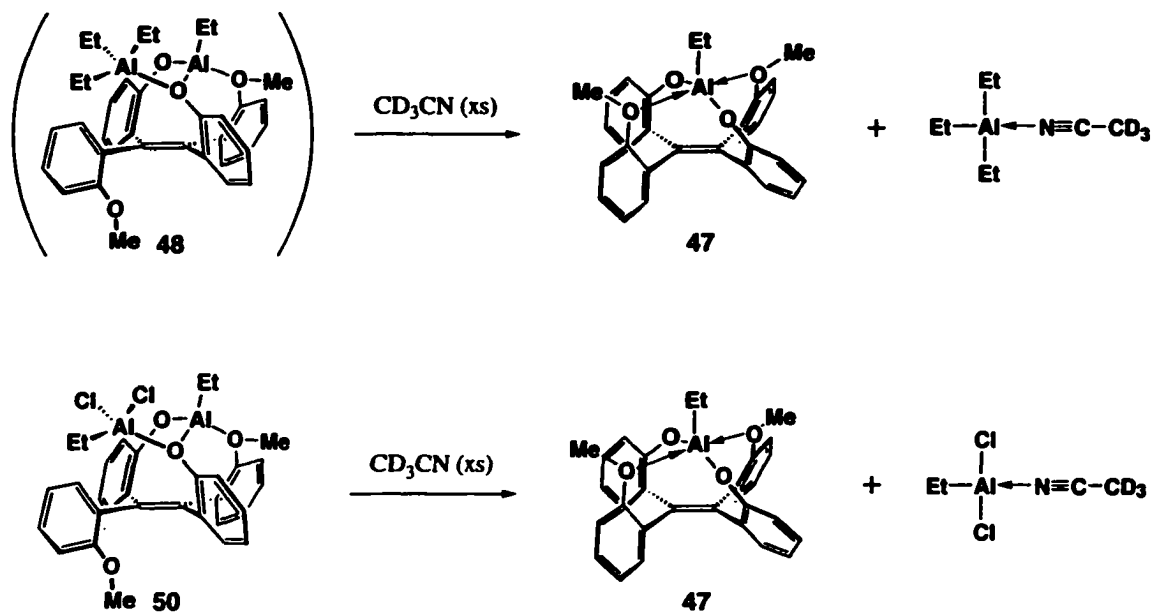
The structure of **50** and the apparent intramolecular disproportionation strongly suggests that similar chemistry occurs to the two-equivalent adduct of Et_3Al (**48**, see **Scheme 4.1**). The greatest difference is that the Et_3Al moiety is not always intact in **48**, but partly dissociates in solution (**Scheme 4.5**). Et_3Al is less Lewis acidic than EtAlCl_2 , thus requiring less stabilization by the oxygen donor of the "core" complex **47**. The dissociation of Et_3Al allows the formation of mononuclear complex **47** in solution, which can be crystallized out by a slow crystallization process (Section 4.1.A-ii).



Scheme 4.5. Proposed structure of **48** and mechanism of the formation.

4.1.C. Aluminum Abstraction by Coordinating Solvent

When dissolved in a coordinating solvent, CD_3CN , the dinuclear complexes **48** and **50** both showed a mixture of mononuclear complex **47** and liberated Et_3Al or EtAlCl_2 , respectively, in the ^1H NMR spectroscopy (**Scheme 4.6**). CD_3CN presumably stabilized the liberated Et_3Al or EtAlCl_2 moieties by coordination, preventing the reaction with **47** from going back to the dinuclear species. This behavior further supports the suggestion that the structure of **48** is an unsymmetrical $(\text{AlEt})(\text{AlEt}_3)$ species (analogous to that of **50**), in which the AlEt_3 unit is "ready" to dissociate.

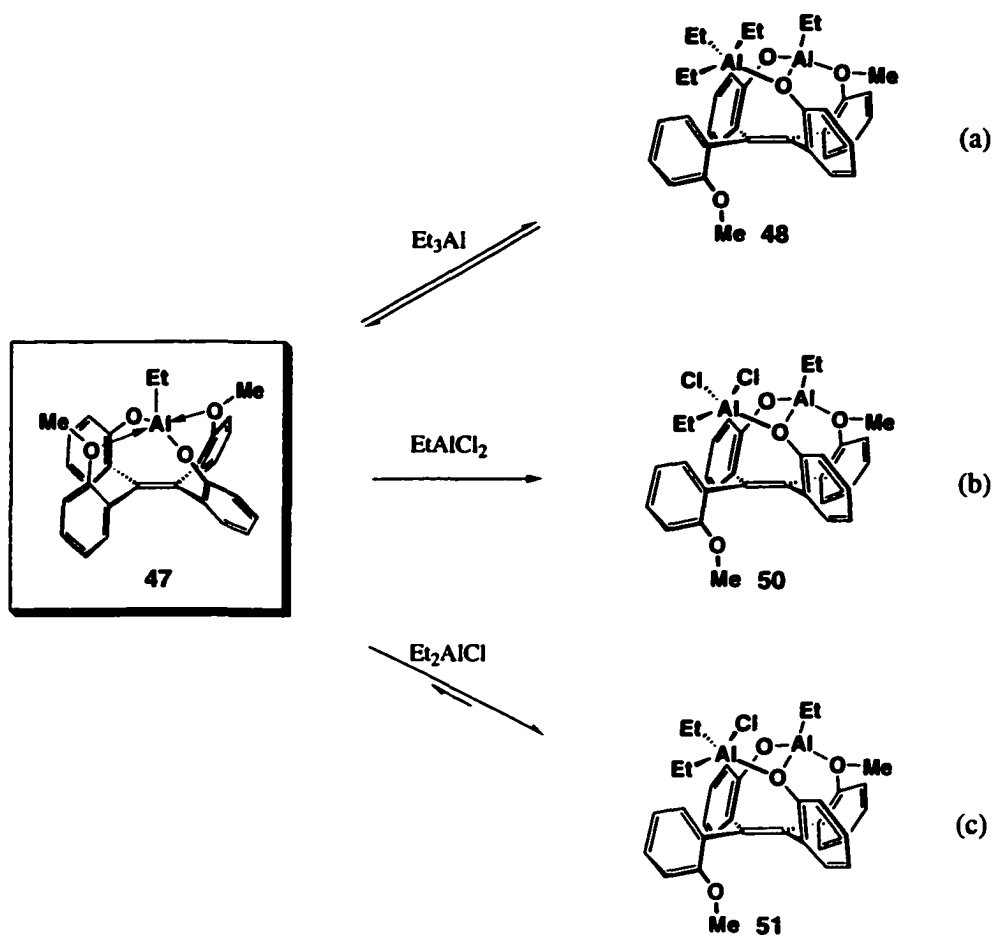


Scheme 4.6. Aluminum abstraction by CD_3CN from **48** and **50**.

4.1.D. From Mononuclear to Dinuclear

It was shown (Section 4.1.A-ii) that the addition of one equivalent of Et_3Al to the mononuclear complex **47** in C_6D_6 produced the same ^1H NMR spectrum as that of the dinuclear complex **48** (Scheme 4.7-a). This "reverse" formation of a dinuclear system from the core mononuclear complex was also successful in converting **47** into **50** (Scheme 4.7-b). The same approach but using Et_2AlCl was used to produce a new dinuclear complex **51**, which cannot be produced from the addition of two equivalents of an alkylaluminum reagent to ligand **3E** (Scheme 4.7-c). The structure of **51** depicted in Scheme 4.7-c is tentatively assigned based on the unsymmetrical ligand framework observed in the ^1H NMR spectrum, the appearance of three different ethyl groups, and by analogy to the other cases shown in the scheme.

The ^1H NMR signals of **51** are all slightly broadened, suggesting some degree of dissociation of the " AlEt_2Cl " unit in solution. The unsymmetrical framework, however, is kept reasonably intact. The degree of dissociation is obviously intermediate between complexes **48** and **50**, reflecting the intermediate Lewis acidity of the corresponding alkyl moiety Et_2AlCl .



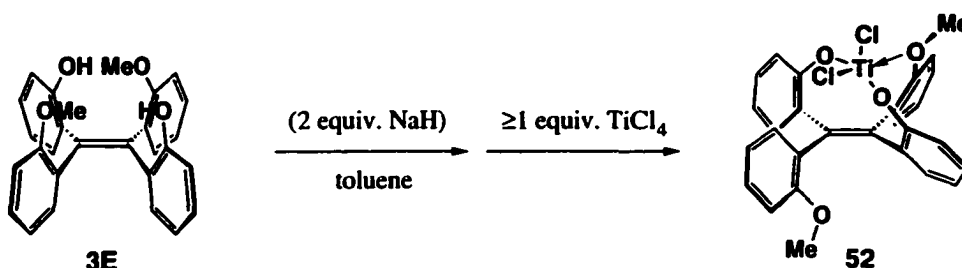
Scheme 4.7. Addition of alkylaluminum reagent to **47**.

4.2. Ti Complexes of Ligands 3E/3Z

The chemical behavior of ligands **3E** and **3Z** toward titanium reagents was quite different. The former showed its capability/preference to form chelating mononuclear complexes, such as "TiCl₂" complex **52**, "CpTiCl" complex **54**, and "TiBn₂" complex **55** (*vide infra*). The latter, in contrast, showed no preference for chelation or formation of discrete complexes.

4.2.A. TiCl_2 Complex of 3E

The mononuclear " TiCl_2 " complex **52** was synthesized by adding one equivalent of TiCl_4 to **3E** in toluene medium, with or without prior deprotonation by two equivalents of NaH (Scheme 4.8). The use of more than one equivalent of TiCl_4 still resulted in the formation of **52**, although use of a large excess (six equivalents) of the reagent increased byproduct formation. The formation of the chelated mononuclear complex in the presence of excess TiCl_4 suggests that the ligand has a strong tendency to chelate one metal rather than to form dinuclear species or intermolecularly bridged aggregates.



Scheme 4.8. Preparation of complex **52**.

The solid state structure of **52** was confirmed by X-ray crystallography (Figure 4.5). The Ti atom takes a pseudo-trigonal bipyramidal coordination geometry, having the two ArO groups and one chloride at the equatorial positions, and one methoxy group and the other chloride at the axial positions. The other methoxy group is not coordinated to the Ti atom, but is turned away from the coordination face, making a "three-up/one down" conformation of the ligand framework. The aryl rings are tilted from the position perpendicular to the olefin plane by approximately 25 to 28°, except for one ring that is off by only ~16°. This least-tilting ring is one of the rings with an anionic oxygen donor. The direction of the ring tilting is helical, like the other crystallographically characterized complexes **47** and **50**.

Although the solid state structure of **52** revealed that the two methoxy groups are inequivalent, the ligand framework appeared symmetrical in solution phase (in C_6D_6) at room temperature, according to ^1H NMR spectroscopy. The single methoxy signal, however, was slightly broadened. The two methoxy groups, one coordinating to the metal center and one not, are presumably exchanging rapidly at room temperature.

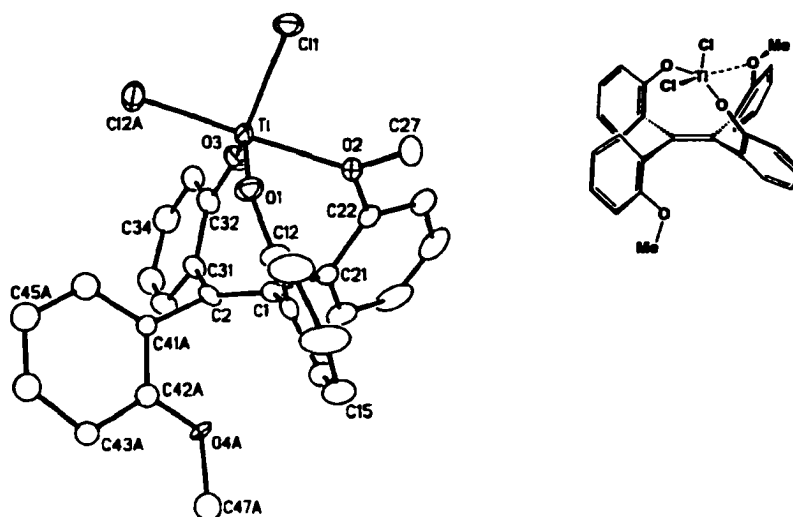


Figure 4.5. X-ray crystallographic structure of **52**.

Bond lengths (Å) Ti-Cl1 = 2.246(2), Ti-Cl2A = 2.281(4), Ti-Cl2B = 2.290(6), Ti-O1 = 1.801(5), Ti-O2 = 2.228(4), Ti-O3 = 1.782(6). Torsional angles of olefin plane (deg): C11-C1-C2-C31 = 167.5(6), C11-C1-C2-C41A = -6.7(11), C11-C1-C2-C41B = -29.7(15), C21-C1-C2-C31 = -13.9(10), C21-C1-C2-C41A = 171.9(7), C21-C1-C2-C41B = 148.9(13). Ring torsion angles (deg): C2-C1-C11-C12 = -77.1(8), C2-C1-C11-C16 = 104.2(8), C2-C1-C21-C22 = 119.2(8), C2-C1-C21-C26 = -62.2(9), C11-C1-C21-C22 = -62.2(8), C2-C1-C21-C26 = 116.5(7), C1-C2-C31-C32 = -56.8(11), C1-C2-C41A-C42A = -67.6(14), C1-C2-C41A-C46A = 117.0(13), C1-C2-C41B-C42B = -47(3), C1-C2-C41B-C46B = 124.9(16).

Low temperature ^1H NMR spectroscopy (toluene- d_6) showed the "frozen" unsymmetrical structure observed in the crystal state. As the temperature was lowered from 25 °C, the methoxy signal became further broadened, split at between 0 °C and -20 °C, and became sharp again at around -60 °C. The methoxy signals broaden again below -80 °C. (No attempt was made to quantify the dissociation energy.)

The reaction that gave complex **52** was reasonably clean, giving a purified yield of ~70%, but was often accompanied by minor byproducts. Mass spectrometry indicates that one byproduct has the formula [**52** - CH_3Cl], suggesting that de-alkylation of the

coordinated methoxy residue. In an attempt to form this suspected byproduct independently, complex **52** was treated with Et_4NCl in toluene- d_8 at 80°C . This reaction was not clean, as was indicated by the emergence of at least four new methoxy signals and a very complicated aromatic region in the ^1H NMR spectrum. The spectrum, however, showed the emergence of a sharp singlet at 2.34 ppm, which was tentatively attributed to CH_3Cl but not confirmed. Prolonged heating led to precipitation of a red solid, which gave a formula of $\text{C}_{27}\text{H}_{19}\text{O}_4\text{TiCl}$ by high-resolution mass spectrometry, although no further confirmation of structure could be attained. Heating in THF, instead of toluene, may have resulted in a cleaner reaction, as Floriani et al. observed such a transformation with the calix[4]arene analogue.¹

4.2.B. CpTiCl_3 Complexes of **3E**

Although introduction of Cp ligand to a titanium complex of **3E** would not improve its potential as a olefin polymerization precatalyst, the reaction of ligand **3E** with CpTiCl_3 was investigated to gain additional insight into the ligand's titanium coordination chemistry. Three separate reactions were performed between a salt of ligand **3E** and one equivalent of CpTiCl_3 . One started with the *in situ* preparation of the sodium salt, and the other two started from the magnesium salt that had been separately prepared.

None of the three reactions gave a clean product. The ^1H NMR spectra of each crude product and the crystallized material showed a mixture containing several methoxy signals and several Cp signals. High resolution mass spectrometry of the products obtained from the magnesium salt showed a parent peak of $\text{C}_{33}\text{H}_{27}\text{O}_4\text{TiCl}$, which corresponds to the mononuclear "CpTiCl" complex **54** (Figure 4.6). Complex **54** is the expected product based on the stoichiometry of the reactions.

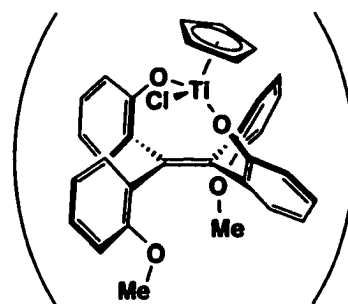


Figure 4.6. Mononuclear "CpTiCl" complex **54**.

X-ray crystallography on a crystal, which was obtained from one of the reactions using the magnesium salt, showed an unexpected structure **53** (Figure 4.7). This structure surprisingly contained one unreacted OH group. An attempt to reproduce this result, however, was not successful. Instead, ^1H NMR spectroscopy of the crystallized product was more supportive of the chelating "CpTiCl" complex **54**. None of the product mixtures, including the one that yielded the crystal of **53**, showed an OH band by IR spectroscopy. We tentatively attribute the formation of complex **53** to incomplete deprotonation of the ligand and slow rotation, which brought the titanium center into reactive proximity to the hydroxy residue.

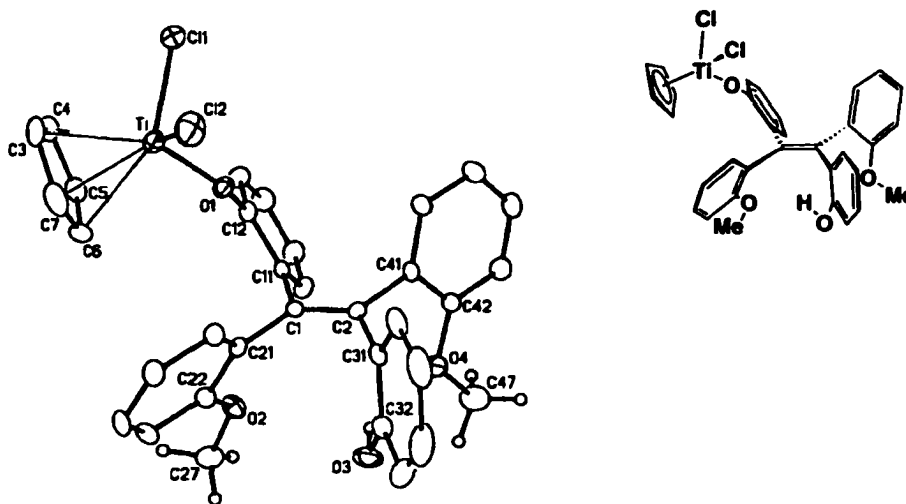


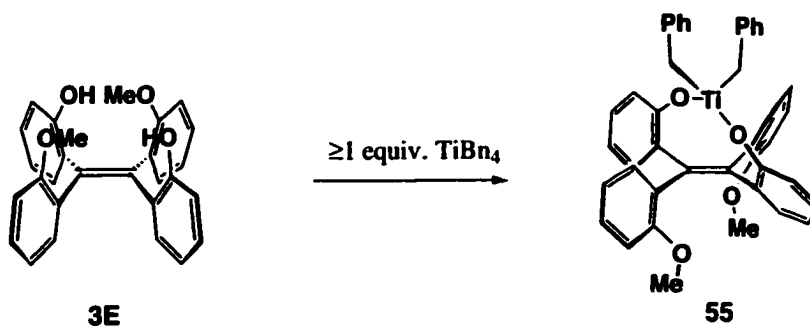
Figure 4.7. X-ray crystallographic structure of the "CpTiCl₂/OH" complex **53**.

Interatomic distances (Å): Ti-C11 = 2.2670(16), Ti-C12 = 2.2490(15), Ti-O1 = 1.787(3), Ti-C3 = 2.341(4), Ti-C4 = 2.347(4), Ti-C5 = 2.317(4), Ti-C6 = 2.319(4), Ti-C7 = 2.332(5), O4-H3O = 2.05*, C1-C2 = 1.353(5). Interatomic angles (deg): C11-Ti-Cl2 = 104.15(6), C11-Ti-O1 = 99.57(10), C12-Ti-O1 = 104.88(9). Torsional angles of olefin plane (deg): C11-C1-C2-C31 = -178.6(4), C11-C1-C2-C41 = 1.9(6), C21-C1-C2-C31 = 2.4(6), C21-C1-C2-C41 = -177.1(3). Ring torsion angles (deg): C2-C1-C11-C12 = -106.1(4), C2-C1-C11-C16 = 70.9(5), C2-C1-C21-C22 = -118.8(4), C2-C1-C21-C26 = 61.2(5), C1-C2-C31-C32 = 72.7(5), C1-C2-C31-C36 = -110.0(5), C1, C2-C41-C42 = -98.7(4), C1-C2-C41-C46 = 83.2(5).

* Nonbonded distance.

4.2.C. TiBn_2 Complex of **3E**

The 1 : 1 reaction of **3E** and TiBn_4 produced the mononuclear " TiBn_2 " complex **55** cleanly (Scheme 4.9). ^1H NMR spectroscopy of this product was consistent with the provided structure, showing a symmetric ligand framework with sharp signals and two identical benzyl groups per ligand. The benzylic methylene protons are split into an AB pattern, consistent with the diastereotopic environment. Crystallization of the product **55**, however, was quite difficult, despite the cleanness of the reaction.

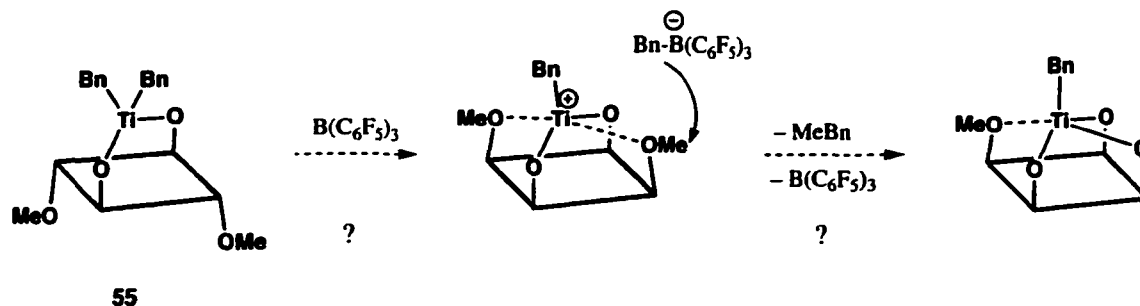


Scheme 4.9. Formation of " TiBn_2 " complex **55**.

The sharpness of the methoxy signal in the ^1H NMR spectrum suggests that neither of the two methoxy groups coordinate to the Ti atom, in contrast to the case of " TiCl_2 " complex **52** (Section 4.2.A). The metal center has two large benzyl groups, leaving little room for extra dative coordination. The metal center is also more electronically fulfilled than in complex **52**, because the benzyl groups are more electron-donating than simple chloride ligands. The relatively upfield chemical shift of the methoxy signal (2.82 ppm for **55**, 3.22 ppm for **52**) also suggests no coordination to titanium.

The addition of two equivalents of TiBn_4 to **3E** did not result in producing a dinuclear " $(\text{TiBn}_3)_2$ " complex. Only the mononuclear product **55** and one equivalent of unreacted reagent was observed in the reaction mixture, confirming that the ligand framework of **3E** prefers to chelate one metal atom, rather than forming a dinuclear complex.

Complex **55** may make an interesting cationic complex upon benzyl abstraction, although the possibility of de-methylation (Scheme 4.10) renders this species an unlikely polymerization catalyst.



Scheme 4.10. Proposed outcome of a reaction between **55** and $B(C_6F_5)_3$.

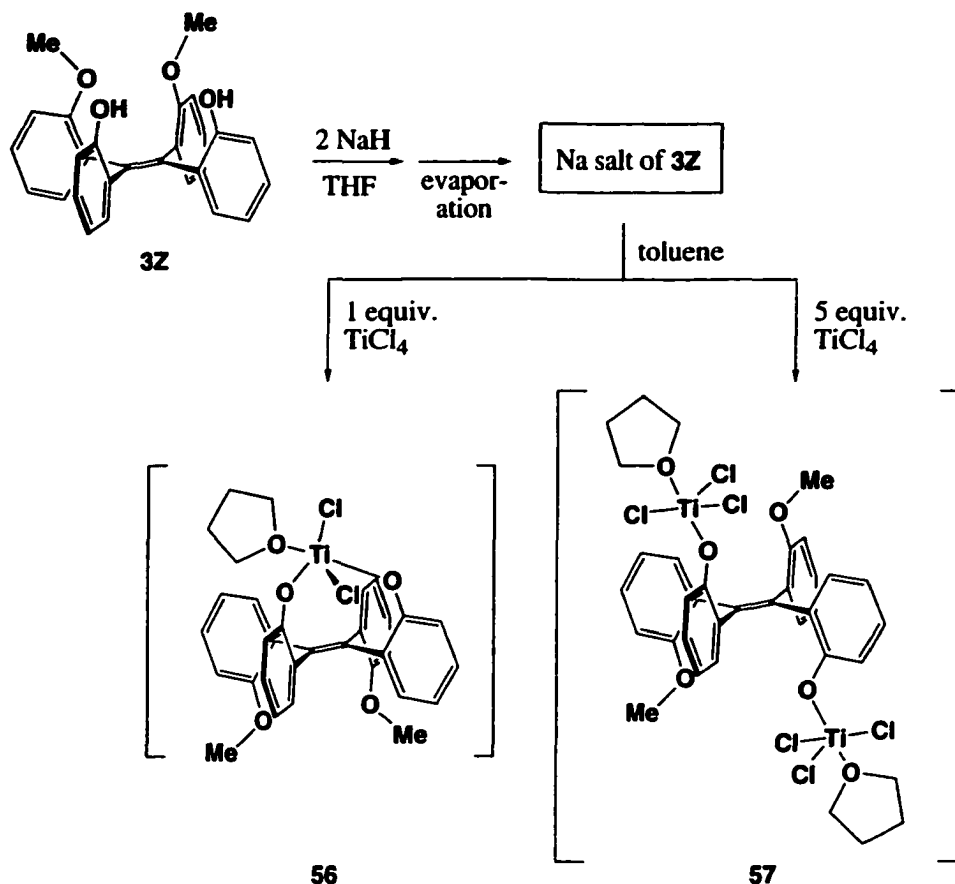
4.2.D. Ti Chemistry of Ligand **3Z**

Small-scale reactions with $TiCl_4$, $TiBn_4$ and $CpTiCl_3$ were performed in the preliminary studies of the coordination behavior of *Z*-ligand **3Z**. The reactivity of the salt of **3Z** toward these titanium reagents was quite different from those of the *E*-isomer **3E**.

i) Reaction with $TiCl_4$. The reaction of the Na salt of ligand **3Z** with one equivalent of $TiCl_4$ resulted in a mixture of compounds. In the 1H NMR spectrum, the major product, labeled **56**, showed a symmetrical ligand framework with sharp signals, while the other product(s) showed only broad signals. Sharp signals for coordinated THF, approximately one equivalent per molecule of **56**, were also present.

The reaction with five equivalents of $TiCl_4$, however, resulted in the formation of different products that showed rather broad signals in the 1H NMR spectrum. The signals were not as broad as those of the minor products from the one-equivalent reaction were, nor did they overlap with them. The product was obviously a mixture, given that at least five methoxy signals were observed. The compound that gave the most significant methoxy and corresponding aromatic signals is assigned as **57**. There are approximately two equivalents of coordinated THF per molecule of **57**.

Scheme 4.11 provides the suggested structures of **56** and **57**. Compound **56** is drawn as a chelating mononuclear complex and **57** as a non-chelating dinuclear complex. Complex **57** is depicted as an alternating "up/down" structure, which would be a likely conformation to minimize steric crowding.



Scheme 4.11. Suggested structures of **56** and **57**.

The fact that the additions of one-equivalent and excess TiCl_4 gave different products alone suggests that the latter is probably a dinuclear species. Apparently, chelating to one Ti atom is not as favorable as doing so is in the case of ligand **3E**. The ligand geometry of **3Z** is probably less suitable for stabilizing the chelated metal center by the additional coordination of the methoxy groups. This hypothesis is supported by the presence of coordinating THF corresponding to the expected number of titanium centers in both **56** and **57**. Ligand **3E** does not retain any THF under analogous reaction

conditions because it receives internal ether donation (**Figure 4.8-a**). However, **3Z** presumably accepts external THF to stabilize the titanium center (**Figure 4.8-b**).

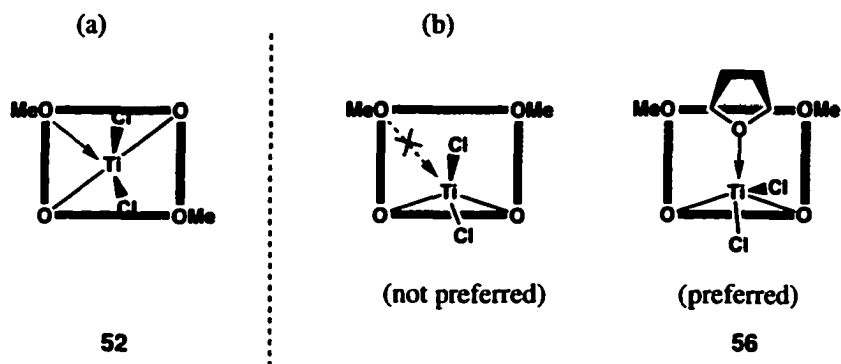


Figure 4.8. Internal and external ether coordination in mononuclear TiCl_2 complexes **52** (E-ligand) and **56** (Z-ligand).

The proposed dinuclear structure of **57** (**Scheme 4.11**) is further supported by the broadening of the ^1H NMR signals, which perhaps comes from the slow rotation of each aryl-ring moiety of the non-rigid structure of **57**. No further data, however, were obtained for **56** and **57** to confirm these suggested structures.

ii) Reaction with CpTiCl_3 . The reaction of the sodium salt of **3Z** with one equivalent of CpTiCl_3 also resulted in a mixture of products, which consists of one major species, a second substantial species, and miscellaneous minor species. Crystallization of the product mixture yielded crystals of dinuclear complex **58**, the structure of which was confirmed by X-ray crystallography (**Figure 4.9**; see Appendix A-22 for details). The ligand conformation is "alternating up/down" to minimize steric congestion.

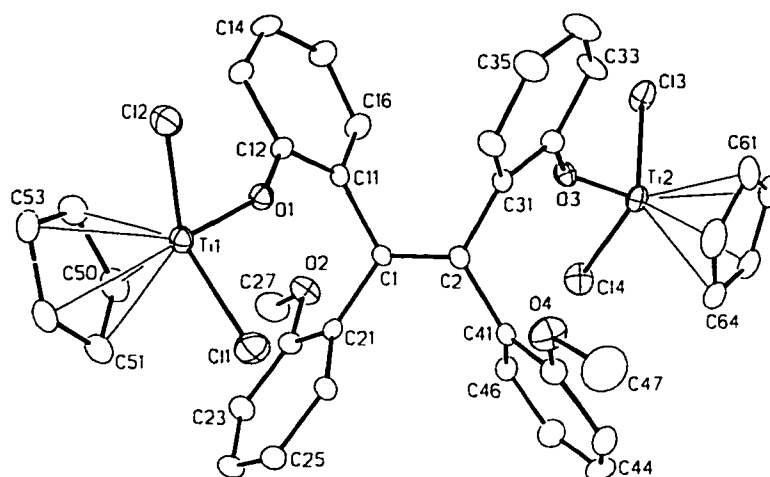


Figure 4.9. X-ray crystallographic structure of **58**.

The formation of dinuclear complex **58**, when only one equivalent of CpTiCl_3 was used, again suggests that the vicinal pair of hydroxy groups is not ideally situated for chelation. No further attempts were made to optimize the conditions to obtain this compound or to identify other components of the product mixture.

iii) Reaction with TiBn_4 . The reaction of ligand **3Z** with one equivalent of TiBn_4 resulted in a product mixture only sparingly soluble in toluene. The addition of two equivalents of the reagent resulted in a mixture of products, from which mainly unreacted TiBn_4 was triturated by toluene. The triturate also contained a small amount of non-discrete species that showed broad signals in the ^1H NMR spectrum. Probably intermolecular bridging dominated to form irregular aggregates.

In summary, the vicinal pair of hydroxy groups in **3Z** is not ideal to chelate about a single titanium atom to form discrete complexes, especially if the ancillary ligands on the metal fragment are big. No attempts to produce metal complexes of other metals were made for ligand **3Z** because of these undesirable coordination preferences and the poor activity obtained in ethylene polymerization reactions by metal derivatives of **3Z** (Chapter 5).

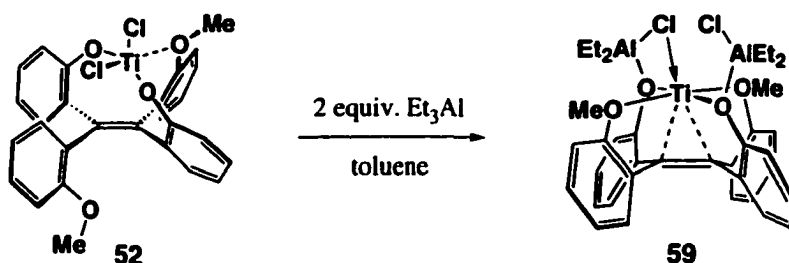
4.3. Attempts to Prepare Al/Ti Complexes of Ligand 3E

Due to the unavailability of discrete magnesium complexes of ligand 3E, attempts to prepare hetero-polymetallic derivatives were limited to the Al/Ti combination. The basic strategy was to start with the well-characterized Al or Ti species and apply Ti or Al reagents to them, respectively. Preliminary studies of the Al/Ti mixed-metal chemistry on ligand 3E are presented in this section.

4.3.A. Reactions of a Ti Complex 52 with Al Reagents

The "TiCl₂" complex 52 was used as a starting titanium complex. Additions of Et₃Al (one and two equivalents) and Me₃Al (one equivalent) in toluene were performed, and the resulting product or product mixtures were analyzed by ¹H NMR spectroscopy.

i) **Two-equivalent adduct of Et₃Al: Al/Ti(II) complex 59.** Among the above-mentioned combinations, only the addition of two equivalents of Et₃Al to 52 resulted in the clean formation of the Al/Ti hetero-polymetallic complex 59 (Scheme 4.12). The structure of complex 59 was determined by X-ray crystallography (Figure 4.10).



Scheme 4.12. Al/Ti hetero-polymetallic complex 59.

The titanium atom of complex 59 was formally reduced to Ti(II). The olefin double bond is quite distorted, due to backbonding from the formally d² Ti atom. The olefin bond length (C1-C2) is accordingly lengthened to 1.44 Å by this backbonding.²

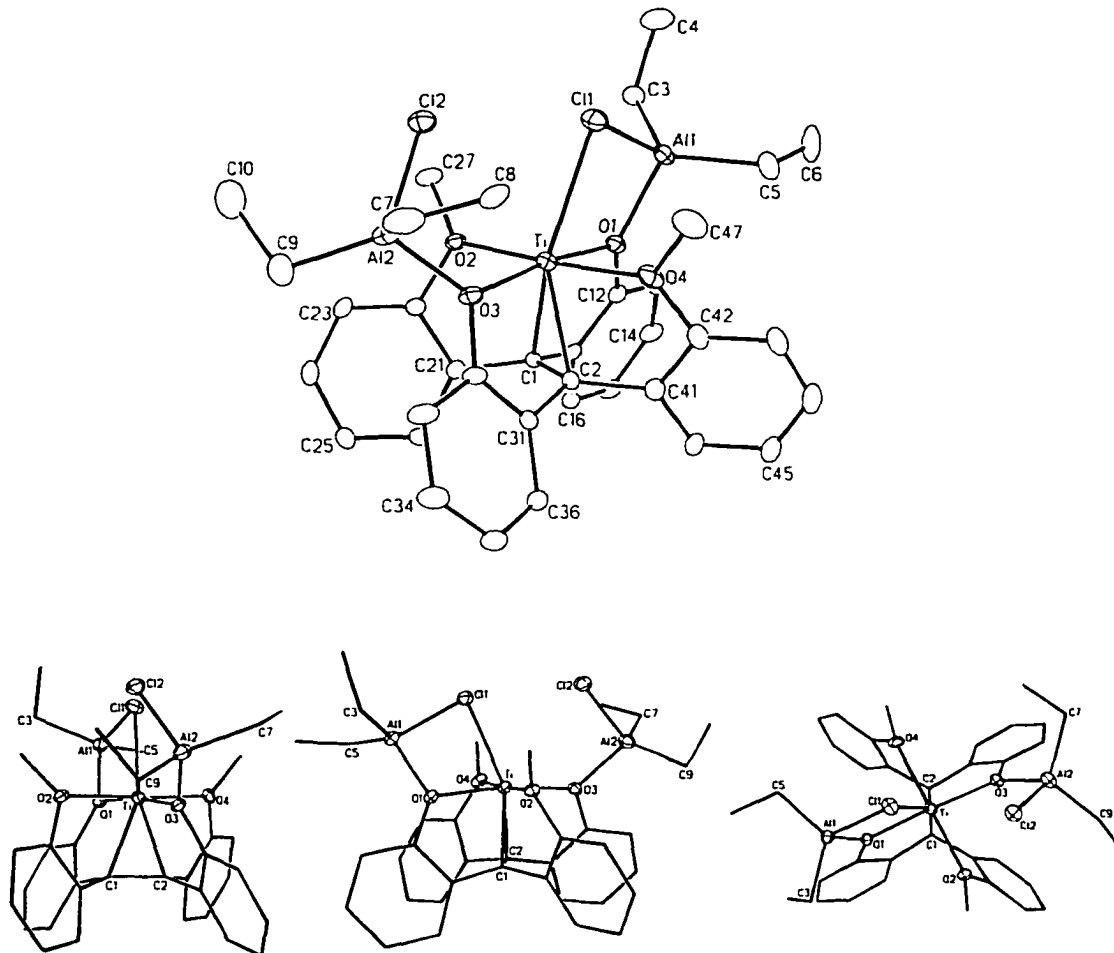


Figure 4.10. X-ray crystallographic structure of the complex **59** with different angle views.

Bond length (Å): C1-C2 = 1.439(5), Ti-Cl1 = 2.6216(13), Ti-Cl2* = 3.5064(14), Ti-O1 = 2.074(3), Ti-O2 = 2.175(3), Ti-O3 = 2.073(3), Ti-O4 = 2.227(3), Ti-C1 = 2.159(4), Ti-C2 = 2.150(4). **Interatomic angle (deg):** O1-Ti-O2 = 91.27(10), O1-Ti-O3 = 171.96(11), O1-Ti-O4 = 88.38(11), O2-Ti-O3 = 87.02(10), O2-Ti-O4 = 177.54(11), O3-Ti-O4 = 93.66(11). **Torsional angle through C1-C2 bond (deg):** C11-C1-C2-C31 = -156.2(4), C11-C1-C2-C41 = 3.4(5), C21-C1-C2-C31 = 3.7(6), C21-C1-C2-C41 = 163.4(4). **Ring torsion angle against C1-C2 bond (deg):** C2-C1-C11-C12 = -71.8(5), C2-C1-C11-C16 = 106.1(4), C2-C1-C21-C22 = 112.6(4), C2-C1-C21-C26 = -69.2(5), C1-C2-C31-C32 = -69.2(5), C1-C2-C31-C36 = 108.8(4), C1-C2-C41-C42 = 114.4(4), C1-C2-C41-C46 = -66.9(5). *Nonbonded distance.

The titanium atom takes a pseudo-octahedral geometry, with the four oxygen donors at equatorial positions. The olefin double bond is located at one axial position, while the opposite axial position is filled with the Cl group from one of the terminal "AlEt₂Cl" units. The Ti-Cl1 interaction was apparently not permanent in solution, for the ¹H/¹³C NMR spectra in C₆D₆ showed a completely symmetrical ligand framework at room temperature. The aryl rings in the solid state structure are tilted from the position perpendicular to the olefin plane, roughly by 15-30° in a helical way.

With an exception of the Ti-olefin interaction, the structure of the complex **59** has much in common with the dinuclear (AlEt)(AlEtCl₂) complex **50** (Figure 4.11). A "core" structure holds one central metal atom (Ti for **59**, Al for **50**) and one or two aluminum moieties are attached to the core complex at the second lone pair of the aryloxy ligands.

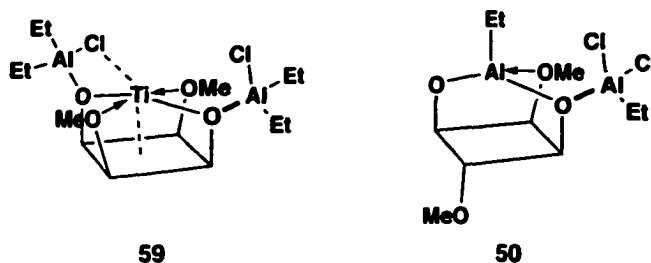


Figure 4.11. The comparison of the structural features of **59** and **50**.

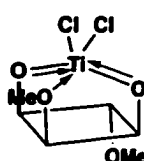
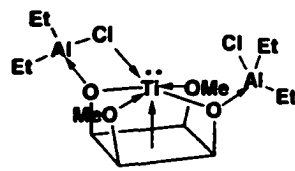
The two ethyl groups on each terminal aluminum moiety in **59** appear separately in the ¹H NMR spectrum, reflecting the diastereotopicity. The methylene protons on each ethyl group are also diastereotopic, as is reflected in the slightly split quartet signals from a ABX₃ pattern. The chemical shifts of the ethyl signals are all close to the normal region for ethyl aluminum reagents (see Section 4.1.A-i). The chemical shifts are also similar to those of the terminal "AlEtCl₂" moiety in the structurally similar complex **50**.

A sharp singlet from the two methoxy groups of **59** appears at 3.96 ppm, which is considerably more downfield than what was observed in other previously discussed complexes. For example, complex **52** (the starting material) shows a methoxy signal at 3.17 ppm; at lower temperature, two differentiated methoxy signals are observed at 3.24 and 3.03 ppm (-60 °C), still in a "normal" region for the methoxy groups of the ligand

system. The structurally similar dinuclear aluminum complex **50** gives methoxy signals at 3.17 and 2.65 ppm.

The strongly downfield shift of the methoxy signal in complex **59** probably comes from stronger donation to the titanium atom. A comparison of the electron count of complexes **52** and **59** may provide a reasonable explanation (Table 4.1). While both formally count as fourteen-electron metal centers, complex **59** has fewer anionic donors and no π -donation of lone pair electrons from the aryloxy anions: these lone pairs are used to bind the aluminum units. The deficiency of electrons requires stronger donation from both neutral methoxy groups, as well as from the chloride bridge and the olefin π -electrons.

Table 4.1. Comparison of the electron counting for **52** and **59**.

	52	59
		
Ti d-electrons	0	2
From anionic donors (ArO, Cl)	8	4
From second lone pair of ArO groups	4	0

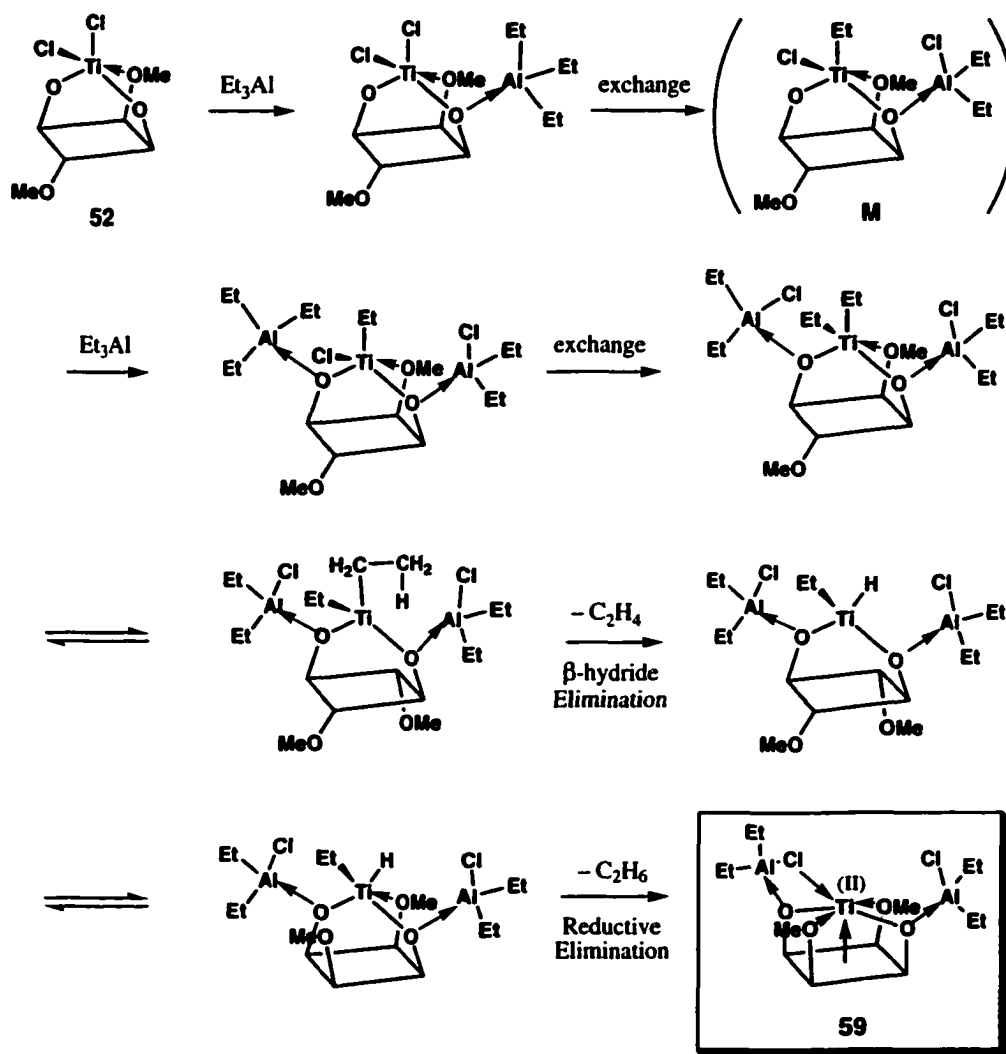
From neutral donors	2 from OMe	4 from OMe x 2
		2 from Al-Cl 2 from C=C

Total electrons	14	14

ii) Reaction of 52 with one equivalent of Et₃Al. The addition of only one equivalent of Et₃Al to **52** resulted in a mixture of three compounds: **M**, **N** and **59** in the ratio of 6 : 1 : 0.9. Because the ratio was determined by the relative integral of the methoxy signals in the ¹H NMR spectrum (C₆D₆), it reflects only soluble species. Some degree of cloudiness

of the solution was noted in the preparation of the C_6D_6 solution, which eventually separated and precipitated. The real ratio of the components, therefore, may be different from the observed ratio.

The dominant product **M** is an unsymmetrical species with two different methoxy groups, both of which are quite downfield (4.16 & 3.96 ppm). Three different ethyl groups belong to **M**. From these observations and the reaction condition, the plausible structure of **M** is suggested to be a 1 : 1 adduct of **52** and Et_3Al , accompanied by a Cl/Et exchange (Scheme 4.13). This same scheme portrays the addition of a second equivalent of Et_3Al to **M** and the mechanism that results in the two-equivalent adduct **59**.



Scheme 4.13. Proposed mechanism of the formation of **59**.

In this proposed mechanism, as soon as the first molecule of Et_3Al approaches complex **52**, an exchange of the aluminum-bound ethyl for titanium-bound chloride occurs. The second Et_3Al molecule does the same: the resulting "Ti(IV) Et_2 " species goes through a β -hydride elimination of ethene, followed by reductive elimination of ethane, to give **59**. The driving force for the reductive elimination may be the steric crowding from the terminal "AlEt₂Cl" groups or simply the irreversible loss of volatile ethene and ethane. This mechanism involves the formation of gaseous ethene and ethane, although no gas evolution was observed in the actual reaction, probably due to the small scale (<10 mg of the starting material). Detection and quantification of the proposed byproducts were not pursued.

The minor byproduct **N** in the 1 : 1 reaction of **52** and Et_3Al showed a symmetrical ligand framework in the ¹H NMR spectrum, to which two equivalent ethyl groups probably belong. Within each ethyl group, the signals are slightly split, indicating a diastereotopic environment. These ethyl groups are assigned to terminally attached aluminum moieties. The single methoxy signal is quite downfield (4.18 ppm). The slight broadness of the methoxy group may suggest that one methoxy group coordinates to a metal atom, but exchanges reasonably fast with another on the NMR time scale. These spectroscopic features narrow down the possibilities for **N** to a few structures, such as **N_a** and **N_b**, presented in **Figure 4.12**.

N_a is analogous to the Ti(II) complex **59**, while **N_b** is analogous to the starting Ti(IV) complex **52**. Considering the limited number of chlorides in the reaction system, **N_a** may be the better candidate. The compound **N_a** could form if the overreaction byproduct **59** (in 1 : 1 reaction) further exchanges its aluminum-bound ethyl groups with the titanium-bound chlorides of the unreacted starting material **52**. Such Al-Et/Ti-Cl exchange should be favorable thermodynamically. If so, **52** must also be transformed into a mononuclear "TiEt₂" complex, although no such species has been detected. It is still possible, however, that the "TiEt₂" complex further decomposes to something insoluble and thus is not detected by ¹H NMR spectroscopy.

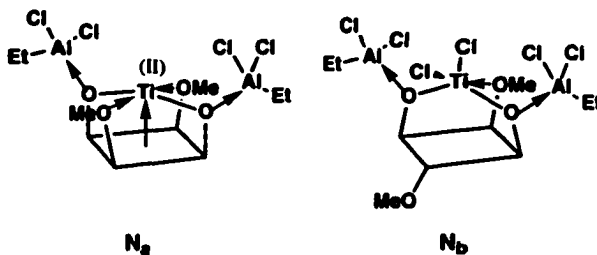
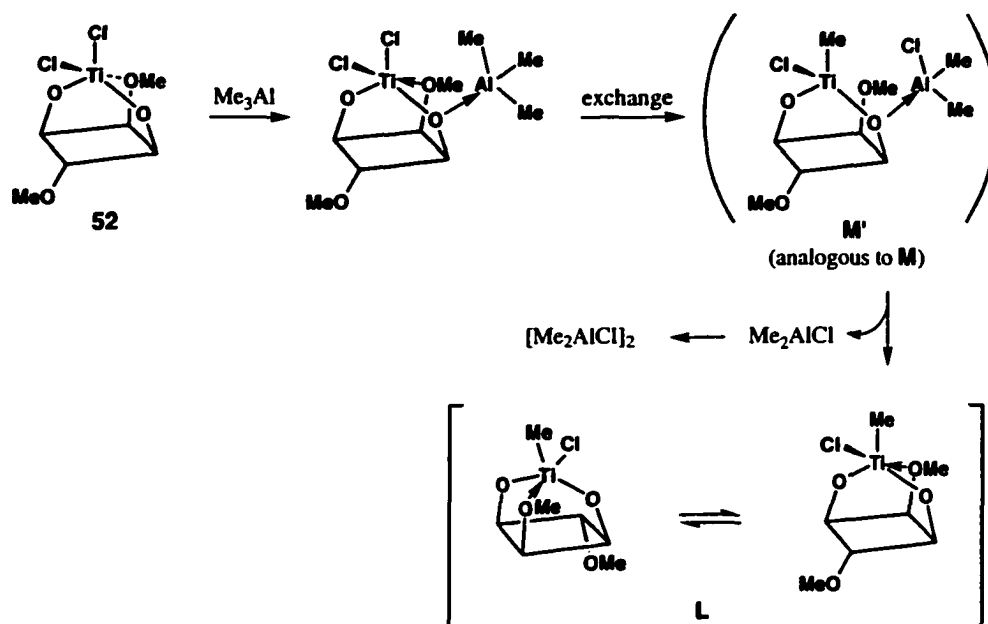


Figure 4.12. Suggested structures of **N**.

iv) **Reaction of 52 with one equivalent of Me₃Al.** The addition of Me₃Al (one equivalent) to **52** was fairly clean, producing one major product **L** with a symmetric ligand framework. The ¹H NMR spectrum showed one titanium-bound methyl group (2.18 ppm) and a broad methoxy signal in a normal region (3.03 ppm).

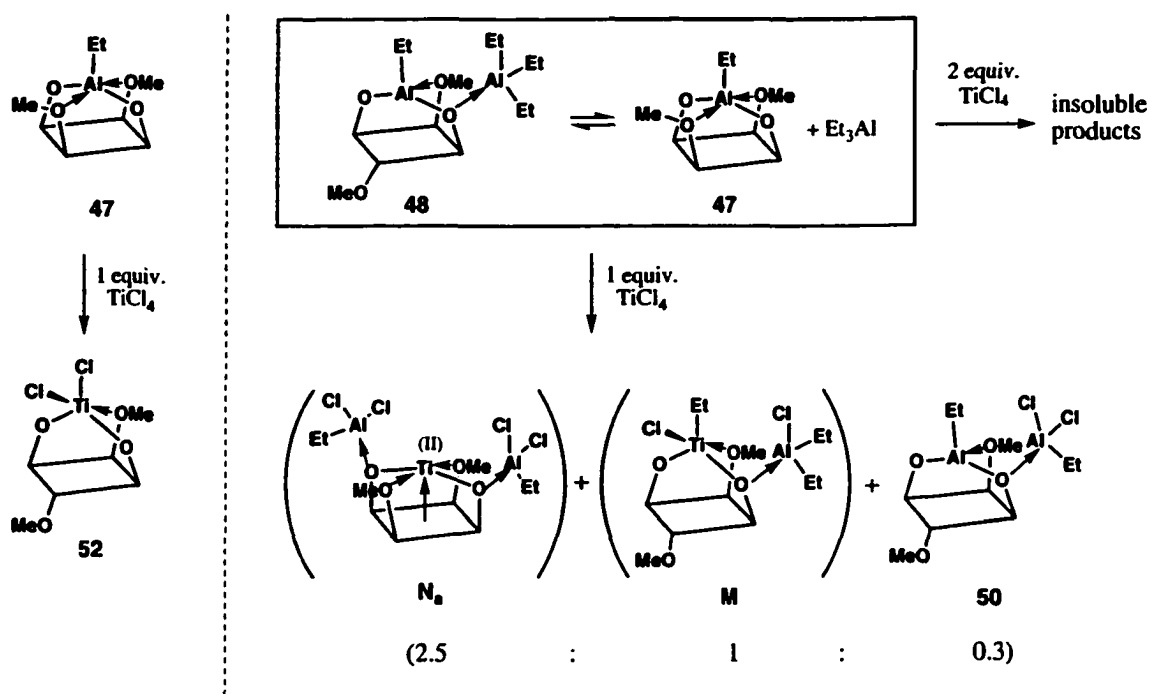
One possibility is that **L** is a mononuclear "TiMeCl" complex, formed by exchange as illustrated **Scheme 4.14**. In this proposed mechanism, the terminal "AlMe₂Cl" moiety in the stage **M'**, analogous to **M** in **Scheme 4.13** does not remain bound to the core molecule. Once dissociated, AlMe₂Cl self-aggregates so the reverse reaction does not compete. It is not certain, however, why the "AlEt₂Cl" moiety in **M** remained intact on the core molecule, while the "AlMe₂Cl" moiety in **M'** did not.



Scheme 4.14. Proposed structure of **L** formed from the reaction between **52** and Me₃Al.

4.3.B. Reactions of Al Complexes with TiCl_4

TiCl_4 was the only titanium reagent used in these attempts. The two aluminum complexes used were the mononuclear "AlEt" complex **47** and the $(\text{AlEt})(\text{AlEt}_3)$ complex **48** that partly dissociates in solution. The results of the reactions between **47** or **48** and TiCl_4 (one or two equivalents) are summarized in **Scheme 4.15**.



Scheme 4.15. Reactions between **47** or **48** and TiCl_4 .

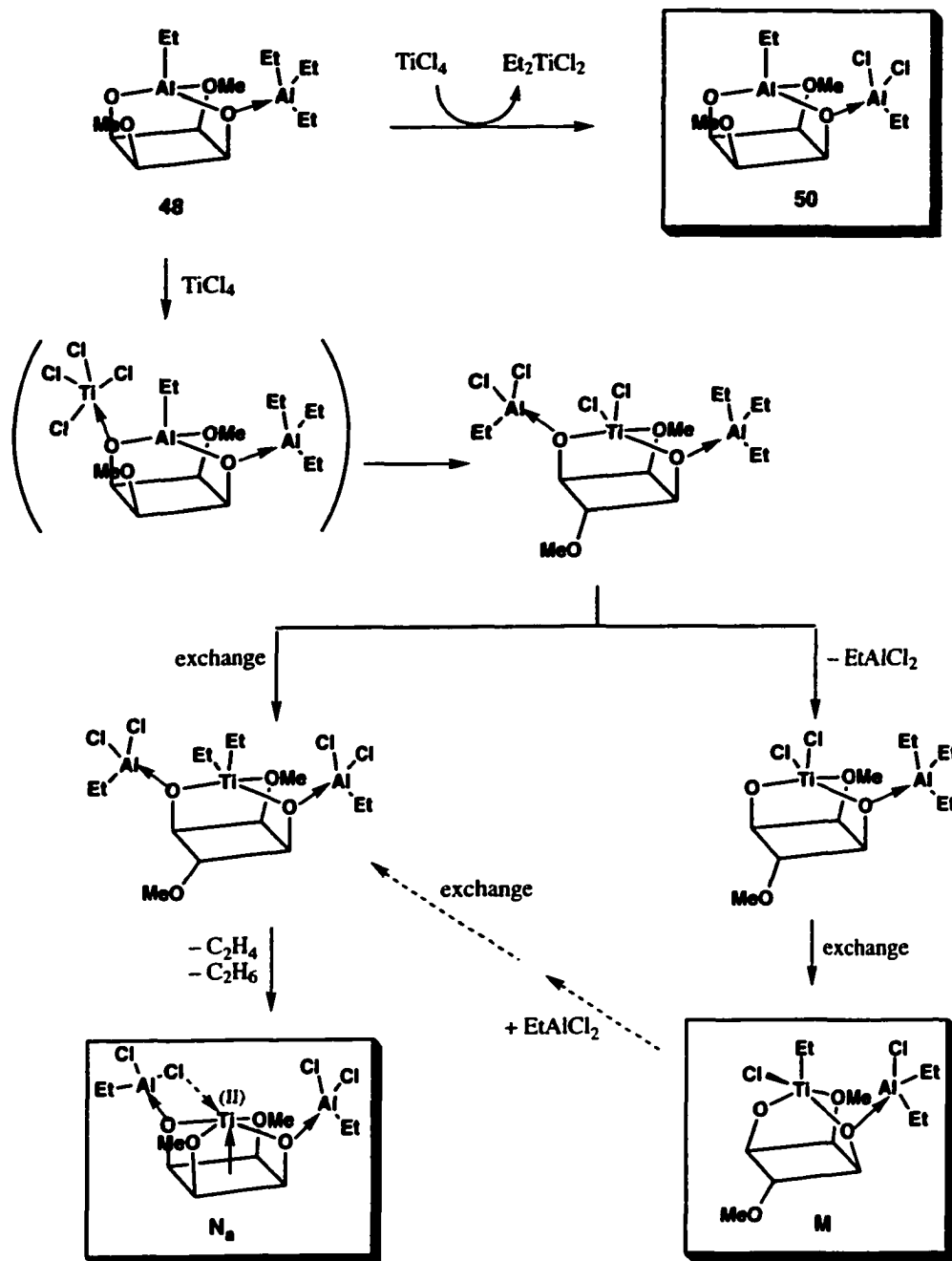
The addition of one equivalent of TiCl_4 to the mononuclear "AlEt" complex **47** cleanly produced the previously characterized mononuclear " TiCl_2 " complex **52**. No aluminum moiety remained intact.

Complex **48** was not the best choice as a starting material for further experiments, because of the dissociation behavior in solution (see **Scheme 4.15**). The addition of two equivalents of TiCl_4 to **48** resulted in toluene-insoluble material. The solution in THF-d_8

or CD₃CN provided only broad signals in ¹H NMR spectroscopy. No further investigation was done for this case.

The reaction of **48** with one equivalent of TiCl₄, however, resulted in a mixture of three compounds: **N**, **M** and **50** (compound **N** is depicted as **N_a** in **Scheme 4.15**). The two major products **N** and **M** were also found in the previously discussed addition of Et₃Al (one equivalent) to the titanium complex **52**. The minor dialuminum complex **50** was crystallographically characterized and discussed in Section 4.1.B.

The proposed mechanism for the formation of these tentatively assigned species is presented in **Scheme 4.16**. The formation of **N** and **M** as major species suggests that the central aluminum atom is promptly replaced by a titanium atom. The minor product **50** can form if two of the ethyl groups on the terminal aluminum are simply replaced by the chlorides from TiCl₄.



Scheme 4.16. Proposed mechanism of the reaction between 48 and one equivalent of TiCl_4 .

4.4. Conclusion

The aluminum and titanium complexes derived from ligand **3E** showed both mono- and polynuclear structures. Some common features were noted in the structurally characterized polymetallic species: (i) a central (core) metal atom, either Al or Ti, and (ii) when applicable, one or two terminal metal Al moieties attached via the lone pair of aryloxy anionic oxygen donors coordinated to the central metal atom.

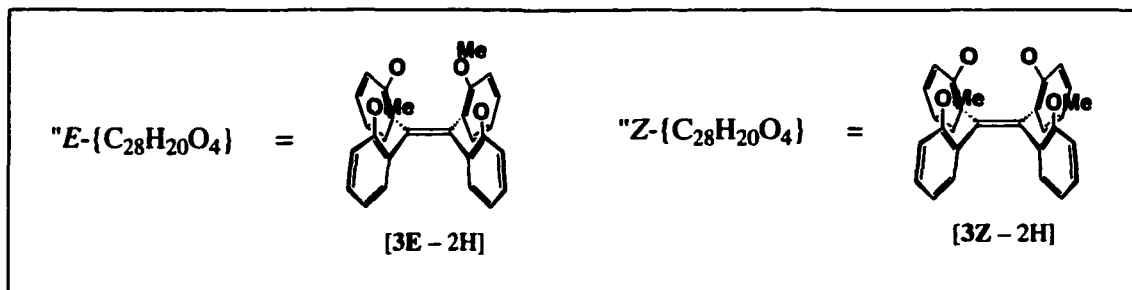
The flexible role of the methoxy donor groups was also noteworthy. Depending on the demand from the metal at the central position and the steric environment, two, one, or none of the methoxy groups were used as required. When binding was unnecessary, they could rotate away to avoid steric crowding. The coordination of the methoxy groups also served to protect the otherwise exposed central metal atom, such as the Ti(II) atom in the hetero-polymetallic complex **59**.

The comparison of *E*-ligand **3E** and *Z*-ligand **3Z** in coordination behavior showed that dialkylation of the tetrahydroxy system in the alternating pattern, as in **3E**, provided a good chelating dianionic ligand framework.

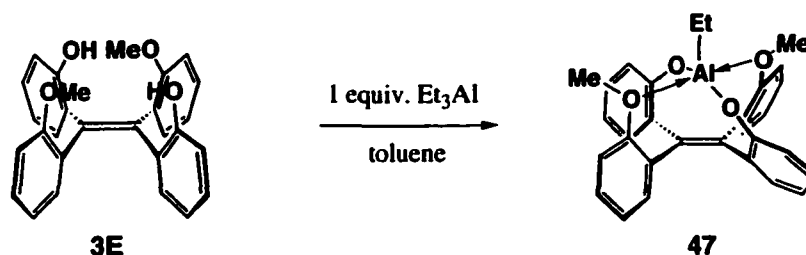
4.5. Experimental

Instrumental, General and Materials: see Chapter 3, Section 3.4 Experimental.

Note: "*E*- or *Z*-{C₂₈H₂₂O₄}" represents the fully deprotonated ligand **3E** or **3Z** i.e., [**3E** – 2H] or [**3Z** – 2H] (see below). The conformation is not restricted to the "all-up" form.



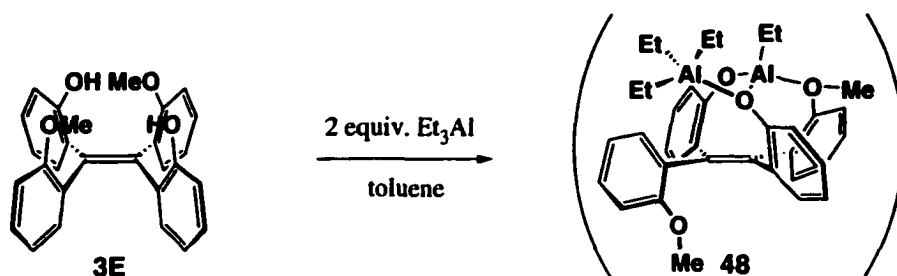
47: *E*-{C₂₈H₂₂O₄}(AlEt)



To a suspension of *E*-bis(2-hydroxyphenyl)-bis(2-methoxyphenyl)ethene (**3E**) (0.0734 g, 0.173 mmol) in 0.5 mL of toluene was slowly added Et₃Al (0.0201 g, 0.176 mmol) dissolved in 1.5 mL of toluene at room temperature. The mixture became a solution within 2 min. Gas evolution was not obvious. After overnight, the volatiles were removed to give a partly crystalline residue. A small amount of toluene was added to dissolve the less crystalline material (but leaving some crystals undissolved), hexane was layered on top for slow diffusion, and the mixture was cooled to –30 °C for crystallization. The crystals were removed from the mother liquor, washed with small amount of pentane, and dried in vacuo. The crystals amounted to 0.0597 g (72%). The mother liquor and the washings were collected and evaporated to leave a shiny crystalline residue, which was also quite pure product (0.0221g, 27%). ¹H NMR (360 MHz, C₆D₆): δ 7.12 (2H, br d, *J* = ~7 Hz), 7.07 (2H, slightly br dd, *J* = 7.5, 1.8 Hz), 6.89 (2H, ddd, *J* = 8, 7, 1.8 Hz), 6.80 (2H, dd, *J* = 8, ~1 Hz), 6.72 (2H, slightly br td, *J* = 8, ~1.8 Hz), 6.65 (2H, td, *J* = 7.5, ~1

Hz), 6.58 (2H, td, $J = 7.5$, ~ 1 Hz), 6.43 (2H, br d, $J = 8$ Hz), 3.18 (6H, s, OCH₃), 1.68 (3H, t, $J = 8$ Hz, AlCH₂CH₃), 0.61 (2H, qd, $J = 8$, 2 Hz, AlCH₂H₂CH₃, AB of ABX₃). ¹H NMR (360 MHz, CD₃CN): δ 7.25 (2H, br d, $J = 7.5$ Hz), 7.18 (2H, slightly br ddd, $J = 8$, 7.5, 1.8 Hz), 7.04 (2H, br), 7.02 (2H, dd, $J = 7.5$, 1.8 Hz), 6.94 (2H, br), 6.94 (2H, ddd, $J = 8$, 7.5, ~ 1 Hz), 6.60 (2H, td, $J = 7.5$, 1 Hz), 6.54 (2H, br d, $J = 8$ Hz), 3.59 (6H, s, OCH₃), 1.30 (3H, t, $J = 8$ Hz, AlCH₂CH₃), 0.19 (2H, q, $J = 8$ Hz, AlCH₂CH₃). ¹³C NMR (75 MHz, C₆D₆): δ 157.5, 156.6, (141.0)?,^c 137.8, (134.4)?,^c 130.2, 129.3, 128.5, 128.4, 125.6, 124.4, 118.8, 117.6, 117.0, 61.0 (OMe), 21.4 (AlCH₂CH₃), 10.6 (AlCH₂CH₃). Anal. Calcd for C₃₀H₂₇AlO₄: C, 75.90; H, 5.69. Found: C, 75.49; H, 5.58. X-ray crystallography: see Appendix A-17. The X-ray analyzed crystals were obtained by slow crystallization of **48** from toluene-hexanes (slow diffusion, r.t. \rightarrow -30 °C).

48: E-{C₂₈H₂₂O₄} \cdot Al₂ \cdot Et₄

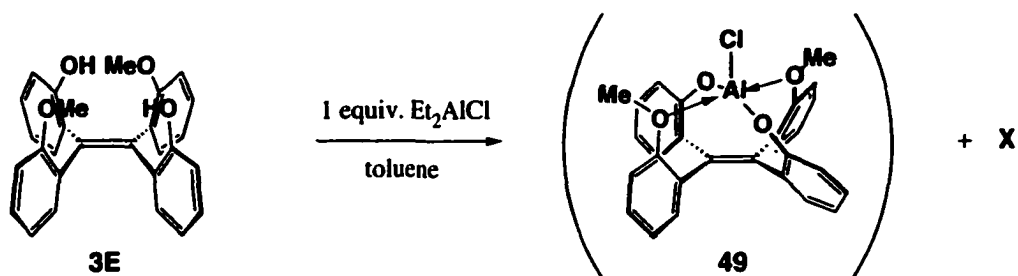


To the stirred suspension of *E*-bis(2-hydroxyphenyl)-bis(2-methoxyphenyl)ethene (**3E**) (0.1254 g, 0.295 mmol) in 2 mL of toluene was added Et₃Al (0.0741 g, 0.649 mmol) dissolved in 1 mL of toluene at room temperature. Gas evolution was observed within 1 min. and the mixture became a solution within 40 min. After 20 h, the solution was concentrated in vacuo until it became slightly cloudy. Hexane was layered on top and the two-phase mixture was cooled to -30 °C. The white precipitate (not crystalline) was collected, washed with cold pentane, and dried in vacuo. The elemental analysis (C/H) was consistent with the composition of the dialuminum product **48**: C₂₈H₂₂O₄Al₂(C₂H₅)₄. The ¹H NMR spectrum at room temperature showed broad signals. From the recrystallization of this material from layered toluene-hexanes at -30 °C, clear prism crystals were produced on the vial wall in the hexane layer, as well as some non-crystalline solid between the solvent layers. The crystals were found to be the monoaluminum product **47**, confirmed by ¹H NMR spectroscopy and X-ray crystallography. Complex **48**: ¹H NMR (400 MHz, C₆D₆, 75 °C): δ 7.19 (2H, slightly br

^c One of these two signals does not belong to the product.

dd, $J = 7.5, \sim 1$ Hz), 7.01 (2H, br dd, $J = \sim 7$ Hz), 6.96 (2H, br), 6.86 (2H, slightly br t, $J = \sim 7$ Hz), 6.78 (2H, br), 6.67 (2H, slightly br t, $J = \sim 7$ Hz), 6.61 (2H, slightly br t, $J = \sim 7.5$ Hz), 6.67 (2H, slightly br t, $J = \sim 7$ Hz), 6.40 (2H, slightly br d, $J = \sim 8$ Hz), 3.09 (6H, br s, OCH₃), 1.46 (3H, t, $J = 8$ Hz, central AlCH₂CH₃), 1.36 (9H, br, terminal Al(CH₂CH₃)₃), 0.75 (1H, m, central AlCH₂H_bCH₃), 0.45 (1H, m, central AlCH₂H_bCH₃), 0.04 (6H, br, terminal Al(CH₂CH₃)₃). Anal. Calcd for C₃₆H₄₂Al₂O₄: C, 72.95; H, 7.14. Found: C, 73.28; H, 7.17.

49: *E*-{C₂₈H₂₂O₄}(AlCl)

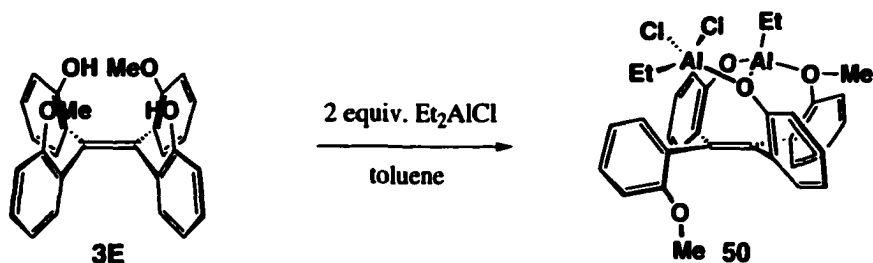


To a suspension of *E*-bis(2-hydroxyphenyl)-bis(2-methoxyphenyl)ethene (**3E**) (0.0098 g, 0.023 mmol) in 0.5 mL of toluene was quickly added Et₂AlCl (0.0028 g, 0.023 mmol) dissolved in 1.5 mL of toluene at room temperature. Gas evolution was not obvious. The cloudy mixture became clear over 30 min. After overnight, the mixture became cloudy again. The volatiles were removed, and the residue was analyzed by ¹H NMR spectroscopy in CD₃CN and mass spectrometry. Both were consistent with the proposed structure of **49**. When a more concentrated solution was prepared in CD₃CN (as a supernatant with a considerable amount of undissolved portion), ¹H NMR spectroscopy showed a mixture of two symmetrical species (**49** and **X**).

49. ¹H NMR (360 MHz, CD₃CN): δ 7.20 (2H, dd, $J = 7.8, 1.8$ Hz), 7.11 (2H, ddd, $J = 8\text{--}8.5, 7.5, 1.8$ Hz), 7.10 (2H, dd, $J = 7.5, 1.8$ Hz), 6.94 (2H, ddd, $J = 8, 7.5, 1.8$ Hz), 6.79 (2H, d, $J = 8$ Hz), 6.77 (2H, dd, $J = 7, 1.2$ Hz), 6.63 (2H, td, $J = 7.5, 1.2$ Hz), 6.60 (2H, dd, $J = 7, 1.2$ Hz), 3.72 (6H, s, OCH₃). HRMS (EI) m/z : Calcd for C₂₈H₂₂AlClO₄: 484.10220. Found: 484.10019 (100%) [M⁺].

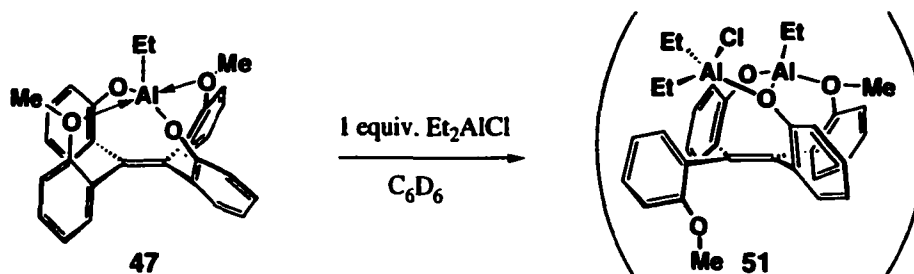
X. ¹H NMR (360 MHz, CD₃CN): ~ 7.18 (2H+2H, overlapping), ~ 7.10 (2H), 6.98 (2H, br), ~ 6.96 (2H, br), 6.92 (2H, ddd, $J = 8, 7.3, 1.8$ Hz), 6.59 (2H, td, $J = \sim 7.5, 1$ Hz), 6.50 (2H, br d, $J = 8$ Hz), 3.68 (6H, br s, OMe).

50: $E\text{-}\{C_{28}H_{22}O_4\}(AlEt)(AlEtCl_2)$



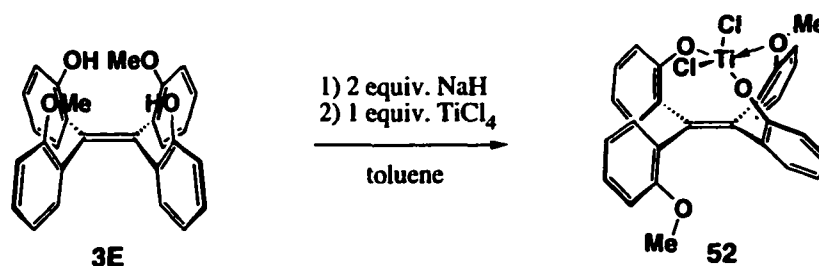
To a suspension of *E*-bis(2-hydroxyphenyl)-bis(2-methoxyphenyl)ethene (**3E**) (0.0386 g, 0.0909 mmol) in 0.5 mL of toluene was quickly added Et_2AlCl (0.0220 g, 0.182 mmol) dissolved in 1.5 mL of toluene at room temperature. Gas evolution was not obvious. The cloudy mixture gradually turned clearer. After overnight, the volatiles were removed from the still slightly cloudy mixture. 1H NMR spectroscopy of the crude product showed a mixture of **50** and **49** in a 7.4 : 1 ratio. The crude product was redissolved in toluene, filtered through a celite-packed pipette, and the filtrate warmed and then allowed to cool to room temperature. Some crystals formed. Pentane was layered on the toluene solution for slow diffusion, and the mixture was cooled to $-30\text{ }^\circ C$. The crystals that formed were removed from the mother liquor, washed with pentane, and dried in vacuo to give reasonably pure product (0.0404 g, 73%). The 1H NMR spectrum of the product showed a mixture of **50** : **49** in a 11 : 1 ratio (8% of **49**). 1H NMR (400 MHz, C_6D_6): δ 7.73 (1H, br d, $J = \sim 8$ Hz), 7.47 (1H, br d, $J = 8$ Hz) 7.22 (1H, br d, $J = \sim 7$ Hz), 7.09 (1H, br d, $J = 8$ Hz), 6.92 (1H, br d, $J = \sim 7$ Hz), 6.79~6.70 (5H, overlapping), 6.56~6.49 (3H, overlapping), 6.29 (1H, br d, $J = 8$ Hz), 6.11 (1H, slightly br dd, $J = 7.5, 1.8$ Hz), 3.13 (3H, s, OCH₃), 2.63 (3H, s, O'CH₃), 1.50 (3H, t, $J = 8$ Hz, AlCH₂CH₃), 1.23 (1H, m, AlCH₂H_bCH₃), 1.2 (3H, br t, $J = \sim 7.5$ Hz, AlC'H₂C'H₃), 0.72 (1H, m, AlCH₂H_bCH₃), -0.62 (1H, br, AlC'H₂H_bC'H₃), -0.86 (1H, br, AlC'H₂H_bC'H₃). ^{13}C NMR (75MHz, C_6D_6): δ 156.4, 155.4, 153.7, 150.0, 141.3, 137.1, 135.1, 133.7, 133.5, 133.3, 133.0, 130.5, 130.4, 129.7, 129.3, 129.0, 128.7, 128.5, 126.7, 123.9, 121.7, 120.2, 120.0, 119.2, 117.6, 110.5, 63.0 (OMe), 54.3 (OMe), 9.4 (AlCH₂CH₃), 8.8 (AlCH₂CH₃), 1.8 (AlCH₂CH₃), 0.11 (AlCH₂CH₃). Anal. Calcd for $C_{32}H_{32}Al_2Cl_2O_4$: C, 63.48; H, 5.33, Cl, 11.71. Found: C, 63.63; H, 5.14, Cl, 11.39.

51: $E\text{-}\{C_{28}H_{22}O_4\}(AlEt)(AlEt_2Cl)$



A solution of **47** (0.0033 g, 0.0069 mmol) and Et_2AlCl (0.0009 g, 0.007 mmol) in C_6D_6 (0.5 mL) was prepared in an NMR tube. The ^1H NMR spectrum was taken after several hours. ^1H NMR (360 MHz, C_6D_6): δ 7.56 (1H, br), 7.27 (1H, br), 7.15~7.10 (1H?), 7.02~6.94 (2H, overlapping, br), 6.94 (1H, br d, $J = 7.5$ Hz), 6.82~6.71 (5H, overlapping br), 6.57~6.53 (3H, overlapping, br), 6.33 (1H, br d, $J = \sim 8$ Hz), 6.21 (1H, br), 3.17 (3H, br s, OCH_3), 2.65 (3H, br s, $\text{O}'\text{CH}_3$), 1.56~1.51 (3H+3H, overlapping, br, AlCH_2CH_3 , $\text{Al}'\text{CH}_2\text{CH}_3$), 1.07 (3H, br, $\text{Al}''\text{CH}_2\text{CH}_3$), 0.76 (1H, br, $\text{AlCH}_2\text{H}'$) 0.67~0.56 (1H+1H+1H, overlapping, br, $\text{AlCH}_2\text{H}'$), -0.70 (1H, br, $\text{AlCH}_2\text{H}'$), -0.97 (1H, br, $\text{AlCH}_2\text{H}'$).

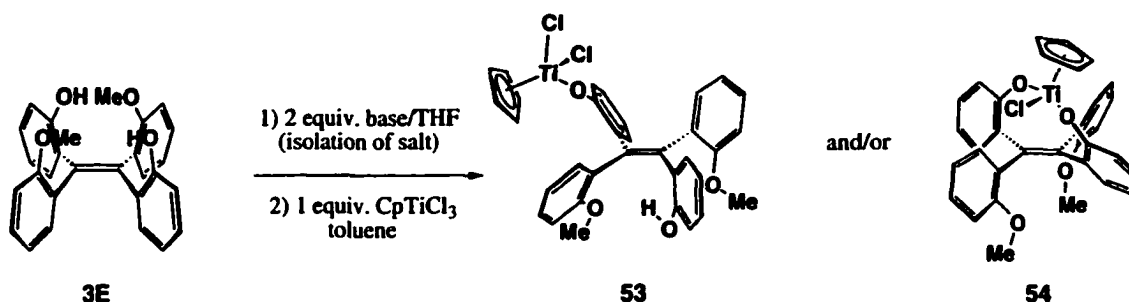
52: $E\text{-}\{C_{28}H_{22}O_4\}(\text{TiCl}_2)$



To a suspension of *E*-bis(2-hydroxyphenyl)-bis(2-methoxyphenyl)ethene (**3E**) (0.1309 g, 0.308 mmol) in toluene (2 mL) was added NaH (0.0152 g, 0.633 mmol) suspended in 2 mL of toluene. No apparent gas evolution was observed. After stirring for 5 min., TiCl_4 (0.0582 g, 0.307 mmol) dissolved in 0.5 mL of toluene was added to the mixture. The color turned to red immediately. After stirring the mixture for 23 h, the mixture was filtered through celite, and the volatiles were removed from the filtrate in vacuo. The residue was crystallized from toluene-hexanes (r.t. \rightarrow -30 $^\circ\text{C}$). After removal of the mother liquor, washing with a small amount of pentane, and drying in vacuo, analytically pure product was obtained (0.1154 g, 69.5 %). ^1H NMR (360 MHz, toluene- d_8): δ 7.38

(2H, br, d), 7.09 (2H, dd, $J = \sim 7, 2.1$ Hz) 6.75 (2H, td, $J = 7.8, 1.8$ Hz), 6.66 ~ 6.58 (2+2+2H, overlapping), 6.39 (2H, dd, $J = \sim 7.7, \sim 1.9$ Hz) 6.34 (2H, dd, $J = \sim 8, <1$ Hz), 3.22 (6H, s, OMe). ^{13}C NMR (125 MHz, toluene- d_8 , APT): δ 171.6, 167.0, 157.2, 140.1, 134.8, 132.8 (3 $^\circ$), 130.0 (3 $^\circ$), 129.6 (3 $^\circ$), 128.9 (3 $^\circ$?), 128.5 (3 $^\circ$), 123.6 (3 $^\circ$), 122.8 (3 $^\circ$, br), 114.8 (3 $^\circ$), 65 ~ 53 (br, OMe). Anal. Calcd for $\text{C}_{28}\text{H}_{22}\text{O}_4\text{Cl}_2\text{Ti}$: C, 62.13; H, 4.10. Found: C, 62.45; H, 4.11. HRMS (EI) m/z : Calcd for $\text{C}_{28}\text{H}_{22}\text{O}_4\text{Cl}_2\text{Ti}$: 540.03748. Found: 540.03713 (100%) [M^+]. X-ray crystallography: see Appendix A-19.

53 and 54: CpTiCl_3 adducts of 3E (unclean)



(1) **From the Mg salt -1.** A magnesium salt, $E\text{-}\{\text{C}_{28}\text{H}_{22}\text{O}_4\}\cdot\text{Mg}$ (FW = 441), was prepared by mixing 3E (0.1665 g, 0.3922 mmol) and CH_3MgCl (0.3M/THF, 2.6 mL, 0.78 mmol) in 1 mL of THF overnight, collecting the precipitate, washing with THF, and drying. The formula weight (FW) was calculated based on the C/H analysis (see Chapter 5, Section 5.4.B). The magnesium salt (0.0135 g, 0.0306 mmol) and CpTiCl_3 (0.0053 g, 0.024 mmol) were mixed in 1.5 mL of toluene for two days. The bright orange, slightly cloudy solution was filtered through a celite-packed pipette, and the volatiles were removed from the filtrate in vacuo. ^1H NMR spectroscopy of the residue showed a mixture of many species, containing the signals assigned to 54 (see below). Crystallization of the residue from toluene-hexanes (r.t. \rightarrow -30 $^\circ\text{C}$) yielded orange-red prism crystals among powder with a lighter color. X-ray crystallography showed the structure of 53, but the HRMS result of the crude product was suggestive of 54. HRMS (EI): Calcd for $\text{C}_{33}\text{H}_{27}\text{O}_4\text{ClTi}$: 570.10974. Found: 570.10899 (31%) [M^+], 505.06751 (100%) [$\text{M} - \text{C}_5\text{H}_5$] $^+$.

(2) **From the Mg salt -2.** The magnesium salt (0.1002 g, 0.227 mmol) and CpTiCl_3 (0.0507 g, 0.231 mmol) were mixed in 5 mL of toluene for four days. The bright orange, cloudy mixture was filtered through a celite-packed pipette, and the volatiles were removed from the filtrate in vacuo. The residue (0.1252 g) was crystallized from toluene-hexanes (r.t. \rightarrow -30 $^\circ\text{C}$). The partly crystalline but mostly powdery solid was separated

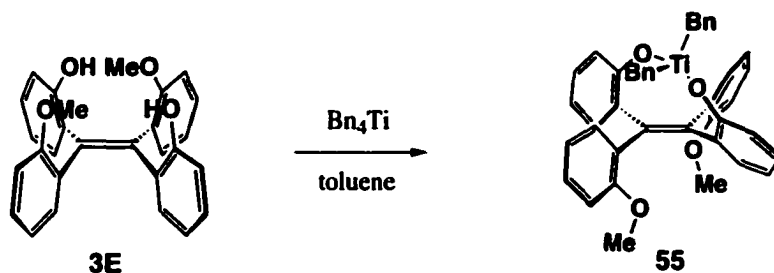
from the mother liquor and dried in vacuo (0.0462 g, 36% if it is exclusively **54**). The powder showed the cleanest ^1H NMR spectrum suggestive of **54**, not **53**. The HRMS result was similar to that of (1), also suggestive of **54**.

(3) From the Na salt. The phenolic ligand **3E** (0.0295 g, 0.0695 mmol) was mixed with NaH (0.0035 g, 0.146 mmol) in 1 mL of THF. Gas evolution was not obvious. After 3.5 h of stirring, the volatiles were removed, then the residue was suspended in toluene (1 mL). To this suspension was added CpTiCl_3 (0.0226 g, 0.103 mmol) dissolved in 1 mL of toluene. The color turned to yellow-orange. After 1.5 h, the volatiles were removed in vacuo, then the residue was triturated with toluene, filtered through a celite-packed pipette, and the volatiles were removed from the filtrate. The residue showed a mixture of many species in the ^1H NMR spectrum (C_6D_6), including signals assigned to **54**.

53: X-ray crystallography: see Appendix A-20.

54 (impure): ^1H NMR (360 MHz, C_6D_6): δ 7.07 (2H, br d, $J = 8$ Hz), 6.87 (2H, dd, $J = 8, 1.5$ Hz), 6.83 (2H, 'td', $J =$ unclear due to overlapping), 6.81 (2H, d?, $J = ?, 1.8$ Hz), 6.67 (2H, td, $J = 6.5, 1$ Hz), 6.66 (2H, br), 6.27 (2H, br d, $J = 8$ Hz), 6.22 (2.5H?, s, the largest Cp signal, but not enough), 3.21 (6H, s, OCH_3).

55: $E\text{-}\{\text{C}_{22}\text{H}_{22}\text{O}_4\}(\text{TiBn}_2)$



To a suspension of *E*-bis(2-hydroxyphenyl)-bis(2-methoxyphenyl)ethene (**3E**) (0.1616 g, 0.3807 mmol) in toluene (1 mL) was added TiBn_4 (0.1585 g, 0.3843 mmol) dissolved in 2 mL of toluene. After stirring the mixture overnight, the volatiles were removed in vacuo to leave dark brown-red residue. ^1H NMR spectroscopy of the crude product showed clean **55** with a trace amount of TiBn_4 . Crystallization attempts from toluene or toluene-hexanes were not successful. The compound was too reactive to allow for mass spectrometric analysis. ^1H NMR (360 MHz, C_6D_6): δ ~7.25 (4H, overlapping), 7.15~6.95 (14H, overlapping), 6.69 (4H, td, $J = 7.5, 1.2$ Hz), 6.53 (2H, td, $J = 7.5, 1$ Hz), 6.15 (2H, dd, $J = 8, 1$ Hz) 3.17 (2H, d, $J = 10.5$ Hz), 3.09 (2H, d, $J = 10.5$ Hz), 2.82 (6H, s, OMe).

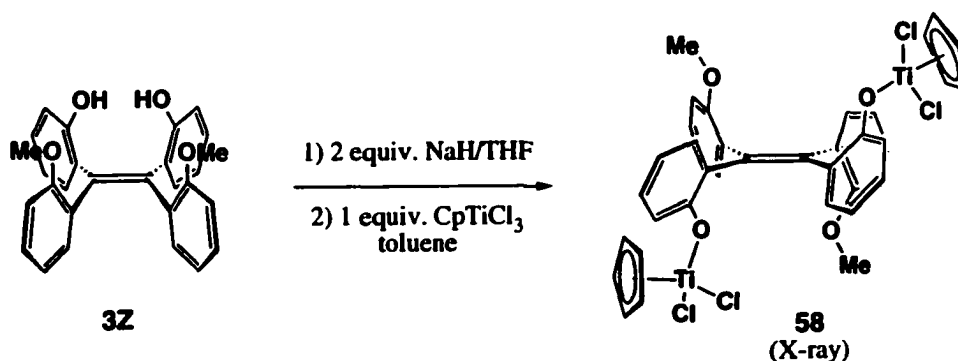
56: Z-{C₂₈H₂₂O₄}[TiCl₂(thf)]? (impure)

To a solution of Z-bis(2-benzyloxyphenyl)-bis(2-methoxyphenyl)ethene (**3Z**) (0.0507 g, 0.119 mmol) in 1 mL of THF was added NaH (0.0059 g, 0.25 mmol) suspended in 1 mL of THF. Gas evolution was observed immediately. The mixture became cloudier within several minutes. After stirring 4 h, the volatiles were removed in vacuo and the residue was suspended in 1 mL of toluene. TiCl₄ (0.0257 g, 0.135 mmol) dissolved in 1 mL of toluene was then added. The color immediately turned dark red. After stirring overnight, the volatiles were removed in vacuo and the residue was triturated with toluene. The triturate was filtered through a celite-packed pipette and evaporated to dryness. The ¹H NMR spectrum of the residue showed a mixture of **56** and other material(s) that show broad signals. The structure of **56** was only tentatively assigned (see Section 4.2.D). ¹H NMR (360 Hz, C₆D₆): δ 7.31 (2H, br d, *J* = -7 Hz), 6.90~6.87 (4H?), 6.71 (2H, dd, *J* = 7.5, 1.8 Hz), 6.69~6.63 (6H?), 6.64 (2H, td, *J* = 7.3, 1.5 Hz), 6.36 (2H, slightly br d, *J* = 8 Hz), 4.06 (4H, m, THF-α), 3.20 (6H, s, OMe), 1.27 (4H, m, THF-β).

57: Z-{C₂₈H₂₂O₄}[TiCl₃(thf)]₂? (impure)

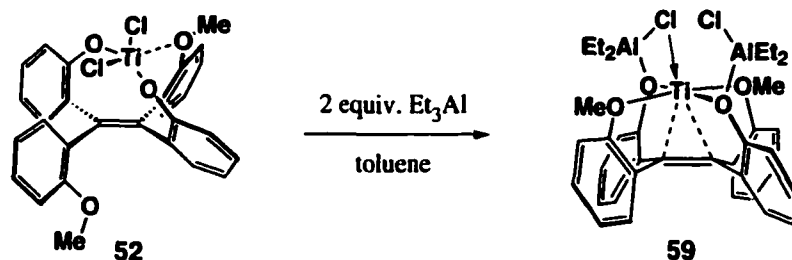
The procedure is the same as above, except for the quantity of the materials. **3Z** (0.0167 g, 0.0393 mmol), NaH (0.0020 g, 0.083 mmol) and TiCl₄ (0.0369 g, 0.195 mmol) were used. The structure of **56** was only tentatively assigned (see Section 4.2.D). ¹H NMR spectroscopy of **57** (360 Hz, C₆D₆): aromatic region is unclear due to broadness of signals and overlapping; δ 3.82 (8H?, br, THF-α), 3.24 (6H, br s, OMe), 1.05 (8H?, br, THF-β). The dinuclear structure was tentatively proposed as one possibility consistent with the limited ¹H NMR spectroscopic information (Section 4.2.D).

58: Z-{C₂₈H₂₂O₄}(CpTiCl₂)₂



To a suspension of *Z*-bis(2-benzyloxyphenyl)-bis(2-methoxyphenyl)ethene (**3Z**) (0.0244 g, 0.0575 mmol) in 1 mL of toluene was added NaH (0.0031 g, 0.13 mmol) suspended in 1 mL of toluene. Immediate gas evolution was observed. The mixture became clear within 5 min, then turned cloudy again. After stirring for 2.5 h, CpTiCl₃ (0.0126 g, 0.0575 mmol) was added in 1 mL of toluene. The color turned yellow-orange, as the mixture became almost homogeneous. After 3 h, the volatiles were removed in vacuo, the residue was triturated with toluene, filtered through a celite-packed pipette, and the filtrate was evaporated in vacuo to dryness. ¹H NMR spectroscopy of this residue showed sharp signals of a mixture, with a 2 : 1 : 2 : 1 ratio of methoxy singlets. The residue was only partially soluble in toluene. Crystallization of the toluene-soluble portion from toluene yielded single crystals analyzed by X-ray crystallography as **58**. The yield was not recorded. ¹H NMR spectroscopy of the major species (360 Hz, C₆D₆): δ 7.84 (1H, br), 7.55 (2H, br d, *J* = ~7 Hz), 6.95–6.60 (XH, unclear due to overlapping), 6.67 (5H, s, Cp), 6.43 (1H?, slightly br, d, *J* = 8 Hz), 6.37 (1H, slightly br, d, *J* = 8 Hz), 5.86 (5H, s, Cp), 3.28 (3H, slightly br s, OMe), 2.99 (3H, s, OMe). Other methoxy signals: 3.27 (3/2 H), 3.17 (3/2 H). X-ray crystallography: see Appendix A-21.

59: *E*-{C₂₈H₂₂O₄}(Ti)(AlEtCl₂)₂



To a solution of **52** (0.0087 g, 0.016 mmol) in 0.5 mL of toluene was added Et₃Al (0.0037 g, 0.032 mmol) dissolved in 1 mL of toluene. The ruby-red color of the starting material immediately turned less reddish, more orange-brown in color. After overnight, the volatiles were removed in vacuo. In the process of removing the volatiles, some crystals were grown. The yield was 0.0109 g (96%). The ¹H NMR spectrum showed a single clean compound. X-ray crystallography of the crystals revealed the structure of the product **59**. ¹H NMR (360 MHz, C₆D₆): δ 7.09 (2H, slightly br d, ~8 Hz), 6.93 (2H, dd, *J* = 6.5–7, ~2.5 Hz), 6.86 (2H, dd, *J* = 7.3, 1.8 Hz), 6.72 (2H, td, *J* = 8, 1.8 Hz), 6.66–6.61 (2H+2H+2H, overlapping), 6.23 (2H, dd, *J* = ~7, ~2 Hz), 3.96 (6H, s, OMe), 1.43 (6H, t, *J* = 8 Hz, AlCH₂CH₃), 0.99 (6H, t, *J* = 8 Hz, Al'CH₂CH₃), 0.50 (4H, m, AlCH₂H₂CH₃),

0.01 (4H, m, Al'CH₂H₂CH₃). ¹³C NMR (100 MHz, C₆D₆): 159.4, 158.1, 145.4, 137.4, 135.1, 133.9, 133.00, 132.97, 124.5, 123.7; one aromatic signal is not found; 69.3 (OMe), 20.6 (AlCH₂CH₃), 20.0 (Al'CH₂CH₃), 14.8 (AlCH₂CH₃), 13.7 (Al'CH₂CH₃). X-ray crystallography: see **Appendix A-21**.

4.6. References

¹ Zanotti-Gerosa, A.; Solari, E.; Giannini, L.; Floriani, C.; Re, N.; Chiesi-Villa, A.; Rizzoli, C. *Inorg. Chim. Acta* **1998**, *270*, 298-311.

² Examples of Ti(II)-(η²-C₂H₄) complexes: (a) Hill, J. E.; Fanwick, P. E.; Rothwell, I. P. *Organometallics* **1992**, *11*, 1771-1773. (b) Alt, H. G.; Schwind, K.-H.; Rausch, M. D.; Thewalt, U. J. *Organomet. Chem.* **1988**, *349*, C7-C10.

Chapter 5

Ethene Polymerization by Derivatives of the Preorganized Polyaryloxy Ligands

Table of Contents

5.0. Introduction and Overview	214
5.1. Titanium Precatalysts	215
5.2. Magnesium Effect	222
5.2.A. Derivatives of the Fluorene-diol Ligand 4	222
5.2.B. Generalization of the "Magnesium Effect"	225
5.2.C. Possible Origins of the Magnesium Effect	235
5.2.D. Isolation of Magnesium-incorporated Titanium Precatalysts	236
5.2.E. Effects of halide and solvated THF/ether	237
5.2.F. In Situ Precatalyst Generation Using Al/Mg complexes: Importance of Mg/Ti Ratio	244
5.2.G. Advantages of Preorganization	246
5.3. Conclusion	254
5.4. Experimental	256
5.4.A. Preparation of Metal Derivatives	256
5.4.B. Composition of Mg salts: Calculations based on Elemental Analysis	262
5.4.C. Small-Scale Polymerization Experiments	264
5.4.D. Large-Scale Polymerization Experiments	266
5.4.E. Complete Data of Polymerization Reactions	270
5.6. References and Notes	282

5.0. Introduction and Overview

The potential of selected metal derivatives described in the previous chapters to be ethene polymerization catalysts, upon activation, was examined, and the results are presented in this chapter. The titanium complexes derived from the preorganized aryloxy ligands are first evaluated and discussed (Section 5.1). Then magnesium-derived precatalysts, which were found to give high polymerization activity, are then discussed (Section 5.2).

Titanium complexes. As discussed in Chapter 2, some aryloxy-based titanium/zirconium complexes are known to give high activity in ethene polymerization. Accordingly, the titanium complexes prepared from the preorganized aryloxy-based ligands *E*- and *Z*-bis(2-hydroxyphenyl)-bis(2-methoxyphenyl)ethene (**3E/3Z**), tetrakis(2-hydroxy-3-propylphenyl)ethene (**7**) and 2,7-bis(1,1-dimethylethyl)-9H-fluorene-1,8-diol (**4**) were evaluated for polymerization activity. Two of the most typical activation methods for Group 4 metal complexes¹ were used to produce the cationic species that served as the actual catalysts. The first method is to activate the titanium halide complex with excess alkylaluminum reagents R₃Al (R = Me or Et) or M-MAO (modified methyl aluminoxane).² The second method is to induce alkyl abstraction from an alkyltitanium precatalyst complex by an electrophilic boron reagent or by protonolysis by using a proton source with inert counterbase and counteranion. Among these trials, only the titanium complexes of the fluorene-diol ligand **4** showed promising levels of activity. Other titanium derivatives from **3E** and **7**, the tetraarylethene based ligands, failed to show comparable polymerization ability.

The magnesium effect. Verkerk observed high polymerization activity when a titanium complex was prepared in situ from the magnesium salt/complex of tetrakis(2-hydroxyphenyl)ethene **2** and several simple chelating bisphenols upon mixing with TiCl₄.³ In contrast, the precatalysts similarly prepared from potassium salts of the same aryloxy ligands showed only poor activity. This phenomenon is termed the "magnesium effect," because the involvement of magnesium is crucial in giving high polymerization activity. We found a similar tendency for the magnesium salts of the above-mentioned ligands.

The magnesium effect, however, was not specific to the preorganized ligands, but was also observed for simpler magnesium phenoxides. The advantage of the preorganized ligand was manifest as a relatively narrower polydispersity of the product polymers and the robustness of the catalyst at higher temperature. The molecular weight of the polymer gained by the magnesium method is usually high, beyond the normal range for high temperature GPC analysis. High temperature experiments, as well as H₂-incorporated experiments, were performed to lower the average molecular weight and obtain analyzable polyethene products.

In this research, we focused on the polymerization activity, using only ethene as a monomer. We did not focus on the polymerization of α -olefins, ethene/ α -olefin copolymerization, or control of polymer quality.

In the experimental section, preparation of the main-group metal salts/complexes and some titanium complexes, our analysis method for the composition of the magnesium salts, and detailed procedures for the polymerization reactions are described.

5.1. Titanium Precatalysts

The titanium complexes tested for ethene polymerization are listed in **Figure 5.1**. The synthesis and characterization of the titanium complexes from the tetraarylethene-based ligands **7** and **3E** were described in Chapters 3 and 4. Because no discrete titanium complex was isolated for ligand **3Z**, only in situ prepared TiCl₄ adducts of the magnesium salt were used. In situ preparation was also used for **30a** and **30**, the titanium chloride derivatives of ligand **7**. Complexes **71** and **72**, titanium derivatives of the fluorene-diol ligand **4**, were prepared from the sodium and magnesium salts in toluene (the coordinated THF in **72** was carried through from the starting magnesium salt). Wuest et al. reported the preparation and crystal structure of the THF-free complex **71** in 1998.⁴ The crystal structure of the THF-coordinated analogue **72** was obtained during our research (see Appendix A-22). This structure is one of several results in this research that confirm the transfer of coordinated THF from Mg to Ti atom upon the reaction of a magnesium salt and TiX₄.

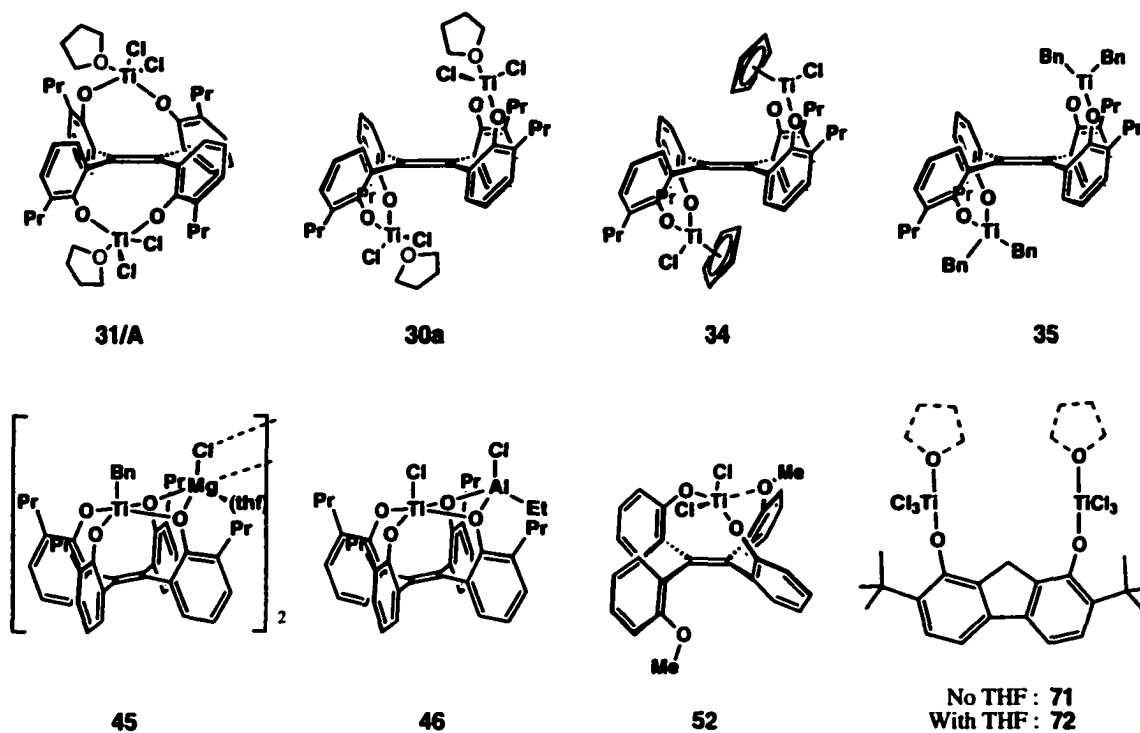


Figure 5.1. Structures of the titanium complexes that appear in **Table 5.1**.

Overall, the titanium complexes from the tetraarylethene-based ligands **7** and **3E** showed poor ethene-polymerization activity. The titanium derivatives of the fluorene-diol ligand **4**, however, displayed promising polymerization activity. **Table 5.1** summarizes the polymerization activity by the above-mentioned titanium complexes upon activation by co-catalysts. The data presented in *entry 21* are from a control run, using TiCl_4 alone, without any ligand support.

Table 5.1. Ethene polymerization trials with titanium complexes derived from ligands 7, 3E and 4.

Entry	Titanium precatalyst	Co-catalyst	(equiv. / Ti)	Activity ^a (kg PE•hr ⁻¹ •mol Ti ⁻¹ •atm ⁻¹)
Derivatives of tetrakis(2-hydroxy-3-propylphenyl)ethene 7				
1	31	Et ₃ Al	200	0
2		M-MAO	200	0
3	30a ^b	Me ₃ Al	100	45
4		M-MAO	200	35
5	30 ^b	Me ₃ Al	100	25
6	34	Me ₃ Al	200	0
7		M-MAO	150	2
8	35	B(C ₆ F ₅) ₃	1.3 (25 min) ^c	0
9		B(C ₆ F ₅) ₃	1 (1 day) ^c	16
10		[PhEt ₂ NH] ⁺ [Y] ^{-d}	1 (< 1 min) ^c	0
11		[PhEt ₂ NH] ⁺ [Y] ^{-d}	1 (1 day) ^c	0
12		[Cp ₂ Fe] ⁺ [Y] ^{-d}	1 (41 min) ^c	0
13		[Ph ₃ C] ⁺ [Y] ^{-d}	1 (20 min) ^c	0
14	45	M-MAO	200	14
15	46	M-MAO	100	8
Derivative of <i>E</i>-bis(2-hydroxyphenyl)-bis(2-methoxyphenyl)ethene 3E				
16	52	Et ₃ Al	200	0
17		M-MAO	200	0
Derivative of <i>Z</i>-bis(2-hydroxyphenyl)-bis(2-methoxyphenyl)ethene 3Z				
18	(57) ^c	Me ₃ Al	100	18
Derivatives of 2,7-bis(1,1-dimethylethyl)-9H-fluorene-1,8-diol 4				
19	71	Me ₃ Al	100	226
20	72	Me ₃ Al	100	156
Control run				
21	TiCl ₄	M-MAO	200	22

General conditions. Solvent: toluene, 5 to 8 mL; catalyst amount: 1 ~ 8 x 10⁻⁶ mol; ethene pressure: 30 psig (~3 atm); polymerization time : 5 ~ 30 min.

^a PE = polyethene.

^b Precatalyst **30a** was prepared in situ from the magnesium salt **25** with 2 equiv. of TiCl₄, mixed for 60 to 80 minutes (long enough for the reaction to complete). Complex **30** was prepared using the sodium salt **40** as a starting material instead of the magnesium salt, mixed for 30 minutes.

^c Reaction time between complex **35** and a co-catalyst before introducing ethene.

^d Y = B(C₆F₅)₄.

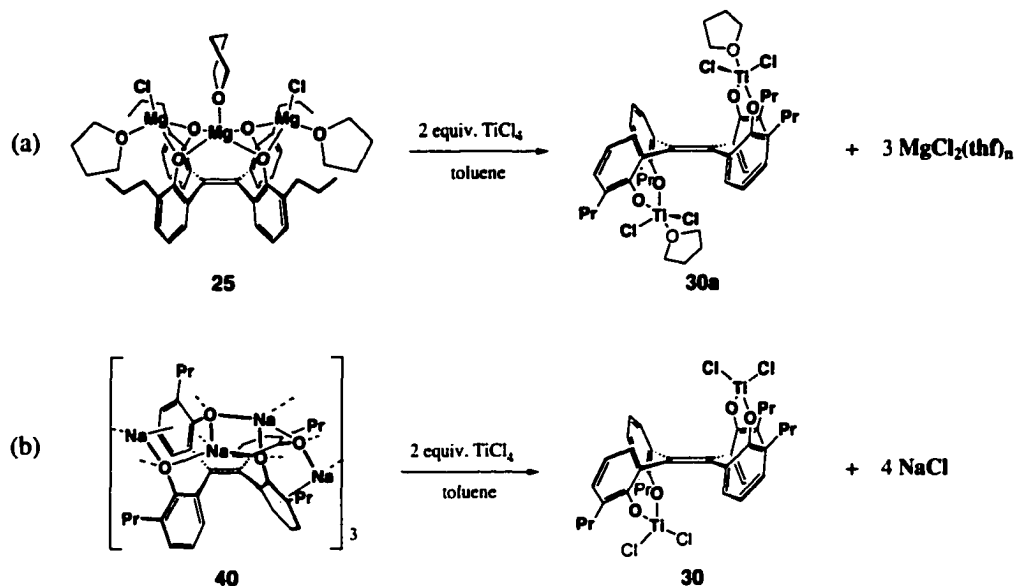
^e Mixture of the magnesium salt of **3Z** (**76**) with 2 equiv. of TiCl₄, with a reaction time of 82 minutes.

i) Titanium complexes of ligand 7. As shown in **Table 5.1**, *entries 1-15*, the titanium complexes derived from tetrakis(2-hydroxy-3-propylphenyl)ethene (**7**) exhibited only low ethene polymerization activity. The activity was typically below that of the control run (22 kg PE•hr⁻¹•mol Ti⁻¹•atm⁻¹). Obviously, the preorganized tetraaryloxy platform does not provide a good catalytic titanium site from the geminal or vicinal "up/down" complexes **30a**, **31**, **34** and **35**, or from the Ti/Mg and Ti/Al complexes **45** and **46**.

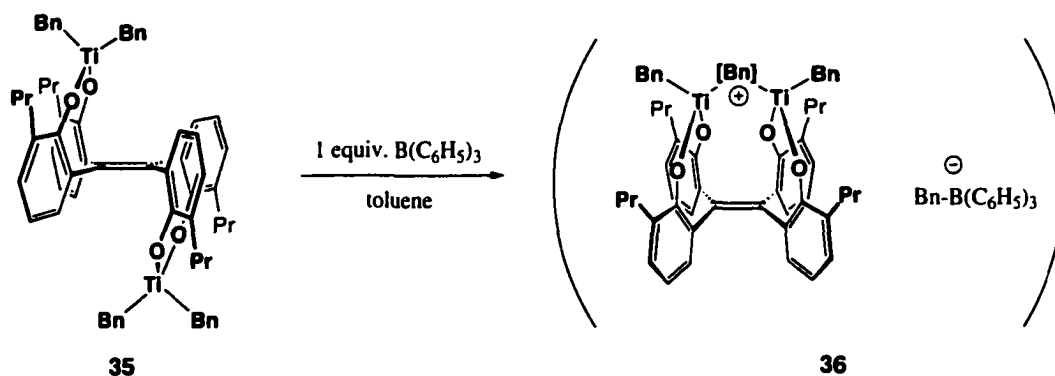
The first four complexes (*entries 1-13*) are in the "up/down" configurations, in which each bidentate chelating unit presumably acts individually. Unlike the bisphenol ligands known to form Ti or Zr complexes that show good polymerization activity (Chapter 2), the pairwise formation of titanium centers in these complexes probably do not provide enough steric protection to form effective catalysts. Replacing one Cl group on each "TiCl₂" fragment in complex **30** with a Cp ligand (**34**), however, did not improve the situation.

Entries 3-4, in which complexes **30a** and **30** were prepared in situ from magnesium complex **25** or sodium salt **40** because both were difficult to isolate, showed relatively higher activities than those of the isolated titanium chloride complexes (**31** and **34**). These activities, however, are suspected to come from the involvement of the byproduct inorganic salts, MgCl₂(thf)_n (n = 0 or 1) for the former and NaCl for the latter (**Scheme 5.1**). The involvement of MgCl₂(thf)_n will be discussed in more detail later as the "magnesium effect."

The di-"TiBn₂" complex **35** was expected to form a discrete [Ti₂]⁺ complex **36** (**Scheme 5.2**) upon reaction with B(C₆F₅)₃, which polymerized THF (see Section 3.1.2.F). However, low to no ethene polymerization was observed when using any of the boron or borate co-catalysts (*entries 8-13*). Only the conditions closest to those under which **36** was synthesized (*entry 9*) gave activity comparable to the control run (*entry 21*). It may be noted that despite the low activity, this was the only experiment that showed any polymerization activity without involvement of inorganic salts, among all titanium complexes of the tetraarylethene-based ligands **7**, **3E**, and **3Z**.



Scheme 5.1. In situ formation of **30a** and **30** accompanied by the formation of inorganic salts.

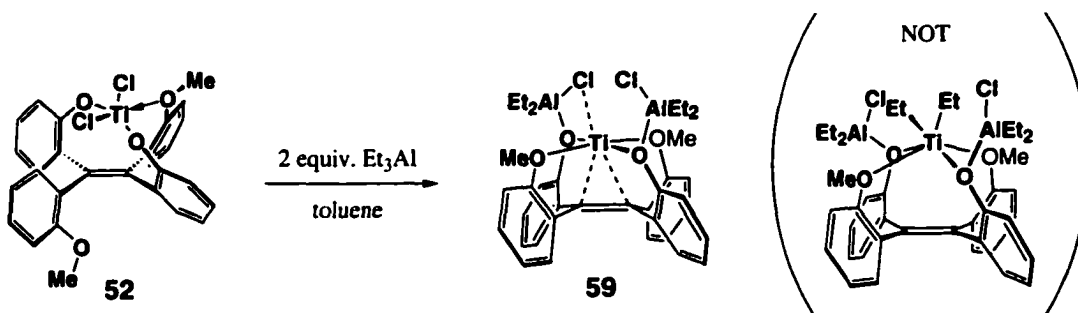


Scheme 5.2. Reaction between **35** and $B(C_6H_5)_3$ and the proposed structure of **36**.

The two hetero-polymetallic complexes, **45** and **46**, did not provide good catalysts, although such hetero-polymetallic species were expected to serve as surface models for heterogeneous Ziegler-Natta catalysts. These particular complexes do not provide suitable environments for catalysis: the titanium atom is surrounded by four oxygen donors in both cases, making three ionic and one dative bonds, probably providing too much electron density to the titanium atom. The pseudo-octahedral

coordination geometry is also apparently not suitable for polymerization, because this geometry does not allow for the creation of two adjacent vacant coordination sites, which are normally required for olefin polymerization.⁵

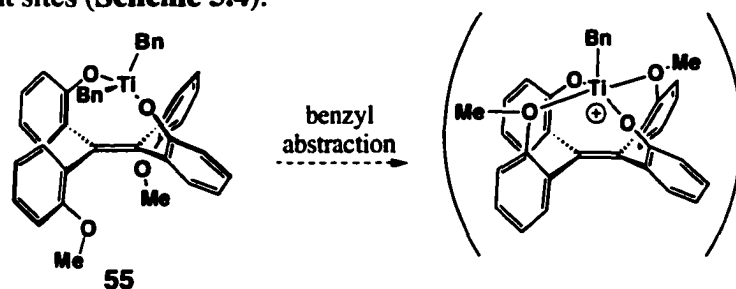
ii) Titanium complexes of ligand 3E. The mononuclear "TiCl₂" complex **52**, in which one of the two methoxy groups are coordinated to the titanium atom to bring some level of steric and electronic protection to the metal, also does not give measurable polymerization (*entries 16-17*). This inertness, however, is well explained by the reactivity of this complex toward Et₃Al, as discussed in Chapter 4, Section 4.3.A. Addition of two equivalents of Et₃Al led to the reduction of the Ti(IV) to Ti(II), resulting in the formation of complex **59** (Scheme 5.3). Formation of a cationic titanium center cannot be expected from this species, even in the presence of excess aluminum co-catalysts. Constructing hetero-polymetallic species was intended to be a potentially new way to introduce steric protection to the titanium center, but with the formation of **59**, the aluminum coordination promotes the reduction of the titanium (see Section 4.3.A). Complex **59** also has a pseudo-octahedral geometry, which again may not be suitable for allowing for the creation of two adjacent vacant sites. The coordination of the olefin in the ligand to the titanium draws the metal "down" into an unsuitable geometry for olefin polymerization. The use of larger zirconium metal may avoid such interaction with the double bond and form a more favorable geometry.



Scheme 5.3. Formation of **59** from **52** and two equivalents of Et₃Al.

The TiBn₂ complex **55** (Scheme 5.4) was not tested for ethene polymerization because the isolation of **55** in analytically pure form was not successful. Upon alkyl abstraction, however, both methoxy groups will presumably be strongly coordinated to the cationic titanium center, forming a pseudo-octahedral coordination geometry

(counting the olefin double bond as one ligand), again unsuitable for forming two adjacent vacant sites (Scheme 5.4).



Scheme 5.4. A proposed 'dead end' cationic titanium from 55.

Although ligand **3E** did not show a suitable environment for polymerization as titanium complexes, use of other metals with larger radii may result in forming a more preferable geometry in which the metal may lie out of the O_4 plane.⁶

iii) Titanium derivatives of ligand 3Z. Only by in situ preparation from the magnesium salt of **3Z** and two equivalents of $TiCl_4$ could polymerization be evaluated because discrete titanium complexes could not be prepared cleanly. The activity observed was low, on the level of the control run (*entry 18*). Still, the activity was relatively higher than that of most isolated titanium complexes that show no measurable activity. This activity is also presumably caused by the presence of the inorganic magnesium byproduct.

iv) Titanium derivatives of the 1,8-fluorene-diol 4. The titanium complexes derived from the fluorene-diol ligand **4**, dinuclear complexes **71** and **72**, showed considerably higher activity (*entries 19-20*) than the catalysts derived from the tetraarylethene-based ligands. These activity values fall within the accepted criteria of "high" activity, according to a review of non-metallocene homogeneous catalysts.⁷

The THF-free complex **71** showed higher activity than THF-solvated **72**. Without repetition of the experiments,^a it is difficult to say that the difference (226 vs. 156 kg

^a Due to the limited availability of ligand **4** and the derivatives **71** and **72**, the reactions were done only once for each case.

PE•hr⁻¹•mol Ti⁻¹•atm⁻¹) is statistically significant; for roughly 10 to 20% error is expected in typical polymerization procedures. Nevertheless, this observation is reasonable because THF is expected to deactivate a cationic titanium center. With excess co-catalyst, however, the effects of a small amount of THF may not be significant.

When the precatalyst was prepared in situ from the magnesium salt of **4**, even higher activity was obtained than from the preformed titanium complexes. The highest value obtained by this method was 821 kg PE•hr⁻¹•mol Ti⁻¹•atm⁻¹, the record performance for all of the small-scale experiments in this research. This is a good example of the "magnesium effect." **Table 5.2** summarizes the comparisons of different precatalysts (either preformed complexes or in situ-prepared) derived from the fluorene-diol ligand **4**. The first two entries (*1* and *2*) are the same as *entries 19* and *20* of **Table 5.1**. This table also serves as an appropriate introduction to the general discussion of the magnesium effect, Section 5.2.

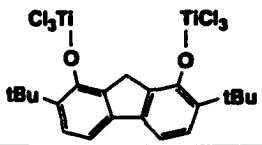
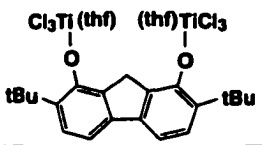
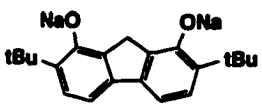
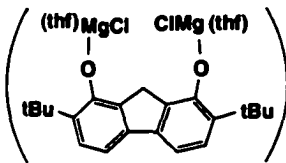
5.2. Magnesium Effect

5.2.A. Derivatives of the Fluorene-diol Ligand **4**

As shown in **Table 5.2**, the in situ preparation of a titanium precatalyst from the magnesium salt of **4** (labeled **74**, *entries 4-13*) gives considerably higher activity than does the use of discrete titanium complex **71** or **72** or the use of precatalysts prepared in situ from the corresponding sodium salt.

The magnesium salt **74** was prepared by mixing ligand **4** and two equivalents of CH₃MgCl in THF overnight. Although crystallization of the THF-soluble product from toluene failed to yield crystals suitable for X-ray analysis, the composition of the resulting substance was calculated as [4 - 2H]•Mg_{2.5}•Cl_{3.0}•(thf)_{2.8} based on the elemental analysis (see Section 5.4.B). From the composition, the salt is tentatively assigned to be a di-MgCl(thf) salt, as drawn in **Table 5.2** (for *entries 4-13*), accompanied by approximately 0.5 equivalent of MgCl₂(thf).

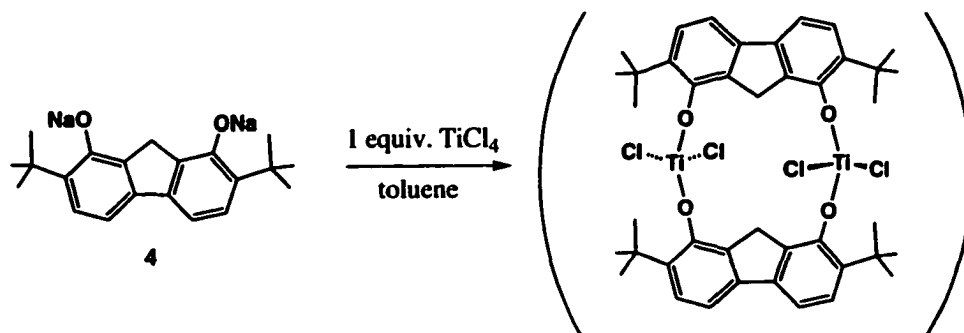
Table 5.2. The different conditions to produce a catalyst from the metal derivatives of **4**. Entries 1 and 2 are the same as entries 19 and 20 of Table 5.1).

Entry	Precatalyst conditions	Co-catalyst and amount (equiv./Ti)	Activity (kg PE·hr ⁻¹ ·mol Ti ⁻¹ ·atm ⁻¹)
1	 (71)	Me ₃ Al 100	226
2	 (72)	Me ₃ Al 100	156
3	 (73)	+ 1 TiCl ₄ (49 min)	Me ₃ Al 100 14
4	 (74)	+ 1 TiCl ₄ (1 min)	Me ₃ Al 100 152
5		+ 1 TiCl ₄ (40 min)	Me ₃ Al 100 360
6		+ 1 TiCl ₄ (58 min)	Me ₃ Al 100 437
7		+ 2 TiCl ₄ (1 min)	Me ₃ Al 100 90
8		+ 2 TiCl ₄ (50 min)	Me ₃ Al 100 343
9		+ 2 TiCl ₄ (65 min)	Me ₃ Al 100 269
10		+ 1 TiCl ₄ (1 min)	M-MAO 200 821
11		+ 1 TiCl ₄ (17 min)	M-MAO 200 53
12		+ 2 TiCl ₄ (1 min)	M-MAO 200 606
13		+ 2 TiCl ₄ (28 min)	M-MAO 200 51

Entries 7-9 and 12-13 are the results obtained from the precatalyst prepared in situ from the magnesium salt **74** and two equivalents of TiCl₄ after a relatively short reaction time ("mixing time"), up to one hour. After prolonged mixing (such as several hours or

complex **72** as a precatalyst, because **72** was prepared in exactly this way. The in situ preparation, however, is accompanied by an insoluble byproduct MgCl_2 , which we assume would self-aggregate and precipitate out of the system after a long enough mixing time, remaining innocent in the polymerization reaction. However, MgCl_2 may not be completely excluded from the system within a short mixing time, somehow incorporated into the newly formed titanium complex. We therefore suspect that the considerably higher polymerization activity obtained from the short-time mixture of the magnesium salt and TiCl_4 arises from the involvement of magnesium chloride in the precatalyst.

This in situ preparation of the Ti precatalyst from a main-group metal salt was only effective with the magnesium salt. The use of sodium salt of ligand **4** (labeled **73**, entry 3) resulted in an activity as low as that obtained from the control experiment lacking any ligand (entry 21, Table 5.1). This result indicates the superiority of the effect of magnesium over that of sodium in giving high polymerization activity. This comparison may not be totally fair, however, because only one set of conditions was evaluated for the sodium salt. The low activity of entry 3 may be due to the formation of a "collapsed" final product as shown in Scheme 5.5. We have not, however, prepared and isolated such dimeric species to confirm the polymerization inertness or activity.



Scheme 5.5. Proposed structure of precatalyst produced in entry 3: the 1 : 1 adduct of TiCl_4 and the sodium salt of ligand **4**.

Nonetheless, the analogous 1 : 1 adduct of the magnesium salt and TiCl_4 , formed in situ (entries 4-6) gave considerably higher activity than that obtained from the sodium salt, supporting the superior effect of the magnesium involvement.

The magnesium effect was found to be considerably sensitive to the mixing time. The best polymerization activity was obtained from mixing times ranging from 1 minute to 1 hour, and typically a decrease in activity was observed after longer mixing time.

Interestingly, the optimal mixing time was greatly affected by the co-catalyst. With Me_3Al , the best activity was obtained after around one hour mixing time, both with one or two equivalents of TiCl_4 per magnesium salt, while a mixing time as short as one minute gave the highest activity when the co-catalyst was M-MAO.

Similar magnesium effects were observed with other phenoxide and polyaryloxyde ligand systems. In the next section, results from magnesium, sodium and aluminum salts of several other ligands systems are discussed in detail.

5.2.B. Generalization of the "Magnesium Effect"

The graphs and tables on the following several pages present the results of the polymerization activity obtained by in situ preparation of precatalyst complexes from salts of the ligand systems shown in **Figure 5.2**: the tetraarylethene-based ligands **7**, **3E**, and **3Z** as preorganized systems; along with phenol, 3,3'-dimethyl-4,4'-biphenol, and hydroquinone. The simpler phenoxide ligand systems provide a control for comparison with the preorganized systems. The non-chelating diols were chosen as a supplemental control template, for comparison with the magnesium effect in various chelating diols as studied by Verkerk.³

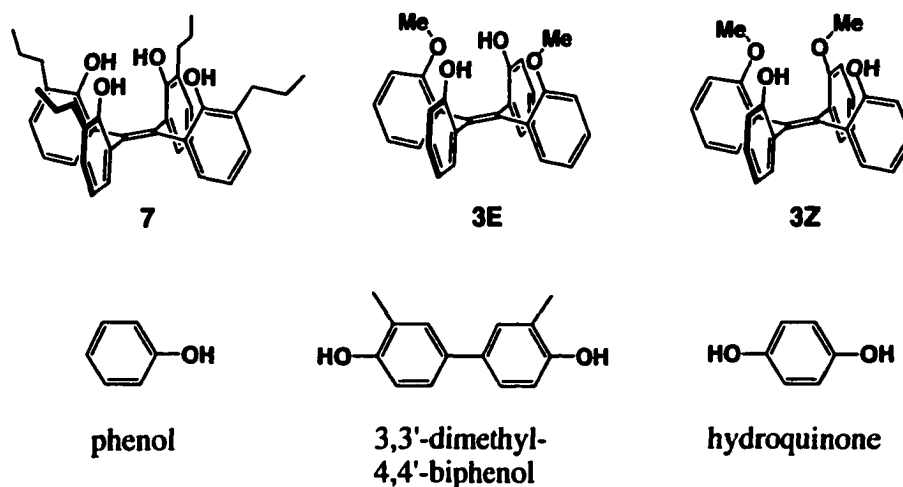


Figure 5.2. Ligand systems evaluated for the magnesium effect.

Chart 1. Results of polymerization by Mg and Na salts of ligand 7.

Composition of the salts.

Mg salt **25**:



Na salt **40**:

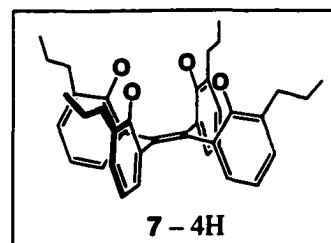


Figure 5.3 (a, b & c). Ethene polymerization activity vs. mixing time: Mg salt of **7 (25)** with $TiCl_4$. The cocatalyst and stoichiometry are specified below.

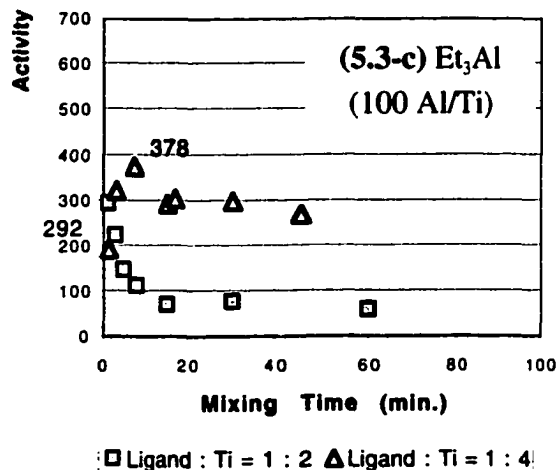
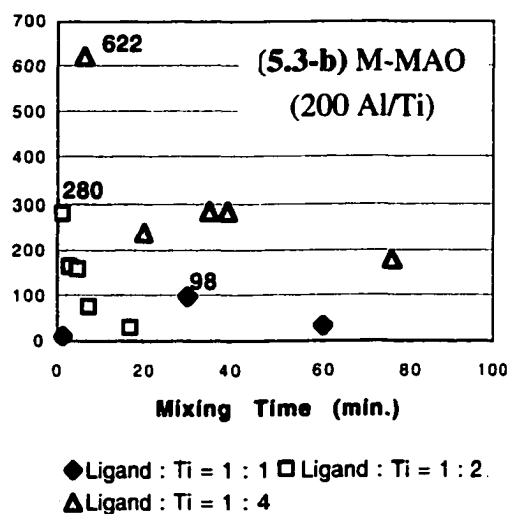
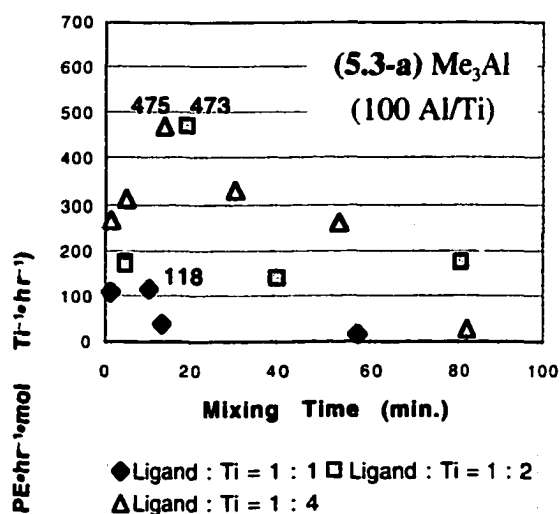


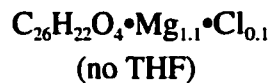
Table 5.3. Control experiments with Na salt of **7 (40)**.

Ligand:Ti	Mix. time (min)	Activity (kg PE·hr ⁻¹ ·mol Ti ⁻¹ ·atm ⁻¹)
1 : 1	1	19
	19	23
1 : 2	1	22
	5	27
	29	25
1 : 4	1	11
	10	13
	38	10
	Co-catalyst: Me_3Al (100Al/Ti)	

Chart 2. Results of polymerization by Mg and Al salts of ligand 3E.

Composition of the salts

Mg salt (75):



Na salt was not evaluated

Al salts:

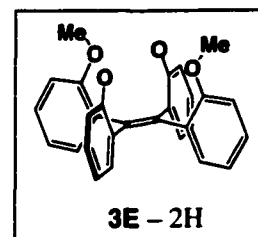
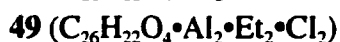
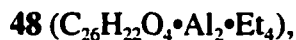
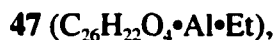


Figure 5.4 (a & b). Ethene polymerization activity vs. mixing time: Mg salt of 3E (75) with TiCl_4 . The cocatalyst and stoichiometry are specified below.

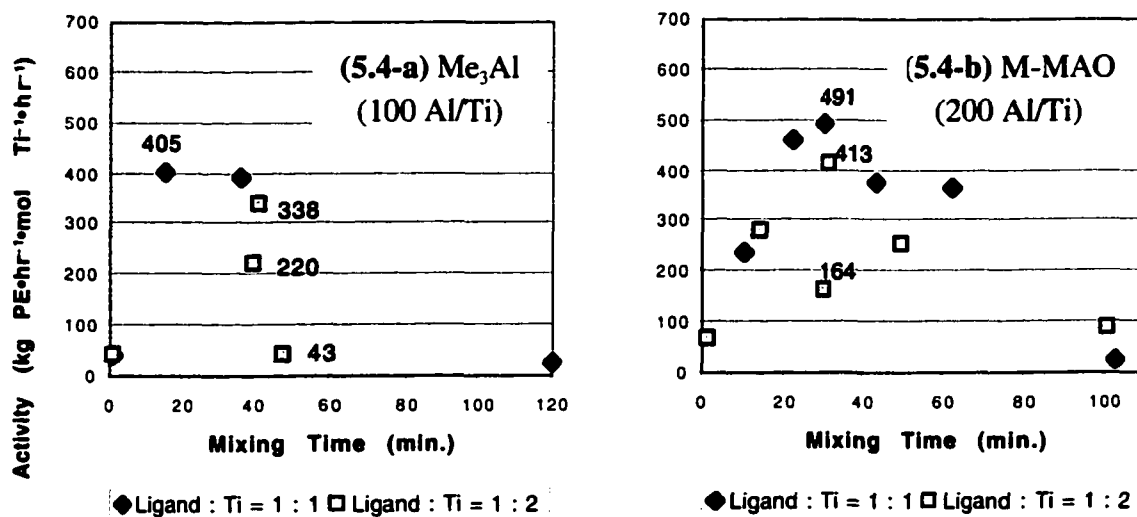


Chart 2. (continued)

Table 5.4. Control experiments with Al salts of 3E.

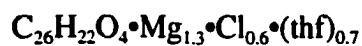
Al compound	Ligand:Ti	Mix. time (min)	Activity (kg PE·hr ⁻¹ ·mol Ti ⁻¹ ·atm ⁻¹)
47	1 : 1	1	26
		103	11
48	1 : 1	1	34
		86	29
	1 : 2	1	37
		87	55
		43 hr	40
50	1 : 1	1	14
		62	18
	1 : 2	1	13
		41	19
		216	30

co-catalyst: M-MAO (200Al/Ti)

Chart 3. Results of polymerization by Mg salt of 3Z

Composition of the salts

Mg salt (76):



Na salt was not evaluated.

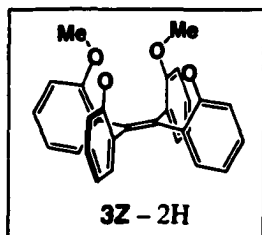


Table 5.5. Control experiments with Mg salt of 3Z (76).

Ligand:Ti	Mix. time (min)	Activity (kg PE·hr ⁻¹ ·mol Ti ⁻¹ ·atm ⁻¹)
1 : 1	14	38
	27	42
	66	21
	208	23
1 : 2	15	41
	29	38
	77	30

co-catalyst: Me₂Al (100Al/Ti)

Chart 4. Results of polymerization by Mg and Na salts of phenol

Composition of the salts

Mg salt (77):



Na salt (80):

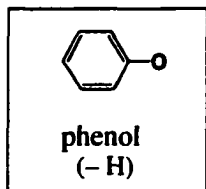
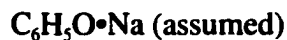


Table 5.6. Control experiments with Na salt of phenol (80).

Ligand:Ti	Mix. time (min)	Activity (kg PE·hr ⁻¹ ·mol Ti ⁻¹ ·atm ⁻¹)
1 : 0.5	79	17
1 : 1	63	19

co-catalyst: Me₃Al (100Al/Ti)

Figure 5.5 (a & b). Ethene polymerization activity vs. mixing time: Mg salt of phenol (77) with TiCl₄. The cocatalyst and stoichiometry are specified below.

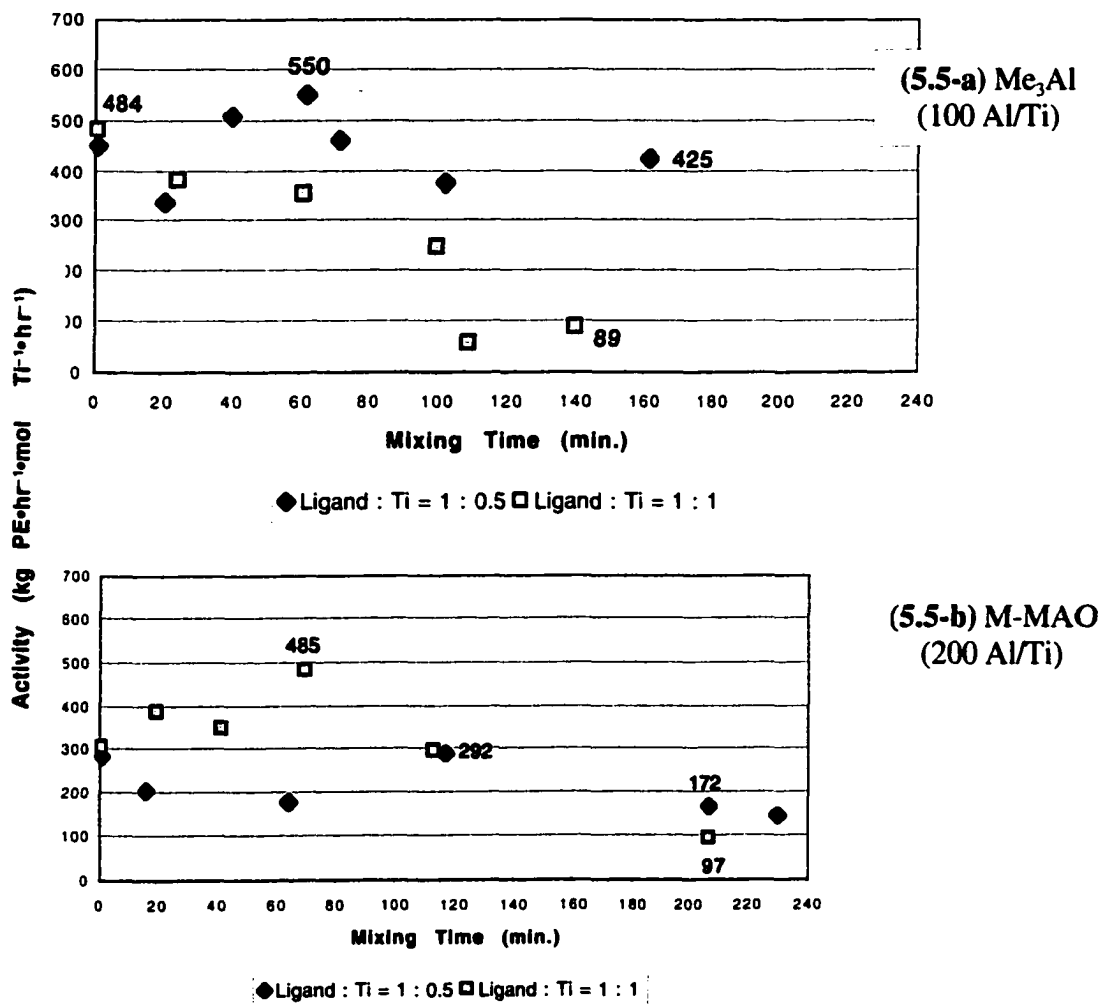


Chart 5. Results of polymerization by Mg salt of 3,3'-dimethyl-4,4'-biphenol

Composition of the salts

Mg salt (**78**):



Na salt was not evaluated

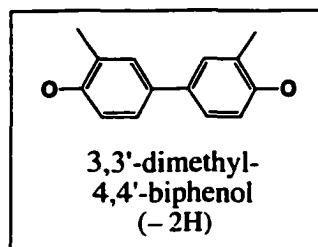


Figure 5.6 (a & b). Ethene polymerization activity vs. mixing time: Mg salt of 3,3'-dimethyl-4,4'-biphenol (**78**) with TiCl_4 . The cocatalyst and stoichiometry are specified below.

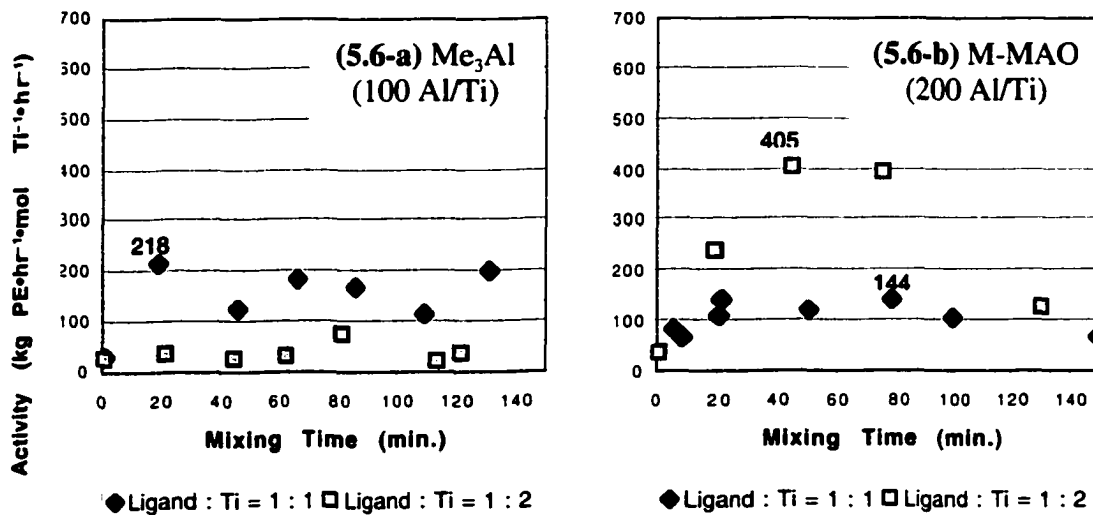
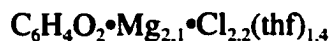


Chart 6. Results of *in situ* method from the salts of hydroquinone

Composition of the salts

Mg salt (**79**):



Na salt (**81**):

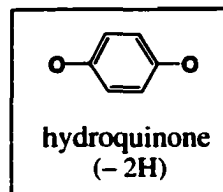
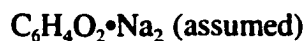


Figure 5.7 (a & b). Ethene polymerization activity vs. mixing time: Mg salt of hydroquinone (**79**) with TiCl_4 . The cocatalyst and stoichiometry are specified below.

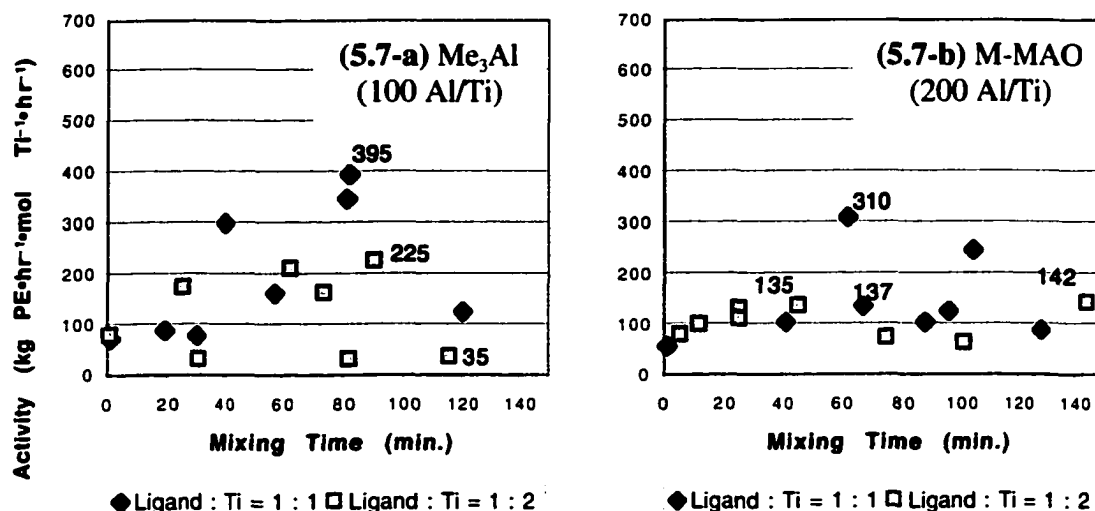


Table 5.7. Control experiments with Na salt of hydroquinone (**81**).

Ligand:Ti	Mix. time (min)	Activity (kg PE·hr ⁻¹ ·mol Ti ⁻¹ ·atm ⁻¹)
1 : 1	49	11
1 : 2	80	20

co-catalyst: Me_3Al (100Al/Ti)

The dependence of the catalyst activity on mixing time was carefully examined for each system to record optimum performance and is summarized in graphs of activity vs. mixing time. The complete data on which the graphs are based are presented in the Experimental section (5.4.E). Results from sodium and aluminum salts were less rigorously evaluated and are given in table form.

Consistent reaction conditions were used: the standard small-scale procedure (detailed in Section 5.4.C) was used throughout, in toluene medium and under 30 psig of ethene pressure. Activation of the in situ-prepared titanium precatalyst was by Me_3Al (100 equiv. Al/Ti), Et_3Al (100 equiv. Al/Ti), or M-MAO (200 equiv. Al/Ti). Different ratios of [ligand : TiCl_4] were evaluated for each system. Because of the small scale, an internal error of 10-20% is reasonably expected. Some salts displayed lower reproducibility than did others.

The formula weight and composition of the magnesium salts were calculated from C/H elemental analysis data (detailed in Section 5.4.B). The formula of the sodium salts was assumed to be "ArONa" when the salt was obtained from the reaction between ArOH and NaH, except for the sodium salt **40**, derived from tetrakis(2-hydroxy-3-propylphenyl)ethene **7**, which was crystallized and analyzed by C/H elemental analysis.

A summary of the noteworthy trends and results determined in this series of experiments appears below.

i) Typical activity. The polymerization activities obtained by the precatalysts prepared in situ from the magnesium salts and TiCl_4 (presented in Charts 1-6) show that the magnesium effect is universal to all phenoxides, preorganized or simple. The optimal activity recorded for each magnesium salt was 400-600 kg PE $\cdot\text{hr}^{-1}\cdot\text{mol Ti}^{-1}\cdot\text{atm}^{-1}$, with few exceptions. Sodium salts, as well as aluminum complexes in some cases, were notably ineffective, similar to the control run level presented in **Table 5.1, entry 21** (~20 kg PE $\cdot\text{hr}^{-1}\cdot\text{mol Ti}^{-1}\cdot\text{atm}^{-1}$) or only slightly higher.

ii) Mixing time dependence. The optimal mixing time clearly varies with the ligand system used. The highest polymerization activities were often obtained after mixing times as short as 1-5 minutes for many precatalysts in the **7** series (see, e.g., **Figure 5.3-c**),

while a prolonged range of "good" mixing times was observed using simple phenol (**Figure 5.5**).

The best mixing time is also a function of titanium stoichiometry and the co-catalyst used. For many cases, however, the graphs show a maximum, and then the activity drops after a longer mixing time. Applying infinite mixing time is presumed to be equivalent to the use of titanium-only complexes, as for ligand **7** in the titanium complex series (**Table 5.1, entries 3-4**). Nevertheless, the diminished activity after a prolonged period of mixing time is still higher compared to that obtained from the use of titanium complexes only, which do not show any measurable activity, and is considered to come from the byproduct $\text{MgCl}_2(\text{thf})_n$ combined with the titanium complexes.

iii) Reproducibility. The reproducibility of the magnesium method seems to depend mainly on the solubility of the starting aryloxymagnesium salt in toluene. Poor reproducibility manifests itself as different activities at a similar mixing time. One example is shown in **Figure 5.4-b (Chart 2)**, at approximately 30 minutes of mixing time (in the series of two equivalents of TiCl_4 per ligand in salt **75**). Activity of $413 \text{ kg PE}\cdot\text{hr}^{-1}\cdot\text{mol Ti}^{-1}\cdot\text{atm}^{-1}$ was observed at one time, but only $164 \text{ kg PE}\cdot\text{hr}^{-1}\cdot\text{mol Ti}^{-1}\cdot\text{atm}^{-1}$ was observed in a different run. The toluene solubility of the magnesium salt in this series was poor, compared to that of the reasonably reproducible cases, such as both ligand **7** and phenol-derived catalysts.

The size of the particles/crystals of the magnesium salts also reflects on the reproducibility. The size mostly impacts the time of maximum activity: the best mixing times occur earlier using finer particles of the magnesium salt. For example, the best mixing time for crystals of magnesium complex **25** (from ligand **7**) with two equivalents of TiCl_4 , activated by Me_3Al (**Figure 5.3-a**), was approximately 20 minutes in this series, while in a separate series of experiments using finer crystals, the best mixing time optimized as early as 1-3 minutes. The larger surface area of finer particles presumably increases the rate of dissolution in toluene, and in turn, the rate of reaction with TiCl_4 .

iv) Inert magnesium derivatives. Although the magnesium effect is typically observed across various aryloxymagnesium salts, consistently poor activity in certain cases was observed at any mixing time. The magnesium salt **76**, derived from ligand **3Z**, in particular, was inert over wide range of mixing times, when either one or two equivalents of TiCl_4 per ligand were used (**Table 5.5**). The initial reaction between the

salt and TiCl_4 appeared to be unusually slow: the color of the mixture did not turn red clearly during the mixing time periods detailed in **Table 5.5**, while the corresponding reactions of the *E*- analogue (**75** from **3E**) immediately turned red. The very poor solubility of the magnesium salt of ligand **3Z** is possibly to blame, but if this is alone responsible, at least some correlation of activity and mixing time would be expected.

Another consistently low activity case is the [Ligand : Ti = 1 : 1] stoichiometry of the magnesium salt **25** derived from ligand **7** as shown in **Figure 5.3-a** and **-b** (**Chart 1**). It is plausible that the reaction at this stoichiometry resulted in the formation of the collapsed "sandwich" type complex **32** (see Chapter 3, Section 3.1.2.D), which is an unsuitable precatalyst.

v) Co-catalysts. Overall, both Me_3Al and M-MAO functioned as co-catalysts, giving comparable polymerization activity. The fact that Me_3Al is as effective as M-MAO suggests that the actual catalyst is functionally more similar to classic heterogeneous Ziegler-Natta catalysts than to metallocene-type homogeneous catalysts. The activity level, up to $600 \text{ kg PE}\cdot\text{hr}^{-1}\cdot\text{mol Ti}^{-1}\cdot\text{atm}^{-1}$ (in large-scale experiments, the highest activity was over $1,000 \text{ kg PE}\cdot\text{hr}^{-1}\cdot\text{mol Ti}^{-1}\cdot\text{atm}^{-1}$), is also similar to the activities reported for "MgCl₂-supported TiCl₄" type heterogeneous catalysts.⁸

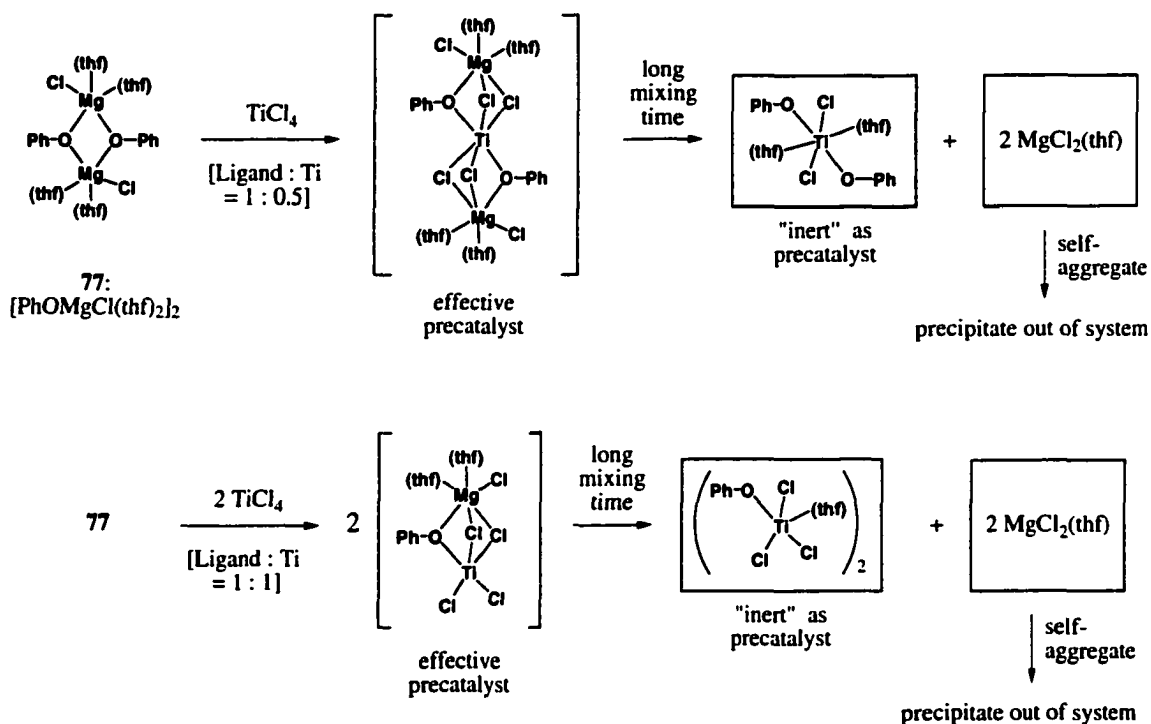
Meanwhile, for other systems, one of the co-catalysts (Me_3Al or M-MAO) gave consistently superior activities. For example, the use of Me_3Al provides better activity for the magnesium salt **77** derived from simple phenol at [Ligand : Ti = 1 : 0.5] (**Figure 5.5-a** and **-b**, **Chart 4**), while M-MAO was clearly superior for the magnesium salt **78** derived from 3,3'-dimethyl-4,4'-biphenol at [Ligand : Ti = 1 : 2] (**Figure 5.6-a** and **-b**, **Chart 5**). The co-catalyst also affected the optimal mixing time and the reproducibility. These observations suggest that the co-catalyst is somehow involved in the actual catalyst structure, affecting the solubility and aggregation tendency, if not the actual catalytic center.

vi) Molecular weight of the polyethene. The polymer products obtained from the magnesium precatalysts have a very high average molecular weight. Analysis by standard high-temperature GPC (gel permeation chromatography) was not possible because the polymer would not dissolve in 1,2,4-trichlorobenzene at temperatures up to 130 °C. High crystallinity of the polymer produced is also suggested by this observation. Modified

polymerization procedures were therefore adopted to lower the molecular weight of the polyethene for analysis of the polydispersity (*vide infra*).

5.2.C. Possible Origins of the Magnesium Effect

Obviously, the direct involvement of magnesium in the catalytic active site is essential to optimize the observed polymerization activity for titanium precatalysts prepared in situ from magnesium salts. We suspect that the magnesium dichloride that is formally produced upon the reaction of the aryloxymagnesium salts with TiCl_4 is intimately involved in the actual catalysts. **Scheme 5.6** provides a proposed scenario for the reaction between magnesium aryloxide, represented by salt **77** derived from simple phenol, and one equivalent of TiCl_4 .



Scheme 5.6. Suggested MgCl_2 -incorporated phenoxytitanium chloride precatalysts produced from the reaction of **77** with TiCl_4 .

The MgCl_2 is considered to be bridged via chlorides and phenolato-oxygens to the newly formed $(\text{ArO})_x\text{TiCl}_{4-x}$ ($x = 1$ or 2) right after the kinetic transmetallation.

Activation of this species by a co-catalyst then produces an active catalyst that still retains bridging magnesium. However, after a long mixing time, the dissociation of magnesium dichloride from the aryloxytitanium unit proceeds. MgCl_2 , as a THF-solvate, subsequently self-aggregates and precipitates out of the system, driving the thermodynamics and preventing re-association to the aryloxytitanium unit. In the scheme, the dissociation of titanium and magnesium units is depicted as being promoted by THF-transfer from magnesium to titanium, although it is not applicable for non-THF magnesium salts. The precipitated MgCl_2 may still be capable of interacting with limited amount of titanium complexes on its surface to create some effective precatalysts, because the precatalyst mixture after long enough mixing time still give the polymerization activity higher than that of titanium-only complexes with no MgCl_2 present.

The rate of this second step is expected to vary among the different aryloxy ligands. The simple phenoxide retained good activity over an exceptionally long mixing time range. Most other cases, however, showed high polymerization activity only for a short time period, between one and sixty minutes. The dissociation of magnesium chloride from the effective precatalyst stage is, apparently, quite fast for most aryloxy systems.

In some ways, these precatalysts prepared by mixing the magnesium salts and TiCl_4 are a microscale version of MgCl_2 -supported TiCl_4 heterogeneous Ziegler-Natta catalysts, in which TiCl_4 is typically supported on fine particles of anhydrous MgCl_2 , or Ti/Mg precatalysts deposited on silica supports.⁹ Small cluster particles or possibly molecular-level MgCl_2 presumably exist for a short time period and serves to "support" the partly aryloxytated titanium chlorides. This system, therefore, may resemble the silica-supported Ti/Mg chloride precatalysts, which are widely used in industry, with the aryloxy ligand replacing the silica structure.

5.2.D. Isolation of Magnesium-incorporated Titanium Precatalysts

Because the magnesium salt **77** [$\text{PhOMgCl}(\text{thf})_2$] derived from phenol showed a minimal correlation of activity and mixing time, in contrast to most other aryloxymagnesium salts, the isolation of the magnesium-incorporated precatalysts was possible. The adducts of the magnesium salt **77** and both 0.5 and 1 equivalent of TiCl_4 per ligand were prepared in hexanes (0.5 equiv.) or toluene (1 equiv.), and the products

were isolated as amorphous precipitates (labeled **84** and **85**, respectively). These precipitates showed ethene polymerization activities of 315 and 277 kg PE•hr⁻¹•mol Ti⁻¹•atm⁻¹, respectively, when activated by ca. 300 equivalents of Et₃Al. Attempts to crystallize these Mg/Ti adducts from non-coordinating hydrocarbon medium were, unfortunately, not successful.

For comparison, the [77 : TiCl₄ = 1 : 2] adduct (labeled **86**) was prepared in hexanes by the same procedure. No in situ preparation of precatalysts in this ratio was evaluated to obtain the mixing-time correlation. This adduct showed an activity of only 22 kg PE•hr⁻¹•mol Ti⁻¹•atm⁻¹. Two equivalents of titanium per aryloxy moiety are apparently not appropriate to produce effective catalysts.

5.2.E. Effects of halide and solvated THF/ether

To specify which part of the MgCl₂(thf)_n was related to the origin of the high polymerization activity, the effects of halide and the solvate ligands (THF or Et₂O) were evaluated by comparing the chloro and bromomagnesium salts, and the THF and Et₂O solvates. The halide effects were also evaluated by using both TiCl₄ and TiBr₄. The two ligand systems used in this study were the *ortho*-propylated ligand **7** and phenol.

i) Halide influences. The aryloxymagnesium chlorides and bromides derived from ligand **7** and phenol (**Table 5.8**), all THF-solvated, were compared for polymerization activity by the preparation of precatalysts with TiCl₄ or TiBr₄. The composition and/or structure of the MgCl and MgBr salts are identical for both ligands, a factor that enabled a fair comparison. For both ligands, the stoichiometry of titanium was adjusted so one equivalent of titanium was provided per two aryloxy moieties. The results are summarized in **Figures 5.8** (for the salts derived from ligand **7**) and **5.9** (for the salts derived from phenol) as a function of the mixing time. The co-catalyst is Me₃Al (100 equiv. Al/Ti) for all cases.

Table 5.8. Composition of the magnesium salts evaluated for the influence of halides on the magnesium effect.

	<i>Salt of ligand 7</i>	<i>Salt of phenol</i>
Mg/Cl/(thf) salt	[7 – 4H]Mg ₃ Cl ₂ (thf) ₃ (25)	C ₆ H ₅ OMgCl(thf) ₂ (77)
Mg/Br/(thf) salt	[7 – 4H]Mg ₃ Br ₂ (thf) ₃ (26)	C ₆ H ₅ OMgBr(thf) ₂ (82)

Different halides in the starting magnesium salts had a minimal effect on the polymerization activity and the mixing-time dependence when TiBr₄ was used as a titanium source (**Figure 5.8-b** and **5.9-b**). With TiCl₄, however, the behavior of MgCl and MgBr salts was quite different. The MgBr salt of ligand **7** gave better activities with TiCl₄ (**Figure 5.8-a**), while the MgBr salt of phenol formed an inefficient precatalyst (**Figure 5.9-a**).

To explain this observation, one hypothesis is that the aryloxytitanium halide (ArO)TiX₂(thf)_n can be active only when incorporated with a certain MgXX' salt. The trends shown in **Figures 5.8** and **5.9** suggest that to be an effective catalyst, (ArO)TiCl₂(thf)_n must be combined with MgCl₂, not MgBr₂ or MgClBr, while (ArO)TiBr₂(thf)_n can be an active catalyst with either MgBr₂ or MgBrCl. **Schemes 5.7** and **5.8** provide a summary of the aryloxytitanium halides and magnesium halides resulting from the precatalyst-preparation reactions. In these schemes, the combination of the MgBr salt of phenol and TiCl₄ (**Scheme 5.8-c**), which gave poor polymerization activities, does not provide a magnesium salt with the halide matching those of the (ArO)₂TiCl₂. The bromide ion, larger in size than chloride, may interfere with the interaction between magnesium and titanium via μ-halide or μ-oxo bridges. With the (ArO)₂TiBr₂, on the other hand, the bromide on the magnesium salt may be able to provide the necessary bridging ligand (**Scheme 5.7-b**).

Although how the different halides bridge or interfere with the structure of the precatalysts is not clear, the influences of mixed-halide systems are another implication that titanium and magnesium interact via μ-halide bridges in the active catalysts.

Figure 5.8. Ethene polymerization activity by the precatalysts prepared in situ from Mg/Cl/(thf) salt (25) and Mg/Br/(thf) salt (26), derived from ligand 7, with 2 equiv. of TiX_4 . Co-catalyst: Me_3Al (100 Al/Ti).

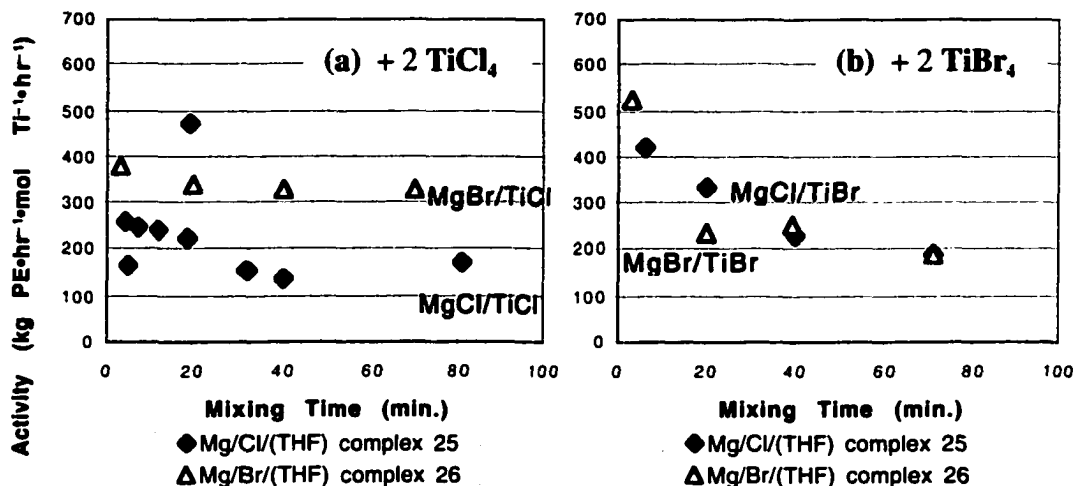
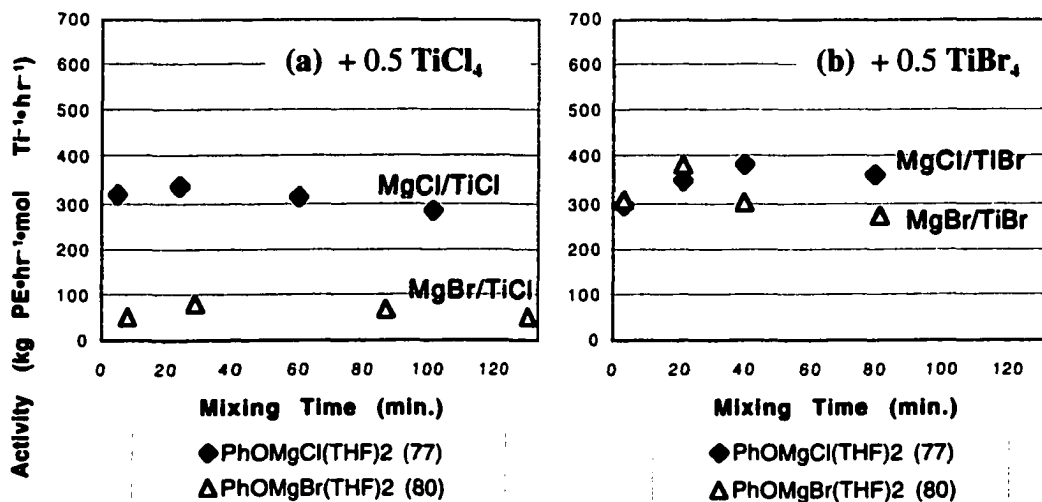
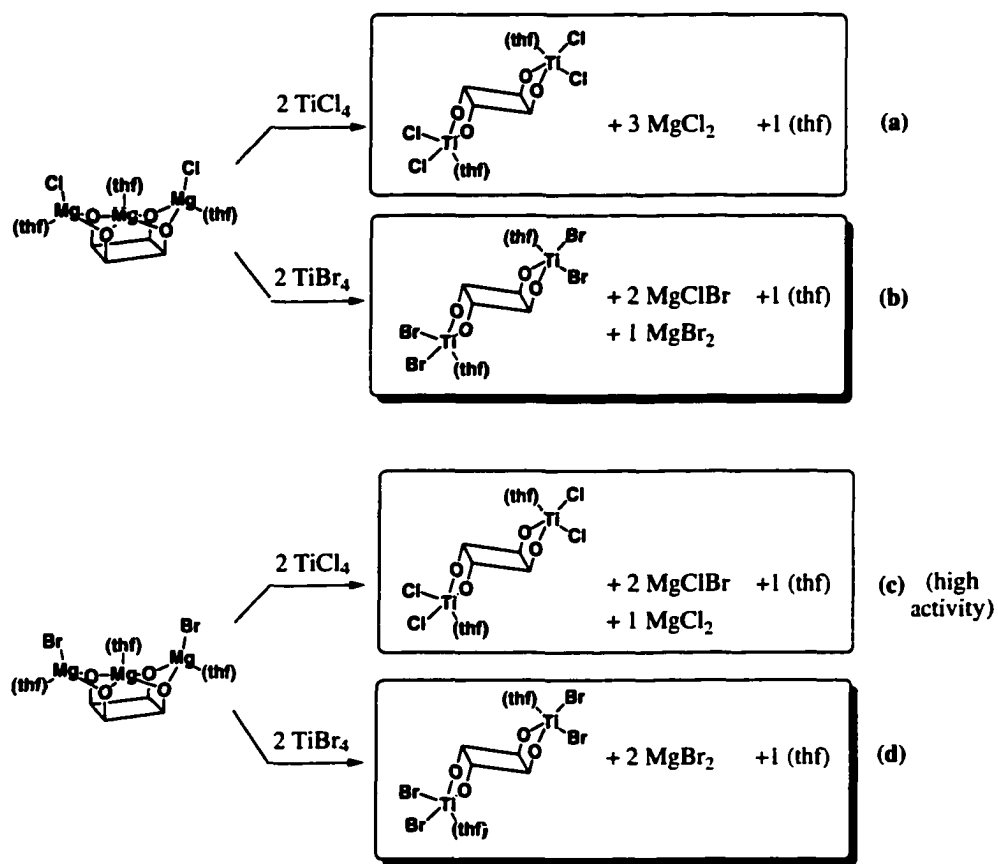
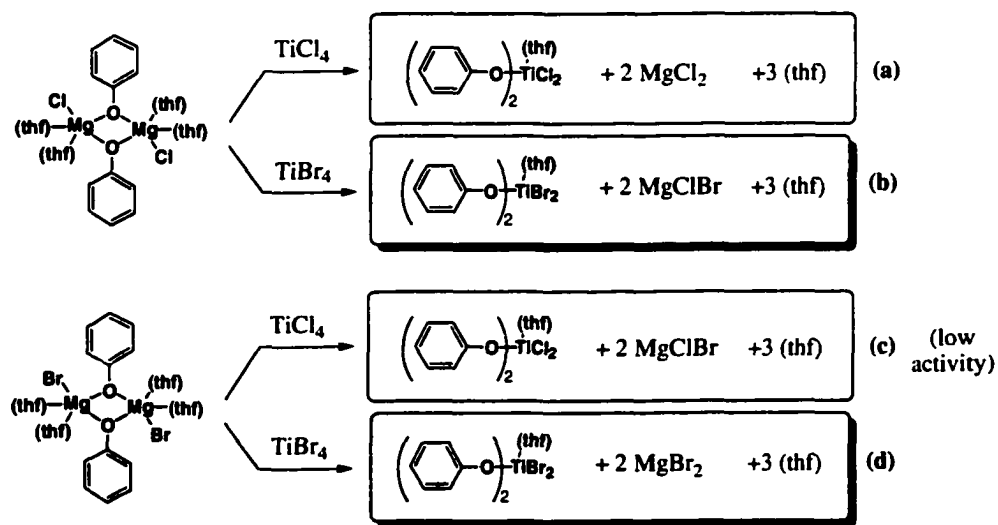


Figure 5.9. Ethene polymerization activity by the precatalysts prepared in situ from Mg/Cl/(thf) salt (77) and Mg/Br/(thf) salt (82) of phenol with 0.5 equiv. of TiX_4 . Co-catalyst: Me_3Al (100 Al/Ti).





Scheme 5.7. Formal balanced equations of the reactions between **25** or **26** and TiCl_4 or TiBr_4 .



Scheme 5.8. Formal balanced equations of the reactions between **77** or **82** and TiCl_4 or TiBr_4 .

ii) Coordination Solvent Influences. The comparison of THF and Et₂O solvates was possible using ligand system **7** because a matching pair of magnesium salts, [7 – 4H]Mg₃Cl₂(thf)₃ (**25**) and [7 – 4H]Mg₃Cl₂(OEt₂)₃ (**27**), was obtained (Table 5.9). For the simple phenol system, however, a desirable match "PhOMgCl(OEt₂)₂" for salt **77** [PhOMgCl(thf)₂] was not obtained from the reaction of PhOH with one equivalent of BnMgCl in Et₂O. Instead, the product of this reaction had the composition of PhO•Mg_{0.6}•Cl_{0.2}•(OEt₂)_{0.1} (**83**) This formula suggests a mixture of (PhO)₂Mg and 0.1 equiv. of MgCl₂(OEt₂). Approximately 0.9 equiv. of MgCl₂(OEt₂) was presumably removed from the product during washing with diethyl ether. Nevertheless, this salt **83** serves as an example of a magnesium salt with no solvation.

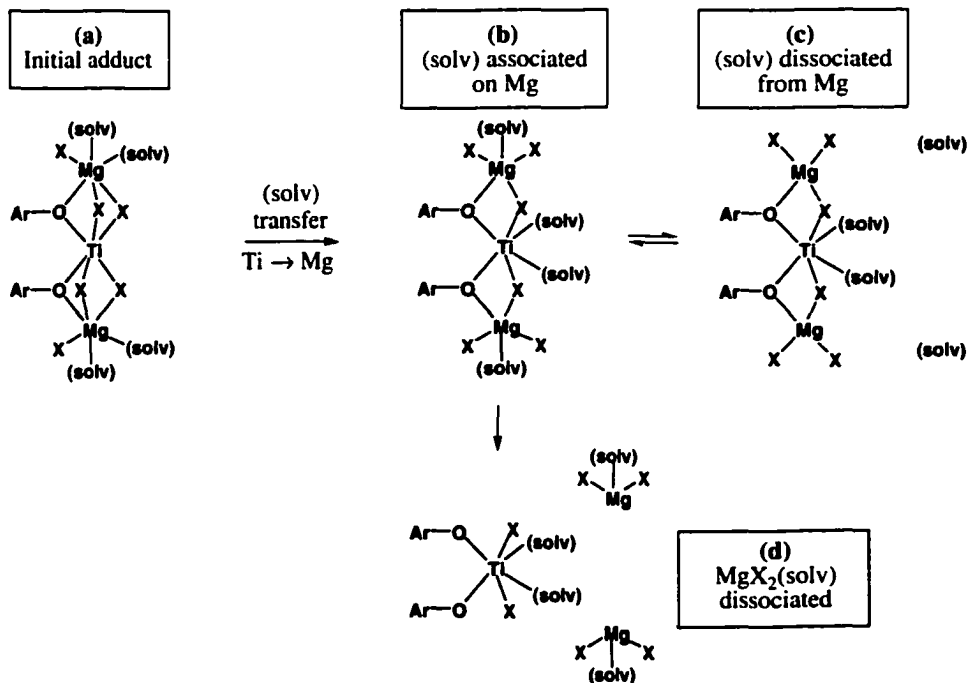
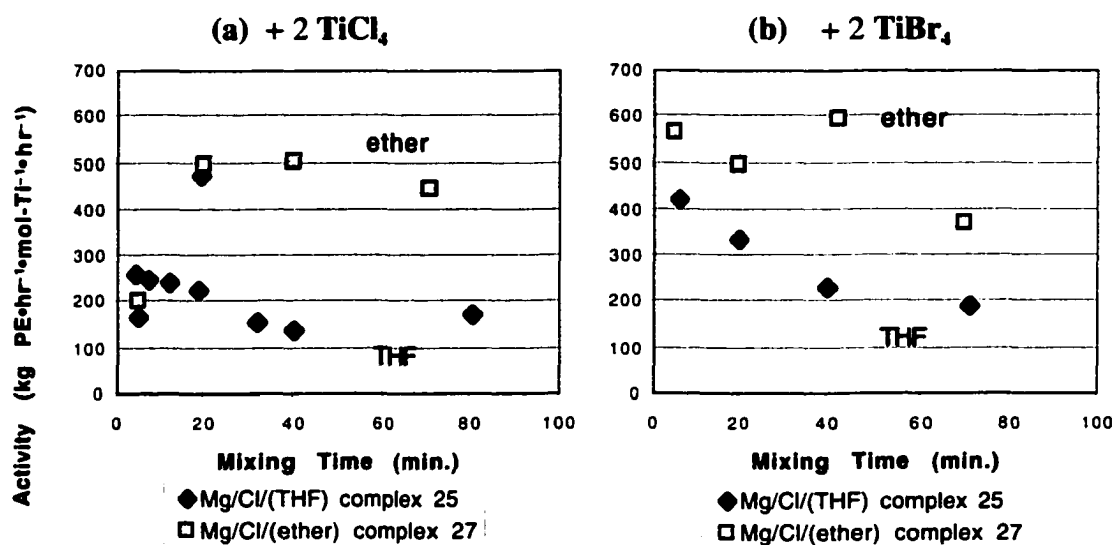
Table 5.9. Composition of the magnesium salts evaluated for the influence of solvating molecules on the magnesium effect.

	<i>Salt of ligand 7</i>	<i>Salt of phenol</i>
Mg/Cl/(thf) salt	[7 – 4H]Mg ₃ Cl ₂ (thf) ₃ (25)	C ₆ H ₅ OMgCl(thf) ₂ (77)
Mg/Cl/(OEt ₂) salt	[7 – 4H]Mg ₃ Cl ₂ (OEt ₂) ₃ (27)	C ₆ H ₅ OMg _{0.6} Cl _{0.2} (OEt ₂) _{0.1} (83)

Figure 5.10 provides the comparison of magnesium salts **25** and **27** in the catalysts derived from two equivalents of TiX₄. The data of **25** are the same as those used in **Figure 5.8**.

It is notable that the ether-solvated salt **27** retained a high level of activity over a prolonged mixing time, compared to that of the THF-solvate **25**, with both TiCl₄ and TiBr₄. Having Et₂O as a solvate, instead of THF, presumably slows the dissociation of the MgX₂(solv)_n moiety from the Mg-Ti incorporated precatalyst compared to the more basic THF. With less efficient coordination by less basic Et₂O, the MgX₂ unit is presumably more strongly coordinated by the μ-heteroatoms between magnesium and titanium in the effective precatalyst (Scheme 5.9, step **b** → **d**), slowing the dissociation of the MgX₂ unit.

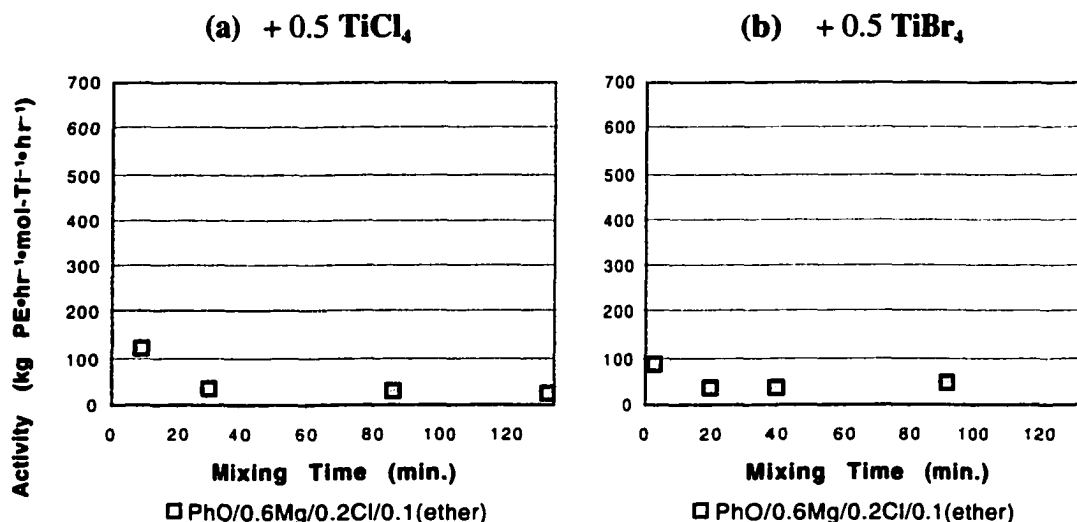
Figure 5.10. Ethene polymerization activity by the precatalysts prepared from Mg/Cl/(thf) salt (**25**) and Mg/Cl/(OEt₂) salt (**27**), derived from ligand **7**, and TiX₄. The data from **25** are the same as those used in **Figure 5.8**. Co-catalyst: Me₃Al (100 Al/Ti).



Scheme 5.9. The suggested transfer-steps of solvate molecules (solv) in the Mg/Ti precatalyst.

The precatalysts prepared from the non-solvated magnesium salt **83** did not show high polymerization activity, as shown in **Figure 5.11**. The lack of solvating ether may affect the solubility of the magnesium salt and/or the precatalyst in toluene.

Figure 5.11. Ethene polymerization activity by the precatalysts prepared from $(\text{PhO})_2\text{Mg}$ (**83**) + $0.1\text{MgCl}_2 \cdot (\text{OEt})_2$ and TiX_4 . Co-catalyst: Me_3Al (100 Al/Ti).



The absence of halide in the starting magnesium salt **83** should not be the problem, because halides are provided by the TiX_4 . The stoichiometry of MgX_2 relative to titanium is obviously affected, but a 1 : 1 ratio of MgX_2 and Ti functions well for many other salts.

The presence of different halides and solvates clearly affected the stability of the precatalysts, but the activity of the catalysts remained at the typical magnesium-effect level. Therefore, it may be concluded that halides and solvate molecules are involved in the precatalysts prepared in situ from the aryloxymagnesium salts and TiX_4 and have secondary influences on the catalyst activity.

5.2.F. In Situ Precatalyst Generation Using Al/Mg complexes: Importance of Mg/Ti Ratio

The Al/Mg hetero-polymetallic complexes **41** and **42** (Figure 5.12) also exhibit high polymerization activity when the precatalysts are generated by analogous in situ methods. Although the presence of aluminum is distinctive, we attribute the high activity to the magnesium effect, based on a similar dependence on mixing-time (effective catalysts are formed only within a short mixing period), similar activity range, and confirmed inertness of the final Al/Ti product **46** (see Table 5.1), that forms after a prolonged mixing time.

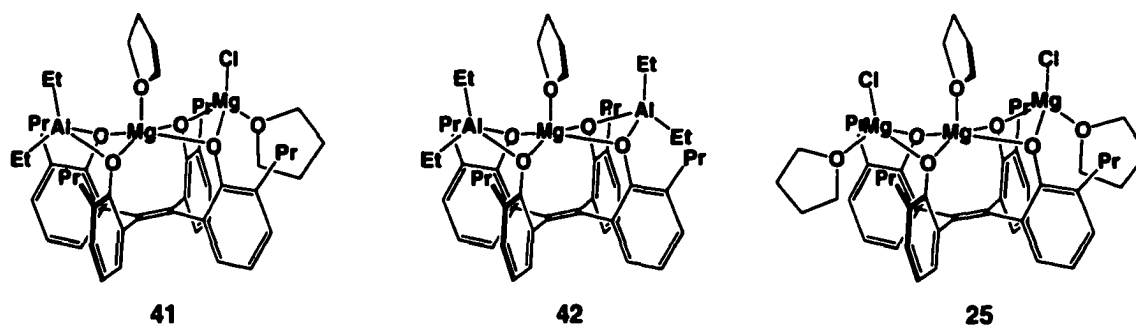


Figure 5.12. Structures of **41**, **42** and **25**.

The polymerization activities at various ligand : titanium ratios and mixing times are summarized in Table 5.10 and 5.11. A short mixing time of 1 minute was evaluated in all series, with the longer mixing time checked only for limited cases. The co-catalyst used was M-MAO in all cases.

Table 5.10. Ethene polymerization activity by the precatalysts prepared from **41** and TiCl₄.

Entry	Ligand:Ti	Mix. time (min)	Activity (kg PE•hr ⁻¹ • mol Ti ⁻¹ •atm ⁻¹)
121	1 : 1	1	335
122		80	31
123	1 : 2	1	518
124		81	43
125	1 : 3	1	445
126	1 : 4	1	425

co-catalyst: M-MAO (200Al/Ti)

Table 5.11. Ethene polymerization activity by the precatalysts prepared from **42** and TiCl₄.

Entry	Ligand:Ti	Mix. time (min)	Activity (kg PE•hr ⁻¹ • mol Ti ⁻¹ •atm ⁻¹)
131	1 : 1	1	715
132		63	75
133	1 : 2	1	659
134		60	324
135		43 hr	61
136	1 : 3	1	443
137	1 : 4	1	354

co-catalyst: M-MAO (200Al/Ti)

The highest activity catalyst derived from the Al/Mg/Mg complex **41** was observed for the ligand : Ti ratio of 1 : 2, whereas for the Al/Mg/Al complex **42**, the ligand : Ti ratio was 1 : 1. For the analogous trinuclear magnesium complex **25** (see **Figure 5.12**), the highest activity with M-MAO was observed at a ligand : Ti stoichiometry of 1 : 4.

We suspect that the best stoichiometry of TiCl₄ is not based on the ratio of ligand : Ti, but instead on the ratio of Mg : Ti. The best ligand : Ti ratios for precatalysts **25**, **41** and **42** convert to Mg : Ti ratios of 1 : 1.3, 1 : 1 and 1 : 1, respectively. In this series of Mg and Al/Mg derivatives from ligand **7**, it thus appears that the ideal ratio of Mg : Ti is about 1 : 1.

The magnesium salt of phenol, **77** [PhOMgCl(thf)₂], also showed the highest activity at a similar Mg : Ti ratio: at 1 : 1 returning 485 kg PE•hr⁻¹•mol Ti⁻¹•atm⁻¹ vs. 282 kg PE•hr⁻¹•mol Ti⁻¹•atm⁻¹ for a Mg : Ti ratio of 2 : 1 (co-catalyst: M-MAO). Using Me₃Al as a co-catalyst, the relative activity was inverted, with higher activity for the greater ratio of Mg : Ti (2 : 1) than for the equimolar case, although the maximum activity was nearly comparable (550 vs. 484 kg PE•hr⁻¹•mol Ti⁻¹•atm⁻¹). The maximum activity was also more comparable for the "isolated" phenoxide Mg/Ti precatalyst series **84**, **85**, and **86** (Section 5.2.D) activated by Et₃Al. The optimal activities for **25**, **41**, **42**, and **77** (both

from in situ preparation of precatalysts and isolated Mg/Ti precatalysts) at various Mg : Ti ratios are compared in the graph of activity vs. Ti/Mg ratio, provided in **Figure 5.13**.

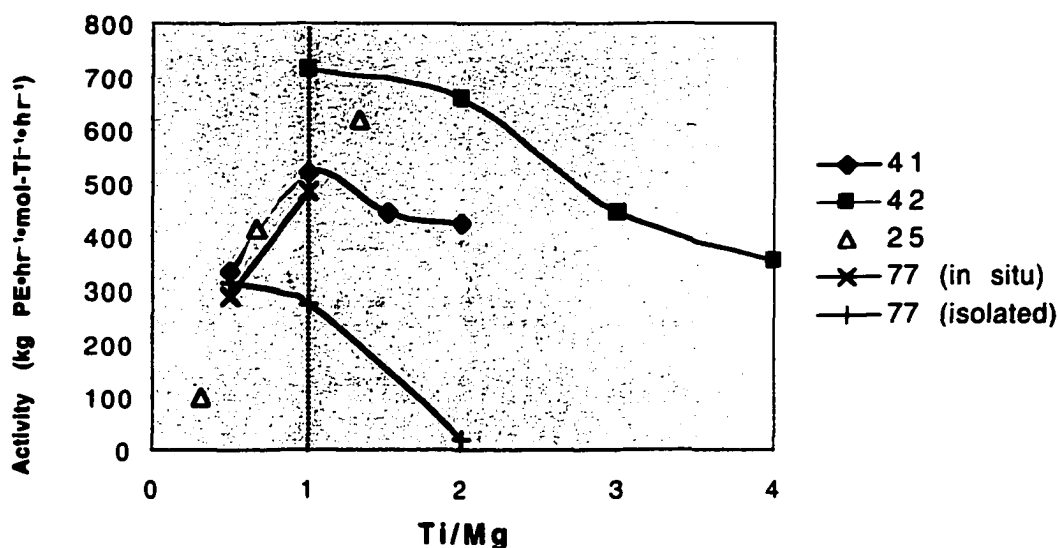


Figure 5.13. Polymerization activity vs. Ti/Mg ratio: from precatalysts prepared in situ from 41, 42, 25 or 77 with TiCl_4 , and the isolated precatalysts [77 + $n\text{TiCl}_4$] ($n = 0.5, 1$ and 2 : 84, 85, and 86 respectively). Co-catalyst is M-MAO, except for the isolated precatalysts, for which Et_3Al was used.

5.2.G. Advantages of Preorganization

5.2.G.1. Polydispersity

It has thus been shown that in the magnesium effect, the aryloxy ligand structure is only of secondary importance, mainly affecting the precatalyst solubility and the best mixing time. One specific advantage of the preorganized ligand system, however, was found to be the narrower molecular weight distribution of the product polyethene.

Because the polyethene product from the magnesium precatalyst method generally had very high molecular weights, both high-temperature polymerization and H_2 -incorporated polymerization reactions were performed to shift the average molecular weight to lower values.¹⁰

i) Results from high temperature polymerization. The polymer obtained from higher temperature conditions (86-87 °C) lowered the molecular weight sufficiently to enable the GPC analysis.¹¹ The data for the polymer from the magnesium salt of ligand **7** (**25**) and from the magnesium phenoxide **77** (as isolated precatalyst **85**) are summarized in **Table 5.12**. Polymerization reactions were performed following the "large-scale" procedure (Section 5.4.D), to provide better control of the temperature and to monitor the temperature change and ethene consumption. The conditions used were selected from the optimized small-scale series of experiments conducted for each magnesium salt. The activity values of each reaction will be discussed in more detail in a later section (5.2.G.2).

Table 5.12. GPC analyses of the polyethene from high temperature polymerization reactions *I* and *II*. Analysis was repeated twice for each sample.

Reaction	Activity (kg PE·hr ⁻¹ · mol Ti ⁻¹ ·atm ⁻¹)	M_n	M_w	M_w/M_n
<i>I</i>	841	6.18 x 10 ⁴	2.26 x 10 ⁵	3.66
		6.73 x 10 ⁴	2.23 x 10 ⁵	3.31
<i>II</i>	275	3.94 x 10 ⁴	1.98 x 10 ⁵	5.04
		3.96 x 10 ⁴	1.99 x 10 ⁵	5.03

Reaction I : **25** + 4 TiCl₄ (5 min); M-MAO (200 Al/Ti); 87 °C.

Reaction II : [**77** + 1 TiCl₄ (isolated precatalyst **85**)] ; Et₃Al (120 Al/Ti); 85 °C.

Definitions:¹²

M_n = number average molecular weight

M_w = weight average molecular weight

M_w/M_n : polydispersity

The polyethene from the preorganized ligand system (*Reaction I*) has polydispersity clearly narrower than that from the simple phenoxide (*Reaction II*). However, the polydispersity of >3 is not narrow enough to indicate the formation of a single site catalyst, the ultimate goal of this ligand design investigation. The difference in polydispersity between these cases probably arises from the reduced degree of randomness imposed by the preorganized aryloxy ligand framework, as compared to the non-organized simple phenoxide.

ii) **Results from H₂-incorporated polymerization.** Hydrogen-incorporation experiments were done by using the small-scale procedure, which allowed the performance of many reactions in order to obtain a more thorough comparison. **Table 5.13** summarizes the precatalyst/co-catalyst combinations and the data from GPC analyses. *Entries 1-8* present the results from the precatalyst prepared from the magnesium salts **25** and **77** with TiCl₄. The partial pressure of hydrogen and ethene was 0.13 and 3 atm, respectively.

Table 5.13. GPC analyses of H₂-incorporated polyethene products.

Entry	Precatalyst (mix. time)	Co-catalyst (Al/Ti)	M_n^a	M_w^a	M_w/M_n^b
1	25 + 2TiCl ₄ (1 min.)	M-MAO (200)	1.08 x 10 ⁵ (5%)	3.36 x 10 ⁵ (4%)	3.18 (0.15)
2	25 + 4TiCl ₄ (2.5 min.)	M-MAO (200)	6.17 x 10 ⁴ (1%)	2.62 x 10 ⁵ (6%)	4.26 (0.26)
3	25 + 2TiCl ₄ (1 min.)	Me ₃ Al (100)	8.93 x 10 ⁴ (2%)	2.71 x 10 ⁵ (0.5%)	3.04 (0.06)
4	25 + 4TiCl ₄ (20 min.)	Me ₃ Al (100)	8.57 x 10 ⁴ (3%)	3.01 x 10 ⁵ (5%)	3.52 (0.24)
5	25 + 2TiCl ₄ (1 min.)	Et ₃ Al (100)	5.47 x 10 ⁴ (7%)	2.62 x 10 ⁵ (5%)	4.79 (0.12)
6	25 + 4TiCl ₄ (7 min.)	Et ₃ Al (100)	3.49 x 10 ⁴ (7%)	1.77 x 10 ⁵ (3%)	5.10 (0.52)
7	77 + 0.5 TiCl ₄ (4 min.)	Et ₃ Al (100)	2.64 x 10 ⁴ (9%)	1.50 x 10 ⁵ (4%)	5.69 (0.38)
8	77 + 1 TiCl ₄ (4 min.)	Et ₃ Al (100)	5.08 x 10 ⁴ (8%)	2.12 x 10 ⁵ (7%)	4.17 (0.14)
9 ^c	[77 + 1 TiCl ₄] (adduct isolated)	Et ₃ Al (120)	4.37 x 10 ⁴ (4%)	2.69 x 10 ⁵ (0.5%)	6.17 (0.20)

^{a, b} Average of four runs. The % Error (a) or standard deviation (b) is given in parentheses.

^c Re-evaluation of the same polymer product obtained from *Reaction II* in **Table 5.10**.

Entry 9 is the repetition of the GPC analysis of the polymer obtained from *Reaction II* of **Table 5.12**, to calibrate the reproducibility of the GPC analysis. Note that this polyethene showed a polydispersity of ~6, broader than that obtained from the

previous analysis by 20%. GPC analysis is affected by machine conditions and the way the baseline is determined.¹³

Under hydrogen partial pressure, the difference between the preorganized system (**25**) and the simple phenoxide (**77**) is not as clear as the difference determined under the high temperature conditions. The polydispersity of the polymer obtained from **25** and both M-MAO and Me₃Al was narrower than that obtained from **77**, while the polydispersity of the polymer obtained from **25** and Et₃Al gave a broader polydispersity.

The presence of hydrogen affected the polymerization performance in these reactions, although the effect is greatly dependent on the co-catalyst used. **Table 5.14** is the summary of polymerization activity obtained in the presence and absence of hydrogen as a function of the co-catalyst. Activity generally diminished for all cases when hydrogen was incorporated, but the extent of the effect for the magnesium salt **25** was most significant when using Et₃Al as a co-catalyst (*entries 5-6*).

Et₃Al thus has a negative effect on both polymerization activity and polydispersity. While it is not certain if a correlation exists between the causes of each effect, this sensitivity toward the co-catalyst nevertheless suggests the co-catalyst's involvement in the structure of the actual catalytic species. The reasons why Et₃Al exerts a more profound influence than either Me₃Al or M-MAO are not well understood at this time.

Table 5.14. Activity of ethene polymerization reactions in the presence and absence of hydrogen partial pressure.

Entry	Precatalyst (mix. time)	Co-catalyst (Al/Ti)	Activity (kg PE·hr ⁻¹ ·mol Ti ⁻¹ ·atm ⁻¹)	
			Non-H ₂	H ₂ -incorporated
1	25 + 2TiCl ₄ (1 min.)	M-MAO (200)	280	127
2	25 + 4TiCl ₄	M-MAO (200)	372 (1 min.) ^a	363 (2.5 min.) ^a
3	25 + 2TiCl ₄ (1 min.)	Me ₃ Al (100)	319	212
4	25 + 4TiCl ₄	Me ₃ Al (100)	325 (14 min.) ^a	204 (20 min.) ^a
5	25 + 2TiCl ₄ (1 min.)	Et ₃ Al (100)	292	65
6	25 + 4TiCl ₄	Et ₃ Al (100)	326 (3 min.) ^a	163 (7 min.) ^a
7	77 + 0.5 TiCl ₄ (4 min.)	Et ₃ Al (100)	413	290
8	77 + 1 TiCl ₄ (4 min.)	Et ₃ Al (100)	430	232

^a The mixing time for the non-H₂ experiment is different from the corresponding H₂-incorporation experiment for these cases.

5.2.G.2. Thermal Robustness of the Catalyst

The magnesium salt **25** from the preorganized ligand system **7** showed a second advantage: high thermal robustness. Both magnesium salts **25** and **77** provided long catalyst lifetimes, but the former retained a high reaction rate at elevated temperature.

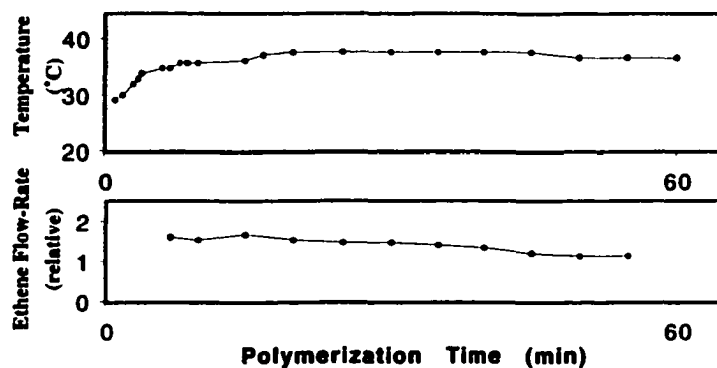
Figures 5.14 and **5.15** provide the temperature and ethene flow-rate¹⁴ profiles of polymerization reactions catalyzed by the precatalysts prepared from magnesium salts **25** (derived from ligand **7**) or **77** (derived from phenol), by using the large-scale procedure (Section 5.4.D). The stoichiometry, co-catalyst, and mixing time were selected from the corresponding small-scale series for optimal performance. Each catalyst was evaluated at

two external temperatures: 31-32 °C and 86-87 °C. The higher temperature experiment using precatalyst **25** is the same one used for the determination of polydispersity, as discussed in 5.2.G.1-i (*Reaction 1, Table 5.12*).

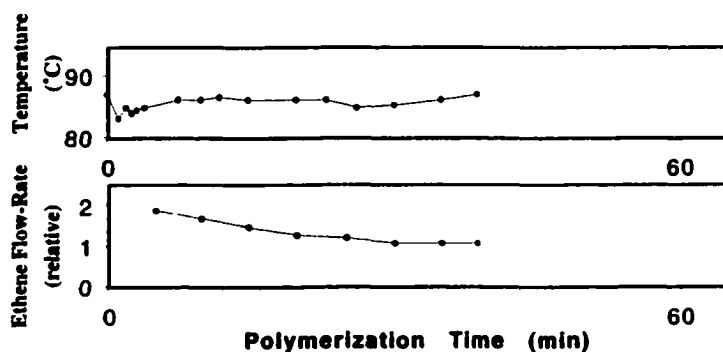
At 31-32 °C, both catalysts maintained strong ethene flow-rates for at least 30 minutes (**Figures 5.14-a** for **25** and **Figure 5.15-a** for **77**). The relative rate of ethene uptake was higher for the former catalyst over the measured period. The higher rate is also reflected in the total activity value over the entire reaction time (640 vs. 548 kg PE•hr⁻¹•mol Ti⁻¹•atm⁻¹). The rate decreased more rapidly, however, was faster for the former catalyst than that of the latter during the polymerization reaction. The catalyst lifetime was longer for the simple phenoxide **77**, which maintained a steady reaction rate for over four hours. The increase in the ethene flow-rate observed after 3 hours is tentatively attributed to the growth in the polymer particles, which absorbed most of the solvent and exposed the catalysts directly to the ethene atmosphere.

At 86-87 °C, despite the expected decrease of ethene solubility in toluene at elevated temperature, the polymerization activity by the catalyst derived from **25** was considerably higher than at 31-32 °C. The activity was 841 kg PE•hr⁻¹•mol Ti⁻¹•atm⁻¹ over 40 minutes at 86-87 °C (**Figure 5.14-b**) while the value of 640 kg PE•hr⁻¹•mol Ti⁻¹•atm⁻¹ was recorded at 31-32 °C. In contrast, the catalyst prepared from simple phenoxide **77** experienced decreased activity at higher temperature (548 kg PE•hr⁻¹•mol Ti⁻¹•atm⁻¹ at 32 °C vs. 241 kg PE•hr⁻¹•mol Ti⁻¹•atm⁻¹ at 86 °C). At high temperature, the preorganized ligand system must contribute to the preservation of active catalytic species, while simple phenoxide does not. The lifetime of the catalyst, however, was again longer for the simple phenoxide system: the rate, although lower, did not drop over a one-hour reaction period, while the rate gradually decreased in polymerization reactions using in the preorganized precatalyst system.

Figures 5.14 (a & b). Temperature/flow-rate profiles of the catalyst prepared from $[7 - 4H]Mg_3Cl_2(thf)_2$ (25) and 4 equiv. of $TiCl_4$; Mixing time 5 min; with co-catalyst M-MAO (200 Al/Ti).

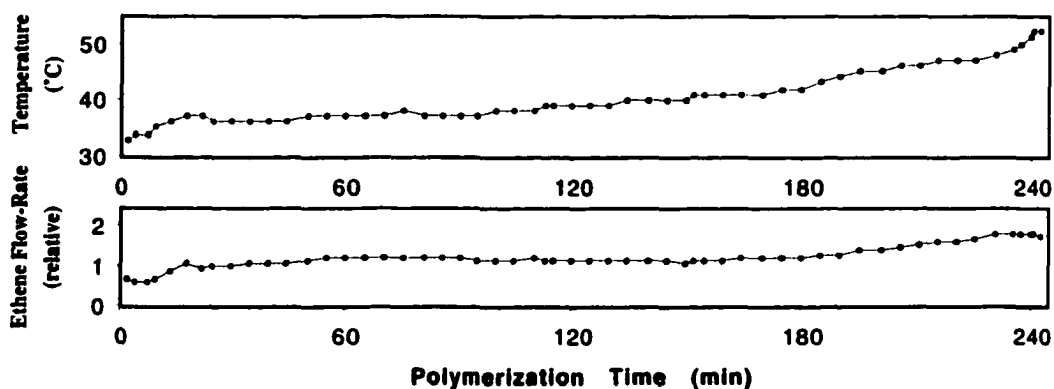


(a) Base temperature : 31.5 °C.
 Polymerization time: 60 min.
 Quantity of Ti : 1.07×10^{-5} moles.
 Activity : 640 kg PE•hr⁻¹•mol Ti⁻¹•atm⁻¹.

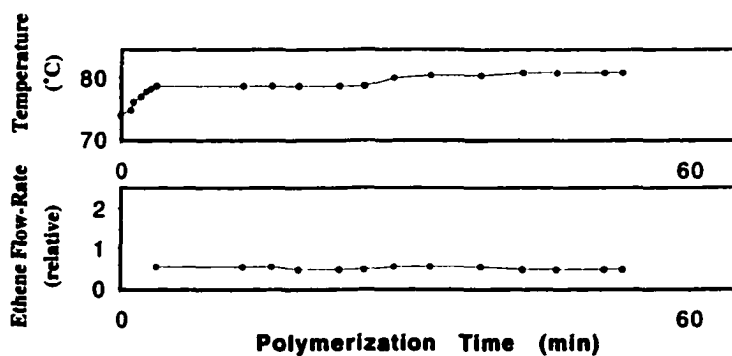


(b) (Reaction I in Table 5.12)
 Base temperature : 87 °C.
 Polymerization time: 40 min.
 Quantity of Ti : 9.06×10^{-6} moles.
 Activity : 841 kg PE•hr⁻¹•mol Ti⁻¹•atm⁻¹.

Figures 5.15 (a & b). Temperature/flow-rate profiles of the catalyst prepared from $C_6H_5OMgCl(thf)_2$ (77) + 0.5 $TiCl_4$; Mixing time 10 min; with co-catalyst Me_3Al (500 Al/Ti)



1. Base temperature : 32 °C.
 Polymerization time: 4 hr 04 min.
 Quantity of Ti : 7.58×10^{-6} moles.
 Activity : 548 kg PE \cdot hr $^{-1}$ \cdot mol Ti $^{-1}$ \cdot atm $^{-1}$.



1. Base temperature : 86 °C
 Polymerization time: 54 min.
 Quantity of Ti : 7.71×10^{-6} moles.
 Activity : 241 kg PE \cdot hr $^{-1}$ \cdot mol Ti $^{-1}$ \cdot atm $^{-1}$.

It should be noted that the activity values obtained from large-scale experiments were generally improved over the corresponding polymerization reactions done at small-scale. A separate large-scale experiment using the conditions reported in **Figure 5.14-a** gave an activity of $1,030 \text{ kg PE}\cdot\text{hr}^{-1}\cdot\text{mol Ti}^{-1}\cdot\text{atm}^{-1}$. This exceptional activity, however, was partly a function of the unusually short polymerization period (11.5 minutes) necessitated by the approximately threefold increase in the quantity of the catalyst (3.20×10^{-5} moles of Ti) compared to that in the other large- and small-scale experiments, and the quick rise in temperature (from $31 \text{ }^\circ\text{C}$ to $76 \text{ }^\circ\text{C}$ within 7.5 minutes) caused by the high exothermicity of the polymerization.

5.3. Conclusion

Tetraarylethene-based Preorganized Polyaryloxiide Ligand Systems. The titanium complexes of the tetraarylethene-based preorganized ligands (**7**, **3E** and **3Z**) were ineffective precatalysts for ethene polymerization. The Mg/Ti and Al/Ti heteropolymetallic complexes developed from ligand **7** were also inert. These systems do not seem to be promising templates for constructing model systems for Ziegler-Natta catalysts based on titanium alone. Other metals with different valencies, such as the Group 3 metals, Ti(III), Group 5, and Group 6 metals in appropriate oxidation states, may be useful for future work. Because the ligand system is oxygen-based, modeling other silica-supported catalysts, such as the chromium-based Phillips catalyst,¹⁵ may be a reasonable subject for future research.

Oxygen atoms as donor groups may also not be ideal to create catalytic species. Nitrogen-based donor groups are used in latest non-metallocene homogeneous catalysts, such as amides and imines,¹⁶ which can give 1,000-fold higher ethene polymerization activities than those of classic heterogeneous Ziegler-Natta catalysts.^{17, 18} Imine-based ligands are particularly useful for late-group metals, often as neutral catalytic species.^{17a} Introduction of donor heteroatoms other than oxygen into the tetraarylethene framework may create different binding sites more suitable for high-activity polymerization catalysts.

Magnesium Effect. The characteristics of the magnesium effect suggest that the actual catalyst formed from magnesium precatalysts resembles the MgCl_2 -supported TiCl_4 heterogeneous Ziegler-Natta catalysts. It is unfortunate that the effective precatalysts have too short a lifetime for isolation, structural characterization, and further investigation as models for such heterogeneous systems. Isolation of the magnesium-incorporated precatalysts was possible for the simple phenoxide system, but structural analyses of the isolated precatalysts were not possible.

Preorganization of multiple phenoxide units contributed to the narrower polydispersity of the polymer and the thermal robustness of the catalyst, but the desired "single-site" behavior was not attained. Preorganization presumably functions to reduce the uncontrolled aggregation of the precatalysts or catalysts, compared to that of the simple phenoxide system.

The Fluorene-Based Ligand System. The titanium complexes from the fluorene-diol ligand **4** showed promising catalytic activity without assistance from magnesium. Further research is warranted to determine if the dinuclear titanium structure is involved in creating the catalytic site and if this system can serve as a model for heterogeneous catalysts. Although the difficulty in synthesizing the ligand discouraged further research, an alternative dibenzofuran-diol system with the same basic structure of the fluorenyl system is currently under investigation.

5.4. Experimental

Instrumental, General and Materials: see Chapter 3, Section 3.4 Experimental.

Instrumental (additional): Gel permeation chromatography (GPC) analysis of polyethene samples were performed at the Department of Chemical and Materials Engineering (Professor Wanke's lab) on Alliance GPCV 2000 using a refractive index detector using 1,2,4-trichlorobenzene as a solvent at a flow-rate of 1 mL/min. and 140 °C. Polymer samples were dissolved in trichlorobenzene at 160 °C before injection.

General (additional): All preparations of the metal derivatives were performed in the drybox. The solutions or suspensions for the polymerization reactions were prepared in the drybox, and the polymerization reactions were performed out of the drybox under the purified ethene atmosphere (see below).

Materials (additional): Ethene and hydrogen gases were purchased from Praxair and purified by passage through a gas purification unit, which consists of columns of copper deoxygenation catalyst and of 13X and 3A molecular sieves. M-MAO as a solution in toluene (7.1 wt% Al) was purchased from Akzo-Nobel and stored in the drybox in the original metal cylinder. Toluene for polymerization experiments was kept "ethereal-solvent-free" as described in Chapter 3, 3.4. Experimental. The synthesis of 2,7-bis(1,1-dimethylethyl)-9*H*-fluorene-1,8-diol **4** is described in Chapter 1.

5.4.A. Preparation of Metal Derivatives

The preparation of the following derivatives were described in earlier chapters: Ti complexes **31**, **34** and **35**, Mg/Ti complex **45**, Al/Ti complex **46**, Mg complexes **25**, **26** and **27**, Na salt **40** and Mg/Al complexes **41** and **42** (Chapter 3); Ti complex **52** and Al complexes **47**, **48** and **50** (Chapter 4).

71: [2,7-di-*t*-butylfluorene-1,8-(OTiCl₂)₂]⁴

To the solution of 2,7-bis(1,1-dimethylethyl)-9*H*-fluorene-1,8-diol (**4**) (0.0245 g, 0.0789 mmol) in 0.5 mL of toluene was added NaH (0.0102 g, 0.425 mmol) suspended in 1 mL

of toluene. After 0.5 h, TiCl_4 (0.30 g, 1.6 mmol) dissolved in toluene (2 mL) was added to the mixture. The color immediately turned dark red. After 0.5 h, the volatiles were removed in vacuo, the residue was triturated with pentane to remove excess TiCl_4 , then triturated with toluene. The pentane triturate, after slow evaporation, resulted in prism crystals. The toluene triturate resulted in semi-crystalline material. Both were identified as **71** by ^1H NMR spectroscopy, identical to the data reported by Wuest et al.⁴ The yields were not recorded.

72: [2,7-di-*t*-butylfluorene-1,8-{OTiCl₃(thf)}₂]

To the suspension of magnesium salt **74** (prepared the same way as presented below, but not analyzed; formula weight was assumed to be 572; 0.020 g, 0.035 mmol) in 3 mL of toluene was added TiCl_4 (0.05 mL, 0.46 mmol). The mixture turned dark red immediately. After 1 h, the mixture was filtered through Celite-packed pipette, and the volatiles were removed from the filtrate in vacuo. The residue was triturated with pentane, filtered, and crystallized from toluene-hexanes (slow evaporation). Large prism crystals of very dark red color were formed. X-ray crystallographic analysis of the crystals revealed the structure of **72** as a THF solvate, with no involvement of magnesium. The yield was not recorded. X-ray crystallography: see Appendix A-23.

74: Mg/Cl(thf) salt of 4

After mixing 2,7-bis(1,1-dimethylethyl)-9*H*-fluorene-1,8-diol (**4**) (0.0234 g, 0.0754 mmol) and CH_3MgCl (0.3M/THF, 0.51 mL, 0.81 mmol) in THF (1 mL) overnight, the volatiles were removed from the clear solution in vacuo, and the residue was crystallized from toluene (r.t. $-30\text{ }^\circ\text{C}$). The white solid produced was, however, not very crystalline. The solid was collected, washed with pentane and dried in vacuo (0.0395 g, 77%). Anal. Found (average of two runs): C, 56.93 (± 0.60); H, 6.88 (± 0.08). Formula: $\text{C}_{21}\text{H}_{24}\text{O}_2 \cdot \text{Mg}_{2.5} \cdot \text{Cl}_{3.0} \cdot (\text{thf})_{2.8}$. Formula weight: 679. For calculation of formula and formula weight, see Section 5.4.B.

General preparation procedure for magnesium salts 75, 76, 77, 78, 79, 82, and 83.

The general form of the magnesium salts of phenolic ligands prepared for this investigation is $[\text{Ar}(\text{O})_o] \cdot \text{Mg}_m \cdot \text{X}_n \cdot (\text{solvent})_p$, in which $[\text{Ar}(\text{O})_o]$ is the deprotonated ligand, o is the number of aryloxy donors per ligand molecule, m , n and p are the stoichiometry of Mg, X (either Cl or Br) and coordinating solvent (either THF or Et_2O) per ligand. $[\text{Ar}(\text{O})_o] \cdot \text{Mg}_m \cdot \text{X}_n \cdot (\text{solvent})_p$ is prepared from a phenolic ligand $[\text{Ar}(\text{OH})_o]$ by adding o equivalent(s) of Grignard reagent $\text{RMgX}/(\text{solvent})$ to the ligand dissolved in the same

solvent, or in some cases toluene, at room temperature for several hours to overnight. The precipitate produced in the reaction was collected, washed with the same reaction solvent to remove excess reagent or ligand, followed by pentane to remove less volatile solvents, and dried in vacuo. The formula and formula weight are calculated from the elemental analysis by the method described in the following section (5.4.B).

75: Mg/Cl salt of 3E

After mixing *E*-bis(2-hydroxyphenyl)-bis(2-methoxyphenyl)ethene (**3E**) (0.1665 g, 0.3922 mmol) and CH₃MgCl (0.3M/THF, 2.6 mL, 0.78 mmol) in THF (1 mL) for overnight, the white precipitate was collected, washed and dried as described in the general procedure. The particles were so tiny, some went through the glass-fritted funnel during the filtration and washing. Yield is not recorded. Anal. Found: C, 74.75; H, 5.00. Formula: C₂₆H₂₂O₄•Mg_{1.1}•Cl_{0.1} (THF content was calculated as below 0.1 equiv.). Formula weight: 452.

76: Mg/Cl/(thf) salt of 3Z

After mixing *Z*-bis(2-hydroxyphenyl)-bis(2-methoxyphenyl)ethene (**3Z**) (0.0582 g, 0.137 mmol) and CH₃MgCl (0.3M/THF, 0.92 mL, 0.28 mmol) in toluene (1 mL) for overnight, the white precipitate was collected, washed and dried as described in the general procedure (0.045 g, 65%). Anal. Found (average of two runs): C, 67.43 (±0.18); H, 4.54 (±0.04). Formula: C₂₆H₂₂O₄•Mg_{1.3}•Cl_{0.6}•(thf)_{0.7}. Formula weight: 505.

77: Mg/Cl/(thf) salt of phenol

After mixing phenol (0.462 g, 4.91 mmol) and CH₃MgCl (3M/THF, 1.7 mL, 5.1 mmol) in THF (5 mL) for overnight, the white precipitate was collected, washed and dried as described in the general procedure (1.09 g, 73%). Anal. Found: C, 55.96; H, 7.08. Formula: C₆H₅O•Mg_{1.05}•Cl_{1.1}(thf)_{2.1}. Formula weight: 306. A small amount of the product was recrystallized from THF (r.t. → -30 °C). Preliminary X-ray analysis of the crystals revealed the dimeric structure (**Figure 5.16**).¹⁹

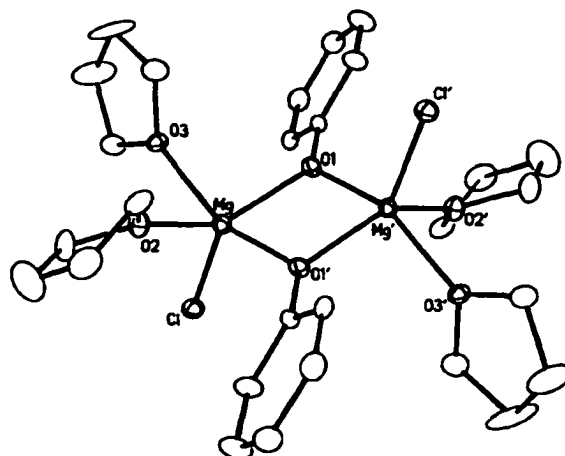


Figure 5.16. Preliminary X-ray crystallographic structure of **77**.

78: Mg/Cl(thf) salt of 3,3'-dimethyl-4,4'-biphenol

After mixing 3,3'-dimethyl-4,4'-biphenol (0.0459 g, 0.214 mmol) and CH_3MgCl (3M/THF, 0.18 mL, 0.54 mmol) in THF (4 mL) for overnight, the white precipitate was collected, washed and dried as described in the general procedure. Yield is not recorded. Anal. Found (average of two runs): C, 55.23 (± 0.32); H, 6.13 (± 0.08). Formula: $\text{C}_{14}\text{H}_{12}\text{O}_2 \cdot \text{Mg}_{1.3} \cdot \text{Cl}_{0.6}(\text{thf})_{2.4}$. Formula weight: 514.

79: Mg/Cl(thf) salt of 4,4'-hydroquinone

After mixing 4,4'-hydroquinone (0.1204 g, 1.09 mmol) and CH_3MgCl (3M/THF, 0.76 mL, 2.3 mmol) in THF (6 mL) for overnight, the white precipitate was collected, washed with THF and dried in vacuo. Yield is not recorded. Anal. Found: C, 41.33; H, 5.17. Formula: $\text{C}_6\text{H}_4\text{O}_2 \cdot \text{Mg}_{2.1} \cdot \text{Cl}_{2.2}(\text{thf})_{1.4}$. Formula weight: 342.

82: Mg/Br(thf) salt of phenol

After mixing phenol (0.3891 g, 4.13 mmol) and $\text{CH}_2=\text{CHCH}_2\text{MgBr}$ (1M/ Et_2O , 4.45 mL, 4.45 mmol) in THF (10 mL) for overnight, the white precipitate was collected, washed with THF and dried in vacuo (1.1244 g, 76.5%). Anal. Found: C, 48.75 (± 0.10); H, 6.20 (± 0.07). Formula: $\text{C}_6\text{H}_5\text{O} \cdot \text{Mg}_{1.0} \cdot \text{Cl}_{1.1}(\text{thf})_{2.1}$. Formula weight: 356.

83: Mg/Cl salt of phenol

After mixing phenol (0.752 g, 7.99 mmol) and BnMgCl (1,0M/ Et_2O , 4.45 mL, 4.45 mmol) in Et_2O (10 mL) for overnight, the white precipitate was collected, washed with

Et₂O, and dried in vacuo (0.4676 g, 48%). Anal. Found (average of two runs): C, 63.96 (±0.62); H, 5.11 (±0.08). Formula: C₆H₅O•Mg_{0.58}•Cl_{0.16}(OEt₂)_{0.12}. Formula weight: 121.

General preparation of sodium salts 73, 80 and 81. Sodium salts **73**, **80** and **81** were prepared by mixing the phenolic ligand [Ar(OH)_o] and *o* equivalent of NaH in toluene. THF was used as a co-solvent only when immediate gas evolution was not observed. The precipitate was collected, washed with toluene, followed by pentane, and dried in vacuo. The formula of the product is assumed as [Ar(ONa)_o]. The formula weight provided is based on this formula.

73: Na salt of 4

After mixing 2,7-bis(1,1-dimethylethyl)-9*H*-fluorene-1,8-diol (**4**) (0.0090 g, 0.029 mmol) and NaH (0.0014 g, 0.058 mmol) in toluene (2 mL) for overnight, co-solvent THF (1 mL) was added and the mixture was stirred again overnight. The slightly pink precipitate was collected, washed and dried as described in the general procedure. The yield was not recorded. Formula (assumed): C₂₁H₂₄O₂•Na₂. Formula weight (assumed): 354.

80: Na salt of phenol

After mixing phenol (0.263 g, 2.80 mmol) and NaH (0.0654 g, 2.73 mmol) in toluene (6 mL) for overnight, the white precipitate was collected, washed and dried as described in the general procedure (0.2632 g, 84%). Formula (assumed): C₆H₅O•Na. Formula weight (assumed): 116.

81: Na salt of 4,4'-hydroquinone.

After mixing 4,4'-hydroquinone (0.1845 g, 1.676 mmol) and NaH (0.0804 g, 3.35 mmol) in toluene (5 mL) for overnight, co-solvent THF (3 mL) was added and the mixture was stirred again overnight. The gray precipitate was collected, washed and dried as described in the general procedure. The yield was not recorded. Formula (assumed): C₆H₄O₂•Na₂. Formula weight (assumed): 154.

84: Isolated Mg/Ti precatalyst of phenoxide ligand (Mg : Ti = 2 : 1)

To the suspension of magnesium salt **77** (0.141 g, 0.461 mmol) in 4 mL of hexanes was added TiCl₄ (0.0440 g, 0.232 mmol) dissolved in 4 mL of hexanes. The color turned orange immediately. After 6 h, the orange precipitate was collected, washed with hexanes, and dried in vacuo (0.1750 g). The supernatant and washings were combined,

and the residue after removal of the volatiles in vacuo weighed 0.0061 g. It is thus assumed that the starting materials were mostly transformed into the precipitate. The yield is 97%, assuming the formula of the adduct to be $(C_6H_5O)_2 \cdot Mg_2 \cdot Ti \cdot Cl_6 \cdot (thf)_4$ (calc. formula weight: 784). Anal. Calc. for $C_{28}H_{42}Cl_6Mg_2O_6Ti$: C. 42.91; H. 5.40. Found (average of two runs): C, 41.60 (± 0.17); H, 5.27 (± 0.06).

85: Isolated Mg/Ti precatalyst of phenoxide ligand (Mg : Ti = 1 : 1)

To the suspension of magnesium salt **77** (0.0854 g, 0.285 mmol) in 3 mL of toluene was added $TiCl_4$ (0.0546 g, 0.288 mmol) dissolved in 1 mL of toluene. The color turned red immediately. After 6 h, the precipitate with brick-red color was collected, washed with toluene, and dried in vacuo (0.1466 g). The supernatant and washings were combined, and the residue after removal of the volatiles in vacuo weighed 0.0071 g. It is thus assumed that the starting materials were mostly transformed into the precipitate. The yield is 97%, assuming the formula of the adduct to be $C_6H_5O \cdot Mg \cdot Ti \cdot Cl_5 \cdot (thf)_2$ (calc. formula weight: 487). Anal. Calc. for $C_{14}H_{21}Cl_5MgO_3Ti$: C. 34.55; H. 4.35. Found (average of two runs): C, 39.26 (± 0.17); H, 4.84 (± 0.04).

86: Isolated Mg/Ti precatalyst of phenoxide ligand (Mg : Ti = 1 : 2)

To the suspension of magnesium salt **77** (0.125 g, 0.408 mmol) in 3 mL of hexanes was added $TiCl_4$ (0.1584 g, 0.8350 mmol) dissolved in 2 mL of hexanes. The color turned orange immediately, then red-orange. After overnight, the precipitate with brick-red/brown color was collected, washed with hexanes, and dried in vacuo (0.2317 g). The supernatant and washings were combined, and the residue after removal of the volatiles in vacuo weighed 0.0086 g. It is thus assumed that the starting materials were mostly transformed into the precipitate. The yield is 84%, assuming the formula of the adduct to be $C_6H_5O \cdot Mg \cdot Ti_2 \cdot Cl_9 \cdot (thf)_2$ (calc. formula weight: 676). Anal. Calc. for $C_{14}H_{21}Cl_9MgO_3Ti_2$: C. 24.86; H. 3.13. Found (average of two runs): C, 27.75 (± 0.06); H, 3.35 (± 0.01).

5.4.B. Composition of Mg salts: Calculations based on Elemental Analysis

The compositions of the magnesium salts were calculated from the carbon/hydrogen elemental analysis data and theoretical charge balance of ions, using the general formulae described below.

For a salt $C_cH_hO_o \cdot Mg_m \cdot X_n \cdot (C_4H_yO)_p$ with formula weight FW :

$C_cH_hO_o$ is the ligand, deprotonated form.

c , h and o are integers specific to the ligand. For example, in deprotonated phenol(C_6H_5O), $c = 6$, $h = 5$ and $o = 1$; in deprotonated ligand 7, $c = 38$, $h = 40$ and $o = 4$.

y is an integer specific to the coordinating solvent: $y = 8$ for THF, $y = 10$ for diethyl ether.

X is halogen atom, either Cl or Br.

m and n are the ratio of Mg and X atoms per ligand.

p is the ratio of the coordination solvent (THF or ether) per ligand.

p , m , n and FW are the unknown values to be calculated.

FW of $C_cH_hO_o \cdot Mg_m \cdot X_n \cdot (C_4H_yO)_p = (c+4p)C \cdot (h+yp)H \cdot (o+p)O \cdot mMg \cdot nX$

Thus:

$$\text{FW} = M_C(c+4p) + M_H(h+yp) + M_O(o+p) + 2 M_{Mg}m + M_Xn \quad (\text{Eq. 5-1})$$

M_C , M_H and M_O and M_{Mg} are atomic weights of C, H and O. $M_C = 12.011$, $M_H = 1.008$ and $M_O = 15.995$.

M_X is an atomic weight of the corresponding halogen atom: $M_X = 34.453$ for Cl, and $M_X = 79.904$ for Br.

$$\text{FW} = 12.011(c+4p) + 1.008(h+yp) + 15.999(o+p) + 24.305m + M_Xn \quad (\text{Eq. 5-1'})$$

Thus:

$$1 = 12.011(c+4p)/\text{FW} + 1.008(h+yp)/\text{FW} + 15.999(o+p)/\text{FW} + 24.305m/\text{FW} + 35.453n/\text{FW} \quad (\text{Eq. 5-1''})$$

The first two terms of the right side are related to C/H elemental analysis data as follows.

$$12.011(c+4p)/FW = [C \text{ EA } \%]/100 \quad (\text{Eq. 5-2})$$

$$1.008(h+yp)/FW = [H \text{ EA } \%]/100 \quad (\text{Eq. 5-3})$$

[C EA %] and [H EA %] are the % elemental compositions of C and H, as determined by combustion analysis.

From Eqs. 5-2 and 5-3,

$$p = \frac{([H \text{ EA } \%] \cdot 12.011 \cdot c - [C \text{ EA } \%] \cdot 1.008 \cdot h)}{([C \text{ EA } \%] \cdot 1.008 \cdot y - [H \text{ EA } \%] \cdot 12.011 \cdot 4)} \quad (\text{Eq. 5-4})$$

$$\frac{FW}{[C \text{ EA } \%]} = \frac{12.011(c+4p) \cdot 100}{[C \text{ EA } \%]} = \frac{1.008(h+yp) \cdot 100}{[H \text{ EA } \%]} \quad (\text{Eq. 5-5})$$

To obtain m and n from FW , p and mass/charge balances,

$$[\text{Mass of Mg} + X] = FW - [\text{mass of deprotonated ligand}] - M_s \cdot p \quad (\text{Eq. 5-6})$$

[Mass of Mg + X] is the portion of Mg plus X in the formula weight of the salt.

M_s is the molecular weight of the coordinating solvent: $M_s = 72.11$ for THF; and $M_s = 74.12$ for diethyl ether.

$$[\text{Mass of Mg, X}] = 24.30m + M_s n \quad (\text{Eq. 5-7})$$

$$2m = o + n \quad (\text{Eq. 5-8})$$

Eq. 5-7 reflects the mass balance of the Mg and X portions in the formula.

Eq. 5-8 reflects the charge balance of the anions (the deprotonated ligand and halide) and the cation (magnesium ion).

5.4.C. Small-Scale Polymerization Experiments

Precatalysts, either Ti complexes or hetero-polymetallic precatalysts prepared in situ, were first examined for ethene polymerization reactivity in the small-scale trials: typically, titanium complexes or main-group metal salts in combination with appropriate stoichiometry of TiCl_4 , both with Ti content of $1\text{--}7 \times 10^{-6}$ mol, were used as precatalysts, along with 5–7 mL of toluene as a solvent. The pressure of ethene was 30 psig for all experiments, including hydrogen-incorporation experiments. The initial temperature was ambient and was uncontrolled during the polymerization reaction. The temperature rises substantially within minutes for very active catalysts. The polymerization time was up to 10 minutes, but when the catalyst was very active, the reaction was terminated after a few minutes to avoid stirring problems.

The pressure-tight reaction vessels purchased from Lab Glass (20 mL, LG-3922-100) were used for all small-scale polymerization reactions. Fitting gaskets and crown caps were used to seal the vessels. Gaskets were wrapped with Teflon tape by at least three-fold to avoid poisoning of the precatalysts. Lubricant-free plastic syringes, purchased from Aldrich (Z23,072-3), were used to convey, measure, and inject toluene-solutions of TiX_4 and aluminum co-catalysts. The co-catalyst was either Me_3Al (100 Al/Ti), Et_3Al (100 Al/Ti), or M-MAO (200 Al/Ti), used as a toluene solution. Purified ethene and hydrogen gases are introduced to the reaction vessel via a gas line equipped with syringe-needle terminals.

Three general procedures are provided in the following: (1) polymerization reaction using Ti complexes as precatalysts; (2) polymerization reaction using precatalysts prepared in situ from main group metal salts and TiX_4 ; and (3) hydrogen-incorporated polymerization reactions. The complete data, including quantities of the precatalysts, the stoichiometry, and the activity of the polymerization catalysis that appear in this chapter will be provided in Section 5.4.E.

(1) Polymerization reaction using Ti complexes or isolated Mg/Ti precatalysts. In the drybox, a solution/suspension of the titanium complex (1 to 5 mg) in 5 mL of toluene was prepared in a pressure-tight reaction vessel which contained a magnetic rod for stirring, and sealed with a gasket and a crown cap. Out of the drybox, ethene (30 psig) was introduced into the reaction vessel via a needle terminal while the

suspension/solution was vigorously stirred. The nitrogen gas was purged by repeatedly pressurizing with ethene to 30 psig and releasing the pressure at least five times. The solution of co-catalyst in toluene was injected into the mixture via syringe to initiate the polymerization. After 10 minutes, or when the mixture became thick with polymer particles to the point stirring became difficult, the reaction vessel was isolated from the ethene source, the pressure was released via a syringe needle through the gasket, and a solution of conc. HCl/EtOH (1/40 ratio, 2 mL) was injected immediately. The polymer was collected, washed with the HCl/EtOH solution, and dried under reduced pressure at 40 °C overnight.

(2) Polymerization reaction using precatalysts prepared in situ from main-group metal salts and TiX_4 . In the drybox, a solution/suspension of the main-group metal salt (ca. 1 to 4 mg) in 5 mL of toluene was prepared in a pressure-tight reaction vessel which contained a magnetic rod for stirring, and sealed with a gasket and a crown cap. Out of the drybox, ethene (30 psig) was introduced to the reaction vessel via a needle terminal while the suspension/solution was vigorously stirred. The nitrogen gas was purged by repeating pressurizing with ethene to 30 psig and venting the pressure at least five times. A solution of TiX_4 in toluene, prepared and measured in the drybox in a lubricant-free disposable syringe, was then injected for a designated mixing time.^a The solution of co-catalyst in toluene was then injected to the mixture via syringe to initiate the polymerization. After 10 minutes, or when the mixture gets thick with polymer particles to the point that stirring is difficult, the reaction vessel was isolated from the ethene source, the pressure was released via a syringe needle through the gasket, and the solution of conc. HCl/EtOH (1/40 ratio, 2 mL) was injected immediately. The polymer was collected, washed with the HCl/EtOH solution, and dried under reduced pressure at 40 °C overnight.

(3) Hydrogen-incorporated polymerization reaction. In the drybox, a solution/suspension of the main-group metal salt (ca. 1 to 4 mg) in 5 mL of toluene was prepared in a pressure-tight reaction vessel which contained a magnetic rod for stirring, and sealed with a gasket and a crown cap. Out of the drybox, ethene (30 psig) was introduced to the reaction vessel via a needle terminal while the suspension/solution was vigorously stirred. The nitrogen gas was purged by repeating pressurizing with ethene to (30 + p) psig (p = designated partial pressure of hydrogen) and venting the pressure at

^a When the designated mixing time is longer than 20 minutes, sometimes TiX_4 was added in the drybox before sealing the reaction vessel. Occasional swirling was applied in such cases, until introduction of ethene gas and addition of the co-catalyst.

least five times. The ethene pressure was released to 0 psig, the stopcock between the reaction vessel and the gas line was closed, then the gas line was filled with hydrogen at the designated pressure (p psig). The hydrogen was introduced by opening the stopcock between the vessel and the gas line, while the mixture was vigorously stirred. The stopcock was closed again, the gas line was flushed with ethene at $(30 + p)$ psig, and the vessel was pressurized by opening the stopcock. A solution of TiX_4 in toluene, prepared and measured in the drybox in a lubricant-free disposable syringe, was then injected to the hydrogen-capped mixture for the designated mixing time. The solution of co-catalyst in toluene was then injected to the mixture via syringe to initiate the polymerization. After 10 minutes, or when the mixture became thick with polymer particles to the point the stirring was difficult, the reaction vessel was isolated from the ethene source, the pressure was released via a syringe needle through the gasket, and the solution of conc. HCl/EtOH (1/40 v/v, 2 mL) was injected immediately. The polymer was collected, washed with the HCl/EtOH solution, and dried under reduced pressure at 40 °C overnight.

5.4.D. Large-Scale Polymerization Experiments

Large-scale experiments were performed for selected catalyst conditions, to obtain temperature and ethene flow-rate profiles and to investigate the catalyst lifetime over a prolonged period. All experiments were to evaluate the precatalysts prepared from selected magnesium salts (25 and 77), under 30 psig of ethene, at a semi-controlled external temperature of either 31-32 °C or 86-87 °C. The external temperature was regulated in an ethylene glycol bath, connected to the Neslab Circulating Cooler RTE-211. These reactions involved the use of similar quantities of precatalysts as used in the small-scale reactions, but using ca. 170 mL of solvent. The reaction vessel was purchased from Andrews Glass Co., equipped with a Lab Crest 110-900-0012 multiported stirring assembly mounted with a type J thermocouple, injection port, vacuum/gas release port combined with a safety valve. To perform polymerization reactions, the reaction vessel was equipped with a pressure-tight addition funnel that can be connected to the reaction vessel via a Swagelok quick-connector fitting and a Parr 4841 controller assembly with mechanical stirrer and temperature control/monitoring devices. The glass container, the stirring blades, and the thermocouple terminal of the reaction vessel were rinsed with neat *tri-iso*-butylaluminum, followed by polymerization-quality toluene in the drybox, prior to

use. Ethene flow-rate (uncalibrated) was detected by an ethene mass flowmeter (Teledyne-Hastings-Raydist) connected to a recorder (Fisher recordall series 5000).

A general procedure is provided below, followed by the specific descriptions of the large-scale polymerization experiments discussed in this chapter.

General procedure of large-scale experiments.

In the drybox, the solution of the designated amount of the co-catalyst in 160 mL of toluene was prepared in the reaction vessel, which was then sealed with the stirring assembly. The pressure-tight addition funnel was also charged with the solution/suspension of the magnesium salt in 6-11 mL of toluene (see specific descriptions below). Out of the drybox, the reaction vessel was equipped with the addition funnel the reaction vessel was placed under ethene pressure (30 psig), and nitrogen gas was purged by repeating pressurizing with ethene and venting the pressure at least five times. The atmosphere of the addition funnel was also flushed with ethene. At the same time, the reaction vessel was placed in the temperature-adjusted ethylene glycol bath. The temperature of the reaction mixture was monitored using the type J thermocouple. When the temperature was equilibrated, the solution of TiCl_4 in toluene, prepared and measured in the drybox in a lubricant-free disposable syringe, was injected to the suspension/solution of the magnesium salt in the addition funnel. Occasional swirling was applied during the designated mixing time. The content of the addition funnel was then added to the co-catalyst solution in the reaction vessel to initiate the polymerization by release the pressure of the vessel slightly and repressurize from the top of the addition funnel. The pressure of the main reactor was regained immediately. The addition funnel was rinsed with 4 mL of fresh toluene, and the rinsing was also added to the reaction vessel by the same procedure. The ethene flow-rate and temperature were recorded during the polymerization, typically over 0.5 h. The reaction was terminated by isolating the reaction vessel from the ethene source, releasing the pressure, and injecting 5 mL of conc. HCl/EtOH (1/40, v/v). The polymer was collected, washed with the HCl/EtOH solution, and dried under reduced pressure at 40 °C overnight.

Polymerization by [25 + 4 TiCl_4 (5 min of mixing time)], M-MAO, 87 °C (Table 5.12, Reaction I).

To the solution of M-MAO (2.31×10^{-3} mol Al/mL toluene, 0.78 mL, 1.8×10^{-3} mol) in toluene (160 mL) in the reaction vessel, vigorously stirred at 87 °C under ethene pressure (30 psig), was added the precatalyst suspension that was prepared by mixing magnesium

salt **25** (FW = 965, 0.0022 g, 2.3×10^{-6} mol) and TiCl_4 (3.35 mol/mL toluene, 0.27 mL, 9.1×10^{-6} mol) in 6 mL of toluene for 5 min in the addition funnel. The addition funnel was rinsed with 4 mL of toluene and the rinsing was added to the reaction mixture. The polymerization reaction was quenched after 40 min by releasing the pressure and injecting the solution of conc.HCl/EtOH (2 mL). The yield of the product polymer was 15.23 g. The polymerization activity was $841 \text{ kg PE}\cdot\text{hr}^{-1}\cdot\text{mol Ti}^{-1}\cdot\text{atm}^{-1}$.

Polymerization by [25 + 4TiCl₄ (5 min of mixing time)], M-MAO, 31.5 °C (Figure 5.14-a).

To the solution of M-MAO (2.31×10^{-3} mol Al/mL toluene, 0.93 mL, 2.1×10^{-3} mol) in toluene (160 mL) in the reaction vessel, vigorously stirred at 31.5 °C under ethene pressure (30 psig), was added the precatalyst suspension that was prepared by mixing magnesium salt **25** (FW = 965, 0.0022 g, 2.3×10^{-6} mol) and TiCl_4 (3.35 mol/mL toluene, 0.32 mL, 1.1×10^{-5} mol) in 11 mL of toluene for 5 min in the addition funnel. The addition funnel was rinsed with 4 mL of toluene and the rinsing was added to the reaction mixture. The polymerization reaction was quenched after 60 min by releasing the pressure and injecting the solution of conc.HCl/EtOH (2 mL). The yield of the product polymer was 20.53 g. The polymerization activity was $640 \text{ kg PE}\cdot\text{hr}^{-1}\cdot\text{mol Ti}^{-1}\cdot\text{atm}^{-1}$.

Polymerization by [25 + 4TiCl₄ (5 min of mixing time)], M-MAO, 31.5 °C (Section 5.2.G.2).

To the solution of M-MAO (7.1 wt% Al, 2.4443 g, 6.4×10^{-3} mol) in toluene (163 mL) in the reaction vessel, vigorously stirred at 31 °C under ethene pressure (30 psig), was added the precatalyst suspension that was prepared by mixing magnesium salt **25** (FW = 939, 0.0075 g, 8.0×10^{-6} mol) and TiCl_4 (3.33×10^{-5} mol/mL toluene, 0.96 mL, 3.2×10^{-5} mol) in 10 mL of toluene for 10 min in the addition funnel. The addition funnel was rinsed with 4 mL of toluene and the rinsing was added to the reaction mixture. Significant rise in temperature up to 66 °C was observed within 7 min, accompanied by rapid formation of polymer particles. The reaction had to be quenched after 11.5 min, because the mixture became thick with polymer particles. The yield of the product polymer was 18.98 g. The polymerization activity was $1,030 \text{ kg PE}\cdot\text{hr}^{-1}\cdot\text{mol Ti}^{-1}\cdot\text{atm}^{-1}$.

Polymerization by Isolated precatalyst **85 [77 + TiCl₄], Et₃Al, 85 °C (Table 5.12, Reaction II).**

To the solution of Et₃Al (1.11×10^{-3} mol Al/mL toluene, 0.58 mL, 6.4×10^{-3} mol) in toluene (160 mL) in the reaction vessel, vigorously stirred at 87.5 °C under ethene pressure (30 psig), was added the precatalyst suspension of **85** (0.0026 g, 5.3×10^{-6} mol)

in 11 mL of toluene. The addition funnel was rinsed with 4 mL of toluene and the rinsing was added to the reaction mixture. The polymerization reaction was quenched after 60 min by releasing the pressure and injecting the solution of conc.HCl/EtOH (2 mL). The polymerization activity was 275 kg PE•hr⁻¹•mol Ti⁻¹•atm⁻¹.

Polymerization by [77 + 0.5TiCl₄ (10 min of mixing time)], Me₃Al, 32 °C (Figure 5.15-a).

To the solution of Me₃Al (0.277 g, 3.85 x 10⁻³ mol) in toluene (160 mL) in the reaction vessel, vigorously stirred at 32 °C under ethene pressure (30 psig), was added the precatalyst suspension that was prepared by mixing magnesium salt 77 (0.0045 g, 1.5 x 10⁻⁶ mol) and TiCl₄ (8.33 x 10⁻⁶ mol/mL toluene, 0.91 mL, 7.6 x 10⁻⁶ mol) in 11 mL of toluene for 10 min in the addition funnel. The addition funnel was rinsed with 4 mL of toluene and the rinsing was added to the reaction mixture. The polymerization reaction was quenched after 244 min by releasing the pressure and injecting the solution of conc.HCl/EtOH (2 mL). The yield of the product polymer was 49.87 g. The polymerization activity was 548 kg PE•hr⁻¹•mol Ti⁻¹•atm⁻¹.

Polymerization by [77 + 0.5TiCl₄ (10 min of mixing time)]; Me₃Al, 86 °C (Figure 5.15-b).

To the solution of Me₃Al (0.279 g, 3.86 x 10⁻³ mol) in toluene (160 mL) in the reaction vessel, vigorously stirred at 86 °C under ethene pressure (30 psig), was added the precatalyst suspension that was prepared by mixing magnesium salt 77 (0.0045 g, 1.5 x 10⁻⁶ mol) and TiCl₄ (3.35 x 10⁻⁵ mol/mL toluene, 0.23 mL, 7.7 x 10⁻⁶ mol) in 11 mL of toluene for 10 min in the addition funnel. The addition funnel was rinsed with 4 mL of toluene and the rinsing was added to the reaction mixture. The polymerization reaction was quenched after 54 min by releasing the pressure and injecting the solution of conc.HCl/EtOH (2 mL). The yield of the product polymer was 5.01 g. The polymerization activity was 241 kg PE•hr⁻¹•mol Ti⁻¹•atm⁻¹.

5.4.E. Complete Data of Polymerization Reactions

This section provides the specific conditions and activity values of all the small-scale polymerization reactions that were presented in this chapter, in the order of appearance. The general procedures were provided in Section 5.4.C. The ethene pressure was consistently 30 psig, which was converted to ca. 45 psia, thus to 3 atm.

(1) Conditions and results for the polymerization reactions in Table 5.1. The first column corresponds to the entries in Table 5.1.

	Precatalyst	mol of Ti	Co-catalyst (Al/Ti)	(Rxn. time with co-catalyst w/o C ₂ H ₄)	Polym. time (hr)	Polymer mass (kg)	Activity (kg PE•hr ⁻¹ •mol Ti ⁻¹ •atm ⁻¹)
1	31	4.46 x 10 ⁻⁶	Et ₃ Al (200)	-	0.167	0	0
2	31	3.18 x 10 ⁻⁶	M-MAO (200)	-	0.167	0	0
3	30a ^a	3.53 x 10 ⁻⁶	Me ₃ Al (100)	-	0.105	5.04 x 10 ⁻⁵	45
4	30a ^a	3.41 x 10 ⁻⁶	M-MAO (200)	-	0.133	4.78 x 10 ⁻⁵	35
5	30 ^a	3.96 x 10 ⁻⁶	Me ₃ Al (100)	-	0.159	4.79 x 10 ⁻⁵	25
6	34	4.18 x 10 ⁻⁶	Me ₃ Al (100)	-	0.169	1.60 x 10 ⁻⁵	8
7	34	4.18 x 10 ⁻⁶	M-MAO (200)	-	0.445	1.23 x 10 ⁻⁵	2
8	35	3.72 x 10 ⁻⁶	B(C ₆ F ₅) ₂ (1.3) ^b	(25 min)	0.168	0	0
9	35	5.48 x 10 ⁻⁶	B(C ₆ F ₅) ₃ (1) ^b	(1 day)	0.167	1.23 x 10 ⁻⁵	16
10	35	8.92 x 10 ⁻⁶	[PhEt ₂ NH][B(C ₆ F ₅) ₄] (1) ^b	(<1 min)	0.50	0	0
11	35	5.10 x 10 ⁻⁶	[PhEt ₂ NH][B(C ₆ F ₅) ₄] (1) ^b	(1 day)	0.167	0	0
12	35	2.74 x 10 ⁻⁶	[Cp ₂ Fe][B(C ₆ F ₅) ₄] (1) ^b	(41 min)	0.282	0	0
13	35	3.72 x 10 ⁻⁶	[Ph ₃ C][B(C ₆ F ₅) ₄] (1) ^b	(20 min)	0.192	0	0
14	45	1.32 x 10 ⁻⁶	M-MAO (200)	-	0.0833	2.3 x 10 ⁻⁶	14
15	46	8 x 10 ⁻⁶	M-MAO (100)	-	0.71	3.33 x 10 ⁻⁵	8
16	52	2.77 x 10 ⁻⁶	Et ₃ Al (200)	-	0.150	0	0
17	52	3.33 x 10 ⁻⁶	M-MAO (200)	-	0.150	0	0
18	(57) ^a	6.72 x 10 ⁻⁶	Me ₃ Al (100)	-	0.164	4.65 x 10 ⁻⁵	18
19	71	1.39 x 10 ⁻⁶	Me ₃ Al (100)	-	0.120	1.131 x 10 ⁻⁴	226
20	72	5.3 x 10 ⁻⁷	Me ₃ Al (100)	-	0.188	4.65 x 10 ⁻⁵	156
21	TiCl ₄	3.56 x 10 ⁻⁶	M-MAO (200)	-	0.0888	2.10 x 10 ⁻⁵	22

^a These titanium complexes were prepared in situ by mixing the corresponding main-group metal salt and TiCl₄ for longer than 30 min. 30a: from 25 and 2 equiv. TiCl₄ (60-80 min), 30: from 40 and 2 equiv. TiCl₄ (30 min), 57: from 76 and 2 equiv. TiCl₄ (82 min).

^b Boron per molecule.

(2) Conditions and results for the polymerization reactions in Table 5.2. The first column corresponds to the entries in Table 5.2.

Salt	Ligand : TiCl ₄	mol of Ti	Mixing time (min)	Co-catalyst (Al/Ti)	Polym. time (hr)	Polymer mass (kg)	Activity (kg PE·hr ⁻¹ · mol Ti ⁻¹ ·atm ⁻¹)	
3	73	1 : 1	3.65 x 10 ⁻⁶	49	Me ₃ Al (100)	0.166	2.63 x 10 ⁻⁵	14
4	74	1 : 1	2.21 x 10 ⁻⁶	1	Me ₃ Al (100)	0.113	1.136 x 10 ⁻⁴	152
5	74	1 : 1	2.80 x 10 ⁻⁶	40	Me ₃ Al (100)	0.0833	2.517 x 10 ⁻⁴	360
6	74	1 : 1	4.27 x 10 ⁻⁶	58	Me ₃ Al (100)	0.0847	4.743 x 10 ⁻⁴	437
7	74	1 : 2	2.79 x 10 ⁻⁶	1	Me ₃ Al (100)	0.113	8.53 x 10 ⁻⁴	90
8	74	1 : 2	3.23 x 10 ⁻⁶	50	Me ₃ Al (100)	0.981	3.261 x 10 ⁻⁴	343
9	74	1 : 2	5.85 x 10 ⁻⁶	65	Me ₃ Al (100)	0.0792	3.741 x 10 ⁻⁴	269
10	74	1 : 1	1.77 x 10 ⁻⁶	1	M-MAO (200)	0.0436	1.901 x 10 ⁻⁴	821
11	74	1 : 1	1.77 x 10 ⁻⁶	17	M-MAO (200)	0.100	2.82 x 10 ⁻⁵	53
12	74	1 : 2	3.23 x 10 ⁻⁶	1	M-MAO (200)	0.0292	1.715 x 10 ⁻⁴	606
13	74	1 : 2	2.67 x 10 ⁻⁶	28	M-MAO (200)	0.104	4.29 x 10 ⁻⁵	51

(3) Conditions and results for the polymerization reactions in Figure 5.3-a.

Salt	Ligand : TiCl ₄	mol of Ti	Mixing time (min)	Co-catalyst (Al/Ti)	Polym. time (hr)	Polymer mass (kg)	Activity (kg PE·hr ⁻¹ · mol Ti ⁻¹ ·atm ⁻¹)
25	1 : 1	1.71 x 10 ⁻⁶	1	Me ₃ Al (100)	0.112	6.44 x 10 ⁻⁵	112
25	1 : 1	9.16 x 10 ⁻⁷	10	Me ₃ Al (100)	0.189	6.14 x 10 ⁻⁵	118
25	1 : 1	1.21 x 10 ⁻⁶	13	Me ₃ Al (100)	0.100	1.40 x 10 ⁻⁵	39
25	1 : 1	1.60 x 10 ⁻⁶	57	Me ₃ Al (100)	0.170	1.43 x 10 ⁻⁵	17
25	1 : 2	4.66 x 10 ⁻⁶	5	Me ₃ Al (100)	0.133	3.269 x 10 ⁻⁴	176
25	1 : 2	4.66 x 10 ⁻⁶	5	Me ₃ Al (100)	0.170	3.985 x 10 ⁻⁴	168
25	1 : 2	5.00 x 10 ⁻⁶	19	Me ₃ Al (100)	0.0750	5.319 x 10 ⁻⁴	473
25	1 : 2	5.00 x 10 ⁻⁶	40	Me ₃ Al (100)	0.177	3.699 x 10 ⁻⁴	139
25	1 : 2	4.66 x 10 ⁻⁶	81	Me ₃ Al (100)	0.170	4.191 x 10 ⁻⁴	176
25	1 : 4	3.10 x 10 ⁻⁶	1	Me ₃ Al (100)	0.0748	2.322 x 10 ⁻⁴	269
25	1 : 4	4.53 x 10 ⁻⁶	5	Me ₃ Al (100)	0.0871	3.857 x 10 ⁻⁴	313
25	1 : 4	4.61 x 10 ⁻⁶	14	Me ₃ Al (100)	0.132	2.960 x 10 ⁻⁴	475
25	1 : 4	4.20 x 10 ⁻⁶	30	Me ₃ Al (100)	0.0931	3.742 x 10 ⁻⁴	335
25	1 : 4	3.58 x 10 ⁻⁶	53	Me ₃ Al (100)	0.0729	6.838 x 10 ⁻⁴	262
25	1 : 4	3.90 x 10 ⁻⁶	82	Me ₃ Al (100)	0.0076	3.300 x 10 ⁻⁴	27

(4) Conditions and results for the polymerization reactions in Figure 5.3-b.

Salt	Ligand : TiCl ₄	mol of Ti	Mixing time (min)	Co-catalyst (Al/Ti)	Polym. time (hr)	Polymer mass (kg)	Activity (kg PE·hr ⁻¹ · mol Ti ⁻¹ ·atm ⁻¹)
25	1 : 1	2.02 x 10 ⁻⁶	1	M-MAO (200)	0.133	1.03 x 10 ⁻⁵	13
25	1 : 1	2.10 x 10 ⁻⁶	30	M-MAO (200)	0.167	1.028 x 10 ⁻⁵	98
25	1 : 1	1.64 x 10 ⁻⁶	60	M-MAO (200)	0.167	2.93 x 10 ⁻⁵	36
25	1 : 2	6.77 x 10 ⁻⁶	1	M-MAO (200)	0.0450	2.430 x 10 ⁻⁴	280
25	1 : 2	6.77 x 10 ⁻⁶	3	M-MAO (200)	0.100	3.334 x 10 ⁻⁴	164
25	1 : 2	5.70 x 10 ⁻⁶	5	M-MAO (200)	0.125	3.412 x 10 ⁻⁴	160
25	1 : 2	6.51 x 10 ⁻⁶	7.5	M-MAO (200)	0.171	2.500 x 10 ⁻⁴	75
25	1 : 2	6.51 x 10 ⁻⁶	17	M-MAO (200)	0.167	1.023 x 10 ⁻⁴	31
25	1 : 4	2.91 x 10 ⁻⁶	6	M-MAO (200)	0.0389	2.112 x 10 ⁻⁴	622
25	1 : 4	2.25 x 10 ⁻⁶	20	M-MAO (200)	0.167	2.726 x 10 ⁻⁴	242
25	1 : 4	4.50 x 10 ⁻⁶	35	M-MAO (200)	0.102	3.938 x 10 ⁻⁴	286
25	1 : 4	3.53 x 10 ⁻⁶	39	M-MAO (200)	0.089	2.724 x 10 ⁻⁴	288
25	1 : 4	5.20 x 10 ⁻⁶	76	M-MAO (200)	0.0469	1.341 x 10 ⁻⁴	183

(5) Conditions and results for the polymerization reactions in Figure 5.3-c.

Salt	Ligand : TiCl ₄	mol of Ti	Mixing time (min)	Co-catalyst (Al/Ti)	Polym. time (hr)	Polymer mass (kg)	Activity (kg PE·hr ⁻¹ · mol Ti ⁻¹ ·atm ⁻¹)
25	1 : 2	6.51 x 10 ⁻⁶	1	Et ₃ Al (100)	0.0500	2.853 x 10 ⁻⁴	292
25	1 : 2	6.77 x 10 ⁻⁶	3	Et ₃ Al (100)	0.0722	3.279 x 10 ⁻⁴	224
25	1 : 2	6.77 x 10 ⁻⁶	5	Et ₃ Al (100)	0.0917	2.078 x 10 ⁻⁴	145
25	1 : 2	6.25 x 10 ⁻⁶	8	Et ₃ Al (100)	0.117	2.472 x 10 ⁻⁴	113
25	1 : 2	7.03 x 10 ⁻⁶	15	Et ₃ Al (100)	0.167	2.580 x 10 ⁻⁴	73
25	1 : 2	7.03 x 10 ⁻⁶	30	Et ₃ Al (100)	0.167	2.647 x 10 ⁻⁴	75
25	1 : 2	6.51 x 10 ⁻⁶	60	Et ₃ Al (100)	0.167	1.839 x 10 ⁻⁴	56
25	1 : 4	5.73 x 10 ⁻⁶	1	Et ₃ Al (100)	0.0958	3.102 x 10 ⁻⁴	196
25	1 : 4	6.25 x 10 ⁻⁶	3	Et ₃ Al (100)	0.0542	3.314 x 10 ⁻⁴	326
25	1 : 4	7.03 x 10 ⁻⁶	7	Et ₃ Al (100)	0.138	5.717 x 10 ⁻⁴	378
25	1 : 4	6.25 x 10 ⁻⁶	15	Et ₃ Al (100)	0.100	5.505 x 10 ⁻⁴	294
25	1 : 4	6.33 x 10 ⁻⁶	17	Et ₃ Al (100)	0.0833	4.871 x 10 ⁻⁴	308
25	1 : 4	6.52 x 10 ⁻⁶	30	Et ₃ Al (100)	0.0611	3.569 x 10 ⁻⁴	299

(6) Conditions and results for the polymerization reactions in Table 5.3.

Salt	Ligand : TiCl ₄	mol of Ti	Mixing time (min)	Co-catalyst (Al/Ti)	Polym. time (hr)	Polymer mass (kg)	Activity (kg PE·hr ⁻¹ · mol Ti ⁻¹ ·atm ⁻¹)
40	1 : 1	3.38 x 10 ⁻⁶	1	Me ₃ Al (100)	0.1589	3.12 x 10 ⁻⁵	19
40	1 : 1	2.13 x 10 ⁻⁶	19	Me ₃ Al (100)	0.1589	2.36 x 10 ⁻⁵	23
40	1 : 2	4.89 x 10 ⁻⁶	1	Me ₃ Al (100)	0.1589	5.18 x 10 ⁻⁵	22
40	1 : 2	4.28 x 10 ⁻⁶	5	Me ₃ Al (100)	0.2356	8.24 x 10 ⁻⁵	27
40	1 : 2	3.96 x 10 ⁻⁶	29	Me ₃ Al (100)	0.1589	4.79 x 10 ⁻⁵	25
40	1 : 4	7.37 x 10 ⁻⁶	1	Me ₃ Al (100)	0.1519	3.94 x 10 ⁻⁵	11
40	1 : 4	6.74 x 10 ⁻⁶	10	Me ₃ Al (100)	0.1928	5.24 x 10 ⁻⁵	13
40	1 : 4	6.75 x 10 ⁻⁶	38	Me ₃ Al (100)	0.1589	3.12 x 10 ⁻⁵	10

(7) Conditions and results for the polymerization reactions in Figure 5.4-a.

Salt	Ligand : TiCl ₄	mol of Ti	Mixing time (min)	Co-catalyst (Al/Ti)	Polym. time (hr)	Polymer mass (kg)	Activity (kg PE·hr ⁻¹ · mol Ti ⁻¹ ·atm ⁻¹)
75	1 : 1	2.83 x 10 ⁻⁶	1	Me ₃ Al (100)	0.159	5.51 x 10 ⁻⁵	41
75	1 : 1	2.13 x 10 ⁻⁶	15	Me ₃ Al (100)	0.117	3.034 x 10 ⁻⁴	405
75	1 : 1	1.94 x 10 ⁻⁶	36	Me ₃ Al (100)	0.117	2.691 x 10 ⁻⁴	394
75	1 : 1	1.78 x 10 ⁻⁶	120	Me ₃ Al (100)	0.0506	6.7 x 10 ⁻⁶	25
75	1 : 2	3.88 x 10 ⁻⁶	1	Me ₃ Al (100)	0.159	7.87 x 10 ⁻⁵	43
75	1 : 2	6.77 x 10 ⁻⁶	40	Me ₃ Al (100)	0.0767	3.429 x 10 ⁻⁴	220
75	1 : 2	3.60 x 10 ⁻⁶	41	Me ₃ Al (100)	0.0650	2.376 x 10 ⁻⁴	338
75	1 : 2	3.19 x 10 ⁻⁶	48	Me ₃ Al (100)	0.159	6.61 x 10 ⁻⁵	43

(8) Conditions and results for the polymerization reactions in Figure 5.4-b.

Salt	Ligand : TiCl ₄	mol of Ti	Mixing time (min)	Co-catalyst (Al/Ti)	Polym. time (hr)	Polymer mass (kg)	Activity (kg PE·hr ⁻¹ · mol Ti ⁻¹ ·atm ⁻¹)
75	1 : 1	2.13 x 10 ⁻⁶	10	M-MAO (200)	0.167	2.526 x 10 ⁻⁴	237
75	1 : 1	2.13 x 10 ⁻⁶	22	M-MAO (200)	0.136	3.988 x 10 ⁻⁴	460
75	1 : 1	3.53 x 10 ⁻⁶	30	M-MAO (200)	0.0278	1.445 x 10 ⁻⁴	491
75	1 : 1	1.94 x 10 ⁻⁶	43	M-MAO (200)	0.159	3.476 x 10 ⁻⁴	376
75	1 : 1	2.83 x 10 ⁻⁶	62	M-MAO (200)	0.118	3.667 x 10 ⁻⁴	365
75	1 : 1	1.58 x 10 ⁻⁶	103	M-MAO (200)	0.181	2.45 x 10 ⁻⁵	29
75	1 : 2	3.88 x 10 ⁻⁶	1	M-MAO (200)	0.1333	1.035 x 10 ⁻⁴	67
75	1 : 2	3.18 x 10 ⁻⁶	14	M-MAO (200)	0.1042	2.817 x 10 ⁻⁴	283
75	1 : 2	3.53 x 10 ⁻⁶	30	M-MAO (200)	0.0750	1.305 x 10 ⁻⁴	164
75	1 : 2	3.58 x 10 ⁻⁶	31	M-MAO (200)	0.1603	7.109 x 10 ⁻⁴	413
75	1 : 2	3.18 x 10 ⁻⁶	50	M-MAO (200)	0.1342	3.264 x 10 ⁻⁴	255
75	1 : 2	2.83 x 10 ⁻⁶	101	M-MAO (200)	0.1708	1.297 x 10 ⁻⁴	89

(9) Conditions and results for the polymerization reactions in Table 5.4.

Salt	Ligand : TiCl ₄	mol of Ti	Mixing time (min)	Co-catalyst (Al/Ti)	Polym. time (hr)	Polymer mass (kg)	Activity (kg PE•hr ⁻¹ • mol Ti ⁻¹ •atm ⁻¹)
47	1 : 1	2.31 x 10 ⁻⁶	1	M-MAO (200)	0.0888	1.58 x 10 ⁻⁵	26
47	1 : 1	4.00 x 10 ⁻⁶	103	M-MAO (200)	0.133	1.72 x 10 ⁻⁵	11
48	1 : 1	3.56 x 10 ⁻⁶	1	M-MAO (200)	0.0833	3.05 x 10 ⁻⁵	34
48	1 : 1	3.75 x 10 ⁻⁶	86	M-MAO (200)	0.217	6.99 x 10 ⁻⁵	29
48	1 : 2	3.56 x 10 ⁻⁶	1	M-MAO (200)	0.0888	3.49 x 10 ⁻⁵	37
48	1 : 2	3.94 x 10 ⁻⁶	87	M-MAO (200)	0.217	1.398 x 10 ⁻⁴	55
48	1 : 2	3.94 x 10 ⁻⁶	43h	M-MAO (200)	0.233	1.101 x 10 ⁻⁴	40
50	1 : 1	3.63 x 10 ⁻⁶	1	M-MAO (200)	0.208	3.21 x 10 ⁻⁵	14
50	1 : 1	4.31 x 10 ⁻⁶	62	M-MAO (200)	0.208	4.97 x 10 ⁻⁵	18
50	1 : 2	4.00 x 10 ⁻⁶	1	M-MAO (200)	0.208	3.31 x 10 ⁻⁵	13
50	1 : 2	4.63 x 10 ⁻⁶	41	M-MAO (200)	0.208	5.44 x 10 ⁻⁵	19
50	1 : 2	4.00 x 10 ⁻⁶	216	M-MAO (200)	0.208	7.37 x 10 ⁻⁵	30

(10) Conditions and results for the polymerization reactions in Table 5.5.

Salt	Ligand : TiCl ₄	mol of Ti	Mixing time (min)	Co-catalyst (Al/Ti)	Polym. time (hr)	Polymer mass (kg)	Activity (kg PE•hr ⁻¹ • mol Ti ⁻¹ •atm ⁻¹)
76	1 : 1	4.83 x 10 ⁻⁶	14	Me ₃ Al (100)	0.178	9.72 x 10 ⁻⁵	38
76	1 : 1	4.83 x 10 ⁻⁶	27	Me ₃ Al (100)	0.18	1.102 x 10 ⁻⁴	42
76	1 : 1	4.83 x 10 ⁻⁶	66	Me ₃ Al (100)	0.176	5.40 x 10 ⁻⁵	21
76	1 : 1	5.00 x 10 ⁻⁶	208	Me ₃ Al (100)	0.183	6.26 x 10 ⁻⁵	23
76	1 : 2	4.83 x 10 ⁻⁶	15	Me ₃ Al (100)	0.178	1.048 x 10 ⁻⁴	41
76	1 : 2	4.83 x 10 ⁻⁶	29	Me ₃ Al (100)	0.183	9.97 x 10 ⁻⁵	38
76	1 : 2	4.83 x 10 ⁻⁶	77	Me ₃ Al (100)	0.175	7.59 x 10 ⁻⁵	30

(11) Conditions and results for the polymerization reactions in Figure 5.5-a.

Salt	Ligand : TiCl ₄	mol of Ti	Mixing time (min)	Co-catalyst (Al/Ti)	Polym. time (hr)	Polymer mass (kg)	Activity (kg PE•hr ⁻¹ • mol Ti ⁻¹ •atm ⁻¹)
77	2 : 1	3.70 x 10 ⁻⁶	1	Me ₃ Al (100)	0.112	5.601 x 10 ⁻⁴	452
77	2 : 1	3.54 x 10 ⁻⁶	21	Me ₃ Al (100)	0.101	3.662 x 10 ⁻⁴	341
77	2 : 1	3.70 x 10 ⁻⁶	40	Me ₃ Al (100)	0.112	6.252 x 10 ⁻⁴	509
77	2 : 1	3.37 x 10 ⁻⁶	62	Me ₃ Al (100)	0.103	5.723 x 10 ⁻⁴	549
77	2 : 1	4.04 x 10 ⁻⁶	71	Me ₃ Al (100)	0.0528	2.950 x 10 ⁻⁴	461
77	2 : 1	3.87 x 10 ⁻⁶	102	Me ₃ Al (100)	0.0733	3.220 x 10 ⁻⁴	378
77	2 : 1	3.70 x 10 ⁻⁶	162	Me ₃ Al (100)	0.0756	3.564 x 10 ⁻⁴	425

(11) Continued.

Salt	Ligand : TiCl ₄	mol of Ti	Mixing time (min)	Co-catalyst (Al/Ti)	Polym. time (hr)	Polymer mass (kg)	Activity (kg PE·hr ⁻¹ · mol Ti ⁻¹ ·atm ⁻¹)
77	1 : 1	3.37 x 10 ⁻⁶	1	Me ₃ Al (100)	0.0872	4.271 x 10 ⁻⁴	484
77	1 : 1	3.70 x 10 ⁻⁶	25	Me ₃ Al (100)	0.0925	3.931 x 10 ⁻⁴	383
77	1 : 1	4.04 x 10 ⁻⁶	61	Me ₃ Al (100)	0.111	4.802 x 10 ⁻⁴	357
77	1 : 1	3.70 x 10 ⁻⁶	100	Me ₃ Al (100)	0.136	3.759 x 10 ⁻⁴	249
77	1 : 1	3.72 x 10 ⁻⁶	109	Me ₃ Al (100)	0.159	1.026 x 10 ⁻⁴	58
77	1 : 1	3.37 x 10 ⁻⁶	140	Me ₃ Al (100)	0.0992	8.89 x 10 ⁻⁵	89

(12) Conditions and results for the polymerization reactions in Figure 5.5-b.

Salt	Ligand : TiCl ₄	mol of Ti	Mixing time (min)	Co-catalyst (Al/Ti)	Polym. time (hr)	Polymer mass (kg)	Activity (kg PE·hr ⁻¹ · mol Ti ⁻¹ ·atm ⁻¹)
77	2 : 1	4.04 x 10 ⁻⁶	1	M-MAO (200)	0.0808	2.833 x 10 ⁻⁴	289
77	2 : 1	4.04 x 10 ⁻⁶	16	M-MAO (200)	0.107	2.681 x 10 ⁻⁴	207
77	2 : 1	4.54 x 10 ⁻⁶	64	M-MAO (200)	0.107	2.613 x 10 ⁻⁴	179
77	2 : 1	3.88 x 10 ⁻⁶	117	M-MAO (200)	0.109	3.708 x 10 ⁻⁴	292
77	2 : 1	3.04 x 10 ⁻⁶	207	M-MAO (200)	0.179	2.816 x 10 ⁻⁴	172
77	2 : 1	4.19 x 10 ⁻⁶	230	M-MAO (200)	0.175	3.314 x 10 ⁻⁴	151
77	1 : 1	5.41 x 10 ⁻⁶	1	M-MAO (200)	0.0686	3.430 x 10 ⁻⁴	308
77	1 : 1	5.41 x 10 ⁻⁶	20	M-MAO (200)	0.0436	2.728 x 10 ⁻⁴	385
77	1 : 1	5.08 x 10 ⁻⁶	42	M-MAO (200)	0.0500	2.671 x 10 ⁻⁴	351
77	1 : 1	3.70 x 10 ⁻⁶	70	M-MAO (200)	0.0694	3.738 x 10 ⁻⁴	485
77	1 : 1	5.08 x 10 ⁻⁶	113	M-MAO (200)	0.0806	3.644 x 10 ⁻⁴	297
77	1 : 1	3.37 x 10 ⁻⁶	207	M-MAO (200)	0.240	2.355 x 10 ⁻⁴	97

(13) Conditions and results for the polymerization reactions in Table 5.6.

Salt	Ligand : TiCl ₄	mol of Ti	Mixing time (min)	Co-catalyst (Al/Ti)	Polym. time (hr)	Polymer mass (kg)	Activity (kg PE·hr ⁻¹ · mol Ti ⁻¹ ·atm ⁻¹)
80	2 : 1	7.76 x 10 ⁻⁶	79	Me ₃ Al (100)	0.236	9.08 x 10 ⁻⁵	17
80	1 : 1	8.61 x 10 ⁻⁶	63	Me ₃ Al (100)	0.237	1.136 x 10 ⁻⁴	19

(14) Conditions and results for the polymerization reactions in Figure 5.6-a.

Salt	Ligand : TiCl ₄	mol of Ti	Mixing time (min)	Co-catalyst (Al/Ti)	Polym. time (hr)	Polymer mass (kg)	Activity (kg PE·hr ⁻¹ · mol Ti ⁻¹ ·atm ⁻¹)
78	1 : 1	3.24 x 10 ⁻⁶	1	Me ₃ Al (100)	0.173	5.00 x 10 ⁻⁵	30
78	1 : 1	3.24 x 10 ⁻⁶	19	Me ₃ Al (100)	0.313	6.620 x 10 ⁻⁴	218
78	1 : 1	4.20 x 10 ⁻⁶	45	Me ₃ Al (100)	0.328	5.225 x 10 ⁻⁴	126
78	1 : 1	8.15 x 10 ⁻⁶	66	Me ₃ Al (100)	0.0928	4.147 x 10 ⁻⁴	183
78	1 : 1	4.20 x 10 ⁻⁶	86	Me ₃ Al (100)	0.317	6.812 x 10 ⁻⁴	171
78	1 : 1	4.22 x 10 ⁻⁶	109	Me ₃ Al (100)	0.168	2.497 x 10 ⁻⁴	117
78	1 : 1	4.20 x 10 ⁻⁶	131	Me ₃ Al (100)	0.342	8.624 x 10 ⁻⁴	200
78	1 : 2	5.45 x 10 ⁻⁶	1	Me ₃ Al (100)	0.202	8.10 x 10 ⁻⁵	25
78	1 : 2	5.45 x 10 ⁻⁶	22	Me ₃ Al (100)	0.178	1.053 x 10 ⁻⁴	36
78	1 : 2	5.45 x 10 ⁻⁶	44	Me ₃ Al (100)	0.186	8.71 x 10 ⁻⁵	29
78	1 : 2	5.45 x 10 ⁻⁶	62	Me ₃ Al (100)	0.134	7.27 x 10 ⁻⁵	33
78	1 : 2	6.91 x 10 ⁻⁶	81	Me ₃ Al (100)	0.124	1.838 x 10 ⁻⁴	72
78	1 : 2	5.91 x 10 ⁻⁶	114	Me ₃ Al (100)	0.119	3.90 x 10 ⁻⁵	19
78	1 : 2	6.03 x 10 ⁻⁶	122	Me ₃ Al (100)	0.113	8.05 x 10 ⁻⁵	39

(15) Conditions and results for the polymerization reactions in Figure 5.6-b.

Salt	Ligand : TiCl ₄	mol of Ti	Mixing time (min)	Co-catalyst (Al/Ti)	Polym. time (hr)	Polymer mass (kg)	Activity (kg PE·hr ⁻¹ · mol Ti ⁻¹ ·atm ⁻¹)
78	1 : 1	4.73 x 10 ⁻⁶	1	M-MAO (200)	0.174	9.36 x 10 ⁻⁵	38
78	1 : 1	4.19 x 10 ⁻⁶	19	M-MAO (200)	0.254	7.572 x 10 ⁻⁴	237
78	1 : 1	4.19 x 10 ⁻⁶	44	M-MAO (200)	0.128	6.513 x 10 ⁻⁴	405
78	1 : 1	3.96 x 10 ⁻⁶	75	M-MAO (200)	0.139	6.526 x 10 ⁻⁴	395
78	1 : 1	4.73 x 10 ⁻⁶	130	M-MAO (200)	0.169	3.011 x 10 ⁻⁴	126
78	1 : 1	3.96 x 10 ⁻⁶	5	M-MAO (200)	0.183	1.899 x 10 ⁻⁴	87
78	1 : 1	7.40 x 10 ⁻⁶	9	M-MAO (200)	0.194	2.892 x 10 ⁻⁴	67
78	1 : 1	3.49 x 10 ⁻⁶	20	M-MAO (200)	0.183	2.127 x 10 ⁻⁴	112
78	1 : 2	6.95 x 10 ⁻⁶	21	M-MAO (200)	0.183	5.430 x 10 ⁻⁴	142
78	1 : 2	3.96 x 10 ⁻⁶	50	M-MAO (200)	0.183	2.625 x 10 ⁻⁴	121
78	1 : 2	8.40 x 10 ⁻⁶	78	M-MAO (200)	0.168	6.088 x 10 ⁻⁴	144
78	1 : 2	8.40 x 10 ⁻⁶	99	M-MAO (200)	0.186	4.991 x 10 ⁻⁴	106
78	1 : 2	4.91 x 10 ⁻⁶	149	M-MAO (200)	0.193	1.993 x 10 ⁻⁴	70

(16) Conditions and results for the polymerization reactions in Figure 5.7-a.

Salt	Ligand : TiCl ₄	mol of Ti	Mixing time (min)	Co-catalyst (Al/Ti)	Polym. time (hr)	Polymer mass (kg)	Activity (kg PE·hr ⁻¹ · mol Ti ⁻¹ ·atm ⁻¹)
79	1 : 1	2.95 x 10 ⁻⁶	1	Me ₃ Al (100)	0.1464	9.48 x 10 ⁻⁵	73
79	1 : 1	2.95 x 10 ⁻⁶	19	Me ₃ Al (100)	0.1464	1.137 x 10 ⁻⁴	88
79	1 : 1	2.72 x 10 ⁻⁶	30	Me ₃ Al (100)	0.1408	8.83 x 10 ⁻⁵	77
79	1 : 1	4.27 x 10 ⁻⁶	40	Me ₃ Al (100)	0.1083	4.149 x 10 ⁻⁴	300
79	1 : 1	3.38 x 10 ⁻⁶	57	Me ₃ Al (100)	0.1494	2.494 x 10 ⁻⁴	165
79	1 : 1	7.45 x 10 ⁻⁶	81	Me ₃ Al (100)	0.0669	5.231 x 10 ⁻⁴	350
79	1 : 1	4.49 x 10 ⁻⁶	82	Me ₃ Al (100)	0.1900	1.0105 x 10 ⁻³	395
79	1 : 1	4.04 x 10 ⁻⁶	120	Me ₃ Al (100)	0.1508	2.279 x 10 ⁻⁴	125
79	1 : 2	4.49 x 10 ⁻⁶	1	Me ₃ Al (100)	0.2692	2.910 x 10 ⁻⁴	80
79	1 : 2	5.43 x 10 ⁻⁶	25	Me ₃ Al (100)	0.0958	2.733 x 10 ⁻⁴	175
79	1 : 2	4.49 x 10 ⁻⁶	31	Me ₃ Al (100)	0.1611	7.19 x 10 ⁻⁵	33
79	1 : 2	4.95 x 10 ⁻⁶	62	Me ₃ Al (100)	0.3333	1.0340 x 10 ⁻³	209
79	1 : 2	5.41 x 10 ⁻⁶	74	Me ₃ Al (100)	0.2761	7.221 x 10 ⁻⁴	161
79	1 : 2	5.43 x 10 ⁻⁶	82	Me ₃ Al (100)	0.1589	8.89 x 10 ⁻⁵	34
79	1 : 2	4.49 x 10 ⁻⁶	90	Me ₃ Al (100)	0.3211	9.629 x 10 ⁻⁴	225
79	1 : 2	7.16 x 10 ⁻⁶	116	Me ₃ Al (100)	0.1628	1.230 x 10 ⁻⁴	35

(17) Conditions and results for the polymerization reactions in Figure 5.7-b.

Salt	Ligand : TiCl ₄	mol of Ti	Mixing time (min)	Co-catalyst (Al/Ti)	Polym. time (hr)	Polymer mass (kg)	Activity (kg PE·hr ⁻¹ · mol Ti ⁻¹ ·atm ⁻¹)
79	1 : 1	3.18 x 10 ⁻⁶	1	M-MAO (200)	0.146	8.01 x 10 ⁻⁵	58
79	1 : 1	3.22 x 10 ⁻⁶	41	M-MAO (200)	0.148	1.492 x 10 ⁻⁴	104
79	1 : 1	2.71 x 10 ⁻⁶	61	M-MAO (200)	0.193	4.866 x 10 ⁻⁴	310
79	1 : 1	2.95 x 10 ⁻⁶	67	M-MAO (200)	0.176	2.136 x 10 ⁻⁴	137
79	1 : 1	2.00 x 10 ⁻⁶	88	M-MAO (200)	0.225	1.408 x 10 ⁻⁴	104
79	1 : 1	3.17 x 10 ⁻⁶	96	M-MAO (200)	0.190	2.237 x 10 ⁻⁴	124
79	1 : 1	3.60 x 10 ⁻⁶	104	M-MAO (200)	0.176	4.650 x 10 ⁻⁴	245
79	1 : 1	3.18 x 10 ⁻⁶	128	M-MAO (200)	0.181	1.538 x 10 ⁻⁴	89
79	1 : 2	3.17 x 10 ⁻⁶	5	M-MAO (200)	0.192	1.883 x 10 ⁻⁴	80
79	1 : 2	4.95 x 10 ⁻⁶	12	M-MAO (200)	0.185	2.695 x 10 ⁻⁴	98
79	1 : 2	4.08 x 10 ⁻⁶	25	M-MAO (200)	0.216	3.514 x 10 ⁻⁴	133
79	1 : 2	3.17 x 10 ⁻⁶	25	M-MAO (200)	0.194	1.986 x 10 ⁻⁴	108
79	1 : 2	2.71 x 10 ⁻⁶	45	M-MAO (200)	0.193	2.127 x 10 ⁻⁴	135
79	1 : 2	4.49 x 10 ⁻⁶	75	M-MAO (200)	0.174	1.732 x 10 ⁻⁴	74
79	1 : 2	4.08 x 10 ⁻⁶	101	M-MAO (200)	0.178	1.374 x 10 ⁻⁴	63
79	1 : 2	4.95 x 10 ⁻⁶	145	M-MAO (200)	0.290	6.127 x 10 ⁻⁴	142

(18) Conditions and results for the polymerization reactions in Table 5.7.

Salt	Ligand : TiCl ₄	mol of Ti	Mixing time (min)	Co-catalyst (Al/Ti)	Polym. time (hr)	Polymer mass (kg)	Activity (kg PE·hr ⁻¹ · mol Ti ⁻¹ ·atm ⁻¹)
81	1 : 1	9.08 x 10 ⁻⁶	49	Me ₃ Al (100)	0.187	5.73 x 10 ⁻⁶	11
81	1 : 2	1.04 x 10 ⁻⁵	80	Me ₃ Al (100)	0.139	8.49 x 10 ⁻⁶	20

(19) Conditions and results for the polymerization reactions in Figure 5.8-a.

Salt	Ligand : TiCl ₄	mol of TiCl ₄	Mixing time (min)	Co-catalyst (Al/Ti)	Polym. time (hr)	Polymer mass (kg)	Activity (kg PE·hr ⁻¹ · mol Ti ⁻¹ ·atm ⁻¹)
25	1 : 2	5.73 x 10 ⁻⁶	4	Me ₃ Al (100)	0.167	7.497	261
25	1 : 2	4.66 x 10 ⁻⁶	5	Me ₃ Al (100)	0.133	3.269 x 10 ⁻⁴	176
25	1 : 2	4.66 x 10 ⁻⁶	5	Me ₃ Al (100)	0.170	3.985 x 10 ⁻⁴	168
25	1 : 2	6.25 x 10 ⁻⁶	7	Me ₃ Al (100)	0.167	7.775 x 10 ⁻⁴	248
25	1 : 2	6.71 x 10 ⁻⁶	12	Me ₃ Al (100)	0.133	6.541 x 10 ⁻⁴	244
25	1 : 2	6.25 x 10 ⁻⁶	18.5	Me ₃ Al (100)	0.129	5.456 x 10 ⁻⁴	226
25	1 : 2	5.00 x 10 ⁻⁶	19	Me ₃ Al (100)	0.0750	5.319 x 10 ⁻⁴	473
25	1 : 2	5.73 x 10 ⁻⁶	32	Me ₃ Al (100)	0.167	4.419 x 10 ⁻⁴	154
25	1 : 2	5.00 x 10 ⁻⁶	40	Me ₃ Al (100)	0.177	3.699 x 10 ⁻⁴	139
25	1 : 2	4.66 x 10 ⁻⁶	81	Me ₃ Al (100)	0.170	4.191 x 10 ⁻⁴	176
26	1 : 2	4.19 x 10 ⁻⁶	3	Me ₃ Al (100)	0.146	7.055 x 10 ⁻⁴	384
26	1 : 2	5.13 x 10 ⁻⁶	20	Me ₃ Al (100)	0.167	8.713 x 10 ⁻⁴	339
26	1 : 2	5.13 x 10 ⁻⁶	40	Me ₃ Al (100)	0.126	6.387 x 10 ⁻⁴	329
26	1 : 2	5.13 x 10 ⁻⁶	70	Me ₃ Al (100)	0.134	6.780 x 10 ⁻⁴	329

Note: some results from 25 are the same as the data presented in Figure 5.3-a.

(20) Conditions and results for the polymerization reactions in Figure 5.8-b.

Salt	Ligand : TiBr ₄	mol of TiBr ₄	Mixing time (min)	Co-catalyst (Al/Ti)	Polym. time (hr)	Polymer mass (kg)	Activity (kg PE·hr ⁻¹ · mol Ti ⁻¹ ·atm ⁻¹)
25	1 : 2	2.75 x 10 ⁻⁶	6	Me ₃ Al (100)	0.125	4.354 x 10 ⁻⁴	422
25	1 : 2	2.75 x 10 ⁻⁶	20	Me ₃ Al (100)	0.180	4.978 x 10 ⁻⁴	335
25	1 : 2	2.75 x 10 ⁻⁶	40	Me ₃ Al (100)	0.183	3.507 x 10 ⁻⁴	232
25	1 : 2	2.75 x 10 ⁻⁶	71	Me ₃ Al (100)	0.117	1.844 x 10 ⁻⁴	191
27	1 : 2	3.86 x 10 ⁻⁶	3	Me ₃ Al (100)	0.0750	4.569 x 10 ⁻⁴	526
27	1 : 2	4.53 x 10 ⁻⁶	20	Me ₃ Al (100)	0.167	5.434 x 10 ⁻⁴	239
27	1 : 2	4.53 x 10 ⁻⁶	39	Me ₃ Al (100)	0.167	5.768 x 10 ⁻⁴	254
27	1 : 2	4.87 x 10 ⁻⁶	71	Me ₃ Al (100)	0.167	4.625 x 10 ⁻⁴	190

(21) Conditions and results for the polymerization reactions in Figure 5.9-a.

Salt	Ligand : TiCl ₄	mol of TiCl ₄	Mixing time (min)	Co-catalyst (Al/Ti)	Polym. time (hr)	Polymer mass (kg)	Activity (kg PE·hr ⁻¹ · mol Ti ⁻¹ ·atm ⁻¹)
77	2 : 1	5.00 x 10 ⁻⁶	5	Me ₃ Al (100)	0.0833	4.016 x 10 ⁻⁴	321
77	2 : 1	4.66 x 10 ⁻⁶	24	Me ₃ Al (100)	0.0847	4.029 x 10 ⁻⁴	340
77	2 : 1	4.66 x 10 ⁻⁶	60	Me ₃ Al (100)	0.0833	3.659 x 10 ⁻⁴	314
77	2 : 1	5.33 x 10 ⁻⁶	102	Me ₃ Al (100)	0.0833	3.813 x 10 ⁻⁴	286
82	2 : 1	5.00 x 10 ⁻⁶	8	Me ₃ Al (100)	0.175	1.305 x 10 ⁻⁴	50
82	2 : 1	5.00 x 10 ⁻⁶	29	Me ₃ Al (100)	0.175	2.084 x 10 ⁻⁴	79
82	2 : 1	5.00 x 10 ⁻⁶	87	Me ₃ Al (100)	0.178	1.921 x 10 ⁻⁴	72
82	2 : 1	5.00 x 10 ⁻⁶	132	Me ₃ Al (100)	0.175	1.341 x 10 ⁻⁴	51

(22) Conditions and results for the polymerization reactions in Figure 5.9-b.

Salt	Ligand : TiBr ₄	mol of TiBr ₄	Mixing time (min)	Co-catalyst (Al/Ti)	Polym. time (hr)	Polymer mass (kg)	Activity (kg PE·hr ⁻¹ · mol Ti ⁻¹ ·atm ⁻¹)
77	2 : 1	5.04 x 10 ⁻⁶	3	Me ₃ Al (100)	0.750	3.351 x 10 ⁻⁴	296
77	2 : 1	5.04 x 10 ⁻⁶	21	Me ₃ Al (100)	0.0583	3.077 x 10 ⁻⁴	349
77	2 : 1	5.04 x 10 ⁻⁶	40	Me ₃ Al (100)	0.0756	4.384 x 10 ⁻⁴	384
77	2 : 1	5.04 x 10 ⁻⁶	80	Me ₃ Al (100)	0.0514	2.802 x 10 ⁻⁴	361
82	2 : 1	5.20 x 10 ⁻⁶	3	Me ₃ Al (100)	0.108	5.199 x 10 ⁻⁴	309
82	2 : 1	4.87 x 10 ⁻⁶	21	Me ₃ Al (100)	0.0667	3.753 x 10 ⁻⁴	385
82	2 : 1	5.04 x 10 ⁻⁶	40	Me ₃ Al (100)	0.108	5.004 x 10 ⁻⁴	306
82	2 : 1	5.37 x 10 ⁻⁶	81	Me ₃ Al (100)	0.0628	2.794 x 10 ⁻⁴	276

(23) Conditions and results for the polymerization reactions in Figure 5.10-a.

Salt	Ligand : TiCl ₄	mol of TiCl ₄	Mixing time (min)	Co-catalyst (Al/Ti)	Polym. time (hr)	Polymer mass (kg)	Activity (kg PE·hr ⁻¹ · mol Ti ⁻¹ ·atm ⁻¹)
27	1 : 2	3.33 x 10 ⁻⁶	5	Me ₃ Al (100)	0.179	3.566 x 10 ⁻⁴	201
27	1 : 2	3.66 x 10 ⁻⁶	20	Me ₃ Al (100)	0.0753	4.106 x 10 ⁻⁴	497
27	1 : 2	3.33 x 10 ⁻⁶	40	Me ₃ Al (100)	0.0833	4.208 x 10 ⁻⁴	506
27	1 : 2	4.50 x 10 ⁻⁶	71	Me ₃ Al (100)	0.0708	4.271 x 10 ⁻⁴	447

(24) Conditions and results for the polymerization reactions in Figure 5.10-b.

Salt	Ligand : TiBr ₄	mol of TiBr ₄	Mixing time (min)	Co-catalyst (Al/Ti)	Polym. time (hr)	Polymer mass (kg)	Activity (kg PE·hr ⁻¹ · mol Ti ⁻¹ ·atm ⁻¹)
27	1 : 2	3.36 x 10 ⁻⁶	5	Me ₃ Al (100)	0.0583	3.338 x 10 ⁻⁴	568
27	1 : 2	3.02 x 10 ⁻⁶	20	Me ₃ Al (100)	0.150	6.748 x 10 ⁻⁴	497
27	1 : 2	2.69 x 10 ⁻⁶	42	Me ₃ Al (100)	0.133	6.373 x 10 ⁻⁴	594
27	1 : 2	4.03 x 10 ⁻⁶	70	Me ₃ Al (100)	0.167	7.498 x 10 ⁻⁴	371

(25) Conditions and results for the polymerization reactions in Figure 5.11-a.

Salt	Ligand : TiCl ₄	mol of TiCl ₄	Mixing time (min)	Co-catalyst (Al/Ti)	Polym. time (hr)	Polymer mass (kg)	Activity (kg PE·hr ⁻¹ · mol Ti ⁻¹ ·atm ⁻¹)
83	2 : 1	6.16 x 10 ⁻⁶	9	Me ₃ Al (100)	0.169	3.720 x 10 ⁻⁴	119
83	2 : 1	5.00 x 10 ⁻⁶	30	Me ₃ Al (100)	0.188	1.011 x 10 ⁻⁴	36
83	2 : 1	5.00 x 10 ⁻⁶	86	Me ₃ Al (100)	0.181	8.45 x 10 ⁻⁵	31
83	2 : 1	6.99 x 10 ⁻⁶	133	Me ₃ Al (100)	0.200	1.070 x 10 ⁻⁴	26

(26) Conditions and results for the polymerization reactions in Figure 5.11-b.

Salt	Ligand : TiBr ₄	mol of TiBr ₄	Mixing time (min)	Co-catalyst (Al/Ti)	Polym. time (hr)	Polymer mass (kg)	Activity (kg PE·hr ⁻¹ · mol Ti ⁻¹ ·atm ⁻¹)
83	2 : 1	5.04 x 10 ⁻⁶	3	Me ₃ Al (100)	0.181	2.415 x 10 ⁻⁴	88
83	2 : 1	6.21 x 10 ⁻⁶	20	Me ₃ Al (100)	0.168	1.023 x 10 ⁻⁴	33
83	2 : 1	5.71 x 10 ⁻⁶	40	Me ₃ Al (100)	0.150	9.53 x 10 ⁻⁵	37
83	2 : 1	6.71 x 10 ⁻⁶	92	Me ₃ Al (100)	0.200	1.776 x 10 ⁻⁴	44

(28) Conditions and results for the polymerization reactions in Tables 5.13 and 5.14.

Salt	Ligand : TiCl ₄	mol of TiCl ₄	Mixing time (min)	Partial P (H ₂) (atm)	Co-catalyst (Al/Ti)	Polym. time (hr)	Polymer mass (kg)	Activity (kg PE·hr ⁻¹ · mol Ti ⁻¹ ·atm ⁻¹)	
1	25	1 : 2	6.77 x 10 ⁻⁶	1	0	M-MAO (200)	0.045	2.430 x 10 ⁻⁴	280
1	25	1 : 2	6.51 x 10 ⁻⁶	1	0.13	M-MAO (200)	0.100	2.476 x 10 ⁻⁴	127
2	25	1 : 4	5.71 x 10 ⁻⁶	1	0	M-MAO (200)	0.0322	2.054 x 10 ⁻⁴	372
2	25	1 : 4	5.24 x 10 ⁻⁶	2.5	0.13	M-MAO (200)	0.0333	1.897 x 10 ⁻⁴	363
3	25	1 : 2	6.19 x 10 ⁻⁶	1	0	Me ₃ Al (100)	0.0972	5.754 x 10 ⁻⁴	319
3	25	1 : 2	6.19 x 10 ⁻⁶	1	0.13	Me ₃ Al (100)	0.167	6.578 x 10 ⁻⁴	212
4	25	1 : 4	5.71 x 10 ⁻⁶	14	0	Me ₃ Al (100)	0.0508	2.827 x 10 ⁻⁴	325
4	25	1 : 4	5.71 x 10 ⁻⁶	20	0.13	Me ₃ Al (100)	0.121	4.228 x 10 ⁻⁴	204
5	25	1 : 2	6.51 x 10 ⁻⁶	1	0	Et ₃ Al (100)	0.050	2.853 x 10 ⁻⁴	292
5	25	1 : 2	6.25 x 10 ⁻⁶	1	0.13	Et ₃ Al (100)	0.167	2.032 x 10 ⁻⁴	65

(28) Continued.

<i>Salt</i>	<i>Ligand :</i> <i>TiCl₄</i>	<i>mol of TiCl₄</i>	<i>Mixing</i> <i>time</i> <i>(min)</i>	<i>Partial</i> <i>P (H₂)</i> <i>(atm)</i>	<i>Co-catalyst</i> <i>(Al/Ti)</i>	<i>Polym.</i> <i>time</i> <i>(hr)</i>	<i>Polymer</i> <i>mass</i> <i>(kg)</i>	<i>Activity</i> <i>(kg PE·hr⁻¹·</i> <i>mol Ti⁻¹·atm⁻¹)</i>	
6	25	1 : 4	6.25 x 10 ⁻⁶	3	0	Et ₃ Al (100)	0.0542	3.314 x 10 ⁻⁴	326
6	25	1 : 4	6.51 x 10 ⁻⁶	7	0.13	Et ₃ Al (100)	0.137	4.195 x 10 ⁻⁴	163
7	77	2 : 1	5.00 x 10 ⁻⁶	4	0	Et ₃ Al (100)	0.0433	2.684 x 10 ⁻⁴	413
7	77	2 : 1	5.24 x 10 ⁻⁶	4	0.13	Et ₃ Al (100)	0.0533	2.427 x 10 ⁻⁴	290
8	77	1 : 1	5.00 x 10 ⁻⁶	4	0	Et ₃ Al (100)	0.0306	1.972 x 10 ⁻⁴	430
8	77	1 : 1	4.76 x 10 ⁻⁶	4	0.13	Et ₃ Al (100)	0.0628	2.085 x 10 ⁻⁴	232

Note: the first column corresponds to the entry numbers of **Tables 5.13** and **5.14**.

5.6. References and Notes

- ¹ Chen, E. Y.-X.; Marks, T. J. *Chem. Rev.* **2000**, *100*, 1391-1434.
- ² Commercially available from Akzo-Nobel.
- ³ Verkerk, U. Ph.D. Dissertation, University of Alberta, 2001.
- ⁴ Saied, O.; Simard, M.; Wuest, J. D. *Inorg. Chem.* **1998**, *37*, 2620-2625.
- ⁵ Brintzinger, H. H.; Fisher, D.; Mülhaupt, R.; Rieger, B.; Waymouth, R. M. *Angew. Chem. Int. Ed. Engl.* **1995**, *34*, 1143-1170; and references therein.
- ⁶ In zirconoporphyrins, for example, the metal center is obviously more 'uplifted' from the plane defined by four porphyrin nitrogens, than in titanoporphyrins, as shown in the following instances: (a) 0.93 Å with Zr(IV) in (OEP)Zr(CH₂SMe₃)₂ (OEP = dianion of octaethylporphyrin); Brand, H.; Arnold, J. J. *Am. Chem. Soc.* **1992**, *114*, 2266-2267; (b) 0.66 Å with Ti(III) in [(TTP)Ti]₂O (TTP = dianion of *meso*-tetra-*p*-tolylporphyrin); Hays, J. A.; Day, C. L.; Young, V. G.; Woo, L. Keith. *Inorg. Chem.* **1996**, *35*, 7601-7607.
- ⁷ Britovsek, G. J. P.; Gibson, V. C.; Wass, D. F. *Angew. Chem. Int. Ed.* **1999**, *38*, 428-447. This review classifies the catalysts according to the activity as: <1 (very low), 1-10 (low), 10-100 (moderate), 100-1000 (high), and >1000 (very high). The unit is g•mmol⁻¹•hr⁻¹•bar⁻¹, which is very close to the unit used in this chapter: kg PE•mol⁻¹•hr⁻¹•atm⁻¹ (1.013 bar = 1 atm).
- ⁸ Tsutsui, T. *Organomet. News* **1998**, 82-85.
- ⁹ (a) Goodall, B. L. "Super High Activity Supported Catalysts for the Stereospecific Polymerization of α -Olefins: History, Development, Mechanistic Aspects, and Characterization" *MMI Press Symp. Ser.*, 4 (Transition Met. Catal. Polym.: Alkenes and Dienes, Part A), **1983**, 355-378. (b) Sobota, P.; Szafer, S. *J Chem. Soc. Dalton Trans.* **2001**, 1379-1386.
- ¹⁰ High-temperature polymerization lowers the molecular weight by promoting thermal cleavage of Ti-C bonds, and H₂-incorporated polymerization by promoting the hydrogenolysis of Ti-C bonds by a σ -bond metathesis.
- ¹¹ GPC analysis was performed at Department of Chemical and Materials Engineering, University of Alberta by N. Bu. See Experimental Section.
- ¹² Painter, P. C.; Coleman, M. M. *Fundamentals of Polymer Science An Introductory Text*, Technomic Publishing Co., Lancaster, 1994.
- ¹³ N. Bu, Department of Chemical and Materials Engineering, University of Alberta, personal communication.
- ¹⁴ Ethene flow-rate, measured by ethene mass flow transducer, directly related to ethene uptake by the reaction mixture. Not calibrated.

¹⁵ Parshall, G. W.; Ittel, S. D. *Homogeneous Catalysis The Application and Chemistry of Catalysis by Soluble Transition Metal Complexes*, 2nd ed., John Wiley & Sons, Inc., New York; 1992.

¹⁶ Chemical Abstract search under "non-metallocene" or "post metallocene" in the last three years resulted mostly in amine- or imine-based ligand systems, other than the variations of magnesium halide- or silica-supported catalysts.

¹⁷ (a) For examples of amide-based non-metallocene homogeneous catalysts, see Lee, C. H.; La, Y.-H.; Park, J. W. *Organometallics* **2000**, *19*, 344-351 and references 1-3 therein.

(b) For examples of imine-based non-metallocene homogeneous catalysts, see the review by Ittel, S. D.; Johnson, L. K.; Brookhart, M. *Chem. Rev.* **2000**, *100*, 1169-1173.

¹⁸ Matsui, S.; Inoue, Y.; Fujita, T. *J. Synth. Org. Chem.* **2001**, *59*, 232-240.

¹⁹ Similar dimeric structure of magnesium phenoxides: Bocelli, G.; Cantoni, A.; Sartori, G.; Maggi, R.; Bigi, F. *Chem. Eur. J.* **1997**, *3*, 1269-1272.

General Conclusion

The modified tetrakis(2-hydroxyphenyl)ethene-based ligands were found to be promising templates for the construction of various discrete mononuclear and polynuclear metal complexes. The *ortho*-propylated derivative, tetrakis(2-hydroxy-3-propylphenyl)ethene (**7**), showed diverse coordination patterns for polynuclear complexes of Mg(II), Ti(IV) and Al(III). The coordination patterns were largely determined by the metal species, probably most affected by the valency of the metal atoms. The dialkylated analogue, *E*-bis(2-hydroxyphenyl)-bis(2-methoxyphenyl)ethene (**3E**), provided several mononuclear Ti and Al complexes, as well as dinuclear and trinuclear species, which possess a mononuclear core attached to extra metal fragment(s) on the periphery. Comparison with the *Z*-analogue of the ligand, **3Z**, showed the advantages of trans-dialkylation in the formation of discrete complexes.

Although the titanium derivatives of these ligands do not show potential as ethene polymerization catalysts, the ligands' capacity as an oxo-surface model merits further exploration. Floriani has investigated potential oxo-surface model chemistry of various transition metal complexes derived from the calix[4]arene ligand system.¹ Very different chemical behavior, however, can be expected from the tetraarylethene-based systems, based on the ability to form polynuclear complexes on a single ligand. The reduced tendency to form collapsed 'sandwich-type' structure in *ortho*-propylated ligand **7** will be particularly advantageous, because such dimerization is a problem often encountered in calix[4]arene systems.

The potential of the divalent *E*-dialkylated ligand **3E** as an alternative ancillary ligand for metallocenes, especially for Group 4 metals, may also be an interesting topic. Little is known about the extent to which the ancillary ligand determines reactivity in organometallic chemistry of the Group 4 metals.² Floriani, *et. al.*, has shown that zirconium complexes of the dialkylated calix-[4]-arene ligand exhibit different reactivity than simple zirconocene complexes in the insertion chemistry of dialkylzirconium complexes³ and butadiene complexes.² The similar but different tetraarylethene framework in ligand **3E** may provide a platform for divergent chemical behavior as well.

The possibilities for coordination chemistry widen upon introduction of other heteroatom binding sites into the tetraarylethene template. The easiest approach is to modify the hydroxy termini with nitrogen- or phosphorous-containing groups, which will be suitable for late transition-metal binding, as recently demonstrated done for calixarene systems.⁴

The newly developed tetrakis(2-hydroxyphenyl)ethene template and metal derivatives may serve as new oxo-surface model templates, as well as new support ligands for various metals in exploratory organometallic chemistry and catalysis.

References

¹ Recent reports of metal-oxo surface model chemistry of calix[4]arene systems by Floriani, *et al.*: (a) Caselli, A.; Solari, E.; Scopelliti, R.; Floriani, C. *J. Am. Chem. Soc.* **2000**, *122*, 538-539. (b) Caselli, A.; Solari, E.; Scopelliti, R.; Floriani, C.; Re, N.; Rizzoli, C.; Chiesi-Villa, A. *J. Am. Chem. Soc.* **2000**, *122*, 3652-3670. (c) Esposito, V.; Solari, E.; Floriani, C.; Re, N.; Rizzoli, C.; Chiesi-Villa, A. *Inorg. Chem.* **2000**, *39*, 2604-2613. (d) Hessechenbrouck, J.; Solari, E.; Floriani, C.; Re, N.; Rizzoli, C.; Chiesi-Villa, A. *Dalton* **2000**, 191-198.

² Caselli, A.; Giannini, L.; Solari, E.; Floriani, C. *Organometallics* **1997**, *16*, 5457-5469.

³ Giannini, L.; Caselli, A.; Solari, E.; Floriani, C.; Chiesi-Villa, A.; Rizzoli, C.; Re, N.; Sgamellotti, A. *J. Am. Chem. Soc.* **1997**, *119*, 9709-9719.

⁴ (a) Wieser, C.; Dieleman, C. B.; Matt, D. *Coord. Chem. Rev.* **1997**, *165*, 93-161. (b) Stolzmar, M.; Floriani, C.; Chiesi-Villa, A.; Rizzoli, C. *Inorg. Chem.* **1997**, *36*, 1694-1701.

University of Alberta

Coordination Chemistry of the New Preorganized Polyphenoxide Ligand Tetrakis(2-hydroxyphenyl)ethene Derivatives. Attempts to Create Surface-Models for Classic Ziegler-Natta Olefin Polymerization Catalysts

Appendices

by

Megumi Fujita

A thesis submitted to the Faculty of Graduate Studies and Research in partial fulfillment of the requirements for the degree of Doctor of Philosophy

Department of Chemistry

Edmonton, Alberta

Fall 2001

Appendices

X-ray Crystallography Data

Note: $[C_{38}H_{40}O_4] = [C_2\{C_6H_3(3\text{-}^n\text{Pr})(2\text{-O-})\}_4]$
 $E\text{- or }Z\text{-}\{C_{28}H_{22}O_4\} = E\text{- or }Z\text{-}\{C_2(C_6H_4\text{-}2\text{-OMe})_2(C_6H_4\text{-}2\text{-O-})_2\}$

			page
A-1	3Z	Z-C ₂ -1,2-(C ₆ H ₄ -2-OH) ₂ -1,2-(C ₆ H ₄ -2-OMe) ₂	287
A-2	13	{C(C ₆ H ₄ -2-OH)(C ₆ H ₄ -2-O-)} ₂	293
A-3	26	[C ₃₈ H ₄₀ O ₄]{Mg(thf)}{MgBr(thf)} ₂	299
A-4	28	[C ₃₈ H ₄₀ O ₄]{Mg(thf)}{MgCH ₃ (thf)} ₂	306
A-5	30a/32	[C ₃₈ H ₄₀ O ₄]-gem-anti-{TiCl ₂ (thf)} ₂ & [C ₃₈ H ₄₀ O ₄] ₂ •Ti ₂	313
A-6	32	[C ₃₈ H ₄₀ O ₄] ₂ Ti ₂	327
A-7	31	[C ₃₈ H ₄₀ O ₄]-vic-anti-{TiCl ₂ (thf)} ₂	336
A-8	33a	[C ₃₈ H ₄₀ O ₄]-gem-anti-{TiBr ₂ (thf)} ₂	345
A-9	34	[C ₃₈ H ₄₀ O ₄]-gem-anti-(CpTiCl) ₂	354
A-10	35	[C ₃₈ H ₄₀ O ₄]-gem-anti-(TiCH ₂ Ph) ₂	362
A-11	38	[C ₃₈ H ₄₀ O ₄](AlEt)(AlEt ₂) ₂	370
A-12	39	[C ₃₈ H ₄₀ O ₄](Al(thf))(AlCl ₂)	379
A-13	41	[C ₃₈ H ₄₀ O ₄]{MgCl(thf)}{Mg(thf)}(AlEt ₂)	387
A-14	42	[C ₃₈ H ₄₀ O ₄]{Mg(thf)}(AlEt ₂) ₂	397
A-15	45	([C ₃₈ H ₄₀ O ₄](TiBn){MgCl(thf)}) ₂	407
A-16	46/46b	[C ₃₈ H ₄₀ O ₄](TiX){AlX'Et}	420
A-17	47	E-{C ₂₈ H ₂₂ O ₄ }(AlEt)	433
A-18	50	E-{C ₂₈ H ₂₂ O ₄ }(AlEt)(AlEtCl ₂)	440
A-19	52	E-{C ₂₈ H ₂₂ O ₄ }(TiCl ₂)	448
A-20	53	E-{C ₂₈ H ₂₂ O ₄ }(TiCl ₃)(H)	456
A-21	59	E-{C ₂₈ H ₂₂ O ₄ }(Ti)(AlEtCl) ₂	464
A-22	58	Z-{C ₂₈ H ₂₂ O ₄ }(CpTiCl ₂) ₂	472
A-23	72	2,7- <i>t</i> Bu ₂ -1,8-((C ₄ H ₈ O)Cl ₃ TiO) ₂ -fluorene	483

A-1: 3Z. Z-1,2-Bis(2-hydroxyphenyl)-1,2-bis(methoxyphenyl)ethene

– Chapter 1 –

SDL Code: JMS9907

Date: 8 July 1999

Compound: Z-C₂(C₆H₄-2-OH)₂(C₆H₄-2-OMe)₂

Formula: C₂₈H₂₄O₄

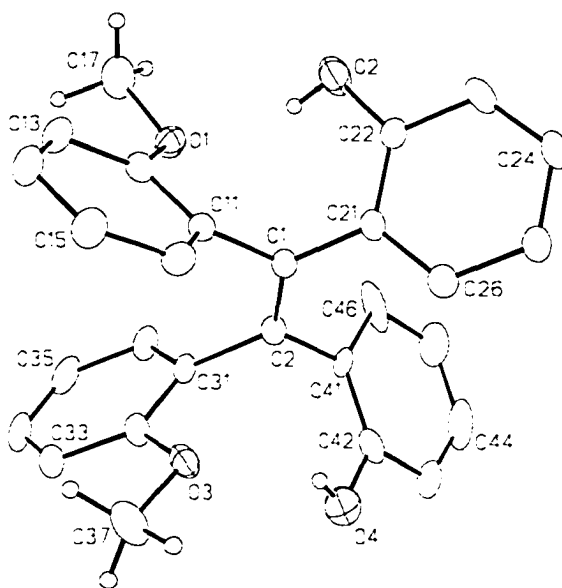


Figure 1. Perspective view of the *cis*-1,2-di(2-hydroxyphenyl)-1,2-di(2-methoxyphenyl)ethene molecule showing the atom labelling scheme. Non-hydrogen atoms are represented by Gaussian ellipsoids at the 20% probability level. Hydroxyl and methyl hydrogen atoms are shown with arbitrarily small thermal parameters; all other hydrogens are not shown.

List of Tables

Table 1. Crystallographic Experimental Details

Table 2. Atomic Coordinates and Equivalent Isotropic Displacement Parameters

Table 3. Selected Interatomic Distances

Table 4. Selected Interatomic Angles

Table 1. Crystallographic Experimental Details

A. Crystal Data

formula	C ₂₈ H ₂₄ O ₄
formula weight	424.47
crystal dimensions (mm)	0.25 × 0.12 × 0.04
crystal system	monoclinic
space group	<i>P</i> 2 ₁ / <i>c</i> (No. 14)
unit cell parameters ^a	
<i>a</i> (Å)	10.9757 (13)
<i>b</i> (Å)	15.4466 (18)
<i>c</i> (Å)	13.6421 (13)
β (deg)	99.547 (2)
<i>V</i> (Å ³)	2280.8 (4)
<i>Z</i>	4
ρ _{calcd} (g cm ⁻³)	1.236
μ (mm ⁻¹)	0.082

B. Data Collection and Refinement Conditions

diffractometer	Bruker P4/RA/SMART 1000 CCD ^b
radiation (λ [Å])	graphite-monochromated Mo Kα (0.71073)
temperature (°C)	-80
scan type	φ rotations (0.3°) / ω scans (0.3°) (30 s exposures)
data collection 2θ limit (deg)	51.60
total data collected	12189 (-13 ≤ <i>h</i> ≤ 13, -18 ≤ <i>k</i> ≤ 18, -16 ≤ <i>l</i> ≤ 15)
independent reflections	4356
number of observations (<i>NO</i>)	1167 [<i>F</i> _o ² ≥ 2σ(<i>F</i> _o ²)]
structure solution method	direct methods (<i>SHELXS-86</i> ^c)

refinement method	full-matrix least-squares on F^2 (<i>SHELXL-93</i> ^d)
absorption correction method	<i>SADABS</i>
range of transmission factors	0.9674–0.6240
data/restraints/parameters	4356 [$F_o^2 \geq -3\sigma(F_o^2)$] / 0 / 292
extinction coefficient (x) ^e	0.0116 (13)
goodness-of-fit (S) ^f	0.771 [$F_o^2 \geq -3\sigma(F_o^2)$]
final R indices ^g	
R_1 [$F_o^2 \geq 2\sigma(F_o^2)$]	0.0659
wR_2 [$F_o^2 \geq -3\sigma(F_o^2)$]	0.1837
largest difference peak and hole	0.631 and -0.276 e \AA^{-3}

^aObtained from least-squares refinement of 1526 centered reflections.

^bPrograms for diffractometer operation, data collection, data reduction and absorption correction were those supplied by Bruker.

^cSheldrick, G. M. *Acta Crystallogr.* **1990**, *A46*, 467–473.

^dSheldrick, G. M. *SHELXL-93*. Program for crystal structure determination. University of Göttingen, Germany, 1993. Refinement on F_o^2 for all reflections (all of these having $F_o^2 \geq -3\sigma(F_o^2)$). Weighted R -factors wR_2 and all goodnesses of fit S are based on F_o^2 ; conventional R -factors R_1 are based on F_o , with F_o set to zero for negative F_o^2 . The observed criterion of $F_o^2 > 2\sigma(F_o^2)$ is used only for calculating R_1 , and is not relevant to the choice of reflections for refinement. R -factors based on F_o^2 are statistically about twice as large as those based on F_o , and R -factors based on ALL data will be even larger.

^e $F_c^* = kF_c[1 + x\{0.001F_c^2\lambda^3/\sin(2\theta)\}]^{-1/4}$ where k is the overall scale factor.

^f $S = [\sum w(F_o^2 - F_c^2)^2/(n - p)]^{1/2}$ (n = number of data; p = number of parameters varied; $w = [\sigma^2(F_o^2) + (0.0622P)^2]^{-1}$ where $P = [\text{Max}(F_o^2, 0) + 2F_c^2]/3$).

^g $R_1 = \sum ||F_o| - |F_c||/\sum |F_o|$; $wR_2 = [\sum w(F_o^2 - F_c^2)^2/\sum w(F_o^4)]^{1/2}$.

Table 2. Atomic Coordinates and Equivalent Isotropic Displacement Parameters

Atom	x	y	z	$U_{eq}, \text{\AA}^2$
O1	0.4055(3)	-0.3307(2)	0.5354(2)	0.0558(10)*
O2	0.3979(4)	-0.1525(2)	0.5096(3)	0.0894(14)*
O3	0.1331(3)	-0.4187(2)	0.2159(3)	0.0636(11)*
O4	-0.0828(4)	-0.3190(3)	0.2451(4)	0.1117(16)*
C1	0.2437(5)	-0.2692(3)	0.3724(3)	0.0399(13)*
C2	0.1420(5)	-0.3140(3)	0.3836(3)	0.0418(13)*
C11	0.3600(4)	-0.3163(3)	0.3630(4)	0.0404(13)*
C12	0.4381(5)	-0.3501(3)	0.4432(4)	0.0454(13)*
C13	0.5421(5)	-0.3962(3)	0.4342(4)	0.0599(16)*
C14	0.5685(5)	-0.4114(4)	0.3389(4)	0.0637(16)*
C15	0.4933(5)	-0.3770(3)	0.2568(4)	0.0610(16)*
C16	0.3895(5)	-0.3307(3)	0.2701(4)	0.0507(14)*
C17	0.4892(5)	-0.3560(4)	0.6235(4)	0.083(2)*
C21	0.2445(5)	-0.1726(3)	0.3628(4)	0.0412(13)*
C22	0.3219(5)	-0.1205(4)	0.4292(4)	0.0512(14)*
C23	0.3226(5)	-0.0317(4)	0.4179(4)	0.0616(16)*
C24	0.2472(5)	0.0072(3)	0.3401(4)	0.0554(15)*
C25	0.1704(5)	-0.0423(4)	0.2723(4)	0.0539(15)*
C26	0.1687(4)	-0.1318(4)	0.2840(4)	0.0505(14)*
C31	0.1442(4)	-0.4117(3)	0.3881(5)	0.0488(14)*
C32	0.1436(5)	-0.4632(4)	0.3046(5)	0.0565(15)*
C33	0.1506(5)	-0.5522(4)	0.3118(5)	0.0648(17)*
C34	0.1545(5)	-0.5912(4)	0.4020(6)	0.077(2)*
C35	0.1512(5)	-0.5427(4)	0.4864(5)	0.0691(18)*
C36	0.1471(4)	-0.4532(4)	0.4797(4)	0.0596(16)*
C37	0.1461(6)	-0.4685(4)	0.1304(4)	0.089(2)*
C41	0.0236(4)	-0.2714(3)	0.4013(4)	0.0495(15)*
C42	-0.0800(6)	-0.2780(3)	0.3311(5)	0.0599(16)*
C43	-0.1949(5)	-0.2457(4)	0.3408(6)	0.0742(19)*
C44	-0.2002(7)	-0.2007(4)	0.4267(6)	0.090(2)*
C45	-0.0962(7)	-0.1918(4)	0.4976(5)	0.084(2)*
C46	0.0218(7)	-0.2269(3)	0.4912(4)	0.080(2)*

Anisotropically-refined atoms are marked with an asterisk (*). The form of the anisotropic displacement parameter is: $\exp[-2\pi^2(h^2a^*U_{11} + k^2b^*U_{22} + l^2c^*U_{33} + 2klb^*c^*U_{23} + 2hla^*c^*U_{13} + 2hka^*b^*U_{12})]$.

Table 3. Selected Interatomic Distances (Å)

Atom1	Atom2	Distance	Atom1	Atom2	Distance
O1	C12	1.395(5)	C21	C26	1.396(6)
O1	C17	1.441(5)	C22	C23	1.381(6)
O2	C22	1.356(5)	C23	C24	1.371(6)
O3	C32	1.380(6)	C24	C25	1.376(6)
O3	C37	1.424(5)	C25	C26	1.393(6)
O4	C42	1.329(6)	C31	C32	1.388(6)
C1	C2	1.344(6)	C31	C36	1.399(6)
C1	C11	1.493(6)	C32	C33	1.379(7)
C1	C21	1.497(6)	C33	C34	1.364(7)
C2	C31	1.511(6)	C34	C35	1.379(7)
C2	C41	1.511(6)	C35	C36	1.387(7)
C11	C12	1.376(6)	C41	C42	1.363(7)
C11	C16	1.378(6)	C41	C46	1.409(7)
C12	C13	1.368(6)	C42	C43	1.382(7)
C13	C14	1.398(6)	C43	C44	1.372(8)
C14	C15	1.384(6)	C44	C45	1.375(8)
C15	C16	1.382(6)	C45	C46	1.421(7)
C21	C22	1.391(6)			

Table 4. Selected Interatomic Angles (deg)

Atom1	Atom2	Atom3	Angle	Atom1	Atom2	Atom3	Angle
C12	O1	C17	118.0(4)	C22	C23	C24	120.6(5)
C32	O3	C37	116.4(4)	C23	C24	C25	120.1(5)
C2	C1	C11	119.8(4)	C24	C25	C26	119.5(5)
C2	C1	C21	122.7(5)	C21	C26	C25	121.3(5)
C11	C1	C21	117.4(4)	C2	C31	C32	122.7(5)
C1	C2	C31	120.7(5)	C2	C31	C36	119.4(5)
C1	C2	C41	123.2(4)	C32	C31	C36	117.8(5)
C31	C2	C41	115.9(4)	O3	C32	C31	115.0(5)
C1	C11	C12	123.1(4)	O3	C32	C33	123.7(6)
C1	C11	C16	119.5(4)	C31	C32	C33	121.3(6)
C12	C11	C16	117.3(5)	C32	C33	C34	119.8(6)
O1	C12	C11	114.5(5)	C33	C34	C35	120.8(6)
O1	C12	C13	122.4(5)	C34	C35	C36	119.5(6)
C11	C12	C13	123.0(5)	C31	C36	C35	120.7(6)
C12	C13	C14	118.4(5)	C2	C41	C42	119.7(5)
C13	C14	C15	120.1(5)	C2	C41	C46	119.2(5)
C14	C15	C16	119.1(5)	C42	C41	C46	121.1(5)
C11	C16	C15	122.0(5)	O4	C42	C41	123.3(6)
C1	C21	C22	122.1(5)	O4	C42	C43	111.7(7)
C1	C21	C26	120.3(5)	C41	C42	C43	125.0(6)
C22	C21	C26	117.5(5)	C42	C43	C44	115.7(6)
O2	C22	C21	122.9(5)	C43	C44	C45	120.2(7)
O2	C22	C23	116.0(5)	C44	C45	C46	125.3(7)
C21	C22	C23	121.1(5)	C41	C46	C45	112.6(6)

A-2: 13. Cis-4b,9b-Dihydro-4b,9b-bis(2-hydroxyphenyl)benzofuro(3,2-b)benzofuran

– Chapter 1 –

SDL Code: JMS9902

Date: 13 April 1999

Compound: $\{C(C_6H_4-2-OH)(C_6H_4-2-O-)\}_2 \cdot Et_2O$

Formula: $C_{30}H_{28}O_5$ ($C_{26}H_{18}O_4 \cdot C_4H_{10}O$)

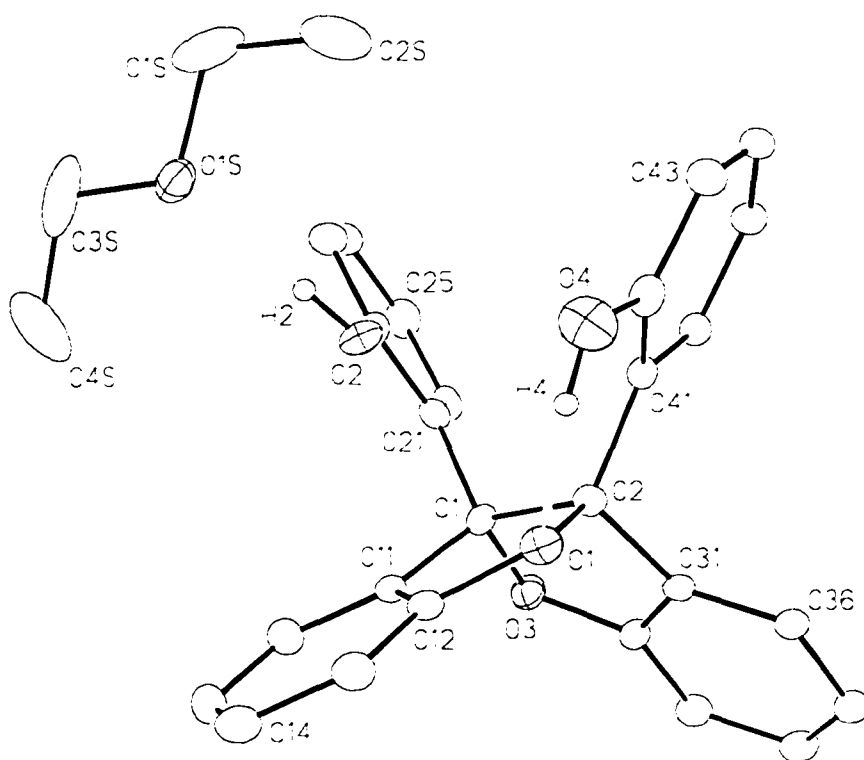


Figure 2. Alternate view showing the intra- ($O1 \cdots H4 = 1.86 \text{ \AA}$) and intermolecular ($O1S \cdots H2 = 1.86 \text{ \AA}$) hydrogen-bonded interactions within and between the $\{C(C_6H_4-2-OH)(C_6H_4-2-O-)\}_2$ molecule and the solvent diethyl ether molecule.

List of Tables

Table 1. Crystallographic Experimental Details

Table 2. Atomic Coordinates and Equivalent Isotropic Displacement Parameters

Table 3. Selected Interatomic Distances

Table 4. Selected Interatomic Angles

Table 1. Crystallographic Experimental Details

A. Crystal Data

formula	C ₃₀ H ₂₈ O ₅
formula weight	468.52
crystal dimensions (mm)	0.28 × 0.08 × 0.04
crystal system	triclinic
space group	PI (No. 2)
unit cell parameters ^a	
<i>a</i> (Å)	8.8406 (10)
<i>b</i> (Å)	9.5462 (11)
<i>c</i> (Å)	16.604 (2)
α (deg)	88.872 (2)
β (deg)	74.665 (2)
γ (deg)	65.160 (2)
<i>V</i> (Å ³)	1219.7 (2)
<i>Z</i>	2
ρ _{calcd} (g cm ⁻³)	1.276
μ (mm ⁻¹)	0.086

B. Data Collection and Refinement Conditions

diffractometer	Bruker P4/RA/SMART 1000 CCD ^b
radiation (λ [Å])	graphite-monochromated Mo Kα (0.71073)
temperature (°C)	-80
scan type	φ rotations (0.3°) / ω scans (0.3°) (30 s exposures)
data collection 2θ limit (deg)	51.40
total data collected	6660 (-9 ≤ <i>h</i> ≤ 10, -11 ≤ <i>k</i> ≤ 10, -20 ≤ <i>l</i> ≤ 19)
independent reflections	4614
number of observations (<i>NO</i>)	1550 [<i>F</i> _o ² ≥ 2σ(<i>F</i> _o ²)]
structure solution method	direct methods (<i>SHELXS-86</i> ^c)

refinement method	full-matrix least-squares on F^2 (SHELXL-93 ^d)
absorption correction method	none ^e
data/restraints/parameters	4614 [$F_o^2 \geq -3\sigma(F_o^2)$] / 0 / 318
goodness-of-fit (S) ^f	0.807 [$F_o^2 \geq -3\sigma(F_o^2)$]
final R indices ^g	
R_1 [$F_o^2 \geq 2\sigma(F_o^2)$]	0.0578
wR_2 [$F_o^2 \geq -3\sigma(F_o^2)$]	0.1516
largest difference peak and hole	0.316 and $-0.303 \text{ e } \text{\AA}^{-3}$

^aObtained from least-squares refinement of 1532 centered reflections.

^bPrograms for diffractometer operation, data collection, data reduction and absorption correction were those supplied by Bruker.

^cSheldrick, G. M. *Acta Crystallogr.* **1990**, A46, 467–473.

^dSheldrick, G. M. *SHELXL-93*. Program for crystal structure determination. University of Göttingen, Germany, 1993. Refinement on F_o^2 for all reflections (all of these having $F_o^2 \geq -3\sigma(F_o^2)$). Weighted R -factors wR_2 and all goodnesses of fit S are based on F_o^2 ; conventional R -factors R_1 are based on F_o , with F_o set to zero for negative F_o^2 . The observed criterion of $F_o^2 > 2\sigma(F_o^2)$ is used only for calculating R_1 , and is not relevant to the choice of reflections for refinement. R -factors based on F_o^2 are statistically about twice as large as those based on F_o , and R -factors based on ALL data will be even larger.

^eNo absorption correction was applied due to the small crystal size and low value of the linear absorption coefficient (μ).

^f $S = [\sum w(F_o^2 - F_c^2)^2 / (n - p)]^{1/2}$ (n = number of data; p = number of parameters varied; $w = [\sigma^2(F_o^2) + (0.466P)^2]^{-1}$ where $P = [\text{Max}(F_o^2, 0) + 2F_c^2]/3$).

^g $R_1 = \sum ||F_o| - |F_c|| / \sum |F_o|$; $wR_2 = [\sum w(F_o^2 - F_c^2)^2 / \sum w(F_o^4)]^{1/2}$.

Table 2. Atomic Coordinates and Equivalent Isotropic Displacement Parameters*(a) atoms of [C(C₆H₄-2-OH)(C₆H₄-2-O-)]₂*

Atom	x	y	z	<i>U</i> _{eq} , Å ²
O1	0.7918(3)	0.4140(3)	0.32005(17)	0.0399(7)*
O2	0.4160(3)	0.6025(3)	0.29920(18)	0.0446(8)*
O3	0.7960(3)	0.1758(3)	0.16455(17)	0.0410(8)*
O4	0.7040(5)	0.7094(4)	0.3249(2)	0.0674(10)*
C1	0.6852(5)	0.3206(4)	0.2198(3)	0.0351(11)*
C2	0.8118(5)	0.3958(4)	0.2299(2)	0.0300(10)*
C11	0.6270(5)	0.2845(5)	0.3084(3)	0.0345(10)*
C12	0.6936(5)	0.3370(5)	0.3604(3)	0.0385(11)*
C13	0.6595(6)	0.3226(5)	0.4452(3)	0.0502(13)*
C14	0.5582(6)	0.2454(6)	0.4765(3)	0.0586(14)*
C15	0.4904(6)	0.1903(6)	0.4249(3)	0.0639(15)*
C16	0.5232(5)	0.2094(5)	0.3405(3)	0.0503(13)*
C21	0.5371(5)	0.4136(5)	0.1823(3)	0.0335(10)*
C22	0.4024(5)	0.5516(5)	0.2257(3)	0.0369(11)*
C23	0.2627(5)	0.6344(5)	0.1949(3)	0.0425(12)*
C24	0.2560(5)	0.5785(5)	0.1204(3)	0.0469(13)*
C25	0.3895(6)	0.4433(5)	0.0755(3)	0.0474(12)*
C26	0.5293(5)	0.3615(5)	0.1069(3)	0.0415(11)*
C31	0.9864(5)	0.2663(4)	0.1877(2)	0.0308(10)*
C32	0.9656(5)	0.1471(5)	0.1545(3)	0.0391(11)*
C33	1.1041(5)	0.0120(5)	0.1110(3)	0.0471(12)*
C34	1.2684(6)	0.0007(5)	0.1037(3)	0.0563(14)*
C35	1.2944(5)	0.1185(5)	0.1370(3)	0.0519(13)*
C36	1.1521(5)	0.2531(5)	0.1792(3)	0.0418(12)*
C41	0.7864(4)	0.5502(5)	0.1942(3)	0.0300(10)*
C42	0.7442(5)	0.6884(5)	0.2397(3)	0.0370(11)*
C43	0.7356(5)	0.8204(5)	0.2007(3)	0.0453(12)*
C44	0.7666(5)	0.8168(5)	0.1155(3)	0.0482(13)*
C45	0.8057(5)	0.6829(5)	0.0675(3)	0.0396(11)*
C46	0.8178(5)	0.5485(5)	0.1061(3)	0.0368(11)*

(b) solvent diethyl ether atoms

Atom	x	y	z	<i>U</i> _{eq} , Å ²
O1S	0.1080(4)	0.8266(4)	0.38901(18)	0.0547(9)*
C1S	0.0678(7)	0.9846(6)	0.3719(4)	0.0840(19)*
C2S	0.2230(8)	1.0116(6)	0.3526(3)	0.0922(19)*
C3S	-0.0383(7)	0.7913(9)	0.4094(4)	0.104(2)*
C4S	0.0152(8)	0.6288(9)	0.4244(5)	0.149(4)*

Anisotropically-refined atoms are marked with an asterisk (*). The form of the

anisotropic displacement parameter is: $\exp[-2\pi^2(h^2a^2U_{11} + k^2b^2U_{22} + l^2c^2U_{33} + 2klb*c*U_{23} + 2hla*c*U_{13} + 2hka*b*U_{12})]$.

Table 3. Selected Interatomic Distances (Å)

(a) within $[C(C_6H_4-2-OH)(C_6H_4-2-O)]_2$

Atom1	Atom2	Distance	Atom1	Atom2	Distance
O1	C2	1.465(4)	C21	C22	1.392(5)
O1	C12	1.397(4)	C21	C26	1.385(5)
O1	H4	1.86 [†]	C22	C23	1.382(5)
O2	C22	1.375(4)	C23	C24	1.382(5)
O3	C1	1.466(4)	C24	C25	1.381(5)
O3	C32	1.369(4)	C25	C26	1.387(5)
O4	C42	1.360(4)	C31	C32	1.374(5)
C1	C2	1.605(5)	C31	C36	1.385(5)
C1	C11	1.509(5)	C32	C33	1.388(5)
C1	C21	1.524(5)	C33	C34	1.382(5)
C2	C31	1.504(5)	C34	C35	1.390(6)
C2	C41	1.527(5)	C35	C36	1.391(5)
C11	C12	1.370(5)	C41	C42	1.388(5)
C11	C16	1.385(5)	C41	C46	1.414(5)
C12	C13	1.376(5)	C42	C43	1.387(5)
C13	C14	1.382(6)	C43	C44	1.367(6)
C14	C15	1.387(6)	C44	C45	1.382(5)
C15	C16	1.378(6)	C45	C46	1.398(5)

(b) within the solvent diethyl ether molecule

Atom1	Atom2	Distance	Atom1	Atom2	Distance
O1S	C1S	1.438(6)	C1S	C2S	1.454(7)
O1S	C3S	1.425(5)	C3S	C4S	1.457(8)
O1S	H2	1.86 [†]			

[†]Nonbonded distance.

Table 4. Selected Interatomic Angles (deg)*(a) within [C(C₆H₄-2-OH)(C₆H₄-2-O)]₂*

Atom1	Atom2	Atom3	Angle	Atom1	Atom2	Atom3	Angle
C2	O1	C12	107.8(3)	O2	C22	C21	117.2(4)
C1	O3	C32	108.0(3)	O2	C22	C23	121.8(4)
O3	C1	C2	106.0(3)	C21	C22	C23	120.9(4)
O3	C1	C11	109.8(3)	C22	C23	C24	119.4(4)
O3	C1	C21	107.0(3)	C23	C24	C25	120.7(4)
C2	C1	C11	101.0(3)	C24	C25	C26	119.3(4)
C2	C1	C21	118.3(3)	C21	C26	C25	121.0(4)
C11	C1	C21	114.3(3)	C2	C31	C32	110.0(3)
O1	C2	C1	106.4(3)	C2	C31	C36	130.4(4)
O1	C2	C31	109.3(3)	C32	C31	C36	119.6(4)
O1	C2	C41	109.2(3)	O3	C32	C31	114.2(4)
C1	C2	C31	100.8(3)	O3	C32	C33	122.7(4)
C1	C2	C41	117.8(3)	C31	C32	C33	123.1(4)
C31	C2	C41	112.7(3)	C32	C33	C34	116.3(4)
C1	C11	C12	110.4(4)	C33	C34	C35	122.1(4)
C1	C11	C16	129.8(4)	C34	C35	C36	119.8(4)
C12	C11	C16	119.8(4)	C31	C36	C35	119.0(4)
O1	C12	C11	113.5(4)	C2	C41	C42	126.0(4)
O1	C12	C13	123.1(4)	C2	C41	C46	116.3(4)
C11	C12	C13	123.2(4)	C42	C41	C46	117.7(4)
C12	C13	C14	116.6(5)	O4	C42	C41	124.4(4)
C13	C14	C15	121.1(5)	O4	C42	C43	113.9(4)
C14	C15	C16	121.1(5)	C41	C42	C43	121.7(4)
C11	C16	C15	118.1(5)	C42	C43	C44	119.9(4)
C1	C21	C22	119.8(4)	C43	C44	C45	120.6(4)
C1	C21	C26	121.6(4)	C44	C45	C46	119.9(4)
C22	C21	C26	118.6(4)	C41	C46	C45	120.2(4)

(b) within the solvent diethyl ether molecule

Atom1	Atom2	Atom3	Angle
C1S	O1S	C3S	114.1(5)
O1S	C1S	C2S	110.7(4)
O1S	C3S	C4S	110.2(5)

List of Tables

Table 1. Crystallographic Experimental Details

Table 2. Atomic Coordinates and Equivalent Isotropic Displacement Parameters

Table 3. Selected Interatomic Distances

Table 4. Selected Interatomic Angles

Table 5. Selected Torsional Angles

Table 6. Least-Squares Planes

Table 1. Crystallographic Experimental Details

A. Crystal Data

formula	$C_{50}H_{64}Br_2Mg_3O_7$
formula weight	1009.76
crystal dimensions (mm)	$0.29 \times 0.18 \times 0.14$
crystal system	monoclinic
space group	$C2/c$ (No. 15)
unit cell parameters ^a	
<i>a</i> (Å)	13.3765 (16)
<i>b</i> (Å)	15.579 (2)
<i>c</i> (Å)	25.739 (3)
β (deg)	94.384 (2)
<i>V</i> (Å ³)	5348.1 (12)
<i>Z</i>	4
ρ_{calcd} (g cm ⁻³)	1.254
μ (mm ⁻¹)	1.596

B. Data Collection and Refinement Conditions

diffractometer	Bruker P4/RA/SMART 1000 CCD ^b
radiation (λ [Å])	graphite-monochromated Mo K α (0.71073)
temperature (°C)	-80
scan type	ϕ rotations (0.3°) / ω scans (0.3°) (30 s exposures)
data collection 2θ limit (deg)	52.90
total data collected	13093 ($-7 \leq h \leq 16, -19 \leq k \leq 16, -32 \leq l \leq 31$)
independent reflections	5477
number of observations (<i>NO</i>)	2768 [$F_o^2 \geq 2\sigma(F_o^2)$]

structure solution method	direct methods (<i>SHELXS-86</i> ^c)
refinement method	full-matrix least-squares on F^2 (<i>SHELXL-93</i> ^d)
absorption correction method	<i>SADABS</i>
range of transmission factors	0.8310–0.4880
data/restraints/parameters	5477 [$F_o^2 \geq -3\sigma(F_o^2)$] / 4 ^e / 328
extinction coefficient (x) ^f	0.0023 (6)
goodness-of-fit (S) ^g	1.045 [$F_o^2 \geq -3\sigma(F_o^2)$]
final R indices ^h	
R_1 [$F_o^2 \geq 2\sigma(F_o^2)$]	0.0959
wR_2 [$F_o^2 \geq -3\sigma(F_o^2)$]	0.3405
largest difference peak and hole	1.497 and -0.528 e Å ⁻³

^aObtained from least-squares refinement of 4979 centered reflections.

^bPrograms for diffractometer operation, data collection, data reduction and absorption correction were those supplied by Bruker.

^cSheldrick, G. M. *Acta Crystallogr.* **1990**, *A46*, 467–473.

^dSheldrick, G. M. *SHELXL-93*. Program for crystal structure determination. University of Göttingen, Germany, 1993. Refinement on F_o^2 for all reflections (all of these having $F_o^2 \geq -3\sigma(F_o^2)$). Weighted R -factors wR_2 and all goodnesses of fit S are based on F_o^2 ; conventional R -factors R_1 are based on F_o , with F_o set to zero for negative F_o^2 . The observed criterion of $F_o^2 > 2\sigma(F_o^2)$ is used only for calculating R_1 , and is not relevant to the choice of reflections for refinement. R -factors based on F_o^2 are statistically about twice as large as those based on F_o , and R -factors based on ALL data will be even larger.

^eDistances within the disordered n -propyl group were given fixed idealized values: $d(\text{C27-C28A}) = d(\text{C28A-C29A}) = d(\text{C27-C28B}) = d(\text{C28B-C29B}) = 1.54$ Å.

^f $F_c^* = kF_c[1 + x\{0.001F_c^2\lambda^3/\sin(2\theta)\}]^{-1/4}$ where k is the overall scale factor.

^g $S = [\sum w(F_o^2 - F_c^2)^2/(n - p)]^{1/2}$ (n = number of data; p = number of parameters varied; $w = [\sigma^2(F_o^2) + (0.2000P)^2]^{-1}$ where $P = [\text{Max}(F_o^2, 0) + 2F_c^2]/3$).

^h $R_1 = \sum ||F_o| - |F_c||/\sum |F_o|$; $wR_2 = [\sum w(F_o^2 - F_c^2)^2/\sum w(F_o^4)]^{1/2}$.

Table 2. Atomic Coordinates and Equivalent Isotropic Displacement Parameters

Atom	x	y	z	U_{eq} , Å ²
Br	0.02725(8)	-0.58136(6)	0.39561(4)	0.0510(4)*
Mg1	0.0000	-0.4061(2)	0.2500	0.0336(9)*
Mg2	0.0235(2)	-0.4362(2)	0.36156(13)	0.0445(8)*
O1	-0.0862(4)	-0.3966(3)	0.3137(3)	0.0409(15)*
O2	0.1132(4)	-0.3966(4)	0.3079(3)	0.0388(14)*
O3	0.0000	-0.5355(5)	0.2500	0.041(2)*
O4	0.0430(7)	-0.3655(5)	0.4266(3)	0.073(2)*
C1	0.0046(6)	-0.2462(5)	0.2764(4)	0.039(2)*
C11	-0.0873(7)	-0.2431(6)	0.3076(4)	0.044(2)*
C12	-0.1289(6)	-0.3195(5)	0.3238(4)	0.042(2)*
C13	-0.2134(7)	-0.3167(6)	0.3541(4)	0.045(2)*
C14	-0.2513(7)	-0.2353(6)	0.3644(4)	0.053(3)*
C15	-0.2102(7)	-0.1615(6)	0.3478(4)	0.049(2)*
C16	-0.1289(7)	-0.1646(6)	0.3201(4)	0.046(2)*
C17	-0.2606(8)	-0.3988(7)	0.3715(5)	0.064(3)*
C18	-0.2139(16)	-0.4287(11)	0.4290(8)	0.122(7)*
C19	-0.2438(19)	-0.3747(14)	0.4693(8)	0.150(8)*
C21	0.1057(6)	-0.2427(5)	0.3058(4)	0.042(2)*
C22	0.1569(6)	-0.3193(5)	0.3199(4)	0.042(2)*
C23	0.2517(7)	-0.3158(6)	0.3478(4)	0.049(2)*
C24	0.2924(7)	-0.2365(6)	0.3613(5)	0.052(3)*
C25	0.2439(8)	-0.1611(7)	0.3482(5)	0.058(3)*
C26	0.1498(7)	-0.1644(6)	0.3209(4)	0.048(2)*
C27	0.3108(7)	-0.3988(7)	0.3613(5)	0.069(4)*
C28A ^a	0.3880(10)	-0.4115(10)	0.3203(6)	0.095(7)*
C29A ^a	0.3487(11)	-0.4273(10)	0.2632(6)	0.121(10)*
C28B ^b	0.4106(18)	-0.399(2)	0.3955(14)	0.036(9)
C29B ^b	0.456(3)	-0.483(2)	0.4178(17)	0.040(10)
C31	0.0898(7)	-0.5888(6)	0.2492(4)	0.049(2)*
C32	0.0518(9)	-0.6763(7)	0.2524(8)	0.099(5)*
C41A ^c	0.035(2)	-0.2802(15)	0.4395(8)	0.072(7)*
C42A ^c	0.069(2)	-0.2657(13)	0.4952(9)	0.091(8)*
C43A ^c	0.1535(16)	-0.3343(13)	0.5008(8)	0.086(6)*
C44A ^c	0.1121(14)	-0.4041(10)	0.4744(6)	0.064(4)*
C41B ^d	0.055(4)	-0.258(3)	0.4226(15)	0.050(12)*
C42B ^d	0.022(5)	-0.228(3)	0.474(2)	0.090(19)*
C43B ^d	-0.049(4)	-0.287(3)	0.4866(19)	0.094(17)*
C44B ^d	-0.032(3)	-0.3738(19)	0.4583(13)	0.050(8)*

Anisotropically-refined atoms are marked with an asterisk (*). The form of the anisotropic displacement parameter is: $\exp[-2\pi^2(h^2a^{*2}U_{11} + k^2b^{*2}U_{22} + l^2c^{*2}U_{33} + 2klb^{*c^{*}}U_{23} + 2hla^{*c^{*}}U_{13} + 2hka^{*b^{*}}U_{12})]$. ^aRefined with an occupancy factor of 0.8.

^bRefined with an occupancy factor of 0.2. ^cRefined with an occupancy factor of 0.7.
^dRefined with an occupancy factor of 0.3.

Table 3. Selected Interatomic Distances (Å)

Atom1	Atom2	Distance	Atom1	Atom2	Distance
Br	Mg2	2.424(3)	C14	C15	1.357(14)
Mg1	O1	2.081(6)	C15	C16	1.346(13)
Mg1	O2	2.047(6)	C17	C18	1.63(2)
Mg1	O3	2.015(8)	C18	C19	1.42(2)
Mg1	C1	2.581(8)	C21	C22	1.410(12)
Mg2	O1	1.942(7)	C21	C26	1.399(12)
Mg2	O2	1.996(7)	C22	C23	1.410(12)
Mg2	O4	2.005(8)	C23	C24	1.384(13)
O1	C12	1.364(10)	C23	C27	1.541(14)
O2	C22	1.364(9)	C24	C25	1.372(15)
O3	C31	1.462(9)	C25	C26	1.395(14)
O4	C41A	1.37(3)	C27	C28A	1.54 [†]
O4	C44A	1.599(19)	C27	C28B	1.54 [†]
O4	C41B	1.68(4)	C28A	C29A	1.54 [†]
O4	C44B	1.34(3)	C28B	C29B	1.54 [†]
C1	C1'	1.355(19)	C31	C32	1.459(14)
C1	C11	1.519(13)	C32	C32'	1.38(2)
C1	C21	1.499(12)	C41A	C42A	1.49(3)
C11	C12	1.392(13)	C42A	C43A	1.55(3)
C11	C16	1.390(12)	C43A	C44A	1.38(3)
C12	C13	1.422(13)	C41B	C42B	1.50(6)
C13	C14	1.398(12)	C42B	C43B	1.38(7)
C13	C17	1.510(14)	C43B	C44B	1.56(5)

Primed atoms are related to unprimed ones via the crystallographic twofold axis (0, y, 1/4).

[†]Distance fixed during refinement.

Table 4. Selected Interatomic Angles (deg)

Atom1	Atom2	Atom3	Angle	Atom1	Atom2	Atom3	Angle
O1	Mg1	O1'	171.8(4)	C1	C11	C16	120.3(8)
O1	Mg1	O2	81.1(2)	C12	C11	C16	120.4(8)
O1	Mg1	O2'	98.3(2)	O1	C12	C11	120.9(8)
O1	Mg1	O3	94.08(18)	O1	C12	C13	119.6(8)
O1	Mg1	C1	74.2(3)	C11	C12	C13	119.4(8)
O1	Mg1	C1'	97.8(3)	C12	C13	C14	116.5(9)
O2	Mg1	O2'	171.7(4)	C12	C13	C17	120.3(8)
O2	Mg1	O3	94.14(18)	C14	C13	C17	123.1(9)
O2	Mg1	C1	74.8(3)	C13	C14	C15	123.2(9)
O2	Mg1	C1'	97.1(3)	C14	C15	C16	120.0(8)
O3	Mg1	C1	164.8(2)	C11	C16	C15	120.5(9)
O3	Mg1	C1'	164.8(2)	C13	C17	C18	111.8(11)
C1	Mg1	C1'	30.4(4)	C17	C18	C19	112.6(16)
Br	Mg2	O1	121.3(2)	C1	C21	C22	120.1(7)
Br	Mg2	O2	122.8(2)	C1	C21	C26	121.2(8)
Br	Mg2	O4	102.3(3)	C22	C21	C26	118.7(8)
O1	Mg2	O2	85.9(3)	O2	C22	C21	119.8(7)
O1	Mg2	O4	113.5(4)	O2	C22	C23	120.2(8)
O2	Mg2	O4	111.2(3)	C21	C22	C23	120.0(8)
Mg1	O1	Mg2	92.3(2)	C22	C23	C24	118.9(9)
Mg1	O1	C12	118.6(5)	C22	C23	C27	120.5(8)
Mg2	O1	C12	117.8(6)	C24	C23	C27	120.5(8)
Mg1	O2	Mg2	91.8(2)	C23	C24	C25	122.3(9)
Mg1	O2	C22	120.6(6)	C24	C25	C26	118.9(9)
Mg2	O2	C22	112.7(6)	C21	C26	C25	121.2(9)
Mg1	O3	C31	124.7(5)	C23	C27	C28A	108.3(10)
C31	O3	C31'	110.7(9)	C23	C27	C28B	122.4(15)
Mg2	O4	C41A	136.4(11)	C27	C28A	C29A	118.3(12)
Mg2	O4	C44A	117.8(8)	C27	C28B	C29B	121(3)
Mg2	O4	C41B	120.1(14)	O3	C31	C32	104.0(8)
Mg2	O4	C44B	113.5(14)	C31	C32	C32'	110.2(6)
C41A	O4	C44A	103.2(13)	O4	C41A	C42A	110.8(18)
C41B	O4	C44B	102(2)	C41A	C42A	C43A	98.8(19)
Mg1	C1	C1'	74.8(2)	C42A	C43A	C44A	103.7(17)
Mg1	C1	C11	99.6(5)	O4	C44A	C43A	105.7(14)
Mg1	C1	C21	99.8(5)	O4	C41B	C42B	103(3)
C1'	C1	C11	121.0(10)	C41B	C42B	C43B	104(4)
C1'	C1	C21	121.0(10)	C42B	C43B	C44B	110(3)
C11	C1	C21	117.9(8)	O4	C44B	C43B	110(3)
C1	C11	C12	119.3(7)				

Primed atoms are related to unprimed ones via the crystallographic twofold axis (0, y, 1/4).

Table 5. Selected Torsional Angles (deg)

Atom1	Atom2	Atom3	Atom4	Angle	Atom1	Atom2	Atom3	Atom4	Angle
Br	Mg2	O1	Mg1	-103.6(2)	C1'	C1	C11	C16	-87.3(9)
Br	Mg2	O1	C12	132.2(5)	C21	C1	C11	C12	-91.3(10)
Br	Mg2	O2	Mg1	101.9(3)	C21	C1	C11	C16	88.2(11)
Br	Mg2	O2	C22	-133.7(5)	C1'	C1	C21	C22	-90.4(9)
O1	Mg2	O2	Mg1	-23.1(3)	C1'	C1	C21	C26	91.3(9)
O1	Mg2	O2	C22	101.4(6)	C11	C1	C21	C22	94.1(10)
O4	Mg2	O2	Mg1	-136.7(4)	C11	C1	C21	C26	-84.2(11)
C11	C1	C1'	C21'	0.3(5)	C1	C11	C12	O1	2.4(14)
C12	C1	C1'	C21'	33.5(5)	C1	C11	C12	C13	178.4(9)
C1'	C1	C11	C12	93.2(9)	C1	C21	C22	O2	-1.6(14)

Primed atoms are related to unprimed ones via the crystallographic twofold axis (0, y, 1/4)

Table 6. Least-Squares Planes

Plane	Coefficients ^a		Defining Atoms with Deviations (Å) ^b	
1	0.0	-15.579(2)	0.0	6.179(4)
			O1	-0.002(4)
			O1'	-0.002(4)
			O2	0.002(4)
			O2'	0.002(4)
			<u>Mg1</u>	0.148(5)
			<u>C1</u>	-2.343(9)

A-4: Complex 28. $[C_{38}H_{40}O_4]\{Mg(thf)\}\{MgMe(thf)\}_2$

– Chapter 3 –

XCL Code: JMS0045

Date: 13 February 2001

Compound: $[C_2\{C_6H_3(3\text{-}^n\text{Pr})(2\text{-}O\text{-})\}_4]\{Mg(OC_4H_8)\}\{Mg(CH_3)(OC_4H_8)\}_2$

Formula: $C_{52}H_{70}Mg_3O_7$

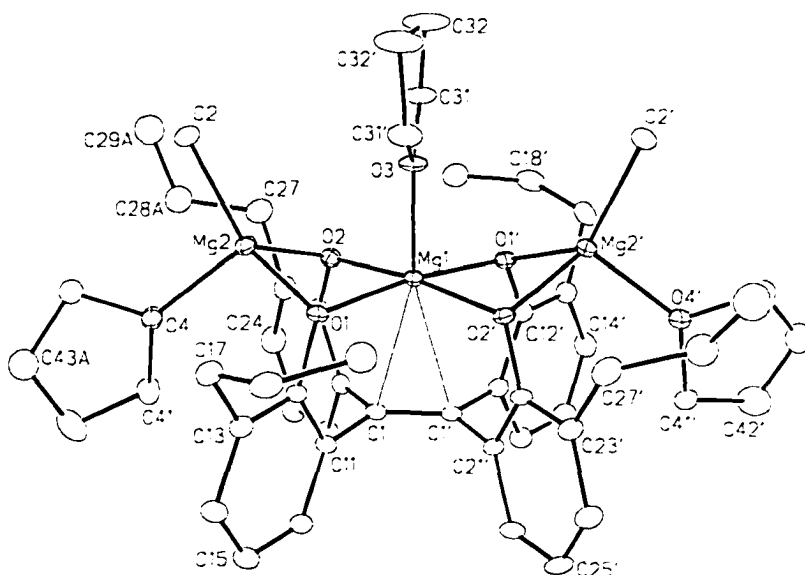


Figure 1. Perspective view of the $[(C_2\{C_6H_3(iPr)O\}_4)\{Mg(OC_4H_8)\}\{MgMe(OC_4H_8)\}_2]$ molecule showing the atom labelling scheme. Non-hydrogen atoms are represented by Gaussian ellipsoids at the 20% probability level. Hydrogen atoms are not shown. Primed atoms are related to unprimed ones via the crystallographic twofold rotational axis $(0, 0, z)$, upon which the Mg1–O3 bond is situated.

List of Tables

- Table 1.** Crystallographic Experimental Details
- Table 2.** Atomic Coordinates and Equivalent Isotropic Displacement Parameters
- Table 3.** Selected Interatomic Distances
- Table 4.** Selected Interatomic Angles
- Table 5.** Selected Torsional Angles
- Table 6.** Least-Squares Planes

Table 1. Crystallographic Experimental Details

A. Crystal Data

<i>formula</i>	<i>C52H70Mg3O7</i>
<i>formula weight</i>	<i>880.01</i>
<i>crystal dimensions (mm)</i>	<i>0.44 _ 0.34 _ 0.31</i>
<i>crystal system</i>	<i>orthorhombic</i>
<i>space group</i>	<i>Fdd2 (No. 43)</i>
<i>unit cell parametersa</i>	
<i>a (Å)</i>	<i>48.907 (6)</i>
<i>b (Å)</i>	<i>12.7642 (15)</i>
<i>c (Å)</i>	<i>15.6366 (18)</i>
<i>V (Å³)</i>	<i>9761 (2)</i>
<i>Z</i>	<i>8</i>
<i>_calcd (g cm⁻³)</i>	<i>1.198</i>
<i>μ (mm⁻¹)</i>	<i>0.112</i>

B. Data Collection and Refinement Conditions

<i>diffractometer</i>	<i>Bruker PLATFORM/SMART 1000 CCDb</i>
<i>radiation (λ [Å])</i>	<i>graphite-monochromated Mo Kα (0.71073)</i>
<i>temperature (°C)</i>	<i>-80</i>
<i>scan type</i>	<i>ω scans (0.2°) (20 s exposures)</i>
<i>data collection 2θ limit (deg)</i>	<i>52.92</i>
<i>total data collected</i>	<i>15670 (-46 ≤ h ≤ 61, -15 ≤ k ≤ 15, -19 ≤ l ≤ 19)</i>
<i>independent reflections</i>	<i>5005</i>
<i>number of observed reflections (NO)</i>	<i>4015 [F_o² ≥ 2σ(F_o²)]</i>
<i>structure solution method</i>	<i>direct methods (SHELXS-86^c)</i>
<i>refinement method</i>	<i>full-matrix least-squares on F² (SHELXL-93^d)</i>

absorption correction method	SADABS
range of transmission factors	0.9662–0.9525
data/restraints/parameters	5005 [$F_o^2 \geq -3\sigma(F_o^2)$] / 0 / 279
Flack absolute structure parameter ^e	–0.2 (3)
goodness-of-fit (S) ^f	1.000 [$F_o^2 \geq -3\sigma(F_o^2)$]
final R indices ^g	
R_1 [$F_o^2 \geq 2\sigma(F_o^2)$]	0.0569
wR_2 [$F_o^2 \geq -3\sigma(F_o^2)$]	0.1487
largest difference peak and hole	0.400 and –0.605 e Å ^{–3}

^aObtained from least-squares refinement of 7006 centered reflections.

^bPrograms for diffractometer operation, data collection, data reduction and absorption correction were those supplied by Bruker.

^cSheldrick, G. M. *Acta Crystallogr.* **1990**, *A46*, 467–473.

^dSheldrick, G. M. *SHELXL-93*. Program for crystal structure determination. University of Göttingen, Germany, 1993. Refinement on F_o^2 for all reflections (all of these having $F_o^2 \geq -3\sigma(F_o^2)$). Weighted R -factors wR_2 and all goodnesses of fit S are based on F_o^2 ; conventional R -factors R_1 are based on F_o , with F_o set to zero for negative F_o^2 . The observed criterion of $F_o^2 > 2\sigma(F_o^2)$ is used only for calculating R_1 , and is not relevant to the choice of reflections for refinement. R -factors based on F_o^2 are statistically about twice as large as those based on F_o , and R -factors based on ALL data will be even larger.

^eFlack, H. D. *Acta Crystallogr.* **1983**, *A39*, 876–881. The Flack parameter will refine to a value near zero if the structure is in the correct configuration and will refine to a value near one for the inverted configuration.

^f $S = [\sum w(F_o^2 - F_c^2)^2 / (n - p)]^{1/2}$ (n = number of data; p = number of parameters varied; $w = [\sigma^2(F_o^2) + (0.0960P)^2]^{-1}$ where $P = [\text{Max}(F_o^2, 0) + 2F_c^2] / 3$).

^g $R_1 = \sum ||F_o| - |F_c|| / \sum |F_o|$; $wR_2 = [\sum w(F_o^2 - F_c^2)^2 / \sum w(F_o^4)]^{1/2}$.

Table 2. Atomic Coordinates and Equivalent Isotropic Displacement Parameters

Atom	x	y	z	U_{eq} , Å ²
Mg1	0.0000	0.0000	0.16436(7)	0.0277(3)*
Mg2	0.059009(17)	0.00706(7)	0.19896(6)	0.0334(2)*
O1	0.03082(3)	0.10811(13)	0.15469(10)	0.0304(4)*
O2	0.03312(3)	-0.10058(13)	0.15522(10)	0.0308(4)*
O3	0.0000	0.0000	0.29324(16)	0.0390(7)*
O4	0.09180(4)	0.01600(16)	0.11732(13)	0.0422(5)*
C1	0.01377(6)	0.0004(2)	0.00487(16)	0.0344(6)*
C2	0.07717(7)	0.0073(2)	0.3215(2)	0.0456(7)*
C11	0.02915(5)	0.1015(2)	0.00175(17)	0.0356(6)*
C12	0.03691(5)	0.1526(2)	0.07825(17)	0.0325(5)*
C13	0.05157(6)	0.2459(2)	0.0740(2)	0.0382(6)*
C14	0.05924(6)	0.2856(3)	-0.0055(2)	0.0466(7)*
C15	0.05210(7)	0.2339(3)	-0.0799(2)	0.0507(8)*
C16	0.03689(6)	0.1446(3)	-0.07629(17)	0.0443(7)*
C17	0.05791(6)	0.3080(2)	0.1541(2)	0.0448(7)*
C18	0.03679(7)	0.3930(2)	0.1724(2)	0.0500(8)*
C19	0.00859(7)	0.3506(3)	0.1892(2)	0.0541(8)*
C21	0.02993(5)	-0.0977(2)	0.00283(17)	0.0359(6)*
C22	0.03942(5)	-0.1450(2)	0.07863(17)	0.0345(6)*
C23	0.05558(6)	-0.2354(2)	0.0758(2)	0.0413(7)*
C24	0.06216(7)	-0.2761(3)	-0.0043(2)	0.0542(9)*
C25	0.05286(7)	-0.2317(3)	-0.0787(2)	0.0562(9)*
C26	0.03707(6)	-0.1431(3)	-0.07596(18)	0.0485(7)*
C27	0.06646(7)	-0.2841(3)	0.1571(2)	0.0542(8)*
C28A ^a	0.09566(13)	-0.2663(5)	0.1758(4)	0.0594(15)
C29A ^a	0.10896(16)	-0.3278(6)	0.2462(5)	0.0750(19)
C28B ^b	0.0910(3)	-0.3450(10)	0.1495(9)	0.092(3)
C29B ^b	0.1017(2)	-0.3801(8)	0.2353(8)	0.072(3)
C31	-0.00046(7)	-0.0925(3)	0.3470(2)	0.0533(8)*
C32	-0.00335(12)	-0.0527(3)	0.4360(2)	0.0946(17)*
C41	0.09500(7)	0.0046(3)	0.0261(2)	0.0605(10)*
C42	0.11962(10)	0.0667(5)	0.0038(3)	0.0990(17)*
C43A ^c	0.13489(18)	0.0780(7)	0.0780(6)	0.067(2)
C44A ^c	0.11988(13)	0.0222(5)	0.1476(4)	0.0413(14)
C43B ^c	0.12773(13)	0.1253(5)	0.0771(5)	0.0457(14)
C44B ^c	0.11537(15)	0.0731(6)	0.1509(5)	0.0546(17)

Anisotropically-refined atoms are marked with an asterisk (*). The form of the anisotropic displacement parameter is: $\exp[-2\pi^2(h^2a^2U_{11} + k^2b^2U_{22} + l^2c^2U_{33} + 2klb^*c^*U_{23} + 2hla^*c^*U_{13} + 2hka^*b^*U_{12})]$. ^aRefined with an occupancy factor of 0.6. ^bRefined with an occupancy factor of 0.4. ^cRefined with an occupancy factor of 0.5.

Table 3. Selected Interatomic Distances (Å)

Atom1	Atom2	Distance	Atom1	Atom2	Distance
Mg1	O1	2.0491(17)	C14	C15	1.382(5)
Mg1	O2	2.0719(16)	C15	C16	1.362(4)
Mg1	O3	2.015(3)	C17	C18	1.525(4)
Mg1	C1	2.583(3)	C18	C19	1.505(5)
Mg2	O1	2.0111(19)	C21	C22	1.409(4)
Mg2	O2	1.989(2)	C21	C26	1.406(4)
Mg2	O4	2.053(2)	C22	C23	1.399(4)
Mg2	C2	2.112(3)	C23	C24	1.394(4)
O1	C12	1.356(3)	C23	C27	1.511(5)
O2	C22	1.360(3)	C24	C25	1.371(5)
O3	C31	1.449(3)	C25	C26	1.370(5)
O4	C41	1.442(4)	C27	C28A	1.475(7)
O4	C44A	1.455(7)	C27	C28B	1.436(13)
O4	C44B	1.462(7)	C28A	C29A	1.501(9)
C1	C1'	1.347(5)	C28B	C29B	1.507(17)
C1	C11	1.495(4)	C31	C32	1.488(5)
C1	C21	1.481(4)	C32	C32'	1.384(9)
C11	C12	1.414(4)	C41	C42	1.483(5)
C11	C16	1.391(4)	C42	C43A	1.388(10)
C12	C13	1.392(4)	C42	C43B	1.426(8)
C13	C14	1.394(4)	C43A	C44A	1.492(10)
C13	C17	1.515(4)	C43B	C44B	1.463(10)

Primed atoms are related to unprimed ones via the crystallographic twofold axis (0, 0, z).

Table 4. Selected Interatomic Angles (deg)

Atom1	Atom2	Atom3	Angle	Atom1	Atom2	Atom3	Angle
O1	Mg1	O1'	171.53(11)	C12	C11	C16	119.1(3)
O1	Mg1	O2	80.63(7)	O1	C12	C11	119.6(2)
O1	Mg1	O2'	98.78(7)	O1	C12	C13	120.9(3)
O1	Mg1	O3	94.23(6)	C11	C12	C13	119.5(2)
O1	Mg1	C1	74.68(8)	C12	C13	C14	119.5(3)
O1	Mg1	C1'	96.99(8)	C12	C13	C17	120.9(3)
O2	Mg1	O2'	172.09(11)	C14	C13	C17	119.5(3)
O2	Mg1	O3	93.96(6)	C13	C14	C15	120.6(3)
O2	Mg1	C1	74.38(8)	C14	C15	C16	120.2(3)
O2	Mg1	C1'	97.81(8)	C11	C16	C15	121.0(3)
O3	Mg1	C1	164.89(6)	C13	C17	C18	112.9(2)
C1	Mg1	C1'	30.21(12)	C17	C18	C19	113.4(3)
O1	Mg2	O2	83.59(8)	C1	C21	C22	121.3(2)
O1	Mg2	O4	106.61(8)	C1	C21	C26	120.0(3)
O1	Mg2	C2	126.85(11)	C22	C21	C26	118.6(3)
O2	Mg2	O4	108.77(8)	O2	C22	C21	119.2(2)
O2	Mg2	C2	125.48(10)	O2	C22	C23	119.9(3)
O4	Mg2	C2	103.63(11)	C21	C22	C23	120.9(3)
Mg1	O1	Mg2	92.69(7)	C22	C23	C24	117.8(3)
Mg1	O1	C12	120.57(15)	C22	C23	C27	120.8(3)
Mg2	O1	C12	114.91(15)	C24	C23	C27	121.4(3)
Mg1	O2	Mg2	92.63(7)	C23	C24	C25	122.1(3)
Mg1	O2	C22	119.73(16)	C24	C25	C26	120.1(3)
Mg2	O2	C22	116.50(15)	C21	C26	C25	120.5(3)
Mg1	O3	C31	125.43(16)	C23	C27	C28A	116.4(4)
C31	O3	C31'	109.1(3)	C23	C27	C28B	116.7(6)
Mg2	O4	C41	133.96(18)	C27	C28A	C29A	119.0(5)
Mg2	O4	C44A	122.6(3)	C27	C28B	C29B	112.3(10)
Mg2	O4	C44B	114.9(3)	O3	C31	C32	105.4(3)
C41	O4	C44A	103.0(3)	C31	C32	C32'	108.0(2)
C41	O4	C44B	108.7(4)	O4	C41	C42	105.5(3)
Mg1	C1	C1'	74.89(6)	C41	C42	C43A	107.2(5)
Mg1	C1	C11	99.46(15)	C41	C42	C43B	108.4(4)
Mg1	C1	C21	99.10(16)	C43A	C42	C43B	28.7(4)
C1'	C1	C11	120.7(3)	C42	C43A	C44A	107.2(6)
C1'	C1	C21	121.8(3)	O4	C44A	C43A	104.7(5)
C11	C1	C21	117.4(2)	C42	C43B	C44B	106.3(5)
C1	C11	C12	120.4(2)	O4	C44B	C43B	105.6(5)
C1	C11	C16	120.5(2)				

Primed atoms are related to unprimed ones via the crystallographic twofold axis (0, 0, z).

Table 5. Selected Torsional Angles (deg)

Atom1	Atom2	Atom3	Atom4	Angle	Atom1	Atom2	Atom3	Atom4	Angle
C2	Mg2	O1	Mg1	-105.61(13)	C1'	C1	C11	C12	91.1(2)
C2	Mg2	O1	C12	128.71(19)	C1'	C1	C11	C16	-91.3(3)
O1	Mg2	O2	Mg1	-24.32(8)	C21	C1	C11	C12	-92.4(3)
O1	Mg2	O2	C22	100.97(18)	C21	C1	C11	C16	85.3(3)
O4	Mg2	O2	Mg1	-129.72(9)	C1'	C1	C21	C22	-94.1(2)
O4	Mg2	O2	C22	-4.4(2)	C1'	C1	C21	C26	88.5(3)
C2	Mg2	O2	Mg1	107.06(13)	C11	C1	C21	C22	89.4(3)
C2	Mg2	O2	C22	-127.7(2)	C11	C1	C21	C26	-87.9(3)
C11	C1	C1'	C11'	175.7(3)	C1	C11	C12	O1	1.4(4)
C11	C1	C1'	C21'	-0.72(16)	C1	C11	C12	C13	179.1(2)
C21	C1	C1'	C21'	-177.1(3)	C1	C21	C22	O2	1.3(4)

Primed atoms are related to unprimed ones via the crystallographic twofold axis (0, 0, z).

Table 6. Least-Squares Planes

Plane	Coefficients ^a			Defining Atoms with Deviations (Å) ^b			
1	0.0	0.0	15.6366(18)	2.4229(12)			
				O1	-0.0042(11)	O2	0.0042(11)
				O1'	-0.0042(11)	O2'	0.0042(11)
				<u>Mg1</u>	0.1471(17)	<u>Mg2</u>	0.6881(15)

^aCoefficients are for the form $ax+by+cz = d$ where x , y and z are crystallographic coordinates.

^bUnderlined atoms were not included in the definition of the plane.

**A-5: Co-crystal of 30a and 32. $[\text{C}_{38}\text{H}_{40}\text{O}_4]$ -gem-anti- $\{\text{TiCl}_2(\text{thf})\}_2 /$
 $[\text{C}_{38}\text{H}_{40}\text{O}_4]_2\text{Ti}_2$**

- Chapter 3 -

XCL Code: JMS0020

Date: 5 April 2001

Compound: $[\text{C}_2\{\text{C}_6\text{H}_3(3\text{-}^n\text{Pr})(2\text{-O-})\}_4]$ -gem-anti- $\{\text{TiCl}_2(\text{OC}_4\text{H}_8)\}_2 \cdot 1/2[\text{C}_2\{\text{C}_6\text{H}_3(3\text{-}^n\text{Pr})(2\text{-O-})\}_4]_2\text{Ti}_2$ cocrystallite, hemitoluene solvate

Formula: $\text{C}_{87.5}\text{H}_{100}\text{Cl}_4\text{O}_{10}\text{Ti}_3$ ($\text{C}_{46}\text{H}_{56}\text{Cl}_4\text{O}_6\text{Ti}_2 \cdot 0.5\text{C}_{76}\text{H}_{80}\text{O}_8\text{Ti}_2 \cdot 0.5\text{C}_7\text{H}_8$)

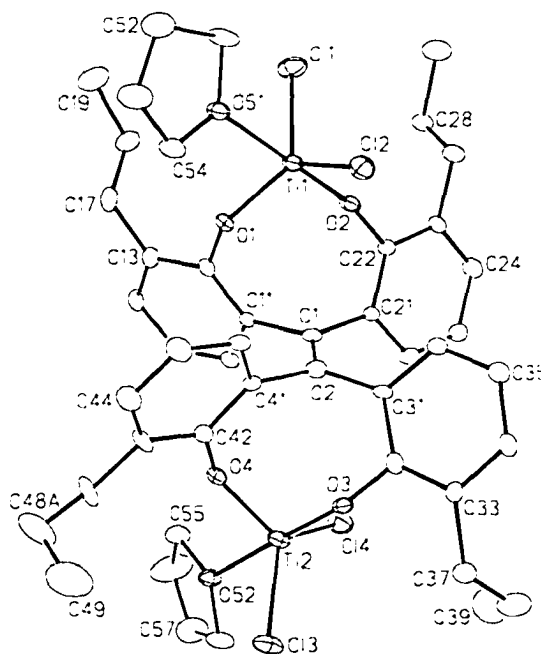


Figure 1. Perspective view of the $[\{\text{C}_2(\text{C}_6\text{H}_3^n\text{Pr}\{\text{O-}\})_4\}\{\text{TiCl}_2(\text{OC}_4\text{H}_8)\}_2]$ molecule showing the atom labelling scheme. Non-hydrogen atoms are represented by Gaussian ellipsoids at the 20% probability level. Hydrogen atoms are not shown.

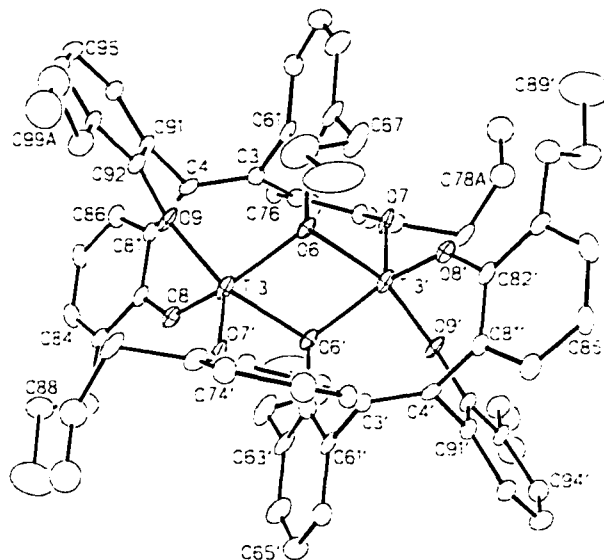


Figure 2. Perspective view of the $[(C_2(C_6H_3^nPr(O^-)))_2Ti_2]$ molecule showing the atom labelling scheme. Primed atoms are related to unprimed ones via the crystallographic inversion center $(0, \frac{1}{2}, \frac{1}{2})$ midway between the Ti3 and Ti3' atoms.

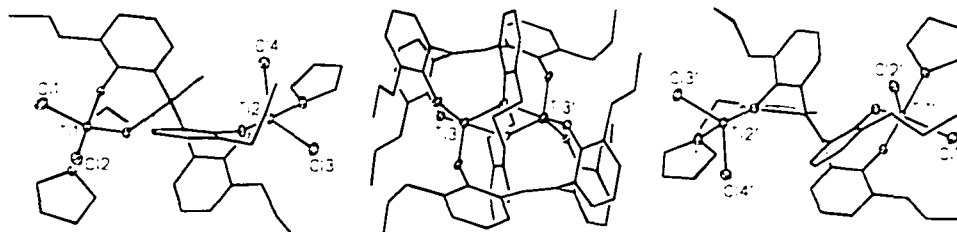


Figure 8. Illustration of the disposition of adjacent $[(C_2(C_6H_3^nPr(O^-)))_4\{TiCl_2(OC_4H_8)\}_2]$ (left and right of diagram) and $[(C_2(C_6H_3^nPr(O^-)))_2Ti_2]$ (center) molecules. The crystallographic asymmetric unit contains one full $[(C_2(C_6H_3^nPr(O^-)))_4\{TiCl_2(OC_4H_8)\}_2]$ molecule and half of a $[(C_2(C_6H_3^nPr(O^-)))_2Ti_2]$ molecule, thus inversion about the $(0, \frac{1}{2}, \frac{1}{2})$ center (as indicated by the primed atoms) generates the full molecules as shown.

List of Tables

Table 1. Crystallographic Experimental Details

Table 2. Atomic Coordinates and Equivalent Isotropic Displacement Parameters

Table 3. Selected Interatomic Distances

Table 4. Selected Interatomic Angles

Table 5. Selected Torsional Angles

Table 1. Crystallographic Experimental Details

A. Crystal Data

formula	$C_{87.5}H_{100}Cl_4O_{10}Ti_3$
formula weight	1597.18
crystal dimensions (mm)	$0.20 \times 0.10 \times 0.07$
crystal system	triclinic
space group	<i>PI</i> (No. 2)
unit cell parameters ^a	
<i>a</i> (Å)	12.1819 (13)
<i>b</i> (Å)	15.6684 (14)
<i>c</i> (Å)	21.641 (2)
α (deg)	88.266 (3)
β (deg)	85.2960 (19)
γ (deg)	87.629 (2)
<i>V</i> (Å ³)	4111.7 (7)
<i>Z</i>	2
ρ_{calcd} (g cm ⁻³)	1.290
μ (mm ⁻¹)	0.471

B. Data Collection and Refinement Conditions

diffractometer	Bruker P4/RA/SMART 1000 CCD ^b
radiation (λ [Å])	graphite-monochromated Mo $K\alpha$ (0.71073)
temperature (°C)	-80
scan type	ϕ rotations (0.3°) / ω scans (0.3°) (30 s exposures)
data collection 2θ limit (deg)	52.94
total data collected	20647 ($-15 \leq h \leq 15$, $-11 \leq k \leq 19$, $-21 \leq l \leq 27$)
independent reflections	16692

number of observed reflections (<i>NO</i>)	4496 [$F_o^2 \geq 2\sigma(F_o^2)$]
structure solution method	direct methods/fragment search (<i>DIRDIF-96</i> ^c)
refinement method	full-matrix least-squares on F^2 (<i>SHELXL-93</i> ^d)
absorption correction method	Gaussian integration (face-indexed)
range of transmission factors	0.9725–0.9118
data/restraints/parameters	16692 [$F_o^2 \geq -3\sigma(F_o^2)$] / 0 / 947
goodness-of-fit (<i>S</i>) ^e	0.777 [$F_o^2 \geq -3\sigma(F_o^2)$]
final <i>R</i> indices ^f	
R_1 [$F_o^2 \geq 2\sigma(F_o^2)$]	0.0732
wR_2 [$F_o^2 \geq -3\sigma(F_o^2)$]	0.1537
largest difference peak and hole	0.432 and $-0.326 \text{ e } \text{\AA}^{-3}$

^aObtained from least-squares refinement of 3750 centered reflections.

^bPrograms for diffractometer operation, data collection, data reduction and absorption correction were those supplied by Bruker.

^cBeurskens, P. T.; Beurskens, G.; Bosman, W. P.; de Gelder, R.; Garcia Granda, S.; Gould, R. O.; Israel, R.; Smits, J. M. M. (1996). The *DIRDIF-96* program system. Crystallography Laboratory, University of Nijmegen, The Netherlands.

^dSheldrick, G. M. *SHELXL-93*. Program for crystal structure determination. University of Göttingen, Germany, 1993. Refinement on F_o^2 for all reflections (all of these having $F_o^2 \geq -3\sigma(F_o^2)$). Weighted *R*-factors wR_2 and all goodnesses of fit *S* are based on F_o^2 ; conventional *R*-factors R_1 are based on F_o , with F_o set to zero for negative F_o^2 . The observed criterion of $F_o^2 > 2\sigma(F_o^2)$ is used only for calculating R_1 , and is not relevant to the choice of reflections for refinement. *R*-factors based on F_o^2 are statistically about twice as large as those based on F_o , and *R*-factors based on ALL data will be even larger.

^e $S = [\sum w(F_o^2 - F_c^2)^2 / (n - p)]^{1/2}$ (n = number of data; p = number of parameters varied; $w = [\sigma^2(F_o^2) + (0.0302P)^2 + \text{FACT}2P]^{-1}$ where $P = [\text{Max}(F_o^2, 0) + 2F_c^2] / 3$).

^f $R_1 = \sum ||F_o| - |F_c|| / \sum |F_o|$; $wR_2 = [\sum w(F_o^2 - F_c^2)^2 / \sum w(F_o^4)]^{1/2}$.

Table 2. Atomic Coordinates and Equivalent Isotropic Displacement Parameters*(a) atoms of $[(C_2(C_6H_3^nPr(O-))_4)\{TiCl_2(OC_4H_8)\}_2]$*

Atom	<i>x</i>	<i>y</i>	<i>z</i>	<i>U</i> _{eq} , Å ²
Ti1	0.47690(11)	-0.30764(7)	0.04330(5)	0.0365(4)*
Ti2	0.16214(11)	0.02039(7)	0.23966(6)	0.0387(4)*
Cl1	0.57356(18)	-0.34105(13)	-0.04668(8)	0.0675(7)*
Cl2	0.36654(17)	-0.40704(11)	0.09134(9)	0.0547(6)*
Cl3	0.08416(17)	0.04504(11)	0.33637(8)	0.0597(7)*
Cl4	0.09152(17)	0.07824(11)	0.15302(8)	0.0579(6)*
O1	0.5204(3)	-0.2224(2)	0.08841(18)	0.0355(12)*
O2	0.3702(4)	-0.2487(2)	0.00907(18)	0.0388(13)*
O3	0.1048(3)	-0.0805(2)	0.23302(18)	0.0370(13)*
O4	0.3057(4)	-0.0147(3)	0.23062(18)	0.0362(12)*
O51	0.6074(4)	-0.3786(3)	0.0872(2)	0.0463(14)*
O52	0.2290(4)	0.1454(3)	0.2454(2)	0.0435(14)*
C1	0.3028(6)	-0.1334(4)	0.0991(3)	0.0304(19)*
C2	0.2620(6)	-0.1604(4)	0.1544(3)	0.0337(19)*
C11	0.4121(6)	-0.0918(4)	0.0910(3)	0.0233(17)*
C12	0.5155(6)	-0.1334(4)	0.0858(3)	0.0320(18)*
C13	0.6144(6)	-0.0912(5)	0.0806(3)	0.0384(19)*
C14	0.6071(6)	-0.0017(4)	0.0767(3)	0.041(2)*
C15	0.5064(7)	0.0411(4)	0.0789(3)	0.042(2)*
C16	0.4083(6)	-0.0019(4)	0.0852(3)	0.0358(19)*
C17	0.7227(6)	-0.1414(5)	0.0745(3)	0.051(2)*
C18	0.7611(6)	-0.1613(4)	0.0082(3)	0.059(2)*
C19	0.8593(6)	-0.2240(5)	0.0036(4)	0.085(3)*
C21	0.2420(5)	-0.1371(4)	0.0416(3)	0.0289(18)*
C22	0.2822(6)	-0.1966(4)	-0.0032(3)	0.0317(19)*
C23	0.2324(6)	-0.2064(4)	-0.0575(3)	0.0335(19)*
C24	0.1420(6)	-0.1530(4)	-0.0691(3)	0.052(2)*
C25	0.1015(6)	-0.0930(4)	-0.0251(3)	0.048(2)*
C26	0.1498(6)	-0.0867(4)	0.0298(3)	0.042(2)*
C27	0.2765(6)	-0.2719(4)	-0.1045(3)	0.049(2)*
C28	0.3567(6)	-0.2393(5)	-0.1547(3)	0.064(3)*
C29	0.4048(7)	-0.3102(5)	-0.1994(4)	0.098(3)*
C31	0.1511(6)	-0.1956(4)	0.1664(3)	0.0277(18)*
C32	0.0729(6)	-0.1553(4)	0.2088(3)	0.0371(19)*
C33	-0.0290(6)	-0.1852(4)	0.2261(3)	0.0345(19)*
C34	-0.0581(6)	-0.2586(4)	0.1972(3)	0.041(2)*
C35	0.0149(6)	-0.2991(4)	0.1537(3)	0.043(2)*
C36	0.1176(6)	-0.2702(4)	0.1392(3)	0.040(2)*
C37	-0.1091(6)	-0.1430(5)	0.2752(3)	0.055(2)*
C38	-0.2087(9)	-0.0982(7)	0.2504(5)	0.119(4)*

Table 2. Atomic Coordinates and Displacement Parameters (continued)

Atom	<i>x</i>	<i>y</i>	<i>z</i>	<i>U</i> _{eq} , Å ²
C39	-0.1872(9)	-0.0188(7)	0.2149(5)	0.136(5)*
C41	0.3322(5)	-0.1642(4)	0.2090(3)	0.0294(18)*
C42	0.3552(6)	-0.0933(4)	0.2428(3)	0.0317(18)*
C43	0.4278(7)	-0.0995(4)	0.2888(3)	0.046(2)*
C44	0.4725(6)	-0.1799(5)	0.3041(3)	0.054(2)*
C45	0.4442(6)	-0.2515(4)	0.2742(3)	0.051(2)*
C46	0.3761(6)	-0.2425(4)	0.2268(3)	0.037(2)*
C47	0.4615(7)	-0.0181(4)	0.3197(4)	0.065(3)*
C48A ^a	0.486(2)	-0.0304(16)	0.3883(11)	0.107(8)*
C48B ^a	0.385(2)	0.0051(12)	0.3718(11)	0.097(8)*
C49	0.3955(12)	-0.0534(7)	0.4307(5)	0.138(5)*
C51	0.6558(8)	-0.4603(4)	0.0685(4)	0.089(4)*
C52	0.7386(8)	-0.4809(5)	0.1140(4)	0.098(4)*
C53	0.7043(8)	-0.4344(5)	0.1697(4)	0.099(4)*
C54	0.6270(7)	-0.3696(5)	0.1521(3)	0.060(3)*
C55	0.3206(7)	0.1734(5)	0.2042(4)	0.063(3)*
C56	0.3039(8)	0.2630(5)	0.1932(5)	0.121(4)*
C57	0.2114(8)	0.2931(5)	0.2302(4)	0.087(3)*
C58	0.1572(7)	0.2200(4)	0.2634(3)	0.061(3)*

(b) atoms of [C₂(C₆H₃ⁿPr(O-))₄]₂Ti₂]

Atom	<i>x</i>	<i>y</i>	<i>z</i>	<i>U</i> _{eq} , Å ²
Ti3	0.04833(12)	0.41869(7)	0.45861(5)	0.0395(4)*
O6	-0.0843(4)	0.4932(2)	0.47478(18)	0.0348(12)*
O7	-0.0585(4)	0.6652(2)	0.48402(18)	0.0400(14)*
O8	0.1847(4)	0.4257(2)	0.41892(19)	0.0366(12)*
O9	-0.0192(4)	0.3654(2)	0.39846(18)	0.0392(13)*
C3	0.0026(6)	0.5802(4)	0.3683(3)	0.0330(18)*
C4	0.0604(6)	0.5177(4)	0.3354(3)	0.0318(18)*
C61	-0.1196(7)	0.5710(4)	0.3810(3)	0.0349(19)*
C62	-0.1577(7)	0.5216(4)	0.4322(3)	0.036(2)*
C63	-0.2690(8)	0.5032(5)	0.4420(3)	0.046(2)*
C64	-0.3408(7)	0.5382(5)	0.4011(4)	0.059(3)*
C65	-0.3054(7)	0.5899(5)	0.3514(4)	0.062(3)*
C66	-0.1922(7)	0.6054(4)	0.3413(3)	0.047(2)*
C67	-0.3151(8)	0.4479(5)	0.4961(4)	0.083(3)*
C68	-0.3038(9)	0.3592(6)	0.4874(4)	0.118(4)*
C69	-0.3613(8)	0.3108(6)	0.5457(5)	0.134(5)*
C71	0.0508(6)	0.6633(4)	0.3851(3)	0.0307(18)*
C72	0.0115(6)	0.7048(4)	0.4403(3)	0.0362(19)*
C73	0.0421(6)	0.7886(4)	0.4513(3)	0.041(2)*
C74	0.1131(6)	0.8274(4)	0.4084(3)	0.045(2)*

Table 2. Atomic Coordinates and Displacement Parameters (continued)

Atom	x	y	z	U_{eq} , Å ²
C75	0.1567(6)	0.7866(4)	0.3557(3)	0.045(2)*
C76	0.1218(6)	0.7064(4)	0.3437(3)	0.039(2)*
C77	-0.0093(7)	0.8356(4)	0.5080(3)	0.053(2)*
C78A ^b	-0.1351(13)	0.8602(9)	0.5038(6)	0.066(4)
C79A ^b	-0.1508(14)	0.9235(9)	0.4568(6)	0.081(5)
C78B ^c	-0.0860(18)	0.9082(14)	0.4865(11)	0.063(6)
C79B ^c	-0.2013(15)	0.8677(13)	0.4602(9)	0.061(6)
C81	0.1818(6)	0.5065(4)	0.3227(3)	0.0322(19)*
C82	0.2389(7)	0.4550(4)	0.3660(3)	0.0341(19)*
C83	0.3518(7)	0.4330(4)	0.3548(3)	0.037(2)*
C84	0.4049(7)	0.4619(4)	0.2999(4)	0.047(2)*
C85	0.3512(7)	0.5104(4)	0.2570(3)	0.046(2)*
C86	0.2422(7)	0.5312(4)	0.2681(3)	0.043(2)*
C87	0.4082(6)	0.3750(4)	0.3997(3)	0.051(2)*
C88	0.3780(8)	0.2797(4)	0.3959(4)	0.079(3)*
C89	0.4296(9)	0.2269(6)	0.4451(5)	0.158(5)*
C91	-0.0037(6)	0.4501(4)	0.3056(3)	0.0325(19)*
C92	-0.0370(6)	0.3777(4)	0.3383(3)	0.038(2)*
C93	-0.0953(6)	0.3141(4)	0.3099(3)	0.036(2)*
C94	-0.1083(6)	0.3270(5)	0.2471(3)	0.048(2)*
C95	-0.0754(6)	0.3989(5)	0.2142(3)	0.048(2)*
C96	-0.0209(6)	0.4616(4)	0.2420(3)	0.040(2)*
C97	-0.1314(6)	0.2366(4)	0.3468(3)	0.049(2)*
C98A ^d	-0.2232(10)	0.1891(7)	0.3226(5)	0.084(4)
C99A ^d	-0.2571(11)	0.1121(7)	0.3653(6)	0.105(5)
C98B ^e	-0.257(4)	0.238(3)	0.363(2)	0.149(19)
C99B ^e	-0.291(4)	0.159(3)	0.401(2)	0.147(19)

(c) solvent toluene atoms

Atom	x	y	z	U_{eq} , Å ²
C10S ^a	0.1310(15)	0.4349(11)	0.0854(8)	0.096(7)
C11S	0.0651(17)	0.4650(19)	0.0439(5)	0.108(6)*
C12S	0.0817(12)	0.5473(15)	0.0203(10)	0.112(6)*
C13S	0.0194(19)	0.5808(8)	-0.0209(11)	0.109(5)*

Anisotropically-refined atoms are marked with an asterisk (*). The form of the anisotropic displacement parameter is: $\exp[-2\pi^2(h^2a^{*2}U_{11} + k^2b^{*2}U_{22} + l^2c^{*2}U_{33} + 2klb^*c^*U_{23} + 2hla^*c^*U_{13} + 2hka^*b^*U_{12})]$. ^aRefined with an occupancy factor of 0.5. ^bRefined with an occupancy factor of 0.6. ^cRefined with an occupancy factor of 0.4. ^dRefined with an occupancy factor of 0.7. ^eRefined with an occupancy factor of 0.3.

Table 3. Selected Interatomic Distances (Å)*(a) within $[(C_2(C_6H_3^nPr(O-))_4)/TiCl_2(OC_4H_8)]_2$*

Atom1	Atom2	Distance	Atom1	Atom2	Distance
Ti1	C11	2.255(2)	C25	C26	1.374(8)
Ti1	C12	2.272(2)	C27	C28	1.493(8)
Ti1	O1	1.800(4)	C28	C29	1.560(8)
Ti1	O2	1.763(4)	C31	C32	1.411(8)
Ti1	O51	2.169(4)	C31	C36	1.415(8)
Ti2	C13	2.264(2)	C32	C33	1.365(8)
Ti2	C14	2.275(2)	C33	C34	1.397(8)
Ti2	O3	1.768(4)	C33	C37	1.529(8)
Ti2	O4	1.809(4)	C34	C35	1.390(8)
Ti2	O52	2.163(4)	C35	C36	1.357(8)
O1	C12	1.393(7)	C37	C38	1.506(11)
O2	C22	1.360(7)	C38	C39	1.464(12)
O3	C32	1.381(7)	C41	C42	1.398(8)
O4	C42	1.376(7)	C41	C46	1.374(8)
O51	C51	1.443(6)	C42	C43	1.383(8)
O51	C54	1.456(7)	C43	C44	1.393(8)
O52	C55	1.444(7)	C43	C47	1.544(8)
O52	C58	1.473(7)	C44	C45	1.383(8)
C1	C2	1.322(8)	C45	C46	1.372(8)
C1	C11	1.502(8)	C47	C48A	1.54(3)
C1	C21	1.503(8)	C47	C48B	1.45(2)
C2	C31	1.480(9)	C48A	C49	1.42(2)
C2	C41	1.513(8)	C48B	C49	1.56(2)
C11	C12	1.392(8)	C51	C52	1.485(9)
C11	C16	1.411(8)	C52	C53	1.451(9)
C12	C13	1.392(9)	C53	C54	1.421(9)
C13	C14	1.402(8)	C55	C56	1.426(9)
C13	C17	1.506(9)	C56	C57	1.401(10)
C14	C15	1.372(9)	C57	C58	1.482(9)
C15	C16	1.392(9)			
C17	C18	1.511(8)			
C18	C19	1.515(8)	C12	H36	2.90†
C21	C22	1.411(7)	C12	H46	3.10†
C21	C26	1.383(8)	C14	H16	3.32†
C22	C23	1.380(8)	C14	H26	2.85†
C23	C24	1.390(8)			
C23	C27	1.518(7)			
C24	C25	1.405(8)			

†Nonbonded distance.

Table 3. Selected Interatomic Distances (continued)*(b) within $[(C_2(C_6H_3^aPr(O^-))_4)_2Ti_2]$*

Atom1	Atom2	Distance	Atom1	Atom2	Distance
Ti3	O6	1.968(4)	C73	C77	1.528(8)
Ti3	O6'	2.110(4)	C74	C75	1.381(8)
Ti3	O7'	1.788(4)	C75	C76	1.381(8)
Ti3	O8	1.813(5)	C77	C78A	1.573(15)
Ti3	O9	1.835(4)	C77	C78B	1.53(2)
O6	C62	1.387(8)	C78A	C79A	1.418(18)
O7	C72	1.373(7)	C78B	C79B	1.71(3)
O8	C82	1.351(7)	C81	C82	1.425(8)
O9	C92	1.343(7)	C81	C86	1.391(8)
C3	C4	1.366(8)	C82	C83	1.408(9)
C3	C61	1.503(9)	C83	C84	1.379(9)
C3	C71	1.517(8)	C83	C87	1.498(8)
C4	C81	1.486(9)	C84	C85	1.372(9)
C4	C91	1.530(8)	C85	C86	1.358(9)
C61	C62	1.391(9)	C87	C88	1.559(9)
C61	C66	1.368(9)	C88	C89	1.493(10)
C62	C63	1.396(9)	C91	C92	1.376(8)
C63	C64	1.382(10)	C91	C96	1.414(8)
C63	C67	1.519(10)	C92	C93	1.429(8)
C64	C65	1.377(10)	C93	C94	1.390(8)
C65	C66	1.408(9)	C93	C97	1.494(8)
C67	C68	1.407(9)	C94	C95	1.370(9)
C68	C69	1.580(11)	C95	C96	1.387(8)
C71	C72	1.416(8)	C97	C98A	1.505(12)
C71	C76	1.376(8)	C97	C98B	1.54(5)
C72	C73	1.412(8)	C98A	C99A	1.546(14)
C73	C74	1.362(8)	C98B	C99B	1.53(5)

Primed atoms are related to unprimed ones via the crystallographic inversion center (0, 1/2, 1/2).

(c) within the solvent toluene molecule

Atom1	Atom2	Distance	Atom1	Atom2	Distance
C10S	C11S	1.316(19)	C11S	C13S''	1.409(17)
C11S	C12S	1.390(16)	C12S	C13S	1.303(15)

Double-primed atoms are related to unprimed ones via the inversion center (0, 1/2, 0).

Table 4. Selected Interatomic Angles (deg)*(a) within $[(C_2(C_6H_3^aPr(O-))_4)(TiCl_2(OC_4H_8))_2]$*

Atom1	Atom2	Atom3	Angle	Atom1	Atom2	Atom3	Angle
C11	Ti1	C12	118.56(9)	C12	C11	C16	117.4(6)
C11	Ti1	O1	119.63(16)	O1	C12	C11	118.0(6)
C11	Ti1	O2	95.85(14)	O1	C12	C13	118.1(6)
C11	Ti1	O51	85.27(13)	C11	C12	C13	123.8(6)
C12	Ti1	O1	118.52(15)	C12	C13	C14	116.9(7)
C12	Ti1	O2	95.66(16)	C12	C13	C17	120.3(7)
C12	Ti1	O51	84.27(14)	C14	C13	C17	122.7(7)
O1	Ti1	O2	96.66(18)	C13	C14	C15	120.7(7)
O1	Ti1	O51	82.30(18)	C14	C15	C16	121.8(7)
O2	Ti1	O51	178.75(17)	C11	C16	C15	119.2(7)
C13	Ti2	C14	122.58(9)	C13	C17	C18	113.2(6)
C13	Ti2	O3	95.84(14)	C17	C18	C19	112.4(7)
C13	Ti2	O4	118.53(15)	C1	C21	C22	117.3(6)
C13	Ti2	O52	84.89(13)	C1	C21	C26	124.8(6)
C14	Ti2	O3	94.70(15)	C22	C21	C26	117.9(6)
C14	Ti2	O4	115.65(15)	O2	C22	C21	118.4(6)
C14	Ti2	O52	83.48(14)	O2	C22	C23	119.1(6)
O3	Ti2	O4	97.52(19)	C21	C22	C23	122.4(6)
O3	Ti2	O52	178.1(2)	C22	C23	C24	118.3(6)
O4	Ti2	O52	83.60(18)	C22	C23	C27	121.2(6)
Ti1	O1	C12	137.1(4)	C24	C23	C27	120.4(6)
Ti1	O2	C22	166.2(4)	C23	C24	C25	119.8(6)
Ti2	O3	C32	162.0(4)	C24	C25	C26	120.8(7)
Ti2	O4	C42	130.3(4)	C21	C26	C25	120.6(6)
Ti1	O51	C51	125.9(4)	C23	C27	C28	115.2(6)
Ti1	O51	C54	122.9(4)	C27	C28	C29	113.2(6)
C51	O51	C54	106.9(5)	C2	C31	C32	119.6(6)
Ti2	O52	C55	122.1(4)	C2	C31	C36	124.1(6)
Ti2	O52	C58	120.9(4)	C32	C31	C36	116.2(6)
C55	O52	C58	109.2(5)	O3	C32	C31	115.7(6)
C2	C1	C11	120.9(6)	O3	C32	C33	119.9(6)
C2	C1	C21	123.3(7)	C31	C32	C33	124.4(6)
C11	C1	C21	115.7(6)	C32	C33	C34	116.8(6)
C1	C2	C31	123.6(7)	C32	C33	C37	123.1(6)
C1	C2	C41	120.7(7)	C34	C33	C37	120.1(7)
C31	C2	C41	115.5(6)	C33	C34	C35	120.9(7)
C1	C11	C12	126.5(6)	C34	C35	C36	121.2(7)
C1	C11	C16	116.1(6)	C31	C36	C35	120.4(6)

Table 4. Selected Interatomic Angles (continued)

Atom1	Atom2	Atom3	Angle				
C33	C37	C38	114.7(6)	C41	C46	C45	122.0(6)
C37	C38	C39	115.4(10)	C43	C47	C48A	114.9(10)
C2	C41	C42	124.3(6)	C43	C47	C48B	111.8(11)
C2	C41	C46	117.9(6)	C47	C48A	C49	116(2)
C42	C41	C46	117.7(6)	C47	C48B	C49	114.1(17)
O4	C42	C41	120.2(6)	O51	C51	C52	104.3(6)
O4	C42	C43	118.2(6)	C51	C52	C53	107.3(7)
C41	C42	C43	121.6(6)	C52	C53	C54	106.3(7)
C42	C43	C44	118.4(6)	O51	C54	C53	109.4(6)
C42	C43	C47	120.0(6)	O52	C55	C56	107.3(6)
C44	C43	C47	121.5(7)	C55	C56	C57	109.6(7)
C43	C44	C45	120.5(7)	C56	C57	C58	109.5(7)
C44	C45	C46	119.5(7)	O52	C58	C57	104.1(6)

(b) within $[(C_2(C_6H_3^nPr(O-))_4)_2Ti_2]$

Atom1	Atom2	Atom3	Angle	Atom1	Atom2	Atom3	Angle
O6	Ti3	O6'	72.9(2)	C62	C61	C66	120.0(8)
O6	Ti3	O7'	112.3(2)	O6	C62	C61	119.2(7)
O6	Ti3	O8	138.02(19)	O6	C62	C63	120.1(8)
O6	Ti3	O9	89.85(19)	C61	C62	C63	120.7(8)
O6'	Ti3	O7'	88.98(17)	C62	C63	C64	118.3(8)
O6'	Ti3	O8	91.89(18)	C62	C63	C67	123.2(9)
O6'	Ti3	O9	162.3(2)	C64	C63	C67	118.5(8)
O7'	Ti3	O8	106.0(2)	C63	C64	C65	121.9(8)
O7'	Ti3	O9	101.55(19)	C64	C65	C66	118.8(8)
O8	Ti3	O9	98.73(19)	C61	C66	C65	120.2(8)
Ti3	O6	Ti3'	107.1(2)	C63	C67	C68	115.3(7)
Ti3	O6	C62	126.9(4)	C67	C68	C69	109.3(8)
Ti3'	O6	C62	116.5(3)	C3	C71	C72	120.4(6)
Ti3'	O7	C72	136.8(4)	C3	C71	C76	121.2(6)
Ti3	O8	C82	142.6(5)	C72	C71	C76	117.8(6)
Ti3	O9	C92	138.5(4)	O7	C72	C71	121.0(6)
C4	C3	C61	117.5(6)	O7	C72	C73	118.3(6)
C4	C3	C71	124.0(7)	C71	C72	C73	120.7(7)
C61	C3	C71	117.9(5)	C72	C73	C74	118.3(6)
C3	C4	C81	128.1(6)	C72	C73	C77	120.1(7)
C3	C4	C91	118.5(6)	C74	C73	C77	121.5(6)
C81	C4	C91	113.3(5)	C73	C74	C75	121.9(7)
C3	C61	C62	118.6(7)	C74	C75	C76	119.3(7)
C3	C61	C66	121.3(7)	C71	C76	C75	121.7(6)

Table 4. Selected Interatomic Angles (continued)

Atom1	Atom2	Atom3	Angle	Atom1	Atom2	Atom3	Angle
C73	C77	C78A	113.0(7)	C87	C88	C89	110.3(7)
C73	C77	C78B	108.9(9)	C4	C91	C92	121.2(6)
C77	C78A	C79A	111.5(14)	C4	C91	C96	117.6(6)
C77	C78B	C79B	110.1(16)	C92	C91	C96	121.0(6)
C4	C81	C82	116.8(7)	O9	C92	C91	121.5(6)
C4	C81	C86	125.7(7)	O9	C92	C93	117.5(6)
C82	C81	C86	116.7(7)	C91	C92	C93	120.9(6)
O8	C82	C81	120.2(7)	C92	C93	C94	116.0(7)
O8	C82	C83	118.6(7)	C92	C93	C97	119.8(6)
C81	C82	C83	121.2(7)	C94	C93	C97	124.0(6)
C82	C83	C84	117.6(7)	C93	C94	C95	123.2(7)
C82	C83	C87	119.9(7)	C94	C95	C96	120.7(7)
C84	C83	C87	122.3(7)	C91	C96	C95	117.8(7)
C83	C84	C85	122.2(8)	C93	C97	C98A	116.3(7)
C84	C85	C86	119.8(7)	C93	C97	C98B	112.4(19)
C81	C86	C85	122.4(7)	C97	C98A	C99A	112.2(9)
C83	C87	C88	113.2(6)	C97	C98B	C99B	111(4)

Primed atoms are related to unprimed ones via the crystallographic inversion center (0, 1/2, 1/2).

(c) within the solvent toluene molecule

Atom1	Atom2	Atom3	Angle	Atom1	Atom2	Atom3	Angle
C10S	C11S	C12S	117(3)	C11S	C12S	C13S	120.4(15)
C10S	C11S	C13S''	125(3)	C11S''	C13S	C12S	121.8(15)
C12S	C11S	C13S''	117.8(12)				

Double-primed atoms are related to unprimed ones via the inversion center (0, 1/2, 0).

Table 5. Selected Torsional Angles (deg)*(a) within $[[C_2(C_6H_3^nPr(O-))_4][TiCl_2(OC_4H_8)]_2]$*

Atom1	Atom2	Atom3	Atom4	Angle	Atom1	Atom2	Atom3	Atom4	Angle
Ti1	O1	C12	C11	63.2(8)	C1	C2	C31	C32	-120.1(7)
Ti1	O1	C12	C13	-119.1(6)	C1	C2	C31	C36	61.9(10)
Ti1	O2	C22	C21	14(2)	C41	C2	C31	C32	65.1(8)
Ti1	O2	C22	C23	-162.8(15)	C41	C2	C31	C36	-112.8(7)
Ti2	O3	C32	C31	41.4(17)	C1	C2	C41	C42	78.2(9)
Ti2	O3	C32	C33	-138.2(12)	C1	C2	C41	C46	-101.8(8)
Ti2	O4	C42	C41	64.5(7)	C31	C2	C41	C42	-106.8(7)
Ti2	O4	C42	C43	-115.6(6)	C31	C2	C41	C46	73.1(8)
C11	C1	C2	C31	175.0(5)	C1	C11	C12	O1	-0.1(9)
C11	C1	C2	C41	-10.5(9)	C1	C11	C12	C13	-177.6(6)
C21	C1	C2	C31	-1.4(10)	C1	C21	C22	O2	2.3(9)
C21	C1	C2	C41	173.1(5)	C1	C21	C22	C23	179.2(6)
C2	C1	C11	C12	82.0(8)	C1	C21	C26	C25	178.1(7)
C2	C1	C11	C16	-101.1(7)	C2	C31	C32	O3	4.6(9)
C21	C1	C11	C12	-101.3(7)	C2	C31	C32	C33	-175.9(7)
C21	C1	C11	C16	75.5(6)	C2	C31	C36	C35	178.7(7)
C2	C1	C21	C22	-109.6(7)	C2	C41	C42	O4	5.7(10)
C2	C1	C21	C26	70.3(9)	C2	C41	C42	C43	-174.2(7)
C11	C1	C21	C22	73.9(7)	C2	C41	C46	C45	177.4(7)
C11	C1	C21	C26	-106.3(8)					

(b) within $[[C_2(C_6H_3^nPr(O-))_4]_2Ti_2]$

Atom1	Atom2	Atom3	Atom4	Angle	Atom1	Atom2	Atom3	Atom4	Angle
O6'	Ti3	O6	Ti3'	0.0	O6'	Ti3	O8	C82	-110.2(6)
O6'	Ti3	O6	C62	144.6(6)	O7'	Ti3	O8	C82	160.3(6)
O7'	Ti3	O6	Ti3'	81.6(2)	O9	Ti3	O8	C82	55.5(6)
O7'	Ti3	O6	C62	-133.8(5)	O6	Ti3	O9	C92	83.0(6)
O8	Ti3	O6	Ti3'	-73.1(3)	O6'	Ti3	O9	C92	70.4(10)
O8	Ti3	O6	C62	71.5(6)	O7'	Ti3	O9	C92	-164.2(6)
O9	Ti3	O6	Ti3'	-176.0(2)	O8	Ti3	O9	C92	-55.7(7)
O9	Ti3	O6	C62	-31.4(5)	Ti3	O6	C62	C61	-60.7(7)
O6	Ti3	O6'	C62'	148.8(6)	Ti3	O6	C62	C63	121.5(6)
O8	Ti3	O6'	C62'	-71.0(5)	Ti3'	O6	C62	C61	81.1(6)
O9	Ti3	O6'	C62'	162.0(6)	Ti3'	O6	C62	C63	-96.7(6)
O6	Ti3	O7'	C72'	19.5(6)	Ti3'	O7	C72	C71	73.9(8)
O8	Ti3	O7'	C72'	-177.8(5)	Ti3'	O7	C72	C73	-107.0(6)
O9	Ti3	O7'	C72'	-75.1(6)	Ti3	O8	C82	C81	7.7(10)
O6	Ti3	O8	C82	-44.1(7)					

Table 5. Selected Torsional Angles (continued)

Atom1	Atom2	Atom3	Atom4	Angle	Atom1	Atom2	Atom3	Atom4	Angle
Ti3	O8	C82	C83	-171.9(4)	C3	C4	C81	C86	-99.1(8)
Ti3	O9	C92	C91	-3.4(11)	C91	C4	C81	C82	-90.6(7)
Ti3	O9	C92	C93	178.7(5)	C91	C4	C81	C86	79.4(8)
C61	C3	C4	C81	-172.7(7)	C3	C4	C91	C92	-86.2(8)
C61	C3	C4	C91	8.8(9)	C3	C4	C91	C96	98.1(7)
C71	C3	C4	C81	15.9(11)	C81	C4	C91	C92	95.1(8)
C71	C3	C4	C91	-162.5(6)	C81	C4	C91	C96	-80.6(8)
C4	C3	C61	C62	84.9(7)	C3	C71	C72	O7	9.7(10)
C4	C3	C61	C66	-90.9(8)	C3	C71	C72	C73	-169.4(6)
C71	C3	C61	C62	-103.2(7)	C3	C71	C76	C75	172.7(6)
C71	C3	C61	C66	81.0(8)	C4	C81	C82	O8	-6.5(8)
C4	C3	C71	C72	-149.5(7)	C4	C81	C82	C83	173.1(6)
C4	C3	C71	C76	39.8(10)	C4	C81	C86	C85	-172.4(6)
C61	C3	C71	C72	39.2(9)	C4	C91	C92	O9	3.2(10)
C61	C3	C71	C76	-131.6(7)	C4	C91	C92	C93	-179.0(6)
C3	C4	C81	C82	90.9(8)	C4	C91	C96	C95	177.6(6)

Primed atoms are related to unprimed ones via the crystallographic inversion center (0, 1/2, 1/2).

A-6: Complex 32. $[\text{C}_{38}\text{H}_{40}\text{O}_4]_2\text{Ti}_2$

– Chapter 3 –

XCL Code: JMS0029

Date: 9 April 2001

Compound: $[\text{C}_2\{\text{C}_6\text{H}_3(3\text{-}^n\text{Pr})(2\text{-O-})\}_4]_2\text{Ti}_2\cdot\text{PhMe}$

Formula: $\text{C}_{83}\text{H}_{88}\text{O}_8\text{Ti}_2$ ($\text{C}_{76}\text{H}_{80}\text{O}_8\text{Ti}_2\cdot\text{C}_7\text{H}_8$)

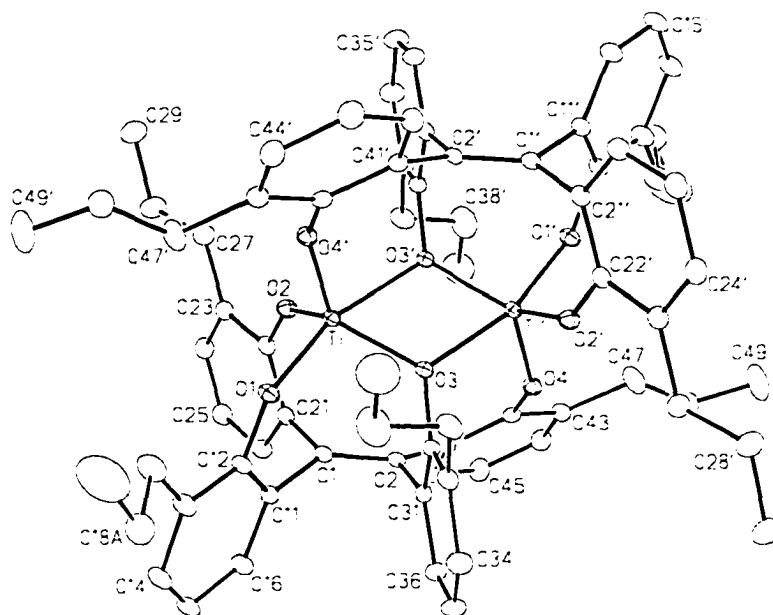


Figure 1. Perspective view of the $[\{\text{C}_2(\text{C}_6\text{H}_3^n\text{Pr}\{\text{O-}\})_4\}_2\text{Ti}_2]$ molecule showing the atom labelling scheme. Non-hydrogen atoms are represented by Gaussian ellipsoids at the 20% probability level. Hydrogen atoms are not shown. Primed atoms are related to unprimed ones via the crystallographic inversion center (0, 0, 0) midway between the Ti and Ti' atoms.

List of Tables

- Table 1.** Crystallographic Experimental Details
- Table 2.** Atomic Coordinates and Equivalent Isotropic Displacement Parameters
- Table 3.** Selected Interatomic Distances
- Table 4.** Selected Interatomic Angles
- Table 5.** Selected Torsional Angles

Table 1. Crystallographic Experimental Details

A. Crystal Data

formula	C ₈₃ H ₈₈ O ₈ Ti ₂
formula weight	1309.33
crystal dimensions (mm)	0.44 × 0.38 × 0.32
crystal system	monoclinic
space group	<i>P</i> 2 ₁ / <i>n</i> (an alternate setting of <i>P</i> 2 ₁ / <i>c</i> [No. 14])
unit cell parameters ^a	
<i>a</i> (Å)	13.5677 (9)
<i>b</i> (Å)	14.6687 (9)
<i>c</i> (Å)	18.2488 (11)
β (deg)	104.2416 (12)
<i>V</i> (Å ³)	3520.3 (4)
<i>Z</i>	2
ρ _{calcd} (g cm ⁻³)	1.235
μ (mm ⁻¹)	0.283

B. Data Collection and Refinement Conditions

diffractometer	Bruker P4/RA/SMART 1000 CCD ^b
radiation (λ [Å])	graphite-monochromated Mo Kα (0.71073)
temperature (°C)	-80
scan type	φ rotations (0.3°) / ω scans (0.3°) (30 s exposures)
data collection 2θ limit (deg)	52.78
total data collected	18162 (-14 ≤ <i>h</i> ≤ 16, -14 ≤ <i>k</i> ≤ 18, -22 ≤ <i>l</i> ≤ 22)
independent reflections	7069
number of observed reflections (<i>NO</i>)	5886 [<i>F</i> _o ² ≥ 2σ(<i>F</i> _o ²)]
structure solution method	direct methods (<i>SHELXS-86</i> ^c)

refinement method	full-matrix least-squares on F^2 (<i>SHELXL-93</i> ^d)
absorption correction method	<i>SADABS</i>
range of transmission factors	0.9148–0.8854
data/restraints/parameters	7069 [$F_o^2 \geq -3\sigma(F_o^2)$] / 0 / 415
goodness-of-fit (S) ^e	1.038 [$F_o^2 \geq -3\sigma(F_o^2)$]
final R indices ^f	
R_1 [$F_o^2 \geq 2\sigma(F_o^2)$]	0.0469
wR_2 [$F_o^2 \geq -3\sigma(F_o^2)$]	0.1370
largest difference peak and hole	0.871 and -0.461 e \AA^{-3}

^aObtained from least-squares refinement of 6150 centered reflections.

^bPrograms for diffractometer operation, data collection, data reduction and absorption correction were those supplied by Bruker.

^cSheldrick, G. M. *Acta Crystallogr.* **1990**, *A46*, 467–473.

^dSheldrick, G. M. *SHELXL-93*. Program for crystal structure determination. University of Göttingen, Germany, 1993. Refinement on F_o^2 for all reflections (all of these having $F_o^2 \geq -3\sigma(F_o^2)$). Weighted R -factors wR_2 and all goodnesses of fit S are based on F_o^2 ; conventional R -factors R_1 are based on F_o , with F_o set to zero for negative F_o^2 . The observed criterion of $F_o^2 > 2\sigma(F_o^2)$ is used only for calculating R_1 , and is not relevant to the choice of reflections for refinement. R -factors based on F_o^2 are statistically about twice as large as those based on F_o , and R -factors based on ALL data will be even larger.

$$^e S = [\sum w(F_o^2 - F_c^2)^2 / (n - p)]^{1/2} \quad (n = \text{number of data}; p = \text{number of parameters varied}; w = [\sigma^2(F_o^2) + (0.0730P)^2 + 2.2511P]^{-1} \text{ where } P = [\text{Max}(F_o^2, 0) + 2F_c^2] / 3).$$

$$^f R_1 = \sum ||F_o| - |F_c|| / \sum |F_o|; wR_2 = [\sum w(F_o^2 - F_c^2)^2 / \sum w(F_o^4)]^{1/2}.$$

Table 2. Atomic Coordinates and Equivalent Isotropic Displacement Parameters*(a) atoms of [(C₂(C₆H₃ⁿPr(O-))₄)₂Ti₂]*

Atom	x	y	z	<i>U</i> _{eq} , Å ²
Ti	0.02741(2)	0.10923(2)	-0.003313(18)	0.02231(11)*
O1	0.14888(10)	0.16717(10)	0.03376(8)	0.0300(3)*
O2	-0.05506(11)	0.18524(10)	0.03325(8)	0.0295(3)*
O3	0.08933(9)	-0.00991(9)	0.02609(7)	0.0238(3)*
O4	-0.00889(11)	-0.12932(10)	0.10339(8)	0.0293(3)*
C1	0.07994(15)	0.13318(14)	0.16791(10)	0.0254(4)*
C2	0.07817(14)	0.04091(14)	0.17156(10)	0.0242(4)*
C11	0.17749(15)	0.18158(14)	0.16720(11)	0.0273(4)*
C12	0.20829(15)	0.19771(14)	0.10094(11)	0.0287(4)*
C13	0.29838(17)	0.24565(17)	0.10155(13)	0.0383(5)*
C14	0.35593(18)	0.27667(19)	0.17112(14)	0.0438(6)*
C15	0.32695(18)	0.26074(17)	0.23737(14)	0.0412(6)*
C16	0.23774(17)	0.21365(16)	0.23549(12)	0.0340(5)*
C17	0.3287(2)	0.2644(2)	0.02863(16)	0.0558(8)*
C18A ^a	0.4430(4)	0.2508(4)	0.0329(3)	0.0613(13)
C18B ^b	0.4291(8)	0.2949(9)	0.0278(6)	0.071(3)
C19	0.4608(4)	0.2721(5)	-0.0454(3)	0.132(2)*
C21	-0.00677(15)	0.19723(14)	0.16786(11)	0.0262(4)*
C22	-0.06825(15)	0.22409(14)	0.09775(11)	0.0263(4)*
C23	-0.14261(16)	0.29243(15)	0.09091(12)	0.0302(4)*
C24	-0.15325(17)	0.33394(15)	0.15728(13)	0.0344(5)*
C25	-0.09294(17)	0.30842(16)	0.22752(13)	0.0360(5)*
C26	-0.01978(16)	0.24125(15)	0.23260(12)	0.0319(5)*
C27	-0.20416(18)	0.31964(17)	0.01305(13)	0.0387(5)*
C28	-0.2689(2)	0.4038(2)	0.00851(17)	0.0584(8)*
C29	-0.3225(3)	0.4281(2)	-0.07288(18)	0.0698(9)*
C31	0.16929(14)	-0.00861(13)	0.15804(11)	0.0251(4)*
C32	0.17582(14)	-0.02649(14)	0.08420(11)	0.0251(4)*
C33	0.26320(16)	-0.06051(16)	0.06701(12)	0.0320(5)*
C34	0.34482(17)	-0.08090(18)	0.12869(14)	0.0404(5)*
C35	0.33921(17)	-0.06741(19)	0.20214(13)	0.0410(6)*
C36	0.25194(16)	-0.03069(16)	0.21733(12)	0.0322(5)*
C37	0.27267(18)	-0.07054(19)	-0.01331(13)	0.0414(6)*
C38	0.3221(3)	0.0060(3)	-0.0401(2)	0.0848(12)*
C39	0.3387(3)	-0.0100(3)	-0.1199(2)	0.0954(14)*
C41	0.00009(14)	-0.01328(14)	0.19734(11)	0.0252(4)*

Table 2. Atomic Coordinates and Displacement Parameters (continued)

Atom	x	y	z	U_{eq} , Å ²
C42	-0.03655(15)	-0.09784(14)	0.16606(11)	0.0253(4)*
C43	-0.09846(16)	-0.15338(15)	0.19833(12)	0.0326(5)*
C44	-0.12432(17)	-0.12224(17)	0.26312(13)	0.0375(5)*
C45	-0.09012(19)	-0.03948(17)	0.29483(13)	0.0394(5)*
C46	-0.02850(17)	0.01428(16)	0.26263(12)	0.0335(5)*
C47	-0.1342(3)	-0.2454(2)	0.16520(16)	0.0633(9)*
C48A ^c	-0.1600(4)	-0.3153(4)	0.2136(3)	0.0488(11)
C48B ^d	-0.1025(6)	-0.3232(5)	0.2119(4)	0.0553(15)
C49	-0.1723(4)	-0.4100(2)	0.1814(2)	0.0905(14)*

(b) solvent toluene atoms

Atom	x	y	z	U_{eq} , Å ²
C10S ^e	0.0978(7)	0.4081(6)	0.0815(5)	0.066(2)
C11S ^e	0.0340(4)	0.4627(4)	0.0271(3)	0.0516(13)
C12S ^e	0.0068(8)	0.4319(8)	-0.0428(6)	0.072(4)
C13S ^e	-0.0568(5)	0.4833(5)	-0.1036(4)	0.0678(17)
C14S ^e	-0.0850(7)	0.5647(7)	-0.0879(5)	0.075(3)
C15S ^e	-0.0585(5)	0.6003(5)	-0.0114(4)	0.0581(14)
C16S ^e	0.0052(7)	0.5489(6)	0.0491(5)	0.051(2)

Anisotropically-refined atoms are marked with an asterisk (*). The form of the anisotropic displacement parameter is: $\exp[-2\pi^2(h^2a^{*2}U_{11} + k^2b^{*2}U_{22} + l^2c^{*2}U_{33} + 2klb^{*c^*}U_{23} + 2hla^{*c^*}U_{13} + 2hka^{*b^*}U_{12})]$. ^aRefined with an occupancy factor of 0.65. ^bRefined with an occupancy factor of 0.35. ^cRefined with an occupancy factor of 0.55. ^dRefined with an occupancy factor of 0.45. ^eRefined with an occupancy factor of 0.5.

Table 3. Selected Interatomic Distances (Å)*(a) within $[(C_2(C_6H_3^nPr(O-))_4)_2Ti_2]$*

Atom1	Atom2	Distance	Atom1	Atom2	Distance
Ti	O1	1.8296(14)	C22	C23	1.406(3)
Ti	O2	1.8187(14)	C23	C24	1.394(3)
Ti	O3	1.9561(14)	C23	C27	1.514(3)
Ti	O3'	2.1166(13)	C24	C25	1.392(3)
Ti	O4'	1.8054(14)	C25	C26	1.385(3)
O1	C12	1.367(2)	C27	C28	1.506(3)
O2	C22	1.359(2)	C28	C29	1.526(4)
O3	C32	1.396(2)	C31	C32	1.397(3)
O4	C42	1.369(2)	C31	C36	1.391(3)
C1	C2	1.356(3)	C32	C33	1.391(3)
C1	C11	1.505(3)	C33	C34	1.403(3)
C1	C21	1.505(3)	C33	C37	1.510(3)
C2	C31	1.506(3)	C34	C35	1.376(3)
C2	C41	1.490(3)	C35	C36	1.389(3)
C11	C12	1.393(3)	C37	C38	1.453(4)
C11	C16	1.393(3)	C38	C39	1.545(5)
C12	C13	1.408(3)	C41	C42	1.404(3)
C13	C14	1.393(3)	C41	C46	1.400(3)
C13	C17	1.512(3)	C42	C43	1.400(3)
C14	C15	1.380(4)	C43	C44	1.391(3)
C15	C16	1.387(3)	C43	C47	1.509(3)
C17	C18A	1.545(6)	C44	C45	1.375(3)
C17	C18B	1.437(11)	C45	C46	1.381(3)
C18A	C19	1.538(7)	C47	C48A	1.451(6)
C18B	C19	1.537(11)	C47	C48B	1.426(7)
C21	C22	1.401(3)	C48A	C49	1.502(6)
C21	C26	1.395(3)	C48B	C49	1.603(7)

Primed atoms are related to unprimed ones via the crystallographic inversion center (0, 0, 0).

(b) within the solvent toluene molecule

Atom1	Atom2	Distance	Atom1	Atom2	Distance
C10S	C11S	1.397(10)	C13S	C14S	1.306(11)
C11S	C12S	1.318(12)	C14S	C15S	1.451(11)
C11S	C16S	1.410(11)	C15S	C16S	1.436(11)
C12S	C13S	1.439(13)			

Table 4. Selected Interatomic Angles (deg)*(a) within $[(C_2(C_6H_3^nPr(O-))_4)_2Ti_2]$*

Atom1	Atom2	Atom3	Angle	Atom1	Atom2	Atom3	Angle
O1	Ti	O2	99.16(7)	C1	C21	C22	117.75(17)
O1	Ti	O3	91.52(6)	C1	C21	C26	123.37(18)
O1	Ti	O3'	162.71(6)	C22	C21	C26	118.17(19)
O1	Ti	O4'	100.76(6)	O2	C22	C21	119.83(18)
O2	Ti	O3	135.12(6)	O2	C22	C23	117.83(18)
O2	Ti	O3'	89.76(6)	C21	C22	C23	122.32(18)
O2	Ti	O4'	109.03(7)	C22	C23	C24	117.4(2)
O3	Ti	O3'	71.88(6)	C22	C23	C27	119.30(19)
O3	Ti	O4'	111.52(6)	C24	C23	C27	123.3(2)
O3'	Ti	O4'	90.14(6)	C23	C24	C25	121.3(2)
Ti	O1	C12	139.72(13)	C24	C25	C26	120.1(2)
Ti	O2	C22	143.04(13)	C21	C26	C25	120.7(2)
Ti	O3	Ti'	108.12(6)	C23	C27	C28	116.6(2)
Ti	O3	C32	126.02(12)	C27	C28	C29	112.1(2)
Ti'	O3	C32	118.55(11)	C2	C31	C32	119.88(17)
Ti'	O4	C42	142.34(13)	C2	C31	C36	121.47(18)
C2	C1	C11	119.85(18)	C32	C31	C36	118.44(18)
C2	C1	C21	126.87(18)	O3	C32	C31	117.34(17)
C11	C1	C21	113.23(17)	O3	C32	C33	119.66(17)
C1	C2	C31	116.65(17)	C31	C32	C33	123.00(18)
C1	C2	C41	124.79(18)	C32	C33	C34	116.34(19)
C31	C2	C41	118.07(17)	C32	C33	C37	122.32(19)
C1	C11	C12	122.68(17)	C34	C33	C37	121.3(2)
C1	C11	C16	118.37(18)	C33	C34	C35	121.9(2)
C12	C11	C16	118.92(19)	C34	C35	C36	120.3(2)
O1	C12	C11	119.09(17)	C31	C36	C35	119.9(2)
O1	C12	C13	119.35(19)	C33	C37	C38	114.1(2)
C11	C12	C13	121.55(19)	C37	C38	C39	112.7(3)
C12	C13	C14	117.5(2)	C2	C41	C42	123.43(17)
C12	C13	C17	120.5(2)	C2	C41	C46	118.81(18)
C14	C13	C17	122.0(2)	C42	C41	C46	117.16(18)
C13	C14	C15	121.8(2)	O4	C42	C41	119.69(17)
C14	C15	C16	119.8(2)	O4	C42	C43	118.13(18)
C11	C16	C15	120.4(2)	C41	C42	C43	122.15(18)
C13	C17	C18A	114.8(3)	C42	C43	C44	118.0(2)
C13	C17	C18B	122.0(5)	C42	C43	C47	121.3(2)
C17	C18A	C19	108.2(4)	C44	C43	C47	120.7(2)
C17	C18B	C19	114.2(7)	C43	C44	C45	121.2(2)

Table 4. Selected Interatomic Angles (continued)

Atom1	Atom2	Atom3	Angle	Atom1	Atom2	Atom3	Angle
C44	C45	C46	120.1(2)	C43	C47	C48B	117.2(3)
C41	C46	C45	121.4(2)	C47	C48A	C49	115.8(4)
C43	C47	C48A	119.3(3)	C47	C48B	C49	111.3(5)

Primed atoms are related to unprimed ones via the crystallographic inversion center (0, 0, 0).

(b) within the solvent toluene molecule

Atom1	Atom2	Atom3	Angle	Atom1	Atom2	Atom3	Angle
C10S	C11S	C12S	118.0(8)	C12S	C13S	C14S	117.5(9)
C10S	C11S	C16S	118.6(7)	C13S	C14S	C15S	121.5(9)
C12S	C11S	C16S	123.4(8)	C14S	C15S	C16S	120.7(7)
C11S	C12S	C13S	122.6(10)	C11S	C16S	C15S	114.1(7)

Table 5. Selected Torsional Angles (deg)

Atom1	Atom2	Atom3	Atom4	Angle	Atom1	Atom2	Atom3	Atom4	Angle
O2	Ti	O1	C12	54.4(2)	C2	C1	C11	C16	-95.3(2)
O3	Ti	O1	C12	-81.8(2)	C21	C1	C11	C12	-96.1(2)
O3'	Ti	O1	C12	-65.8(3)	C21	C1	C11	C16	82.1(2)
O4'	Ti	O1	C12	166.0(2)	C2	C1	C21	C22	-92.6(3)
O1	Ti	O2	C22	-54.6(2)	C2	C1	C21	C26	97.1(3)
O3	Ti	O2	C22	46.9(3)	C11	C1	C21	C22	90.2(2)
O3'	Ti	O2	C22	110.5(2)	C11	C1	C21	C26	-80.0(2)
O4'	Ti	O2	C22	-159.4(2)	C1	C2	C31	C32	-83.4(2)
O1	Ti	O3	Ti'	175.05(7)	C1	C2	C31	C36	91.2(2)
O1	Ti	O3	C32	25.79(14)	C41	C2	C31	C32	104.3(2)
O2	Ti	O3	Ti'	70.44(10)	C41	C2	C31	C36	-81.2(2)
O2	Ti	O3	C32	-78.83(16)	C1	C2	C41	C42	144.3(2)
O3'	Ti	O3	Ti'	0.0	C1	C2	C41	C46	-44.9(3)
O3'	Ti	O3	C32	-149.27(17)	C31	C2	C41	C42	-44.1(3)
O4'	Ti	O3	Ti'	-82.75(7)	C31	C2	C41	C46	126.7(2)
O4'	Ti	O3	C32	127.98(14)	C1	C11	C12	O1	-1.2(3)
O1	Ti	O3'	C32'	-168.80(19)	C1	C11	C12	C13	178.0(2)
O2	Ti	O3'	C32'	69.74(13)	C1	C11	C16	C15	-178.3(2)
O3	Ti	O3'	C32'	-151.93(16)	C1	C21	C22	O2	6.7(3)
O1	Ti	O4'	C42'	81.4(2)	C1	C21	C22	C23	-171.57(18)
O2	Ti	O4'	C42'	-174.9(2)	C1	C21	C26	C25	171.4(2)
O3	Ti	O4'	C42'	-14.5(2)	C2	C31	C32	O3	-9.8(3)
C11	C1	C2	C31	-12.7(3)	C2	C31	C32	C33	170.97(19)
C11	C1	C2	C41	159.12(18)	C2	C31	C36	C35	-173.0(2)
C21	C1	C2	C31	170.36(18)	C2	C41	C42	O4	-7.3(3)
C21	C1	C2	C41	-17.9(3)	C2	C41	C42	C43	170.48(19)
C2	C1	C11	C12	86.6(3)	C2	C41	C46	C45	-171.4(2)

Primed atoms are related to unprimed ones via the crystallographic inversion center (0, 0, 0).

A-7 Complex 31. [C₃₈H₄₀O₄]-vic-anti-{TiCl₂(thf)}₂

– Chapter 3 –

XCL Code: JMS9922

Date: 3 April 2001

Compound: [C₂{C₆H₃(3-*n*Pr)(2-O-)}₄]-vic-anti-{TiCl₂(OC₄H₈)}₂

Formula: C₄₆H₅₆Cl₄O₆Ti₂

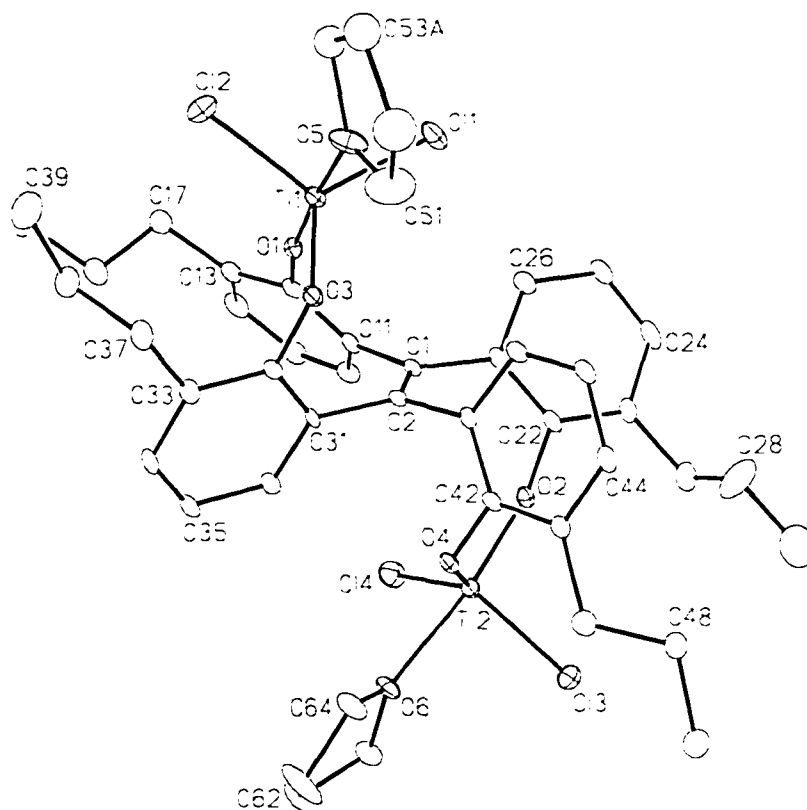


Figure 1. Perspective view of the [(C₂(C₆H₃^{*n*}PrO)₄){TiCl₂(OC₄H₈)}₂] molecule showing the atom labelling scheme. Non-hydrogen atoms are represented by Gaussian ellipsoids at the 20% probability level. Hydrogen atoms are not shown.

List of Tables

Table 1. Crystallographic Experimental Details

Table 2. Atomic Coordinates and Equivalent Isotropic Displacement Parameters

Table 3. Selected Interatomic Distances

Table 4. Selected Interatomic Angles

Table 5. Selected Torsional Angles

Table 1. Crystallographic Experimental Details

A. Crystal Data

formula	$C_{46}H_{56}Cl_4O_6Ti_2$
formula weight	942.51
crystal dimensions (mm)	$0.26 \times 0.18 \times 0.18$
crystal system	monoclinic
space group	$P2_1/n$ (an alternate setting of $P2_1/c$ [No. 14])
unit cell parameters ^a	
a (Å)	10.6883 (14)
b (Å)	12.1674 (15)
c (Å)	36.098 (5)
β (deg)	97.806 (2)
V (Å ³)	4651.0 (10)
Z	4
ρ_{calcd} (g cm ⁻³)	1.346
μ (mm ⁻¹)	0.618

B. Data Collection and Refinement Conditions

diffractometer	Bruker P4/RA/SMART 1000 CCD ^b
radiation (λ [Å])	graphite-monochromated Mo K α (0.71073)
temperature (°C)	-80
scan type	ϕ rotations (0.3°) / ω scans (0.3°) (30 s exposures)
data collection 2θ limit (deg)	53.04
total data collected	20116 ($-11 \leq h \leq 13, -15 \leq k \leq 7, -42 \leq l \leq 45$)
independent reflections	9524
number of observed reflections (NO)	5118 [$F_o^2 \geq 2\sigma(F_o^2)$]
structure solution method	direct methods (<i>SHELXS-86</i> ^c)

refinement method	full-matrix least-squares on F^2 (SHELXL-93 ^d)
absorption correction method	SADABS
range of transmission factors	0.9077–0.5769
data/restraints/parameters	9524 [$F_o^2 \geq -3\sigma(F_o^2)$] / 6 ^e / 521
goodness-of-fit (S) ^f	0.951 [$F_o^2 \geq -3\sigma(F_o^2)$]
final R indices ^g	
R_1 [$F_o^2 \geq 2\sigma(F_o^2)$]	0.0674
wR_2 [$F_o^2 \geq -3\sigma(F_o^2)$]	0.1943
largest difference peak and hole	0.777 and $-1.010 \text{ e } \text{\AA}^{-3}$

^aObtained from least-squares refinement of 4407 centered reflections.

^bPrograms for diffractometer operation, data collection, data reduction and absorption correction were those supplied by Bruker.

^cSheldrick, G. M. *Acta Crystallogr.* **1990**, *A46*, 467–473.

^dSheldrick, G. M. *SHELXL-93*. Program for crystal structure determination. University of Göttingen, Germany, 1993. Refinement on F_o^2 for all reflections (all of these having $F_o^2 \geq -3\sigma(F_o^2)$). Weighted R -factors wR_2 and all goodnesses of fit S are based on F_o^2 ; conventional R -factors R_1 are based on F_o , with F_o set to zero for negative F_o^2 . The observed criterion of $F_o^2 > 2\sigma(F_o^2)$ is used only for calculating R_1 , and is not relevant to the choice of reflections for refinement. R -factors based on F_o^2 are statistically about twice as large as those based on F_o , and R -factors based on ALL data will be even larger.

^eAn idealized geometry was imposed upon the disordered tetrahydrofuran ligand through use of the following restraints: $d(\text{C52A}-\text{C53A}) = d(\text{C53A}-\text{C54A}) = d(\text{C52B}-\text{C53B}) = d(\text{C53B}-\text{C54B}) = 1.54 \text{ \AA}$; $d(\text{C52A}\cdots\text{C54A}) = d(\text{C52A}\cdots\text{C54A}) = 2.51 \text{ \AA}$.

^f $S = [\sum w(F_o^2 - F_c^2)^2 / (n - p)]^{1/2}$ (n = number of data; p = number of parameters varied; $w = [\sigma^2(F_o^2) + (0.1006P)^2]^{-1}$ where $P = [\text{Max}(F_o^2, 0) + 2F_c^2]/3$).

^g $R_1 = \sum ||F_o| - |F_c|| / \sum |F_o|$; $wR_2 = [\sum w(F_o^2 - F_c^2)^2 / \sum w(F_o^4)]^{1/2}$.

Table 2. Atomic Coordinates and Equivalent Isotropic Displacement Parameters

Atom	x	y	z	U_{eq} , Å ²
Ti1	-0.19123(8)	0.29033(7)	0.43962(2)	0.0314(2)*
Ti2	-0.35300(8)	-0.13519(7)	0.30482(2)	0.0287(2)*
Cl1	-0.34473(13)	0.23302(12)	0.47262(4)	0.0474(4)*
Cl2	-0.03907(16)	0.39068(13)	0.47242(4)	0.0630(5)*
Cl3	-0.49424(14)	-0.23708(12)	0.26801(4)	0.0515(4)*
Cl4	-0.18363(14)	-0.23657(11)	0.32990(4)	0.0481(4)*
O1	-0.1094(3)	0.1643(2)	0.44023(8)	0.0290(7)*
O2	-0.4262(3)	-0.1335(2)	0.34598(8)	0.0319(7)*
O3	-0.2157(3)	0.3031(2)	0.38874(8)	0.0284(7)*
O4	-0.3678(3)	0.0135(2)	0.29783(8)	0.0272(7)*
O5	-0.3003(4)	0.4418(3)	0.43304(10)	0.0562(11)*
O6	-0.2485(3)	-0.1112(2)	0.25781(9)	0.0345(8)*
C1	-0.2688(4)	0.0049(3)	0.39816(12)	0.0245(10)*
C2	-0.2809(4)	0.0811(3)	0.37113(11)	0.0224(9)*
C11	-0.1472(4)	-0.0226(4)	0.42061(12)	0.0283(10)*
C12	-0.0676(4)	0.0586(4)	0.43925(12)	0.0307(11)*
C13	0.0526(5)	0.0338(4)	0.45758(12)	0.0341(11)*
C14	0.0883(5)	-0.0752(5)	0.45953(14)	0.0459(14)*
C15	0.0109(5)	-0.1575(5)	0.44348(14)	0.0419(13)*
C16	-0.1050(5)	-0.1312(4)	0.42390(13)	0.0373(12)*
C17	0.1415(5)	0.1248(5)	0.47294(14)	0.0435(13)*
C18	0.2131(5)	0.1714(5)	0.44275(16)	0.0509(15)*
C19	0.3023(6)	0.2644(6)	0.45757(19)	0.0694(19)*
C21	-0.3829(4)	-0.0563(3)	0.40709(12)	0.0276(10)*
C22	-0.4613(4)	-0.1177(4)	0.38052(13)	0.0289(10)*
C23	-0.5732(5)	-0.1650(4)	0.38838(14)	0.0351(12)*
C24	-0.6033(5)	-0.1548(4)	0.42457(15)	0.0449(14)*
C25	-0.5257(5)	-0.0987(4)	0.45210(15)	0.0422(13)*
C26	-0.4151(5)	-0.0490(4)	0.44321(13)	0.0360(12)*
C27	-0.6644(5)	-0.2167(5)	0.35799(16)	0.0530(15)*
C28	-0.7649(7)	-0.1285(6)	0.3409(2)	0.082(2)*
C29	-0.8539(8)	-0.1699(7)	0.3100(2)	0.099(3)*
C31	-0.1689(4)	0.1373(3)	0.35821(12)	0.0229(9)*
C32	-0.1439(4)	0.2473(3)	0.36569(12)	0.0249(10)*
C33	-0.0475(4)	0.3052(4)	0.35133(13)	0.0310(11)*
C34	0.0285(5)	0.2449(4)	0.33032(14)	0.0379(12)*
C35	0.0100(5)	0.1341(4)	0.32383(14)	0.0373(12)*
C36	-0.0884(4)	0.0796(4)	0.33757(12)	0.0305(11)*

Table 2. Atomic Coordinates and Displacement Parameters (continued)

Atom	x	y	z	$U_{eq}, \text{\AA}^2$
C37	-0.0220(5)	0.4262(4)	0.35980(15)	0.0415(13)*
C38	0.0971(6)	0.4463(4)	0.38657(16)	0.0510(15)*
C39	0.1106(7)	0.5641(5)	0.4000(2)	0.083(2)*
C41	-0.4071(4)	0.1150(3)	0.35129(12)	0.0226(9)*
C42	-0.4465(4)	0.0812(3)	0.31470(12)	0.0251(10)*
C43	-0.5621(4)	0.1110(4)	0.29452(12)	0.0294(10)*
C44	-0.6414(5)	0.1782(4)	0.31319(14)	0.0348(12)*
C45	-0.6066(4)	0.2109(4)	0.34986(13)	0.0340(11)*
C46	-0.4911(4)	0.1787(4)	0.36902(12)	0.0288(10)*
C47	-0.6003(5)	0.0719(5)	0.25498(14)	0.0439(13)*
C48	-0.7365(5)	0.0562(6)	0.24203(15)	0.0590(17)*
C49	-0.7650(6)	0.0074(5)	0.20342(15)	0.0551(16)*
C51	-0.3849(8)	0.4729(6)	0.4021(2)	0.097(3)*
C52A ^a	-0.4276(17)	0.5854(13)	0.4044(3)	0.092(6)
C53A ^a	-0.3772(14)	0.6208(9)	0.4446(3)	0.071(4)
C54A ^a	-0.2900(12)	0.5306(10)	0.4634(3)	0.056(3)
C52B ^a	-0.4850(17)	0.5547(14)	0.4092(3)	0.095(6)
C53B ^a	-0.4408(16)	0.5785(12)	0.4507(3)	0.099(6)
C54B ^a	-0.3412(15)	0.4930(12)	0.4662(4)	0.081(5)
C61	-0.1962(6)	-0.1988(4)	0.23708(15)	0.0451(13)*
C62	-0.1106(6)	-0.1415(5)	0.21328(18)	0.0598(17)*
C63	-0.1593(8)	-0.0316(5)	0.2077(2)	0.086(3)*
C64	-0.2347(6)	-0.0072(4)	0.23874(15)	0.0483(15)*

Anisotropically-refined atoms are marked with an asterisk (*). The form of the anisotropic displacement parameter is: $\exp[-2\pi^2(h^2a^{*2}U_{11} + k^2b^{*2}U_{22} + l^2c^{*2}U_{33} + 2klb^{*c^{*}}U_{23} + 2hla^{*c^{*}}U_{13} + 2hka^{*b^{*}}U_{12})]$. ^aRefined with an occupancy factor of 0.5.

Table 3. Selected Interatomic Distances (Å)

Atom1	Atom2	Distance	Atom1	Atom2	Distance
Ti1	C11	2.2646(16)	C24	C25	1.385(7)
Ti1	C12	2.2394(16)	C25	C26	1.403(7)
Ti1	O1	1.764(3)	C27	C28	1.584(9)
Ti1	O3	1.826(3)	C28	C29	1.454(9)
Ti1	O5	2.177(4)	C31	C32	1.385(6)
Ti2	C13	2.2443(15)	C31	C36	1.401(6)
Ti2	C14	2.2745(15)	C32	C33	1.404(6)
Ti2	O2	1.771(3)	C33	C34	1.393(7)
Ti2	O4	1.830(3)	C33	C37	1.520(6)
Ti2	O6	2.175(3)	C34	C35	1.378(7)
O1	C12	1.364(5)	C35	C36	1.390(6)
O2	C22	1.364(5)	C37	C38	1.510(7)
O3	C32	1.384(5)	C38	C39	1.513(7)
O4	C42	1.378(5)	C41	C42	1.393(6)
O5	C51	1.389(7)	C41	C46	1.404(6)
O5	C54A	1.533(12)	C42	C43	1.394(6)
O5	C54B	1.466(15)	C43	C44	1.413(6)
O6	C61	1.457(6)	C43	C47	1.508(6)
O6	C64	1.457(6)	C44	C45	1.384(6)
C1	C2	1.339(6)	C45	C46	1.387(6)
C1	C11	1.473(6)	C47	C48	1.480(7)
C1	C21	1.501(6)	C48	C49	1.508(7)
C2	C31	1.506(6)	C51	C52A	1.449(16)
C2	C41	1.497(6)	C51	C52B	1.508(17)
C11	C12	1.413(7)	C52A	C53A	1.54†
C11	C16	1.396(6)	C53A	C54A	1.54†
C12	C13	1.396(7)	C52B	C53B	1.54†
C13	C14	1.379(7)	C53B	C54B	1.54†
C13	C17	1.514(7)	C61	C62	1.508(7)
C14	C15	1.376(8)	C62	C63	1.440(8)
C15	C16	1.378(7)	C63	C64	1.495(7)
C17	C18	1.525(7)	C11	H26	2.98††
C18	C19	1.528(8)	C12	H16	3.01††
C21	C22	1.401(6)	C13	H46	2.98††
C21	C26	1.396(6)	C14	H36	3.05††
C22	C23	1.391(6)			
C23	C24	1.393(7)			
C23	C27	1.503(7)			

†Distance fixed during refinement.

††Nonbonded distance..

Table 4. Selected Interatomic Angles (deg)

Atom1	Atom2	Atom3	Angle	Atom1	Atom2	Atom3	Angle
C11	Ti1	C12	114.56(7)	C1	C11	C16	120.8(4)
C11	Ti1	O1	96.86(11)	C12	C11	C16	117.0(4)
C11	Ti1	O3	122.70(11)	O1	C12	C11	119.6(4)
C11	Ti1	O5	84.40(12)	O1	C12	C13	118.3(4)
C12	Ti1	O1	98.27(11)	C11	C12	C13	122.1(4)
C12	Ti1	O3	118.68(11)	C12	C13	C14	117.5(5)
C12	Ti1	O5	86.32(13)	C12	C13	C17	120.5(5)
O1	Ti1	O3	95.13(14)	C14	C13	C17	121.9(5)
O1	Ti1	O5	174.17(14)	C13	C14	C15	122.2(5)
O3	Ti1	O5	79.45(14)	C14	C15	C16	119.6(5)
C13	Ti2	C14	111.78(6)	C11	C16	C15	121.4(5)
C13	Ti2	O2	99.49(11)	C13	C17	C18	111.2(4)
C13	Ti2	O4	115.21(11)	C17	C18	C19	112.0(5)
C13	Ti2	O6	89.29(10)	C1	C21	C22	123.1(4)
C14	Ti2	O2	95.21(12)	C1	C21	C26	118.7(4)
C14	Ti2	O4	129.79(11)	C22	C21	C26	118.2(4)
C14	Ti2	O6	85.30(10)	O2	C22	C21	119.2(4)
O2	Ti2	O4	93.71(14)	O2	C22	C23	118.6(4)
O2	Ti2	O6	170.27(13)	C21	C22	C23	122.1(4)
O4	Ti2	O6	78.66(12)	C22	C23	C24	118.0(5)
Ti1	O1	C12	169.5(3)	C22	C23	C27	121.0(5)
Ti2	O2	C22	167.6(3)	C24	C23	C27	120.8(5)
Ti1	O3	C32	123.2(3)	C23	C24	C25	121.7(5)
Ti2	O4	C42	125.2(3)	C24	C25	C26	119.3(5)
Ti1	O5	C51	126.8(3)	C21	C26	C25	120.6(5)
Ti1	O5	C54A	122.2(4)	C23	C27	C28	109.8(5)
Ti1	O5	C54B	119.0(5)	C27	C28	C29	113.7(6)
C51	O5	C54A	111.0(5)	C2	C31	C32	121.3(4)
C51	O5	C54B	107.8(6)	C2	C31	C36	120.6(4)
Ti2	O6	C61	125.2(3)	C32	C31	C36	118.1(4)
Ti2	O6	C64	125.5(3)	O3	C32	C31	118.9(4)
C61	O6	C64	108.8(3)	O3	C32	C33	118.1(4)
C2	C1	C11	123.3(4)	C31	C32	C33	123.1(4)
C2	C1	C21	119.9(4)	C32	C33	C34	116.6(4)
C11	C1	C21	116.8(4)	C32	C33	C37	122.1(4)
C1	C2	C31	122.5(4)	C34	C33	C37	121.2(4)
C1	C2	C41	122.1(4)	C33	C34	C35	121.8(5)
C31	C2	C41	115.4(3)	C34	C35	C36	120.3(5)
C1	C11	C12	122.1(4)	C31	C36	C35	120.0(4)

Table 4. Selected Interatomic Angles (continued)

Atom1	Atom2	Atom3	Angle	Atom1	Atom2	Atom3	Angle
C33	C37	C38	113.4(4)	C43	C47	C48	117.9(4)
C37	C38	C39	113.2(5)	C47	C48	C49	114.2(5)
C2	C41	C42	120.6(4)	O5	C51	C52A	112.8(6)
C2	C41	C46	121.6(4)	O5	C51	C52B	116.4(7)
C42	C41	C46	117.7(4)	C51	C52A	C53A	104.2(6)
O4	C42	C41	118.1(4)	C52A	C53A	C54A	109.3 [†]
O4	C42	C43	118.4(4)	O5	C54A	C53A	101.9(6)
C41	C42	C43	123.5(4)	C51	C52B	C53B	99.1(7)
C42	C43	C44	116.6(4)	C52B	C53B	C54B	109.3 [†]
C42	C43	C47	121.3(4)	O5	C54B	C53B	105.1(7)
C44	C43	C47	122.1(4)	O6	C61	C62	105.0(4)
C43	C44	C45	121.4(4)	C61	C62	C63	105.8(5)
C44	C45	C46	120.1(4)	C62	C63	C64	107.5(5)
C41	C46	C45	120.6(4)	O6	C64	C63	106.3(4)

[†]Angle fixed during refinement.

Table 5. Selected Torsional Angles (deg)

Atom1	Atom2	Atom3	Atom4	Angle	Atom1	Atom2	Atom3	Atom4	Angle
Ti1	O1	C12	C11	20.0(18)	C41	C2	C31	C32	70.5(5)
Ti1	O1	C12	C13	-158.7(14)	C41	C2	C31	C36	-108.3(5)
Ti2	O2	C22	C21	-3.8(17)	C1	C2	C41	C42	-106.2(5)
Ti2	O2	C22	C23	177.3(12)	C1	C2	C41	C46	71.9(6)
Ti1	O3	C32	C31	78.0(5)	C31	C2	C41	C42	73.0(5)
Ti1	O3	C32	C33	-101.3(4)	C31	C2	C41	C46	-109.0(5)
Ti2	O4	C42	C41	80.4(4)	C1	C11	C12	O1	7.5(7)
Ti2	O4	C42	C43	-98.7(4)	C1	C11	C12	C13	-173.9(4)
C11	C1	C2	C31	6.9(6)	C16	C11	C12	O1	-173.3(4)
C11	C1	C2	C41	-174.0(4)	C16	C11	C12	C13	5.3(7)
C21	C1	C2	C31	-173.8(4)	C1	C11	C16	C15	177.2(4)
C21	C1	C2	C41	5.3(6)	C1	C21	C22	O2	7.5(6)
C2	C1	C11	C12	52.0(6)	C1	C21	C22	C23	-173.7(4)
C2	C1	C11	C16	-127.2(5)	C1	C21	C26	C25	175.7(4)
C21	C1	C11	C12	-127.4(5)	C2	C31	C32	O3	6.7(6)
C21	C1	C11	C16	53.5(6)	C2	C31	C32	C33	-174.1(4)
C2	C1	C21	C22	57.4(6)	C2	C31	C36	C35	176.0(4)
C2	C1	C21	C26	-120.5(5)	C2	C41	C42	O4	1.8(6)
C11	C1	C21	C22	-123.2(5)	C2	C41	C42	C43	-179.2(4)
C11	C1	C21	C26	58.9(6)	C2	C41	C46	C45	178.8(4)
C1	C2	C31	C32	-110.4(5)					
C1	C2	C31	C36	70.8(6)					

A-8: Complex 33a. $[C_{38}H_{40}O_4]$ -gem-anti- $\{TiBr_2(thf)\}_2$

– Chapter 3 –

XCL Code: JMS0010

Date: 12 April 2000

Compound: $[C_2\{C_6H_3(3\text{-}^n\text{Pr})(2\text{-}O\text{-})\}_4]\{TiBr_2(OC_4H_8)\}_2 \cdot PhMe$

Formula: $C_{53}H_{64}Br_4O_6Ti_2$ ($C_{46}H_{56}Br_4O_6Ti_2 \cdot C_7H_8$)

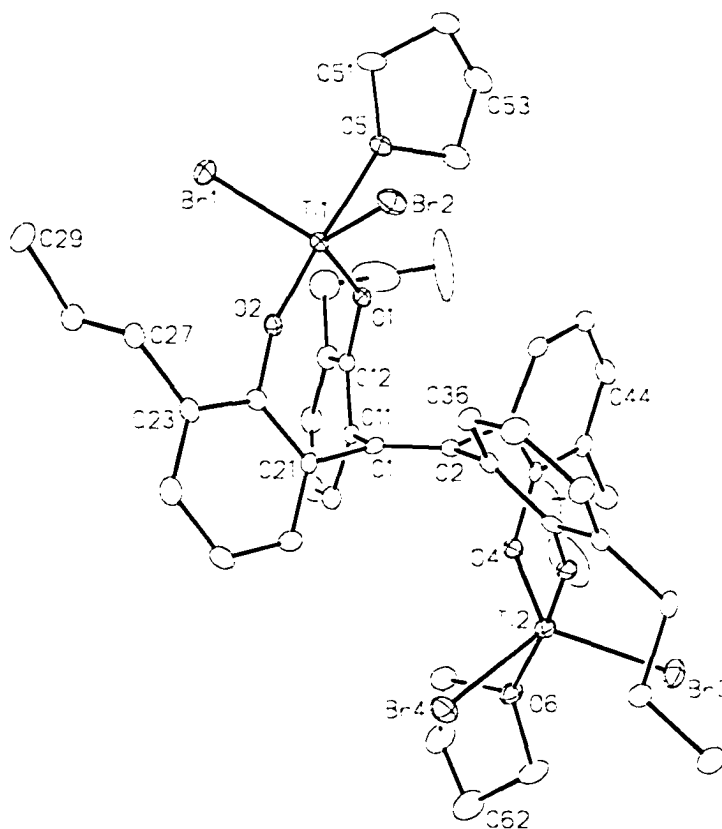


Figure 1. Perspective view of the $[(C_2\{C_6H_3(^n\text{Pr})(O\text{-})\}_4)\{TiBr_2(OC_4H_8)\}_2]$ molecule showing the atom labelling scheme. Non-hydrogen atoms are represented by Gaussian ellipsoids at the 20% probability level. Hydrogen atoms are not shown.

List of Tables

Table 1. Crystallographic Experimental Details

Table 2. Atomic Coordinates and Equivalent Isotropic Displacement Parameters

Table 3. Selected Interatomic Distances

Table 4. Selected Interatomic Angles

Table 5. Selected Torsional Angles

Table 1. Crystallographic Experimental Details

A. Crystal Data

formula	C ₅₃ H ₆₄ Br ₄ O ₆ Ti ₂
formula weight	1212.48
crystal dimensions (mm)	0.12 × 0.11 × 0.08
crystal system	triclinic
space group	PI (No. 2)
unit cell parameters ^a	
<i>a</i> (Å)	13.5182 (11)
<i>b</i> (Å)	14.5632 (11)
<i>c</i> (Å)	15.6882 (13)
α (deg)	71.8273 (19)
β (deg)	70.8232 (14)
γ (deg)	74.7699 (16)
<i>V</i> (Å ³)	2727.1 (4)
<i>Z</i>	2
ρ _{calcd} (g cm ⁻³)	1.477
μ (mm ⁻¹)	3.268

B. Data Collection and Refinement Conditions

diffractometer	Bruker P4/RA/SMART 1000 CCD ^b
radiation (λ [Å])	graphite-monochromated Mo Kα (0.71073)
temperature (°C)	-80
scan type	φ rotations (0.3°) / ω scans (0.3°) (30 s exposures)
data collection 2θ limit (deg)	52.78
total data collected	13662 (-16 ≤ <i>h</i> ≤ 16, -18 ≤ <i>k</i> ≤ 10, -18 ≤ <i>l</i> ≤ 19)

independent reflections	11069
number of observations (<i>NO</i>)	4609 [$F_o^2 \geq 2\sigma(F_o^2)$]
structure solution method	direct methods (<i>SHELXS-86</i> ^c)
refinement method	full-matrix least-squares on F^2 (<i>SHELXL-93</i> ^d)
absorption correction method	Gaussian integration (face-indexed)
range of transmission factors	0.7954–0.6484
data/restraints/parameters	11069 [$F_o^2 \geq -3\sigma(F_o^2)$] / 0 / 587
goodness-of-fit (<i>S</i>) ^e	0.808 [$F_o^2 \geq -3\sigma(F_o^2)$]
final <i>R</i> indices ^f	
R_1 [$F_o^2 \geq 2\sigma(F_o^2)$]	0.0516
wR_2 [$F_o^2 \geq -3\sigma(F_o^2)$]	0.1069
largest difference peak and hole	0.921 and –0.680 e Å ⁻³

^aObtained from least-squares refinement of 4774 centered reflections.

^bPrograms for diffractometer operation, data collection, data reduction and absorption correction were those supplied by Bruker.

^cSheldrick, G. M. *Acta Crystallogr.* **1990**, *A46*, 467–473.

^dSheldrick, G. M. *SHELXL-93*. Program for crystal structure determination. University of Göttingen, Germany, 1993. Refinement on F_o^2 for all reflections (all of these having $F_o^2 \geq -3\sigma(F_o^2)$). Weighted *R*-factors wR_2 and all goodnesses of fit *S* are based on F_o^2 ; conventional *R*-factors R_1 are based on F_o , with F_o set to zero for negative F_o^2 . The observed criterion of $F_o^2 > 2\sigma(F_o^2)$ is used only for calculating R_1 , and is not relevant to the choice of reflections for refinement. *R*-factors based on F_o^2 are statistically about twice as large as those based on F_o , and *R*-factors based on ALL data will be even larger.

^e $S = [\sum w(F_o^2 - F_c^2)^2 / (n - p)]^{1/2}$ (n = number of data; p = number of parameters varied; $w = [\sigma^2(F_o^2) + (0.0270P)^2]^{-1}$ where $P = [\text{Max}(F_o^2, 0) + 2F_c^2]/3$).

^f $R_1 = \sum ||F_o| - |F_c|| / \sum |F_o|$; $wR_2 = [\sum w(F_o^2 - F_c^2)^2 / \sum w(F_o^4)]^{1/2}$.

Table 2. Atomic Coordinates and Equivalent Isotropic Displacement Parameters*(a) atoms of [(C₂{C₆H₃(ⁿPr)(O-)}₄){TiBr₂(OC₄H₈)}₂]*

Atom	x	y	z	<i>U</i> _{eq} , Å ²
Br1	0.05397(6)	0.18027(4)	0.40466(5)	0.0581(2)*
Br2	-0.13906(6)	0.30117(5)	0.22073(5)	0.0469(2)*
Br3	-0.29114(6)	1.01206(4)	0.10412(5)	0.0510(2)*
Br4	-0.41182(6)	0.84296(5)	0.37568(5)	0.0545(2)*
Ti1	-0.03160(9)	0.32232(6)	0.30995(7)	0.0282(3)*
Ti2	-0.27270(9)	0.86847(6)	0.23004(7)	0.0306(3)*
O1	0.0233(3)	0.4312(2)	0.2808(2)	0.0275(10)*
O2	-0.1454(3)	0.3547(2)	0.3976(2)	0.0272(9)*
O3	-0.3137(3)	0.7899(2)	0.1880(2)	0.0277(10)*
O4	-0.1405(3)	0.7991(2)	0.2239(2)	0.0283(10)*
O5	0.0997(3)	0.2878(3)	0.1935(3)	0.0379(11)*
O6	-0.2242(3)	0.9556(2)	0.2902(3)	0.0413(12)*
C1	-0.1786(5)	0.5583(3)	0.3369(4)	0.0270(15)*
C2	-0.1980(4)	0.6075(3)	0.2547(4)	0.0227(14)*
C11	-0.0783(5)	0.5601(4)	0.3557(4)	0.0252(14)*
C12	0.0195(5)	0.4986(4)	0.3271(4)	0.0246(14)*
C13	0.1114(5)	0.5048(4)	0.3447(4)	0.0346(16)*
C14	0.1065(5)	0.5716(4)	0.3925(4)	0.0398(17)*
C15	0.0095(6)	0.6305(4)	0.4235(4)	0.0461(19)*
C16	-0.0810(5)	0.6245(4)	0.4065(4)	0.0344(16)*
C17	0.2172(6)	0.4407(5)	0.3124(5)	0.063(2)*
C18	0.2982(7)	0.4922(7)	0.2409(8)	0.129(4)*
C19	0.2864(10)	0.5271(8)	0.1536(7)	0.192(8)*
C21	-0.2565(5)	0.5070(3)	0.4190(4)	0.0244(14)*
C22	-0.2361(5)	0.4034(4)	0.4477(4)	0.0273(14)*
C23	-0.3030(5)	0.3498(4)	0.5219(4)	0.0316(15)*
C24	-0.3911(5)	0.4022(4)	0.5738(4)	0.0379(17)*
C25	-0.4124(5)	0.5044(4)	0.5501(4)	0.0434(18)*
C26	-0.3464(5)	0.5547(4)	0.4721(4)	0.0378(17)*
C27	-0.2797(5)	0.2379(4)	0.5471(4)	0.0367(17)*
C28	-0.2013(5)	0.1948(4)	0.6046(4)	0.0448(18)*
C29	-0.1732(6)	0.0821(4)	0.6217(5)	0.073(3)*
C31	-0.2970(4)	0.6149(4)	0.2285(4)	0.0230(14)*
C32	-0.3508(5)	0.7096(4)	0.1905(4)	0.0257(14)*
C33	-0.4353(5)	0.7231(4)	0.1543(4)	0.0271(15)*
C34	-0.4714(5)	0.6394(4)	0.1602(4)	0.0374(16)*
C35	-0.4249(5)	0.5474(4)	0.2014(4)	0.0386(17)*

Table 2. Atomic Coordinates and Displacement Parameters (continued)

Atom	x	y	z	$U_{eq}, \text{\AA}^2$
C36	-0.3396(5)	0.5361(4)	0.2347(4)	0.0315(16)*
C37	-0.4838(5)	0.8245(4)	0.1092(4)	0.0331(16)*
C38	-0.5671(5)	0.8777(4)	0.1791(4)	0.0433(18)*
C39	-0.6088(6)	0.9833(4)	0.1320(5)	0.062(2)*
C41	-0.1090(4)	0.6488(3)	0.1770(4)	0.0221(14)*
C42	-0.0811(5)	0.7395(4)	0.1650(4)	0.0232(14)*
C43	0.0053(5)	0.7730(4)	0.0923(4)	0.0300(15)*
C44	0.0625(5)	0.7133(4)	0.0323(4)	0.0385(17)*
C45	0.0356(5)	0.6248(4)	0.0413(4)	0.0340(16)*
C46	-0.0502(4)	0.5944(4)	0.1127(4)	0.0284(15)*
C47	0.0330(5)	0.8694(4)	0.0822(4)	0.0472(19)*
C48	0.1040(8)	0.8569(5)	0.1466(5)	0.087(3)*
C49	0.1047(9)	0.9603(9)	0.1452(7)	0.175(5)*
C51	0.1328(6)	0.1928(4)	0.1696(5)	0.059(2)*
C52	0.1900(6)	0.2144(5)	0.0673(5)	0.061(2)*
C53	0.2271(5)	0.3105(5)	0.0487(5)	0.056(2)*
C54	0.1347(5)	0.3628(4)	0.1109(4)	0.0499(19)*
C61	-0.2840(6)	1.0524(4)	0.3022(5)	0.060(2)*
C62	-0.2654(7)	1.0629(5)	0.3879(5)	0.080(3)*
C63	-0.1569(7)	0.9999(5)	0.3875(5)	0.080(3)*
C64	-0.1612(6)	0.9157(4)	0.3560(4)	0.0486(19)*

(b) solvent toluene atoms

Atom	x	y	z	$U_{eq}, \text{\AA}^2$
C10S	0.6056(10)	0.2947(7)	0.1063(9)	0.190(7)*
C11S	0.5438(11)	0.2605(8)	0.1929(9)	0.109(4)*
C12S	0.5536(9)	0.2759(6)	0.2733(10)	0.084(3)*
C13S	0.4829(11)	0.2398(8)	0.3547(9)	0.102(4)*
C14S	0.4055(15)	0.1918(11)	0.3569(14)	0.168(8)*
C15S	0.394(2)	0.1723(17)	0.2926(18)	0.225(12)*
C16S	0.4606(12)	0.2094(9)	0.2043(11)	0.113(4)*

Anisotropically-refined atoms are marked with an asterisk (*). The form of the anisotropic displacement parameter is: $\exp[-2\pi^2(h^2a^*{}^2U_{11} + k^2b^*{}^2U_{22} + l^2c^*{}^2U_{33} + 2klb^*c^*U_{23} + 2hla^*c^*U_{13} + 2hka^*b^*U_{12})]$.

Table 3. Selected Interatomic Distances (Å)*(a) within [(C₂[C₆H₃(ⁿPr)(O-)]₄)(TiBr₂(OC₄H₈))₂]*

Atom1	Atom2	Distance	Atom1	Atom2	Distance
Br1	Ti1	2.4041(11)	C14	C15	1.394(8)
Br2	Ti1	2.4503(13)	C15	C16	1.363(8)
Br2	H46	3.64†	C17	C18	1.455(9)
Br2	H36	2.99†	C18	C19	1.352(12)
Br3	Ti2	2.4105(11)	C21	C22	1.412(6)
Br4	Ti2	2.4311(13)	C21	C26	1.381(7)
Br4	H26	3.01†	C22	C23	1.376(7)
Ti1	O1	1.794(3)	C23	C24	1.391(8)
Ti1	O2	1.765(4)	C23	C27	1.524(7)
Ti1	O5	2.171(4)	C24	C25	1.392(7)
Ti1	H46	3.64†	C25	C26	1.377(7)
Ti2	O3	1.760(4)	C27	C28	1.502(7)
Ti2	O4	1.795(4)	C28	C29	1.540(7)
Ti2	O6	2.127(4)	C31	C32	1.425(7)
Ti2	H16	4.07†	C31	C36	1.377(7)
O1	C12	1.373(6)	C32	C33	1.379(7)
O1	H46	3.20†	C33	C34	1.395(7)
O2	C22	1.371(6)	C33	C37	1.502(6)
O2	H36	3.33†	C34	C35	1.375(7)
O3	C32	1.374(6)	C35	C36	1.368(7)
O3	H26	4.06†	C37	C38	1.527(7)
O4	C42	1.378(6)	C38	C39	1.529(6)
O4	H16	3.20†	C41	C42	1.409(7)
O5	C51	1.464(6)	C41	C46	1.386(7)
O5	C54	1.442(6)	C42	C43	1.407(7)
O6	C61	1.463(6)	C43	C44	1.384(8)
O6	C64	1.438(6)	C43	C47	1.496(7)
C1	C2	1.338(7)	C44	C45	1.383(7)
C1	C11	1.488(7)	C45	C46	1.379(7)
C1	C21	1.500(7)	C47	C48	1.552(9)
C2	C31	1.493(7)	C48	C49	1.501(12)
C2	C41	1.501(7)	C51	C52	1.508(8)
C11	C12	1.411(7)	C52	C53	1.520(8)
C11	C16	1.394(7)	C53	C54	1.502(8)
C12	C13	1.389(7)	C61	C62	1.506(9)
C13	C14	1.379(8)			
C13	C17	1.514(8)			

Table 4. Selected Interatomic Angles (continued)

Atom1	Atom2	Distance	Atom1	Atom2	Distance
C62	C63	1.512(9)	C63	C64	1.478(8)

†Nonbonded distance.

(b) within the solvent toluene molecule

Atom1	Atom2	Distance	Atom1	Atom2	Distance
C10S	C11S	1.357(13)	C13S	C14S	1.389(17)
C11S	C12S	1.400(14)	C14S	C15S	1.20(2)
C11S	C16S	1.441(17)	C15S	C16S	1.41(3)
C12S	C13S	1.365(12)			

Table 4. Selected Interatomic Angles (deg)

(a) within $[(C_2[C_6H_3(^nPr)(O-)]_4)\{TiBr_2(OC_4H_8)\}_2]$

Atom1	Atom2	Atom3	Angle	Atom1	Atom2	Atom3	Angle
Br1	Ti1	Br2	119.58(5)	Ti2	O4	C42	128.2(3)
Br1	Ti1	O1	114.76(12)	Ti1	O5	C51	125.1(3)
Br1	Ti1	O2	98.55(11)	Ti1	O5	C54	121.7(3)
Br1	Ti1	O5	85.86(10)	C51	O5	C54	108.6(4)
Br2	Ti1	O1	122.50(12)	Ti2	O6	C61	122.8(4)
Br2	Ti1	O2	92.35(13)	Ti2	O6	C64	123.8(3)
Br2	Ti1	O5	83.16(11)	C61	O6	C64	108.8(4)
O1	Ti1	O2	97.11(16)	C2	C1	C11	120.5(5)
O1	Ti1	O5	83.32(16)	C2	C1	C21	124.7(5)
O2	Ti1	O5	174.87(16)	C11	C1	C21	114.5(5)
Br3	Ti2	Br4	121.69(5)	C1	C2	C31	125.7(5)
Br3	Ti2	O3	96.66(11)	C1	C2	C41	118.3(5)
Br3	Ti2	O4	116.22(11)	C31	C2	C41	115.5(5)
Br3	Ti2	O6	87.38(10)	C1	C11	C12	123.7(5)
Br4	Ti2	O3	92.26(12)	C1	C11	C16	118.5(5)
Br4	Ti2	O4	120.11(12)	C12	C11	C16	117.8(5)
Br4	Ti2	O6	84.84(12)	O1	C12	C11	119.0(5)
O3	Ti2	O4	95.22(16)	O1	C12	C13	119.6(5)
O3	Ti2	O6	175.86(15)	C11	C12	C13	121.5(5)
O4	Ti2	O6	83.73(16)	C12	C13	C14	119.1(6)
Ti1	O1	C12	135.6(3)	C12	C13	C17	121.9(6)
Ti1	O2	C22	164.5(3)	C14	C13	C17	119.0(6)
Ti2	O3	C32	157.8(3)	C13	C14	C15	119.7(6)

Table 4. Selected Interatomic Angles (continued)

Atom1	Atom2	Atom3	Angle	Atom1	Atom2	Atom3	Angle
C14	C15	C16	121.4(6)	C33	C34	C35	121.0(6)
C11	C16	C15	120.5(6)	C34	C35	C36	120.4(6)
C13	C17	C18	115.4(6)	C31	C36	C35	122.0(5)
C17	C18	C19	118.0(10)	C33	C37	C38	112.9(5)
C1	C21	C22	119.1(5)	C37	C38	C39	111.7(5)
C1	C21	C26	124.1(5)	C2	C41	C42	124.3(5)
C22	C21	C26	116.7(5)	C2	C41	C46	118.2(5)
O2	C22	C21	117.6(5)	C42	C41	C46	117.5(5)
O2	C22	C23	119.2(5)	O4	C42	C41	120.0(5)
C21	C22	C23	123.3(5)	O4	C42	C43	118.3(5)
C22	C23	C24	117.2(5)	C41	C42	C43	121.7(5)
C22	C23	C27	121.1(5)	C42	C43	C44	117.6(5)
C24	C23	C27	121.7(5)	C42	C43	C47	120.1(6)
C23	C24	C25	121.4(6)	C44	C43	C47	122.3(6)
C24	C25	C26	119.2(6)	C43	C44	C45	122.0(6)
C21	C26	C25	122.0(5)	C44	C45	C46	119.1(6)
C23	C27	C28	113.2(5)	C41	C46	C45	122.0(5)
C27	C28	C29	111.5(5)	C43	C47	C48	110.3(5)
C2	C31	C32	118.8(5)	C47	C48	C49	104.0(7)
C2	C31	C36	125.0(5)	O5	C51	C52	105.6(5)
C32	C31	C36	116.2(5)	C51	C52	C53	104.0(6)
O3	C32	C31	117.6(5)	C52	C53	C54	100.9(5)
O3	C32	C33	119.5(5)	O5	C54	C53	105.5(5)
C31	C32	C33	122.9(5)	O6	C61	C62	105.4(5)
C32	C33	C34	117.3(5)	C61	C62	C63	102.1(6)
C32	C33	C37	120.4(5)	C62	C63	C64	102.7(6)
C34	C33	C37	122.3(5)	O6	C64	C63	105.7(5)

(b) within the solvent toluene molecule

Atom1	Atom2	Atom3	Angle	Atom1	Atom2	Atom3	Angle
C10S	C11S	C12S	123.1(17)	C12S	C13S	C14S	121.7(13)
C10S	C11S	C16S	119.7(18)	C13S	C14S	C15S	127(3)
C12S	C11S	C16S	117.1(11)	C14S	C15S	C16S	116(3)
C11S	C12S	C13S	115.9(11)	C11S	C16S	C15S	122.3(18)

Table 5. Selected Torsional Angles (deg)

Atom1	Atom2	Atom3	Atom4	Angle	Atom1	Atom2	Atom3	Atom4	Angle
Ti1	O1	C12	C11	-66.7(6)	C11	C1	C21	C26	102.7(6)
Ti1	O1	C12	C13	113.3(5)	C1	C2	C31	C32	128.8(6)
Ti1	O2	C22	C21	-20.5(17)	C1	C2	C31	C36	-53.8(8)
Ti1	O2	C22	C23	158.6(11)	C41	C2	C31	C32	-59.2(7)
Ti2	O3	C32	C31	-52.8(12)	C41	C2	C31	C36	118.1(6)
Ti2	O3	C32	C33	129.1(8)	C1	C2	C41	C42	-83.7(6)
Ti2	O4	C42	C41	-71.1(5)	C1	C2	C41	C46	96.3(6)
Ti2	O4	C42	C43	107.4(5)	C1	C11	C12	O1	-1.4(7)
C11	C1	C2	C31	-177.4(5)	C1	C11	C12	C13	178.6(5)
C11	C1	C2	C41	10.9(7)	C1	C11	C16	C15	-178.3(5)
C21	C1	C2	C31	-3.9(8)	C1	C21	C22	O2	-0.7(8)
C21	C1	C2	C41	-175.6(5)	C1	C21	C22	C23	-179.8(5)
C2	C1	C11	C12	-82.7(6)	C1	C21	C26	C25	-176.2(6)
C2	C1	C11	C16	98.9(6)	C2	C31	C32	O3	-5.8(7)
C21	C1	C11	C12	103.2(6)	C2	C31	C32	C33	172.2(5)
C21	C1	C11	C16	-75.2(6)	C2	C31	C36	C35	-173.7(5)
C2	C1	C21	C22	111.7(6)	C2	C41	C42	O4	-3.5(8)
C2	C1	C21	C26	-71.2(8)	C2	C41	C42	C43	178.0(5)
C11	C1	C21	C22	-74.4(7)	C2	C41	C46	C45	-177.4(5)

A-9: Complex 34. $C_{38}H_{40}O_4 \cdot (CpTiCl)_2$

– Chapter 3 –

XCL Code: JMS9917

Date: 27 April 2001

Compound: $[[C_2(C_6H_3^mPr\{O-\})_4](CpTiCl)_2] \cdot 2PhMe$

Formula: $C_{62}H_{66}Cl_2O_4Ti_2$ ($C_{48}H_{50}Cl_2O_4Ti_2 \cdot 2C_7H_8$)

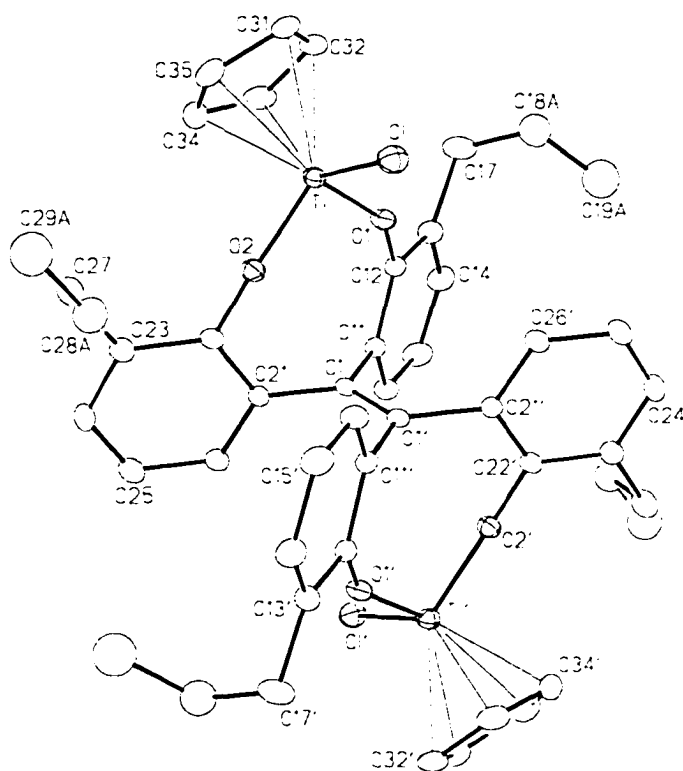


Figure 1. Perspective view of the $[[C_2(C_6H_3^mPr\{O-\})_4](CpTiCl)_2]$ molecule/ion showing the atom labelling scheme. Non-hydrogen atoms are represented by Gaussian ellipsoids at the 20% probability level. Hydrogen atoms are not shown. Primed atoms are related to unprimed ones via the crystallographic inversion center $(0, 0, 1/2)$ at the midpoint of the $C1-C1'$ bond.

List of Tables

Table 1. Crystallographic Experimental Details

Table 2. Atomic Coordinates and Equivalent Isotropic Displacement Parameters

Table 3. Selected Interatomic Distances

Table 4. Selected Interatomic Angles

Table 5. Selected Torsional Angles

Table 1. Crystallographic Experimental Details

A. Crystal Data

formula	C ₆₂ H ₆₆ Cl ₂ O ₄ Ti ₂
formula weight	1041.85
crystal dimensions (mm)	0.40 × 0.14 × 0.13
crystal system	monoclinic
space group	<i>P</i> 2 ₁ / <i>n</i> (an alternate setting of <i>P</i> 2 ₁ / <i>c</i> [No. 14])
unit cell parameters ^a	
<i>a</i> (Å)	12.705 (3)
<i>b</i> (Å)	18.114 (4)
<i>c</i> (Å)	12.779 (3)
β (deg)	110.227 (4)
<i>V</i> (Å ³)	2759.7 (12)
<i>Z</i>	2
ρ _{calcd} (g cm ⁻³)	1.254
μ (mm ⁻¹)	0.432

B. Data Collection and Refinement Conditions

diffractometer	Bruker P4/RA/SMART 1000 CCD ^b
radiation (λ [Å])	graphite-monochromated Mo Kα (0.71073)
temperature (°C)	-80
scan type	φ rotations (0.3°) / ω scans (0.3°) (30 s exposures)
data collection 2θ limit (deg)	52.80
total data collected	13336 (-15 ≤ <i>h</i> ≤ 15, -8 ≤ <i>k</i> ≤ 22, -15 ≤ <i>l</i> ≤ 15)

independent reflections	5629
number of observed reflections (<i>NO</i>)	3617 [$F_o^2 \geq 2\sigma(F_o^2)$]
structure solution method	direct methods (<i>SHELXS-86^c</i>)
refinement method	full-matrix least-squares on F^2 (<i>SHELXL-93^d</i>)
absorption correction method	<i>SADABS</i>
range of transmission factors	0.9280–0.6880
data/restraints/parameters	5629 [$F_o^2 \geq -3\sigma(F_o^2)$] / 15 ^e / 295
goodness-of-fit (<i>S</i>) ^f	1.042 [$F_o^2 \geq -3\sigma(F_o^2)$]
final <i>R</i> indices ^g	
R_1 [$F_o^2 \geq 2\sigma(F_o^2)$]	0.0706
wR_2 [$F_o^2 \geq -3\sigma(F_o^2)$]	0.2306
largest difference peak and hole	1.031 and $-0.852 \text{ e } \text{Å}^{-3}$

^aObtained from least-squares refinement of 4097 centered reflections.

^bPrograms for diffractometer operation, data collection, data reduction and absorption correction were those supplied by Bruker.

^cSheldrick, G. M. *Acta Crystallogr.* **1990**, *A46*, 467–473.

^dSheldrick, G. M. *SHELXL-93*. Program for crystal structure determination. University of Göttingen, Germany, 1993. Refinement on F_o^2 for all reflections (all of these having $F_o^2 \geq -3\sigma(F_o^2)$). Weighted *R*-factors wR_2 and all goodnesses of fit *S* are based on F_o^2 ; conventional *R*-factors R_1 are based on F_o , with F_o set to zero for negative F_o^2 . The observed criterion of $F_o^2 > 2\sigma(F_o^2)$ is used only for calculating R_1 , and is not relevant to the choice of reflections for refinement. *R*-factors based on F_o^2 are statistically about twice as large as those based on F_o , and *R*-factors based on ALL data will be even larger.

^eAn idealized geometry was imposed on the disordered *n*-propyl groups of the $C_2(C_6H_3^nPr(O-))_4$ ligand through use of the following distance conditions: $d(C17-C18A) = d(C18A-C19A) = d(C17-C18B) = d(C18B-C19B) = d(C27-C28A) = d(C28A-C29A) = d(C27-C28B) = d(C28B-C29B) = 1.54 \text{ Å}$; $d(C17 \cdots C19A) = d(C17 \cdots C19B) = d(C27 \cdots C29A) = d(C27 \cdots C29B) = 2.52 \text{ Å}$. The ring carbons of one of the solvent toluene molecules (containing C21S through C26S, and disordered about the crystallographic inversion center (0, $1/2$, $1/2$)) were refined as an idealized hexagon with a bond distance of 1.39 Å, and the geometry of the methyl carbon was also idealized ($d(C20S-C21S) = 1.54 \text{ Å}$; $d(C20S \cdots C22S) = d(C20S \cdots C26S) = 2.54 \text{ Å}$).

^f $S = [\sum w(F_o^2 - F_c^2)^2 / (n - p)]^{1/2}$ (*n* = number of data; *p* = number of parameters varied; $w = [\sigma^2(F_o^2) + (0.1420P)^2]^{-1}$ where $P = [\text{Max}(F_o^2, 0) + 2F_c^2] / 3$).

^g $R_1 = \sum ||F_o| - |F_c|| / \sum |F_o|$; $wR_2 = [\sum w(F_o^2 - F_c^2)^2 / \sum w(F_o^4)]^{1/2}$.

Table 2. Atomic Coordinates and Equivalent Isotropic Displacement Parameters*(a) atoms of [(C₂(C₆H₃ⁿPr(O-))₄)(CpTiCl)₂]*

Atom	x	y	z	<i>U</i> _{eq} , Å ²
Ti	0.24469(6)	0.05371(4)	0.41573(6)	0.0316(2)*
Cl	0.36121(9)	0.07784(7)	0.59411(9)	0.0493(3)*
O1	0.1927(2)	-0.03827(14)	0.4217(2)	0.0369(7)*
O2	0.1234(2)	0.10914(14)	0.4043(2)	0.0367(7)*
C1	-0.0128(3)	-0.00120(18)	0.4444(3)	0.0280(8)*
C11	0.0033(3)	-0.07157(19)	0.3906(3)	0.0302(8)*
C12	0.1085(3)	-0.08870(19)	0.3840(3)	0.0312(8)*
C13	0.1297(3)	-0.1571(2)	0.3440(4)	0.0381(9)*
C14	0.0421(4)	-0.2071(2)	0.3077(4)	0.0440(11)*
C15	-0.0643(4)	-0.1896(2)	0.3078(4)	0.0468(11)*
C16	-0.0832(4)	-0.1229(2)	0.3497(4)	0.0396(10)*
C17	0.2472(4)	-0.1765(2)	0.3498(4)	0.0556(13)*
C18A ^{a,b}	0.3318(6)	-0.1915(5)	0.4675(5)	0.075(2)
C19A ^{a,c}	0.2935(10)	-0.2589(6)	0.5185(7)	0.104(3)
C18B ^{b,d}	0.3074(9)	-0.2074(10)	0.4678(6)	0.075(2)
C19B ^{c,d}	0.4279(8)	-0.2302(10)	0.4803(11)	0.104(3)
C21	-0.0605(3)	0.06421(18)	0.3729(3)	0.0301(8)*
C22	0.0108(3)	0.11921(19)	0.3585(3)	0.0322(8)*
C23	-0.0314(4)	0.1844(2)	0.2986(4)	0.0407(10)*
C24	-0.1467(4)	0.1911(2)	0.2494(4)	0.0459(11)*
C25	-0.2189(4)	0.1361(2)	0.2588(4)	0.0480(11)*
C26	-0.1758(3)	0.0736(2)	0.3217(4)	0.0382(9)*
C27	0.0473(4)	0.2487(2)	0.2995(4)	0.0612(14)*
C28A ^e	0.0859(6)	0.2867(3)	0.4145(4)	0.067(2)
C29A ^e	0.1603(7)	0.3536(4)	0.4136(7)	0.099(3)
C28B ^f	0.0450(18)	0.3207(5)	0.3625(10)	0.066(6)
C29B ^f	0.098(2)	0.3076(11)	0.4891(8)	0.088(8)
C31	0.4064(4)	0.0807(3)	0.3660(4)	0.0511(12)*
C32	0.3640(4)	0.0131(3)	0.3180(4)	0.0492(11)*
C33	0.2559(4)	0.0253(3)	0.2402(4)	0.0548(12)*
C34	0.2331(4)	0.1006(3)	0.2423(4)	0.0546(13)*
C35	0.3244(4)	0.1343(3)	0.3195(4)	0.0543(12)*

(b) solvent toluene atoms

Atom	x	y	z	<i>U</i> _{eq} , Å ²
C10S ^g	-0.0646(14)	0.1531(7)	-0.0164(12)	0.099(5)*
C11S	-0.0310(5)	0.0746(4)	-0.0075(5)	0.0732(17)*

Table 2. Atomic Coordinates and Displacement Parameters (continued)

Atom	x	y	z	U_{eq} , Å ²
C12S	-0.0613(5)	0.0276(4)	0.0633(5)	0.0764(17)*
C13S	-0.0295(5)	-0.0467(4)	0.0691(5)	0.0713(16)*
C20S ^{g,h}	-0.1208(12)	0.4083(8)	0.5506(13)	0.131(2)
C21S ^{g,h}	-0.0476(10)	0.4671(7)	0.5216(10)	0.131(2)
C22S ^{g,h}	-0.0670(11)	0.4851(7)	0.4108(10)	0.131(2)
C23S ^{g,h}	0.0049(12)	0.5333(6)	0.3838(11)	0.131(2)
C24S ^{g,h}	0.0961(11)	0.5635(6)	0.4676(13)	0.131(2)
C25S ^{g,h}	0.1155(9)	0.5455(6)	0.5785(12)	0.131(2)
C26S ^{g,h}	0.0437(10)	0.4973(7)	0.6055(10)	0.131(2)

Anisotropically-refined atoms are marked with an asterisk (*). The form of the anisotropic displacement parameter is: $\exp[-2\pi^2(h^2a^{*2}U_{11} + k^2b^{*2}U_{22} + l^2c^{*2}U_{33} + 2klb^{*c^*}U_{23} + 2hla^{*c^*}U_{13} + 2hka^{*b^*}U_{12})]$. ^aRefined with an occupancy factor of 0.6. ^bThe methylene carbons C18A and C18B were refined with a common isotropic displacement parameter. ^cThe methyl carbons C19A and C19B were refined with a common isotropic displacement parameter. ^dRefined with an occupancy factor of 0.4. ^eRefined with an occupancy factor of 0.75. ^fRefined with an occupancy factor of 0.25. ^gRefined with an occupancy factor of 0.5. ^hCarbon atoms of this disordered solvent toluene molecule were refined with a common isotropic displacement parameter.

Table 3. Selected Interatomic Distances (Å)*(a) within $[(C_2(C_6H_3^nPr(O-))_4)(CpTiCl)_2]$*

Atom1	Atom2	Distance	Atom1	Atom2	Distance
Ti	Cl	2.2903(14)	C17	C18A	1.54†
Ti	O1	1.804(3)	C17	C18B	1.54†
Ti	O2	1.802(3)	C18A	C19A	1.54†
Ti	C31	2.402(4)	C18B	C19B	1.54†
Ti	C32	2.389(4)	C21	C22	1.401(5)
Ti	C33	2.354(5)	C21	C26	1.393(5)
Ti	C34	2.330(5)	C22	C23	1.409(5)
Ti	C35	2.351(4)	C23	C24	1.386(6)
O1	C12	1.361(4)	C23	C27	1.532(6)
O2	C22	1.358(4)	C24	C25	1.388(6)
C1	C1'	1.344(8)	C25	C26	1.386(6)
C1	C11	1.495(5)	C27	C28A	1.54†
C1	C21	1.491(5)	C27	C28B	1.54†
C11	C12	1.402(5)	C28A	C29A	1.54†
C11	C16	1.396(5)	C28B	C29B	1.54†
C12	C13	1.403(5)	C31	C32	1.391(7)
C13	C14	1.384(6)	C31	C35	1.398(7)
C13	C17	1.510(6)	C32	C33	1.407(7)
C14	C15	1.390(6)	C33	C34	1.396(7)
C15	C16	1.376(5)	C34	C35	1.379(7)

Primed atoms are related to unprimed ones via the crystallographic inversion center (0, 0, 1/2). †Distance fixed during refinement.

(b) within the solvent toluene molecules

Atom1	Atom2	Distance	Atom1	Atom2	Distance
C10S	C11S	1.478(14)	C11S	C13S''	1.372(9)
C11S	C12S	1.390(9)	C12S	C13S	1.400(9)

Double-primed atoms are related to unprimed ones via the inversion center (0, 0, 0).

Table 4. Selected Interatomic Angles (deg)*(a) within $[(C_2(C_6H_3^nPr(O-))_4)(CpTiCl)_2]$*

Atom1	Atom2	Atom3	Angle	Atom1	Atom2	Atom3	Angle
Cl	Ti	O1	104.73(10)	C11	C12	C13	121.7(3)
Cl	Ti	O2	102.41(10)	C12	C13	C14	117.8(4)
Cl	Ti	C31	84.65(13)	C12	C13	C17	119.9(4)
Cl	Ti	C32	105.70(13)	C14	C13	C17	122.1(4)
Cl	Ti	C33	139.39(13)	C13	C14	C15	121.3(4)
Cl	Ti	C34	133.14(14)	C14	C15	C16	120.1(4)
Cl	Ti	C35	98.92(14)	C11	C16	C15	120.6(4)
O1	Ti	O2	101.68(12)	C13	C17	C18A	115.7(5)
O1	Ti	C31	123.96(15)	C13	C17	C18B	106.3(5)
O1	Ti	C32	92.64(15)	C17	C18A	C19A	109.8†
O1	Ti	C33	89.00(16)	C17	C18B	C19B	109.8†
O1	Ti	C34	118.25(17)	C1	C21	C22	120.1(3)
O1	Ti	C35	145.69(16)	C1	C21	C26	121.6(3)
O2	Ti	C31	130.62(15)	C22	C21	C26	118.3(3)
O2	Ti	C32	143.92(16)	O2	C22	C21	118.8(3)
O2	Ti	C33	112.10(16)	O2	C22	C23	119.5(3)
O2	Ti	C34	87.05(15)	C21	C22	C23	121.7(4)
O2	Ti	C35	97.03(16)	C22	C23	C24	117.6(4)
C31	Ti	C32	33.76(16)	C22	C23	C27	120.5(4)
C31	Ti	C33	56.82(17)	C24	C23	C27	121.5(4)
C31	Ti	C34	56.82(17)	C23	C24	C25	121.6(4)
C31	Ti	C35	34.20(16)	C24	C25	C26	119.8(4)
C32	Ti	C33	34.50(17)	C21	C26	C25	120.8(4)
C32	Ti	C34	57.16(17)	C23	C27	C28A	109.7(4)
C32	Ti	C35	56.76(17)	C23	C27	C28B	121.1(9)
C33	Ti	C34	34.68(18)	C27	C28A	C29A	109.8†
C33	Ti	C35	57.19(18)	C27	C28B	C29B	109.8†
C34	Ti	C35	34.25(18)	Ti	C31	C32	72.6(3)
Ti	O1	C12	149.2(3)	Ti	C31	C35	70.9(3)
Ti	O2	C22	148.6(2)	C32	C31	C35	107.8(4)
Cl'	C1	C11	119.5(4)	Ti	C32	C31	73.6(3)
Cl'	C1	C21	121.3(4)	Ti	C32	C33	71.4(3)
C11	C1	C21	119.1(3)	C31	C32	C33	108.0(4)
Cl	C11	C12	120.0(3)	Ti	C33	C32	74.1(3)
Cl	C11	C16	121.6(3)	Ti	C33	C34	71.8(3)
C12	C11	C16	118.3(3)	C32	C33	C34	107.4(5)
O1	C12	C11	118.6(3)				
O1	C12	C13	119.7(3)				

Table 4. Selected Interatomic Angles (continued)

Atom1	Atom2	Atom3	Angle	Atom1	Atom2	Atom3	Angle
Ti	C34	C33	73.6(3)	Ti	C35	C31	74.9(3)
Ti	C34	C35	73.7(3)	Ti	C35	C34	72.1(3)
C33	C34	C35	108.5(4)	C31	C35	C34	108.4(4)

Primed atoms are related to unprimed ones via the crystallographic inversion center (0, 0, 1/2). †Angle fixed during refinement.

(b) within the solvent toluene molecules

Atom1	Atom2	Atom3	Angle	Atom1	Atom2	Atom3	Angle
C10S	C11S	C12S	120.1(9)	C11S	C12S	C13S	118.9(6)
C10S	C11S	C13S''	120.9(9)	C11S''	C13S	C12S	122.1(6)
C12S	C11S	C13S''	119.0(6)				

Double-primed atoms are related to unprimed ones via the inversion center (0, 0, 0).

Table 5. Selected Torsional Angles (deg)

Atom1	Atom2	Atom3	Atom4	Angle	Atom1	Atom2	Atom3	Atom4	Angle
Ti	O1	C12	C11	-57.4(6)	C1'	C1	C21	C26	-93.9(5)
Ti	O1	C12	C13	125.1(4)	C11	C1	C21	C22	-98.0(4)
Ti	O2	C22	C21	57.7(6)	C11	C1	C21	C26	84.0(5)
Ti	O2	C22	C23	-122.6(5)	C1	C11	C12	O1	-3.7(5)
C11	C1	C1'	C21'	2.1(7)	C1	C11	C12	C13	173.8(4)
C1'	C1	C11	C12	-85.2(5)	C1	C11	C16	C15	-175.3(4)
C1'	C1	C11	C16	92.3(6)	C1	C21	C22	O2	4.5(5)
C21	C1	C11	C12	96.8(4)	C1	C21	C22	C23	-175.1(4)
C21	C1	C11	C16	-85.6(5)	C1	C21	C26	C25	177.7(4)
C1'	C1	C21	C22	84.1(6)					

Primed atoms are related to unprimed ones via the crystallographic inversion center (0, 0, 1/2). Double-primed atoms are related to unprimed ones via the inversion center (0, 0, 0).

A-10: Complex 35. $[C_{38}H_{40}O_4]$ -gem-anti-(TiCH₂Ph)₂

– Chapter 3 –

XCL Code: JMS9913

Date: 6 April 2001

Compound: $[[C_2(C_6H_3^iPr(O-))_4]\{Ti(CH_2Ph)_2\}_2]\cdot PhMe$

Formula: $C_{73}H_{76}O_4Ti_2$ ($C_{66}H_{68}O_4Ti_2\cdot C_7H_8$)

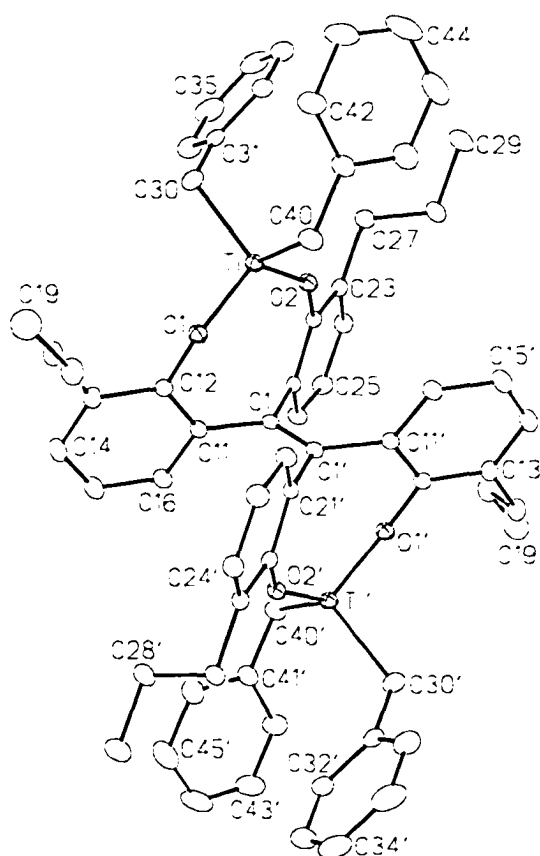


Figure 1. Perspective view of the $[[C_2(C_6H_3^iPr(O-))_4]\{Ti(CH_2Ph)_2\}_2]$ molecule showing the atom labelling scheme. Non-hydrogen atoms are represented by Gaussian ellipsoids at the 20% probability level. Hydrogen atoms are not shown.

List of Tables

Table 1. Crystallographic Experimental Details

Table 2. Atomic Coordinates and Equivalent Isotropic Displacement Parameters

Table 3. Selected Interatomic Distances

Table 4. Selected Interatomic Angles

Table 5. Selected Torsional Angles

Table 6. Selected Non-Bonded Distances and Angles

Table 1. Crystallographic Experimental Details

A. Crystal Data

formula	C ₇₃ H ₇₆ O ₄ Ti ₂
formula weight	1113.14
crystal dimensions (mm)	0.36 × 0.25 × 0.15
crystal system	triclinic
space group	PI (No. 2)
unit cell parameters ^a	
<i>a</i> (Å)	11.8707 (9)
<i>b</i> (Å)	12.2967 (10)
<i>c</i> (Å)	12.6151 (10)
α (deg)	91.2072 (16)
β (deg)	116.1191 (16)
γ (deg)	108.1636 (15)
<i>V</i> (Å ³)	1543.7 (2)
<i>Z</i>	1
ρ _{calcd} (g cm ⁻³)	1.197
μ (mm ⁻¹)	0.307

B. Data Collection and Refinement Conditions

diffractometer	Bruker P4/RA/SMART 1000 CCD ^b
radiation (λ [Å])	graphite-monochromated Mo Kα (0.71073)
temperature (°C)	-80
scan type	φ rotations (0.3°) / ω scans (0.3°) (30 s exposures)

data collection 2θ limit (deg)	51.40
total data collected	8323 ($-14 \leq h \leq 13$, $-14 \leq k \leq 14$, $-15 \leq l \leq 14$)
independent reflections	5824
number of observed reflections (<i>NO</i>)	4240 [$F_o^2 \geq 2\sigma(F_o^2)$]
structure solution method	direct methods/fragment search (<i>DIRDIF-96^c</i>)
refinement method	full-matrix least-squares on F^2 (<i>SHELXL-93^d</i>)
absorption correction method	Gaussian integration (face-indexed)
range of transmission factors	0.9586–0.9168
data/restraints/parameters	5824 [$F_o^2 \geq -3\sigma(F_o^2)$] / 0 / 355
goodness-of-fit (<i>S</i>) ^e	0.981 [$F_o^2 \geq -3\sigma(F_o^2)$]
final <i>R</i> indices ^f	
R_1 [$F_o^2 \geq 2\sigma(F_o^2)$]	0.0553
wR_2 [$F_o^2 \geq -3\sigma(F_o^2)$]	0.1527
largest difference peak and hole	0.364 and $-0.344 \text{ e } \text{\AA}^{-3}$

^aObtained from least-squares refinement of 3256 centered reflections.

^bPrograms for diffractometer operation, data collection, data reduction and absorption correction were those supplied by Bruker.

^cBeurskens, P. T.; Beurskens, G.; Bosman, W. P.; de Gelder, R.; Garcia Granda, S.; Gould, R. O.; Israel, R.; Smits, J. M. M. (1996). The *DIRDIF-96* program system. Crystallography Laboratory, University of Nijmegen, The Netherlands.

^dSheldrick, G. M. *SHELXL-93*. Program for crystal structure determination. University of Göttingen, Germany, 1993. Refinement on F_o^2 for all reflections (all of these having $F_o^2 \geq -3\sigma(F_o^2)$). Weighted *R*-factors wR_2 and all goodnesses of fit *S* are based on F_o^2 ; conventional *R*-factors R_1 are based on F_o , with F_o set to zero for negative F_o^2 . The observed criterion of $F_o^2 > 2\sigma(F_o^2)$ is used only for calculating R_1 , and is not relevant to the choice of reflections for refinement. *R*-factors based on F_o^2 are statistically about twice as large as those based on F_o , and *R*-factors based on ALL data will be even larger.

$${}^e S = [\sum w(F_o^2 - F_c^2)^2 / (n - p)]^{1/2} \quad (n = \text{number of data}; p = \text{number of parameters varied}; w = [\sigma^2(F_o^2) + (0.0888P)^2]^{-1} \text{ where } P = [\text{Max}(F_o^2, 0) + 2F_c^2] / 3).$$

$${}^f R_1 = \sum ||F_o| - |F_c|| / \sum |F_o|; \quad wR_2 = [\sum w(F_o^2 - F_c^2)^2 / \sum w(F_o^4)]^{1/2}.$$

Table 2. Atomic Coordinates and Equivalent Isotropic Displacement Parameters*(a) atoms of $[[C_2(C_6H_3^nPr(O-))_4][Ti(CH_2Ph)_2]_2]$*

Atom	x	y	z	$U_{eq}, \text{\AA}^2$
Ti	0.20431(4)	0.28103(4)	0.18141(4)	0.02850(16)*
O1	0.26392(17)	0.20354(15)	0.10853(16)	0.0323(4)*
O2	0.07375(17)	0.18556(15)	0.20722(16)	0.0305(4)*
C1	0.0439(2)	-0.0058(2)	0.0536(2)	0.0241(5)*
C11	0.1790(2)	-0.0044(2)	0.0740(2)	0.0271(5)*
C12	0.2820(2)	0.1009(2)	0.0943(2)	0.0286(6)*
C13	0.4047(2)	0.1045(2)	0.1023(2)	0.0332(6)*
C14	0.4240(3)	-0.0012(3)	0.0952(3)	0.0416(7)*
C15	0.3261(3)	-0.1052(3)	0.0802(3)	0.0434(7)*
C16	0.2038(3)	-0.1074(2)	0.0687(2)	0.0357(6)*
C17	0.5097(3)	0.2189(3)	0.1163(3)	0.0426(7)*
C18	0.4740(3)	0.2712(3)	0.0027(3)	0.0471(8)*
C19	0.5836(4)	0.3842(3)	0.0191(4)	0.0654(10)*
C21	0.0088(2)	-0.0204(2)	0.1540(2)	0.0257(5)*
C22	0.0194(2)	0.0759(2)	0.2241(2)	0.0258(5)*
C23	-0.0239(2)	0.0638(2)	0.3118(2)	0.0297(6)*
C24	-0.0769(3)	-0.0485(2)	0.3282(2)	0.0355(6)*
C25	-0.0836(3)	-0.1441(2)	0.2639(3)	0.0381(6)*
C26	-0.0416(3)	-0.1306(2)	0.1768(2)	0.0331(6)*
C27	-0.0179(3)	0.1685(2)	0.3797(2)	0.0357(6)*
C28	-0.1321(3)	0.2112(3)	0.3081(3)	0.0471(8)*
C29	-0.1256(4)	0.3166(3)	0.3781(3)	0.0661(10)*
C30	0.3730(3)	0.3685(3)	0.3451(3)	0.0438(7)*
C31	0.3515(3)	0.3744(2)	0.4523(2)	0.0381(7)*
C32	0.2985(3)	0.4529(3)	0.4743(3)	0.0467(7)*
C33	0.2787(4)	0.4578(3)	0.5733(4)	0.0650(10)*
C34	0.3118(4)	0.3859(4)	0.6544(4)	0.0747(12)*
C35	0.3642(4)	0.3069(3)	0.6344(3)	0.0679(11)*
C36	0.3831(3)	0.3011(3)	0.5337(3)	0.0520(8)*
C40	0.1414(3)	0.4012(2)	0.0754(3)	0.0404(7)*
C41	0.1334(3)	0.4918(2)	0.1482(2)	0.0392(7)*
C42	0.2372(4)	0.5999(3)	0.2013(3)	0.0523(8)*
C43	0.2305(5)	0.6825(3)	0.2714(3)	0.0658(10)*
C44	0.1217(5)	0.6596(4)	0.2907(3)	0.0750(13)*
C45	0.0177(5)	0.5537(4)	0.2402(4)	0.0722(12)*
C46	0.0238(3)	0.4700(3)	0.1694(3)	0.0517(8)*

Table 2. Atomic Coordinates and Displacement Parameters (continued)*(b) solvent toluene atoms*

Atom	x	y	z	$U_{eq}, \text{\AA}^2$
C10S ^a	0.2978(11)	-0.0229(11)	0.4755(11)	0.084(4)
C11S ^a	0.4284(7)	-0.0055(6)	0.4973(6)	0.0549(16)
C12S ^a	0.4445(11)	0.0374(8)	0.4123(9)	0.062(3)
C13S ^a	0.5790(10)	0.0608(8)	0.4164(9)	0.084(2)
C14S ^a	0.6775(14)	0.0399(11)	0.4916(11)	0.088(4)
C15S ^a	0.6530(9)	-0.0073(7)	0.5916(8)	0.075(2)
C16S ^a	0.5232(10)	-0.0336(8)	0.5925(8)	0.053(3)

Anisotropically-refined atoms are marked with an asterisk (*). The form of the anisotropic displacement parameter is: $\exp[-2\pi^2(h^2a^{*2}U_{11} + k^2b^{*2}U_{22} + l^2c^{*2}U_{33} + 2klb^{*c^*}U_{23} + 2hla^{*c^*}U_{13} + 2hka^{*b^*}U_{12})]$. ^aRefined with an occupancy factor of 0.5.

Table 3. Selected Interatomic Distances (Å)*(a) within $[(C_2(C_6H_3^nPr(O-))_4)[Ti(CH_2Ph)_2]_2]$*

Atom1	Atom2	Distance	Atom1	Atom2	Distance
Ti	O1	1.7917(18)	C23	C24	1.391(4)
Ti	O2	1.7923(17)	C23	C27	1.496(4)
Ti	C30	2.086(3)	C24	C25	1.374(4)
Ti	C40	2.103(3)	C25	C26	1.387(4)
O1	C12	1.365(3)	C27	C28	1.521(4)
O2	C22	1.368(3)	C28	C29	1.515(4)
C1	C1'	1.341(5)	C30	C31	1.486(4)
C1	C11	1.502(3)	C31	C32	1.388(4)
C1	C21	1.495(3)	C31	C36	1.385(4)
C11	C12	1.400(4)	C32	C33	1.372(5)
C11	C16	1.394(3)	C33	C34	1.373(6)
C12	C13	1.401(3)	C34	C35	1.378(6)
C13	C14	1.396(4)	C35	C36	1.389(5)
C13	C17	1.505(4)	C40	C41	1.481(4)
C14	C15	1.376(4)	C41	C42	1.396(4)
C15	C16	1.385(4)	C41	C46	1.389(4)
C17	C18	1.524(4)	C42	C43	1.376(5)
C18	C19	1.514(4)	C43	C44	1.365(6)
C21	C22	1.402(3)	C44	C45	1.377(6)
C21	C26	1.392(3)	C45	C46	1.389(5)
C22	C23	1.404(3)			

Primed atoms are related to unprimed ones via the crystallographic inversion center (0, 0, 0).

(b) within the solvent toluene molecule

Atom1	Atom2	Distance	Atom1	Atom2	Distance
C10S	C11S	1.393(13)	C13S	C14S	1.247(14)
C11S	C12S	1.267(11)	C14S	C15S	1.504(16)
C11S	C16S	1.377(11)	C15S	C16S	1.478(13)
C12S	C13S	1.509(14)			

Table 4. Selected Interatomic Angles (deg)*(a) within $[(C_2(C_6H_3^iPr(O-))_4)\{Ti(CH_2Ph)_2\}_2]$*

Atom1	Atom2	Atom3	Angle	Atom1	Atom2	Atom3	Angle
O1	Ti	O2	112.40(8)	O2	C22	C23	118.4(2)
O1	Ti	C30	104.25(10)	C21	C22	C23	122.2(2)
O1	Ti	C40	107.56(10)	C22	C23	C24	117.2(2)
O2	Ti	C30	109.93(10)	C22	C23	C27	120.4(2)
O2	Ti	C40	112.17(10)	C24	C23	C27	122.3(2)
C30	Ti	C40	110.22(12)	C23	C24	C25	121.7(2)
Ti	O1	C12	143.88(16)	C24	C25	C26	120.2(2)
Ti	O2	C22	145.33(16)	C21	C26	C25	120.6(3)
C1'	C1	C11	120.1(3)	C23	C27	C28	113.1(2)
C1'	C1	C21	120.5(3)	C27	C28	C29	112.6(3)
C11	C1	C21	119.3(2)	Ti	C30	C31	116.98(19)
C1	C11	C12	120.6(2)	C30	C31	C32	121.4(3)
C1	C11	C16	121.2(2)	C30	C31	C36	121.1(3)
C12	C11	C16	118.2(2)	C32	C31	C36	117.5(3)
O1	C12	C11	119.4(2)	C31	C32	C33	121.2(3)
O1	C12	C13	118.6(2)	C32	C33	C34	121.0(4)
C11	C12	C13	122.0(2)	C33	C34	C35	119.0(4)
C12	C13	C14	117.5(2)	C34	C35	C36	120.1(3)
C12	C13	C17	120.4(2)	C31	C36	C35	121.3(3)
C14	C13	C17	122.0(2)	Ti	C40	C41	109.49(18)
C13	C14	C15	121.4(3)	C40	C41	C42	121.5(3)
C14	C15	C16	120.3(3)	C40	C41	C46	120.8(3)
C11	C16	C15	120.6(3)	C42	C41	C46	117.7(3)
C13	C17	C18	113.6(2)	C41	C42	C43	121.1(4)
C17	C18	C19	112.1(3)	C42	C43	C44	120.2(4)
C1	C21	C22	121.0(2)	C43	C44	C45	120.3(4)
C1	C21	C26	120.9(2)	C44	C45	C46	119.8(4)
C22	C21	C26	118.0(2)	C41	C46	C45	120.9(4)
O2	C22	C21	119.4(2)				

Primed atoms are related to unprimed ones via the crystallographic inversion center (0, 0, 0).

Table 4. Selected Interatomic Angles (continued)*(b) within the solvent toluene molecule*

Atom1	Atom2	Atom3	Angle	Atom1	Atom2	Atom3	Angle
C10S	C11S	C12S	108.4(9)	C12S	C13S	C14S	128.3(11)
C10S	C11S	C16S	126.2(9)	C13S	C14S	C15S	111.4(11)
C12S	C11S	C16S	125.4(8)	C14S	C15S	C16S	122.9(9)
C11S	C12S	C13S	117.3(9)	C11S	C16S	C15S	114.5(8)

Table 5. Selected Torsional Angles (deg)

Atom1	Atom2	Atom3	Atom4	Angle	Atom1	Atom2	Atom3	Atom4	Angle
O1	Ti	C30	C31	-140.8(2)	C21	C1	C11	C12	-102.0(3)
O2	Ti	C30	C31	-20.1(3)	C21	C1	C11	C16	80.5(3)
C40	Ti	C30	C31	104.0(2)	C1'	C1	C21	C22	-80.6(4)
O1	Ti	C40	C41	-161.74(19)	C1'	C1	C21	C26	96.2(3)
O2	Ti	C40	C41	74.2(2)	C11	C1	C21	C22	99.4(3)
C30	Ti	C40	C41	-48.7(2)	C11	C1	C21	C26	-83.8(3)
Ti	O1	C12	C11	44.8(4)	C1	C11	C12	O1	7.1(4)
Ti	O1	C12	C13	-134.3(2)	C1	C11	C12	C13	-173.8(2)
Ti	O2	C22	C21	-41.4(4)	C1	C11	C16	C15	175.9(2)
Ti	O2	C22	C23	138.5(2)	C1	C21	C22	O2	-5.8(3)
C11	C1	C1'	C21'	0.0(5)	C1	C21	C22	C23	174.3(2)
C1'	C1	C11	C12	77.9(4)	C1	C21	C26	C25	-175.0(2)
C1'	C1	C11	C16	-99.5(3)					

Primed atoms are related to unprimed ones via the crystallographic inversion center (0, 0, 0).

Table 6. Selected Non-Bonded Distances and Angles

(Centroid of C31~C36)-(centroid of C41~C46) = 74.4°

H32-(centroid of C41~C46) = 2.72 Å

(Plane of C31~C36) ⊥ (plane of C41~C46) = 4.95 Å

List of Tables

Table 1. Crystallographic Experimental Details

Table 2. Atomic Coordinates and Equivalent Isotropic Displacement Parameters

Table 3. Selected Interatomic Distances

Table 4. Selected Interatomic Angles

Table 5. Selected Torsional Angles

Table 1. Crystallographic Experimental Details

A. Crystal Data

formula	C ₄₈ H ₆₅ Al ₃ O ₄
formula weight	786.94
crystal dimensions (mm)	0.37 × 0.36 × 0.28
crystal system	monoclinic
space group	<i>P</i> 2 ₁ / <i>n</i> (an alternate setting of <i>P</i> 2 ₁ / <i>c</i> [No. 14])
unit cell parameters ^a	
<i>a</i> (Å)	12.5164 (9)
<i>b</i> (Å)	20.1607 (14)
<i>c</i> (Å)	18.4010 (12)
β (deg)	104.5430 (13)
<i>V</i> (Å ³)	4494.5 (5)
<i>Z</i>	4
ρ _{calcd} (g cm ⁻³)	1.163
μ (mm ⁻¹)	0.125

B. Data Collection and Refinement Conditions

diffractometer	Bruker P4/RA/SMART 1000 CCD ^b
radiation (λ [Å])	graphite-monochromated Mo Kα (0.71073)
temperature (°C)	-80
scan type	φ rotations (0.3°) / ω scans (0.3°) (30 s exposures)
data collection 2θ limit (deg)	52.76
total data collected	23542 (-15 ≤ h ≤ 15, -25 ≤ k ≤ 24, -18 ≤ l ≤ 23)
independent reflections	9168
number of observed reflections (<i>NO</i>)	5054 [<i>F</i> _o ² ≥ 2σ(<i>F</i> _o ²)]

structure solution method	direct methods (<i>SHELXS-86</i> ^c)
refinement method	full-matrix least-squares on F^2 (<i>SHELXL-93</i> ^d)
absorption correction method	<i>SADABS</i>
range of transmission factors	0.9703–0.8192
data/restraints/parameters	9168 [$F_o^2 \geq -3\sigma(F_o^2)$] / 0 / 496
goodness-of-fit (S) ^e	1.036 [$F_o^2 \geq -3\sigma(F_o^2)$]
final R indices ^f	
R_1 [$F_o^2 \geq 2\sigma(F_o^2)$]	0.0672
wR_2 [$F_o^2 \geq -3\sigma(F_o^2)$]	0.1869
largest difference peak and hole	0.586 and -0.372 e Å ⁻³

^aObtained from least-squares refinement of 5991 centered reflections.

^bPrograms for diffractometer operation, data collection, data reduction and absorption correction were those supplied by Bruker.

^cSheldrick, G. M. *Acta Crystallogr.* **1990**, *A46*, 467–473.

^dSheldrick, G. M. *SHELXL-93*. Program for crystal structure determination. University of Göttingen, Germany, 1993. Refinement on F_o^2 for all reflections (all of these having $F_o^2 \geq -3\sigma(F_o^2)$). Weighted R -factors wR_2 and all goodnesses of fit S are based on F_o^2 ; conventional R -factors R_1 are based on F_o , with F_o set to zero for negative F_o^2 . The observed criterion of $F_o^2 > 2\sigma(F_o^2)$ is used only for calculating R_1 , and is not relevant to the choice of reflections for refinement. R -factors based on F_o^2 are statistically about twice as large as those based on F_o , and R -factors based on ALL data will be even larger.

$$^eS = [\sum w(F_o^2 - F_c^2)^2 / (n - p)]^{1/2} \quad (n = \text{number of data}; p = \text{number of parameters varied}; w = [\sigma^2(F_o^2) + (0.0920P)^2]^{-1} \text{ where } P = [\text{Max}(F_o^2, 0) + 2F_c^2] / 3).$$

$$^fR_1 = \sum ||F_o| - |F_c|| / \sum |F_o|; wR_2 = [\sum w(F_o^2 - F_c^2)^2 / \sum w(F_o^4)]^{1/2}.$$

Table 2. Atomic Coordinates and Equivalent Isotropic Displacement Parameters

Atom	x	y	z	$U_{eq}, \text{\AA}^2$
Al1	0.03788(7)	-0.33357(5)	0.21365(4)	0.0372(2)*
Al2	-0.09936(8)	-0.20675(5)	0.25721(5)	0.0480(3)*
Al3	-0.20153(8)	-0.36314(5)	0.24820(5)	0.0428(3)*
O1	0.16875(16)	-0.36385(11)	0.23799(10)	0.0442(6)*
O2	0.03440(16)	-0.24922(10)	0.25440(10)	0.0395(5)*
O3	-0.05609(15)	-0.38879(10)	0.24935(10)	0.0369(5)*
O4	-0.15425(16)	-0.28262(11)	0.29554(11)	0.0451(6)*
C1	0.1515(4)	-0.3232(2)	0.38139(17)	0.0672(11)*
C2	0.0601(3)	-0.3446(2)	0.38985(16)	0.0645(12)*
C11	0.2423(3)	-0.36777(17)	0.37041(17)	0.0460(8)*
C12	0.2497(2)	-0.38306(17)	0.29877(17)	0.0434(8)*
C13	0.3385(3)	-0.4196(2)	0.2869(2)	0.0646(11)*
C14	0.4217(3)	-0.4384(2)	0.3486(2)	0.0771(13)*
C15	0.4169(3)	-0.4209(2)	0.4205(2)	0.0699(12)*
C16	0.3273(3)	-0.38668(19)	0.43164(19)	0.0574(10)*
C17	0.3380(3)	-0.4441(2)	0.2053(3)	0.0773(13)*
C18	0.3764(4)	-0.3914(3)	0.1648(3)	0.0968(16)*
C19	0.3651(5)	-0.4193(3)	0.0810(3)	0.127(2)*
C21	0.1710(3)	-0.24962(17)	0.37413(17)	0.0522(9)*
C22	0.1257(3)	-0.21918(16)	0.30558(16)	0.0417(8)*
C23	0.1648(3)	-0.15940(17)	0.28635(17)	0.0454(8)*
C24	0.2451(3)	-0.12734(19)	0.3416(2)	0.0586(10)*
C25	0.2863(3)	-0.1551(2)	0.4114(2)	0.0648(11)*
C26	0.2529(3)	-0.21617(19)	0.42634(19)	0.0665(11)*
C27	0.1288(3)	-0.12989(18)	0.20879(18)	0.0574(10)*
C28	0.2132(3)	-0.1419(3)	0.1627(2)	0.0787(13)*
C29	0.1749(4)	-0.1145(3)	0.0834(2)	0.0951(16)*
C31	0.0394(3)	-0.42100(17)	0.37479(17)	0.0457(8)*
C32	-0.0164(2)	-0.43971(16)	0.30268(15)	0.0385(7)*
C33	-0.0365(3)	-0.50581(18)	0.28216(18)	0.0489(8)*
C34	0.0009(3)	-0.55272(19)	0.3388(2)	0.0623(10)*
C35	0.0542(3)	-0.5349(2)	0.4108(2)	0.0642(11)*
C36	0.0744(3)	-0.4700(2)	0.4294(2)	0.0588(10)*
C37	-0.0913(3)	-0.5251(2)	0.20317(19)	0.0614(10)*
C38	-0.0106(4)	-0.5296(2)	0.1534(2)	0.0781(13)*
C39	-0.0670(5)	-0.5453(2)	0.0726(2)	0.1055(18)*
C41	-0.0281(3)	-0.30558(17)	0.41771(16)	0.0459(8)*
C42	-0.1295(3)	-0.28193(16)	0.37533(17)	0.0472(8)*
C43	-0.2085(3)	-0.25447(19)	0.4075(2)	0.0607(10)*

Atom	x	y	z	$U_{eq}, \text{Å}^2$
C44	-0.1817(4)	-0.2513(2)	0.4865(2)	0.0783(13)*
Table 2. Atomic Coordinates and Displacement Parameters (continued)				
C45	-0.0836(4)	-0.2743(2)	0.5290(2)	0.0787(13)*
C46	-0.0060(3)	-0.30037(19)	0.49551(18)	0.0607(10)*
C47	-0.3174(3)	-0.2281(2)	0.3611(3)	0.0765(12)*
C48	-0.4153(4)	-0.2706(2)	0.3580(3)	0.0885(14)*
C49	-0.5224(4)	-0.2416(3)	0.3092(3)	0.1021(17)*
C50	-0.0179(3)	-0.32934(19)	0.10523(16)	0.0493(9)*
C51	0.0552(4)	-0.3001(3)	0.0630(2)	0.117(2)*
C52	-0.1869(3)	-0.1853(2)	0.1562(2)	0.0713(12)*
C53A ^a	-0.2073(5)	-0.1151(3)	0.1366(3)	0.0725(16)
C53B ^b	-0.2819(11)	-0.1458(7)	0.1531(7)	0.072(4)
C54	-0.0844(3)	-0.1297(2)	0.3225(2)	0.0774(13)*
C55	-0.0237(4)	-0.1215(3)	0.3992(3)	0.1034(17)*
C56	-0.2910(3)	-0.3466(2)	0.14608(17)	0.0570(10)*
C57	-0.3248(4)	-0.4081(3)	0.0979(2)	0.1038(17)*
C58	-0.2718(3)	-0.42474(18)	0.30383(17)	0.0512(9)*
C59	-0.2389(3)	-0.43780(19)	0.38846(18)	0.0596(10)*

Anisotropically-refined atoms are marked with an asterisk (*). The form of the anisotropic displacement parameter is: $\exp[-2\pi^2(h^2a^2U_{11} + k^2b^2U_{22} + l^2c^2U_{33} + 2klb^*c^*U_{23} + 2hla^*c^*U_{13} + 2hka^*b^*U_{12})]$. ^aRefined with an occupancy factor of 0.7. ^bRefined with an occupancy factor of 0.3.

Table 3. Selected Interatomic Distances (Å)

Atom1	Atom2	Distance	Atom1	Atom2	Distance
A11	O1	1.699(2)	C22	C23	1.380(4)
A11	O2	1.863(2)	C23	C24	1.396(5)
A11	O3	1.855(2)	C23	C27	1.507(4)
A11	C50	1.943(3)	C24	C25	1.376(5)
A12	O2	1.893(2)	C25	C26	1.350(5)
A12	O4	1.885(2)	C27	C28	1.531(5)
A12	C52	1.955(4)	C28	C29	1.521(5)
A12	C54	1.943(4)	C31	C32	1.388(4)
A13	O3	1.887(2)	C31	C36	1.398(4)
A13	O4	1.867(2)	C32	C33	1.391(5)
A13	C56	1.960(3)	C33	C34	1.398(5)
A13	C58	1.954(3)	C33	C37	1.494(5)
O1	C12	1.363(3)	C34	C35	1.373(5)
O2	C22	1.421(3)	C35	C36	1.361(5)
O3	C32	1.421(3)	C37	C38	1.527(5)
O4	C42	1.422(4)	C38	C39	1.511(6)
C1	C2	1.268(5)	C41	C42	1.395(5)
C1	C11	1.502(5)	C41	C46	1.392(4)
C1	C21	1.514(5)	C42	C43	1.389(5)
C2	C31	1.574(5)	C43	C44	1.408(5)
C2	C41	1.545(5)	C43	C47	1.512(5)
C11	C12	1.380(4)	C44	C45	1.361(6)
C11	C16	1.395(4)	C45	C46	1.378(5)
C12	C13	1.395(5)	C47	C48	1.484(6)
C13	C14	1.386(5)	C48	C49	1.529(6)
C13	C17	1.580(5)	C50	C51	1.464(5)
C14	C15	1.384(6)	C52	C53A	1.466(7)
C15	C16	1.375(5)	C52	C53B	1.421(13)
C17	C18	1.448(6)	C54	C55	1.435(6)
C18	C19	1.614(6)	C56	C57	1.522(6)
C21	C22	1.389(4)	C58	C59	1.530(4)
C21	C26	1.391(5)			

Table 4. Selected Interatomic Angles (deg)

Atom1	Atom2	Atom3	Angle	Atom1	Atom2	Atom3	Angle
O1	Al1	O2	109.88(10)	C11	C12	C13	121.0(3)
O1	Al1	O3	110.24(10)	C12	C13	C14	118.7(3)
O1	Al1	C50	111.13(12)	C12	C13	C17	120.0(3)
O2	Al1	O3	108.91(9)	C14	C13	C17	121.1(4)
O2	Al1	C50	109.54(13)	C13	C14	C15	120.6(4)
O3	Al1	C50	107.08(12)	C14	C15	C16	120.2(3)
O2	Al2	O4	92.93(10)	C11	C16	C15	120.1(3)
O2	Al2	C52	111.26(14)	C13	C17	C18	109.7(4)
O2	Al2	C54	115.47(15)	C17	C18	C19	106.0(4)
O4	Al2	C52	111.44(15)	C1	C21	C22	118.3(3)
O4	Al2	C54	113.87(15)	C1	C21	C26	121.4(3)
C52	Al2	C54	110.80(19)	C22	C21	C26	118.3(3)
O3	Al3	O4	92.36(10)	O2	C22	C21	119.3(3)
O3	Al3	C56	112.02(13)	O2	C22	C23	118.7(3)
O3	Al3	C58	112.34(13)	C21	C22	C23	121.9(3)
O4	Al3	C56	109.71(14)	C22	C23	C24	117.0(3)
O4	Al3	C58	116.10(13)	C22	C23	C27	123.1(3)
C56	Al3	C58	112.73(15)	C24	C23	C27	119.7(3)
Al1	O1	C12	141.9(2)	C23	C24	C25	121.5(3)
Al1	O2	Al2	122.28(11)	C24	C25	C26	119.9(3)
Al1	O2	C22	124.02(18)	C21	C26	C25	120.9(3)
Al2	O2	C22	111.02(18)	C23	C27	C28	112.2(3)
Al1	O3	Al3	121.81(11)	C27	C28	C29	112.3(4)
Al1	O3	C32	122.38(17)	C2	C31	C32	117.1(3)
Al3	O3	C32	111.99(16)	C2	C31	C36	123.8(3)
Al2	O4	Al3	129.32(11)	C32	C31	C36	119.1(3)
Al2	O4	C42	111.89(18)	O3	C32	C31	117.9(3)
Al3	O4	C42	116.84(19)	O3	C32	C33	119.8(3)
C2	C1	C11	123.2(4)	C31	C32	C33	122.2(3)
C2	C1	C21	121.0(4)	C32	C33	C34	116.2(3)
C11	C1	C21	115.5(3)	C32	C33	C37	121.4(3)
C1	C2	C31	115.2(4)	C34	C33	C37	122.4(3)
C1	C2	C41	127.5(4)	C33	C34	C35	122.2(4)
C31	C2	C41	117.2(3)	C34	C35	C36	120.6(3)
C1	C11	C12	119.8(3)	C31	C36	C35	119.6(3)
C1	C11	C16	120.3(3)	C33	C37	C38	112.8(3)
C12	C11	C16	119.4(3)	C37	C38	C39	112.8(4)
O1	C12	C11	120.4(3)	C2	C41	C42	127.9(3)
O1	C12	C13	118.7(3)	C2	C41	C46	113.9(3)

Table 4. Selected Interatomic Angles (continued)

Atom1	Atom2	Atom3	Angle	Atom1	Atom2	Atom3	Angle
C42	C41	C46	117.8(3)	C41	C46	C45	120.5(4)
O4	C42	C41	120.4(3)	C43	C47	C48	115.9(4)
O4	C42	C43	116.7(3)	C47	C48	C49	113.3(4)
C41	C42	C43	122.9(3)	Al1	C50	C51	116.8(3)
C42	C43	C44	116.5(4)	Al2	C52	C53A	117.9(3)
C42	C43	C47	122.5(3)	Al2	C52	C53B	115.2(6)
C44	C43	C47	120.9(4)	Al2	C54	C55	130.2(4)
C43	C44	C45	121.7(4)	Al3	C56	C57	115.4(3)
C44	C45	C46	120.5(4)	Al3	C58	C59	126.9(2)

Table 5. Torsional Angles (deg)

Atom1	Atom2	Atom3	Atom4	Angle	Atom1	Atom2	Atom3	Atom4	Angle
O2	Al1	O1	C12	64.4(4)	C56	Al3	O4	C42	154.8(2)
O3	Al1	O1	C12	-55.7(4)	C58	Al3	O4	Al2	-171.80(15)
C50	Al1	O1	C12	-174.2(3)	C58	Al3	O4	C42	25.5(3)
O1	Al1	O2	Al2	-166.90(12)	C11	C1	C2	C31	-9.8(4)
O1	Al1	O2	C22	-7.1(2)	C11	C1	C2	C41	166.1(3)
O3	Al1	O2	Al2	-46.05(14)	C21	C1	C2	C31	164.1(3)
O3	Al1	O2	C22	113.7(2)	C21	C1	C2	C41	-20.0(5)
C50	Al1	O2	Al2	70.76(16)	C2	C1	C11	C12	93.8(4)
C50	Al1	O2	C22	-129.5(2)	C2	C1	C11	C16	-94.7(4)
O1	Al1	O3	Al3	168.79(11)	C21	C1	C11	C12	-80.4(4)
O1	Al1	O3	C32	12.6(2)	C21	C1	C11	C16	91.1(4)
O2	Al1	O3	Al3	48.17(14)	C2	C1	C21	C22	-78.0(4)
O2	Al1	O3	C32	-108.0(2)	C2	C1	C21	C26	118.0(4)
C50	Al1	O3	Al3	-70.20(17)	C11	C1	C21	C22	96.4(4)
C50	Al1	O3	C32	133.6(2)	C11	C1	C21	C26	-67.7(4)
O4	Al2	O2	Al1	47.56(13)	C1	C2	C31	C32	-92.4(4)
O4	Al2	O2	C22	-114.57(18)	C1	C2	C31	C36	87.1(4)
C52	Al2	O2	Al1	-66.80(19)	C41	C2	C31	C32	91.3(3)
C52	Al2	O2	C22	131.1(2)	C41	C2	C31	C36	-89.2(4)
C54	Al2	O2	Al1	165.80(17)	C1	C2	C41	C42	105.0(4)
C54	Al2	O2	C22	3.7(2)	C1	C2	C41	C46	-82.2(4)
O2	Al2	O4	Al3	-70.36(15)	C31	C2	C41	C42	-79.2(4)
O2	Al2	O4	C42	93.0(2)	C31	C2	C41	C46	93.6(4)
C52	Al2	O4	Al3	43.8(2)	C1	C11	C12	O1	-7.0(5)
C52	Al2	O4	C42	-152.8(2)	C1	C11	C12	C13	174.4(4)
C54	Al2	O4	Al3	170.07(18)	C1	C11	C16	C15	-172.3(4)
C54	Al2	O4	C42	-26.6(3)	C1	C21	C22	O2	21.8(5)
O4	Al3	O3	Al1	-51.12(13)	C1	C21	C22	C23	-160.1(3)
O4	Al3	O3	C32	107.32(19)	C1	C21	C26	C25	165.2(4)
C56	Al3	O3	Al1	61.26(18)	C2	C31	C32	O3	-3.6(4)
C56	Al3	O3	C32	-140.3(2)	C2	C31	C32	C33	178.0(3)
C58	Al3	O3	Al1	-170.65(14)	C2	C31	C36	C35	-179.0(4)
C58	Al3	O3	C32	-12.2(2)	C2	C41	C42	O4	-10.8(5)
O3	Al3	O4	Al2	71.86(15)	C2	C41	C42	C43	171.8(4)
O3	Al3	O4	C42	-90.8(2)	C2	C41	C46	C45	-171.9(4)
C56	Al3	O4	Al2	-42.6(2)					

A-12: Complex 39. C₃₈H₄₀O₄[Al(thf)][AlCl₂]

– Chapter 3–

XCL Code: JMS0050

Date: 3 June 2001

Compound: [[C₂(C₆H₃ⁿPr{O-})₄]{Al(OC₄H₈)}(AlCl₂)]

Formula: C₄₂H₄₈Al₂Cl₂O₅

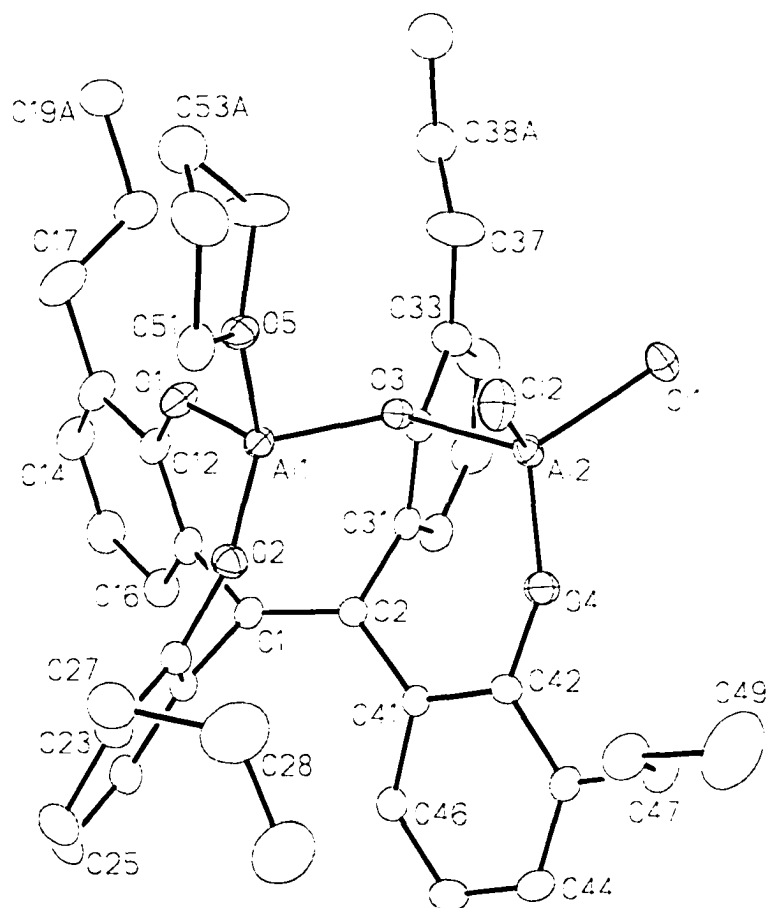


Figure 1. Perspective view of the [[C₂(C₆H₃ⁿPr{O-})₄]{Al(OC₄H₈)}(AlCl₂)] molecule showing the atom labelling scheme. Non-hydrogen atoms are represented by Gaussian ellipsoids at the 20% probability level. Hydrogen atoms are not shown.

List of Tables

Table 1. Crystallographic Experimental Details

Table 2. Atomic Coordinates and Equivalent Isotropic Displacement Parameters

Table 3. Selected Interatomic Distances

Table 4. Selected Interatomic Angles

Table 5. Selected Torsional Angles

Table 1. Crystallographic Experimental Details

A. Crystal Data

formula	C ₄₂ H ₄₈ Al ₂ Cl ₂ O ₅
formula weight	757.66
crystal dimensions (mm)	0.45 × 0.38 × 0.15
crystal system	monoclinic
space group	<i>P</i> 2 ₁ / <i>n</i> (an alternate setting of <i>P</i> 2 ₁ / <i>c</i> [No. 14])
unit cell parameters ^a	
<i>a</i> (Å)	13.6750 (8)
<i>b</i> (Å)	12.7435 (8)
<i>c</i> (Å)	22.9049 (14)
β (deg)	94.0180 (14)
<i>V</i> (Å ³)	3981.8 (4)
<i>Z</i>	4
ρ _{calcd} (g cm ⁻³)	1.264
μ (mm ⁻¹)	0.250

B. Data Collection and Refinement Conditions

diffractometer	Bruker PLATFORM/SMART 1000 CCD ^b
radiation (λ [Å])	graphite-monochromated Mo Kα (0.71073)
temperature (°C)	-80
scan type	ω scans (0.2°) (20 s exposures)
data collection 2θ limit (deg)	52.82
total data collected	21354 (-17 ≤ <i>h</i> ≤ 17, -15 ≤ <i>k</i> ≤ 15, -18 ≤ <i>l</i> ≤ 28)

independent reflections	8128
number of observed reflections (<i>NO</i>)	5395 [$F_o^2 \geq 2\sigma(F_o^2)$]
structure solution method	direct methods (<i>SHELXS-86</i> ^c)
refinement method	full-matrix least-squares on F^2 (<i>SHELXL-93</i> ^d)
absorption correction method	empirical (<i>SADABS</i>)
range of transmission factors	0.9635–0.8958
data/restraints/parameters	8128 [$F_o^2 \geq -3\sigma(F_o^2)$] / 0 / 466
goodness-of-fit (<i>S</i>) ^e	1.031 [$F_o^2 \geq -3\sigma(F_o^2)$]
final <i>R</i> indices ^f	
R_1 [$F_o^2 \geq 2\sigma(F_o^2)$]	0.0592
wR_2 [$F_o^2 \geq -3\sigma(F_o^2)$]	0.1625
largest difference peak and hole	0.642 and $-0.333 \text{ e } \text{\AA}^{-3}$

^aObtained from least-squares refinement of 5589 centered reflections.

^bPrograms for diffractometer operation, data collection, data reduction and absorption correction were those supplied by Bruker.

^cSheldrick, G. M. *Acta Crystallogr.* **1990**, *A46*, 467–473.

^dSheldrick, G. M. *SHELXL-93*. Program for crystal structure determination. University of Göttingen, Germany, 1993. Refinement on F_o^2 for all reflections (all of these having $F_o^2 \geq -3\sigma(F_o^2)$). Weighted *R*-factors wR_2 and all goodnesses of fit *S* are based on F_o^2 ; conventional *R*-factors R_1 are based on F_o , with F_o set to zero for negative F_o^2 . The observed criterion of $F_o^2 > 2\sigma(F_o^2)$ is used only for calculating R_1 , and is not relevant to the choice of reflections for refinement. *R*-factors based on F_o^2 are statistically about twice as large as those based on F_o , and *R*-factors based on ALL data will be even larger.

^e $S = [\sum w(F_o^2 - F_c^2)^2 / (n - p)]^{1/2}$ (n = number of data; p = number of parameters varied; $w = [\sigma^2(F_o^2) + (0.0759P)^2 + 2.2850P]^{-1}$ where $P = [\text{Max}(F_o^2, 0) + 2F_c^2] / 3$).

^f $R_1 = \sum ||F_o| - |F_c|| / \sum |F_o|$; $wR_2 = [\sum w(F_o^2 - F_c^2)^2 / \sum w(F_o^4)]^{1/2}$.

Table 2. Atomic Coordinates and Equivalent Isotropic Displacement Parameters

Atom	x	y	z	U_{eq} , Å ²
C11	0.19869(6)	0.58294(6)	0.08429(4)	0.0502(2)*
C12	0.31669(7)	0.49706(6)	0.21420(4)	0.0550(2)*
A11	0.26312(6)	0.22467(7)	0.16756(4)	0.0348(2)*
A12	0.28875(6)	0.46475(6)	0.12403(4)	0.0352(2)*
O1	0.18634(16)	0.12395(17)	0.14722(9)	0.0465(5)*
O2	0.38457(14)	0.20698(16)	0.18827(9)	0.0408(5)*
O3	0.22528(13)	0.33650(15)	0.12159(8)	0.0342(4)*
O4	0.38968(15)	0.44544(16)	0.08838(11)	0.0484(6)*
O5	0.21891(15)	0.26699(16)	0.23694(9)	0.0435(5)*
C1	0.3483(2)	0.1290(2)	0.07514(13)	0.0364(7)*
C2	0.3500(2)	0.2264(2)	0.05161(12)	0.0341(6)*
C11	0.2629(2)	0.0560(2)	0.06494(14)	0.0420(7)*
C12	0.1866(2)	0.0553(2)	0.10205(14)	0.0443(8)*
C13	0.1096(3)	-0.0170(3)	0.09448(16)	0.0566(9)*
C14	0.1121(3)	-0.0875(3)	0.04816(18)	0.0672(11)*
C15	0.1873(3)	-0.0879(3)	0.01146(18)	0.0651(11)*
C16	0.2630(3)	-0.0163(3)	0.01926(16)	0.0537(9)*
C17	0.0279(3)	-0.0163(4)	0.13441(19)	0.0766(13)*
C18A ^a	-0.0433(5)	0.0578(7)	0.1211(3)	0.089(2)*
C19A ^a	-0.1324(6)	0.0548(7)	0.1575(4)	0.099(3)*
C18B ^b	-0.0680(13)	-0.0554(16)	0.1211(8)	0.118(6)
C19B ^b	-0.1528(14)	-0.0223(16)	0.1588(9)	0.121(6)
C21	0.4326(2)	0.0898(2)	0.11353(15)	0.0419(7)*
C22	0.4475(2)	0.1334(2)	0.16960(14)	0.0426(7)*
C23	0.5275(3)	0.1026(3)	0.20726(17)	0.0564(9)*
C24	0.5893(3)	0.0257(3)	0.1885(2)	0.0703(12)*
C25	0.5737(3)	-0.0203(3)	0.1344(2)	0.0711(12)*
C26	0.4954(3)	0.0104(3)	0.09685(17)	0.0566(9)*
C27	0.5477(3)	0.1560(4)	0.26572(17)	0.0703(11)*
C28	0.5863(4)	0.2685(5)	0.2602(3)	0.1075(18)*
C29	0.6702(4)	0.2825(5)	0.2268(3)	0.121(2)*
C31	0.2552(2)	0.2707(2)	0.02569(13)	0.0367(7)*
C32	0.1902(2)	0.3156(2)	0.06219(13)	0.0374(7)*
C33	0.0945(2)	0.3439(3)	0.04450(16)	0.0504(8)*
C34	0.0678(3)	0.3303(3)	-0.01490(18)	0.0645(11)*
C35	0.1324(3)	0.2906(3)	-0.05297(17)	0.0619(10)*
C36	0.2246(3)	0.2599(3)	-0.03322(14)	0.0486(8)*
C37	0.0239(2)	0.3840(4)	0.0867(2)	0.0788(14)*
C38A ^a	-0.0807(5)	0.3630(6)	0.0763(3)	0.0678(17)

Table 2. Atomic Coordinates and Displacement Parameters (continued)

Atom	x	y	z	$U_{eq}, \text{\AA}^2$
C39A ^a	-0.1393(7)	0.3981(7)	0.1262(4)	0.082(2)
C38B ^b	-0.0521(8)	0.3200(10)	0.0960(5)	0.062(3)
C39B ^b	-0.1311(12)	0.3572(13)	0.1342(7)	0.081(5)
C41	0.4433(2)	0.2850(2)	0.04737(13)	0.0358(6)*
C42	0.4601(2)	0.3887(2)	0.06592(13)	0.0348(6)*
C43	0.5515(2)	0.4366(2)	0.06016(14)	0.0410(7)*
C44	0.6223(2)	0.3826(3)	0.03331(16)	0.0510(8)*
C45	0.6068(3)	0.2819(3)	0.01267(17)	0.0586(10)*
C46	0.5189(2)	0.2336(3)	0.02050(15)	0.0485(8)*
C47	0.5698(2)	0.5462(3)	0.08323(15)	0.0505(8)*
C48	0.5918(3)	0.5515(3)	0.14875(18)	0.0652(10)*
C49	0.6149(5)	0.6613(5)	0.1694(2)	0.120(2)*
C51	0.2767(3)	0.2723(3)	0.29369(14)	0.0523(8)*
C52	0.2032(4)	0.3147(4)	0.33376(18)	0.0947(17)*
C53A ^c	0.1144(5)	0.2820(6)	0.3132(3)	0.0734(19)
C53B ^d	0.1255(8)	0.3676(9)	0.3001(5)	0.070(3)
C54	0.1166(3)	0.2944(5)	0.2451(2)	0.0900(16)*

Anisotropically-refined atoms are marked with an asterisk (*). The form of the anisotropic displacement parameter is: $\exp[-2\pi^2(h^2a^*U_{11} + k^2b^*U_{22} + l^2c^*U_{33} + 2klb^*c^*U_{23} + 2hla^*c^*U_{13} + 2hka^*b^*U_{12})]$. ^aRefined with an occupancy factor of 0.65. ^bRefined with an occupancy factor of 0.35. ^cRefined with an occupancy factor of 0.6. ^dRefined with an occupancy factor of 0.4.

Table 3. Selected Interatomic Distances (Å)

Atom1	Atom2	Distance	Atom1	Atom2	Distance
C11	A12	2.1111(11)	C22	C23	1.401(4)
C12	A12	2.1142(12)	C23	C24	1.383(5)
A11	O1	1.703(2)	C23	C27	1.510(6)
A11	O2	1.710(2)	C24	C25	1.373(6)
A11	O3	1.825(2)	C25	C26	1.383(5)
A11	O5	1.821(2)	C27	C28	1.536(7)
A12	O3	1.850(2)	C28	C29	1.433(7)
A12	O4	1.670(2)	C31	C32	1.385(4)
O1	C12	1.355(4)	C31	C36	1.391(4)
O2	C22	1.361(4)	C32	C33	1.390(4)
O3	C32	1.435(3)	C33	C34	1.395(5)
O4	C42	1.336(3)	C33	C37	1.502(5)
O5	C51	1.475(4)	C34	C35	1.380(5)
O5	C54	1.466(4)	C35	C36	1.367(5)
C1	C2	1.354(4)	C37	C38A	1.459(7)
C1	C11	1.499(4)	C37	C38B	1.350(12)
C1	C21	1.486(4)	C38A	C39A	1.509(11)
C2	C31	1.498(4)	C38B	C39B	1.512(19)
C2	C41	1.488(4)	C41	C42	1.403(4)
C11	C12	1.392(5)	C41	C46	1.402(4)
C11	C16	1.394(4)	C42	C43	1.405(4)
C12	C13	1.401(4)	C43	C44	1.369(5)
C13	C14	1.393(5)	C43	C47	1.508(4)
C13	C17	1.493(5)	C44	C45	1.380(5)
C14	C15	1.373(6)	C45	C46	1.374(5)
C15	C16	1.381(5)	C47	C48	1.511(5)
C17	C18A	1.374(8)	C48	C49	1.503(6)
C17	C18B	1.416(17)	C51	C52	1.507(5)
C18A	C19A	1.524(10)	C52	C53A	1.339(8)
C18B	C19B	1.55(2)	C52	C53B	1.436(11)
C21	C22	1.401(4)	C53A	C54	1.571(9)
C21	C26	1.398(4)	C53B	C54	1.566(11)

Table 4. Selected Interatomic Angles (deg)

Atom1	Atom2	Atom3	Angle	Atom1	Atom2	Atom3	Angle
O1	A11	O2	123.02(11)	C13	C17	C18A	114.7(5)
O1	A11	O3	106.64(10)	C13	C17	C18B	125.9(9)
O1	A11	O5	103.06(10)	C17	C18A	C19A	116.3(6)
O2	A11	O3	119.58(10)	C17	C18B	C19B	120.0(15)
O2	A11	O5	99.93(10)	C1	C21	C22	117.8(3)
O3	A11	O5	100.03(10)	C1	C21	C26	123.2(3)
C11	A12	C12	110.02(5)	C22	C21	C26	119.0(3)
C11	A12	O3	111.04(7)	O2	C22	C21	120.4(3)
C11	A12	O4	111.80(10)	O2	C22	C23	118.9(3)
C12	A12	O3	104.71(8)	C21	C22	C23	120.7(3)
C12	A12	O4	114.03(10)	C22	C23	C24	118.4(4)
O3	A12	O4	104.90(10)	C22	C23	C27	120.4(3)
A11	O1	C12	131.4(2)	C24	C23	C27	121.2(3)
A11	O2	C22	128.8(2)	C23	C24	C25	121.5(4)
A11	O3	A12	123.99(10)	C24	C25	C26	120.4(4)
A11	O3	C32	117.68(16)	C21	C26	C25	119.9(4)
A12	O3	C32	108.50(16)	C23	C27	C28	112.9(4)
A12	O4	C42	155.6(2)	C27	C28	C29	117.0(5)
A11	O5	C51	126.35(19)	C2	C31	C32	119.3(3)
A11	O5	C54	124.0(2)	C2	C31	C36	122.6(3)
C51	O5	C54	109.5(3)	C32	C31	C36	117.7(3)
C2	C1	C11	122.8(3)	O3	C32	C31	117.6(2)
C2	C1	C21	120.6(3)	O3	C32	C33	118.2(3)
C11	C1	C21	116.6(2)	C31	C32	C33	124.1(3)
C1	C2	C31	117.8(3)	C32	C33	C34	115.4(3)
C1	C2	C41	121.6(3)	C32	C33	C37	122.4(3)
C31	C2	C41	120.5(2)	C34	C33	C37	122.2(3)
C1	C11	C12	121.2(3)	C33	C34	C35	121.8(3)
C1	C11	C16	119.1(3)	C34	C35	C36	120.8(3)
C12	C11	C16	119.6(3)	C31	C36	C35	120.0(3)
O1	C12	C11	120.3(3)	C33	C37	C38A	120.1(4)
O1	C12	C13	118.5(3)	C33	C37	C38B	115.8(6)
C11	C12	C13	121.2(3)	C37	C38A	C39A	113.0(6)
C12	C13	C14	117.4(3)	C37	C38B	C39B	119.4(11)
C12	C13	C17	120.6(3)	C2	C41	C42	125.2(3)
C14	C13	C17	122.0(3)	C2	C41	C46	117.1(3)
C13	C14	C15	121.9(3)	C42	C41	C46	117.6(3)
C14	C15	C16	120.3(3)	O4	C42	C41	121.3(3)
C11	C16	C15	119.6(3)	O4	C42	C43	118.1(3)

Table 4. Selected Interatomic Angles (continued)

Atom1	Atom2	Atom3	Angle	Atom1	Atom2	Atom3	Angle
C41	C42	C43	120.6(3)	C47	C48	C49	112.1(4)
C42	C43	C44	119.1(3)	O5	C51	C52	102.4(3)
C42	C43	C47	119.8(3)	C51	C52	C53A	107.5(5)
C44	C43	C47	121.1(3)	C51	C52	C53B	109.9(5)
C43	C44	C45	121.7(3)	C52	C53A	C54	103.8(5)
C44	C45	C46	119.1(3)	C52	C53B	C54	99.5(7)
C41	C46	C45	121.8(3)	O5	C54	C53A	100.8(4)
C43	C47	C48	114.0(3)	O5	C54	C53B	102.9(5)

Table 5. Selected Torsional Angles (deg)

Atom1	Atom2	Atom3	Atom4	Angle	Atom1	Atom2	Atom3	Atom4	Angle
C11	C1	C2	C31	13.7(4)	C1	C2	C41	C42	-130.1(3)
C11	C1	C2	C41	-161.9(3)	C1	C2	C41	C46	52.7(4)
C21	C1	C2	C31	-165.6(3)	C31	C2	C41	C42	54.5(4)
C21	C1	C2	C41	18.9(4)	C31	C2	C41	C46	-122.8(3)
C2	C1	C11	C12	-90.2(4)	C1	C11	C12	O1	2.5(5)
C2	C1	C11	C16	93.4(4)	C1	C11	C12	C13	-176.3(3)
C21	C1	C11	C12	89.1(4)	C1	C11	C16	C15	176.4(3)
C21	C1	C11	C16	-87.3(4)	C1	C21	C22	O2	1.8(4)
C2	C1	C21	C22	71.5(4)	C1	C21	C22	C23	-177.8(3)
C2	C1	C21	C26	-110.2(4)	C1	C21	C26	C25	178.5(3)
C11	C1	C21	C22	-107.8(3)	C2	C31	C32	O3	12.3(4)
C11	C1	C21	C26	70.5(4)	C2	C31	C32	C33	-169.4(3)
C1	C2	C31	C32	81.1(3)	C2	C31	C36	C35	172.0(3)
C1	C2	C31	C36	-92.4(4)	C2	C41	C42	O4	-1.7(5)
C41	C2	C31	C32	-103.3(3)	C2	C41	C42	C43	179.7(3)
C41	C2	C31	C36	83.2(4)	C2	C41	C46	C45	177.9(3)

A-13: Complex 41. $C_{38}H_{40}O_4 \cdot [MgCl(thf)] \cdot [Mg(thf)] \cdot [AlEt_2]$

– Chapter 3 –

XCL Code: JMS0046

Date: 13 February 2001

Compound: $[(C_2\{C_6H_3(iPr)O\}_4)\{Mg(OC_4H_8)\}\{MgCl(OC_4H_8)\}(AlEt_2)] \cdot PhMe$

Formula: $C_{57}H_{74}AlClMg_2O_6$ ($C_{50}H_{66}AlClMg_2O_6 \cdot C_7H_8$)

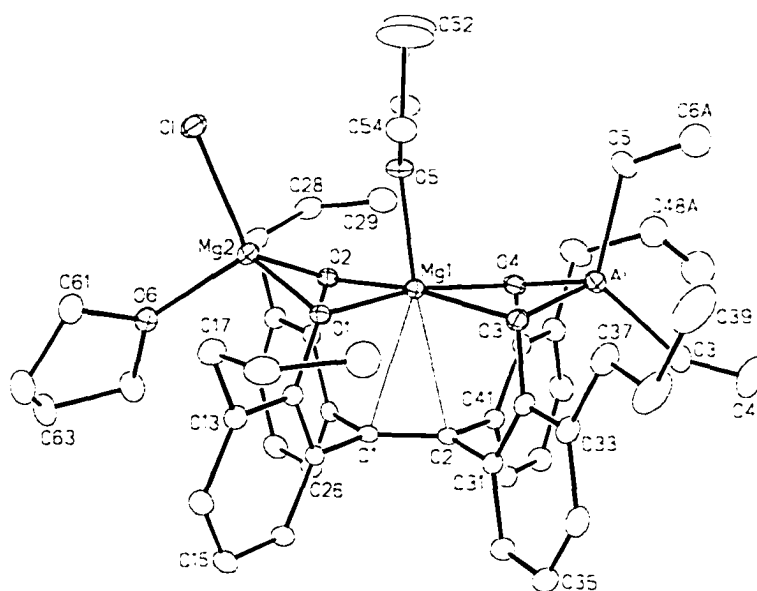


Figure 1. Perspective view of the $[(C_2\{C_6H_3(iPr)O\}_4)\{Mg(OC_4H_8)\}\{MgCl(OC_4H_8)\}(AlEt_2)]$ molecule showing the atom labelling scheme. Non-hydrogen atoms are represented by Gaussian ellipsoids at the 20% probability level. Hydrogen atoms are not shown.

List of Tables

- Table 1.** Crystallographic Experimental Details
Table 2. Atomic Coordinates and Equivalent Isotropic Displacement Parameters
Table 3. Selected Interatomic Distances
Table 4. Selected Interatomic Angles
Table 5. Selected Torsional Angles
Table 6. Least-Squares Planes
-

Table 1. Crystallographic Experimental Details

A. Crystal Data

formula	C ₅₇ H ₇₄ AlClMg ₂ O ₆
formula weight	966.21
crystal dimensions (mm)	0.50 × 0.34 × 0.13
crystal system	monoclinic
space group	<i>P</i> 2 ₁ / <i>n</i> (an alternate setting of <i>P</i> 2 ₁ / <i>c</i> [No. 14])
unit cell parameters ^a	
<i>a</i> (Å)	13.5529 (13)
<i>b</i> (Å)	15.4878 (15)
<i>c</i> (Å)	25.538 (2)
β (deg)	98.9741 (19)
<i>V</i> (Å ³)	5295.0 (9)
<i>Z</i>	4
ρ _{calcd} (g cm ⁻³)	1.212
μ (mm ⁻¹)	0.161

B. Data Collection and Refinement Conditions

diffractometer	Bruker PLATFORM/SMART 1000 CCD ^b
radiation (λ [Å])	graphite-monochromated Mo Kα (0.71073)
temperature (°C)	-80
scan type	ω scans (0.2°) (20 s exposures)
data collection 2θ limit (deg)	52.84
total data collected	34499 (-16 ≤ <i>h</i> ≤ 16, -13 ≤ <i>k</i> ≤ 19, -31 ≤ <i>l</i> ≤ 31)

independent reflections	10857
number of observed reflections (<i>NO</i>)	7541 [$F_o^2 \geq 2\sigma(F_o^2)$]
structure solution method	direct methods/fragment search (<i>DIRDIF-96</i> ^c)
refinement method	full-matrix least-squares on F^2 (<i>SHELXL-93</i> ^d)
absorption correction method	<i>SADABS</i>
range of transmission factors	0.9793–0.9238
data/restraints/parameters	10857 [$F_o^2 \geq -3\sigma(F_o^2)$] / 0 / 603
goodness-of-fit (<i>S</i>) ^e	1.031 [$F_o^2 \geq -3\sigma(F_o^2)$]
final <i>R</i> indices ^f	
R_1 [$F_o^2 \geq 2\sigma(F_o^2)$]	0.0602
wR_2 [$F_o^2 \geq -3\sigma(F_o^2)$]	0.1557
largest difference peak and hole	0.573 and –0.392 e Å ⁻³

^aObtained from least-squares refinement of 4497 centered reflections.

^bPrograms for diffractometer operation, data collection, data reduction and absorption correction were those supplied by Bruker.

^cBeurskens, P. T.; Beurskens, G.; Bosman, W. P.; de Gelder, R.; Garcia Granda, S.; Gould, R. O.; Israel, R.; Smits, J. M. M. (1996). The *DIRDIF-96* program system. Crystallography Laboratory, University of Nijmegen, The Netherlands.

^dSheldrick, G. M. *SHELXL-93*. Program for crystal structure determination. University of Göttingen, Germany, 1993. Refinement on F_o^2 for all reflections (all of these having $F_o^2 \geq -3\sigma(F_o^2)$). Weighted *R*-factors wR_2 and all goodnesses of fit *S* are based on F_o^2 ; conventional *R*-factors R_1 are based on F_o , with F_o set to zero for negative F_o^2 . The observed criterion of $F_o^2 > 2\sigma(F_o^2)$ is used only for calculating R_1 , and is not relevant to the choice of reflections for refinement. *R*-factors based on F_o^2 are statistically about twice as large as those based on F_o , and *R*-factors based on ALL data will be even larger.

^e $S = [\sum w(F_o^2 - F_c^2)^2 / (n - p)]^{1/2}$ (n = number of data; p = number of parameters varied; $w = [\sigma^2(F_o^2) + (0.0578P)^2 + 4.9804P]^{-1}$ where $P = [\text{Max}(F_o^2, 0) + 2F_c^2] / 3$).

^f $R_1 = \sum ||F_o| - |F_c|| / \sum |F_o|$; $wR_2 = [\sum w(F_o^2 - F_c^2)^2 / \sum w(F_o^4)]^{1/2}$.

Table 2. Atomic Coordinates and Equivalent Isotropic Displacement Parameters*(a) atoms of [(C₂[C₆H₃(ⁱPr)O]₄){Mg(OC₄H₈)}{MgCl(OC₄H₈)}(AlEt₂)]*

Atom	x	y	z	<i>U</i> _{eq} , Å ²
Cl	-0.04540(6)	-0.06620(5)	-0.38707(3)	0.04352(19)*
Al	0.03577(8)	0.07965(6)	-0.12188(3)	0.0433(2)*
Mg1	0.01057(6)	0.09612(6)	-0.23714(3)	0.0274(2)*
Mg2	-0.01805(6)	0.06602(6)	-0.34931(3)	0.0313(2)*
O1	0.09844(12)	0.09780(11)	-0.29514(7)	0.0271(4)*
O2	-0.09960(12)	0.11839(11)	-0.30008(7)	0.0288(4)*
O3	0.12205(14)	0.09546(12)	-0.17039(7)	0.0348(4)*
O4	-0.06732(14)	0.11585(12)	-0.17349(7)	0.0358(4)*
O5	-0.00954(13)	-0.03205(12)	-0.25082(8)	0.0351(4)*
O6	-0.01413(15)	0.13956(13)	-0.41425(7)	0.0409(5)*
C1	0.02338(18)	0.25929(16)	-0.26393(10)	0.0258(5)*
C2	0.03842(19)	0.25692(16)	-0.21064(10)	0.0264(5)*
C3	0.0590(3)	0.1602(2)	-0.06200(12)	0.0544(9)*
C4	0.1506(4)	0.1488(3)	-0.01982(16)	0.0931(16)*
C5	0.0169(4)	-0.0442(2)	-0.10883(15)	0.0860(15)*
C6A ^a	0.0774(5)	-0.0863(4)	-0.0653(2)	0.0695(16)
C6B ^b	-0.0102(10)	-0.0745(9)	-0.0687(5)	0.081(4)
C11	0.10789(18)	0.25245(17)	-0.29572(10)	0.0267(5)*
C12	0.14284(18)	0.17173(17)	-0.30896(10)	0.0272(5)*
C13	0.22187(19)	0.16622(18)	-0.33896(10)	0.0318(6)*
C14	0.2598(2)	0.2431(2)	-0.35616(11)	0.0385(7)*
C15	0.2242(2)	0.3228(2)	-0.34393(11)	0.0384(7)*
C16	0.1488(2)	0.32699(18)	-0.31315(11)	0.0337(6)*
C17	0.2675(2)	0.0815(2)	-0.35033(12)	0.0403(7)*
C18	0.3665(2)	0.0663(2)	-0.31407(14)	0.0493(8)*
C19	0.3552(3)	0.0584(3)	-0.25659(15)	0.0612(10)*
C21	-0.07939(18)	0.27181(17)	-0.29529(9)	0.0271(5)*
C22	-0.13690(18)	0.19862(17)	-0.31264(10)	0.0276(5)*
C23	-0.23126(19)	0.20868(19)	-0.34417(11)	0.0338(6)*
C24	-0.2646(2)	0.2917(2)	-0.35737(12)	0.0411(7)*
C25	-0.2085(2)	0.3637(2)	-0.34045(12)	0.0419(7)*
C26	-0.1163(2)	0.35361(18)	-0.30932(11)	0.0353(6)*
C27	-0.2945(2)	0.1308(2)	-0.36298(12)	0.0421(7)*
C28	-0.3770(2)	0.1155(2)	-0.32966(14)	0.0501(8)*
C29	-0.3393(3)	0.0934(2)	-0.27268(15)	0.0610(10)*
C31	0.14299(19)	0.24821(17)	-0.18050(10)	0.0286(6)*
C32	0.1817(2)	0.16809(18)	-0.16301(10)	0.0319(6)*
C33	0.2807(2)	0.15946(19)	-0.13680(11)	0.0382(7)*
C34	0.3374(2)	0.2344(2)	-0.12828(11)	0.0425(7)*
C35	0.2991(2)	0.3144(2)	-0.14422(11)	0.0419(7)*
C36	0.2028(2)	0.32112(19)	-0.17089(11)	0.0356(6)*

C37 0.3192(2) 0.0712(2) -0.11909(13) 0.0505(8)*

Table 2. Atomic Coordinates and Displacement Parameters (continued)

Atom	x	y	z	$U_{eq}, \text{\AA}^2$
C38	0.4270(3)	0.0668(3)	-0.09305(18)	0.0870(16)*
C39	0.4581(4)	-0.0249(3)	-0.0745(2)	0.107(2)*
C41	-0.04870(19)	0.26915(17)	-0.18136(10)	0.0297(6)*
C42	-0.1020(2)	0.19822(18)	-0.16637(10)	0.0342(6)*
C43	-0.1894(2)	0.2098(2)	-0.14423(12)	0.0447(7)*
C44	-0.2192(2)	0.2936(2)	-0.13554(12)	0.0491(8)*
C45	-0.1643(2)	0.3643(2)	-0.14797(12)	0.0434(7)*
C46	-0.0806(2)	0.35213(18)	-0.17134(11)	0.0346(6)*
C47	-0.2506(3)	0.1330(3)	-0.13149(17)	0.0719(12)*
C48A ^c	-0.2336(5)	0.1013(4)	-0.0771(2)	0.0732(16)
C49A ^c	-0.2690(6)	0.1568(5)	-0.0403(3)	0.101(2)
C48B ^d	-0.294(3)	0.134(2)	-0.0822(14)	0.202(14)
C49B ^d	-0.3085(9)	0.0625(8)	-0.0496(5)	0.059(3)
C51	-0.1034(2)	-0.0781(2)	-0.25199(14)	0.0467(8)*
C52	-0.0766(3)	-0.1711(3)	-0.2501(3)	0.0962(17)*
C53	0.0240(4)	-0.1802(3)	-0.2500(3)	0.107(2)*
C54	0.0722(2)	-0.0938(2)	-0.24828(14)	0.0462(8)*
C61	0.0415(3)	0.1090(2)	-0.45527(13)	0.0537(9)*
C62	0.0664(4)	0.1882(3)	-0.48368(16)	0.0785(13)*
C63	-0.0212(4)	0.2459(3)	-0.48020(14)	0.0713(12)*
C64	-0.0452(3)	0.2275(2)	-0.42602(13)	0.0609(10)*

(b) solvent toluene atoms

Atom	x	y	z	$U_{eq}, \text{\AA}^2$
C10S	0.4327(4)	0.1560(3)	-0.4798(2)	0.0981(16)*
C11S	0.3841(3)	0.0700(3)	-0.47833(14)	0.0575(9)*
C12S	0.2917(3)	0.0541(3)	-0.50718(14)	0.0637(11)*
C13S	0.2449(3)	-0.0236(3)	-0.50526(16)	0.0749(12)*
C14S	0.2905(3)	-0.0891(3)	-0.47429(17)	0.0752(12)*
C15S	0.3831(3)	-0.0748(3)	-0.44550(14)	0.0648(10)*
C16S	0.4296(3)	0.0031(3)	-0.44777(13)	0.0580(10)*

Anisotropically-refined atoms are marked with an asterisk (*). The form of the anisotropic displacement parameter is: $\exp[-2\pi^2(h^2a^2U_{11} + k^2b^2U_{22} + l^2c^2U_{33} + 2klb^*c^*U_{23} + 2hla^*c^*U_{13} + 2hka^*b^*U_{12})]$. ^aRefined with an occupancy factor of 0.65. ^bRefined with an occupancy factor of 0.35. ^cRefined with an occupancy factor of 0.7. ^dRefined with an occupancy factor of 0.3.

Table 3. Selected Interatomic Distances (Å)*(a) within [(C₂[C₆H₃(ⁱPr)O]₄)[Mg(OC₄H₈)]{MgCl(OC₄H₈)}(AlEt₂)]*

Atom1	Atom2	Distance	Atom1	Atom2	Distance
Cl	Mg2	2.2694(12)	C17	C18	1.525(4)
Al	O3	1.848(2)	C18	C19	1.505(5)
Al	O4	1.852(2)	C21	C22	1.407(4)
Al	C3	1.961(3)	C21	C26	1.388(4)
Al	C5	1.970(4)	C22	C23	1.410(4)
Mg1	O1	2.0402(18)	C23	C24	1.387(4)
Mg1	O2	2.0453(19)	C23	C27	1.514(4)
Mg1	O3	2.0943(19)	C24	C25	1.380(4)
Mg1	O4	2.094(2)	C25	C26	1.382(4)
Mg1	O5	2.027(2)	C27	C28	1.525(4)
Mg1	C1	2.631(3)	C28	C29	1.504(5)
Mg1	C2	2.593(3)	C31	C32	1.393(4)
Mg2	O1	1.9918(18)	C31	C36	1.389(4)
Mg2	O2	1.9732(19)	C32	C33	1.409(4)
Mg2	O6	2.019(2)	C33	C34	1.390(4)
O1	C12	1.365(3)	C33	C37	1.507(4)
O2	C22	1.361(3)	C34	C35	1.380(4)
O3	C32	1.381(3)	C35	C36	1.380(4)
O4	C42	1.381(3)	C37	C38	1.509(5)
O5	C51	1.455(3)	C38	C39	1.536(6)
O5	C54	1.457(3)	C41	C42	1.400(4)
O6	C61	1.462(4)	C41	C46	1.392(4)
O6	C64	1.443(4)	C42	C43	1.402(4)
C1	C2	1.345(3)	C43	C44	1.386(5)
C1	C11	1.507(3)	C43	C47	1.514(5)
C1	C21	1.507(3)	C44	C45	1.388(4)
C2	C31	1.509(3)	C45	C46	1.374(4)
C2	C41	1.505(4)	C47	C48A	1.457(7)
C3	C4	1.522(5)	C47	C48B	1.47(4)
C5	C6A	1.431(7)	C48A	C49A	1.413(10)
C5	C6B	1.235(13)	C48B	C49B	1.42(3)
C11	C12	1.397(4)	C51	C52	1.485(5)
C11	C16	1.384(4)	C52	C53	1.370(6)
C12	C13	1.413(4)	C53	C54	1.487(5)
C13	C14	1.395(4)	C61	C62	1.490(5)
C13	C17	1.499(4)	C62	C63	1.500(6)
C14	C15	1.378(4)	C63	C64	1.497(5)
C15	C16	1.384(4)			

Table 3. Selected Interatomic Distances (continued)*(b) within the solvent toluene molecule*

Atom1	Atom2	Distance	Atom1	Atom2	Distance
C10S	C11S	1.490(6)	C13S	C14S	1.372(6)
C11S	C12S	1.372(5)	C14S	C15S	1.370(6)
C11S	C16S	1.382(5)	C15S	C16S	1.366(6)
C12S	C13S	1.366(6)			

Table 4. Selected Interatomic Angles (deg)*(a) within [(C₂{C₆H₃(ⁱPr)O)₄][Mg(OC₄H₈)]{MgCl(OC₄H₈)}(AlEt₂)]*

Atom1	Atom2	Atom3	Angle	Atom1	Atom2	Atom3	Angle
O3	Al	O4	88.21(9)	Cl	Mg2	O6	100.57(7)
O3	Al	C3	113.40(13)	O1	Mg2	O2	85.30(8)
O3	Al	C5	110.79(17)	O1	Mg2	O6	108.15(9)
O4	Al	C3	111.95(13)	O2	Mg2	O6	112.36(9)
O4	Al	C5	108.16(16)	Mg1	O1	Mg2	90.68(7)
C3	Al	C5	119.80(15)	Mg1	O1	C12	121.94(15)
O1	Mg1	O2	82.22(7)	Mg2	O1	C12	111.17(14)
O1	Mg1	O3	99.34(8)	Mg1	O2	Mg2	91.06(8)
O1	Mg1	O4	169.61(8)	Mg1	O2	C22	122.55(15)
O1	Mg1	O5	88.02(8)	Mg2	O2	C22	116.72(15)
O1	Mg1	C1	74.30(8)	Al	O3	Mg1	95.44(9)
O1	Mg1	C2	95.71(8)	Al	O3	C32	115.77(16)
O2	Mg1	O3	170.44(9)	Mg1	O3	C32	116.09(15)
O2	Mg1	O4	101.00(8)	Al	O4	Mg1	95.32(9)
O2	Mg1	O5	88.15(8)	Al	O4	C42	114.85(16)
O2	Mg1	C1	72.74(8)	Mg1	O4	C42	117.38(15)
O2	Mg1	C2	95.85(8)	Mg1	O5	C51	125.28(17)
O3	Mg1	O4	75.86(8)	Mg1	O5	C54	123.68(17)
O3	Mg1	O5	101.30(8)	C51	O5	C54	109.6(2)
O3	Mg1	C1	98.50(8)	Mg2	O6	C61	119.27(19)
O3	Mg1	C2	74.63(8)	Mg2	O6	C64	131.24(18)
O4	Mg1	O5	101.89(8)	C61	O6	C64	108.8(2)
O4	Mg1	C1	97.09(8)	Mg1	C1	C2	73.53(15)
O4	Mg1	C2	74.20(8)	Mg1	C1	C11	99.15(15)
O5	Mg1	C1	155.32(9)	Mg1	C1	C21	99.72(15)
O5	Mg1	C2	174.85(9)	C2	C1	C11	122.4(2)
C1	Mg1	C2	29.83(8)	C2	C1	C21	121.5(2)
Cl	Mg2	O1	125.27(7)	C11	C1	C21	116.1(2)
Cl	Mg2	O2	124.83(7)	Mg1	C2	C1	76.65(15)

Table 4. Selected Interatomic Angles (continued)

Atom1	Atom2	Atom3	Angle	Atom1	Atom2	Atom3	Angle
Mg1	C2	C31	97.71(15)	C23	C27	C28	112.0(2)
Mg1	C2	C41	99.03(16)	C27	C28	C29	114.1(3)
Mg1	C2	C1	76.65(15)	C2	C31	C32	121.3(2)
Mg1	C2	C31	97.71(15)	C2	C31	C36	119.5(2)
Mg1	C2	C41	99.03(16)	C32	C31	C36	119.2(2)
C1	C2	C31	120.0(2)	O3	C32	C31	119.9(2)
C1	C2	C41	119.5(2)	O3	C32	C33	118.8(2)
C31	C2	C41	120.3(2)	C31	C32	C33	121.3(3)
Al	C3	C4	119.4(3)	C32	C33	C34	117.2(3)
Al	C5	C6A	120.1(4)	C32	C33	C37	119.2(3)
Al	C5	C6B	125.1(7)	C34	C33	C37	123.6(3)
C1	C11	C12	120.5(2)	C33	C34	C35	122.0(3)
C1	C11	C16	119.4(2)	C34	C35	C36	119.8(3)
C12	C11	C16	120.0(2)	C31	C36	C35	120.5(3)
O1	C12	C11	120.5(2)	C33	C37	C38	116.0(3)
O1	C12	C13	119.4(2)	C37	C38	C39	112.2(4)
C11	C12	C13	120.0(2)	C2	C41	C42	121.0(2)
C12	C13	C14	117.8(3)	C2	C41	C46	119.9(2)
C12	C13	C17	121.9(2)	C42	C41	C46	119.0(2)
C14	C13	C17	120.2(2)	O4	C42	C41	119.2(2)
C13	C14	C15	122.3(3)	O4	C42	C43	119.9(3)
C14	C15	C16	119.1(3)	C41	C42	C43	120.9(3)
C11	C16	C15	120.8(3)	C42	C43	C44	118.0(3)
C13	C17	C18	111.6(2)	C42	C43	C47	120.7(3)
C17	C18	C19	113.0(3)	C44	C43	C47	121.3(3)
C1	C21	C22	119.0(2)	C43	C44	C45	121.4(3)
C1	C21	C26	121.3(2)	C44	C45	C46	120.0(3)
C22	C21	C26	119.6(2)	C41	C46	C45	120.5(3)
O2	C22	C21	119.6(2)	C43	C47	C48A	117.3(4)
O2	C22	C23	120.4(2)	C43	C47	C48B	118.8(15)
C21	C22	C23	120.0(2)	C47	C48A	C49A	114.2(6)
C22	C23	C24	118.3(3)	C47	C48B	C49B	127(3)
C22	C23	C27	120.8(3)	O5	C51	C52	105.4(3)
C24	C23	C27	121.0(2)	C51	C52	C53	109.8(3)
C23	C24	C25	122.0(3)	C52	C53	C54	109.8(3)
C24	C25	C26	119.6(3)	O5	C54	C53	105.2(3)
C21	C26	C25	120.6(3)	O6	C61	C62	105.3(3)

Table 4. Selected Interatomic Angles (continued)

Atom1	Atom2	Atom3	Angle	Atom1	Atom2	Atom3	Angle
C61	C62	C63	102.7(3)	O6	C64	C63	105.9(3)
C62	C63	C64	103.3(3)				

(b) within the solvent toluene molecule

Atom1	Atom2	Atom3	Angle	Atom1	Atom2	Atom3	Angle
C10S	C11S	C12S	121.1(4)	C12S	C13S	C14S	120.1(4)
C10S	C11S	C16S	121.6(4)	C13S	C14S	C15S	118.9(4)
C12S	C11S	C16S	117.3(4)	C14S	C15S	C16S	120.6(4)
C11S	C12S	C13S	121.9(4)	C11S	C16S	C15S	121.1(4)

Table 5. Selected Torsional Angles (deg)

Atom1	Atom2	Atom3	Atom4	Angle	Atom1	Atom2	Atom3	Atom4	Angle
O4	Al	O3	Mg1	-17.99(9)	O2	Mg1	O3	Al	88.3(5)
O4	Al	O3	C32	104.46(17)	O2	Mg1	O3	C32	-33.9(6)
O3	Al	O4	Mg1	17.99(9)	O4	Mg1	O3	Al	16.35(8)
O3	Al	O4	C42	-105.53(18)	O4	Mg1	O3	C32	-105.86(18)
O3	Al	C3	C4	-72.7(3)	O5	Mg1	O3	Al	-83.23(9)
O2	Mg1	O1	Mg2	-24.02(7)	O5	Mg1	O3	C32	154.57(17)
O2	Mg1	O1	C12	91.65(17)	O1	Mg1	O4	Al	-79.8(5)
O3	Mg1	O1	Mg2	165.52(8)	O1	Mg1	O4	C42	41.7(5)
O3	Mg1	O1	C12	-78.82(17)	O2	Mg1	O4	Al	172.94(8)
O4	Mg1	O1	Mg2	-132.9(4)	O2	Mg1	O4	C42	-65.48(19)
O4	Mg1	O1	C12	-17.2(5)	O3	Mg1	O4	Al	-16.31(8)
O5	Mg1	O1	Mg2	64.38(8)	O3	Mg1	O4	C42	105.27(19)
O5	Mg1	O1	C12	-179.95(17)	O5	Mg1	O4	Al	82.52(9)
O1	Mg1	O2	Mg2	24.26(8)	O5	Mg1	O4	C42	-155.90(18)
O1	Mg1	O2	C22	-98.78(18)	O1	Mg1	O5	C51	-139.3(2)
O3	Mg1	O2	Mg2	124.4(5)	O1	Mg1	O5	C54	55.9(2)
O3	Mg1	O2	C22	1.3(6)	O2	Mg1	O5	C51	-57.1(2)
O4	Mg1	O2	Mg2	-165.75(8)	O2	Mg1	O5	C54	138.2(2)
O4	Mg1	O2	C22	71.20(18)	O3	Mg1	O5	C51	121.5(2)
O5	Mg1	O2	Mg2	-63.99(8)	O3	Mg1	O5	C54	-43.2(2)
O5	Mg1	O2	C22	172.96(18)	O4	Mg1	O5	C51	43.8(2)
O1	Mg1	O3	Al	-173.07(8)	O4	Mg1	O5	C54	-120.9(2)
O1	Mg1	O3	C32	64.73(18)	C11	C1	C2	C31	0.7(4)

Table 5. Torsional Angles (continued)

Atom1	Atom2	Atom3	Atom4	Angle	Atom1	Atom2	Atom3	Atom4	Angle
C11	C1	C2	C41	176.6(2)	C41	C2	C31	C32	88.1(3)
C21	C1	C2	Mg1	91.4(2)	C41	C2	C31	C36	-93.2(3)
C21	C1	C2	C31	-177.3(2)	Mg1	C2	C41	C42	13.4(3)
C21	C1	C2	C41	-1.5(4)	Mg1	C2	C41	C46	-163.1(2)
Mg1	C1	C11	C12	9.4(2)	C1	C2	C41	C42	93.1(3)
Mg1	C1	C11	C16	-172.5(2)	C1	C2	C41	C46	-83.4(3)
C2	C1	C11	C12	85.7(3)	C31	C2	C41	C42	-91.0(3)
C2	C1	C11	C16	-96.3(3)	C31	C2	C41	C46	92.4(3)
C21	C1	C11	C12	-96.2(3)	C1	C11	C12	O1	2.6(3)
C21	C1	C11	C16	81.9(3)	C1	C11	C12	C13	179.8(2)
Mg1	C1	C21	C22	-15.9(2)	C1	C11	C16	C15	-177.8(2)
Mg1	C1	C21	C26	167.0(2)	C1	C21	C22	O2	1.1(3)
C2	C1	C21	C22	-92.5(3)	C1	C21	C22	C23	-177.0(2)
C2	C1	C21	C26	90.4(3)	C1	C21	C26	C25	176.6(2)
C11	C1	C21	C22	89.3(3)	C2	C31	C32	O3	-3.9(4)
C11	C1	C21	C26	-87.7(3)	C2	C31	C32	C33	177.3(2)
Mg1	C2	C31	C32	-17.1(3)	C2	C31	C36	C35	-178.9(2)
Mg1	C2	C31	C36	161.5(2)	C2	C41	C42	O4	7.1(4)
C1	C2	C31	C32	-96.1(3)	C2	C41	C42	C43	-173.1(2)
C1	C2	C31	C36	82.6(3)	C2	C41	C46	C45	175.4(2)

Table 6. Least-Squares Plane

Plane	Coefficients ^a			Defining Atoms with Deviations				
(Å) ^b								
1	1.627(9)	15.374(2)	-0.063(14)	1.680(4)	O1	-0.0027(9)	O2	-0.0026(9)
					O3	-0.0028(9)	O4	0.0028(9)
					<u>Mg1</u>	0.1697(13)	<u>Mg2</u>	-0.672(2)
					<u>Al</u>	-0.389(2)		

^aCoefficients are for the form $ax+by+cz = d$ where x , y and z are crystallographic coordinates.

^bUnderlined atoms were not included in the definition of the plane.

A-14: Complex 42. $(C_2\{C_6H_3(iPr)O\}_4)\{Mg(OC_4H_8)\}(AlEt_2)_2$

– Chapter 3 –

XCL Code: JMS0048

Date: 13 February 2001

Compound: $[(C_2\{C_6H_3(iPr)O\}_4)\{Mg(OC_4H_8)\}(AlEt_2)_2]$

Formula: $C_{50}H_{68}Al_2MgO_5$

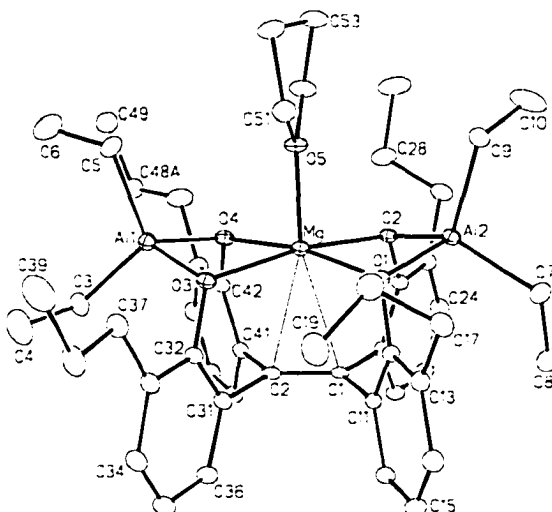


Figure 1. Perspective view of the $[(C_2\{C_6H_3(iPr)O\}_4)\{Mg(OC_4H_8)\}(AlEt_2)_2]$ molecule showing the atom labelling scheme. Non-hydrogen atoms are represented by Gaussian ellipsoids at the 20% probability level. Hydrogen atoms are not shown.

List of Tables

Table 1. Crystallographic Experimental Details

Table 2. Atomic Coordinates and Equivalent Isotropic Displacement Parameters

Table 3. Selected Interatomic Distances

Table 4. Selected Interatomic Angles

Table 5. Selected Torsional Angles

Table 6. Least-Squares Planes

Table 1. Crystallographic Experimental Details

A. Crystal Data

formula	C ₅₀ H ₆₈ Al ₂ MgO ₅
formula weight	827.31
crystal dimensions (mm)	0.47 × 0.29 × 0.19
crystal system	monoclinic
space group	<i>P</i> 2 ₁ / <i>c</i> (No. 14)
unit cell parameters ^a	
<i>a</i> (Å)	12.2996 (15)
<i>b</i> (Å)	19.454 (2)
<i>c</i> (Å)	19.634 (2)
β (deg)	90.590 (2)
<i>V</i> (Å ³)	4697.6 (10)
<i>Z</i>	4
ρ _{calcd} (g cm ⁻³)	1.170
μ (mm ⁻¹)	0.119

B. Data Collection and Refinement Conditions

diffractometer	Bruker PLATFORM/SMART 1000 CCD ^b
radiation (λ [Å])	graphite-monochromated Mo Kα (0.71073)
temperature (°C)	-80
scan type	ω scans (0.2°) (20 s exposures)
data collection 2θ limit (deg)	52.82
total data collected	26560 (-15 ≤ <i>h</i> ≤ 15, -24 ≤ <i>k</i> ≤ 23, -24 ≤ <i>l</i> ≤ 23)

independent reflections	9592
number of observed reflections (<i>NO</i>)	5262 [$F_o^2 \geq 2\sigma(F_o^2)$]
structure solution method	direct methods (<i>SHELXS-86</i> ^c)
refinement method	full-matrix least-squares on F^2 (<i>SHELXL-93</i> ^d)
absorption correction method	<i>SADABS</i>
range of transmission factors	0.9777–0.9460
data/restraints/parameters	9592 [$F_o^2 \geq -3\sigma(F_o^2)$] / 0 / 522
goodness-of-fit (<i>S</i>) ^e	1.005 [$F_o^2 \geq -3\sigma(F_o^2)$]
final <i>R</i> indices ^f	
R_1 [$F_o^2 \geq 2\sigma(F_o^2)$]	0.0647
wR_2 [$F_o^2 \geq -3\sigma(F_o^2)$]	0.1754
largest difference peak and hole	0.734 and –0.283 e Å ⁻³

^aObtained from least-squares refinement of 5029 centered reflections.

^bPrograms for diffractometer operation, data collection, data reduction and absorption correction were those supplied by Bruker.

^cSheldrick, G. M. *Acta Crystallogr.* **1990**, *A46*, 467–473.

^dSheldrick, G. M. *SHELXL-93*. Program for crystal structure determination. University of Göttingen, Germany, 1993. Refinement on F_o^2 for all reflections (all of these having $F_o^2 \geq -3\sigma(F_o^2)$). Weighted *R*-factors wR_2 and all goodnesses of fit *S* are based on F_o^2 ; conventional *R*-factors R_1 are based on F_o , with F_o set to zero for negative F_o^2 . The observed criterion of $F_o^2 > 2\sigma(F_o^2)$ is used only for calculating R_1 , and is not relevant to the choice of reflections for refinement. *R*-factors based on F_o^2 are statistically about twice as large as those based on F_o , and *R*-factors based on ALL data will be even larger.

^e $S = [\sum w(F_o^2 - F_c^2)^2 / (n - p)]^{1/2}$ (n = number of data; p = number of parameters varied; $w = [\sigma^2(F_o^2) + (0.0836P)^2 + 0.1586P]^{-1}$ where $P = [\text{Max}(F_o^2, 0) + 2F_c^2]/3$).

^f $R_1 = \sum ||F_o| - |F_c|| / \sum |F_o|$; $wR_2 = [\sum w(F_o^2 - F_c^2)^2 / \sum w(F_o^4)]^{1/2}$.

Table 2. Atomic Coordinates and Equivalent Isotropic Displacement Parameters

Atom	x	y	z	$U_{eq}, \text{\AA}^2$
Al1	-0.05994(7)	0.37263(5)	0.18938(5)	0.0284(2)*
Al2	-0.49991(7)	0.36388(5)	0.29151(4)	0.0248(2)*
Mg	-0.28041(8)	0.37852(5)	0.24020(5)	0.0226(2)*
O1	-0.36492(15)	0.38228(10)	0.33053(9)	0.0233(5)*
O2	-0.44135(15)	0.38878(9)	0.20887(9)	0.0224(5)*
O3	-0.12103(15)	0.38658(10)	0.27411(9)	0.0248(5)*
O4	-0.19524(16)	0.39359(10)	0.15158(9)	0.0250(5)*
O5	-0.28027(17)	0.27630(10)	0.22910(10)	0.0301(5)*
C1	-0.3329(2)	0.50849(14)	0.25898(14)	0.0228(7)*
C2	-0.2312(2)	0.51039(14)	0.23470(14)	0.0234(7)*
C3	0.0478(3)	0.4413(2)	0.16310(18)	0.0432(9)*
C4	0.1538(4)	0.4433(3)	0.1993(3)	0.0915(17)*
C5	-0.0144(3)	0.27663(18)	0.17518(19)	0.0460(9)*
C6	0.0734(4)	0.2670(2)	0.1252(3)	0.0891(17)*
C7	-0.6180(3)	0.41824(18)	0.32942(17)	0.0395(9)*
C8	-0.6379(3)	0.49279(19)	0.3252(2)	0.0542(11)*
C9	-0.5402(3)	0.26609(16)	0.29318(17)	0.0344(8)*
C10	-0.6418(4)	0.2494(2)	0.2514(3)	0.0794(16)*
C11	-0.3505(2)	0.50555(15)	0.33454(15)	0.0246(7)*
C12	-0.3613(2)	0.44259(15)	0.36844(14)	0.0232(7)*
C13	-0.3698(2)	0.43930(17)	0.43862(15)	0.0287(7)*
C14	-0.3693(3)	0.50093(18)	0.47472(16)	0.0360(8)*
C15	-0.3609(3)	0.56345(18)	0.44194(17)	0.0372(8)*
C16	-0.3507(3)	0.56583(17)	0.37282(16)	0.0322(8)*
C17	-0.3802(3)	0.37068(17)	0.47404(15)	0.0358(8)*
C18	-0.2759(3)	0.32772(19)	0.47298(17)	0.0436(9)*
C19	-0.1804(3)	0.3628(2)	0.50782(19)	0.0554(11)*
C21	-0.4274(2)	0.51218(15)	0.20997(14)	0.0221(7)*
C22	-0.4745(2)	0.45184(15)	0.18334(14)	0.0228(7)*
C23	-0.5524(2)	0.45450(16)	0.13172(14)	0.0261(7)*
C24	-0.5867(2)	0.51892(17)	0.10914(16)	0.0314(8)*
C25	-0.5446(3)	0.57863(16)	0.13699(16)	0.0314(8)*
C26	-0.4653(3)	0.57516(16)	0.18639(16)	0.0296(7)*
C27	-0.5931(3)	0.38928(17)	0.09984(16)	0.0358(8)*
C28	-0.5172(3)	0.36244(19)	0.04544(19)	0.0536(11)*
C29	-0.5531(4)	0.2946(2)	0.0149(2)	0.0792(15)*
C31	-0.1362(2)	0.50943(16)	0.28395(15)	0.0268(7)*
C32	-0.0877(2)	0.44782(15)	0.30498(14)	0.0245(7)*
C33	-0.0058(2)	0.44621(17)	0.35463(16)	0.0311(8)*

Table 2. Atomic Coordinates and Displacement Parameters (continued)

Atom	x	y	z	$U_{eq}, \text{\AA}^2$
C34	0.0275(3)	0.50797(18)	0.38187(17)	0.0377(8)*
C35	-0.0158(3)	0.56983(19)	0.36062(17)	0.0417(9)*
C36	-0.0980(3)	0.57086(17)	0.31215(17)	0.0349(8)*
C37	0.0431(3)	0.37744(17)	0.37448(16)	0.0360(8)*
C38	0.1217(3)	0.3784(2)	0.43381(18)	0.0463(10)*
C39	0.1671(3)	0.3076(2)	0.4487(2)	0.0730(14)*
C41	-0.2122(2)	0.51627(15)	0.15982(15)	0.0251(7)*
C42	-0.1990(2)	0.45739(15)	0.11990(15)	0.0260(7)*
C43	-0.1867(3)	0.46141(16)	0.04969(15)	0.0295(7)*
C44	-0.1857(3)	0.52698(18)	0.02072(16)	0.0349(8)*
C45	-0.1972(3)	0.58491(17)	0.05894(17)	0.0347(8)*
C46	-0.2104(2)	0.58059(17)	0.12840(16)	0.0317(7)*
C47	-0.1731(3)	0.39713(19)	0.00805(17)	0.0504(10)*
C48A ^a	-0.1116(5)	0.4032(3)	-0.0576(3)	0.0426(15)
C48B ^b	-0.0759(7)	0.3850(5)	-0.0217(5)	0.042(2)
C49	-0.0773(3)	0.3335(2)	-0.0839(2)	0.0624(12)*
C51	-0.2422(3)	0.22621(16)	0.27909(17)	0.0364(8)*
C52	-0.2412(3)	0.15820(18)	0.24243(19)	0.0492(10)*
C53	-0.3296(3)	0.16624(18)	0.18837(19)	0.0502(10)*
C54	-0.3198(3)	0.24066(17)	0.16834(17)	0.0430(9)*

Anisotropically-refined atoms are marked with an asterisk (*). The form of the anisotropic displacement parameter is: $\exp[-2\pi^2(h^2a^{*2}U_{11} + k^2b^{*2}U_{22} + l^2c^{*2}U_{33} + 2klb^{*c^*}U_{23} + 2hla^{*c^*}U_{13} + 2hka^{*b^*}U_{12})]$. ^aRefined with an occupancy factor of 0.6. ^bRefined with an occupancy factor of 0.4.

Table 3. Selected Interatomic Distances (Å)

Atom1	Atom2	Distance	Atom1	Atom2	Distance
Al1	O3	1.852(2)	C15	C16	1.365(4)
Al1	O4	1.860(2)	C17	C18	1.531(5)
Al1	C3	1.954(4)	C18	C19	1.516(5)
Al1	C5	1.970(3)	C21	C22	1.407(4)
Al2	O1	1.856(2)	C21	C26	1.389(4)
Al2	O2	1.847(2)	C22	C23	1.388(4)
Al2	C7	1.951(3)	C23	C24	1.394(4)
Al2	C9	1.966(3)	C23	C27	1.499(4)
Mg	O1	2.066(2)	C24	C25	1.382(4)
Mg	O2	2.076(2)	C25	C26	1.370(4)
Mg	O3	2.070(2)	C27	C28	1.519(5)
Mg	O4	2.061(2)	C28	C29	1.515(5)
Mg	O5	2.001(2)	C31	C32	1.399(4)
Mg	C1	2.636(3)	C31	C36	1.396(4)
Mg	C2	2.638(3)	C32	C33	1.395(4)
O1	C12	1.390(3)	C33	C34	1.376(4)
O2	C22	1.385(3)	C33	C37	1.516(4)
O3	C32	1.396(3)	C34	C35	1.379(5)
O4	C42	1.389(3)	C35	C36	1.381(4)
O5	C51	1.457(3)	C37	C38	1.506(4)
O5	C54	1.459(3)	C38	C39	1.514(5)
C1	C2	1.344(4)	C41	C42	1.398(4)
C1	C11	1.503(4)	C41	C46	1.395(4)
C1	C21	1.503(4)	C42	C43	1.390(4)
C2	C31	1.509(4)	C43	C44	1.397(4)
C2	C41	1.495(4)	C43	C47	1.504(4)
C3	C4	1.480(5)	C44	C45	1.362(5)
C5	C6	1.478(5)	C45	C46	1.378(4)
C7	C8	1.473(5)	C47	C48A	1.506(6)
C9	C10	1.522(5)	C47	C48B	1.356(9)
C11	C12	1.401(4)	C48A	C49	1.514(7)
C11	C16	1.393(4)	C48B	C49	1.581(9)
C12	C13	1.384(4)	C51	C52	1.506(5)
C13	C14	1.393(4)	C52	C53	1.520(5)
C13	C17	1.511(4)	C53	C54	1.505(5)
C14	C15	1.380(5)			

Table 4. Selected Interatomic Angles (deg)

Atom1	Atom2	Atom3	Angle	Atom1	Atom2	Atom3	Angle
O3	All	O4	87.52(9)	All	O3	Mg	95.26(9)
O3	All	C3	114.81(13)	All	O3	C32	113.26(17)
O3	All	C5	112.60(13)	Mg	O3	C32	118.48(17)
O4	All	C3	110.56(13)	All	O4	Mg	95.30(9)
O4	All	C5	113.94(14)	All	O4	C42	113.57(17)
C3	All	C5	114.56(16)	Mg	O4	C42	119.37(17)
O1	Al2	O2	87.52(9)	Mg	O5	C51	126.31(18)
O1	Al2	C7	113.86(13)	Mg	O5	C54	124.11(18)
O1	Al2	C9	113.85(12)	C51	O5	C54	109.6(2)
O2	Al2	C7	119.46(13)	Mg	C1	C2	75.32(17)
O2	Al2	C9	111.66(12)	Mg	C1	C11	98.02(17)
C7	Al2	C9	109.22(15)	Mg	C1	C21	98.35(17)
O1	Mg	O2	76.38(8)	C2	C1	C11	119.7(3)
O1	Mg	O3	101.79(8)	C2	C1	C21	119.2(3)
O1	Mg	O4	169.77(9)	C11	C1	C21	121.0(2)
O1	Mg	O5	97.45(9)	Mg	C2	C1	75.16(17)
O1	Mg	C1	73.74(9)	Mg	C2	C31	97.95(17)
O1	Mg	C2	96.80(9)	Mg	C2	C41	98.79(17)
O2	Mg	O3	170.03(9)	C1	C2	C31	119.3(3)
O2	Mg	O4	103.15(8)	C1	C2	C41	120.4(3)
O2	Mg	O5	93.74(9)	C31	C2	C41	120.2(3)
O2	Mg	C1	73.45(9)	All	C3	C4	119.2(3)
O2	Mg	C2	96.49(9)	All	C5	C6	115.1(3)
O3	Mg	O4	76.87(8)	Al2	C7	C8	129.5(3)
O3	Mg	O5	96.22(9)	Al2	C9	C10	113.8(2)
O3	Mg	C1	96.60(9)	C1	C11	C12	121.2(3)
O3	Mg	C2	73.89(9)	C1	C11	C16	120.1(3)
O4	Mg	O5	92.78(9)	C12	C11	C16	118.6(3)
O4	Mg	C1	96.26(9)	O1	C12	C11	119.1(2)
O4	Mg	C2	73.04(9)	O1	C12	C13	119.4(3)
O5	Mg	C1	165.71(10)	C11	C12	C13	121.5(3)
O5	Mg	C2	164.08(10)	C12	C13	C14	117.8(3)
C1	Mg	C2	29.52(9)	C12	C13	C17	120.4(3)
Al2	O1	Mg	95.43(9)	C14	C13	C17	121.8(3)
Al2	O1	C12	114.01(17)	C13	C14	C15	121.4(3)
Mg	O1	C12	118.43(17)	C14	C15	C16	120.1(3)
Al2	O2	Mg	95.38(9)	C11	C16	C15	120.6(3)
Al2	O2	C22	115.73(17)	C13	C17	C18	113.6(3)
Mg	O2	C22	117.95(17)	C17	C18	C19	113.2(3)

Table 4. Selected Interatomic Angles (continued)

Atom1	Atom2	Atom3	Angle	Atom1	Atom2	Atom3	Angle
C1	C21	C22	120.7(3)	C34	C35	C36	119.9(3)
C1	C21	C26	120.7(3)	C31	C36	C35	120.1(3)
C22	C21	C26	118.5(3)	C33	C37	C38	115.9(3)
O2	C22	C21	119.0(3)	C37	C38	C39	111.7(3)
O2	C22	C23	119.7(3)	C2	C41	C42	120.6(3)
C21	C22	C23	121.2(3)	C2	C41	C46	120.4(3)
C22	C23	C24	118.1(3)	C42	C41	C46	119.0(3)
C22	C23	C27	119.9(3)	O4	C42	C41	119.0(3)
C24	C23	C27	122.0(3)	O4	C42	C43	119.4(3)
C23	C24	C25	121.2(3)	C41	C42	C43	121.6(3)
C24	C25	C26	120.0(3)	C42	C43	C44	117.2(3)
C21	C26	C25	120.9(3)	C42	C43	C47	120.4(3)
C23	C27	C28	112.3(3)	C44	C43	C47	122.4(3)
C27	C28	C29	113.5(4)	C43	C44	C45	122.0(3)
C2	C31	C32	121.6(3)	C44	C45	C46	120.6(3)
C2	C31	C36	119.9(3)	C41	C46	C45	119.7(3)
C32	C31	C36	118.4(3)	C43	C47	C48A	117.3(4)
O3	C32	C31	118.7(3)	C43	C47	C48B	118.8(5)
O3	C32	C33	119.4(3)	C47	C48A	C49	111.5(4)
C31	C32	C33	121.9(3)	C47	C48B	C49	116.1(6)
C32	C33	C34	117.5(3)	O5	C51	C52	105.6(3)
C32	C33	C37	118.8(3)	C51	C52	C53	103.5(3)
C34	C33	C37	123.7(3)	C52	C53	C54	102.9(3)
C33	C34	C35	122.2(3)	O5	C54	C53	105.7(3)

Table 5. Torsional Angles (deg)

Atom1	Atom2	Atom3	Atom4	Angle	Atom1	Atom2	Atom3	Atom4	Angle
O4	All	O3	Mg	17.62(9)	O1	Mg	O4	C42	-21.0(6)
O4	All	O3	C32	-106.49(19)	O2	Mg	O4	All	-174.03(9)
O3	All	O4	Mg	-17.70(9)	O2	Mg	O4	C42	65.1(2)
O3	All	O4	C42	107.59(19)	O3	Mg	O4	All	16.21(9)
O2	All	O1	Mg	-18.16(9)	O3	Mg	O4	C42	-104.7(2)
O2	All	O1	C12	106.31(18)	O5	Mg	O4	All	-79.53(10)
O1	All	O2	Mg	18.07(9)	O5	Mg	O4	C42	159.6(2)
O1	All	O2	C22	-106.54(19)	O1	Mg	O5	C51	-53.9(2)
O2	Mg	O1	All	16.56(8)	O1	Mg	O5	C54	125.8(2)
O2	Mg	O1	C12	-104.53(19)	O2	Mg	O5	C51	-130.7(2)
O3	Mg	O1	All	-173.49(9)	O2	Mg	O5	C54	49.0(2)
O3	Mg	O1	C12	65.4(2)	O3	Mg	O5	C51	48.9(2)
O4	Mg	O1	All	105.1(5)	O3	Mg	O5	C54	-131.4(2)
O4	Mg	O1	C12	-16.0(6)	O4	Mg	O5	C51	126.0(2)
O5	Mg	O1	All	-75.50(10)	O4	Mg	O5	C54	-54.4(2)
O5	Mg	O1	C12	163.41(19)	All	O2	C22	C21	78.6(3)
O1	Mg	O2	All	-16.64(8)	All	O2	C22	C23	-102.1(3)
O1	Mg	O2	C22	106.28(19)	Mg	O2	C22	C21	-33.3(3)
O3	Mg	O2	All	-97.2(5)	Mg	O2	C22	C23	146.0(2)
O3	Mg	O2	C22	25.7(6)	All	O3	C32	C31	79.0(3)
O4	Mg	O2	All	173.86(9)	All	O3	C32	C33	-99.6(3)
O4	Mg	O2	C22	-63.22(19)	Mg	O3	C32	C31	-31.3(3)
O5	Mg	O2	All	80.13(9)	Mg	O3	C32	C33	150.1(2)
O5	Mg	O2	C22	-156.95(18)	All	O4	C42	C41	-80.8(3)
O1	Mg	O3	All	174.10(9)	All	O4	C42	C43	97.6(3)
O1	Mg	O3	C32	-65.8(2)	Mg	O4	C42	C41	30.4(3)
O2	Mg	O3	All	-107.6(5)	Mg	O4	C42	C43	-151.2(2)
O2	Mg	O3	C32	12.5(6)	Mg	O5	C51	C52	-170.6(2)
O4	Mg	O3	All	-16.28(9)	C54	O5	C51	C52	9.7(3)
O4	Mg	O3	C32	103.79(19)	Mg	O5	C54	C53	-166.7(2)
O5	Mg	O3	All	75.13(10)	C51	O5	C54	C53	13.0(4)
O5	Mg	O3	C32	-164.80(19)					
O1	Mg	O4	All	99.8(5)					

Table 5. Torsional Angles (continued)

Atom1	Atom2	Atom3	Atom4	Angle	Atom1	Atom2	Atom3	Atom4	Angle
C11	C1	C2	C31	0.1(4)	C1	C2	C41	C42	-92.6(4)
C11	C1	C2	C41	-177.5(3)	C1	C2	C41	C46	85.7(4)
C21	C1	C2	Mg	-91.5(2)	C1	C11	C12	O1	-5.5(4)
C21	C1	C2	C31	177.7(2)	C1	C11	C12	C13	175.3(3)
C21	C1	C2	C41	0.1(4)	C1	C11	C16	C15	-176.5(3)
C2	C1	C11	C12	-92.3(4)	C1	C21	C22	O2	7.6(4)
C2	C1	C11	C16	84.4(4)	C1	C21	C22	C23	-171.7(3)
C21	C1	C11	C12	90.2(3)	C1	C21	C26	C25	173.8(3)
C21	C1	C11	C16	-93.2(3)	C2	C31	C32	O3	6.8(4)
C2	C1	C21	C22	91.8(3)	C2	C31	C32	C33	-174.7(3)
C2	C1	C21	C26	-83.8(4)	C36	C31	C32	O3	-176.3(3)
C11	C1	C21	C22	-90.7(3)	C36	C31	C32	C33	2.3(4)
C11	C1	C21	C26	93.8(3)	C2	C31	C36	C35	175.7(3)
C1	C2	C31	C32	90.8(4)	C2	C41	C42	O4	-4.9(4)
C1	C2	C31	C36	-86.1(4)	C2	C41	C42	C43	176.7(3)
C41	C2	C31	C32	-91.7(3)	C2	C41	C46	C45	-177.4(3)
C41	C2	C31	C36	91.4(4)					

Table 6. Least-Square Plane Calculation and Selected Atom Deviations for O1-O2-O3-O4

Plane	Coefficients ^a			Defining Atoms with Deviations				
(Å) ^b								
1	-0.098(8)	19.421(2)	1.135(14)	7.833(4)	O1	0.0022(9)	O2	-0.0022(9)
					O3	-0.0022(9)	O4	0.0022(9)
					<u>Al1</u>	0.1697(13)	<u>Al2</u>	-0.672(2)
					<u>Mg</u>	-0.1815(13)		

^aCoefficients are for the form $ax+by+cz = d$ where x , y and z are crystallographic coordinates.

^bUnderlined atoms were not included in the definition of the plane.

A-15: Complex 45. $([C_{38}H_{40}O_4](TiBn)\{MgCl(thf)\})_2$

– Chapter 3 –

PRELIMINARY STRUCTURE REPORT – NOT FOR PUBLICATION

XCL Code: JMS0036

Date: 1 June 2001

Compound: $[[C_2(C_6H_3\{^nPr\}\{O-\})_4](TiCH_2Ph)\{Mg(OC_4H_8)(\mu-Cl)\}]_2 \cdot 0.5PhMe$

Formula: $C_{101.5}H_{114}Cl_2Mg_2O_{10}Ti_2 (C_9H_{11}ClMg_2O_{10}Ti_2 \cdot 0.5C_7H_8)$

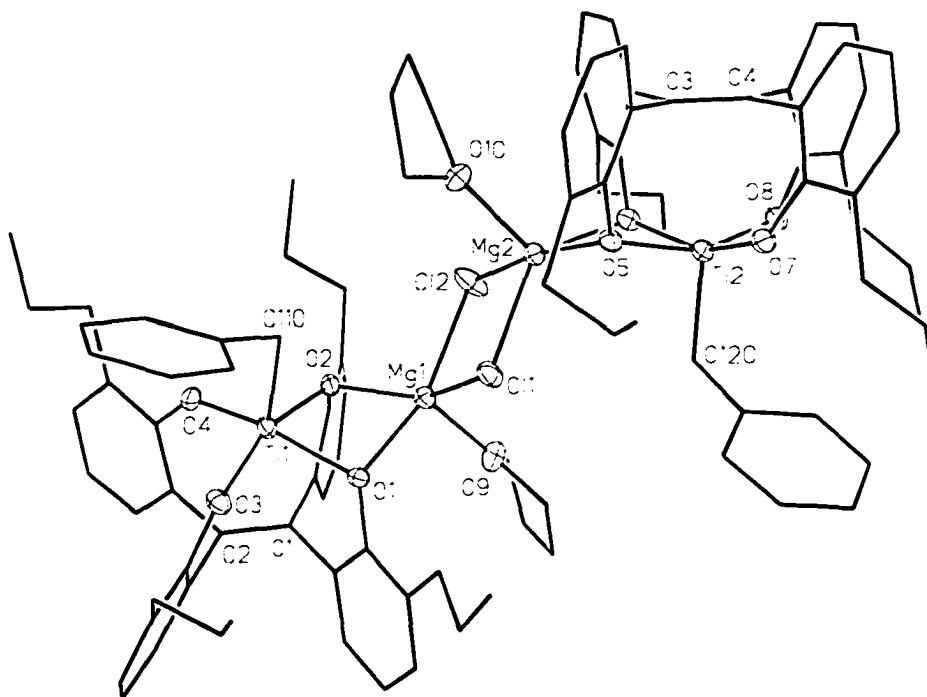


Figure 1. ‘Framework’ view of the $[[C_2(C_6H_3\{^nPr\}\{O-\})_4](TiCH_2Ph)\{Mg(OC_4H_8)(\mu-Cl)\}]_2$ molecule showing the atom labelling scheme. Ti, Cl, Mg and O atoms are represented by Gaussian ellipsoids at the 20% probability level; carbon thermal ellipsoids have been omitted, and hydrogen atom positions are not shown.

* **Numbering Scheme:** carbon atoms on the aryl ring with OX are named CX1–CX6.

Appendix A-15 page 407

List of Tables

Table 1. Crystallographic Experimental Details

Table 2. Atomic Coordinates and Equivalent Isotropic Displacement Parameters

Table 3. Selected Interatomic Distances

Table 4. Selected Interatomic Angles

Table 5. Selected Torsional Angles

Table 1. Crystallographic Experimental Details

A. Crystal Data

formula	$C_{101.5}H_{114}Cl_2Mg_2O_{10}Ti_2$
formula weight	1709.25
crystal dimensions (mm)	$0.21 \times 0.18 \times 0.17$
crystal system	monoclinic
space group	$P2_1/n$ (an alternate setting of $P2_1/c$ [No. 14])
unit cell parameters ^a	
<i>a</i> (Å)	19.4964 (18)
<i>b</i> (Å)	21.667 (2)
<i>c</i> (Å)	25.383 (2)
β (deg)	111.0813 (19)
<i>V</i> (Å ³)	10005.0 (16)
<i>Z</i>	4
ρ_{calcd} (g cm ⁻³)	1.135
μ (mm ⁻¹)	0.279

B. Data Collection and Refinement Conditions

diffractometer	Bruker P4/RA/SMART 1000 CCD ^b
radiation (λ [Å])	graphite-monochromated Mo K α (0.71073)
temperature (°C)	-80
scan type	ϕ rotations (0.3°) / ω scans (0.3°) (30 s exposures)
data collection 2θ limit (deg)	52.92
total data collected	49147 ($-24 \leq h \leq 17, -27 \leq k \leq 18, -28 \leq l \leq 31$)
independent reflections	20421
number of observed reflections (<i>NO</i>)	6390 [$F_o^2 \geq 2\sigma(F_o^2)$]

structure solution method	direct methods/fragment search (<i>DIRDIF-96</i> ^c)
refinement method	full-matrix least-squares on F^2 (<i>SHELXL-93</i> ^d)
absorption correction method	empirical (<i>SADABS</i>)
range of transmission factors	0.9622–0.8043
data/restraints/parameters	20421 [$F_o^2 \geq -3\sigma(F_o^2)$] / 0 / 943
goodness-of-fit (S) ⁱ	0.944 [$F_o^2 \geq -3\sigma(F_o^2)$]
final R indices ^j	
R_1 [$F_o^2 \geq 2\sigma(F_o^2)$]	0.1164
wR_2 [$F_o^2 \geq -3\sigma(F_o^2)$]	0.3944
largest difference peak and hole	2.022 and $-0.650 \text{ e } \text{\AA}^{-3}$

^aObtained from least-squares refinement of 4707 centered reflections.

^bPrograms for diffractometer operation, data collection, data reduction and absorption correction were those supplied by Bruker.

^cBeurskens, P. T.; Beurskens, G.; Bosman, W. P.; de Gelder, R.; Garcia Granda, S.; Gould, R. O.; Israel, R.; Smits, J. M. M. (1996). The *DIRDIF-96* program system. Crystallography Laboratory, University of Nijmegen, The Netherlands.

^dSheldrick, G. M. *SHELXL-93*. Program for crystal structure determination. University of Göttingen, Germany, 1993. Refinement on F_o^2 for all reflections (all of these having $F_o^2 \geq -3\sigma(F_o^2)$). Weighted R -factors wR_2 and all goodnesses of fit S are based on F_o^2 ; conventional R -factors R_1 are based on F_o , with F_o set to zero for negative F_o^2 . The observed criterion of $F_o^2 > 2\sigma(F_o^2)$ is used only for calculating R_1 , and is not relevant to the choice of reflections for refinement. R -factors based on F_o^2 are statistically about twice as large as those based on F_o , and R -factors based on ALL data will be even larger.

^e $S = [\sum w(F_o^2 - F_c^2)^2 / (n - p)]^{1/2}$ (n = number of data; p = number of parameters varied; $w = [\sigma^2(F_o^2) + (0.2000P)^2]^{-1}$ where $P = [\text{Max}(F_o^2, 0) + 2F_c^2] / 3$).

^f $R_1 = \sum ||F_o| - |F_c|| / \sum |F_o|$; $wR_2 = [\sum w(F_o^2 - F_c^2)^2 / \sum w(F_o^4)]^{1/2}$.

Table 2. Atomic Coordinates and Equivalent Isotropic Displacement Parameters*(a) atoms of $[(C_2(C_6H_3(^nPr)(O-))_4)(TiCH_2Ph)(Mg(OC_4H_8)(\mu-Cl))]_2$*

Atom	x	y	z	$U_{eq}, \text{\AA}^2$
Ti1	0.12331(8)	-0.13997(7)	0.25106(6)	0.0409(4)*
Ti2	-0.11243(8)	0.19915(7)	0.26286(7)	0.0457(4)*
Cl1	0.03377(12)	0.03496(11)	0.29940(9)	0.0537(6)*
Cl2	-0.04215(14)	0.02633(14)	0.16131(11)	0.0817(9)*
Mg1	0.07770(15)	-0.00419(13)	0.22684(12)	0.0450(7)*
Mg2	-0.08610(15)	0.06389(12)	0.23404(12)	0.0451(7)*
O1	0.1597(3)	-0.0557(2)	0.2836(2)	0.0423(14)*
O2	0.0829(3)	-0.0835(2)	0.1825(2)	0.0401(13)*
O3	0.1959(3)	-0.1754(3)	0.3122(2)	0.0525(16)*
O4	0.1109(3)	-0.2063(2)	0.2033(2)	0.0480(15)*
O5	-0.1133(3)	0.1132(2)	0.2930(2)	0.0406(13)*
O6	-0.1306(3)	0.1460(3)	0.1941(2)	0.0479(15)*
O7	-0.1330(3)	0.2296(3)	0.3238(2)	0.0528(16)*
O8	-0.1508(3)	0.2658(3)	0.2165(3)	0.0555(16)*
O9	0.1371(4)	0.0656(3)	0.2124(3)	0.0656(18)*
O10	-0.1537(4)	-0.0090(3)	0.2256(3)	0.0657(18)*
C1	0.2379(4)	-0.1046(4)	0.2189(3)	0.0381(19)*
C2	0.2529(4)	-0.1660(4)	0.2271(4)	0.041(2)*
C3	-0.2549(4)	0.1535(4)	0.2305(4)	0.051(2)*
C4	-0.2671(4)	0.2146(5)	0.2346(4)	0.052(2)*
C11	0.2722(5)	-0.0612(4)	0.2659(4)	0.046(2)*
C12	0.2332(5)	-0.0405(4)	0.3007(4)	0.047(2)*
C13	0.2661(5)	-0.0058(4)	0.3493(4)	0.052(2)*
C14	0.3406(5)	0.0097(4)	0.3622(4)	0.064(3)*
C15	0.3796(5)	-0.0082(4)	0.3298(5)	0.064(3)*
C16	0.3466(5)	-0.0438(4)	0.2825(4)	0.062(3)*
C17	0.2256(6)	0.0101(6)	0.3870(5)	0.082(4)*
C18	0.2676(13)	0.0258(14)	0.4443(9)	0.265(15)*
C19	0.2170(11)	0.0382(14)	0.4799(7)	0.278(16)*
C21	0.1931(5)	-0.0827(4)	0.1607(4)	0.044(2)*
C22	0.1164(5)	-0.0777(4)	0.1435(4)	0.042(2)*
C23	0.0732(6)	-0.0675(4)	0.0871(4)	0.059(3)*
C24	0.1096(7)	-0.0559(4)	0.0486(4)	0.071(3)*
C25	0.1885(8)	-0.0550(5)	0.0681(5)	0.081(3)*
C26	0.2270(6)	-0.0689(4)	0.1221(4)	0.065(3)*
C27	-0.0085(6)	-0.0724(5)	0.0650(4)	0.072(3)*
C28	-0.0367(8)	-0.1340(8)	0.0558(8)	0.155(7)*

Table 2. Atomic Coordinates and Displacement Parameters (continued)

Atom	x	y	z	$U_{eq}, \text{\AA}^2$
C29	-0.1208(10)	-0.1341(9)	0.0285(9)	0.201(9)*
C31	0.2988(5)	-0.1898(4)	0.2834(4)	0.049(2)*
C32	0.2678(5)	-0.1945(4)	0.3259(4)	0.054(2)*
C33	0.3069(6)	-0.2178(5)	0.3802(4)	0.068(3)*
C34	0.3769(7)	-0.2374(5)	0.3913(5)	0.084(3)*
C35	0.4103(6)	-0.2341(5)	0.3522(5)	0.088(4)*
C36	0.3711(5)	-0.2113(5)	0.2976(5)	0.066(3)*
C37	0.2726(7)	-0.2204(6)	0.4241(5)	0.093(4)*
C38	0.2909(12)	-0.1649(10)	0.4614(7)	0.190(9)*
C39	0.2602(10)	-0.1611(9)	0.5069(7)	0.178(8)*
C41	0.2205(5)	-0.2129(4)	0.1829(4)	0.045(2)*
C42	0.1488(5)	-0.2335(4)	0.1732(4)	0.045(2)*
C43	0.1160(6)	-0.2791(4)	0.1346(4)	0.062(3)*
C44	0.1560(6)	-0.3062(4)	0.1040(4)	0.070(3)*
C45	0.2275(6)	-0.2875(5)	0.1141(5)	0.074(3)*
C46	0.2599(5)	-0.2415(4)	0.1523(4)	0.058(3)*
C47	0.0358(5)	-0.3016(5)	0.1250(5)	0.079(3)*
C48	0.0379(6)	-0.3506(5)	0.1685(6)	0.103(4)*
C49	-0.0391(7)	-0.3740(7)	0.1611(7)	0.142(6)*
C51	-0.2420(5)	0.1120(4)	0.2785(4)	0.054(2)*
C52	-0.1696(5)	0.0953(4)	0.3108(4)	0.048(2)*
C53	-0.1534(5)	0.0617(4)	0.3610(4)	0.058(3)*
C54	-0.2131(6)	0.0434(5)	0.3763(5)	0.069(3)*
C55	-0.2811(7)	0.0597(5)	0.3470(5)	0.076(3)*
C56	-0.2988(5)	0.0940(5)	0.2962(4)	0.062(3)*
C57	-0.0732(6)	0.0468(5)	0.3998(4)	0.075(3)*
C58	-0.0384(7)	0.1010(7)	0.4343(5)	0.109(5)*
C59A ^a	-0.0594(17)	0.1052(14)	0.4883(12)	0.132(11)
C59B ^a	0.0360(18)	0.0864(15)	0.4743(14)	0.148(12)
C61	-0.2603(5)	0.1296(5)	0.1726(4)	0.058(3)*
C62	-0.1997(5)	0.1332(4)	0.1550(4)	0.055(2)*
C63	-0.2095(6)	0.1230(5)	0.0973(4)	0.065(3)*
C64	-0.2757(7)	0.1008(6)	0.0616(5)	0.087(4)*
C65	-0.3346(7)	0.0928(6)	0.0786(6)	0.104(4)*
C66	-0.3277(6)	0.1091(6)	0.1349(5)	0.084(3)*
C67	-0.1480(6)	0.1383(5)	0.0762(4)	0.077(3)*
C68	-0.1545(11)	0.2029(10)	0.0548(9)	0.185(9)*
C69	-0.1030(11)	0.2198(9)	0.0324(8)	0.186(8)*
C71	-0.2629(5)	0.2428(4)	0.2895(4)	0.047(2)*

Table 2. Atomic Coordinates and Displacement Parameters (continued)

Atom	<i>x</i>	<i>y</i>	<i>z</i>	<i>U</i> _{eq} , Å ²
C72	-0.1952(5)	0.2483(4)	0.3321(4)	0.051(2)*
C73	-0.1898(6)	0.2741(5)	0.3837(4)	0.066(3)*
C74	-0.2525(7)	0.2939(5)	0.3916(5)	0.087(4)*
C75	-0.3207(6)	0.2879(6)	0.3484(5)	0.090(4)*
C76	-0.3267(5)	0.2631(5)	0.2972(4)	0.066(3)*
C77	-0.1152(7)	0.2814(6)	0.4307(5)	0.095(4)*
C78	-0.0806(8)	0.3410(9)	0.4326(8)	0.183(9)*
C79	-0.0122(8)	0.3476(7)	0.4824(7)	0.142(6)*
C81	-0.2805(6)	0.2591(5)	0.1868(4)	0.065(3)*
C82	-0.2171(6)	0.2860(5)	0.1817(4)	0.062(3)*
C83	-0.2236(7)	0.3298(5)	0.1410(5)	0.086(4)*
C84	-0.2933(7)	0.3489(7)	0.1059(5)	0.112(5)*
C85	-0.3567(8)	0.3239(7)	0.1105(6)	0.124(6)*
C86	-0.3496(6)	0.2796(6)	0.1510(5)	0.097(4)*
C87	-0.1546(7)	0.3572(6)	0.1359(6)	0.103(5)*
C88	-0.1160(7)	0.4030(6)	0.1870(7)	0.120(6)*
C89	-0.0449(7)	0.4334(7)	0.1877(7)	0.138(6)*
C91	0.1763(6)	0.1125(5)	0.2515(5)	0.074(3)*
C92	0.2373(8)	0.1314(7)	0.2333(7)	0.116(5)*
C93	0.2187(10)	0.1110(7)	0.1764(9)	0.143(7)*
C94	0.1408(8)	0.0842(5)	0.1574(5)	0.100(4)*
C101	-0.1508(6)	-0.0562(5)	0.2666(5)	0.079(3)*
C102	-0.2280(8)	-0.0761(7)	0.2525(8)	0.119(5)*
C103	-0.2683(9)	-0.0618(7)	0.1925(9)	0.149(7)*
C104	-0.2095(8)	-0.0302(6)	0.1738(6)	0.110(5)*
C110	0.0237(5)	-0.1404(4)	0.2661(4)	0.057(3)*
C111 ^b	0.0282(6)	-0.1910(5)	0.3079(5)	0.143(3)
C112 ^b	0.0460(6)	-0.1800(4)	0.3652(5)	0.143(3)
C113 ^b	0.0531(6)	-0.2291(6)	0.4021(3)	0.143(3)
C114 ^b	0.0426(6)	-0.2892(5)	0.3816(5)	0.143(3)
C115 ^b	0.0248(6)	-0.3002(4)	0.3243(5)	0.143(3)
C116 ^b	0.0176(6)	-0.2511(6)	0.2874(3)	0.143(3)
C120	-0.0016(5)	0.2084(4)	0.2774(4)	0.061(3)*
C121 ^b	0.0380(5)	0.2462(5)	0.3256(4)	0.123(2)
C122 ^b	0.0752(5)	0.2231(3)	0.3795(5)	0.123(2)
C123 ^b	0.1106(5)	0.2632(5)	0.4236(3)	0.123(2)
C124 ^b	0.1087(5)	0.3265(4)	0.4139(4)	0.123(2)
C125 ^b	0.0715(5)	0.3496(3)	0.3601(4)	0.123(2)
C126 ^b	0.0361(5)	0.3095(5)	0.3159(3)	0.123(2)

Table 2. Atomic Coordinates and Displacement Parameters (continued)*(b) solvent toluene atoms*

Atom	<i>x</i>	<i>y</i>	<i>z</i>	<i>U</i> _{eq} , Å ²
C10S ^c	0.1784(14)	-0.4408(12)	0.4733(10)	0.105(3)
C11S ^c	0.1177(8)	-0.4605(8)	0.4344(6)	0.105(3)
C12S ^c	0.0545(10)	-0.4861(8)	0.4388(6)	0.105(3)
C13S ^c	-0.0041(8)	-0.5023(8)	0.3904(8)	0.105(3)
C14S ^c	0.0004(8)	-0.4930(8)	0.3375(6)	0.105(3)
C15S ^c	0.0635(10)	-0.4674(8)	0.3331(6)	0.105(3)
C16S ^c	0.1222(8)	-0.4512(8)	0.3816(8)	0.105(3)

Anisotropically-refined atoms are marked with an asterisk (*). The form of the anisotropic displacement parameter is: $\exp[-2\pi^2(h^2a^{*2}U_{11} + k^2b^{*2}U_{22} + l^2c^{*2}U_{33} + 2klb^{*c^*}U_{23} + 2hla^{*c^*}U_{13} + 2hka^{*b^*}U_{12})]$. ^aRefined with an occupancy factor of 0.5. ^bThe benzyl group rings were refined as an idealized hexagon ($d(\text{C}-\text{C}) = 1.39 \text{ \AA}$); each set of ring carbons was refined with a common isotropic displacement parameter. ^cThe ring carbons of the solvent toluene molecule were refined as an idealized hexagon ($d(\text{C}-\text{C}) = 1.39 \text{ \AA}$); all solvent toluene carbons were refined with an occupancy factor of 0.5 and with a common isotropic displacement parameter.

Table 3. Selected Interatomic Distances (Å)*(a) within $[[C_2(C_6H_3(^nPr)(O-))_4](TiCH_2Ph)(Mg(OC_4H_8)(\mu-Cl))]_2$*

Atom1	Atom2	Distance	Atom1	Atom2	Distance
Ti1	O1	2.025(5)	C3	C4	1.356(12)
Ti1	O2	2.040(5)	C3	C51	1.463(13)
Ti1	O3	1.849(6)	C3	C61	1.526(12)
Ti1	O4	1.840(5)	C4	C71	1.498(12)
Ti1	C110	2.110(8)	C4	C81	1.497(13)
Ti2	O5	2.017(5)	C11	C12	1.429(11)
Ti2	O6	2.013(6)	C11	C16	1.408(11)
Ti2	O7	1.853(5)	C12	C13	1.388(11)
Ti2	O8	1.844(6)	C13	C14	1.410(12)
Ti2	C120	2.068(9)	C13	C17	1.485(13)
Cl1	Mg1	2.445(3)	C14	C15	1.362(13)
Cl1	Mg2	2.412(4)	C15	C16	1.376(12)
Cl2	Mg1	2.422(4)	C17	C18	1.43(2)
Cl2	Mg2	2.438(3)	C18	C19	1.58(2)
Mg1	O1	2.054(6)	C21	C22	1.403(11)
Mg1	O2	2.077(6)	C21	C26	1.396(12)
Mg1	O9	2.017(7)	C22	C23	1.393(12)
Mg2	O5	2.057(6)	C23	C24	1.424(13)
Mg2	O6	2.076(6)	C23	C27	1.489(13)
Mg2	O10	2.018(7)	C24	C25	1.436(15)
Mg2	C62	2.826(10)	C25	C26	1.338(13)
O1	C12	1.379(10)	C27	C28	1.431(17)
O2	C22	1.372(9)	C28	C29	1.53(2)
O3	C32	1.381(10)	C31	C32	1.417(12)
O4	C42	1.373(9)	C31	C36	1.403(12)
O5	C52	1.384(9)	C32	C33	1.406(13)
O6	C62	1.384(10)	C33	C34	1.359(14)
O7	C72	1.363(9)	C33	C37	1.493(14)
O8	C82	1.349(11)	C34	C35	1.370(15)
O9	C91	1.434(11)	C35	C36	1.409(14)
O9	C94	1.479(12)	C37	C38	1.492(19)
O10	C101	1.446(11)	C38	C39	1.481(18)
O10	C104	1.448(13)	C41	C42	1.403(11)
C1	C2	1.363(10)	C41	C46	1.417(11)
C1	C11	1.476(11)	C42	C43	1.376(12)
C1	C21	1.498(11)	C43	C44	1.410(12)
C2	C31	1.479(12)			
C2	C41	1.477(11)			

Table 3. Selected Interatomic Distances (continued)

Atom1	Atom2	Distance	Atom1	Atom2	Distance
C43	C47	1.570(13)	C77	C78	1.450(19)
C44	C45	1.385(13)	C78	C79	1.477(18)
C45	C46	1.376(13)	C81	C82	1.413(13)
C47	C48	1.524(15)	C81	C86	1.399(14)
C48	C49	1.530(15)	C82	C83	1.376(14)
C51	C52	1.401(12)	C83	C84	1.394(15)
C51	C56	1.391(12)	C83	C87	1.518(15)
C52	C53	1.402(12)	C84	C85	1.393(16)
C53	C54	1.410(13)	C85	C86	1.376(15)
C53	C57	1.552(14)	C87	C88	1.591(18)
C54	C55	1.314(14)	C88	C89	1.530(16)
C55	C56	1.420(14)	C91	C92	1.482(16)
C57	C58	1.476(15)	C92	C93	1.426(18)
C58	C59A	1.57(3)	C93	C94	1.533(19)
C58	C59B	1.48(3)	C101	C102	1.481(16)
C61	C62	1.407(12)	C102	C103	1.47(2)
C61	C66	1.391(13)	C103	C104	1.551(18)
C62	C63	1.425(12)	C110	C111	1.506(11)
C63	C64	1.370(14)	C111	C112	1.39†
C63	C67	1.515(14)	C111	C116	1.39†
C64	C65	1.376(16)	C112	C113	1.39†
C65	C66	1.431(15)	C113	C114	1.39†
C67	C68	1.490(19)	C114	C115	1.39†
C68	C69	1.37(2)	C115	C116	1.39†
C71	C72	1.378(12)	C120	C121	1.444(11)
C71	C76	1.397(11)	C121	C122	1.39†
C72	C73	1.393(12)	C121	C126	1.39†
C73	C74	1.378(13)	C122	C123	1.39†
C73	C77	1.523(15)	C123	C124	1.39†
C74	C75	1.393(15)	C124	C125	1.39†
C75	C76	1.371(14)	C125	C126	1.39†

(b) within the solvent toluene molecule

Atom1	Atom2	Distance	Atom1	Atom2	Distance
C10S	C11S	1.31(3)	C13S	C14S	1.39†
C11S	C12S	1.39†	C14S	C15S	1.39†
C11S	C16S	1.39†	C15S	C16S	1.39†
C12S	C13S	1.39†			

†Idealized aromatic C–C distance.

Table 4. Selected Interatomic Angles (deg)*(a) within $[(C_2(C_6H_3(^nPr)(O-))_4)(TiCH_2Ph)(Mg(OC_4H_8)(\mu-Cl))]_2$*

Atom1	Atom2	Atom3	Angle	Atom1	Atom2	Atom3	Angle
O1	Ti1	O2	77.2(2)	O5	Mg2	O6	74.8(2)
O1	Ti1	O3	89.0(2)	O5	Mg2	O10	98.8(3)
O1	Ti1	O4	156.6(2)	O5	Mg2	C62	84.2(2)
O1	Ti1	C110	98.1(3)	O6	Mg2	O10	118.4(3)
O2	Ti1	O3	155.4(2)	O6	Mg2	C62	27.8(2)
O2	Ti1	O4	89.3(2)	O10	Mg2	C62	91.4(3)
O2	Ti1	C110	93.4(3)	Ti1	O1	Mg1	97.7(2)
O3	Ti1	O4	96.2(3)	Ti1	O1	C12	121.0(5)
O3	Ti1	C110	108.8(3)	Mg1	O1	C12	123.3(5)
O4	Ti1	C110	101.8(3)	Ti1	O2	Mg1	96.5(2)
O5	Ti2	O6	77.1(2)	Ti1	O2	C22	122.2(5)
O5	Ti2	O7	88.8(2)	Mg1	O2	C22	116.4(4)
O5	Ti2	O8	155.4(2)	Ti1	O3	C32	137.5(5)
O5	Ti2	C120	99.9(3)	Ti1	O4	C42	137.1(5)
O6	Ti2	O7	154.6(2)	Ti2	O5	Mg2	99.4(2)
O6	Ti2	O8	89.5(3)	Ti2	O5	C52	119.9(5)
O6	Ti2	C120	93.3(3)	Mg2	O5	C52	122.4(5)
O7	Ti2	O8	95.4(3)	Ti2	O6	Mg2	98.9(2)
O7	Ti2	C120	110.0(3)	Ti2	O6	C62	124.0(5)
O8	Ti2	C120	101.3(3)	Mg2	O6	C62	107.9(5)
Mg1	Cl1	Mg2	95.01(12)	Ti2	O7	C72	134.9(6)
Mg1	Cl2	Mg2	94.94(13)	Ti2	O8	C82	138.1(6)
Cl1	Mg1	Cl2	84.83(11)	Mg1	O9	C91	127.0(6)
Cl1	Mg1	O1	93.15(18)	Mg1	O9	C94	127.0(6)
Cl1	Mg1	O2	142.6(2)	C91	O9	C94	105.5(7)
Cl1	Mg1	O9	104.9(2)	Mg2	O10	C101	128.5(6)
Cl2	Mg1	O1	160.9(2)	Mg2	O10	C104	126.4(7)
Cl2	Mg1	O2	94.42(19)	C101	O10	C104	104.6(8)
Cl2	Mg1	O9	98.3(2)	C2	C1	C11	119.2(8)
O1	Mg1	O2	75.7(2)	C2	C1	C21	118.5(7)
O1	Mg1	O9	100.5(3)	C11	C1	C21	122.0(7)
O2	Mg1	O9	112.2(3)	C1	C2	C31	120.7(8)
Cl1	Mg2	Cl2	85.21(11)	C1	C2	C41	123.0(8)
Cl1	Mg2	O5	94.24(19)	C31	C2	C41	116.1(7)
Cl1	Mg2	O6	133.6(2)	C4	C3	C51	121.3(8)
Cl1	Mg2	O10	107.7(2)	C4	C3	C61	116.8(9)
Cl1	Mg2	C62	160.8(2)	C51	C3	C61	121.8(8)
Cl2	Mg2	O5	167.7(2)	C3	C4	C71	121.2(9)
Cl2	Mg2	O6	96.64(19)	C3	C4	C81	123.4(9)
Cl2	Mg2	O10	93.0(2)				
Cl2	Mg2	C62	92.2(2)				

Table 4. Selected Interatomic Angles (continued)

Atom1	Atom2	Atom3	Angle	Atom1	Atom2	Atom3	Angle
C71	C4	C81	115.3(8)	C37	C38	C39	117.9(16)
C1	C11	C12	120.8(7)	C2	C41	C42	118.7(7)
C1	C11	C16	122.1(8)	C2	C41	C46	123.3(8)
C12	C11	C16	116.8(8)	C42	C41	C46	117.8(8)
O1	C12	C11	117.0(8)	O4	C42	C41	117.8(8)
O1	C12	C13	120.3(7)	O4	C42	C43	120.0(8)
C11	C12	C13	122.7(8)	C41	C42	C43	122.2(8)
C12	C13	C14	116.4(8)	C42	C43	C44	118.9(9)
C12	C13	C17	121.0(8)	C42	C43	C47	121.0(8)
C14	C13	C17	122.5(8)	C44	C43	C47	120.2(9)
C13	C14	C15	122.9(9)	C43	C44	C45	119.8(9)
C14	C15	C16	119.9(9)	C44	C45	C46	121.2(9)
C11	C16	C15	121.3(9)	C41	C46	C45	120.1(9)
C13	C17	C18	117.9(11)	C43	C47	C48	109.8(9)
C17	C18	C19	111.9(17)	C47	C48	C49	111.9(11)
C1	C21	C22	120.5(7)	C3	C51	C52	118.7(8)
C1	C21	C26	120.3(8)	C3	C51	C56	121.6(9)
C22	C21	C26	119.1(9)	C52	C51	C56	119.4(9)
O2	C22	C21	120.0(7)	O5	C52	C51	119.2(8)
O2	C22	C23	119.1(8)	O5	C52	C53	119.7(8)
C21	C22	C23	121.0(8)	C51	C52	C53	121.1(8)
C22	C23	C24	117.8(10)	C52	C53	C54	117.2(10)
C22	C23	C27	123.1(9)	C52	C53	C57	122.0(9)
C24	C23	C27	118.9(10)	C54	C53	C57	120.7(10)
C23	C24	C25	120.1(10)	C53	C54	C55	122.3(11)
C24	C25	C26	119.2(10)	C54	C55	C56	121.3(10)
C21	C26	C25	122.2(10)	C51	C56	C55	118.6(9)
C23	C27	C28	115.1(10)	C53	C57	C58	110.8(10)
C27	C28	C29	111.1(15)	C57	C58	C59A	110.9(15)
C2	C31	C32	119.0(7)	C57	C58	C59B	111.6(18)
C2	C31	C36	124.4(8)	C3	C61	C62	120.8(8)
C32	C31	C36	116.5(9)	C3	C61	C66	119.5(8)
O3	C32	C31	117.3(8)	C62	C61	C66	119.5(9)
O3	C32	C33	119.8(8)	Mg2	C62	O6	44.4(4)
C31	C32	C33	122.8(9)	Mg2	C62	C61	106.2(6)
C32	C33	C34	117.7(10)	Mg2	C62	C63	115.4(6)
C32	C33	C37	121.0(10)	O6	C62	C61	119.6(8)
C34	C33	C37	121.3(10)	O6	C62	C63	120.3(8)
C33	C34	C35	122.5(11)	C61	C62	C63	120.0(9)
C34	C35	C36	120.0(10)	C62	C63	C64	118.7(10)
C31	C36	C35	120.5(10)				
C33	C37	C38	112.1(12)				

Table 4. Selected Interatomic Angles (continued)

Atom1	Atom2	Atom3	Angle	Atom1	Atom2	Atom3	Angle
C62	C63	C67	119.9(9)	C84	C85	C86	118.8(12)
C64	C63	C67	121.3(10)	C81	C86	C85	121.3(11)
C63	C64	C65	122.0(11)	C83	C87	C88	110.3(11)
C64	C65	C66	119.5(11)	C87	C88	C89	115.9(12)
C61	C66	C65	119.5(11)	O9	C91	C92	105.5(9)
C63	C67	C68	111.1(10)	C91	C92	C93	106.8(12)
C67	C68	C69	115.1(17)	C92	C93	C94	107.4(12)
C4	C71	C72	118.7(7)	O9	C94	C93	100.7(10)
C4	C71	C76	120.3(8)	O10	C101	C102	105.0(10)
C72	C71	C76	121.0(9)	C101	C102	C103	107.9(12)
O7	C72	C71	120.6(8)	C102	C103	C104	103.4(13)
O7	C72	C73	119.6(9)	O10	C104	C103	104.9(12)
C71	C72	C73	119.8(8)	Ti1	C110	C111	107.9(6)
C72	C73	C74	119.6(10)	C110	C111	C112	122.8(9)
C72	C73	C77	120.5(9)	C110	C111	C116	117.1(9)
C74	C73	C77	120.0(10)	C112	C111	C116	120.0 [†]
C73	C74	C75	120.0(10)	C111	C112	C113	120.0 [†]
C74	C75	C76	121.0(10)	C112	C113	C114	120.0 [†]
C71	C76	C75	118.6(10)	C113	C114	C115	120.0 [†]
C73	C77	C78	114.9(12)	C114	C115	C116	120.0 [†]
C77	C78	C79	112.4(15)	C111	C116	C115	120.0 [†]
C4	C81	C82	115.9(9)	Ti2	C120	C121	114.3(6)
C4	C81	C86	125.1(9)	C120	C121	C122	124.0(9)
C82	C81	C86	118.7(10)	C120	C121	C126	116.0(9)
O8	C82	C81	118.1(9)	C122	C121	C126	120.0 [†]
O8	C82	C83	121.5(9)	C121	C122	C123	120.0 [†]
C81	C82	C83	120.4(10)	C122	C123	C124	120.0 [†]
C82	C83	C84	119.4(11)	C123	C124	C125	120.0 [†]
C82	C83	C87	119.3(11)	C124	C125	C126	120.0 [†]
C84	C83	C87	121.3(11)	C121	C126	C125	120.0 [†]
C83	C84	C85	121.4(12)				

(b) within the solvent toluene molecule

Atom1	Atom2	Atom3	Angle	Atom1	Atom2	Atom3	Angle
C10S	C11S	C12S	131.0(18)	C12S	C13S	C14S	120.0 [†]
C10S	C11S	C16S	109.0(17)	C13S	C14S	C15S	120.0 [†]
C12S	C11S	C16S	120.0 [†]	C14S	C15S	C16S	120.0 [†]
C11S	C12S	C13S	120.0 [†]	C11S	C16S	C15S	120.0 [†]

[†]Idealized aromatic C–C–C angle.

Table 5. Selected Torsional Angles (deg)

Atom1	Atom2	Atom3	Atom4	Angle	Atom1	Atom2	Atom3	Atom4	Angle
C11	C1	C2	C31	4.3(11)	C3	C4	C71	C76	-109.5(10)
C11	C1	C2	C41	179.2(7)	C81	C4	C71	C72	-105.5(9)
C21	C1	C2	C31	178.1(7)	C81	C4	C71	C76	74.6(11)
C21	C1	C2	C41	-7.0(11)	C3	C4	C81	C82	-87.8(12)
C2	C1	C11	C12	-97.3(9)	C3	C4	C81	C86	98.3(13)
C2	C1	C11	C16	75.6(11)	C71	C4	C81	C82	88.0(10)
C21	C1	C11	C12	89.1(10)	C71	C4	C81	C86	-85.8(13)
C21	C1	C11	C16	-98.0(10)	C1	C11	C12	O1	-8.9(12)
C2	C1	C21	C22	92.1(9)	C1	C11	C12	C13	172.1(8)
C2	C1	C21	C26	-85.9(10)	C1	C11	C16	C15	-173.5(9)
C11	C1	C21	C22	-94.3(9)	C1	C21	C22	O2	10.1(11)
C11	C1	C21	C26	87.7(10)	C1	C21	C22	C23	-169.2(8)
C1	C2	C31	C32	75.5(10)	C1	C21	C26	C25	173.4(9)
C1	C2	C31	C36	-107.7(10)	C2	C31	C32	O3	-0.8(12)
C41	C2	C31	C32	-99.8(9)	C2	C31	C32	C33	178.6(9)
C41	C2	C31	C36	77.0(11)	C2	C31	C36	C35	-179.0(9)
C1	C2	C41	C42	-80.4(10)	C2	C41	C42	O4	3.7(11)
C1	C2	C41	C46	104.3(10)	C2	C41	C42	C43	-176.9(8)
C31	C2	C41	C42	94.8(9)	C2	C41	C46	C45	176.0(9)
C31	C2	C41	C46	-80.6(10)	C3	C51	C52	O5	-6.7(12)
C51	C3	C4	C71	4.2(12)	C3	C51	C52	C53	172.5(8)
C51	C3	C4	C81	179.9(8)	C3	C51	C56	C55	-172.5(9)
C61	C3	C4	C71	-179.8(7)	C3	C61	C62	Mg2	60.1(10)
C61	C3	C4	C81	-4.1(12)	C3	C61	C62	O6	13.8(14)
C4	C3	C51	C52	-99.7(10)	C3	C61	C62	C63	-166.8(9)
C4	C3	C51	C56	73.7(12)	C3	C61	C66	C65	173.6(10)
C61	C3	C51	C52	84.5(10)	C4	C71	C72	O7	1.5(13)
C61	C3	C51	C56	-102.1(10)	C4	C71	C72	C73	-179.6(9)
C4	C3	C61	C62	84.9(11)	C4	C71	C76	C75	179.2(10)
C4	C3	C61	C66	-89.5(12)	C4	C81	C82	O8	5.7(13)
C51	C3	C61	C62	-99.2(11)	C4	C81	C82	C83	-176.8(10)
C51	C3	C61	C66	86.4(12)	C4	C81	C86	C85	175.4(12)
C3	C4	C71	C72	70.4(11)					

A-16: Complex 46. [C₃₈H₄₀O₄](TiX)(AlX'Et)

– Chapter 3 –

PRELIMINARY STRUCTURE REPORT – NOT FOR PUBLICATION

XCL Code: JMS0049

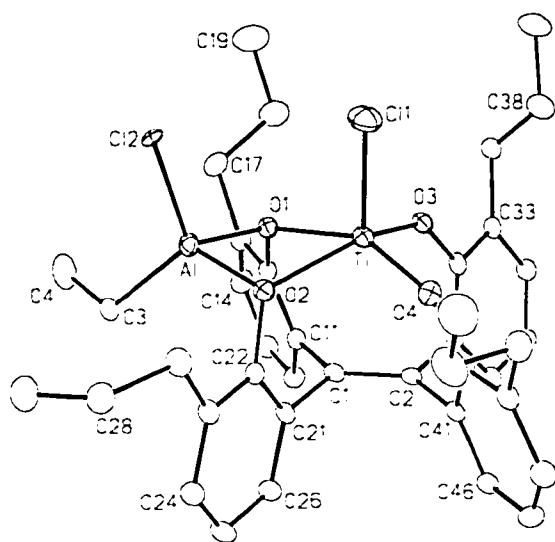
Date: 4 June 2001

Compound: [(C₂(C₆H₃ⁿPr{O-})₄)(TiX)(AlXEt)] (X = Cl, 50%; Et, 50%)

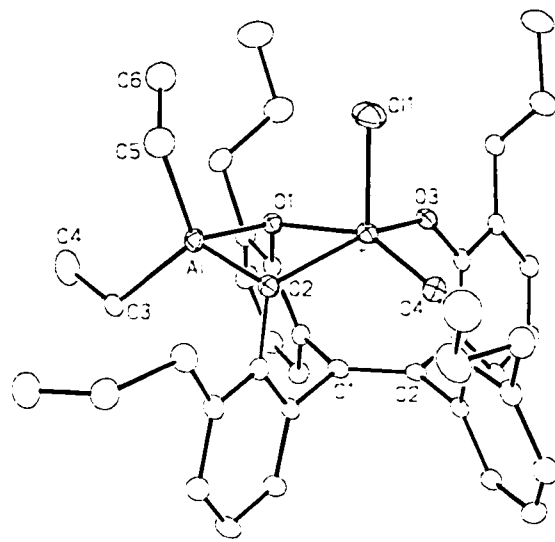
Formula: C₄₂H₅₀AlClO₄Ti

Figure 1. (See next page)

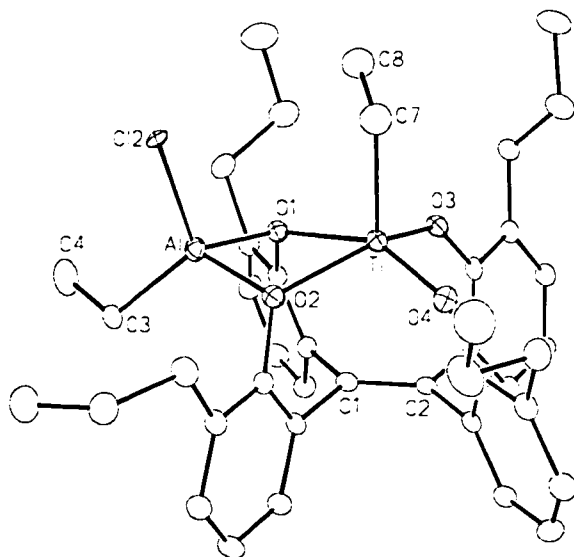
Illustration of the four possible permutations of [(C₂(C₆H₃ⁿPr{O-})₄)(TiX)(AlXEt)] (X = Cl or Et) for one of the two crystallographically-independent molecules (molecule A) showing the atom labelling scheme. Non-hydrogen atoms are represented by Gaussian ellipsoids at the 20% probability level. Hydrogen atoms are not shown. Since the disordered Cl and Et groups are each refined with an occupancy factor of 50%, each of these permutations is equally abundant. The second crystallographically-independent molecule (molecule B) is essentially identical aside from minor conformational differences involving the Et and ⁿPr groups, so will not be shown.



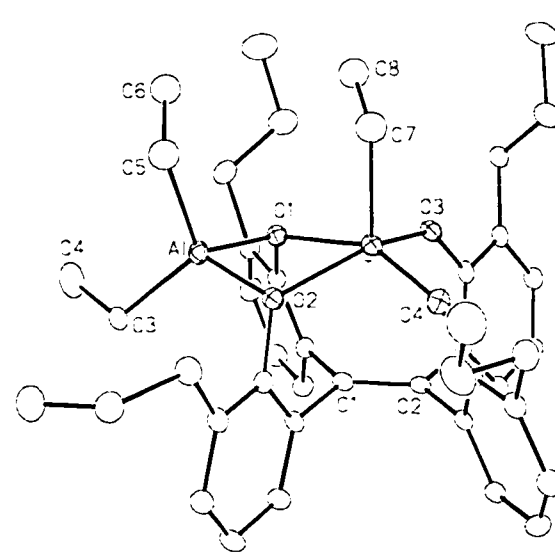
$[[C_2(C_6H_3^iPr)(O^-)_4](TiCl)(AlClEt)]$



$[[C_2(C_6H_3^iPr)(O^-)_4](TiCl)(AlEt_2)]$



$[[C_2(C_6H_3^iPr)(O^-)_4](TiEt)(AlClEt)]$



$[[C_2(C_6H_3^iPr)(O^-)_4](TiEt)(AlEt_2)]$

List of Tables

Table 1. Crystallographic Experimental Details

Table 2. Atomic Coordinates and Equivalent Isotropic Displacement Parameters

Table 3. Selected Interatomic Distances

Table 4. Selected Interatomic Angles

Table 5. Selected Torsional Angles

Table 1. Crystallographic Experimental Details

A. Crystal Data

formula	C ₄₂ H ₅₀ AlClO ₄ Ti
formula weight	729.15
crystal dimensions (mm)	0.34 × 0.19 × 0.18
crystal system	triclinic
space group	PI (No. 2)
unit cell parameters ^a	
<i>a</i> (Å)	9.8169 (7)
<i>b</i> (Å)	20.5020 (14)
<i>c</i> (Å)	21.3722 (14)
α (deg)	102.9549 (13)
β (deg)	100.0276 (13)
γ (deg)	100.5909 (14)
<i>V</i> (Å ³)	4015.1 (5)
<i>Z</i>	4
ρ _{calcd} (g cm ⁻³)	1.206
μ (mm ⁻¹)	0.340

B. Data Collection and Refinement Conditions

diffractometer	Bruker PLATFORM/SMART 1000 CCD ^b
radiation (λ [Å])	graphite-monochromated Mo Kα (0.71073)
temperature (°C)	-80
scan type	ω scans (0.2°) (20 s exposures)
data collection 2θ limit (deg)	52.86
total data collected	26132 (-12 ≤ <i>h</i> ≤ 11, -25 ≤ <i>k</i> ≤ 25, -26 ≤ <i>l</i> ≤ 26)

independent reflections	15979
number of observed reflections (<i>NO</i>)	9002 [$F_o^2 \geq 2\sigma(F_o^2)$]
structure solution method	direct methods (<i>SHELXS-86</i> ^c)
refinement method	full-matrix least-squares on F^2 (<i>SHELXL-93</i> ^d)
absorption correction method	Gaussian integration (face-indexed)
range of transmission factors	0.9399–0.8768
data/restraints/parameters	15979 [$F_o^2 \geq -3\sigma(F_o^2)$] / 12 ^e / 889
goodness-of-fit (<i>S</i>) ^f	1.019 [$F_o^2 \geq -3\sigma(F_o^2)$]
final <i>R</i> indices ^g	
R_1 [$F_o^2 \geq 2\sigma(F_o^2)$]	0.0828
wR_2 [$F_o^2 \geq -3\sigma(F_o^2)$]	0.2918
largest difference peak and hole	1.385 and -1.340 e Å ⁻³

^aObtained from least-squares refinement of 7624 centered reflections.

^bPrograms for diffractometer operation, data collection, data reduction and absorption correction were those supplied by Bruker.

^cSheldrick, G. M. *Acta Crystallogr.* **1990**, *A46*, 467–473.

^dSheldrick, G. M. *SHELXL-93*. Program for crystal structure determination. University of Göttingen, Germany, 1993. Refinement on F_o^2 for all reflections (all of these having $F_o^2 \geq -3\sigma(F_o^2)$). Weighted *R*-factors wR_2 and all goodnesses of fit *S* are based on F_o^2 ; conventional *R*-factors R_1 are based on F_o , with F_o set to zero for negative F_o^2 . The observed criterion of $F_o^2 > 2\sigma(F_o^2)$ is used only for calculating R_1 , and is not relevant to the choice of reflections for refinement. *R*-factors based on F_o^2 are statistically about twice as large as those based on F_o , and *R*-factors based on ALL data will be even larger.

^eAn idealized geometry was imposed upon the disordered ethyl groups through application of the following restraints: $d(\text{Ti}-\text{CH}_2) = 2.15$ Å; $d(\text{Al}-\text{CH}_2) = 1.95$ Å; $d(\text{CH}_2-\text{CH}_3) = 1.54$ Å; $d(\text{Ti}\cdots\text{CH}_3) = 3.03$ Å; $d(\text{Al}\cdots\text{CH}_3) = 2.90$ Å.

^f $S = [\sum w(F_o^2 - F_c^2)^2 / (n - p)]^{1/2}$ (n = number of data; p = number of parameters varied; $w = [\sigma^2(F_o^2) + (0.1775P)^2]^{-1}$ where $P = [\text{Max}(F_o^2, 0) + 2F_c^2] / 3$).

^g $R_1 = \sum ||F_o| - |F_c|| / \sum |F_o|$; $wR_2 = [\sum w(F_o^2 - F_c^2)^2 / \sum w(F_o^4)]^{1/2}$.

Table 2. Atomic Coordinates and Equivalent Isotropic Displacement Parameters*(a) Molecule A*

Atom	<i>x</i>	<i>y</i>	<i>z</i>	<i>U</i> _{eq} , Å ²
Ti	0.33972(9)	0.20885(4)	0.23999(4)	0.0292(2)*
C11 ^a	0.1114(4)	0.1994(8)	0.2194(3)	0.0642(11)*
C12 ^a	0.1982(3)	0.3827(3)	0.28655(18)	0.0317(6)*
Al	0.40199(17)	0.36113(8)	0.30021(8)	0.0352(4)*
O1	0.3996(4)	0.28404(16)	0.33057(15)	0.0309(7)*
O2	0.4148(4)	0.30355(16)	0.22239(15)	0.0319(8)*
O3	0.3560(4)	0.14522(16)	0.28525(16)	0.0340(8)*
O4	0.3713(4)	0.16617(17)	0.16193(15)	0.0361(8)*
C1	0.6309(5)	0.2430(2)	0.2802(2)	0.0279(10)*
C2	0.6151(5)	0.1756(2)	0.2517(2)	0.0278(10)*
C3	0.5602(6)	0.4399(2)	0.3442(3)	0.0387(12)*
C4	0.5515(8)	0.4769(3)	0.4135(3)	0.067(2)*
C5 ^b	0.2144(15)	0.3817(17)	0.2868(10)	0.064(2)
C6 ^b	0.1394(8)	0.3708(7)	0.3424(6)	0.064(2)
C7 ^b	0.1143(12)	0.201(3)	0.2227(9)	0.064(2)
C8 ^b	0.0653(8)	0.2018(7)	0.2875(6)	0.064(2)
C11	0.6370(5)	0.2670(2)	0.3521(2)	0.0301(11)*
C12	0.5220(5)	0.2846(2)	0.3758(2)	0.0296(10)*
C13	0.5234(6)	0.3025(3)	0.4425(2)	0.0367(12)*
C14	0.6481(6)	0.3030(3)	0.4868(3)	0.0432(13)*
C15	0.7642(6)	0.2866(3)	0.4639(3)	0.0428(13)*
C16	0.7609(6)	0.2688(3)	0.3985(2)	0.0361(12)*
C17	0.3925(7)	0.3170(3)	0.4665(3)	0.0469(14)*
C18	0.2901(9)	0.2524(4)	0.4652(5)	0.084(3)*
C19	0.1561(11)	0.2653(5)	0.4858(6)	0.113(4)*
C21	0.6609(5)	0.2954(2)	0.2415(2)	0.0299(10)*
C22	0.5522(5)	0.3214(2)	0.2109(2)	0.0314(11)*
C23	0.5762(6)	0.3678(2)	0.1729(2)	0.0349(11)*
C24	0.7157(6)	0.3907(3)	0.1689(2)	0.0386(12)*
C25	0.8257(6)	0.3671(3)	0.1994(3)	0.0419(13)*
C26	0.7975(6)	0.3184(3)	0.2345(2)	0.0361(12)*
C27	0.4506(6)	0.3892(3)	0.1370(3)	0.0453(14)*
C28	0.4847(7)	0.4560(3)	0.1180(3)	0.0505(15)*
C29	0.5330(9)	0.5180(3)	0.1758(4)	0.070(2)*
C31	0.5853(5)	0.1224(2)	0.2890(2)	0.0290(10)*
C32	0.4534(5)	0.1098(2)	0.3050(2)	0.0303(11)*
C33	0.4166(6)	0.0623(2)	0.3406(2)	0.0329(11)*
C34	0.5177(6)	0.0256(2)	0.3578(2)	0.0366(12)*

Table 2. Atomic Coordinates and Displacement Parameters (continued)

Atom	x	y	z	$U_{eq}, \text{\AA}^2$
C35	0.6480(6)	0.0367(3)	0.3412(3)	0.0410(13)*
C36	0.6830(6)	0.0849(3)	0.3068(2)	0.0379(12)*
C37	0.2763(6)	0.0523(3)	0.3602(3)	0.0391(12)*
C38	0.1524(7)	0.0096(3)	0.3068(3)	0.0586(17)*
C39	0.0114(8)	0.0033(4)	0.3288(4)	0.081(2)*
C41	0.6079(5)	0.1495(2)	0.1798(2)	0.0293(10)*
C42	0.4800(5)	0.1451(2)	0.1356(2)	0.0316(11)*
C43	0.4624(6)	0.1214(3)	0.0683(2)	0.0381(12)*
C44	0.5764(7)	0.1003(3)	0.0455(3)	0.0458(14)*
C45	0.7018(7)	0.1046(3)	0.0876(3)	0.0456(14)*
C46	0.7182(6)	0.1289(3)	0.1553(2)	0.0360(12)*
C47	0.3276(7)	0.1187(3)	0.0215(3)	0.0460(14)*
C48	0.3339(8)	0.1845(4)	-0.0008(4)	0.073(2)*
C49	0.2008(9)	0.1829(4)	-0.0502(4)	0.076(2)*

(b) Molecule B

Atom	x	y	z	$U_{eq}, \text{\AA}^2$
Ti	0.17193(10)	-0.22291(5)	0.22590(4)	0.0362(3)*
Cl1 ^a	-0.0501(6)	-0.2129(6)	0.2209(3)	0.0591(10)*
Cl2 ^a	-0.1464(4)	-0.3845(5)	0.1210(4)	0.086(2)*
Al	0.07235(18)	-0.36972(9)	0.14357(8)	0.0414(4)*
O1	0.1599(4)	-0.28544(19)	0.13154(16)	0.0386(8)*
O2	0.1440(4)	-0.32402(17)	0.23130(15)	0.0333(8)*
O3	0.2561(5)	-0.1495(2)	0.2027(2)	0.0526(11)*
O4	0.2451(4)	-0.19586(18)	0.31430(17)	0.0392(9)*
C1	0.4252(5)	-0.2623(2)	0.2261(2)	0.0293(10)*
C2	0.4772(5)	-0.1947(2)	0.2566(2)	0.0308(11)*
C3	0.1536(6)	-0.4487(3)	0.1116(3)	0.0420(13)*
C4	0.1003(10)	-0.5138(4)	0.1299(4)	0.092(3)*
C5 ^b	-0.1319(7)	-0.3764(14)	0.1215(11)	0.063(2)
C6 ^b	-0.2061(7)	-0.4324(6)	0.0572(5)	0.063(2)
C7 ^b	-0.0430(18)	-0.211(2)	0.2152(15)	0.063(2)
C8 ^b	-0.1066(8)	-0.2337(7)	0.2699(6)	0.063(2)
C11	0.4092(5)	-0.2865(2)	0.1530(2)	0.0287(10)*
C12	0.2821(6)	-0.2939(3)	0.1080(2)	0.0347(11)*
C13	0.2706(6)	-0.3137(3)	0.0408(2)	0.0401(12)*
C14	0.3888(6)	-0.3280(3)	0.0183(3)	0.0447(14)*
C15	0.5155(6)	-0.3225(3)	0.0617(3)	0.0437(13)*
C16	0.5254(6)	-0.3021(2)	0.1286(2)	0.0339(11)*

Table 2. Atomic Coordinates and Displacement Parameters (continued)

Atom	x	y	z	$U_{eq}, \text{\AA}^2$
C17	0.1322(7)	-0.3212(3)	-0.0075(3)	0.0519(15)*
C18	0.1128(10)	-0.2540(4)	-0.0200(4)	0.081(2)*
C19	-0.0215(11)	-0.2628(6)	-0.0722(4)	0.115(4)*
C21	0.3963(5)	-0.3140(2)	0.2650(2)	0.0296(10)*
C22	0.2581(5)	-0.3439(2)	0.2661(2)	0.0298(11)*
C23	0.2281(6)	-0.3928(3)	0.3000(2)	0.0376(12)*
C24	0.3423(6)	-0.4116(3)	0.3344(3)	0.0404(13)*
C25	0.4810(6)	-0.3819(3)	0.3347(3)	0.0401(13)*
C26	0.5088(6)	-0.3330(2)	0.3005(2)	0.0326(11)*
C27	0.0763(6)	-0.4238(3)	0.2999(3)	0.0498(15)*
C28	0.0176(7)	-0.3767(4)	0.3496(3)	0.072(2)*
C29	-0.1413(8)	-0.4028(5)	0.3421(4)	0.110(4)*
C31	0.5039(6)	-0.1422(2)	0.2177(2)	0.0330(11)*
C32	0.3850(7)	-0.1206(3)	0.1930(3)	0.0458(14)*
C33	0.3944(9)	-0.0699(4)	0.1580(4)	0.068(2)*
C34	0.5273(9)	-0.0437(3)	0.1488(3)	0.063(2)*
C35	0.6454(8)	-0.0653(3)	0.1729(3)	0.0529(16)*
C36	0.6336(7)	-0.1149(3)	0.2076(2)	0.0435(13)*
C37 ^a	0.246(2)	-0.0644(10)	0.1150(10)	0.079(5)
C38 ^a	0.208(4)	0.0018(16)	0.1247(17)	0.174(12)
C37' ^a	0.2794(15)	-0.0272(7)	0.1539(7)	0.056(3)
C38' ^a	0.195(3)	-0.0547(17)	0.0883(15)	0.157(12)
C39	0.0712(10)	-0.0014(6)	0.0928(6)	0.143(5)*
C41	0.4977(5)	-0.1673(2)	0.3290(2)	0.0309(11)*
C42	0.3769(6)	-0.1702(2)	0.3560(2)	0.0329(11)*
C43	0.3878(6)	-0.1479(3)	0.4239(2)	0.0375(12)*
C44	0.5214(6)	-0.1211(3)	0.4635(2)	0.0447(14)*
C45	0.6417(7)	-0.1155(3)	0.4382(3)	0.0472(14)*
C46	0.6308(6)	-0.1386(3)	0.3713(2)	0.0364(12)*
C47	0.2552(7)	-0.1529(3)	0.4509(3)	0.0461(14)*
C48	0.1902(9)	-0.0912(4)	0.4494(4)	0.071(2)*
C49	0.0546(10)	-0.0976(4)	0.4767(5)	0.093(3)*

Anisotropically-refined atoms are marked with an asterisk (*). The form of the anisotropic displacement parameter is: $\exp[-2\pi^2(h^2a^2U_{11} + k^2b^2U_{22} + l^2c^2U_{33} + 2klb^*c^*U_{23} + 2hla^*c^*U_{13} + 2hka^*b^*U_{12})]$. ^aRefined with an occupancy factor of 0.5. ^bAtoms of the disordered ethyl groups of both independent molecules were refined with a common isotropic displacement parameter.

Table 3. Selected Interatomic Distances (Å)

<i>(a) Molecule A</i>			<i>(b) Molecule B</i>		
Atom1	Atom2	Distance	Atom1	Atom2	Distance
Ti	Cl1	2.171(3)	Ti	Cl1	2.213(3)
Ti	O1	2.098(3)	Ti	O1	2.104(3)
Ti	O2	2.086(3)	Ti	O2	2.072(3)
Ti	O3	1.803(3)	Ti	O3	1.793(4)
Ti	O4	1.808(3)	Ti	O4	1.818(4)
Ti	C7	2.15†	Ti	C7	2.15†
Cl2	Al	2.112(3)	Cl2	Al	2.066(4)
Al	O1	1.836(3)	Al	O1	1.876(4)
Al	O2	1.850(3)	Al	O2	1.844(3)
Al	C3	1.948(5)	Al	C3	1.973(5)
Al	C5	1.95†	Al	C5	1.95†
O1	C12	1.402(6)	O1	C12	1.404(6)
O2	C22	1.410(6)	O2	C22	1.410(6)
O3	C32	1.369(6)	O3	C32	1.366(7)
O4	C42	1.383(6)	O4	C42	1.372(6)
C1	C2	1.347(6)	C1	C2	1.351(7)
C1	C11	1.492(6)	C1	C11	1.500(6)
C1	C21	1.514(6)	C1	C21	1.503(6)
C2	C31	1.505(6)	C2	C31	1.515(6)
C2	C41	1.493(6)	C2	C41	1.487(6)
C3	C4	1.530(8)	C3	C4	1.502(9)
C5	C6	1.54†	C5	C6	1.54†
C7	C8	1.54†	C7	C8	1.54†
C11	C12	1.388(7)	C11	C12	1.396(7)
C11	C16	1.417(7)	C11	C16	1.394(7)
C12	C13	1.386(7)	C12	C13	1.380(7)
C13	C14	1.408(8)	C13	C14	1.387(8)
C13	C17	1.519(7)	C13	C17	1.516(8)
C14	C15	1.382(8)	C14	C15	1.386(8)
C15	C16	1.357(7)	C15	C16	1.377(7)
C17	C18	1.500(9)	C17	C18	1.502(9)
C18	C19	1.506(11)	C18	C19	1.524(11)
C21	C22	1.405(7)	C21	C22	1.389(7)
C21	C26	1.382(7)	C21	C26	1.395(7)
C22	C23	1.398(7)	C22	C23	1.381(7)
C23	C24	1.387(7)	C23	C24	1.394(8)
C23	C27	1.523(7)	C23	C27	1.509(8)
C24	C25	1.383(8)	C24	C25	1.383(8)

Table 3. Selected Interatomic Distances (continued)

<i>(a) Molecule A</i>			<i>(b) Molecule B</i>		
Atom1	Atom2	Distance	Atom1	Atom2	Distance
C25	C26	1.394(7)	C25	C26	1.383(7)
C27	C28	1.511(7)	C27	C28	1.533(9)
C28	C29	1.496(9)	C28	C29	1.520(10)
C31	C32	1.389(7)	C31	C32	1.384(8)
C31	C36	1.390(7)	C31	C36	1.366(8)
C32	C33	1.398(7)	C32	C33	1.410(8)
C33	C34	1.399(7)	C33	C34	1.382(10)
C33	C37	1.501(7)	C33	C37	1.62(2)
			C33	C37'	1.552(15)
C34	C35	1.378(7)	C34	C35	1.374(10)
C35	C36	1.387(7)	C35	C36	1.387(7)
C37	C38	1.492(8)	C37	C38	1.45(4)
C38	C39	1.531(9)	C38	C39	1.38(3)
			C37'	C38'	1.43(3)
			C38'	C39	1.78(3)
C41	C42	1.408(7)	C41	C42	1.403(7)
C41	C46	1.376(7)	C41	C46	1.392(7)
C42	C43	1.381(6)	C42	C43	1.399(7)
C43	C44	1.396(8)	C43	C44	1.370(8)
C43	C47	1.497(8)	C43	C47	1.509(8)
C44	C45	1.368(8)	C44	C45	1.378(8)
C45	C46	1.391(7)	C45	C46	1.379(7)
C47	C48	1.524(8)	C47	C48	1.522(8)
C48	C49	1.519(10)	C48	C49	1.539(9)

†Distance fixed during refinement.

Table 4. Selected Interatomic Angles (deg)

<i>(a) Molecule A</i>				<i>(b) Molecule B</i>			
Atom1	Atom2	Atom3	Angle	Atom1	Atom2	Atom3	Angle
Cl1	Ti	O1	99.8(3)	Cl1	Ti	O1	102.4(3)
Cl1	Ti	O2	102.1(4)	Cl1	Ti	O2	98.5(3)
Cl1	Ti	O3	101.2(3)	Cl1	Ti	O3	104.3(3)
Cl1	Ti	O4	103.6(3)	Cl1	Ti	O4	101.5(2)
O1	Ti	O2	71.94(12)	O1	Ti	O2	71.96(13)
O1	Ti	O3	88.03(14)	O1	Ti	O3	89.73(17)
O1	Ti	O4	152.56(15)	O1	Ti	O4	150.85(15)
O1	Ti	C7	98.1(12)	O1	Ti	C7	100.2(11)
O2	Ti	O3	151.43(15)	O2	Ti	O3	153.40(17)
O2	Ti	O4	89.21(14)	O2	Ti	O4	88.29(14)
O2	Ti	C7	102.0(16)	O2	Ti	C7	100.9(11)
O3	Ti	O4	101.09(16)	O3	Ti	O4	100.21(18)
O3	Ti	C7	100.8(13)	O3	Ti	C7	101.3(8)
O4	Ti	C7	105.4(9)	O4	Ti	C7	104.5(9)
Cl2	Al	O1	110.56(17)	Cl2	Al	O1	110.7(4)
Cl2	Al	O2	108.16(17)	Cl2	Al	O2	110.0(2)
Cl2	Al	C3	115.7(2)	Cl2	Al	C3	117.7(3)
O1	Al	O2	83.63(15)	O1	Al	O2	82.54(16)
O1	Al	C3	116.5(2)	O1	Al	C3	116.0(2)
O1	Al	C5	111.2(7)	O1	Al	C5	106.3(11)
O2	Al	C3	118.1(2)	O2	Al	C3	114.7(2)
O2	Al	C5	107.9(8)	O2	Al	C5	109.3(5)
C3	Al	C5	115.4(10)	C3	Al	C5	121.3(6)
Ti	O1	Al	99.16(14)	Ti	O1	Al	98.08(15)
Ti	O1	C12	118.7(3)	Ti	O1	C12	121.9(3)
Al	O1	C12	116.3(3)	Al	O1	C12	108.1(3)
Ti	O2	Al	99.13(15)	Ti	O2	Al	100.27(16)
Ti	O2	C22	121.2(3)	Ti	O2	C22	118.6(3)
Al	O2	C22	110.1(3)	Al	O2	C22	118.0(3)
Ti	O3	C32	139.2(3)	Ti	O3	C32	140.0(3)
Ti	O4	C42	139.8(3)	Ti	O4	C42	137.3(3)
C2	C1	C11	120.0(4)	C2	C1	C11	119.0(4)
C2	C1	C21	120.0(4)	C2	C1	C21	121.0(4)
C11	C1	C21	119.5(4)	C11	C1	C21	119.7(4)
C1	C2	C31	121.1(4)	C1	C2	C31	121.3(4)
C1	C2	C41	121.6(4)	C1	C2	C41	122.0(4)
C31	C2	C41	116.8(4)	C31	C2	C41	116.5(4)
Al	C3	C4	114.0(4)	Al	C3	C4	116.8(5)

Table 4. Selected Interatomic Angles (continued)

<i>(a) Molecule A</i>				<i>(b) Molecule B</i>			
Atom1	Atom2	Atom3	Angle	Atom1	Atom2	Atom3	Angle
Al	C5	C6	111.9†	Al	C5	C6	111.9†
Ti	C7	C8	109.3†	Ti	C7	C8	109.3†
C1	C11	C12	122.1(4)	C1	C11	C12	122.7(4)
C1	C11	C16	119.6(4)	C1	C11	C16	119.0(4)
C12	C11	C16	118.2(4)	C12	C11	C16	118.3(4)
O1	C12	C11	118.8(4)	O1	C12	C11	119.2(4)
O1	C12	C13	118.7(4)	O1	C12	C13	118.7(5)
C11	C12	C13	122.5(4)	C11	C12	C13	121.9(5)
C12	C13	C14	117.5(5)	C12	C13	C14	118.1(5)
C12	C13	C17	121.1(5)	C12	C13	C17	121.5(5)
C14	C13	C17	121.3(5)	C14	C13	C17	120.4(5)
C13	C14	C15	120.6(5)	C13	C14	C15	121.2(5)
C14	C15	C16	121.3(5)	C14	C15	C16	119.8(5)
C11	C16	C15	120.0(5)	C11	C16	C15	120.5(5)
C13	C17	C18	112.3(5)	C13	C17	C18	112.6(6)
C17	C18	C19	113.3(7)	C17	C18	C19	112.1(7)
C1	C21	C22	121.7(4)	C1	C21	C22	121.0(4)
C1	C21	C26	120.4(4)	C1	C21	C26	120.2(5)
C22	C21	C26	117.9(4)	C22	C21	C26	118.8(4)
O2	C22	C21	118.7(4)	O2	C22	C21	119.1(4)
O2	C22	C23	118.3(4)	O2	C22	C23	118.6(5)
C21	C22	C23	122.8(5)	C21	C22	C23	122.3(5)
C22	C23	C24	116.9(5)	C22	C23	C24	117.8(5)
C22	C23	C27	119.4(5)	C22	C23	C27	120.5(5)
C24	C23	C27	123.6(5)	C24	C23	C27	121.7(5)
C23	C24	C25	121.7(5)	C23	C24	C25	121.0(5)
C24	C25	C26	120.0(5)	C24	C25	C26	120.3(5)
C21	C26	C25	120.6(5)	C21	C26	C25	119.8(5)
C23	C27	C28	116.2(5)	C23	C27	C28	112.0(5)
C27	C28	C29	113.5(5)	C27	C28	C29	111.8(6)
C2	C31	C32	118.2(4)	C2	C31	C32	114.9(5)
C2	C31	C36	122.6(4)	C2	C31	C36	124.9(5)
C32	C31	C36	119.2(4)	C32	C31	C36	120.1(5)
O3	C32	C31	118.8(4)	O3	C32	C31	119.0(5)
O3	C32	C33	118.8(5)	O3	C32	C33	119.6(6)
C31	C32	C33	122.4(4)	C31	C32	C33	121.4(6)
C34	C33	C37	121.9(4)	C32	C33	C34	116.7(6)

Table 4. Selected Interatomic Angles (continued)

<i>(a) Molecule A</i>				<i>(b) Molecule B</i>			
Atom1	Atom2	Atom3	Angle	Atom1	Atom2	Atom3	Angle
C32	C33	C34	116.8(5)	C32	C33	C37	116.1(9)
C32	C33	C37	121.3(4)	C32	C33	C37'	120.0(8)
				C34	C33	C37	124.7(9)
				C34	C33	C37'	119.5(8)
C33	C34	C35	121.3(5)	C33	C34	C35	122.0(6)
C34	C35	C36	120.9(5)	C34	C35	C36	120.2(6)
C31	C36	C35	119.4(5)	C31	C36	C35	119.6(6)
C33	C37	C38	115.2(5)	C33	C37	C38	119(2)
C37	C38	C39	113.0(6)	C37	C38	C39	114(3)
				C33	C37'	C38'	104.5(17)
				C37'	C38'	C39	98(2)
C2	C41	C42	117.5(4)	C2	C41	C42	118.4(4)
C2	C41	C46	123.4(4)	C2	C41	C46	123.2(5)
C42	C41	C46	119.1(4)	C42	C41	C46	118.4(5)
O4	C42	C41	117.6(4)	O4	C42	C41	118.7(4)
O4	C42	C43	120.4(4)	O4	C42	C43	119.5(5)
C41	C42	C43	122.0(5)	C41	C42	C43	121.7(5)
C42	C43	C44	117.0(5)	C42	C43	C44	117.5(5)
C42	C43	C47	121.7(5)	C42	C43	C47	120.0(5)
C44	C43	C47	121.2(5)	C44	C43	C47	122.5(5)
C43	C44	C45	121.9(5)	C43	C44	C45	122.1(5)
C44	C45	C46	120.4(5)	C44	C45	C46	120.3(5)
C41	C46	C45	119.6(5)	C41	C46	C45	120.0(5)
C43	C47	C48	111.7(5)	C43	C47	C48	112.2(5)
C47	C48	C49	113.4(6)	C47	C48	C49	111.3(6)

† Angle fixed during refinement.

Table 5. Torsional Angles (deg)

<i>(a) Molecule A</i>					<i>(b) Molecule B</i>				
Atom1	Atom2	Atom3	Atom4	Angle	Atom1	Atom2	Atom3	Atom4	Angle
C11	C1	C2	C31	7.7(7)	C11	C1	C2	C31	6.9(7)
C11	C1	C2	C41	179.7(4)	C11	C1	C2	C41	-179.2(4)
C21	C1	C2	C31	180.0(4)	C21	C1	C2	C31	-178.8(4)
C21	C1	C2	C41	-8.0(7)	C21	C1	C2	C41	-4.9(7)
C2	C1	C11	C12	-103.2(6)	C2	C1	C11	C12	-94.2(6)
C2	C1	C11	C16	73.6(6)	C2	C1	C11	C16	85.7(6)
C21	C1	C11	C12	84.5(6)	C21	C1	C11	C12	91.4(6)
C21	C1	C11	C16	-98.8(5)	C21	C1	C11	C16	-88.7(6)
C2	C1	C21	C22	97.9(6)	C2	C1	C21	C22	106.5(6)
C2	C1	C21	C26	-81.1(6)	C2	C1	C21	C26	-73.8(6)
C11	C1	C21	C22	-89.8(6)	C11	C1	C21	C22	-79.2(6)
C11	C1	C21	C26	91.2(6)	C11	C1	C21	C26	100.5(5)
C1	C2	C31	C32	69.2(6)	C1	C2	C31	C32	81.9(6)
C1	C2	C31	C36	-112.2(6)	C1	C2	C31	C36	-99.7(6)
C41	C2	C31	C32	-103.2(5)	C41	C2	C31	C32	-92.3(5)
C41	C2	C31	C36	75.5(6)	C41	C2	C31	C36	86.1(6)
C1	C2	C41	C42	-75.8(6)	C1	C2	C41	C42	-66.3(6)
C1	C2	C41	C46	105.1(6)	C1	C2	C41	C46	114.0(6)
C31	C2	C41	C42	96.6(5)	C31	C2	C41	C42	107.9(5)
C31	C2	C41	C46	-82.5(6)	C31	C2	C41	C46	-71.9(6)
C1	C11	C12	O1	-4.2(7)	C1	C11	C12	O1	-6.7(7)
C1	C11	C12	C13	175.6(4)	C1	C11	C12	C13	177.5(4)
C1	C11	C16	C15	-176.1(4)	C1	C11	C16	C15	-178.2(4)
C1	C21	C22	O2	6.7(7)	C1	C21	C22	O2	-1.4(6)
C1	C21	C22	C23	-177.5(4)	C1	C21	C22	C23	178.3(4)
C1	C21	C26	C25	-179.5(4)	C1	C21	C26	C25	-178.4(4)
C2	C31	C32	O3	1.1(6)	C2	C31	C32	O3	-2.7(7)
C2	C31	C32	C33	-178.9(4)	C2	C31	C32	C33	177.5(5)
C2	C31	C36	C35	180.0(4)	C2	C31	C36	C35	-177.8(5)
C2	C41	C42	O4	0.8(6)	C2	C41	C42	O4	-2.4(6)
C2	C41	C42	C43	-179.8(4)	C2	C41	C42	C43	177.5(4)
C2	C41	C46	C45	179.3(4)	C2	C41	C46	C45	-178.7(5)

A-17: Complex 47. $[\{E-C_2(C_6H_4-2-O-)_2(C_6H_4-2-OMe)_2\}AlEt]$

– Chapter 4 –

XCL Code: JMS0051

Date: 6 April 2001

Compound: $[\{C_2(C_6H_4-2-O-)_2(C_6H_4-2-OMe)_2\}AlEt]$

Formula: $C_{30}H_{27}AlO_4$

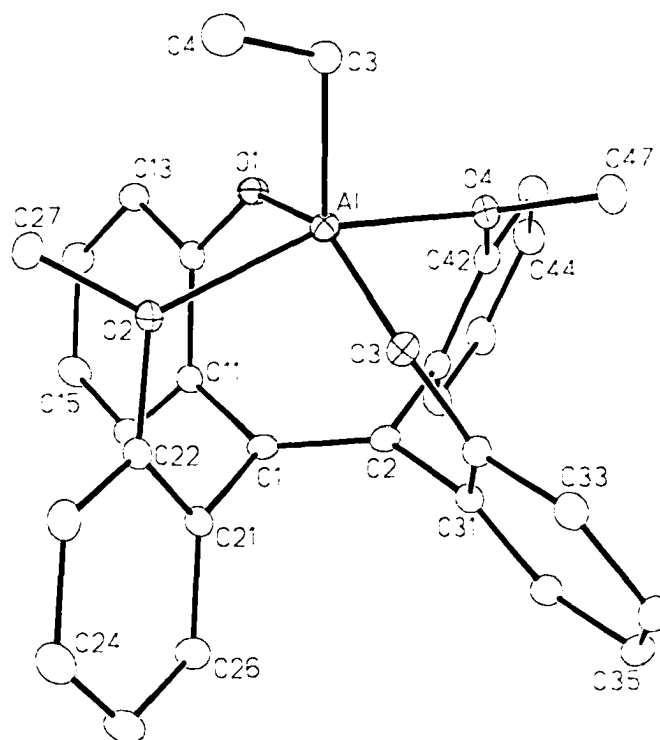


Figure 1. Perspective view of the $[\{C_2(C_6H_4-2-O-)_2(C_6H_4-2-OMe)_2\}AlEt]$ molecule showing the atom labelling scheme. Non-hydrogen atoms are represented by Gaussian ellipsoids at the 20% probability level. Hydrogen atoms are not shown.

List of Tables

Table 1. Crystallographic Experimental Details

Table 2. Atomic Coordinates and Equivalent Isotropic Displacement Parameters

Table 3. Selected Interatomic Distances

Table 4. Selected Interatomic Angles

Table 5. Selected Torsional Angles

Table 1. Crystallographic Experimental Details

A. Crystal Data

formula	C ₃₀ H ₂₇ AlO ₄
formula weight	478.50
crystal dimensions (mm)	0.42 × 0.20 × 0.13
crystal system	monoclinic
space group	P2 ₁ (No. 4)
unit cell parameters ^a	
<i>a</i> (Å)	9.3302 (5)
<i>b</i> (Å)	9.0757 (5)
<i>c</i> (Å)	14.3749 (8)
β (deg)	95.5040 (11)
<i>V</i> (Å ³)	1211.63 (11)
<i>Z</i>	2
ρ _{calcd} (g cm ⁻³)	1.312
μ (mm ⁻¹)	0.119

B. Data Collection and Refinement Conditions

diffractometer	Bruker PLATFORM/SMART 1000 CCD ^b
radiation (λ [Å])	graphite-monochromated Mo Kα (0.71073)
temperature (°C)	-80
scan type	ω scans (0.2°) (20 s exposures)
data collection 2θ limit (deg)	52.80
total data collected	8089 (-11 ≤ <i>h</i> ≤ 11, -11 ≤ <i>k</i> ≤ 11, -17 ≤ <i>l</i> ≤ 17)
independent reflections	4891
number of observed reflections (NO)	4503 [<i>F</i> _o ² ≥ 2σ(<i>F</i> _o ²)]

structure solution method	direct methods (<i>SHELXS-86</i> ^c)
refinement method	full-matrix least-squares on F^2 (<i>SHELXL-93</i> ^d)
absorption correction method	<i>SADABS</i>
range of transmission factors	0.9847–0.9517
data/restraints/parameters	4891 [$F_o^2 \geq -3\sigma(F_o^2)$] / 0 / 316
Flack absolute structure parameter ^e	0.11 (14)
goodness-of-fit (S) ^f	1.030 [$F_o^2 \geq -3\sigma(F_o^2)$]
final R indices ^g	
R_1 [$F_o^2 \geq 2\sigma(F_o^2)$]	0.0335
wR_2 [$F_o^2 \geq -3\sigma(F_o^2)$]	0.0855
largest difference peak and hole	0.294 and $-0.155 \text{ e } \text{\AA}^{-3}$

^aObtained from least-squares refinement of 7587 centered reflections.

^bPrograms for diffractometer operation, data collection, data reduction and absorption correction were those supplied by Bruker.

^cSheldrick, G. M. *Acta Crystallogr.* **1990**, *A46*, 467–473.

^dSheldrick, G. M. *SHELXL-93*. Program for crystal structure determination. University of Göttingen, Germany, 1993. Refinement on F_o^2 for all reflections (all of these having $F_o^2 \geq -3\sigma(F_o^2)$). Weighted R -factors wR_2 and all goodnesses of fit S are based on F_o^2 ; conventional R -factors R_1 are based on F_o , with F_o set to zero for negative F_o^2 . The observed criterion of $F_o^2 > 2\sigma(F_o^2)$ is used only for calculating R_1 , and is not relevant to the choice of reflections for refinement. R -factors based on F_o^2 are statistically about twice as large as those based on F_o , and R -factors based on ALL data will be even larger.

^eFlack, H. D. *Acta Crystallogr.* **1983**, *A39*, 876–881. The Flack parameter will refine to a value near zero if the structure is in the correct configuration and will refine to a value near one for the inverted configuration.

^f $S = [\sum w(F_o^2 - F_c^2)^2 / (n - p)]^{1/2}$ (n = number of data; p = number of parameters varied; $w = [\sigma^2(F_o^2) + (0.0469P)^2 + 0.1476P]^{-1}$ where $P = [\text{Max}(F_o^2, 0) + 2F_c^2] / 3$).

^g $R_1 = \sum ||F_o| - |F_c|| / \sum |F_o|$; $wR_2 = [\sum w(F_o^2 - F_c^2)^2 / \sum w(F_o^4)]^{1/2}$.

Table 2. Atomic Coordinates and Equivalent Isotropic Displacement Parameters

Atom	<i>x</i>	<i>y</i>	<i>z</i>	<i>U</i> _{eq} , Å ²
Al	-0.23585(5)	-0.15320(6)	0.13498(3)	0.02223(12)*
O1	-0.09048(14)	-0.27806(14)	0.12302(9)	0.0252(3)*
O2	-0.33661(14)	-0.32276(14)	0.20323(9)	0.0258(3)*
O3	-0.32620(13)	-0.03104(15)	0.20791(9)	0.0255(3)*
O4	-0.08312(13)	0.01127(14)	0.12119(9)	0.0250(3)*
C1	-0.09777(18)	-0.2314(2)	0.31610(12)	0.0223(4)*
C2	-0.05674(18)	-0.0911(2)	0.30433(12)	0.0228(4)*
C3	-0.34644(18)	-0.1484(2)	0.01143(12)	0.0284(4)*
C4	-0.4936(2)	-0.2239(3)	-0.00083(16)	0.0418(5)*
C11	-0.01554(18)	-0.3554(2)	0.27978(12)	0.0228(4)*
C12	-0.01393(18)	-0.3688(2)	0.18204(12)	0.0234(4)*
C13	0.0692(2)	-0.4803(2)	0.14737(13)	0.0298(4)*
C14	0.1486(2)	-0.5759(2)	0.20780(14)	0.0340(4)*
C15	0.1449(2)	-0.5641(2)	0.30367(14)	0.0352(5)*
C16	0.0615(2)	-0.4545(2)	0.33897(13)	0.0291(4)*
C21	-0.23479(18)	-0.2664(2)	0.35844(12)	0.0229(4)*
C22	-0.35315(19)	-0.3160(2)	0.29921(13)	0.0244(4)*
C23	-0.48234(19)	-0.3525(2)	0.33247(14)	0.0305(4)*
C24	-0.4949(2)	-0.3422(3)	0.42732(15)	0.0369(5)*
C25	-0.3804(2)	-0.2919(3)	0.48735(15)	0.0366(5)*
C26	-0.2517(2)	-0.2533(2)	0.45267(13)	0.0302(4)*
C27	-0.3473(2)	-0.4703(2)	0.16532(15)	0.0359(5)*
C31	-0.14434(18)	0.0369(2)	0.32912(12)	0.0240(4)*
C32	-0.27905(18)	0.0601(2)	0.27740(12)	0.0232(4)*
C33	-0.3606(2)	0.1814(2)	0.30011(14)	0.0296(4)*
C34	-0.3101(2)	0.2771(2)	0.37120(14)	0.0332(4)*
C35	-0.1760(2)	0.2554(2)	0.42020(14)	0.0344(4)*
C36	-0.0940(2)	0.1360(2)	0.39792(13)	0.0294(4)*
C41	0.07465(18)	-0.0564(2)	0.25633(12)	0.0242(4)*
C42	0.05843(18)	-0.0029(2)	0.16526(13)	0.0246(4)*
C43	0.1744(2)	0.0317(2)	0.11669(15)	0.0315(4)*
C44	0.3125(2)	0.0141(2)	0.16179(16)	0.0360(5)*
C45	0.3313(2)	-0.0395(2)	0.25204(16)	0.0368(5)*
C46	0.21378(19)	-0.0753(2)	0.29926(14)	0.0307(4)*
C47	-0.1235(2)	0.1625(2)	0.09694(14)	0.0318(4)*

Anisotropically-refined atoms are marked with an asterisk (*). The form of the anisotropic displacement parameter is: $\exp[-2\pi^2(h^2a^{*2}U_{11} + k^2b^{*2}U_{22} + l^2c^{*2}U_{33} + 2klb^{*c^{*}}U_{23} + 2hla^{*c^{*}}U_{13} + 2hka^{*b^{*}}U_{12})]$.

Table 3. Selected Interatomic Distances (Å)

Atom1	Atom2	Distance	Atom1	Atom2	Distance
Al	O1	1.7883(13)	C14	C15	1.386(3)
Al	O2	2.0956(14)	C15	C16	1.389(3)
Al	O3	1.7912(14)	C21	C22	1.402(2)
Al	O4	2.0862(13)	C21	C26	1.384(3)
Al	C3	1.9671(17)	C22	C23	1.379(2)
O1	C12	1.339(2)	C23	C24	1.383(3)
O2	C22	1.404(2)	C24	C25	1.385(3)
O2	C27	1.445(2)	C25	C26	1.388(3)
O3	C32	1.338(2)	C31	C32	1.413(2)
O4	C42	1.415(2)	C31	C36	1.384(3)
O4	C47	1.457(2)	C32	C33	1.395(3)
C1	C2	1.345(3)	C33	C34	1.389(3)
C1	C11	1.485(3)	C34	C35	1.390(3)
C1	C21	1.502(2)	C35	C36	1.382(3)
C2	C31	1.484(3)	C41	C42	1.391(3)
C2	C41	1.497(2)	C41	C46	1.393(2)
C3	C4	1.530(3)	C42	C43	1.379(2)
C11	C12	1.412(2)	C43	C44	1.395(3)
C11	C16	1.390(3)	C44	C45	1.381(3)
C12	C13	1.396(3)	C45	C46	1.383(3)
C13	C14	1.390(3)			

Table 4. Selected Interatomic Angles (deg)

Atom1	Atom2	Atom3	Angle	Atom1	Atom2	Atom3	Angle
O1	Al	O2	87.60(6)	C14	C15	C16	119.12(18)
O1	Al	O3	148.47(6)	C11	C16	C15	120.99(17)
O1	Al	O4	85.01(5)	C1	C21	C22	118.25(16)
O1	Al	C3	105.33(7)	C1	C21	C26	124.05(16)
O2	Al	O3	85.59(6)	C22	C21	C26	117.70(16)
O2	Al	O4	155.66(5)	O2	C22	C21	117.13(15)
O2	Al	C3	102.66(7)	O2	C22	C23	120.82(17)
O3	Al	O4	88.67(6)	C21	C22	C23	122.02(17)
O3	Al	C3	106.20(8)	C22	C23	C24	119.01(18)
O4	Al	C3	101.66(7)	C23	C24	C25	120.23(18)
Al	O1	C12	133.82(11)	C24	C25	C26	120.10(19)
Al	O2	C22	121.64(11)	C21	C26	C25	120.89(19)
Al	O2	C27	121.44(11)	C2	C31	C32	118.21(15)
C22	O2	C27	113.61(14)	C2	C31	C36	121.54(16)
Al	O3	C32	132.84(11)	C32	C31	C36	120.17(17)
Al	O4	C42	120.62(10)	O3	C32	C31	120.85(16)
Al	O4	C47	122.26(10)	O3	C32	C33	120.98(16)
C42	O4	C47	113.66(13)	C31	C32	C33	118.16(16)
C2	C1	C11	120.69(16)	C32	C33	C34	120.78(17)
C2	C1	C21	121.02(16)	C33	C34	C35	120.63(18)
C11	C1	C21	118.07(16)	C34	C35	C36	119.02(18)
C1	C2	C31	122.77(15)	C31	C36	C35	121.18(17)
C1	C2	C41	120.83(16)	C2	C41	C42	119.17(16)
C31	C2	C41	116.14(16)	C2	C41	C46	122.65(17)
Al	C3	C4	118.77(14)	C42	C41	C46	118.19(16)
C1	C11	C12	118.07(16)	O4	C42	C41	117.76(15)
C1	C11	C16	121.97(16)	O4	C42	C43	119.79(17)
C12	C11	C16	119.94(17)	C41	C42	C43	122.42(16)
O1	C12	C11	121.45(16)	C42	C43	C44	118.26(19)
O1	C12	C13	120.04(16)	C43	C44	C45	120.33(18)
C11	C12	C13	118.51(16)	C44	C45	C46	120.59(18)
C12	C13	C14	120.69(17)	C41	C46	C45	120.19(18)
C13	C14	C15	120.72(18)				

Table 5. Selected Torsional Angles (deg)

Atom1	Atom2	Atom3	Atom4	Angle	Atom1	Atom2	Atom3	Atom4	Angle
C3	Al	O1	C12	-150.35(16)	C1	C2	C31	C36	116.8(2)
C3	Al	O2	C22	-144.19(13)	C41	C2	C31	C32	107.99(18)
C3	Al	O2	C27	57.66(15)	C41	C2	C31	C36	-69.0(2)
C3	Al	O3	C32	-144.99(17)	C1	C2	C41	C42	104.9(2)
C3	Al	O4	C42	-144.91(13)	C1	C2	C41	C46	-75.2(3)
C3	Al	O4	C47	57.40(15)	C31	C2	C41	C42	-69.5(2)
C11	C1	C2	C31	172.56(15)	C31	C2	C41	C46	110.4(2)
C11	C1	C2	C41	-1.4(3)	C1	C11	C12	O1	-3.7(2)
C21	C1	C2	C31	-1.9(3)	C1	C11	C12	C13	176.66(16)
C21	C1	C2	C41	-175.89(15)	C1	C11	C16	C15	-175.96(18)
C2	C1	C11	C12	-65.6(2)	C1	C21	C22	O2	-2.9(2)
C2	C1	C11	C16	112.8(2)	C1	C21	C22	C23	179.12(18)
C21	C1	C11	C12	109.07(19)	C1	C21	C26	C25	-178.10(19)
C21	C1	C11	C16	-72.6(2)	C2	C31	C32	O3	0.0(2)
C2	C1	C21	C22	105.4(2)	C2	C31	C32	C33	-179.33(16)
C2	C1	C21	C26	-74.8(3)	C2	C31	C36	C35	179.62(18)
C11	C1	C21	C22	-69.2(2)	C2	C41	C42	O4	-2.2(3)
C11	C1	C21	C26	110.6(2)	C2	C41	C42	C43	179.88(18)
C1	C2	C31	C32	-66.3(2)	C2	C41	C46	C45	-179.1(2)

A-18: Complex 50. $[[E-C_2(C_6H_4-2-O)_2(C_6H_4-2-OMe)_2](AlEt)(AlEtCl_2)]$

– Chapter 4 –

XCL Code: JMS0101

Date: 18 May 2001

Compound: $[[C_2(C_6H_4-2-OMe)_2(C_6H_4-2-O)_2](AlEt)(AlCl_2Et)]$

Formula: $C_{32}H_{32}Al_2Cl_2O_4$

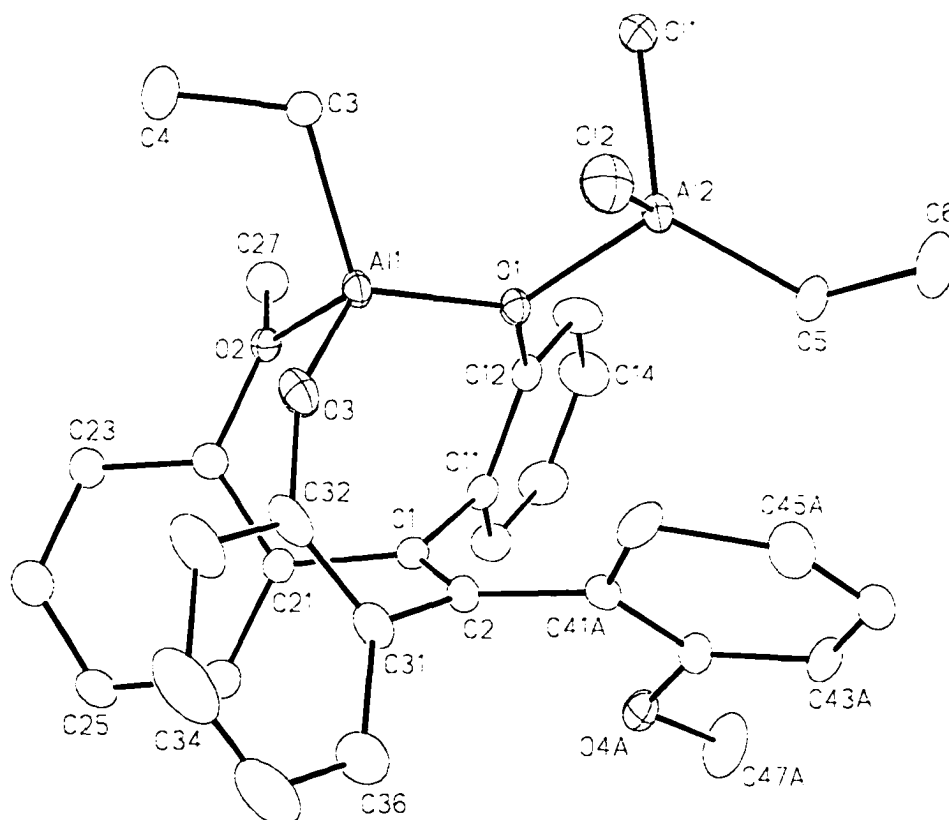


Figure 1. Perspective view of the $[[C_2(C_6H_4-2-OMe)_2(C_6H_4-2-O)_2](AlEt)(AlCl_2Et)]$ molecule showing the atom labelling scheme. Non-hydrogen atoms are represented by Gaussian ellipsoids at the 20% probability level. Hydrogen atoms are not shown.

List of Tables

Table 1. Crystallographic Experimental Details

Table 2. Atomic Coordinates and Equivalent Isotropic Displacement Parameters

Table 3. Selected Interatomic Distances

Table 4. Selected Interatomic Angles

Table 5. Selected Torsional Angles

Table 1. Crystallographic Experimental Details

A. Crystal Data

formula	C ₃₂ H ₃₂ Al ₂ Cl ₂ O ₄
formula weight	605.44
crystal dimensions (mm)	0.17 × 0.14 × 0.14
crystal system	monoclinic
space group	C2/c (No. 15)
unit cell parameters ^a	
<i>a</i> (Å)	17.4675 (12)
<i>b</i> (Å)	9.9042 (7)
<i>c</i> (Å)	36.299 (3)
β (deg)	101.1720 (16)
<i>V</i> (Å ³)	6160.8 (8)
<i>Z</i>	8
ρ _{calcd} (g cm ⁻³)	1.305
μ (mm ⁻¹)	0.303

B. Data Collection and Refinement Conditions

diffractometer	Bruker PLATFORM/SMART 1000 CCD ^b
radiation (λ [Å])	graphite-monochromated Mo Kα (0.71073)
temperature (°C)	-80
scan type	ω scans (0.2°) (30 s exposures)
data collection 2θ limit (deg)	52.80
total data collected	14085 (-21 ≤ <i>h</i> ≤ 18, -12 ≤ <i>k</i> ≤ 11, -41 ≤ <i>l</i> ≤ 45)
independent reflections	6304
number of observed reflections (<i>NO</i>)	3920 [<i>F</i> _o ² ≥ 2σ(<i>F</i> _o ²)]

structure solution method	direct methods/fragment search (<i>DIRDIF-96</i> ^c)
refinement method	full-matrix least-squares on F^2 (<i>SHELXL-93</i> ^d)
absorption correction method	<i>SADABS</i>
range of transmission factors	0.9588–0.9503
data/restraints/parameters	6304 [$F_o^2 \geq -3\sigma(F_o^2)$] / 0 / 393
goodness-of-fit (S) ^e	1.167 [$F_o^2 \geq -3\sigma(F_o^2)$]
final R indices ^f	
R_1 [$F_o^2 \geq 2\sigma(F_o^2)$]	0.0969
wR_2 [$F_o^2 \geq -3\sigma(F_o^2)$]	0.1995
largest difference peak and hole	0.358 and $-0.277 \text{ e } \text{\AA}^{-3}$

^aObtained from least-squares refinement of 4627 centered reflections.

^bPrograms for diffractometer operation, data collection, data reduction and absorption correction were those supplied by Bruker.

^cBeurskens, P. T.; Beurskens, G.; Bosman, W. P.; de Gelder, R.; Garcia Granda, S.; Gould, R. O.; Israel, R.; Smits, J. M. M. (1996). The *DIRDIF-96* program system. Crystallography Laboratory, University of Nijmegen, The Netherlands.

^dSheldrick, G. M. *SHELXL-93*. Program for crystal structure determination. University of Göttingen, Germany, 1993. Refinement on F_o^2 for all reflections (all of these having $F_o^2 \geq -3\sigma(F_o^2)$). Weighted R -factors wR_2 and all goodnesses of fit S are based on F_o^2 ; conventional R -factors R_1 are based on F_o , with F_o set to zero for negative F_o^2 . The observed criterion of $F_o^2 > 2\sigma(F_o^2)$ is used only for calculating R_1 , and is not relevant to the choice of reflections for refinement. R -factors based on F_o^2 are statistically about twice as large as those based on F_o , and R -factors based on ALL data will be even larger.

^e $S = [\sum w(F_o^2 - F_c^2)^2 / (n - p)]^{1/2}$ (n = number of data; p = number of parameters varied; $w = [\sigma^2(F_o^2) + (0.0278P)^2 + 41.1247P]^{-1}$ where $P = [\text{Max}(F_o^2, 0) + 2F_c^2]/3$).

^f $R_1 = \sum ||F_o| - |F_c|| / \sum |F_o|$; $wR_2 = [\sum w(F_o^2 - F_c^2)^2 / \sum w(F_o^4)]^{1/2}$.

Table 2. Atomic Coordinates and Equivalent Isotropic Displacement Parameters

Atom	x	y	z	$U_{eq}, \text{\AA}^2$
C11	0.12462(9)	0.31788(18)	0.18250(5)	0.0562(5)*
C12	0.20479(11)	0.14923(17)	0.11539(5)	0.0641(5)*
A11	0.21909(9)	0.46983(17)	0.09414(4)	0.0340(4)*
A12	0.23268(10)	0.27075(18)	0.16500(5)	0.0396(4)*
O1	0.26182(19)	0.4291(4)	0.14364(9)	0.0324(8)*
O2	0.2362(2)	0.6613(4)	0.09727(11)	0.0385(9)*
O3	0.2636(2)	0.4248(4)	0.05808(10)	0.0469(10)*
O4A ^a	0.5271(8)	0.4372(15)	0.1679(4)	0.049(3)*
O4B ^b	0.4121(10)	0.178(2)	0.1189(5)	0.023(5)
C1	0.3875(3)	0.5540(6)	0.11743(14)	0.0348(13)*
C2	0.4126(3)	0.4357(6)	0.10732(17)	0.0439(15)*
C3	0.1064(3)	0.4620(6)	0.08400(16)	0.0452(15)*
C4	0.0702(4)	0.5440(9)	0.0494(2)	0.099(3)*
C5	0.3135(4)	0.2075(7)	0.20583(17)	0.0519(17)*
C6	0.3140(5)	0.0543(8)	0.2128(2)	0.082(3)*
C11	0.3718(3)	0.5841(6)	0.15551(15)	0.0380(13)*
C12	0.3082(3)	0.5247(6)	0.16745(14)	0.0361(13)*
C13	0.2867(4)	0.5590(7)	0.20070(17)	0.0522(17)*
C14	0.3303(4)	0.6548(8)	0.22367(18)	0.066(2)*
C15	0.3932(4)	0.7154(8)	0.21270(19)	0.068(2)*
C16	0.4132(4)	0.6835(7)	0.17896(17)	0.0518(17)*
C21	0.3693(3)	0.6658(5)	0.08988(15)	0.0356(13)*
C22	0.2945(3)	0.7207(6)	0.08009(17)	0.0431(15)*
C23	0.2742(4)	0.8181(8)	0.0533(2)	0.082(3)*
C24	0.3326(5)	0.8689(9)	0.0365(3)	0.102(3)*
C25	0.4066(4)	0.8195(8)	0.0445(2)	0.073(2)*
C26	0.4249(4)	0.7202(6)	0.07138(18)	0.0492(16)*
C27	0.1994(4)	0.7534(6)	0.1202(2)	0.0583(18)*
C31	0.4044(4)	0.4063(6)	0.06675(18)	0.0501(16)*
C32	0.3291(4)	0.4034(6)	0.04388(18)	0.0504(17)*
C33	0.3202(5)	0.3753(7)	0.00557(19)	0.066(2)*
C34	0.3857(7)	0.3511(9)	-0.0097(2)	0.090(3)*
C35	0.4578(7)	0.3544(9)	0.0118(3)	0.094(3)*
C36	0.4682(5)	0.3805(8)	0.0502(2)	0.074(2)*
C41A ^a	0.4341(5)	0.3082(11)	0.1287(3)	0.036(2)*
C42A ^a	0.4935(5)	0.3171(10)	0.1623(3)	0.040(2)*
C43A ^a	0.5171(7)	0.1984(12)	0.1826(4)	0.053(3)*
C44A ^a	0.4850(7)	0.0769(12)	0.1713(3)	0.057(3)*
C45A ^a	0.4311(7)	0.0654(10)	0.1388(3)	0.059(3)*

Table 2. Atomic Coordinates and Displacement Parameters (continued)

Atom	<i>x</i>	<i>y</i>	<i>z</i>	<i>U</i> _{eq} , Å ²
C46A ^a	0.3932(10)	0.1797(19)	0.1139(5)	0.047(4)*
C47A ^a	0.5767(7)	0.4567(12)	0.2057(4)	0.088(4)*
C41B ^b	0.4662(11)	0.3631(18)	0.1404(6)	0.035(4)
C42B ^b	0.4565(11)	0.233(2)	0.1413(5)	0.043(4)
C43B ^b	0.5050(14)	0.144(3)	0.1665(6)	0.045(6)
C44B ^b	0.5585(13)	0.207(2)	0.1966(7)	0.057(6)
C45B ^b	0.5681(14)	0.346(3)	0.1967(7)	0.077(6)
C46B ^b	0.516(2)	0.431(4)	0.1753(11)	0.031(8)
C47B ^b	0.3942(12)	0.036(2)	0.1102(6)	0.063(5)

Anisotropically-refined atoms are marked with an asterisk (*). The form of the anisotropic displacement parameter is: $\exp[-2\pi^2(h^2a^{*2}U_{11} + k^2b^{*2}U_{22} + l^2c^{*2}U_{33} + 2klb^{*c^{*}}U_{23} + 2hla^{*c^{*}}U_{13} + 2hka^{*b^{*}}U_{12})]$. ^aRefined with an occupancy factor of 0.65. ^bRefined with an occupancy factor of 0.35.

Table 3. Selected Interatomic Distances (Å)

Atom1	Atom2	Distance	Atom1	Atom2	Distance
C11	Al2	2.156(2)	C13	C14	1.389(9)
C12	Al2	2.142(3)	C14	C15	1.378(9)
Al1	O1	1.852(4)	C15	C16	1.374(9)
Al1	O2	1.920(4)	C21	C22	1.396(7)
Al1	O3	1.707(4)	C21	C26	1.392(8)
Al1	C3	1.934(5)	C22	C23	1.367(8)
Al2	O1	1.864(4)	C23	C24	1.379(9)
Al2	C5	1.942(6)	C24	C25	1.360(10)
O1	C12	1.424(6)	C25	C26	1.378(9)
O2	C22	1.420(6)	C31	C32	1.412(9)
O2	C27	1.464(7)	C31	C36	1.389(9)
O3	C32	1.359(7)	C32	C33	1.397(9)
O4A	C42A	1.325(16)	C33	C34	1.385(11)
O4A	C47A	1.487(18)	C34	C35	1.347(12)
O4B	C42B	1.15(2)	C35	C36	1.395(11)
O4B	C47B	1.46(3)	C41A	C42A	1.442(13)
C1	C2	1.328(8)	C41A	C46A	1.51(2)
C1	C11	1.490(7)	C42A	C43A	1.407(13)
C1	C21	1.485(7)	C43A	C44A	1.357(17)
C2	C31	1.480(8)	C44A	C45A	1.362(15)
C2	C41A	1.492(11)	C45A	C46A	1.52(2)
C2	C41B	1.55(2)	C41B	C42B	1.30(3)
C3	C4	1.525(8)	C41B	C46B	1.54(5)
C5	C6	1.539(9)	C42B	C43B	1.43(3)
C11	C12	1.399(7)	C43B	C44B	1.44(3)
C11	C16	1.406(8)	C44B	C45B	1.39(3)
C12	C13	1.374(8)	C45B	C46B	1.37(5)

Table 4. Selected Interatomic Angles (deg)

Atom1	Atom2	Atom3	Angle	Atom1	Atom2	Atom3	Angle
O1	A11	O2	97.40(17)	C1	C21	C22	122.0(5)
O1	A11	O3	122.0(2)	C1	C21	C26	122.3(5)
O1	A11	C3	112.3(2)	C22	C21	C26	115.7(5)
O2	A11	O3	102.40(19)	O2	C22	C21	116.3(5)
O2	A11	C3	101.1(2)	O2	C22	C23	119.7(5)
O3	A11	C3	116.3(2)	C21	C22	C23	123.8(6)
Cl1	A12	Cl2	107.44(10)	C22	C23	C24	117.4(6)
Cl1	A12	O1	105.41(14)	C23	C24	C25	121.8(7)
Cl1	A12	C5	113.2(2)	C24	C25	C26	119.3(6)
Cl2	A12	O1	99.15(14)	C21	C26	C25	121.9(6)
Cl2	A12	C5	118.3(2)	C2	C31	C32	119.3(5)
O1	A12	C5	111.8(2)	C2	C31	C36	122.3(7)
A11	O1	A12	119.72(19)	C32	C31	C36	118.4(6)
A11	O1	C12	121.3(3)	O3	C32	C31	122.0(5)
A12	O1	C12	118.4(3)	O3	C32	C33	117.9(7)
A11	O2	C22	120.0(3)	C31	C32	C33	120.1(6)
A11	O2	C27	124.6(4)	C32	C33	C34	119.3(8)
C22	O2	C27	115.0(4)	C33	C34	C35	121.2(8)
A11	O3	C32	150.9(4)	C34	C35	C36	120.5(8)
C42A	O4A	C47A	114.9(12)	C31	C36	C35	120.4(8)
C42B	O4B	C47B	134(2)	C2	C41A	C42A	117.1(9)
C2	C1	C11	124.3(5)	C2	C41A	C46A	118.3(9)
C2	C1	C21	120.8(5)	C42A	C41A	C46A	124.6(11)
C11	C1	C21	114.9(5)	O4A	C42A	C41A	114.2(11)
C1	C2	C31	118.3(5)	O4A	C42A	C43A	126.4(11)
C1	C2	C41A	131.8(6)	C41A	C42A	C43A	118.8(10)
C1	C2	C41B	112.2(8)	C42A	C43A	C44A	121.3(12)
C31	C2	C41A	108.6(6)	C43A	C44A	C45A	120.8(11)
C31	C2	C41B	127.4(8)	C44A	C45A	C46A	127.0(12)
A11	C3	C4	112.3(4)	C41A	C46A	C45A	107.1(11)
A12	C5	C6	115.0(5)	C2	C41B	C42B	114.7(19)
C1	C11	C12	120.2(5)	C2	C41B	C46B	126(2)
C1	C11	C16	122.5(5)	C42B	C41B	C46B	118(2)
C12	C11	C16	116.9(5)	O4B	C42B	C41B	122(2)
O1	C12	C11	119.0(5)	O4B	C42B	C43B	113(2)
O1	C12	C13	118.5(5)	C41B	C42B	C43B	125(2)
C11	C12	C13	122.4(5)	C42B	C43B	C44B	116(2)
C12	C13	C14	119.0(6)	C43B	C44B	C45B	120(2)
C13	C14	C15	120.0(6)	C44B	C45B	C46B	123(3)
C14	C15	C16	120.8(6)	C41B	C46B	C45B	114(3)
C11	C16	C15	120.8(6)				

Table 5. Selected Torsional Angles (deg)

Atom1	Atom2	Atom3	Atom4	Angle	Atom1	Atom2	Atom3	Atom4	Angle
C11	C1	C2	C31	162.8(5)	C31	C2	C41A	C42A	137.5(7)
C11	C1	C2	C41A	-2.3(11)	C31	C2	C41A	C46A	-41.9(11)
C11	C1	C2	C41B	-32.3(10)	C1	C2	C41B	C42B	141.5(13)
C21	C1	C2	C31	-14.3(8)	C1	C2	C41B	C46B	-25(2)
C21	C1	C2	C41A	-179.4(7)	C31	C2	C41B	C42B	-55.3(18)
C21	C1	C2	C41B	150.6(8)	C31	C2	C41B	C46B	137.7(19)
C2	C1	C11	C12	-70.0(7)	C1	C11	C12	O1	3.8(8)
C2	C1	C11	C16	117.7(7)	C1	C11	C12	C13	-173.5(6)
C21	C1	C11	C12	107.2(6)	C1	C11	C16	C15	175.1(6)
C21	C1	C11	C16	-65.1(7)	C1	C21	C22	O2	-1.5(8)
C2	C1	C21	C22	118.2(7)	C1	C21	C22	C23	-176.0(7)
C2	C1	C21	C26	-59.9(8)	C1	C21	C26	C25	176.8(6)
C11	C1	C21	C22	-59.0(7)	C2	C31	C32	O3	-1.0(9)
C11	C1	C21	C26	122.8(6)	C2	C31	C32	C33	-179.7(6)
C1	C2	C31	C32	-61.1(8)	C2	C31	C36	C35	-179.5(7)
C1	C2	C31	C36	119.3(7)	C2	C41A	C42A	O4A	-6.1(13)
C41A	C2	C31	C32	107.2(7)	C2	C41A	C42A	C43A	-178.1(8)
C41A	C2	C31	C36	-72.4(8)	C2	C41A	C46A	C45A	175.0(9)
C41B	C2	C31	C32	136.6(10)	C2	C41B	C42B	O4B	1(3)
C41B	C2	C31	C36	-43.0(13)	C2	C41B	C42B	C43B	172.7(16)
C1	C2	C41A	C42A	-56.3(11)	C2	C41B	C46B	C45B	-168.7(19)
C1	C2	C41A	C46A	124.3(11)					

A-19: Complex 52. $[\{C_2(C_6H_4-2-O)_2(C_6H_4-2-OMe)_2\}TiCl_2]$

– Chapter 4 –

XCL Code: JMS0009

Date: 4 April 2000

Compound: $[\{C_2(C_6H_4-2-OMe)_2(C_6H_4-2-O)_2\}TiCl_2] \cdot 0.25C_6H_{14}$

Formula: $C_{29.5}H_{25.5}Cl_2O_4Ti (C_{28}H_{22}Cl_2O_4Ti \cdot 0.25C_6H_{14})$

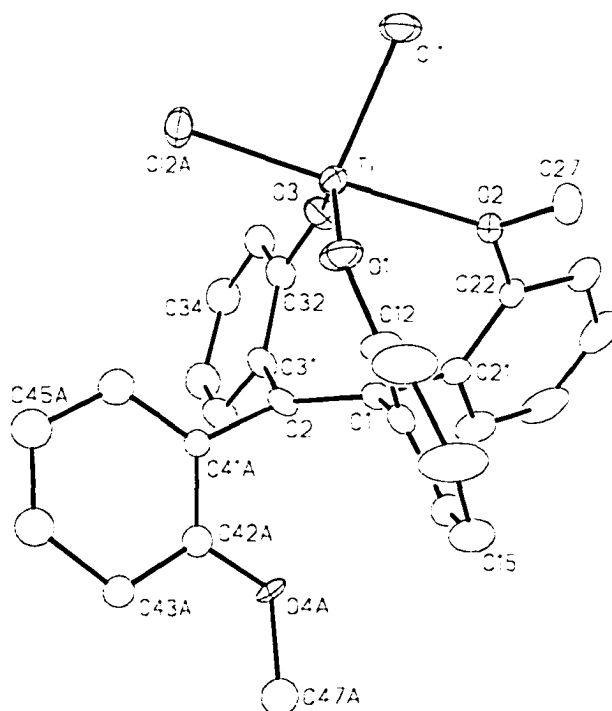


Figure 1. Perspective view of the $[\{C_2(C_6H_4-2-OMe)_2(C_6H_4-2-O)_2\}TiCl_2]$ molecule showing the atom labelling scheme. Non-hydrogen atoms are represented by Gaussian ellipsoids at the 20% probability level. Hydrogen atoms are not shown.

This structure determination was carried out by graduate research assistant Robert Lam.

List of Tables

Table 1. Crystallographic Experimental Details

Table 2. Atomic Coordinates and Equivalent Isotropic Displacement Parameters

Table 3. Selected Interatomic Distances

Table 4. Selected Interatomic Angles

Table 5. Selected Torsional Angles

Table 1. Crystallographic Experimental Details

A. Crystal Data

formula	C _{29.5} H _{25.5} Cl ₂ O ₄ Ti
formula weight	562.80
crystal dimensions (mm)	0.16 × 0.16 × 0.15
crystal system	triclinic
space group	PI (No. 2)
unit cell parameters ^a	
<i>a</i> (Å)	8.9668 (10)
<i>b</i> (Å)	10.6965 (10)
<i>c</i> (Å)	16.2572 (17)
α (deg)	77.314 (2)
β (deg)	89.3273 (19)
γ (deg)	74.8256 (19)
<i>V</i> (Å ³)	1466.4 (3)
<i>Z</i>	2
ρ _{calcd} (g cm ⁻³)	1.275
μ (mm ⁻¹)	0.505

B. Data Collection and Refinement Conditions

diffractometer	Bruker P4/RA/SMART 1000 CCD ^b
radiation (λ [Å])	graphite-monochromated Mo Kα (0.71073)
temperature (°C)	-80
scan type	φ rotations (0.3°) / ω scans (0.3°) (30 s exposures)
data collection 2θ limit (deg)	52.80
total data collected	9881 (-11 ≤ <i>h</i> ≤ 11, -13 ≤ <i>k</i> ≤ 5, -20 ≤ <i>l</i> ≤ 19)

independent reflections	5935
number of observations (<i>NO</i>)	2412 [$F_o^2 \geq 2\sigma(F_o^2)$]
structure solution method	direct methods (<i>SHELXS-86</i> ^c)
refinement method	full-matrix least-squares on F^2 (<i>SHELXL-93</i> ^d)
absorption correction method	Gaussian integration (face-indexed)
range of transmission factors	0.9511–0.8902
data/restraints/parameters	5935 [$F_o^2 \geq -3\sigma(F_o^2)$] / 5 ^e / 336
goodness-of-fit (<i>S</i>) ^f	0.951 [$F_o^2 \geq -3\sigma(F_o^2)$]
final <i>R</i> indices ^g	
R_1 [$F_o^2 \geq 2\sigma(F_o^2)$]	0.0855
wR_2 [$F_o^2 \geq -3\sigma(F_o^2)$]	0.3076
largest difference peak and hole	1.475 and $-0.411 \text{ e } \text{\AA}^{-3}$

^aObtained from least-squares refinement of 2675 centered reflections.

^bPrograms for diffractometer operation, data collection, data reduction and absorption correction were those supplied by Bruker.

^cSheldrick, G. M. *Acta Crystallogr.* **1990**, *A46*, 467–473.

^dSheldrick, G. M. *SHELXL-93*. Program for crystal structure determination. University of Göttingen, Germany, 1993. Refinement on F_o^2 for all reflections (all of these having $F_o^2 \geq -3\sigma(F_o^2)$). Weighted *R*-factors wR_2 and all goodnesses of fit *S* are based on F_o^2 ; conventional *R*-factors R_1 are based on F_o , with F_o set to zero for negative F_o^2 . The observed criterion of $F_o^2 > 2\sigma(F_o^2)$ is used only for calculating R_1 , and is not relevant to the choice of reflections for refinement. *R*-factors based on F_o^2 are statistically about twice as large as those based on F_o , and *R*-factors based on ALL data will be even larger.

^eDistances within the solvent *n*-hexane molecule were assigned fixed idealized values: $d(\text{C1S}-\text{C2S}) = d(\text{C2S}-\text{C3S}) = d(\text{C3S}-\text{C3S}') = 1.50 \text{ \AA}$; $d(\text{C1S}\cdots\text{C3S}) = d(\text{C2S}\cdots\text{C3S}') = 2.45 \text{ \AA}$ (primed atoms are related to unprimed ones via the crystallographic inversion center (0, 0, 0)).

^f $S = [\sum w(F_o^2 - F_c^2)^2 / (n - p)]^{1/2}$ (n = number of data; p = number of parameters varied; $w = [\sigma^2(F_o^2) + (0.1655P)^2]^{-1}$ where $P = [\text{Max}(F_o^2, 0) + 2F_c^2]/3$).

^g $R_1 = \sum ||F_o| - |F_c|| / \sum |F_o|$; $wR_2 = [\sum w(F_o^2 - F_c^2)^2 / \sum w(F_o^4)]^{1/2}$.

Table 2. Atomic Coordinates and Equivalent Isotropic Displacement Parameters*(a) atoms of [(C₂(C₆H₄-2-OMe)₂(C₆H₄-2-O)₂)]TiCl₂*

Atom	x	y	z	<i>U</i> _{eq} , Å ²
Ti	-0.43983(14)	0.00844(11)	0.23766(9)	0.0512(5)*
Cl1	-0.5706(3)	0.22244(16)	0.19077(14)	0.0694(7)*
Cl2A ^a	-0.2091(5)	0.0527(5)	0.2023(3)	0.0628(12)*
Cl2B ^b	-0.1919(7)	0.0198(7)	0.2581(5)	0.0698(19)*
O1	-0.4276(6)	-0.0848(4)	0.1569(3)	0.0650(15)*
O2	-0.6731(5)	-0.0288(4)	0.2489(3)	0.0468(12)*
O3	-0.4223(6)	-0.0397(4)	0.3500(3)	0.0603(15)*
O4A ^a	-0.2560(15)	-0.5561(12)	0.3121(9)	0.050(3)*
O4B ^b	-0.308(2)	-0.5761(17)	0.3384(13)	0.046(5)*
C1	-0.4610(8)	-0.2789(6)	0.2979(4)	0.0412(16)*
C2	-0.3170(8)	-0.3063(6)	0.3321(5)	0.054(2)*
C11	-0.4852(7)	-0.2922(6)	0.2102(4)	0.0394(16)*
C12	-0.4643(9)	-0.1937(6)	0.1413(5)	0.0534(19)*
C13	-0.4848(13)	-0.2025(8)	0.0591(6)	0.091(3)*
C14	-0.5300(14)	-0.3099(8)	0.0425(6)	0.096(4)*
C15	-0.5510(10)	-0.4072(7)	0.1083(5)	0.066(2)*
C16	-0.5317(8)	-0.3979(6)	0.1912(4)	0.0456(17)*
C21	-0.5996(8)	-0.2381(6)	0.3445(4)	0.0432(16)*
C22	-0.7091(8)	-0.1161(6)	0.3185(5)	0.0459(17)*
C23	-0.8426(9)	-0.0791(8)	0.3592(6)	0.070(2)*
C24	-0.8724(12)	-0.1634(11)	0.4288(7)	0.091(3)*
C25	-0.7652(15)	-0.2848(10)	0.4603(6)	0.089(3)*
C26	-0.6311(11)	-0.3228(8)	0.4180(5)	0.067(2)*
C27	-0.7863(9)	0.0179(8)	0.1796(6)	0.076(3)*
C31	-0.2929(8)	-0.2667(7)	0.4120(5)	0.057(2)*
C32	-0.3459(8)	-0.1345(7)	0.4174(5)	0.058(2)*
C33	-0.3193(9)	-0.0977(8)	0.4919(6)	0.067(2)*
C34	-0.2416(10)	-0.1928(9)	0.5625(6)	0.074(3)*
C35	-0.1828(10)	-0.3246(9)	0.5561(6)	0.080(3)*
C36	-0.2083(9)	-0.3579(7)	0.4806(5)	0.068(2)*
C41A ^a	-0.1696(16)	-0.3681(12)	0.2848(8)	0.034(3)
C42A ^a	-0.1497(15)	-0.4941(12)	0.2753(9)	0.045(3)
C43A ^a	-0.0187(19)	-0.5635(13)	0.2407(8)	0.043(3)
C44A ^a	0.0902(17)	-0.4876(16)	0.2139(9)	0.061(4)
C45A ^a	0.0776(18)	-0.3661(15)	0.2231(10)	0.066(4)
C46A ^a	-0.0536(17)	-0.3045(15)	0.2576(9)	0.059(4)
C47A ^a	-0.2468(17)	-0.6900(13)	0.3010(9)	0.063(4)

Table 2. Atomic Coordinates and Displacement Parameters (continued)

Atom	x	y	z	$U_{eq}, \text{\AA}^2$
C41B ^b	-0.194(2)	-0.398(2)	0.3100(14)	0.045(6)
C42B ^b	-0.190(2)	-0.5260(17)	0.3033(12)	0.019(4)
C43B ^b	-0.076(3)	-0.602(2)	0.2638(13)	0.060(6)
C44B ^b	0.044(3)	-0.539(2)	0.2301(13)	0.047(5)
C45B ^b	0.057(3)	-0.424(3)	0.2474(15)	0.071(6)
C46B ^b	-0.073(3)	-0.345(2)	0.2834(14)	0.056(6)
C47B ^b	-0.318(3)	-0.698(2)	0.3330(15)	0.071(6)

(b) solvent n-hexane atoms

Atom	x	y	z	$U_{eq}, \text{\AA}^2$
C1S ^c	-0.027(4)	0.2875(16)	0.017(3)	0.250
C2S ^c	0.051(4)	0.1636(18)	-0.012(3)	0.250
C3S ^c	-0.039(3)	0.0625(19)	0.014(3)	0.250

Anisotropically-refined atoms are marked with an asterisk (*). The form of the anisotropic displacement parameter is: $\exp[-2\pi^2(h^2a^{*2}U_{11} + k^2b^{*2}U_{22} + l^2c^{*2}U_{33} + 2klb^*c^*U_{23} + 2hla^*c^*U_{13} + 2hka^*b^*U_{12})]$. ^aRefined with an occupancy factor of 0.6. ^bRefined with an occupancy factor of 0.4. ^cAtoms of the solvent *n*-hexane molecule were refined with an occupancy factor of 0.5 and a common fixed isotropic displacement parameter.

Table 3. Selected Interatomic Distances (Å)

Atom1	Atom2	Distance	Atom1	Atom2	Distance
Ti	C11	2.246(2)	C13	C14	1.393(12)
Ti	C12A	2.281(4)	C14	C15	1.368(11)
Ti	C12B	2.290(6)	C15	C16	1.390(10)
Ti	O1	1.801(5)	C21	C22	1.394(9)
Ti	O2	2.228(4)	C21	C26	1.407(10)
Ti	O3	1.782(6)	C22	C23	1.369(10)
Ti	C46A	4.097(15) [†]	C23	C24	1.355(12)
Ti	H46A	3.54 [†]	C24	C25	1.393(14)
C12A	H46A	2.78 [†]	C25	C26	1.389(13)
O1	C12	1.365(7)	C31	C32	1.391(9)
O1	H46A	3.48 [†]	C31	C36	1.388(10)
O2	C22	1.393(8)	C32	C33	1.394(10)
O2	C27	1.436(8)	C33	C34	1.404(11)
O3	C32	1.366(9)	C34	C35	1.396(11)
O3	H46A	3.69 [†]	C35	C36	1.388(11)
O4A	C42A	1.360(15)	C41A	C42A	1.356(17)
O4A	C47A	1.463(18)	C41A	C46A	1.40(2)
O4B	C42B	1.38(2)	C42A	C43A	1.399(19)
O4B	C47B	1.35(3)	C43A	C44A	1.43(2)
C1	C2	1.346(9)	C44A	C45A	1.32(2)
C1	C11	1.488(9)	C45A	C46A	1.369(19)
C1	C21	1.466(9)	C41B	C42B	1.39(3)
C2	C31	1.486(10)	C41B	C46B	1.37(3)
C2	C41A	1.586(15)	C42B	C43B	1.38(3)
C2	C41B	1.37(2)	C43B	C44B	1.45(3)
C11	C12	1.407(9)	C44B	C45B	1.35(3)
C11	C16	1.396(8)	C45B	C46B	1.45(3)
C12	C13	1.377(11)			

[†]Nonbonded distance.

Table 4. Selected Interatomic Angles (deg)

Atom1	Atom2	Atom3	Angle	Atom1	Atom2	Atom3	Angle
C11	Ti	C12A	92.09(14)	C13	C14	C15	119.5(8)
C11	Ti	C12B	103.07(19)	C14	C15	C16	120.6(7)
C11	Ti	O1	111.99(19)	C11	C16	C15	121.4(7)
C11	Ti	O2	84.90(13)	C1	C21	C22	122.8(6)
C11	Ti	O3	112.41(16)	C1	C21	C26	121.2(6)
C12A	Ti	O1	90.9(2)	C22	C21	C26	116.0(7)
C12A	Ti	O2	170.38(18)	O2	C22	C21	116.0(6)
C12A	Ti	O3	103.2(2)	O2	C22	C23	120.5(6)
C12B	Ti	O1	104.5(3)	C21	C22	C23	123.5(7)
C12B	Ti	O2	166.7(2)	C22	C23	C24	119.6(8)
C12B	Ti	O3	80.7(3)	C23	C24	C25	120.1(9)
O1	Ti	O2	81.9(2)	C24	C25	C26	120.1(8)
O1	Ti	O3	132.6(2)	C21	C26	C25	120.7(8)
O2	Ti	O3	86.4(2)	C2	C31	C32	120.3(7)
Ti	O1	C12	140.9(5)	C2	C31	C36	121.2(6)
Ti	O2	C22	121.8(4)	C32	C31	C36	118.4(7)
Ti	O2	C27	122.0(4)	O3	C32	C31	120.6(6)
C22	O2	C27	115.5(5)	O3	C32	C33	119.5(6)
Ti	O3	C32	144.6(4)	C31	C32	C33	119.9(7)
C42A	O4A	C47A	118.4(13)	C32	C33	C34	120.9(7)
C42B	O4B	C47B	121(2)	C33	C34	C35	119.3(8)
C2	C1	C11	120.4(6)	C34	C35	C36	118.5(8)
C2	C1	C21	122.5(6)	C31	C36	C35	122.9(7)
C11	C1	C21	117.0(5)	C2	C41A	C42A	117.5(12)
C1	C2	C31	119.8(6)	C2	C41A	C46A	124.3(10)
C1	C2	C41A	121.4(7)	C42A	C41A	C46A	118.0(13)
C1	C2	C41B	122.6(10)	O4A	C42A	C41A	115.2(13)
C31	C2	C41A	118.5(7)	O4A	C42A	C43A	121.2(13)
C31	C2	C41B	115.5(10)	C41A	C42A	C43A	123.1(14)
C1	C11	C12	119.9(6)	C42A	C43A	C44A	113.8(12)
C1	C11	C16	123.4(6)	C43A	C44A	C45A	125.4(15)
C12	C11	C16	116.7(6)	C44A	C45A	C46A	117.5(16)
O1	C12	C11	118.7(6)	C41A	C46A	C45A	122.2(14)
O1	C12	C13	119.5(7)	C2	C41B	C42B	127.2(18)
C11	C12	C13	121.8(6)	C2	C41B	C46B	112.4(16)
C12	C13	C14	120.0(8)				

Table 4. Selected Interatomic Angles (deg)

Atom1	Atom2	Atom3	Angle	Atom1	Atom2	Atom3	Angle
C42B	C41B	C46B	120.0(19)	C42B	C43B	C44B	115.1(19)
O4B	C42B	C41B	116.4(19)	C43B	C44B	C45B	123(2)
O4B	C42B	C43B	120.2(19)	C44B	C45B	C46B	118(2)
C41B	C42B	C43B	123(2)	C41B	C46B	C45B	119(2)

Table 5. Selected Torsional Angles (deg)

Atom1	Atom2	Atom3	Atom4	Angle	Atom1	Atom2	Atom3	Atom4	Angle
O2	Ti	O1	C12	-41.4(8)	C41B	C2	C31	C32	139.2(12)
O3	Ti	O1	C12	36.0(9)	C41B	C2	C31	C36	-36.2(14)
Ti	O2	C22	C21	-45.7(7)	C1	C2	C41A	C42A	-67.6(14)
Ti	O2	C22	C23	132.2(6)	C1	C2	C41A	C46A	117.0(13)
C27	O2	C22	C21	124.5(7)	C31	C2	C41A	C42A	118.2(11)
C27	O2	C22	C23	-57.7(9)	C31	C2	C41A	C46A	-57.2(15)
C11	C1	C2	C31	167.5(6)	C1	C2	C41B	C42B	-47(3)
C11	C1	C2	C41A	-6.7(11)	C1	C2	C41B	C46B	124.9(16)
C11	C1	C2	C41B	-29.7(15)	C1	C11	C12	O1	-2.5(10)
C21	C1	C2	C31	-13.9(10)	C1	C11	C12	C13	179.7(8)
C21	C1	C2	C41A	171.9(7)	C1	C11	C16	C15	-179.1(6)
C21	C1	C2	C41B	148.9(13)	C1	C21	C22	O2	-5.3(9)
C2	C1	C11	C12	-77.1(8)	C1	C21	C22	C23	176.9(7)
C2	C1	C11	C16	104.2(8)	C1	C21	C26	C25	-178.1(7)
C21	C1	C11	C12	104.2(7)	C2	C31	C32	O3	0.9(11)
C21	C1	C11	C16	-74.5(8)	C2	C31	C32	C33	-178.3(7)
C2	C1	C21	C22	119.2(8)	C2	C31	C36	C35	179.7(8)
C2	C1	C21	C26	-62.2(9)	C2	C41A	C42A	O4A	-3.5(18)
C11	C1	C21	C22	-62.2(8)	C2	C41A	C42A	C43A	-174.9(11)
C11	C1	C21	C26	116.5(7)	C2	C41A	C46A	C45A	174.6(12)
C1	C2	C31	C32	-56.8(11)	C2	C41B	C42B	O4B	-14(3)
C1	C2	C31	C36	127.8(8)	C2	C41B	C42B	C43B	165.7(18)
C41A	C2	C31	C32	117.5(9)	C2	C41B	C46B	C45B	-172.0(18)
C41A	C2	C31	C36	-57.9(11)					

A-20: Complex 53. $[\{C_2(C_6H_4-2-O)_2(C_6H_4-2-OMe)_2\}(CpTiCl_2)(H)]$

– Chapter 4 –

XCL Code: JMS9918

Date: 18 May 2001

Compound: $[\{C_2(C_6H_4-2-OMe)_2(C_6H_4-2-OH)(C_6H_4-2-OTiCl_2Cp)\} \cdot PhMe]$

Formula: $C_{40}H_{36}Cl_2O_4Ti (C_{33}H_{28}Cl_2O_4Ti \cdot C_7H_8)$

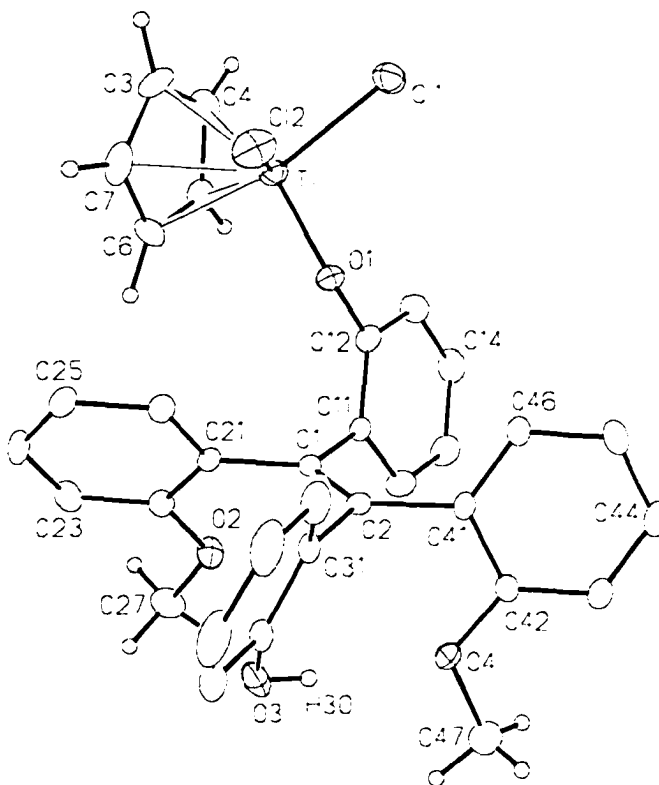


Figure 1. Perspective view of the $[\{C_2(C_6H_4-2-OMe)_2(C_6H_4-2-OH)(C_6H_4-2-OTiCl_2Cp)\}]$ molecule showing the atom labelling scheme. Non-hydrogen atoms are represented by Gaussian ellipsoids at the 20% probability level. Hydrogen atoms are shown with arbitrarily small thermal parameters except for phenyl hydrogens, which are not shown.

List of Tables

- Table 1.** Crystallographic Experimental Details
Table 2. Atomic Coordinates and Equivalent Isotropic Displacement Parameters
Table 3. Selected Interatomic Distances
Table 4. Selected Interatomic Angles
Table 5. Torsional Angles
-

Table 1. Crystallographic Experimental Details

A. Crystal Data

formula	C ₄₀ H ₃₆ Cl ₂ O ₄ Ti
formula weight	699.49
crystal dimensions (mm)	0.41 × 0.11 × 0.04
crystal system	monoclinic
space group	<i>P</i> 2 ₁ / <i>c</i> (No. 14)
unit cell parameters ^a	
<i>a</i> (Å)	9.2513 (8)
<i>b</i> (Å)	24.1558 (17)
<i>c</i> (Å)	16.1144 (13)
β (deg)	104.2728 (16)
<i>V</i> (Å ³)	3490.0 (5)
<i>Z</i>	4
ρ _{calcd} (g cm ⁻³)	1.331
μ (mm ⁻¹)	0.439

B. Data Collection and Refinement Conditions

diffractometer	Bruker P4/RA/SMART 1000 CCD ^b
radiation (λ [Å])	graphite-monochromated Mo Kα (0.71073)
temperature (°C)	-80
scan type	φ rotations (0.3°) / ω scans (0.3°) (30 s exposures)
data collection 2θ limit (deg)	52.84
total data collected	18909 (-11 ≤ <i>h</i> ≤ 11, -30 ≤ <i>k</i> ≤ 25, -20 ≤ <i>l</i> ≤ 20)
independent reflections	7166
number of observed reflections (<i>NO</i>)	2547 [<i>F</i> _o ² ≥ 2σ(<i>F</i> _o ²)]

structure solution method	direct methods/fragment search (<i>DIRDIF-96</i> ^c)
refinement method	full-matrix least-squares on F^2 (<i>SHELXL-93</i> ^d)
absorption correction method	<i>SADABS</i>
range of transmission factors	0.9678–0.5871
data/restraints/parameters	7166 [$F_o^2 \geq -3\sigma(F_o^2)$] / 1 ^e / 425
goodness-of-fit (S) ^f	0.788 [$F_o^2 \geq -3\sigma(F_o^2)$]
final R indices ^g	
R_1 [$F_o^2 \geq 2\sigma(F_o^2)$]	0.0543
wR_2 [$F_o^2 \geq -3\sigma(F_o^2)$]	0.1195
largest difference peak and hole	0.256 and $-0.276 \text{ e } \text{\AA}^{-3}$

^aObtained from least-squares refinement of 3966 centered reflections.

^bPrograms for diffractometer operation, data collection, data reduction and absorption correction were those supplied by Bruker.

^cBeurskens, P. T.; Beurskens, G.; Bosman, W. P.; de Gelder, R.; Garcia Granda, S.; Gould, R. O.; Israel, R.; Smits, J. M. M. (1996). The *DIRDIF-96* program system. Crystallography Laboratory, University of Nijmegen, The Netherlands.

^dSheldrick, G. M. *SHELXL-93*. Program for crystal structure determination. University of Göttingen, Germany, 1993. Refinement on F_o^2 for all reflections (all of these having $F_o^2 \geq -3\sigma(F_o^2)$). Weighted R -factors wR_2 and all goodnesses of fit S are based on F_o^2 ; conventional R -factors R_1 are based on F_o , with F_o set to zero for negative F_o^2 . The observed criterion of $F_o^2 > 2\sigma(F_o^2)$ is used only for calculating R_1 , and is not relevant to the choice of reflections for refinement. R -factors based on F_o^2 are statistically about twice as large as those based on F_o , and R -factors based on ALL data will be even larger.

^eAn idealized geometry was imposed upon the intramolecular hydrogen-bonded interaction (O3–H3O···O4) by constraining the atoms O3, O4, C32 and H3O to lie in the same plane (more precisely, to occupy a tetrahedron of volume no larger than 0.05 \AA^3).

$$fS = [\sum w(F_o^2 - F_c^2)^2 / (n - p)]^{1/2} \quad (n = \text{number of data}; p = \text{number of parameters varied}; w = [\sigma^2(F_o^2) + (0.0340P)^2]^{-1} \text{ where } P = [\text{Max}(F_o^2, 0) + 2F_c^2] / 3).$$

$$gR_1 = \sum ||F_o| - |F_c|| / \sum |F_o|; wR_2 = [\sum w(F_o^2 - F_c^2)^2 / \sum w(F_o^4)]^{1/2}.$$

Table 2. Atomic Coordinates and Equivalent Isotropic Displacement Parameters*(a) atoms of [(C₂(C₆H₄-2-OMe)₂(C₆H₄-2-OH)(C₆H₄-2-OTiCl₂Cp)]*

Atom	x	y	z	<i>U</i> _{eq} , Å ²
Ti	0.25508(9)	0.10679(3)	0.44906(5)	0.0432(2)*
C11	0.49505(15)	0.07723(4)	0.48223(9)	0.0700(4)*
C12	0.20151(16)	0.12077(5)	0.30675(8)	0.0716(4)*
O1	0.2812(3)	0.17454(9)	0.49484(17)	0.0423(8)*
O2	-0.0581(3)	0.28361(11)	0.59658(18)	0.0482(8)*
O3	-0.0897(3)	0.38585(12)	0.4503(2)	0.0690(10)*
O4	0.2133(3)	0.41444(10)	0.52693(17)	0.0464(8)*
C1	0.1289(4)	0.27722(14)	0.4889(2)	0.0289(10)*
C2	0.1613(5)	0.31834(14)	0.4395(2)	0.0311(10)*
C3	0.1353(7)	0.02093(19)	0.4421(4)	0.0700(18)*
C4	0.2165(6)	0.02797(19)	0.5260(4)	0.0614(15)*
C5	0.1581(5)	0.07367(19)	0.5590(3)	0.0509(13)*
C6	0.0403(5)	0.09456(17)	0.4968(3)	0.0475(13)*
C7	0.0246(6)	0.0623(2)	0.4239(3)	0.0671(16)*
C11	0.2442(4)	0.25793(14)	0.5662(3)	0.0307(10)*
C12	0.3171(5)	0.20741(15)	0.5662(3)	0.0371(11)*
C13	0.4285(5)	0.19032(17)	0.6354(3)	0.0473(13)*
C14	0.4687(5)	0.22388(19)	0.7065(3)	0.0536(14)*
C15	0.3990(5)	0.27343(18)	0.7087(3)	0.0512(13)*
C16	0.2879(5)	0.29058(16)	0.6393(3)	0.0427(12)*
C21	-0.0205(5)	0.24948(14)	0.4675(3)	0.0299(10)*
C22	-0.1129(5)	0.25176(16)	0.5251(3)	0.0355(11)*
C23	-0.2489(5)	0.22485(17)	0.5072(3)	0.0437(12)*
C24	-0.2962(5)	0.19698(16)	0.4306(3)	0.0476(13)*
C25	-0.2094(5)	0.19486(15)	0.3722(3)	0.0425(12)*
C26	-0.0718(5)	0.22107(14)	0.3916(3)	0.0371(11)*
C27	-0.1519(5)	0.29282(18)	0.6528(3)	0.0575(14)*
C31	0.0492(5)	0.34032(15)	0.3623(3)	0.0342(11)*
C32	-0.0675(5)	0.37272(17)	0.3717(3)	0.0447(12)*
C33	-0.1707(6)	0.39273(19)	0.3011(4)	0.0749(18)*
C34	-0.1554(8)	0.3813(2)	0.2198(4)	0.089(2)*
C35	-0.0370(7)	0.3506(2)	0.2098(3)	0.0747(19)*
C36	0.0661(5)	0.32990(18)	0.2804(3)	0.0522(13)*
C41	0.3123(5)	0.34457(15)	0.4578(2)	0.0323(11)*
C42	0.3350(5)	0.39506(16)	0.5019(2)	0.0333(10)*
C43	0.4717(5)	0.42039(17)	0.5190(3)	0.0473(13)*
C44	0.5851(5)	0.39706(18)	0.4899(3)	0.0516(13)*
C45	0.5657(5)	0.34817(18)	0.4458(3)	0.0516(13)*

Table 2. Atomic Coordinates and Displacement Parameters (continued)

Atom	x	y	z	$U_{eq}, \text{\AA}^2$
C46	0.4285(5)	0.32162(16)	0.4308(3)	0.0418(12)*
C47	0.2267(6)	0.46544(18)	0.5711(3)	0.0858(19)*

(b) solvent toluene atoms

Atom	x	y	z	$U_{eq}, \text{\AA}^2$
C10S	-0.1095(7)	0.0161(3)	0.1686(3)	0.106(2)*
C11S	-0.2408(7)	0.0106(2)	0.2044(3)	0.0628(15)*
C12S	-0.3072(8)	-0.0404(2)	0.2078(3)	0.0717(18)*
C13S	-0.4306(8)	-0.0444(3)	0.2428(4)	0.087(2)*
C14S	-0.4886(7)	0.0012(3)	0.2730(4)	0.091(2)*
C15S	-0.4230(7)	0.0514(2)	0.2680(4)	0.0775(18)*
C16S	-0.3039(7)	0.0563(2)	0.2333(3)	0.0646(16)*

Anisotropically-refined atoms are marked with an asterisk (*). The form of the anisotropic displacement parameter is: $\exp[-2\pi^2(h^2a^*{}^2U_{11} + k^2b^*{}^2U_{22} + l^2c^*{}^2U_{33} + 2klb^*c^*U_{23} + 2hla^*c^*U_{13} + 2hka^*b^*U_{12})]$.

Table 3. Selected Interatomic Distances (Å)*(a) within [(C₂(C₆H₄-2-OMe)₂(C₆H₄-2-OH)(C₆H₄-2-OTiCl₂Cp)]*

Atom1	Atom2	Distance	Atom1	Atom2	Distance
Ti	C11	2.2670(16)	C11	C12	1.394(5)
Ti	C12	2.2490(15)	C11	C16	1.392(5)
Ti	O1	1.787(3)	C12	C13	1.382(5)
Ti	C3	2.341(4)	C13	C14	1.378(5)
Ti	C4	2.347(4)	C14	C15	1.364(5)
Ti	C5	2.317(4)	C15	C16	1.384(5)
Ti	C6	2.319(4)	C21	C22	1.409(5)
Ti	C7	2.332(5)	C21	C26	1.381(5)
O1	C12	1.369(4)	C22	C23	1.382(5)
O2	C22	1.374(4)	C23	C24	1.380(5)
O2	C27	1.417(5)	C24	C25	1.381(6)
O3	C32	1.369(5)	C25	C26	1.387(5)
O4	C42	1.368(4)	C31	C32	1.371(5)
O4	C47	1.413(4)	C31	C36	1.391(5)
O4	H3O	2.05 [†]	C32	C33	1.380(6)
C1	C2	1.353(5)	C33	C34	1.382(7)
C1	C11	1.500(5)	C34	C35	1.364(7)
C1	C21	1.497(5)	C35	C36	1.385(6)
C2	C31	1.506(5)	C41	C42	1.401(5)
C2	C41	1.495(5)	C41	C46	1.372(5)
C3	C4	1.385(6)	C42	C43	1.370(5)
C3	C7	1.410(6)	C43	C44	1.372(6)
C4	C5	1.391(6)	C44	C45	1.367(5)
C5	C6	1.382(5)	C45	C46	1.389(5)
C6	C7	1.386(6)			

†Nonbonded distance.

(b) within the solvent toluene molecule

Atom1	Atom2	Distance	Atom1	Atom2	Distance
C10S	C11S	1.474(7)	C13S	C14S	1.366(7)
C11S	C12S	1.384(7)	C14S	C15S	1.368(7)
C11S	C16S	1.381(6)	C15S	C16S	1.358(7)
C12S	C13S	1.395(7)			

Table 4. Selected Interatomic Angles (deg)*(a) within [(C₂(C₆H₄-2-OMe)₂(C₆H₄-2-OH)(C₆H₄-2-OTiCl₂Cp)]*

Atom1	Atom2	Atom3	Angle	Atom1	Atom2	Atom3	Angle
C11	Ti	C12	104.15(6)	Ti	C3	C7	72.1(3)
C11	Ti	O1	99.57(10)	C4	C3	C7	107.9(5)
C11	Ti	C3	99.01(17)	Ti	C4	C3	72.6(3)
C11	Ti	C4	83.54(13)	Ti	C4	C5	71.5(2)
C11	Ti	C5	104.60(13)	C3	C4	C5	107.6(5)
C11	Ti	C6	138.66(12)	Ti	C5	C4	73.8(3)
C11	Ti	C7	134.13(16)	Ti	C5	C6	72.7(3)
C12	Ti	O1	104.88(9)	C4	C5	C6	108.8(4)
C12	Ti	C3	95.83(17)	Ti	C6	C5	72.6(3)
C12	Ti	C4	129.52(16)	Ti	C6	C7	73.2(3)
C12	Ti	C5	143.33(13)	C5	C6	C7	108.0(4)
C12	Ti	C6	111.45(13)	Ti	C7	C3	72.8(3)
C12	Ti	C7	85.98(13)	Ti	C7	C6	72.2(3)
O1	Ti	C3	147.71(16)	C3	C7	C6	107.6(5)
O1	Ti	C4	123.21(18)	C1	C11	C12	121.2(4)
O1	Ti	C5	92.23(15)	C1	C11	C16	121.7(3)
O1	Ti	C6	91.12(15)	C12	C11	C16	117.1(4)
O1	Ti	C7	121.21(18)	O1	C12	C11	119.3(4)
C3	Ti	C4	34.37(16)	O1	C12	C13	118.9(4)
C3	Ti	C5	57.50(17)	C11	C12	C13	121.8(4)
C3	Ti	C6	57.92(17)	C12	C13	C14	119.4(4)
C3	Ti	C7	35.12(16)	C13	C14	C15	120.4(4)
C4	Ti	C5	34.70(14)	C14	C15	C16	120.2(4)
C4	Ti	C6	57.81(16)	C11	C16	C15	121.2(4)
C4	Ti	C7	57.75(18)	C1	C21	C22	120.4(4)
C5	Ti	C6	34.68(14)	C1	C21	C26	121.5(4)
C5	Ti	C7	57.59(17)	C22	C21	C26	118.1(4)
C6	Ti	C7	34.67(15)	O2	C22	C21	114.6(4)
Ti	O1	C12	149.1(2)	O2	C22	C23	124.5(4)
C22	O2	C27	117.8(4)	C21	C22	C23	120.9(4)
C42	O4	C47	118.1(3)	C22	C23	C24	119.2(4)
C2	C1	C11	120.1(4)	C23	C24	C25	121.3(4)
C2	C1	C21	121.3(4)	C24	C25	C26	119.0(4)
C11	C1	C21	118.6(3)	C21	C26	C25	121.5(4)
C1	C2	C31	122.5(4)	C2	C31	C32	120.7(4)
C1	C2	C41	121.8(3)	C2	C31	C36	120.3(4)
C31	C2	C41	115.7(3)				
Ti	C3	C4	73.0(3)				

Table 4. Selected Interatomic Angles (continued)

Atom1	Atom2	Atom3	Angle	Atom1	Atom2	Atom3	Angle
C32	C31	C36	119.0(4)	C2	C41	C46	122.2(4)
O3	C32	C31	122.4(4)	C42	C41	C46	118.8(4)
O3	C32	C33	116.7(5)	O4	C42	C41	114.6(4)
C31	C32	C33	120.8(5)	O4	C42	C43	125.0(4)
C32	C33	C34	120.0(6)	C41	C42	C43	120.4(4)
C33	C34	C35	119.6(6)	C42	C43	C44	119.6(4)
C34	C35	C36	120.6(6)	C43	C44	C45	121.3(5)
C31	C36	C35	119.9(5)	C44	C45	C46	119.1(5)
C2	C41	C42	119.0(4)	C41	C46	C45	120.8(4)

(b) within the solvent toluene molecule

Atom1	Atom2	Atom3	Angle	Atom1	Atom2	Atom3	Angle
C10S	C11S	C12S	120.8(6)	C12S	C13S	C14S	121.4(6)
C10S	C11S	C16S	121.2(6)	C13S	C14S	C15S	118.3(6)
C12S	C11S	C16S	118.0(6)	C14S	C15S	C16S	121.3(6)
C11S	C12S	C13S	119.5(6)	C11S	C16S	C15S	121.5(5)

Table 5. Selected Torsional Angles (deg)

Atom1	Atom2	Atom3	Atom4	Angle	Atom1	Atom2	Atom3	Atom4	Angle
C11	C1	C2	C31	-178.6(4)	C1	C2	C41	C42	-98.7(4)
C11	C1	C2	C41	1.9(6)	C1	C2	C41	C46	83.2(5)
C21	C1	C2	C31	2.4(6)	C31	C2	C41	C42	81.8(5)
C21	C1	C2	C41	-177.1(3)	C31	C2	C41	C46	-96.3(4)
C2	C1	C11	C12	-106.1(4)	C1	C11	C12	O1	-0.9(6)
C2	C1	C11	C16	70.9(5)	C1	C11	C12	C13	176.9(4)
C21	C1	C11	C12	72.9(5)	C1	C11	C16	C15	-177.1(4)
C21	C1	C11	C16	-110.0(4)	C1	C21	C22	O2	3.9(5)
C2	C1	C21	C22	-118.8(4)	C1	C21	C22	C23	-178.0(3)
C2	C1	C21	C26	61.2(5)	C1	C21	C26	C25	179.3(3)
C11	C1	C21	C22	62.1(5)	C2	C31	C32	O3	-1.2(6)
C11	C1	C21	C26	-117.8(4)	C2	C31	C32	C33	-179.8(4)
C1	C2	C31	C32	72.7(5)	C2	C31	C36	C35	-179.6(4)
C1	C2	C31	C36	-110.0(5)	C2	C41	C42	O4	2.4(5)
C41	C2	C31	C32	-107.8(4)	C2	C41	C42	C43	-179.4(4)
C41	C2	C31	C36	69.5(5)	C2	C41	C46	C45	177.3(4)

A-21: Complex 59. [*E*-{C₂(C₆H₄-2-O-)₂(C₆H₄-2-OMe)₂}Ti(AlClEt₂)₂]

– Chapter 4 –

XCL Code: JMS0104

Date: 6 April 2001

Compound: [(C₂(C₆H₄-2-O-)₂(C₆H₄-2-OMe)₂)Ti(AlClEt₂)₂]

Formula: C₃₆H₄₂Al₂Cl₂O₄Ti

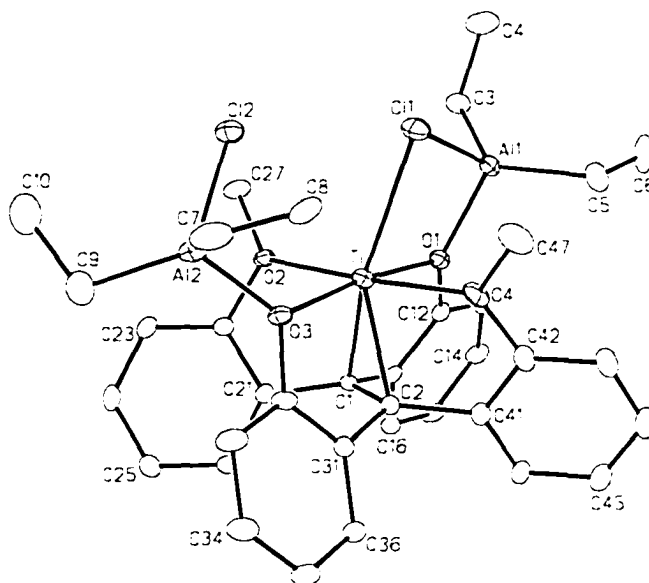


Figure 1. Perspective view of the [(C₂(C₆H₄-2-O-)₂(C₆H₄-2-OMe)₂)Ti(AlClEt₂)₂] molecule showing the atom labelling scheme. Non-hydrogen atoms are represented by Gaussian ellipsoids at the 20% probability level. Hydrogen atoms are not shown.

List of Tables

Table 1. Crystallographic Experimental Details

Table 2. Atomic Coordinates and Equivalent Isotropic Displacement Parameters

Table 3. Selected Interatomic Distances

Table 4. Selected Interatomic Angles

Table 5. Selected Torsional Angles

Table 1. Crystallographic Experimental Details

A. Crystal Data

formula	C ₃₆ H ₄₂ Al ₂ Cl ₂ O ₄ Ti
formula weight	711.46
crystal dimensions (mm)	0.24 × 0.18 × 0.07
crystal system	triclinic
space group	PI (No. 2)
unit cell parameters ^a	
<i>a</i> (Å)	9.3788 (8)
<i>b</i> (Å)	12.5078 (11)
<i>c</i> (Å)	15.9986 (14)
α (deg)	72.9295 (15)
β (deg)	80.9868 (16)
γ (deg)	87.6047 (18)
<i>V</i> (Å ³)	1771.9 (3)
<i>Z</i>	2
ρ _{calcd} (g cm ⁻³)	1.333
μ (mm ⁻¹)	0.479

B. Data Collection and Refinement Conditions

diffractometer	Bruker PLATFORM/SMART 1000 CCD ^b
radiation (λ [Å])	graphite-monochromated Mo Kα (0.71073)
temperature (°C)	-80
scan type	ω scans (0.2°) (20 s exposures)
data collection 2θ limit (deg)	52.84
total data collected	12197 (-9 ≤ <i>h</i> ≤ 11, -15 ≤ <i>k</i> ≤ 15, -20 ≤ <i>l</i> ≤ 20)

independent reflections	7200
number of observed reflections (<i>NO</i>)	4136 [$F_o^2 \geq 2\sigma(F_o^2)$]
structure solution method	direct methods (<i>SHELXS-86</i> ^c)
refinement method	full-matrix least-squares on F^2 (<i>SHELXL-93</i> ^d)
absorption correction method	Gaussian integration (face-indexed)
range of transmission factors	0.9670–0.8854
data/restraints/parameters	7200 [$F_o^2 \geq -3\sigma(F_o^2)$] / 0 / 406
goodness-of-fit (<i>S</i>) ^e	0.979 [$F_o^2 \geq -3\sigma(F_o^2)$]
final <i>R</i> indices ^f	
R_1 [$F_o^2 \geq 2\sigma(F_o^2)$]	0.0637
wR_2 [$F_o^2 \geq -3\sigma(F_o^2)$]	0.1603
largest difference peak and hole	1.205 and –0.631 e Å ⁻³

^aObtained from least-squares refinement of 4282 centered reflections.

^bPrograms for diffractometer operation, data collection, data reduction and absorption correction were those supplied by Bruker.

^cSheldrick, G. M. *Acta Crystallogr.* **1990**, *A46*, 467–473.

^dSheldrick, G. M. *SHELXL-93*. Program for crystal structure determination. University of Göttingen, Germany, 1993. Refinement on F_o^2 for all reflections (all of these having $F_o^2 \geq -3\sigma(F_o^2)$). Weighted *R*-factors wR_2 and all goodnesses of fit *S* are based on F_o^2 ; conventional *R*-factors R_1 are based on F_o , with F_o set to zero for negative F_o^2 . The observed criterion of $F_o^2 > 2\sigma(F_o^2)$ is used only for calculating R_1 , and is not relevant to the choice of reflections for refinement. *R*-factors based on F_o^2 are statistically about twice as large as those based on F_o , and *R*-factors based on ALL data will be even larger.

^e $S = [\sum w(F_o^2 - F_c^2)^2 / (n - p)]^{1/2}$ (n = number of data; p = number of parameters varied; $w = [\sigma^2(F_o^2) + (0.0753P)^2]^{-1}$ where $P = [\text{Max}(F_o^2, 0) + 2F_c^2] / 3$).

^f $R_1 = \sum ||F_o| - |F_c|| / \sum |F_o|$; $wR_2 = [\sum w(F_o^2 - F_c^2)^2 / \sum w(F_o^4)]^{1/2}$.

Table 2. Atomic Coordinates and Equivalent Isotropic Displacement Parameters

Atom	x	y	z	U_{eq} , Å ²
Ti	0.35132(8)	0.25738(6)	0.25291(5)	0.0282(2)*
C11	0.10988(12)	0.33152(10)	0.32265(8)	0.0438(3)*
C12	0.03336(12)	0.21416(9)	0.17734(8)	0.0442(3)*
A11	0.25000(15)	0.45513(11)	0.34917(8)	0.0339(3)*
A12	0.17735(15)	0.07823(11)	0.16208(10)	0.0426(4)*
O1	0.4014(3)	0.3978(2)	0.28666(17)	0.0296(6)*
O2	0.3484(3)	0.3560(2)	0.11631(17)	0.0306(7)*
O3	0.3315(3)	0.1172(2)	0.21150(18)	0.0321(7)*
O4	0.3447(3)	0.1589(2)	0.39418(18)	0.0401(8)*
C1	0.5750(4)	0.2864(3)	0.1942(2)	0.0223(8)*
C2	0.5619(4)	0.1863(3)	0.2678(2)	0.0240(9)*
C3	0.1856(5)	0.6032(4)	0.2861(3)	0.0400(11)*
C4	0.0364(5)	0.6285(5)	0.3287(4)	0.0651(16)*
C5	0.2752(6)	0.4243(4)	0.4728(3)	0.0567(14)*
C6	0.2867(8)	0.5284(5)	0.5013(4)	0.082(2)*
C7	0.0852(5)	-0.0595(4)	0.2415(4)	0.0606(15)*
C8	0.0555(5)	-0.0588(4)	0.3352(3)	0.0436(12)*
C9	0.2343(6)	0.0871(5)	0.0355(3)	0.0632(15)*
C10	0.1183(8)	0.1447(7)	-0.0222(4)	0.110(3)*
C11	0.6287(4)	0.3910(3)	0.2047(2)	0.0242(9)*
C12	0.5367(4)	0.4445(3)	0.2563(2)	0.0282(9)*
C13	0.5787(5)	0.5394(3)	0.2738(3)	0.0351(10)*
C14	0.7154(5)	0.5835(4)	0.2370(3)	0.0386(11)*
C15	0.8083(5)	0.5313(3)	0.1850(3)	0.0372(11)*
C16	0.7659(4)	0.4355(3)	0.1685(3)	0.0301(9)*
C21	0.5828(4)	0.2839(3)	0.1004(2)	0.0246(9)*
C22	0.4655(4)	0.3291(3)	0.0588(3)	0.0277(9)*
C23	0.4621(5)	0.3419(3)	-0.0293(3)	0.0347(10)*
C24	0.5788(5)	0.3034(4)	-0.0757(3)	0.0402(11)*
C25	0.6953(5)	0.2535(3)	-0.0360(3)	0.0368(11)*
C26	0.6974(4)	0.2437(3)	0.0523(3)	0.0304(9)*
C27	0.2455(5)	0.4362(4)	0.0764(3)	0.0408(11)*
C31	0.5646(4)	0.0755(3)	0.2518(2)	0.0256(9)*
C32	0.4484(4)	0.0444(3)	0.2196(3)	0.0315(10)*
C33	0.4512(5)	-0.0548(4)	0.1971(4)	0.0490(13)*
C34	0.5683(5)	-0.1247(4)	0.2109(4)	0.0502(13)*
C35	0.6815(5)	-0.0981(4)	0.2465(3)	0.0402(11)*
C36	0.6809(4)	0.0027(3)	0.2651(3)	0.0293(9)*
C41	0.5933(5)	0.1861(3)	0.3566(3)	0.0307(10)*

Table 2. Atomic Coordinates and Displacement Parameters (continued)

Atom	<i>x</i>	<i>y</i>	<i>z</i>	<i>U</i> _{eq} , Å ²
C42	0.4765(5)	0.1647(3)	0.4243(3)	0.0367(11)*
C43	0.4902(6)	0.1543(4)	0.5108(3)	0.0506(13)*
C44	0.6244(7)	0.1709(4)	0.5291(3)	0.0582(15)*
C45	0.7440(6)	0.1962(4)	0.4628(3)	0.0488(13)*
C46	0.7276(5)	0.2031(3)	0.3768(3)	0.0358(10)*
C47	0.2227(6)	0.1144(4)	0.4620(3)	0.0578(15)*

Anisotropically-refined atoms are marked with an asterisk (*). The form of the anisotropic displacement parameter is: $\exp[-2\pi^2(h^2a^{*2}U_{11} + k^2b^{*2}U_{22} + l^2c^{*2}U_{33} + 2klb^*c^*U_{23} + 2hla^*c^*U_{13} + 2hka^*b^*U_{12})]$.

Table 3. Selected Interatomic Distances (Å)

Atom1	Atom2	Distance	Atom1	Atom2	Distance
Ti	C11	2.6216(13)	C1	C11	1.484(5)
Ti	C12	3.5064(14)†	C1	C21	1.501(5)
Ti	O1	2.074(3)	C2	C31	1.480(5)
Ti	O2	2.175(3)	C2	C41	1.494(5)
Ti	O3	2.073(3)	C3	C4	1.520(6)
Ti	O4	2.227(3)	C5	C6	1.513(7)
Ti	C1	2.159(4)	C7	C8	1.484(7)
Ti	C2	2.150(4)	C9	C10	1.554(8)
C11	A11	2.2420(17)	C11	C12	1.388(5)
C12	A12	2.1732(17)	C11	C16	1.392(5)
A11	O1	1.850(3)	C12	C13	1.383(5)
A11	C3	1.953(4)	C13	C14	1.388(6)
A11	C5	1.951(5)	C14	C15	1.387(6)
A12	O3	1.896(3)	C15	C16	1.385(6)
A12	C7	1.955(5)	C21	C22	1.389(5)
A12	C9	1.983(5)	C21	C26	1.386(5)
O1	C12	1.375(5)	C22	C23	1.377(5)
O2	C22	1.414(5)	C23	C24	1.376(6)
O2	C27	1.443(5)	C24	C25	1.384(6)
O3	C32	1.392(5)	C25	C26	1.385(5)
O4	C42	1.407(5)	C31	C32	1.391(5)
O4	C47	1.451(5)	C31	C36	1.393(5)
C1	C2	1.439(5)			

†Nonbonded distance.

Table 3. Selected Interatomic Distances (continued)

Atom1	Atom2	Distance	Atom1	Atom2	Distance
C32	C33	1.389(6)	C41	C46	1.388(6)
C33	C34	1.378(6)	C42	C43	1.379(6)
C34	C35	1.376(6)	C43	C44	1.372(7)
C35	C36	1.377(6)	C44	C45	1.394(7)
C41	C42	1.388(6)	C45	C46	1.386(6)

Table 4. Selected Interatomic Angles (deg)

Atom1	Atom2	Atom3	Angle	Atom1	Atom2	Atom3	Angle
C11	Ti	O1	72.54(8)	C3	Al1	C5	119.2(2)
C11	Ti	O2	97.77(8)	C12	Al2	O3	97.50(10)
C11	Ti	O3	115.48(8)	C12	Al2	C7	106.50(18)
C11	Ti	O4	79.80(8)	C12	Al2	C9	111.06(19)
C11	Ti	C1	148.99(10)	O3	Al2	C7	109.6(2)
C11	Ti	C2	149.06(10)	O3	Al2	C9	112.1(2)
O1	Ti	O2	91.27(10)	C7	Al2	C9	118.0(3)
O1	Ti	O3	171.96(11)	Ti	O1	Al1	115.06(14)
O1	Ti	O4	88.38(11)	Ti	O1	C12	118.9(2)
O1	Ti	C1	77.62(12)	Al1	O1	C12	125.8(2)
O1	Ti	C2	92.69(12)	Ti	O2	C22	111.6(2)
O2	Ti	O3	87.02(10)	Ti	O2	C27	131.2(3)
O2	Ti	O4	177.54(11)	C22	O2	C27	117.1(3)
O2	Ti	C1	74.39(12)	Ti	O3	Al2	128.22(14)
O2	Ti	C2	109.87(12)	Ti	O3	C32	115.1(2)
O3	Ti	O4	93.66(11)	Al2	O3	C32	116.6(2)
O3	Ti	C1	94.35(12)	Ti	O4	C42	111.8(2)
O3	Ti	C2	80.53(12)	Ti	O4	C47	130.3(3)
O4	Ti	C1	107.89(13)	C42	O4	C47	116.1(3)
O4	Ti	C2	72.58(12)	Ti	C1	C2	70.2(2)
C1	Ti	C2	39.02(13)	Ti	C1	C11	110.8(2)
Ti	C11	Al1	85.48(5)	Ti	C1	C21	106.0(2)
C11	Al1	O1	86.28(10)	C2	C1	C11	119.6(3)
C11	Al1	C3	106.31(15)	C2	C1	C21	122.4(3)
C11	Al1	C5	114.60(18)	C11	C1	C21	115.1(3)
O1	Al1	C3	114.73(17)	Ti	C2	C1	70.8(2)
O1	Al1	C5	111.04(19)	Ti	C2	C31	108.3(3)

Table 4. Selected Interatomic Angles (continued)

Atom1	Atom2	Atom3	Angle	Atom1	Atom2	Atom3	Angle
Ti	C2	C41	108.0(3)	C22	C23	C24	117.3(4)
C1	C2	C31	119.9(3)	C23	C24	C25	121.8(4)
C1	C2	C41	121.7(3)	C24	C25	C26	119.8(4)
C31	C2	C41	115.5(3)	C21	C26	C25	119.8(4)
Al1	C3	C4	110.9(3)	C2	C31	C32	118.6(4)
Al1	C5	C6	113.8(4)	C2	C31	C36	122.6(4)
Al2	C7	C8	113.1(3)	C32	C31	C36	118.7(4)
Al2	C9	C10	112.7(4)	O3	C32	C31	116.8(3)
C1	C11	C12	117.1(3)	O3	C32	C33	122.6(4)
C1	C11	C16	124.0(4)	C31	C32	C33	120.6(4)
C12	C11	C16	118.9(4)	C32	C33	C34	119.0(4)
O1	C12	C11	115.2(3)	C33	C34	C35	121.4(4)
O1	C12	C13	122.9(4)	C34	C35	C36	119.3(4)
C11	C12	C13	121.8(4)	C31	C36	C35	120.9(4)
C12	C13	C14	118.8(4)	C2	C41	C42	115.9(4)
C13	C14	C15	120.0(4)	C2	C41	C46	125.9(4)
C14	C15	C16	120.7(4)	C42	C41	C46	118.2(4)
C11	C16	C15	119.7(4)	O4	C42	C41	112.8(4)
C1	C21	C22	115.9(3)	O4	C42	C43	124.5(4)
C1	C21	C26	125.7(3)	C41	C42	C43	122.6(5)
C22	C21	C26	118.4(4)	C42	C43	C44	117.9(5)
O2	C22	C21	113.7(3)	C43	C44	C45	121.5(5)
O2	C22	C23	123.5(4)	C44	C45	C46	119.3(5)
C21	C22	C23	122.8(4)	C41	C46	C45	120.4(5)

Table 5. Selected Torsional Angles (deg)

Atom1	Atom2	Atom3	Atom4	Angle	Atom1	Atom2	Atom3	Atom4	Angle
O1	Ti	C11	Al1	-5.08(9)	C2	C1	C11	C16	106.1(4)
O2	Ti	C11	Al1	-93.96(9)	C21	C1	C11	C12	126.9(4)
O3	Ti	C11	Al1	175.65(9)	C21	C1	C11	C16	-55.3(5)
O4	Ti	C11	Al1	86.44(9)	C2	C1	C21	C22	112.6(4)
C11	Ti	O1	Al1	6.78(11)	C2	C1	C21	C26	-69.2(5)
C11	Ti	O1	C12	-168.5(3)	C11	C1	C21	C22	-86.6(4)
O3	Ti	O1	Al1	-177.9(7)	C11	C1	C21	C26	91.6(5)
O3	Ti	O1	C12	6.8(9)	C1	C2	C31	C32	-69.2(5)
C11	Ti	O3	Al2	34.5(2)	C1	C2	C31	C36	108.8(4)
C11	Ti	O3	C32	-147.1(2)	C41	C2	C31	C32	129.9(4)
O1	Ti	O3	Al2	-140.5(7)	C41	C2	C31	C36	-52.1(5)
O1	Ti	O3	C32	37.9(9)	C1	C2	C41	C42	114.4(4)
O2	Ti	O3	Al2	-62.69(19)	C1	C2	C41	C46	-66.9(5)
O2	Ti	O3	C32	115.7(3)	C1	C11	C12	O1	-4.5(5)
C11	Al1	O1	Ti	-7.58(13)	C1	C11	C12	C13	176.8(3)
C12	Al2	O3	Ti	-5.3(2)	C1	C11	C16	C15	-177.3(4)
C27	O2	C22	C21	159.1(3)	C1	C21	C22	O2	-8.4(5)
C27	O2	C22	C23	-23.5(5)	C1	C21	C22	C23	174.2(4)
C47	O4	C42	C41	167.7(3)	C1	C21	C26	C25	-175.4(4)
C47	O4	C42	C43	-14.4(6)	C2	C31	C32	O3	-5.1(5)
C11	C1	C2	C31	-156.2(4)	C2	C31	C32	C33	175.0(4)
C11	C1	C2	C41	3.4(5)	C2	C31	C36	C35	-177.7(4)
C21	C1	C2	C31	3.7(6)	C2	C41	C42	O4	-6.5(5)
C21	C1	C2	C41	163.4(4)	C2	C41	C42	C43	175.5(4)
C2	C1	C11	C12	-71.8(5)	C2	C41	C46	C45	-177.2(4)

A-22: Complex 59. $[[Z-C_2(C_6H_4-2-O)_2(C_6H_4-2-OMe)_2](CpTiCl_2)_2]$

– Chapter 4 –

XCL Code: JMS0006

Date: 18 May 2001

Compound: $[[C_2(C_6H_4-2-OMe)_2(C_6H_4-2-OTiCl_2Cp)_2] \cdot 1.5PhMe$

Formula: $C_{48.5}H_{44}Cl_4O_4Ti_2 (C_{38.5}H_{32}Cl_4O_4Ti_2 \cdot 1.5C_7H_8)$

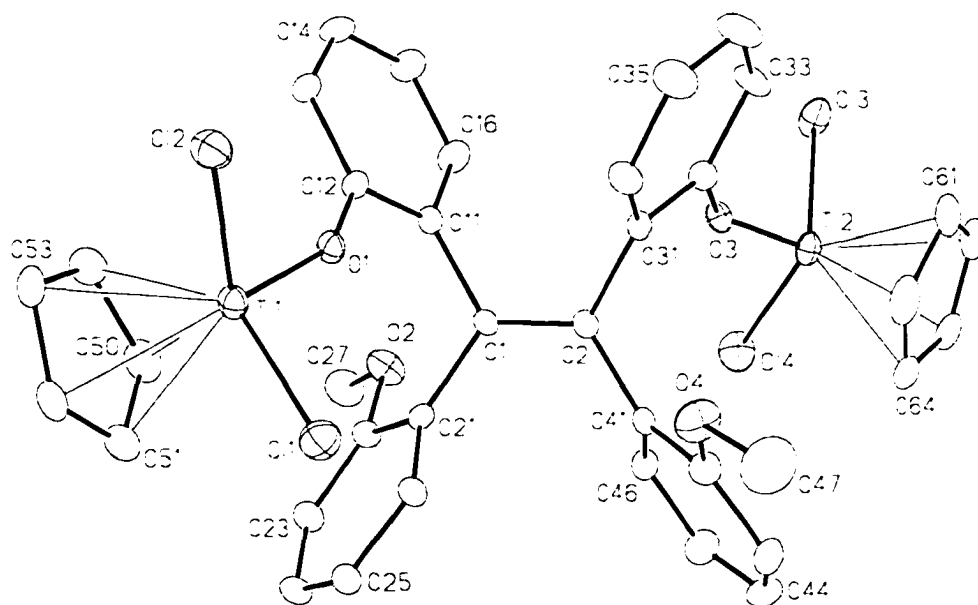


Figure 1. Perspective view of the $[[C_2(C_6H_4-2-OMe)_2(C_6H_4-2-OTiCl_2Cp)_2]$ molecule showing the atom labelling scheme. Non-hydrogen atoms are represented by Gaussian ellipsoids at the 20% probability level. Hydrogen atoms are not shown.

List of Tables

Table 1. Crystallographic Experimental Details

Table 2. Atomic Coordinates and Equivalent Isotropic Displacement Parameters

Table 3. Selected Interatomic Distances

Table 4. Selected Interatomic Angles

Table 5. Selected Torsional Angles

Table 1. Crystallographic Experimental Details

A. Crystal Data

formula	C _{48.5} H ₄₄ Cl ₄ O ₄ Ti ₂
formula weight	928.44
crystal dimensions (mm)	0.16 × 0.14 × 0.13
crystal system	triclinic
space group	PI (No. 2)
unit cell parameters ^a	
<i>a</i> (Å)	9.6893 (8)
<i>b</i> (Å)	14.8937 (14)
<i>c</i> (Å)	17.1040 (15)
α (deg)	108.9234 (16)
β (deg)	98.200 (2)
γ (deg)	96.8737 (18)
<i>V</i> (Å ³)	2274.4 (3)
<i>Z</i>	2
ρ _{calcd} (g cm ⁻³)	1.356
μ (mm ⁻¹)	0.628

B. Data Collection and Refinement Conditions

diffractometer	Bruker P4/RA/SMART 1000 CCD ^b
radiation (λ [Å])	graphite-monochromated Mo Kα (0.71073)
temperature (°C)	-80
scan type	φ rotations (0.3°) / ω scans (0.3°) (30 s exposures)
data collection 2θ limit (deg)	52.80
total data collected	11467 (-5 ≤ <i>h</i> ≤ 12, -18 ≤ <i>k</i> ≤ 18, -21 ≤ <i>l</i> ≤ 17)

independent reflections	9254
number of observed reflections (<i>NO</i>)	3318 [$F_o^2 \geq 2\sigma(F_o^2)$]
structure solution method	direct methods/fragment search (<i>DIRDIF-96</i> ^c)
refinement method	full-matrix least-squares on F^2 (<i>SHELXL-93</i> ^d)
absorption correction method	Gaussian integration (face-indexed)
range of transmission factors	0.9383–0.8968
data/restraints/parameters	9254 [$F_o^2 \geq -3\sigma(F_o^2)$] / 0 / 517
goodness-of-fit (<i>S</i>) ^e	0.805 [$F_o^2 \geq -3\sigma(F_o^2)$]
final <i>R</i> indices ^f	
R_1 [$F_o^2 \geq 2\sigma(F_o^2)$]	0.0599
wR_2 [$F_o^2 \geq -3\sigma(F_o^2)$]	0.1382
largest difference peak and hole	0.680 and –0.296 e Å ⁻³

^aObtained from least-squares refinement of 3067 centered reflections.

^bPrograms for diffractometer operation, data collection, data reduction and absorption correction were those supplied by Bruker.

^cBeurskens, P. T.; Beurskens, G.; Bosman, W. P.; de Gelder, R.; Garcia Granda, S.; Gould, R. O.; Israel, R.; Smits, J. M. M. (1996). The *DIRDIF-96* program system. Crystallography Laboratory, University of Nijmegen, The Netherlands.

^dSheldrick, G. M. *SHELXL-93*. Program for crystal structure determination. University of Göttingen, Germany, 1993. Refinement on F_o^2 for all reflections (all of these having $F_o^2 \geq -3\sigma(F_o^2)$). Weighted *R*-factors wR_2 and all goodnesses of fit *S* are based on F_o^2 ; conventional *R*-factors R_1 are based on F_o , with F_o set to zero for negative F_o^2 . The observed criterion of $F_o^2 > 2\sigma(F_o^2)$ is used only for calculating R_1 , and is not relevant to the choice of reflections for refinement. *R*-factors based on F_o^2 are statistically about twice as large as those based on F_o , and *R*-factors based on ALL data will be even larger.

^e $S = [\sum w(F_o^2 - F_c^2)^2 / (n - p)]^{1/2}$ (n = number of data; p = number of parameters varied; $w = [\sigma^2(F_o^2) + (0.0369P)^2]^{-1}$ where $P = [\text{Max}(F_o^2, 0) + 2F_c^2]/3$).

^f $R_1 = \sum ||F_o| - |F_c|| / \sum |F_o|$; $wR_2 = [\sum w(F_o^2 - F_c^2)^2 / \sum w(F_o^4)]^{1/2}$.

Table 2. Atomic Coordinates and Equivalent Isotropic Displacement Parameters*(a) atoms of [(C₂(C₆H₄-2-OMe)₂(C₆H₄-2-OTiCl₂Cp)₂]*

Atom	x	y	z	<i>U</i> _{eq} , Å ²
Ti1	0.15565(10)	0.59610(7)	-0.24897(6)	0.0357(3)*
Ti2	0.23827(10)	0.01411(7)	-0.14833(6)	0.0391(3)*
Cl1	-0.04674(14)	0.59434(12)	-0.19828(10)	0.0555(5)*
Cl2	0.29835(15)	0.72443(11)	-0.14845(10)	0.0528(4)*
Cl3	0.45618(16)	-0.02414(12)	-0.13374(11)	0.0645(5)*
Cl4	0.13497(18)	-0.07750(11)	-0.28184(10)	0.0650(5)*
O1	0.2331(3)	0.5000(2)	-0.2322(2)	0.0343(9)*
O2	0.1583(4)	0.1902(3)	-0.4261(2)	0.0520(11)*
O3	0.2774(3)	0.1340(2)	-0.1485(2)	0.0342(9)*
O4	-0.0614(4)	0.3293(3)	-0.0901(3)	0.0622(13)*
C1	0.1512(5)	0.2983(3)	-0.2605(3)	0.0240(12)*
C2	0.1237(5)	0.2683(3)	-0.1974(3)	0.0283(13)*
C11	0.2998(5)	0.3454(4)	-0.2572(3)	0.0283(13)*
C12	0.3356(5)	0.4423(4)	-0.2445(3)	0.0313(13)*
C13	0.4739(5)	0.4853(4)	-0.2402(3)	0.0377(15)*
C14	0.5780(5)	0.4292(4)	-0.2450(4)	0.0456(16)*
C15	0.5463(6)	0.3330(4)	-0.2574(4)	0.0486(17)*
C16	0.4078(5)	0.2915(4)	-0.2631(3)	0.0417(15)*
C21	0.0414(5)	0.2915(4)	-0.3330(3)	0.0297(13)*
C22	0.0486(5)	0.2420(4)	-0.4165(4)	0.0351(14)*
C23	-0.0506(6)	0.2414(4)	-0.4822(4)	0.0440(15)*
C24	-0.1623(6)	0.2917(4)	-0.4667(4)	0.0499(17)*
C25	-0.1713(5)	0.3394(4)	-0.3845(4)	0.0425(16)*
C26	-0.0721(5)	0.3393(4)	-0.3184(3)	0.0368(14)*
C27	0.1613(6)	0.1302(5)	-0.5098(4)	0.067(2)*
C31	0.2325(5)	0.2959(4)	-0.1190(3)	0.0299(13)*
C32	0.3068(5)	0.2295(4)	-0.0985(3)	0.0341(14)*
C33	0.4132(6)	0.2584(5)	-0.0265(4)	0.0478(16)*
C34	0.4436(6)	0.3540(5)	0.0259(4)	0.0583(18)*
C35	0.3683(6)	0.4200(4)	0.0072(4)	0.0541(17)*
C36	0.2653(6)	0.3900(4)	-0.0655(4)	0.0403(15)*
C41	-0.0151(5)	0.2064(4)	-0.2046(3)	0.0309(13)*
C42	-0.1052(6)	0.2385(5)	-0.1469(4)	0.0464(16)*
C43	-0.2292(6)	0.1757(5)	-0.1522(4)	0.0591(19)*
C44	-0.2638(6)	0.0872(5)	-0.2137(5)	0.065(2)*
C45	-0.1783(6)	0.0571(5)	-0.2719(4)	0.0593(19)*
C46	-0.0551(6)	0.1173(4)	-0.2666(4)	0.0420(15)*
C47	-0.1453(7)	0.3626(6)	-0.0290(4)	0.101(3)*

Table 2. Atomic Coordinates and Displacement Parameters (continued)

Atom	x	y	z	$U_{eq}, \text{\AA}^2$
C50	0.1397(7)	0.5171(5)	-0.3925(3)	0.0529(17)*
C51	0.0213(6)	0.5607(5)	-0.3831(4)	0.0495(16)*
C52	0.0634(6)	0.6602(5)	-0.3504(4)	0.0487(17)*
C53	0.2106(6)	0.6810(5)	-0.3383(4)	0.0499(17)*
C54	0.2581(6)	0.5925(5)	-0.3637(4)	0.0511(17)*
C60	0.1072(9)	0.0787(5)	-0.0476(5)	0.068(2)*
C61	0.2223(7)	0.0530(6)	-0.0071(4)	0.062(2)*
C62	0.2103(7)	-0.0463(5)	-0.0397(4)	0.0540(18)*
C63	0.0906(7)	-0.0841(5)	-0.1003(5)	0.059(2)*
C64	0.0241(7)	-0.0057(7)	-0.1053(5)	0.071(2)*

(b) solvent toluene atoms

Atom	x	y	z	$U_{eq}, \text{\AA}^2$
C10S	0.3315(8)	0.2273(6)	0.2278(6)	0.125(4)*
C11S	0.3633(7)	0.2673(7)	0.3171(6)	0.088(3)*
C12S	0.3334(6)	0.3565(6)	0.3579(5)	0.065(2)*
C13S	0.3658(8)	0.3951(7)	0.4424(6)	0.097(3)*
C14S	0.4235(9)	0.3465(9)	0.4909(8)	0.128(4)*
C15S	0.4573(10)	0.2590(11)	0.4529(10)	0.148(6)*
C16S	0.4279(9)	0.2187(7)	0.3680(8)	0.098(4)*
C20S	0.3940(13)	0.0070(10)	0.6026(9)	0.189(5)
C21S ^a	0.4643(15)	0.0096(11)	0.5516(9)	0.060(4)
C22S	0.4013(8)	-0.0685(6)	0.4612(6)	0.099(3)
C23S ^a	0.4598(15)	-0.0714(11)	0.4042(9)	0.066(4)
C24S ^a	0.6481(17)	0.0529(13)	0.4697(13)	0.097(5)

Anisotropically-refined atoms are marked with an asterisk (*). The form of the anisotropic displacement parameter is: $\exp[-2\pi^2(h^2a^*{}^2U_{11} + k^2b^*{}^2U_{22} + l^2c^*{}^2U_{33} + 2klb^*c^*U_{23} + 2hla^*c^*U_{13} + 2hka^*b^*U_{12})]$. ^aRefined with an occupancy factor of 0.5.

Table 3. Selected Interatomic Distances (Å)*(a) within $[(C_2(C_6H_4-2-OMe)_2(C_6H_4-2-OTiCl_2Cp)_2]$*

Atom1	Atom2	Distance	Atom1	Atom2	Distance
Ti1	C11	2.2551(15)	C14	C15	1.368(7)
Ti1	C12	2.2536(18)	C15	C16	1.385(6)
Ti1	O1	1.776(3)	C21	C22	1.396(6)
Ti1	C50	2.327(6)	C21	C26	1.389(6)
Ti1	C51	2.331(6)	C22	C23	1.368(7)
Ti1	C52	2.358(6)	C23	C24	1.396(7)
Ti1	C53	2.354(5)	C24	C25	1.374(7)
Ti1	C54	2.311(5)	C25	C26	1.376(7)
Ti2	C13	2.2526(17)	C31	C32	1.394(7)
Ti2	C14	2.253(2)	C31	C36	1.372(7)
Ti2	O3	1.782(3)	C32	C33	1.397(7)
Ti2	C60	2.313(6)	C33	C34	1.383(7)
Ti2	C61	2.327(6)	C34	C35	1.382(7)
Ti2	C62	2.347(6)	C35	C36	1.385(7)
Ti2	C63	2.340(6)	C41	C42	1.416(7)
Ti2	C64	2.316(5)	C41	C46	1.372(7)
O1	C12	1.384(5)	C42	C43	1.404(7)
O2	C22	1.384(6)	C43	C44	1.360(8)
O2	C27	1.427(6)	C44	C45	1.382(8)
O3	C32	1.370(6)	C45	C46	1.378(7)
O4	C42	1.358(6)	C50	C51	1.389(7)
O4	C47	1.416(6)	C50	C54	1.412(7)
C1	C2	1.342(6)	C51	C52	1.388(7)
C1	C11	1.509(6)	C52	C53	1.393(7)
C1	C21	1.481(7)	C53	C54	1.404(7)
C2	C31	1.488(7)	C60	C61	1.387(8)
C2	C41	1.502(6)	C60	C64	1.389(9)
C11	C12	1.379(6)	C61	C62	1.385(8)
C11	C16	1.389(6)	C62	C63	1.363(8)
C12	C13	1.395(6)	C63	C64	1.419(8)
C13	C14	1.380(7)			

(b) within the solvent toluene molecules

Atom1	Atom2	Distance	Atom1	Atom2	Distance
C10S	C11S	1.419(10)	C13S	C14S	1.370(12)
C11S	C12S	1.373(9)	C14S	C15S	1.357(15)
C11S	C16S	1.425(11)	C15S	C16S	1.351(13)
C12S	C13S	1.345(9)	C20S	C21S	1.189(15)

Table 3. Selected Interatomic Distances (continued)

Atom1	Atom2	Distance	Atom1	Atom2	Distance
C20S'	C23S	1.654(17)	C21S	C22S'	1.564(15)
C20S'	C24S	1.243(19)	C22S	C23S	1.187(12)
C21S	C22S	1.585(16)	C22S'	C24S	1.301(17)

Primed atoms are related to unprimed ones via the crystallographic inversion center ($1/2, 0, 1/2$).

Table 4. Selected Interatomic Angles (deg)

(a) within $[(C_2(C_6H_4-2-OMe)_2(C_6H_4-2-OTiCl_2Cp)_2)]$

Atom1	Atom2	Atom3	Angle	Atom1	Atom2	Atom3	Angle
Cl1	Ti1	Cl2	101.70(7)	C52	Ti1	C54	57.6(2)
Cl1	Ti1	O1	106.35(11)	C53	Ti1	C54	35.02(18)
Cl1	Ti1	C50	117.58(17)	Cl3	Ti2	Cl4	103.88(7)
Cl1	Ti1	C51	88.94(15)	Cl3	Ti2	O3	101.52(11)
Cl1	Ti1	C52	92.30(15)	Cl3	Ti2	C60	130.2(2)
Cl1	Ti1	C53	123.95(16)	Cl3	Ti2	C61	95.8(2)
Cl1	Ti1	C54	146.20(17)	Cl3	Ti2	C62	84.80(17)
Cl2	Ti1	O1	100.96(12)	Cl3	Ti2	C63	108.10(19)
Cl2	Ti1	C50	135.74(17)	Cl3	Ti2	C64	141.51(19)
Cl2	Ti1	C51	137.58(17)	Cl4	Ti2	O3	105.75(12)
Cl2	Ti1	C52	103.54(17)	Cl4	Ti2	C60	122.0(2)
Cl2	Ti1	C53	83.42(16)	Cl4	Ti2	C61	145.38(18)
Cl2	Ti1	C54	100.31(17)	Cl4	Ti2	C62	119.0(2)
O1	Ti1	C50	87.45(19)	Cl4	Ti2	C63	89.2(2)
O1	Ti1	C51	115.3(2)	Cl4	Ti2	C64	90.4(2)
O1	Ti1	C52	145.34(19)	O3	Ti2	C60	84.9(2)
O1	Ti1	C53	127.67(18)	O3	Ti2	C61	97.7(2)
O1	Ti1	C54	94.20(19)	O3	Ti2	C62	131.9(2)
C50	Ti1	C51	34.69(18)	O3	Ti2	C63	142.45(19)
C50	Ti1	C52	57.9(2)	O3	Ti2	C64	108.7(2)
C50	Ti1	C53	58.6(2)	C60	Ti2	C61	34.8(2)
C50	Ti1	C54	35.45(18)	C60	Ti2	C62	57.7(2)
C51	Ti1	C52	34.42(18)	C60	Ti2	C63	58.4(2)
C51	Ti1	C53	57.5(2)	C60	Ti2	C64	34.9(2)
C51	Ti1	C54	57.7(2)	C61	Ti2	C62	34.5(2)
C52	Ti1	C53	34.40(17)	C61	Ti2	C63	57.4(2)

Table 4. Selected Interatomic Angles (continued)

Atom1	Atom2	Atom3	Angle	Atom1	Atom2	Atom3	Angle
C61	Ti2	C64	57.6(2)	C31	C32	C33	120.9(5)
C62	Ti2	C63	33.81(19)	C32	C33	C34	119.5(6)
C62	Ti2	C64	57.3(2)	C33	C34	C35	120.0(6)
C63	Ti2	C64	35.5(2)	C34	C35	C36	119.4(6)
Ti1	O1	C12	149.9(3)	C31	C36	C35	122.2(6)
C22	O2	C27	116.6(4)	C2	C41	C42	120.5(5)
Ti2	O3	C32	144.1(3)	C2	C41	C46	120.3(4)
C42	O4	C47	117.3(5)	C42	C41	C46	119.2(5)
C2	C1	C11	119.4(5)	O4	C42	C41	115.6(5)
C2	C1	C21	123.5(4)	O4	C42	C43	125.8(5)
C11	C1	C21	117.1(4)	C41	C42	C43	118.7(6)
C1	C2	C31	119.7(5)	C42	C43	C44	120.2(6)
C1	C2	C41	121.2(5)	C43	C44	C45	121.1(6)
C31	C2	C41	119.1(4)	C44	C45	C46	119.3(6)
C1	C11	C12	122.7(4)	C41	C46	C45	121.4(5)
C1	C11	C16	119.7(4)	Ti1	C50	C51	72.8(3)
C12	C11	C16	117.6(5)	Ti1	C50	C54	71.7(3)
O1	C12	C11	119.4(4)	C51	C50	C54	106.3(6)
O1	C12	C13	118.4(5)	Ti1	C51	C50	72.5(3)
C11	C12	C13	122.1(5)	Ti1	C51	C52	73.8(4)
C12	C13	C14	118.2(5)	C50	C51	C52	109.5(6)
C13	C14	C15	121.2(5)	Ti1	C52	C51	71.7(3)
C14	C15	C16	119.5(5)	Ti1	C52	C53	72.7(3)
C11	C16	C15	121.4(5)	C51	C52	C53	108.3(6)
C1	C21	C22	123.2(4)	Ti1	C53	C52	72.9(3)
C1	C21	C26	119.2(5)	Ti1	C53	C54	70.8(3)
C22	C21	C26	117.6(5)	C52	C53	C54	107.0(6)
O2	C22	C21	114.5(5)	Ti1	C54	C50	72.9(3)
O2	C22	C23	123.7(5)	Ti1	C54	C53	74.2(3)
C21	C22	C23	121.7(5)	C50	C54	C53	108.8(5)
C22	C23	C24	120.0(5)	Ti2	C60	C61	73.2(3)
C23	C24	C25	118.6(5)	Ti2	C60	C64	72.7(4)
C24	C25	C26	121.3(5)	C61	C60	C64	107.3(6)
C21	C26	C25	120.7(5)	Ti2	C61	C60	72.0(4)
C2	C31	C32	122.2(5)	Ti2	C61	C62	73.5(4)
C2	C31	C36	119.9(5)	C60	C61	C62	108.4(7)
C32	C31	C36	117.9(5)	Ti2	C62	C61	72.0(3)
O3	C32	C31	120.8(5)	Ti2	C62	C63	72.8(4)
O3	C32	C33	118.3(5)	C61	C62	C63	109.3(7)

Table 4. Selected Interatomic Angles (continued)

Atom1	Atom2	Atom3	Angle	Atom1	Atom2	Atom3	Angle
Ti2	C63	C62	73.4(4)	Ti2	C64	C60	72.4(3)
Ti2	C63	C64	71.3(3)	Ti2	C64	C63	73.2(3)
C62	C63	C64	107.0(7)	C60	C64	C63	108.0(7)

(b) within the solvent toluene molecules

Atom1	Atom2	Atom3	Angle	Atom1	Atom2	Atom3	Angle
C10S	C11S	C12S	120.2(11)	C11S	C16S	C15S	121.1(11)
C10S	C11S	C16S	122.6(10)	C20S	C21S	C22S	113.5(14)
C12S	C11S	C16S	117.3(8)	C20S	C21S	C22S'	142.2(17)
C11S	C12S	C13S	120.1(9)	C22S	C21S	C22S'	104.2(10)
C12S	C13S	C14S	122.1(10)	C21S	C22S	C23S	119.9(11)
C13S	C14S	C15S	119.4(13)	C20S'	C23S	C22S	132.5(14)
C14S	C15S	C16S	119.9(12)	C20S'	C24S	C22S'	132.7(17)

Primed atoms are related to unprimed ones via the crystallographic inversion center ($1/2, 0, 1/2$).

Table 5. Torsional Angles (deg)

Atom1	Atom2	Atom3	Atom4	Angle	Atom1	Atom2	Atom3	Atom4	Angle
C11	Ti1	O1	C12	171.9(6)	C54	Ti1	C52	C53	-37.8(3)
C12	Ti1	O1	C12	-82.3(7)	C11	Ti1	C53	C52	-26.2(4)
C50	Ti1	O1	C12	53.9(7)	C11	Ti1	C53	C54	-141.7(3)
C51	Ti1	O1	C12	75.1(7)	C12	Ti1	C53	C52	-125.8(4)
C52	Ti1	O1	C12	52.0(8)	C12	Ti1	C53	C54	118.6(4)
C53	Ti1	O1	C12	7.8(7)	O1	Ti1	C53	C52	135.4(4)
C54	Ti1	O1	C12	19.0(7)	O1	Ti1	C53	C54	19.8(5)
C11	Ti1	C50	C51	37.7(4)	C50	Ti1	C53	C52	77.9(4)
C11	Ti1	C50	C54	152.0(3)	C50	Ti1	C53	C54	-37.7(3)
C12	Ti1	C50	C51	-112.1(4)	C51	Ti1	C53	C52	36.8(3)
C12	Ti1	C50	C54	2.2(5)	C51	Ti1	C53	C54	-78.8(4)
O1	Ti1	C50	C51	144.8(4)	C52	Ti1	C53	C54	-115.6(5)
O1	Ti1	C50	C54	-100.9(4)	C54	Ti1	C53	C52	115.6(5)
C51	Ti1	C50	C54	114.3(5)	C11	Ti1	C54	C50	-48.5(5)
C52	Ti1	C50	C51	-36.4(3)	C11	Ti1	C54	C53	67.5(5)
C52	Ti1	C50	C54	77.9(4)	C12	Ti1	C54	C50	-178.4(3)
C53	Ti1	C50	C51	-77.1(4)	C12	Ti1	C54	C53	-62.4(4)
C53	Ti1	C50	C54	37.2(3)	O1	Ti1	C54	C50	79.6(4)
C54	Ti1	C50	C51	-114.3(5)	O1	Ti1	C54	C53	-164.4(4)
C11	Ti1	C51	C50	-147.2(4)	C50	Ti1	C54	C53	116.0(5)
C11	Ti1	C51	C52	95.6(3)	C51	Ti1	C54	C50	-37.8(3)
C12	Ti1	C51	C50	106.5(4)	C51	Ti1	C54	C53	78.1(4)
C12	Ti1	C51	C52	-10.7(5)	C52	Ti1	C54	C50	-78.8(4)
O1	Ti1	C51	C50	-39.6(4)	C52	Ti1	C54	C53	37.1(3)
O1	Ti1	C51	C52	-156.8(3)	C53	Ti1	C54	C50	-116.0(5)
C50	Ti1	C51	C52	-117.2(5)	C13	Ti2	O3	C32	-91.9(5)
C52	Ti1	C51	C50	117.2(5)	C14	Ti2	O3	C32	160.0(5)
C53	Ti1	C51	C50	80.4(4)	C60	Ti2	O3	C32	38.1(6)
C53	Ti1	C51	C52	-36.7(3)	C61	Ti2	O3	C32	5.7(6)
C54	Ti1	C51	C50	38.7(3)	C62	Ti2	O3	C32	1.5(6)
C54	Ti1	C51	C52	-78.5(4)	C63	Ti2	O3	C32	49.9(7)
C11	Ti1	C52	C51	-84.8(3)	C64	Ti2	O3	C32	64.0(6)
C11	Ti1	C52	C53	158.5(4)	C13	Ti2	C60	C61	-10.6(6)
C12	Ti1	C52	C51	172.6(3)	C13	Ti2	C60	C64	-125.4(5)
C12	Ti1	C52	C53	55.9(4)	C14	Ti2	C60	C61	143.3(4)
O1	Ti1	C52	C51	38.8(5)	C14	Ti2	C60	C64	28.4(5)
O1	Ti1	C52	C53	-77.9(5)	O3	Ti2	C60	C61	-111.3(5)
C50	Ti1	C52	C51	36.7(3)	O3	Ti2	C60	C64	133.8(5)
C50	Ti1	C52	C53	-80.0(4)	C61	Ti2	C60	C64	-114.9(6)
C51	Ti1	C52	C53	-116.7(5)	C62	Ti2	C60	C61	37.0(4)
C53	Ti1	C52	C51	116.7(5)	C62	Ti2	C60	C64	-77.9(4)
C54	Ti1	C52	C51	78.9(4)	C63	Ti2	C60	C61	77.0(4)

Table 5. Torsional Angles (continued)

Atom1	Atom2	Atom3	Atom4	Angle	Atom1	Atom2	Atom3	Atom4	Angle
C63	Ti2	C60	C64	-37.8(4)	C41	C2	C31	C36	-111.1(5)
C64	Ti2	C60	C61	114.9(6)	C1	C2	C41	C42	-120.0(6)
C11	C1	C2	C31	10.0(7)	C1	C2	C41	C46	60.9(7)
C11	C1	C2	C41	-169.5(4)	C31	C2	C41	C42	60.5(7)
C21	C1	C2	C31	-167.4(4)	C31	C2	C41	C46	-118.6(5)
C21	C1	C2	C41	13.1(7)	C1	C11	C12	O1	1.4(8)
C2	C1	C11	C12	-110.0(6)	C1	C11	C12	C13	178.9(5)
C2	C1	C11	C16	66.8(6)	C1	C11	C16	C15	-177.7(5)
C21	C1	C11	C12	67.5(6)	C1	C21	C22	O2	7.1(7)
C21	C1	C11	C16	-115.6(5)	C1	C21	C22	C23	-176.4(5)
C2	C1	C21	C22	-122.4(5)	C1	C21	C26	C25	176.0(5)
C2	C1	C21	C26	60.2(7)	C2	C31	C32	O3	-3.0(7)
C11	C1	C21	C22	60.2(6)	C2	C31	C32	C33	176.9(5)
C11	C1	C21	C26	-117.3(5)	C2	C31	C36	C35	-178.4(5)
C1	C2	C31	C32	-108.7(6)	C2	C41	C42	O4	4.0(8)
C1	C2	C31	C36	69.4(6)	C2	C41	C42	C43	-175.6(5)
C41	C2	C31	C32	70.8(6)	C2	C41	C46	C45	176.6(5)

Primed atoms are related to unprimed ones via the crystallographic inversion center ($1/2$, 0 , $1/2$).

A-23: Complex 72. [2,7-^tBu₂-1,8-((C₄H₈O)Cl₃TiO)₂-fluorene]

– Chapter 5 –

XCL Code: JMS9812

Date: 26 November 1998

Compound: [2,7-^tBu₂-1,8-((C₄H₈O)Cl₃TiO)₂-fluorene]

Formula: C₂₉H₄₀Cl₆O₄Ti₂

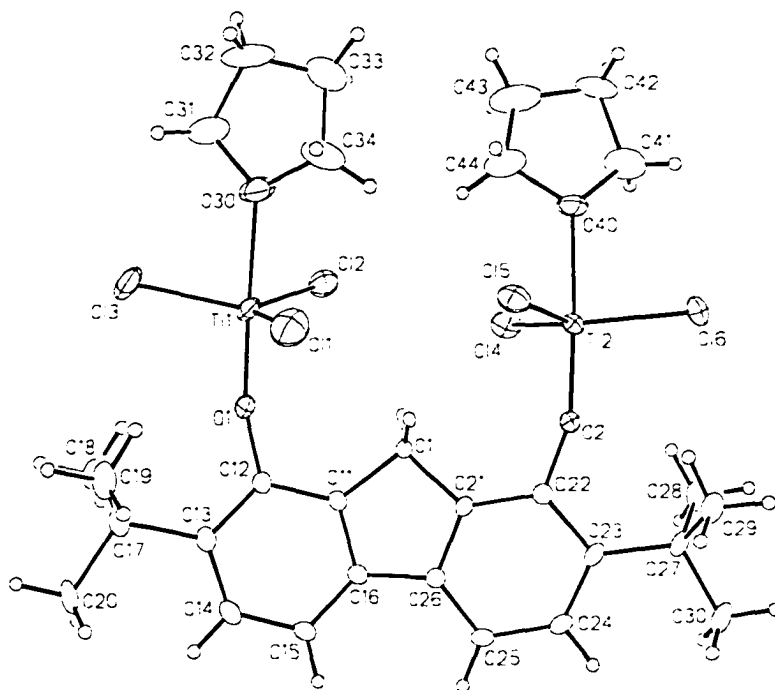


Figure 1. Perspective view of the [2,7-^tBu₂-1,8-((C₄H₈O)Cl₃TiO)₂-fluorene] molecule showing the atom labelling scheme. Non-hydrogen atoms are represented by Gaussian ellipsoids at the 20% probability level. Hydrogen atoms are shown with arbitrarily small thermal parameters.

List of Tables

Table 1. Crystallographic Experimental Details

Table 2. Atomic Coordinates and Equivalent Isotropic Displacement Parameters

Table 3. Selected Interatomic Distances

Table 4. Selected Interatomic Angles

Table 1. Crystallographic Experimental Details

A. Crystal Data

formula	C ₂₉ H ₄₀ Cl ₆ O ₄ Ti ₂
formula weight	761.11
crystal dimensions (mm)	0.50 × 0.28 × 0.27
crystal system	monoclinic
space group	<i>P</i> 2 ₁ / <i>n</i> (an alternate setting of <i>P</i> 2 ₁ / <i>c</i> [No. 14])
unit cell parameters ^a	
<i>a</i> (Å)	13.5437 (9)
<i>b</i> (Å)	8.9759 (7)
<i>c</i> (Å)	29.725 (2)
β (deg)	101.749 (5)
<i>V</i> (Å ³)	3537.8 (4)
<i>Z</i>	4
ρ _{calcd} (g cm ⁻³)	1.429
μ (mm ⁻¹)	0.936

B. Data Collection and Refinement Conditions

diffractometer	Siemens P4/RA ^b
radiation (λ [Å])	graphite-monochromated Mo Kα (0.71073)
temperature (°C)	-60
scan type	ω
data collection 2θ limit (deg)	50.0
total data collected	6523 (0 ≤ <i>h</i> ≤ 16, 0 ≤ <i>k</i> ≤ 10, -35 ≤ <i>l</i> ≤ 34)
independent reflections	6238
number of observed reflections (<i>NO</i>)	3577 [<i>F</i> ₀ ² ≥ 2σ(<i>F</i> ₀ ²)]
structure solution method	direct methods (<i>SHELXS-86</i> ^c)

refinement method	full-matrix least-squares on F^2 (SHELXL-93 ^d)
absorption correction method	Gaussian integration (face-indexed)
range of transmission factors	0.8298–0.7189
data/restraints/parameters	6232 [$F_o^2 \geq -3\sigma(F_o^2)$] / 0 / 370
goodness-of-fit (S) ^e	1.036 [$F_o^2 \geq -3\sigma(F_o^2)$]
final R indices ^f	
R_1 [$F_o^2 \geq 2\sigma(F_o^2)$]	0.0796
wR_2 [$F_o^2 \geq -3\sigma(F_o^2)$]	0.2177
largest difference peak and hole	0.865 and -0.636 e \AA^{-3}

^aObtained from least-squares refinement of 40 reflections with $22.0^\circ < 2\theta < 25.8^\circ$.

^bPrograms for diffractometer operation, data collection, data reduction and absorption correction were those supplied by Siemens.

^cSheldrick, G. M. *Acta Crystallogr.* **1990**, *A46*, 467–473.

^dSheldrick, G. M. *SHELXL-93*. Program for crystal structure determination. University of Göttingen, Germany, 1993. Refinement on F_o^2 for all reflections except for 6 having $F_o^2 < -3\sigma(F_o^2)$. Weighted R -factors wR_2 and all goodnesses of fit S are based on F_o^2 ; conventional R -factors R_1 are based on F_o , with F_o set to zero for negative F_o^2 . The observed criterion of $F_o^2 > 2\sigma(F_o^2)$ is used only for calculating R_1 , and is not relevant to the choice of reflections for refinement. R -factors based on F_o^2 are statistically about twice as large as those based on F_o , and R -factors based on ALL data will be even larger.

^e $S = [\sum w(F_o^2 - F_c^2)^2 / (n - p)]^{1/2}$ (n = number of data; p = number of parameters varied; $w = [\sigma^2(F_o^2) + (0.0728P)^2 + 13.7401P]^{-1}$ where $P = [\text{Max}(F_o^2, 0) + 2F_c^2]/3$).

^f $R_1 = \sum ||F_o| - |F_c|| / \sum |F_o|$; $wR_2 = [\sum w(F_o^2 - F_c^2)^2 / \sum w(F_o^4)]^{1/2}$.

Table 2. Atomic Coordinates and Equivalent Isotropic Displacement Parameters

Atom	x	y	z	$U_{eq}, \text{\AA}^2$
Ti1	-0.06961(11)	0.1535(2)	0.16163(5)	0.0626(5)*
Ti2	0.26974(10)	-0.00164(15)	0.07441(5)	0.0421(4)*
C11	-0.0975(2)	0.2894(4)	0.09550(9)	0.0967(9)*
C12	0.0455(2)	-0.0242(3)	0.17675(10)	0.0840(8)*
C13	-0.1852(2)	0.1404(4)	0.20449(11)	0.1228(14)*
C14	0.2950(2)	-0.0943(2)	0.14499(7)	0.0613(6)*
C15	0.1195(2)	0.0976(2)	0.04190(7)	0.0599(6)*
C16	0.3718(2)	-0.0678(3)	0.02769(10)	0.0922(9)*
O1	0.0046(3)	0.2959(5)	0.1915(2)	0.0442(12)*
O2	0.3271(3)	0.1699(5)	0.0926(2)	0.0405(12)*
O30	-0.1620(6)	-0.0077(10)	0.1190(2)	0.120(3)*
O40	0.1956(4)	-0.2117(6)	0.0542(2)	0.066(2)*
C1	0.1931(5)	0.2823(7)	0.1541(2)	0.034(2)*
C11	0.1626(5)	0.3980(7)	0.1860(2)	0.0319(15)*
C12	0.0742(5)	0.4081(7)	0.2032(2)	0.0330(15)*
C13	0.0552(5)	0.5298(8)	0.2296(2)	0.038(2)*
C14	0.1323(6)	0.6339(8)	0.2404(2)	0.047(2)*
C15	0.2224(5)	0.6250(8)	0.2251(2)	0.043(2)*
C16	0.2365(5)	0.5062(7)	0.1973(2)	0.0341(15)*
C17	-0.0449(5)	0.5502(9)	0.2456(2)	0.048(2)*
C18	-0.0599(5)	0.4247(9)	0.2784(3)	0.053(2)*
C19	-0.1329(6)	0.5543(11)	0.2032(3)	0.066(3)*
C20	-0.0468(6)	0.6989(10)	0.2713(3)	0.069(3)*
C21	0.2937(4)	0.3449(7)	0.1471(2)	0.0307(14)*
C22	0.3552(5)	0.2948(7)	0.1181(2)	0.034(2)*
C23	0.4451(5)	0.3739(8)	0.1148(2)	0.041(2)*
C24	0.4676(5)	0.4972(8)	0.1431(2)	0.044(2)*
C25	0.4076(5)	0.5479(8)	0.1723(2)	0.041(2)*
C26	0.3184(5)	0.4724(7)	0.1733(2)	0.0325(15)*
C27	0.5134(5)	0.3240(9)	0.0822(2)	0.046(2)*
C28	0.5580(6)	0.1702(9)	0.0960(3)	0.057(2)*
C29	0.4524(6)	0.3237(10)	0.0325(2)	0.056(2)*
C30	0.6017(6)	0.4318(11)	0.0833(3)	0.070(3)*
C31	-0.2355(9)	-0.1009(12)	0.1304(4)	0.106(4)*
C32	-0.2627(12)	-0.2070(16)	0.0918(5)	0.143(6)*
C33	-0.1777(14)	-0.2168(16)	0.0718(5)	0.147(6)*
C34	-0.1477(13)	-0.0475(19)	0.0745(5)	0.189(9)*
C41	0.2410(10)	-0.3430(12)	0.0412(6)	0.135(5)*
C42	0.1618(9)	-0.4628(11)	0.0354(4)	0.101(4)*

Table 2. Atomic Coordinates and Displacement Parameters (continued)

Atom	<i>x</i>	<i>y</i>	<i>z</i>	<i>U</i> _{eq} , Å ²
C43	0.0944(11)	-0.4101(13)	0.0647(6)	0.137(6)*
C44	0.1026(12)	-0.2486(15)	0.0652(6)	0.171(8)*

Anisotropically-refined atoms are marked with an asterisk (*). The form of the anisotropic displacement parameter is: $\exp[-2\pi^2(h^2a^{*2}U_{11} + k^2b^{*2}U_{22} + l^2c^{*2}U_{33} + 2klb^{*c^*}U_{23} + 2hla^{*c^*}U_{13} + 2hka^{*b^*}U_{12})]$.

Table 3. Selected Interatomic Distances (Å)

Atom1	Atom2	Distance	Atom1	Atom2	Distance
Ti1	C11	2.279(3)	C14	C15	1.390(9)
Ti1	C12	2.211(3)	C15	C16	1.385(9)
Ti1	C13	2.213(3)	C16	C26	1.469(8)
Ti1	O1	1.753(5)	C17	C18	1.529(10)
Ti1	O30	2.149(6)	C17	C19	1.549(10)
Ti2	C14	2.218(2)	C17	C20	1.540(11)
Ti2	C15	2.251(2)	C21	C22	1.389(8)
Ti2	C16	2.231(2)	C21	C26	1.386(9)
Ti2	O2	1.759(5)	C22	C23	1.430(9)
Ti2	O40	2.163(5)	C23	C24	1.387(10)
O1	C12	1.374(8)	C23	C27	1.537(9)
O2	C22	1.364(8)	C24	C25	1.381(9)
O30	C31	1.394(11)	C25	C26	1.390(9)
O30	C34	1.421(13)	C27	C28	1.530(11)
O40	C41	1.418(11)	C27	C29	1.540(10)
O40	C44	1.405(13)	C27	C30	1.533(10)
C1	C11	1.520(8)	C31	C32	1.48(2)
C1	C21	1.526(8)	C32	C33	1.40(2)
C11	C12	1.398(8)	C33	C34	1.57(2)
C11	C16	1.386(9)	C41	C42	1.503(14)
C12	C13	1.398(9)	C42	C43	1.46(2)
C13	C14	1.389(10)	C43	C44	1.45(2)
C13	C17	1.537(9)			

Table 4. Selected Interatomic Angles (deg)

Atom1	Atom2	Atom3	Angle	Atom1	Atom2	Atom3	Angle
C11	Ti1	C12	123.20(12)	C14	C15	C16	118.5(6)
C11	Ti1	C13	120.83(15)	C11	C16	C15	120.3(6)
C11	Ti1	O1	91.4(2)	C11	C16	C26	108.5(5)
C11	Ti1	O30	83.0(3)	C15	C16	C26	131.2(6)
C12	Ti1	C13	113.38(15)	C13	C17	C18	110.5(6)
C12	Ti1	O1	96.6(2)	C13	C17	C19	109.3(6)
C12	Ti1	O30	86.3(3)	C13	C17	C20	111.2(6)
C13	Ti1	O1	98.4(2)	C18	C17	C19	110.8(7)
C13	Ti1	O30	84.8(2)	C18	C17	C20	107.8(6)
O1	Ti1	O30	174.3(3)	C19	C17	C20	107.1(7)
C14	Ti2	C15	120.42(10)	C1	C21	C22	129.0(6)
C14	Ti2	C16	119.56(12)	C1	C21	C26	110.4(5)
C14	Ti2	O2	93.6(2)	C22	C21	C26	120.6(6)
C14	Ti2	O40	84.8(2)	O2	C22	C21	118.4(6)
C15	Ti2	C16	117.33(11)	O2	C22	C23	121.0(6)
C15	Ti2	O2	95.1(2)	C21	C22	C23	120.6(6)
C15	Ti2	O40	84.2(2)	C22	C23	C24	116.0(6)
C16	Ti2	O2	97.7(2)	C22	C23	C27	122.0(6)
C16	Ti2	O40	84.6(2)	C24	C23	C27	122.0(6)
O2	Ti2	O40	177.6(2)	C23	C24	C25	124.0(6)
Ti1	O1	C12	162.9(4)	C24	C25	C26	118.5(6)
Ti2	O2	C22	161.2(4)	C16	C26	C21	108.9(5)
Ti1	O30	C31	128.3(7)	C16	C26	C25	130.9(6)
Ti1	O30	C34	123.0(7)	C21	C26	C25	120.2(6)
C31	O30	C34	108.3(9)	C23	C27	C28	110.4(6)
Ti2	O40	C41	126.7(6)	C23	C27	C29	109.3(6)
Ti2	O40	C44	121.9(6)	C23	C27	C30	111.7(6)
C41	O40	C44	109.1(8)	C28	C27	C29	111.2(7)
C11	C1	C21	101.4(5)	C28	C27	C30	107.5(6)
C1	C11	C12	129.4(6)	C29	C27	C30	106.6(6)
C1	C11	C16	110.8(5)	O30	C31	C32	106.0(10)
C12	C11	C16	119.7(6)	C31	C32	C33	105.9(11)
O1	C12	C11	117.0(5)	C32	C33	C34	98.3(12)
O1	C12	C13	121.3(6)	O30	C34	C33	102.0(11)
C11	C12	C13	121.6(6)	O40	C41	C42	106.7(9)
C12	C13	C14	116.2(6)	C41	C42	C43	102.5(9)
C12	C13	C17	122.7(6)	C42	C43	C44	105.9(12)
C14	C13	C17	121.1(6)	O40	C44	C43	107.6(12)
C13	C14	C15	123.6(6)				